Ollscoil na Gaillimhe
University of Galway

Provided by the author(s) and University of Galway in accordance with publisher policies. Please cite the published version when available.

Title	Glycosylation in the injured and regenerating spinal cord, and the influence of biomaterial treatment
Author(s)	Ronan, Rachel
Publication Date	2020-02-04
Publisher	NUI Galway
Item record	http://hdl.handle.net/10379/15758

Downloaded 2024-04-26T13:24:40Z

Some rights reserved. For more information, please see the item record link above.

Glycosylation In The Injured And Regenerating Spinal Cord, And The Influence Of Biomaterial Treatment

Rachel Ronan

August 2019

Discipline of Anatomy
College of Medicine, Nursing and Health Sciences
National University of Ireland, Galway

Thesis submitted in fulfilment of the requirements for the degree of Doctor of Philosophy

Thesis supervisors:

Dr Siobhán McMahon
Prof Abhay Pandit

Table of Contents

Declaration vii

Abstract ix

Acknowledgements xi

List of Abbreviations xiii

Research dissemination xvii

Publication xvii

Conference presentations xvii

1 Chapter 1 – Introduction 1

1.1 Spinal cord injury 1

1.1.1 Incidence and statistics 1

1.1.2 Pathophysiology of SCI 1

1.2 Mammalian models of SCI 4

1.2.1 The scarring process following SCI in mammals 5

1.2.2 The inflammatory response and macrophage polarisation following SCI in mammals 6

1.3 Biomaterial treatment strategies for SCI 10

1.3.1 Collagen for treatment of SCI 11

1.3.2 Biomaterial therapies in clinical trials 12

1.4 SCI and the regenerative capacity of non-mammalian species 13

1.4.1 Metamorphosis and the regenerative potential of Xenopus laevis 14

1.4.2 Mechanisms of regeneration in tadpole Xenopus laevis 15

1.4.3 Scarring and inflammation in non-mammalian SCI 17

1.5 Glycobiology 20

1.5.1 Basic glycochemistry 20

1.5.2 Glycans found in tissue 22

1.5.3 N-glycan biosynthesis 25

1.5.4 Glycan nomenclature 33

1.5.5 Glycobiology of the healthy CNS 36

1.5.6 Glycobiology of the injured or diseased CNS 38

1.5.7 Glycans and inflammation 41

1.6 Phases and rationale for the project 48

2 Chapter 2 - Materials and Methods 49

2.1 *In vivo* modelling of SCI in *Xenopus laevis* 49

2.1.1 Growth of Xenopus laevis 49

2.1.2 Spinal cord injury stage 50 tadpole 49

2.1.3 Spinal cord injury stage 66 froglet 50

2.1.4 Euthanasia: Xenopus laevis 51

2.1.5 Processing of Xenopus laevis tissue 52

2.2 *In vivo* modelling of SCI in the rat 53

2.2.1 Spinal cord transection injury, collagen hydrogel implantation and sham injury in the rat 53

2.2.2 Euthanasia: rat 54

2.2.3 Tissue harvesting and processing of rat tissue 55

2.2.4 Collagen hydrogel preparation 56

2.3 Immunohistochemistry 56

2.3.1 Immunohistochemistry: Xenopus laevis 57

2.3.2 Immunohistochemistry: rat 57

2.4 Lectin histochemistry 59

2.5 Combined lectin- and immuno-histochemistry 60

2.6 Histology 60

2.6.1 Alcian blue 60

2.6.2 Masson's trichrome 60

2.7 Image acquisition and analysis 61

2.7.1 High magnification image acquisition for Xenopus laevis experiments 61

2.7.2 Analysis of timeline of neuronal growth in tadpole Xenopus laevis 63

2.7.3 Analysis of astrocyte response to SCI in Xenopus laevis 64

2.7.4 Analysis of lectin histochemistry in Xenopus laevis 64

2.7.5 Histological analysis of scar tissue in the rat 65

2.7.6 Analysis of microglia / macrophage phenotype in the rat 65

2.8 *N*-glycan analysis of the rat spinal cord 68

2.8.1 Sample preparation 69

2.8.2 Weak anion exchange high performance liquid chromatography (WAX-HPLC) 70

2.8.3 Exoglycosidase digestions 70

2.8.4 Hydrophilic interaction liquid chromatography-ultra-performance liquid chromatography (HILIC-UPLC) separation and quantification of released, labelled N-glycans ... 72

2.8.5 Integration, assignments and analysis of UPLC data 72

2.8.6 Liquid chromatography coupled mass spectrometry (LC-MS) 73

2.8.7 DMB assay 74

2.9 Statistical analysis 75

3 Chapter 3 - The cellular response to spinal cord transection in regenerative and non-regenerative stages of *Xenopus laevis* 76
3.1 Introduction 76
3.2 Hypotheses 78
3.3 Objectives 78
3.4 Experimental design 78
3.5 Results 80
3.5.1 Timeline of regeneration following spinal cord transection in stage 50 tadpole 80
3.5.2 Astrocytes increase following spinal cord transection in stage 66 froglet 88
3.6 Discussion 95
4 Chapter 4 - The Glycosylation Response to Spinal Cord Transection in Pre- and Post-Metamorphic *Xenopus Laevis* 98
4.1 Introduction 98
4.2 Hypothesis 98
4.3 Objectives 98
4.4 Experimental design 99
4.5 Results 100
4.5.1 Galactose in and around the lesion increases following SCI but decreases as regeneration proceeds in tadpole 100
4.5.2 β(1-4) GlcNAc in and around the lesion increases following SCI but decreases over time in both tadpole and froglet 108
4.5.3 α(2-6) sialic acid increases in and around the lesion following SCI in tadpole and to a greater extent in froglet 116
4.5.4 GalNAc is increased following SCI in tadpole, but decreased following SCI in froglet 124

4.5.5 Sugar abundance in sham injured tissue 132

4.5.6 Lectin signal does not co-localise with tubulin positive neurons or GFAP positive astroglia 135

4.6 Discussion 135

5 Chapter 5 - Inflammation and Scar Deposition following SCI and Collagen Hydrogel Implantation in a Rat Transection Model 145

5.1 Introduction 145

5.2 Hypothesis 146

5.3 Objectives 146

5.4 Experimental design 146

5.5 Results 148

5.5.1 Scar deposition and extracellular matrix composition 148

5.5.2 Time-course of microglia and macrophage polarisation in injured rat spinal cord 153

5.5.3 Collagen hydrogel reduced bleeding at the site of injury 161

5.6 Discussion 162

6 Chapter 6 - *N*-glycosylation of the healthy, injured and collagen treated rat spinal cord 166

6.1 Introduction 166

6.2 Hypotheses 167

6.3 Objectives 167

6.4 Experimental design 167

6.5 Results 171

6.5.1 Method development to analyse spinal cord N-glycosylation 171

6.5.2 Characterisation of spinal cord of the healthy adult female rat 175

6.5.3 Changes in N-glycosylation as a result of transection and treatment with aligned collagen hydrogel at the lesion epicentre 205

6.6 Discussion 238

7 Chapter 7 – Conclusions 245

7.1 Future directions 250

8 Chapter 8 - Bibliography 252

Appendices 268

Appendix I: Microglia and macrophage polarisation in rodent models of SCI 268

Appendix II: Collagen biomaterials in pre-clinical models of SCI 273

Appendix III: Reagents, equipment and consumables required for *Xenopus laevis* growth and surgery 286

Appendix IV: Reagents, equipment and consumables required for rat surgery and tissue processing 287

Appendix V: Reagents and consumables for tissue processing, histology and lectin- and immuno-histochemistry 288

Appendix VI: Protocols for histological stains 290

Alcian Blue 290

Masson's trichrome 291

Appendix VII: Reagents and consumables required for *N*-glycosylation studies 292

Appendix VIII: Recipes 293

Appendix IX: Macros 296

Macro to create maximum projection with desired brightness and contrast for analysis of time line of repair in Xenopus laevis tadpoles 296

Macro for analysis of lectin histochemistry 297

Appendix X: Spinal cord *N*-glycome 298

Appendix XI: Mass data for spinal cord *N*-glycans 313

Declaration

I declare that the work described in this thesis was carried out in accordance with the regulations of the National University of Ireland, Galway. All data and ideas described herein are the results of my own work, unless otherwise indicated or acknowledged as a referenced work. This thesis has not been submitted to any other academic institution or non-academic institution for any degree or qualification.

The table below indicates the people involved in each stage of the experimental work.

Growth of *Xenopus laevis*	Rachel Ronan, Aniket Kshirsagar
Development of spinal cord transection model in tadpole	Dr Gerhard Schlosser, Aniket Kshirsagar, Rachel Ronan
Surgical procedure and aftercare for tadpole and froglet *Xenopus laevis* for the data shown in this work	Rachel Ronan
Euthanasia and tissue processing for *Xenopus laevis* tissue used in this work	Rachel Ronan
Behavioural analysis of *Xenopus laevis* pre- and post-transection	Ana Lúcia Rebelo (MSc project with supervision of RR)
Cryosectioning, immuno- and lectin-histochemistry and imaging of *Xenopus laevis* tissue	Rachel Ronan
Image quantification of lectin histochemistry	Rachel Ronan
Image quantification of GFAP	Seamus Cawley (BSc project with supervision of RR)
Image quantification of GAP43	Claire McHugh (BSc project with supervision of RR)
Surgical procedures to model SCI in the rat, and implant collage hydrogels	Dr Abbah Sunny
Fabrication of collagen hydrogels	Aniket Kshirsagar
Post-procedural care, rat	Rachel Ronan, Aniket Kshirsagar
Euthanasia and tissue processing, rat	Rachel Ronan, Aniket Kshirsagar

Cryosectioning, rat tissue	Rachel Ronan, Aniket Kshirsagar
Immuno-histochemistry and lectin histochemistry, image acquisition, rat tissue	Rachel Ronan
Image quantification, microglia/macrophage study	Rachel Ronan
Alcian blue and masson's trichrome staining	Heather Morrison (BSc project with supervision of RR)
Image acquisition alcian blue and masson's trichrome	Rachel Ronan, Heather Morrison
Image analysis alcian blue and masson's trichrome	Heather Morrison (BSc project with supervision of RR)
Method development for *N*-glycan analysis of CNS tissue	Rachel Ronan, Juhi Samal, Dr Róisín O'Flaherty (NIBRT), Dr Radka Saldova (NIBRT)
Sample preparation: *N*-glycan release, labelling, clean up and UPLC for characterisation and SCI studies	Rachel Ronan
Exoglycosidase digestions	Rachel Ronan
DMB analysis	Paula Kenny (NIBRT)
Mass spectrometry (experimental run)	Jo Withers (NIBRT)
Mass spectrometry (analysis)	Rachel Ronan
N-glycome characterisation of healthy tissue	Rachel Ronan, with support from Dr Radka Saldova (NIBRT)
Analysis of *N*-glycosylation changes in SCI	Rachel Ronan

Abstract

Traumatic spinal cord injury (SCI) results in disruption of tissue integrity leading to a loss of function. There has been minimal success in treating these injuries clinically, due to the inhibitory environment which develops over time. In this work, we study the glycosylation response to SCI in two models: *Xenopus laevis* is used to compare successful to failed regeneration, by comparing the response to injury pre- and post-metamorphosis, while we use a rat model to understand the pathophysiology of the injury and how this may be modified by treatment with an aligned collagen hydrogel. We hypothesise that glycosylation is altered in response to injury, that it has a role in determining the success of regeneration, and that biomaterial treatment can influence this glycosylation response. Complete transection was used to model SCI in pre- and post-metamorphic stages of *Xenopus laevis* and in adult rat. Collagen hydrogels with aligned or non-aligned fibres were placed at the transection site in the rat spinal cord only. Lectin histochemistry was used to investigate glycosylation changes in *Xenopus laevis.* HILIC-UPLC *N*-glycoprofiling was used to characterise the normal *N*-glycome of the healthy adult rat, and to investigate changes in response to SCI and collagen hydrogel treatment. Immunohistochemistry was used to investigate neuronal or glial changes in response to the injury in each species.

In the healthy rat spinal cord UPLC *N*-glycoprofiling identified all three major categories of *N*-glycan, i.e. complex, hybrid and high mannose. Many of the complex structures terminated in galactose and were commonly decorated with core and outer arm fucose residues. There was a low level of sialylation. Following SCI there was a decrease in complex glycans in the rat spinal cord and a corresponding increase in high mannose and hybrid structures, with and without core fucose. There was a loss of outer arm fucosylation, while bisecting GlcNAc and sialic acid were increased. Treatment with aligned collagen hydrogel lead to small changes in the glycosylation response.

Pre-metamorphic *Xenopus laevis* regenerated the spinal cord within 10 days, with a thin tissue bridge seen at 7 days. There was significantly more GFAP in the non-regenerating froglet spinal cord. In both tadpole and froglet *Xenopus* there was an early increase in sialic acid following SCI but this was far more pronounced in the non-regenerative froglet. In the rat injury also resulted in an increase in sialic acid, which was found to be associated with microglia or macrophages. Sugars carrying GlcNAc were increased during the tadpole regenerative response but were decreased in the froglet. This may relate to *N*-glycan complexity which was decreased following SCI in the rat. There were also differences in GalNAc decoration depending on the regenerative potential, being increased in the tadpole but decreased in the froglet. This sugar was not identified on rat *N*-glycans. This work suggests that glycosylation may influence the success of regeneration. In particular an early but transient increase

in sialic acid may be important for repair, and the loss of complexity in rat spinal cord glycans may be a contributing factor to the failure of regeneration.

Acknowledgements

Firstly I would like to express my gratitude to my supervisors Dr Siobhán McMahon and Prof Abhay Pandit for their instruction, guidance and support over the past number of years. Thank you for giving me a chance when I came to you as a naïve student with little idea of what a PhD entails, and then for the encouragement, and for pushing me when it was needed.

Thank you also to Dr Radka Saldova, without whose guidance and endless corrections the glycosylation study would simply not have been possible, and to Dr Róisín O' Flaherty for all of the advice over the last two years, scientific and otherwise. Thank you to Dr Gerhard Schlosser for introducing me to working with *Xenopus laevis,* and helping me to understand this probably under-used model. Thank you to Dr Michelle Kilcoyne for teaching me how to use and understand lectins.

This work would never have reached completion if not for the never-ending support from the friends and colleagues I have been fortunate enough to be surrounded by for the past six years.

Thank you to all members of the anatomy department for scientific help and guidance, and just generally making sure coming to work could be fun! Thank you especially to Mr Mark Canney for answering all of my many histology and tissue processing questions, to Prof Peter Dockery for the advice on image analysis, and to Dr Kerry Thompson for teaching me to use a microscope, still my favourite toy! Dr Yolanda Garcia, thank you for your support during the *in vivo* study. Your advice, patience and guidance was hugely appreciated and made the whole process so much easier. To all the students of the anatomy department who I have worked beside, in particular my office buddies Azim, Joana and Silvia, it was a pleasure. To all of the CÚRAM people I have worked beside, thank you too… there are just too many to name! But a special thank you to Dr Abbah Sunny for sharing your incredible knowledge and skills, and for your kind advice during the toughest stage of this entire PhD. Thank you also to Dr Oliver Carroll for somehow always having time to answer questions and give help when needed, and to Aniket with whom I worked side by side through much of this study.

To my most recent workmates, the NIBRT Contract Research group, thank you all so very much for your patience, understanding, kind words (and of course the nuggets of glycan wisdom!) over the past 9 months, and for knowing that once the big headphones went on that I was no longer 'at work'!

To my dearest friends, an enormous thank you for all your support during these years.

To Ian, Emma H, Emma Mc and Eva for always being there to remind me that there is a world outside of science, a world of hikes and gigs in the Róisín and all kinds of adventures!

To Ana Lucia and Grazia, we have come through this journey together, with all its ups and downs, and you two keep smiling and singing even when anyone else would do the opposite. Thanks for keeping me smiling too. To Vaibhav and to Adriona, you both always manage to brighten the day.

To my ‘neuro girls’, Amy, Jen, Katie and Alicia, thank you for always being there for chats and activities. They’re not so frequent any more, but we make them count! Here’s to many more.

To Fiona, we started our educational journey side by side as tiny humans in a tiny play school on Skough Hill, and I’m so pleased that we finished this side by side here in Galway. I’m sure our parents are relieved that we can do no more!

To João, you have been an immense support over the past couple of years, I cannot thank you enough. I just hope I can do the same for you.

Finally, to my family. Mam, Dad, Daniel and Olivia, my god-mother Leish and my grandmother Mollie. Thank you for teaching me the value and importance of hard work, and for understanding completely when visits became less and less frequent as that hard work slowly took over. I have taken comfort in you so many times over the past while, and knowing you were all just a bus trip or a phone call away made this journey ten times easier. I love you all, this is for you.

List of Abbreviations

2AB	2-aminobenzamide
A	Antennae (glcnac)
ABS	Arthrobacter ureafaciens sialidase
AD	Alzheimer's disease
AIA	Artocarpus integrifolia agglutinin
AMF	Almond meal α-fucosidase
ANOVA	Analysis of variance
ASIA	American spinal injury association
B	Bisect
BBB	Basso beattie bresnahan
BKF	Bovine kidney α-fucosidase
BrdU	Bromodeoxyuridine
BSA	Bovine serum albumin
BSCB	Blood spinal cord barrier
BTG	Bovine testes β-galactosidase
C	Carbon
CBG	Coffee bean α-galactosidase
CCR2	CC chemokine receptor 2
CFG	Consortium for Functional Glycomics
CNS	Central nervous system
CSPG	Chondroitin sulphate proteoglycans
CV	Coefficient of variation
dHex	Deoxy-hexoses
DMB	1,2-diamino-4,5-methylenedioxybenzene.2hcl
dpi	Days post injury
DPX	Plasticiser and xylene
DSA	Datura stramonium agglutinin
DTT	Dithiothreitol
ECM	Extracellular matrix
ER	Endoplasmic reticulum
F	Fucose
FITC	Fluorescein isothiocyanate
G	Galactose
Ga	Alpha linked galactose
GAG	Glycosaminoglycan
Gal	Galactose
Gal-1	Galectin-1

Gal-3	Galectin-3
GalCer	Galactosylceramide
GalNAc	*N*-acetyl galactosamine
GAP43	Growth associated protein 43
GFAP	Glial fibrillary acidic protein
GlcNAc	*N*-acetylglucosamine
GnT	Glcnac-transferase
GP	Glycan peak
GPI	Glycosylphosphatidylinositol
GU	Glucose unit
GUH	Streptococcus pneumonia hexosamindase
HD	Huntington's disease
HILIC	Hydrophilic interaction liquid chromatography
HNK-1	Human natural killer cell epitope-1
HPLC	High performance liquid chromatography
HSPG	Heparan sulphate proteoglycan
IAA	Iodoacetamide
IFNγ	Interferon-γ
IL	Interleukin
iNOS	Inducible nitric oxide synthase
ITAM	Immunoreceptor tyrosine-based activatory motif
ITIM	Immunoreceptor tyrosine-based inhibitory motif
JBH	Jack bean β-N-acetylhexoaminidase
JBM	Jack bean mannosidase
Lac	Lacosamine
LC-MS	Liquid chromatography-mass spectrometry
M	Mannose
MALDI	Matrix assisted laser desorption/ionisation
MBS	Modified Barth solution
MCAO	Middle cerebral artery occlusion
MCP-1	Monocyte chemoattractant protein-1
MS222	Tricaine methanesulfonate
MSCs	Mesenchymal stem cells
NADPH	Dihydronicotinamide-adenine dinucleotide phosphate
NAN-1	Recombinant sialidase
NCAM	Neural cell adhesion molecule
NEB	New england biolabs
Neu5Ac	*N*-acetyl neuraminic acid
Neu5Gc	*N*-glycolyl neuraminic acid
NF	Nieuwkoop and Faber

NSPCs	Neural stem and progenitor cells
NT-3	Neurotrophin-3
OCT	Optimal cutting temperature
P	Phosphate
PBS	Phosphate buffered saline
PBS-T	Triton X-100 in 1X PBS
PCL	Polycaprolactone
PEG	Poly ethylene glycol
PFA	Paraformaldehyde
PGA	Poly glycolic acid
pHEMA	Poly(2-hydroxyethyl methacrylate)
PIC	Protease inhibitor cocktail
PLA	Poly lactic acid
PLGA	Poly(lactic-co-glycolic acid)
PNA	Peanut agglutinin
PNGaseF	Peptide N-glycosidase F
PSGL-1	P-selectin glycoprotein ligand-1
RIPA	Radioimmunoprecipitation assay buffer
ROI	Region of interest
S	Sialic acid
SCI	Spinal cord injury
SEM	Standard error of the mean
SII	Spinal injuries Ireland
SNA-I	Sambucus nigra agglutinin
SPG	Streptococcus pneumoniae β-galactosidase
T	Thoracic vertebra
TBI	Traumatic brain injury
TBS	Tris buffered saline
TBS-T	Triton-X-100 in TBS
TEMED	Tetramethylethylenediamine
TIM-1	T-cell immunoglobulin and mucin domain-1
TNF-α	Tumour necrosis factor-α
UDP	Uridine diphosphate
UMP	Uridine monophosphate
UND	Undigested
UPLC	Ultra performance liquid chromatography
Vv	Volume fraction
WAX	Weak anion exchange
WFA	Wisteria floribunda agglutinin
WHO	World health organisation

WT	Wild-type

Research dissemination

Publication

BA. Breen, H Kraskiewicz, R Ronan, A Kshiragar, A Patar, T Sargeant, A Pandit and S McMahon "Therapeutic Effect of Neurotrophin 3 Treatment in an Injectable Collagen Scaffold Following Rat Spinal Cord Hemisection Injury" ACS Biomater. Sci. Eng. 2017, 3 (7), pp 1287–1295.

Conference presentations

R Ronan, A Kshirsagar, M Kilcoyne, G Schlosser, R O'Flaherty, R Saldova, A Pandit, S McMahon "Glycan and glial regulation of the regenerative process following spinal cord injury, and the influence of biomaterial treatment" Poster presentation, Gordon Research Seminar on Neurobiology of Brain Disorders, Gordon Research Conference on Neurobiology of Brain Disorders, Castelldefels, Spain, 2018

R Ronan, A Kshirsagar, M Kilcoyne, R O'Flaherty, R Saldova, G Schlosser, A Pandit, S McMahon "Glycobiology in Spinal Cord Injury and Repair" Poster presentation, Eurocarb, Barcelona, Spain, 2017

R Ronan, A Kshirsagar, AL Rebelo, M Kilcoyne, G Schlosser, A Pandit, S McMahon. "Cellular and glycomic facilitators of regeneration in a *Xenopus laevis* model of spinal cord injury" Poster and datablitz (first prize) presentations, Neuroscience Ireland, Galway, Ireland, 2017

R Ronan, A Kshirsagar, AL Rebelo, M Kilcoyne, G Schlosser, S McMahon, A Pandit "Establishment of *Xenopus laevis* as a model to study cellular and molecular facilitators of spinal cord regeneration" Podium presentation, TERMIS, Uppsala, Sweden, 2016

A Kshirsagar, R Ronan, AL Rebelo, M Kilcoyne, G Schlosser, S McMahon, A Pandit "Standardisation of *Xenopus laevis* spinal cord injury model for proteomic and glycomic profiling during spinal cord regeneration" Poster presentation, FENS, Copenhagen, Denmark, 2016

AL Rebelo, A Kshirsagar, R Ronan, G Schlosser, A Pandit "Study of pain markers and motor function recovery after spinal cord injury in *Xenopus laevis* tadpole" RAMI Biomedical Sciences, Cork, Ireland, 2016

AL Rebelo, R Ronan, A Kshirsagar, G Schlosser, A Pandit "Assessment of Functional Recovery Following Spinal Cord Injury in *Xenopus laevis* tadpoles" Poster presentation, Young Neuroscientists Symposium, Dublin, Ireland, 2016

R Ronan, A Kshirsagar, AL Rebelo, G Schlosser, S McMahon, A Pandit, "Studying regeneration in tadpole *Xenopus laevis* for improved biomaterial therapy design for the injured spinal cord" Podium presentation, Bioengineering in Ireland, Galway, Ireland, 2016

R Ronan, A Kshirsagar, M Kilcoyne, A Pandit, S McMahon “Glycobiology of the spinal cord in tadpole *Xenopus laevis*” Poster presentation (first prize, life sciences), Microscopy Society of Ireland Symposium, Limerick, Ireland, 2015

A Kshirsagar, R Ronan, AL Rebelo, G Schlosser, S McMahon, A Pandit “Development of non-mammalian model system *Xenopus laevis* to study spinal cord regeneration” Poster presentation, Neuroscience Ireland, Dublin, Ireland, 2015

R Ronan, H Kraskiewicz, B Breen, A Kshiragar, T Sargeant, A Pandit, S McMahon “A collagen-based multimodal delivery system provides therapeutic factors and physical support for treatment of spinal cord injury in the rat” Poster presentation, Advanced Functional Polymers in Medicine, Galway, Ireland, 2015

R Ronan, H Kraskiewicz, B Breen, T Sargeant, A Pandit, S McMahon “A collagen-based multimodal delivery system provides therapeutic factors as well as physical support for treatment of spinal cord injury in the rat” Datablitz presentation, Network for European CNS Transplantation & Restoration, Galway, Ireland, 2014

R Ronan, H Kraskiewicz, B Breen, T Sargeant, A Pandit, S McMahon “A collagen-based multimodal delivery system provides therapeutic factors as well as physical support for treatment of spinal cord injury in the rat” Podium presentation, European Society for Biomaterials, Liverpool, UK, 2014

1 Chapter 1 – Introduction

1.1 Spinal cord injury

1.1.1 Incidence and statistics

The World Health Organisation (WHO) estimates that between 250,000 and 500,000 new patients suffer a spinal cord injury (SCI) due to trauma or disease each year. Trauma is by far the most common and will be the focus of this work. Traumatic SCI most commonly occurs due to road traffic accidents, falls which may be related to sporting or workplace accidents, or violence. It is more common for males to suffer an SCI than females, in an estimated 2:1 ratio worldwide, although this varies depending on the data set examined, a ratio of 5:1 has also been reported (Norenberg *et al.*, 2004). For both males and females injury is most common in youth (20-29 years for males, 15-19 years for females) or after the age of 60 (WHO factsheet, SCI). In Ireland, many SCI patients utilise the Spinal Injuries Ireland (SII) support service. Between 2005 and 2015 804 patients accessed the services of SII, suggesting an average of 80 new patients per year, and between January 2015 and 2016 61 new patients joined, suggesting a similar trend. The total number of patients that SII worked with in 2016 was 1822. Of these the vast majority (1294) were male and unfortunately most suffered a cervical (673) or thoracic (770) injury (SII, private communication, April 2016).

Following a SCI motor and sensory function may be impaired below the level of the injury. Therefore cervical and thoracic injuries tend to cause the greatest detriment to the patient. The extent of impairment varies between patients and depends on the type and severity of injury acquired. The American Spinal Injury Association (ASIA) have classified SCI into 5 categories based on the extent of function remaining below the level of the injury. Category A is a complete injury with no function remaining at S4-S5 (sacral level 4-5), category B is incomplete with only sensory function remaining at S4-S5, category C is also incomplete with only motor function remaining at S4-S5 level. Category D also describes an incomplete injury but with motor function maintained below the level of injury with the muscles affected having a score greater than 3. Category E describes normal motor and sensory function (American Spinal Injury Association).

1.1.2 Pathophysiology of SCI

The pathophysiology of human SCI is reasonably well understood and reviewed (Dumont *et al.*, 2001; Norenberg *et al.*, 2004; Ahuja *et al.*, 2017). The pathology which forms as a result of mechanical

trauma to the spinal cord occurs across two phases. The first very brief phase results directly from the initial mechanical insult. The second phase takes place over the following days, weeks and months and most of the pathological changes take place here. Four categories of human SCI have been suggested based on the type of mechanical insult and the resulting gross and histological pathology (Bunge *et al.*, 1993). The first is an injury where damage is only evident at the histological level, the second is the contusion injury, which is most common and is characterised by the presence of cysts resulting from necrosis. Haemorrhage, particularly in the grey matter regions, is common in this type of injury also, while from the outside there tends to be little evidence of damage. The third is massive compression resulting in complete distortion and crushing of the cord. The fourth type is laceration where part of the cord is severed and continuity is immediately disrupted. Complete severing of the cord is highly unusual in human cases although it makes for a useful animal model and will be discussed later. While most of the pathology of human SCI is common to all four of these types of injury there are some minor differences between them: cyst formation is particularly characteristic of the contusion injuries, while formation of a collagenous mesenchymal scar is a feature of laceration and massive compression (Dumont *et al.*, 2001; Norenberg *et al.*, 2004; Ahuja *et al.*, 2017).

The primary injury phase from the time of mechanical trauma to approximately 2 hours post impact produces very little pathology. There may also be some alterations to normal vascular physiology at this stage, vessels may be impacted, they may dilate and there may be an accumulation of blood in some regions. There may also be small surface bleeds on the spinal cord. Except in the case of laceration injuries there are usually very few changes to the cord during this primary phase (Norenberg *et al.*, 2004).

The features of the secondary injury phase can be assorted chronologically. During the acute phase, from the immediate hours to 2 dpi (days post injury) much pathology develops. Oedema may be observed extracellularly or intracellularly (mainly in astrocytes) and bleeding continues. The extent of haemorrhage depends on the nature of the injury and there is a breakdown of the blood spinal cord barrier (BSCB). Unsurprisingly, some neuronal cell death occurs during this phase, and injured axons form retraction buds. From reviews of the literature neuronal death has been reported to be mainly necrotic (Norenberg *et al.*, 2004) but also apoptotic (Kwon *et al.*, 2004) but likely depends on the type and severity of insult. Oligodendrocytes also die during the acute stage by both necrosis and apoptosis. The inflammatory phase begins here with the transient invasion of neutrophils at 1 dpi, but by 3 dpi most are gone. Resident microglia also become activated at 1 dpi (Norenberg *et al.*, 2004).

In the sub-acute or intermediate phase occurring over the following days to weeks the priorities are the clearing of debris from the earlier cell death and tissue destruction and the restoration of the

BSCB. Glia and peripheral immune cells are recruited for these roles. The resident microglia become phagocytic and together with the blood derived monocytes and macrophages they phagocytose the debris surrounding the injury. These cell types have been observed to remain in the injured spinal cord for many months. Astrocytes become hypertrophic within a few days after injury and attempt to restore homeostasis by removing the excess neurotransmitters and free radicals and returning the normal ionic balance. They may also play a supportive role by producing growth and neurotrophic factors and assisting with BSCB repair (Dumont *et al.*, 2001; Norenberg *et al.*, 2004).

Cyst and scar formation takes place in the late phase of weeks to months in parallel with the process of Wallerian degeneration. Cysts are formed once necrotic debris has been cleared away. They consist of an accumulation of extracellular fluid and are contained within a wall of glia. The astroglial scar is formed from astrocyte processes tightly adherent to each other through tight junctions, with extracellular matrix (ECM) all around. This scar begins to form after the peak hypertrophic stage at 2-3 weeks. Humans do not exhibit the same extent of astrogliosis and scarring that is seen in rodent models. The fibrotic scar is made up of fibrous connective tissue and collagen and is particularly evident after laceration type injuries. This scar is thought to result from disruption of the glia limitans, is likely produced by fibroblasts and is thought to contribute more to the prevention of axonal growth (Dumont *et al.*, 2001; Norenberg *et al.*, 2004).

As well as these cellular level observations, many biochemical aspects of pathology also develop during the secondary phase. A common feature of traumatic central nervous system (CNS) injury is the release of excessive amounts of the excitatory neurotransmitter glutamate which can happen within minutes of the injury (Kwon *et al.*, 2004). Glutamate binding to its ionotropic receptor triggers Ca^{2+} influx from the extracellular environment and also possibly Ca^{2+} release from intracellular stores. This imbalance sets off a range of signalling events in the cell which often leads to death of neurons and oligodendrocytes in a phenomenon known as excitotoxicity (McDonald and Sadowsky, 2002). Glutamate toxicity can also lead to Na^{+} becoming overly concentrated intracellularly leading to influx of water and axonal swelling (Kwon *et al.*, 2004). One of the downstream effects of excitotoxicity is the production of free radicals (McDonald and Sadowsky, 2002). The presence of free radicals can propagate the production of more free radicals through peroxidation of membrane lipids and lead to oxidative stress (Kwon *et al.*, 2004). Neurons may be particularly vulnerable to oxidative stress and this may contribute to their death (McDonald and Sadowsky, 2002).

1.2 Mammalian models of SCI

The rat is the most commonly used mammalian model of traumatic SCI and is used in 72% of SCI studies. The mouse is the second most commonly used model organism used in 16% of studies. Other less popular animal models include rabbit, dog, cat, pig, guinea pig and non-human primate. The thoracic region is the most common spinal cord area to induce injury, being performed in 81% of studies, followed by the cervical region. The vast majority of SCI models use a mechanical insult to induce pathology, with contusion being the most popular model followed by transection and then compression (Sharif-Alhoseini *et al.*, 2017). Non-mechanical injury models include ischaemia-reperfusion, and photochemically induced damage (Zhang *et al.*, 2014).

Contusion injuries are considered the most clinically relevant since the induction and resulting pathology is the closest to clinical observations. Contusion injury generally requires some kind of apparatus and usually utilises a weight-drop system. Commercially produced weight-drop systems are available such as the Ohio State University, New York University or Infinite Horizon impactors. Compression can be carried out using a clip, forceps or balloon, or using a similar apparatus to weight drop but maintaining pressure on the cord for an extended period of time. With both contusion and compression models the severity can be controlled by varying the contusive force exerted or the duration of compression (Zhang *et al.*, 2014; Kjell and Olson, 2016). Traction is another method of mechanically inducing SCI although not very popular (Sharif-Alhoseini *et al.*, 2017). Traction may involve stretching the spinal cord by pushing two vertebrae in opposing directions (Zhang *et al.*, 2014).

Although laceration injuries are not the most common to occur in humans (Norenberg *et al.*, 2004) hemisection (lateral or dorsal), transection or resection of the cord can be very useful in the research environment. These are particularly useful models to examine the efficacy of biomaterial or tissue engineering strategies. Transection or resection are most beneficial as any observed repair at the structural or the functional level can be considered 'true' regeneration since all continuity was disrupted at the time of injury (Talac *et al.*, 2004). With contusion, compression or even hemisection injuries it is possible that any improvement in functionality is a result of sprouting or plasticity rather than axonal regrowth. A disadvantage with hemisection injuries is the difficulty in creating a consistent injury between animals and in ensuring completeness across half of the cord, however it is a less severe injury for the animal to undergo and urinary function is preserved (Talac *et al.*, 2004).

The rat response to SCI is more similar to the human condition than the mouse response. In rats the development of cysts is common, as in human SCI, and fibrosis at the injury epicentre when the meningeal layers are disrupted is also seen in both. In the mouse, cysts do not usually develop and a

proliferative response to transection is observed which is not evident in the rat or the human. From a regenerative point of view, unassisted return of function following transection of the cord has not been reported in rats or in human, while this has been observed in the mouse (Kjell and Olson, 2016). The advantage gained with mouse models is the established techniques to alter gene expression. The rat is a useful model for testing potential treatments for SCI in terms of functional recovery, and there are many behavioural tests well established for testing both motor function and sensory function. The Basso Beattie Bresnahan (BBB) scale is the most widely used motor test (Sharif-Alhoseini *et al.*, 2017) and allows for subtle improvements in hindlimb function to be detected in a minimally stressful environment for the animal. Von Frey filament test, hot plate test and the pinch reflex are useful sensory assessments while the grid walk is a popular test for which the animal needs to have both sensory and motor capability (Sharif-Alhoseini *et al.*, 2017).

A key difference between experimental and clinical SCI is the controlled conditions experimental SCI is carried out under and the necessity of performing laminectomy for many of the surgical procedures. This may perhaps impact on the resultant pathology as the injury is often very clean with no fragments of bone remaining, whereas in the human situation fragmented or displaced vertebrae may impinge on the cord for hours, days or weeks before surgical intervention.

1.2.1 The scarring process following SCI in mammals

Traumatic SCI in mammals results in two types of scar formation, the glial scar and the fibrotic scar. The fibrotic scar, which is rapidly established within the first 3-7 dpi is most prominent in transection type injuries when there is a disruption of the meningeal sheaths, leading to an infiltration of fibroblast-like cells and the deposition of dense ECM made up of collagens, laminin, fibronectin, tenascin, nidogen, heparan sulphate proteoglycans (HSPGs) and chondroitin sulphate proteoglycans (CSPGs). However the fibrotic scar may also appear after contusion injuries when the meninges remain intact (Hermanns *et al.*, 2001; Kjell and Olson, 2016). Of the collagens present, type IV collagen is particularly abundant but collagens I, III, V and VI are also found (Hermanns *et al.*, 2001). In the cases of contusion injury it is possible that this scar is produced by vasculature associated pericytes or meningeal-like (Fawcett, 2006; Kjell and Olson, 2016). The fibrotic scar has been proposed to contribute to the failure of axon regeneration due to the observed expression of semaphorin III A and the ephrins and their receptors which are proposed axon repellents (Hermanns *et al.*, 2001).

The glial scar has been more widely studied in the context of SCI, forming at about 2 – 3 weeks post injury in the rat, after astrocyte reactivity has already peaked. Human glial scars may take months to

form, but remain for years (Kjell and Olson, 2016). Many studies have suggested that the glial scar is responsible for the failure of axonal growth across injuries of the CNS, however there are also studies to suggest the opposite (Fawcett, 2006; Anderson *et al.*, 2016). The morphology of the scar does suggest that it is inhibitory for growth, being composed mainly of tightly interconnected astrocytes and their processes connected by tight or gap junctions and enclosed in ECM (Fawcett and Asher, 1999; Norenberg *et al.*, 2004). Additionally it is abundant in various CSPG species, many of which have been shown to be growth inhibitory (Bradbury *et al.*, 2002) as well as other inhibitory molecules such as the ECM constituent tenascin-R and the myelin proteins Nogo-A and MAG (Fawcett and Asher, 1999; Fawcett, 2006). Although astrocytes are the dominant cell type in the glial scar, microglia, oligodendrocyte progenitors, endothelial cells and meningeal cells are also present, all of which become reactive in some manner (Fawcett and Asher, 1999; Fawcett, 2006). The work of the Sofroniew group has suggested that the astrocytic scar may not be as detrimental for repair as previously thought. Using genetic mouse models to either prevent scar formation or to ablate the established scar did not restore axonal growth of either descending or ascending tracts. Preventing scar formation led to a much larger lesion cavity and actually caused further death or retraction of axons and surprisingly did not reduce the amount of total CSPG present. It was then shown that CSPGs of both a growth inhibitory and growth promoting nature were produced by both astrocytes and non-astrocyte cells around spinal cord crush injuries, although only one of the growth inhibitory CSPGS was increased in astrocytes while two of the growth promoting CSPGs were increased (Anderson *et al.*, 2016). Again using transgenic mice in which astrocytes could be selectively ablated the glial scar was shown to be necessary for a number of protective mechanisms following stab injury in the brain. Without astrocytes and their protective functions there was extensive oedema, vasodilation and infiltration of many inflammatory cells, including monocytes and macrophages, neutrophils and lymphocytes. Degeneration of neurons was widespread in the astrocyte ablated animals, while in controls reactive astrocytes were observed in close proximity to healthy neurons, suggesting a protective function (Bush *et al.*, 1999).

1.2.2 The inflammatory response and macrophage polarisation following SCI in mammals

As expected for any traumatic injury there is a significant inflammatory response following SCI in mammals. Many cell types are involved but the most focus has been on the resident microglia which become activated in response to injury and on the infiltrating monocyte-derived macrophages, which become indistinguishable from the activated amoeboid microglia around the lesion. In contrast to many other injuries however, inflammation which occurs due to a SCI does not appear to resolve and

the tissue remains chronically inflamed. A second wave of macrophage infiltration has even been observed at approximately 60 dpi (Kjell and Olson, 2016). The numbers and time to resolution for neutrophils, microglia/macrophages and T cells have been characterised following an incomplete transection injury in the rat, using immunohistochemistry at a range of time-points over the first month post injury, and again at 70 dpi. Both neutrophils and T cells peaked at 3 days, and were cleared rapidly: 50% of neutrophils had been removed 1.2 days later and had been completely eliminated by 14 dpi. 50% of T cells had been cleared by 1.5 days and only 10% of the peak number remained in the injured tissue chronically. Macrophages and microglia peaked at 7 days, but it took 55 days for these numbers to decrease by half and 45% of the macrophage/microglia numbers remained even at 70 dpi, indicating a chronic inflammatory environment (Prüss *et al.*, 2011). Another study has shown a T cell peak at 3-7 dpi in both Sprague-Dawley and Lewis rats (Popovich *et al.*, 1997) while in human T cells have been detected as late as 6 months post injury (Fleming *et al.*, 2006). The differences in timing of T cell response may be due to variations in mode of injury and strain or species.

Macrophage responses have been shown to be polarised in many other tissues, existing along a spectrum between classical, pro-inflammatory activation 'M1' or alternative, anti-inflammatory activation 'M2', with the former thought to cause tissue damage and the latter thought to contribute to wound healing and resolution of inflammation (Gensel and Zhang, 2015). M1 macrophages have been proposed to mediate their effects by production of a range of pro-inflammatory cytokines, reactive oxygen species (via NADPH oxidases and iNOS) and ECM modifying enzymes (David and Kroner, 2011; Gensel and Zhang, 2015). M2 type macrophages on the other hand produce much lower amounts of pro-inflammatory cytokines and reactive oxygen species, and instead release anti-inflammatory and growth factors, produce ECM components and carry out phagocytosis (Gensel and Zhang, 2015).

Macrophage polarisation specifically in relation to SCI was first investigated by (Kigerl *et al.*, 2009). Here a contusion injury model was employed in mouse and expression of various M1 and M2 markers was investigated over a range of time-points (1, 3, 7, 14, 28 dpi). Using a gene array they showed that both M1 and M2 associated genes were mostly upregulated after injury, but while M1 genes were mostly chronically expressed, M2 genes were upregulated only briefly. Even within the M1/M2 categories differential timing in peak expression could be seen showing the complexity of the macrophage response to injury and suggesting that a range of markers may be required to build a picture of the inflammatory environment of SCI. In particular, of the M2 markers Arginase-1 peaked rapidly at 1-3 dpi after which it returned to sham levels, while CD206 peaked at 7-14 dpi. Arginase-1 was far more highly expressed than CD206. Of the M1 markers, inducible nitric oxide synthase (iNOS)

peaked early at 1-3 dpi while CD16 and CD32 were highest from 7-28 dpi and CD86 did not become significantly elevated until 28 dpi. A similar pattern of expression was seen at the protein level in the lesion epicentre. The ratio of M1/M2 cells was approximately equal until 7 dpi after which M1 markers became predominant (Kigerl *et al.*, 2009). A number of other studies later went on to investigate the polarisation profile of macrophages and microglia in the injured spinal cord in mouse and rat models. Many of these investigate how an intervention may impact the polarisation of these cells. The main findings in relation to the injury itself (i.e. the control group data) is summarised in the table in Appendix I. From the data presented in this table it can be seen that there is great variation in macrophage and microglia polarisation in response to experimental SCI. This variation makes it difficult to interpret a 'normal' response, and may be due to any number of factors such as severity of the injury, differences in age, strain or gender of animals, surgical technique, post-operative care or method of analysis. The results were generated from flow cytometry, immunohistochemistry, gene array or PCR data. Variation may also stem from which marker and time-point combination was chosen, because as noted in the work of (Kigerl *et al.*, 2009) each individual marker has a slightly different time profile of expression. Despite the great variation in results between injury models, time-points etc., these types of studies may still be informative when interpreted within an experiment, for example to test a particular treatment strategy against a control.

The polarisation status of circulating monocytes in human SCI patients has also been investigated in the acute phase (1-7 dpi). Using flow cytometry M1 type monocytes were defined as CD14low/CD16+, and M2 type monocytes were defined as CD14high/CD16+, and it was found that M1 type cells were far higher in SCI patients than in controls while there was little difference in M2 type. The plasma cytokine levels reflected the flow cytometry result. Additionally the sum of circulating monocytes was greater in injured patients than in controls (Huang *et al.*, 2014). This suggests that the use of these markers in rodent models is justified from a translational point of view.

A small number of studies have investigated transplanting macrophages polarised in one direction or the other into the injured spinal cord to investigate whether they can retain their phenotype in the injured environment and whether they can modify the repair process. M2 polarised macrophages transplanted at 7 dpi into contused mouse spinal cord had lost their M2 phenotype three days later, while they maintained expression of M2 markers when transplanted into intact tissue (Kigerl *et al.*, 2009). In a mouse crush injury model co-transplantation of neural stem and progenitor cells (NSPCs) with M2 macrophages led to more NSPCs differentiating into neurons or oligodendrocytes, resulting in an improvement in functional recovery. M1 macrophages greatly reduced differentiation into neurons or oligodendrocytes but slightly increased differentiation into astrocytes. This was the case

in both intact and injured spinal cord. (Zhang *et al.*, 2015b). In the contused rat spinal cord macrophages transplanted at 7dpi maintained their phenotype seven days later. Transplantation of M2 macrophages influenced polarisation of T cells: there were less Th1 and more Th2 type T cells. M1 or M2 transplantation differentially influenced production of interferon-γ (IFNγ), tumour necrosis factor-α (TNF-α), interleukin-10, -6 and -13 (IL-10, IL-6, IL-13) & iNOS. M2 macrophage transplantation reduced the lesion volume, improved motor neuron survival at 3-4mm from injury (but not at the injury epicentre), reduced demyelination and improved functional recovery (Ma *et al.*, 2015).

1.3 Biomaterial treatment strategies for SCI

Interest in using biomaterials to treat the injured spinal cord has been growing in recent years. Biomaterials can be used in various forms which may suit different kinds of injuries. They can be used as 'bridges' to aid axons or glia to cross the injured site, as drug, neurotrophic factor or cell delivery systems or as a combination therapy (Madigan *et al.*, 2009; Siebert *et al.*, 2015). They can also be useful in sealing off the injured area reducing the influx of peripheral inflammatory cells (Pires and Pego, 2015). A number of different natural materials have been studied for SCI applications, including ECM constituents such as collagen, fibronectin, or hyaluronic acid, blood derived fibrin or fibrinogen, or the polysaccharides agarose, alginate, or chitosan which may be derived from marine plants or animals. Synthetic biomaterials are also popular and may include poly lactic acid (PLA), poly glycolic acid (PGA), PLGA which is a combination of PLA and PGA, poly ethylene glycol (PEG), Poly(2-hydroxyethyl methacrylate) (pHEMA), or polycaprolactone (PCL). Key considerations when choosing any material is that it, along with any substances produced during the degradation process, will not elicit a detrimental effect on the tissue, and also that the material degrades in a timely manner to allow space for regenerating tissue (Madigan *et al.*, 2009; Shrestha *et al.*, 2014; Pires and Pego, 2015; Siebert *et al.*, 2015).

These materials can be used in different formulations depending on the application or the type of injury. Hydrogels are popular as their mechanical properties are similar to those of CNS tissue, they can fill irregularly shaped injuries especially when designed as an injectable formulation, they can be infused with cells, neurotrophic factors or other therapeutic of choice. Those produced with fibrillar proteins offer a structure and substrate for cells to grow and migrate on, and the degradation rate or stiffness can be controlled by altering monomer/polymer and cross-linker concentrations or porosity (Madigan *et al.*, 2009; Shrestha *et al.*, 2014; Pires and Pego, 2015; Ziemba and Gilbert, 2017). Fibrillar proteins can also be organised into a particular alignment to offer guidance to migrating cells and growth cones. This property is utilised in this work. Scaffolds and conduits are also popular choices. The aim of these is usually to promote axonal regeneration and this is reflected in the architecture of these at both the macro and micro level. They may take the form of a guidance tube similar to those used in peripheral nerve strategies, or they may be more solid with pores or channels arranged longitudinally. Scaffolds and conduits can also be used as a drug delivery system or to deliver cells (Madigan *et al.*, 2009; Siebert *et al.*, 2015). Another strategy which primarily aims to offer guidance to regrowing axons is the use of fibres which may be produced by electrospinning for example. These fibres can also be supplemented with therapeutic factors (Ziemba and Gilbert, 2017). Micro- or nano-particles may also be used as drug delivery vehicles to treat SCI, and may be embedded within

hydrogels. These kind of systems permit controlled sustained release of therapeutic over time, and help to prolong the life of the therapeutic in the injured tissue (Madigan *et al.*, 2009; Tam *et al.*, 2014; Ziemba and Gilbert, 2017; Ham and Leipzig, 2018). Chemically or physically attaching the therapeutic to the biomaterial is another method of controlling the release profile. The release profile of the desired therapeutic should always be matched to the target pathology (Ziemba and Gilbert, 2017).

Biomaterial systems can specifically be employed to interfere with the secondary injury events which follow a SCI. This may be achieved by carefully choosing the therapeutic they are supplemented with, but in some cases the material itself may modulate inflammation, oxidative stress or offer neuroprotection (Ham and Leipzig, 2018). This has been seen in a previous study by our own group where delivery of a collagen hydrogel reduced the amount of positive Iba-1 staining and NG2 proteoglycan and even led to improved motor function. Inclusion of NT-3 contained within collagen microspheres distributed through the hydrogel additionally increased neuronal survival and/or sprouting within the lesion site (Breen *et al.*, 2016).

1.3.1 Collagen for treatment of SCI

In our work, we use a collagen hydrogel for treatment of SCI in the rat. Although collagen is a very minor constituent of the CNS ECM (Ruoslahti, 1996) it is well tolerated, not eliciting any obvious foreign body response (Hoban *et al.*, 2013; Breen *et al.*, 2016; Moriarty *et al.*, 2017), and has been FDA approved for peripheral nerve treatments (Kehoe *et al.*, 2012). The table in Appendix II summarises the collagen based treatment strategies reported for SCI so far.

It can be seen from the studies outlined in Appendix II that the primary aim is for the collagen to act as a bridge or scaffold to physically support the injured spinal cord tissue. In many cases collagen alone can offer some benefit in terms of repair but many groups have recognised the necessity of combinatorial treatment, including cells or growth factors with the biomaterial bridge. An additional advantage of collagen is that it is a fibrillar protein and so there is the possibility to align the fibres, as mentioned above. This can be performed to mimic structural properties of the tissue of interest (Denning *et al.*, 2012) or in the case of SCI alignment of fibres can provide a surface guidance cue for migrating cells or growing axons and so aid in repair of the injured spinal cord (Yoshii *et al.*, 2004; Han *et al.*, 2009; Fan *et al.*, 2010; Liu *et al.*, 2012; Yao *et al.*, 2013; Fan *et al.*, 2017; Snider *et al.*, 2017).

1.3.2 Biomaterial therapies in clinical trials

The linear ordered collagen scaffold developed by the Dai group is currently in clinical trial, to test safety and plausibility, with results of the one-year follow up published in 2016 (Xiao *et al.*, 2016). In this report the response of five patients with severe complete SCI (ASIA grade A) to the removal of scar tissue and implantation of the 'NeuroRegen' scaffold was described. The scaffold was delivered together with patient derived bone-marrow mononuclear cells. No adverse effects of the procedure were observed and there were some improvements in electrophysiology (somatosensory evoked potential) for all patients. This suggests that collagen in scaffold form may hold promise as a therapy for SCI. This scaffold is being tested alone or in combination with a cell therapy (bone-marrow derived cells or mesenchymal stem cells (MSCs)).

There are many other trials ongoing for SCI. Some are investigating pharmacological therapies, but there is a stronger focus on cell therapies (stem cells or more commonly MSCs from various sources) and the use of devices designed to aid in neurotransmission across the injury including robotics or exoskeleton type devices, deep brain stimulation, transcranial magnetic stimulation and others (www.clinicaltrials.gov).

1.4 SCI and the regenerative capacity of non-mammalian species

Although the majority of research in the field of SCI is carried out in non-regenerating rodents there are a number of groups investigating the mechanisms of how repair and regeneration of the spinal cord can occur spontaneously using non-mammalian vertebrates as models. The most popular of these models are zebrafish, urodele amphibians including newt and salamander, and the anuran amphibian *Xenopus laevis.* There was some early interest in these models from the 1960s to early 1990s, but the majority of work has been published in the past ten to fifteen years. The earlier studies establish the regenerative capacity following various methods of injury, while the more modern work seeks to define the essential signalling pathways involved and the role of individual cell types. Some of these studies utilise high-throughput 'omics' approaches to try to understand the mechanisms of spontaneous regeneration (Lee-Liu *et al.*, 2014; Lee-Liu *et al.*, 2018) and the methods to model injury are being improved and developed for *Xenopus laevis*, zebrafish and urodele (Fang *et al.*, 2012; Khattak *et al.*, 2013; Edwards-Faret *et al.*, 2017).

In *Xenopus laevis* and in urodeles spinal cord regeneration may be investigated following focal injury to the spinal cord, usually transection, or following tail amputation, while in zebrafish transection injury is the most common. The time line and morphological stages of regeneration following spinal cord transection in *Xenopus laevis* are described below, and following tail amputation (Beck *et al.*, 2003). *Xenopus laevis* is a particularly useful model to study regeneration due to the ability to compare successful and failed regeneration in the same species: repair after spinal cord transection is successful in pre-metamorphic tadpoles but not in the post-metamorphic froglet (Beattie *et al.*, 1990; Gibbs *et al.*, 2011), Figure 1.1, and tail regeneration is successful in tadpoles up to stage 42 and at stage 48 or later but not in between (Beck *et al.*, 2003). Here the cellular responses during regeneration following SCI or tail amputation are described in *Xenopus laevis*.

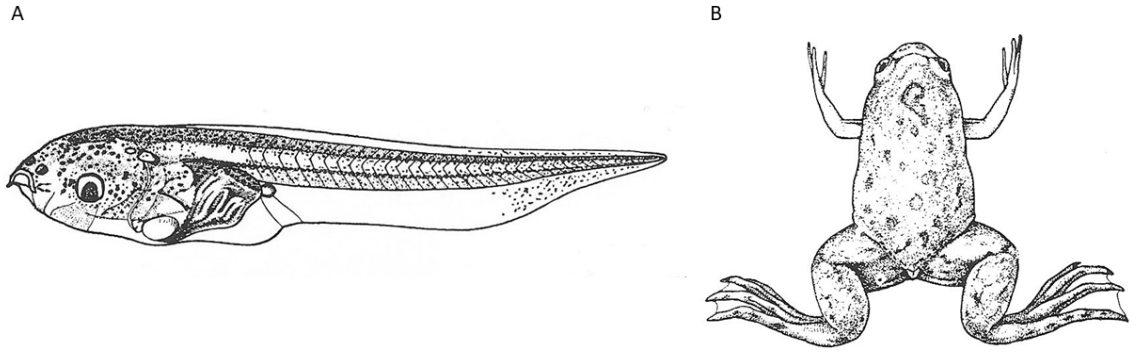

Figure 1.1 *Xenopus laevis* as a pre-metamorphic tadpole (stage 50, A) and as a post-metamorphic froglet (stage 66, B). Illustrations are from Nieuwkoop and Faber (1994) Normal Table of *Xenopus laevis* (Daudin) Garland Publishing Inc, New York ISBN 0-8153-1896-0. Digital versions were accessed via the Xenbase anatomy and development resource. Illustrations are not to scale. Stages 50 and 66 are provided as reference here, as these are the developmental stages studied in this work, however studies of SCI and tail amputation at other stages of development have been reported, see following sections.

1.4.1 Metamorphosis and the regenerative potential of Xenopus laevis

The ability of *Xenopus laevis* tadpoles to regenerate and the loss of this capacity after metamorphosis was demonstrated as early as 1962 by Sims. Pre-metamorphic tadpoles were found to be capable of structural and functional repair while juvenile froglets were not (Sims, 1962). More recent studies have confirmed this observation (Beattie *et al.*, 1990; Gaete *et al.*, 2012; Lee-Liu *et al.*, 2014; Munoz *et al.*, 2015). The process of metamorphosis itself may have an impact on the process of CNS regeneration and has been investigated (Gibbs *et al.*, 2011). The progressive decline in regenerative ability moving from stage 50 pre-metamorphic tadpoles to stage 66 post-metamorphic froglets was demonstrated histologically (Munoz *et al.*, 2015). In contrast to central neurons, peripheral dorsal root ganglion axons successfully regenerate into the spinal cord even in adult frogs (Katzenstein and Bohn, 1984).

Some “baseline” pre-injury differences between tadpoles and froglets may be important in the different responses to SCI seen between the two. The fact that tadpoles are still in an embryonic phase with much growth and patterning of the nervous system still ongoing may be the reason they are capable of such efficient repair. These differences encompass expression of a variety of neuronal and glial markers (including vimentin), proliferation rate, distribution of radial glial cells, ultrastructural

differences, and the presence of cilia on ependymal cells. Any one or more of these differences could be worth future investigation in relation to the loss of regenerative potential after metamorphosis (Edwards-Faret *et al.*, 2018).

1.4.2 Mechanisms of regeneration in tadpole Xenopus laevis

In tadpole *Xenopus laevis* following spinal cord transection the regenerative response begins rapidly and has been reported as being complete by 20-28 dpi (Gaete *et al.*, 2012; Munoz *et al.*, 2015) with reconnection reported at approximately around 7 dpi (Sims, 1962), 10 dpi (Munoz *et al.*, 2015), within 20 dpi (Lee-Liu *et al.*, 2014), or between 5 and 12 dpi (Beattie *et al.*, 1990). Differences in timing of repair between these studies may be due to injury being induced at a variety of stages from stage 50 to 56, or to the temperature at which animals were kept as this is known to affect their rate of development and so likely influences the rate of regeneration.

Regeneration of the spinal cord in tadpole *Xenopus laevis* involved regrowth and sprouting of severed axons (Sims, 1962; Michel and Reier, 1979; Gibbs and Szaro, 2006; Lee-Liu *et al.*, 2014) as well as population of the lesion with proliferative cells (Michel and Reier, 1979; Gaete *et al.*, 2012; Munoz *et al.*, 2015).

Between 2 and 6 dpi the cut ends of the cord and open central canal were sealed off by axons (Lee-Liu *et al.*, 2014; Munoz *et al.*, 2015) and a layer of cell bodies (Munoz *et al.*, 2015). Although retraction buds were observed in the white matter at 1 dpi some sprouting could be seen from the cut surface of the cord from 3 dpi (Sims, 1962) or from 6 dpi (Lee-Liu *et al.*, 2014). Cells in the lesion core appeared to facilitate regrowing neurites by forming 'channels' which were also seen in intact spinal cord tissue (Michel and Reier, 1979; Munoz *et al.*, 2015). These channel-forming cells populating the lesion were identified as ependymal cells which had migrated out into the lesion from the cut cord (Michel and Reier, 1979). Following SCI ependymal cells were found to be positive for Sox2/3 and highly proliferative (Gaete *et al.*, 2012; Munoz *et al.*, 2015). The morphology (large and stretched) and location (along the central canal) of Sox2/3 positive nuclei suggested that these are neural stem cells in stage 50 tadpoles. Sox2/3 positive cells became highly proliferative early after injury at 2 dpi (Munoz *et al.*, 2015) but this burst of cell division was transient: at 4-6 dpi Sox2/3 positive cells showed very little colocalisation with bromodeoxyuridine (BrdU) (Gaete *et al.*, 2012; Munoz *et al.*, 2015). By 6 dpi many Sox2/3 positive cells had migrated into the middle of the lesion, forming apparently organised structures (Munoz *et al.*, 2015).

The activity of Sox2/3 seems to be important for recovery after injury as animals treated with a morpholino to knock down expression of this protein exhibited impaired axonal regrowth and motor function recovery (Munoz *et al.*, 2015). It is possible that Sox2/3 positive cells differentiate into neurons to populate the lesion site (Munoz *et al.*, 2015). In support of this, following SCI in non-regenerative froglet expression of Sox2/3 was almost half of that seen in regenerative tadpole (Gaete *et al.*, 2012; Munoz *et al.*, 2015) and Sox2/3 positive nuclei were more rounded and dispersed, i.e. they no longer showed characteristics of neural stem cells (Munoz *et al.*, 2015). Proliferation of Sox2/3 positive cells was also very limited in froglet as compared to tadpole, and was delayed until 6 dpi (Munoz *et al.*, 2015).

Cell transplantation studies have been performed to determine whether cells from regeneration competent stages could promote repair in the non-regenerative stage. Dissociated spinal cords of stage 50 tadpoles were transplanted into the resected (1 mm) spinal cord of stage 66 froglets. As early as 10 dpi the transplanted cells were observed to self-organise into structures which resembled multiple 'mini' neural tubes: there was a dense packing of cells which were Sox2/3 positive, with lengthened nuclei surrounding an apparently empty space. Sox2/3 expression was graded from one side of this structure to the other, which was reminiscent of the dorso-ventral patterning observed in normal developing spinal cord. Along with the other grafted cells these structures remained in place up to 60 dpi although they apparently decreased in size. By 40 dpi the grafted spinal cord cells appeared to have differentiated into a neuronal phenotype: there was an abundance of NeuN positive nuclei and NF-H signal. This was maintained at 60 dpi (Mendez-Olivos *et al.*, 2017).

It can be concluded that this ability of spinal cord cells to survive and differentiate after transplantation is lost following metamorphosis as cells transplanted from healthy stage 66 froglet to injured stage 66 froglet had much fewer cells present even by 20 dpi and there were only occasional neural tube-like structures formed (Mendez-Olivos *et al.*, 2017).

The Larrain group have performed transcriptomic (Lee-Liu *et al.*, 2014) and proteomic studies (Lee-Liu *et al.*, 2018) comparing the response to spinal cord transection in the tadpole and froglet, to try to understand some of the mechanisms responsible for the respective regenerative success and failure. In both of these studies they performed analysis using only tissue isolated from caudal to the injury. Since it has been shown that growth is more efficient in descending tracts from the rostral side, (Beattie *et al.*, 1990) it is possible that much information was lost in these studies. Unsurprisingly, almost all of these studies found changes in metabolism related transcripts during regeneration of the various tissues as well as genes related to the inflammatory response, wound healing, the cell cycle and proliferation. Changes in genes related to developmental processes and axial or dorso-ventral

patterning have also been identified (Tazaki *et al.*, 2005; Love *et al.*, 2011; Lee-Liu *et al.*, 2014; Chang *et al.*, 2017). Many transcripts relating to neuronal differentiation, microtubules and neuronal projections, synaptic plasticity and transport of neurotransmitters were upregulated as early as 6 hours post amputation in *Xenopus tropicalis* (Chang *et al.*, 2017). Although no transcripts related to neurogenesis or the growth cone were identified in the undirected transcriptomic analysis following SCI, manually searching for transcripts relating to these processes revealed some differences between tadpole and froglet. Differentially regulated neurogenesis related genes were generally upregulated following injury in tadpole while being unchanged, down regulated or delayed in their expression in the froglet. Growth cone related transcripts displayed very little change in the tadpole or at early time-points in the froglet but were greatly reduced at 6 dpi in froglet (Lee-Liu *et al.*, 2014).

1.4.3 Scarring and inflammation in non-mammalian SCI

A glial scar like that observed following SCI in mammals does not form in the regenerative *Xenopus laevis* models discussed above. Instead the ependymoglia, the ECM and possibly the meninges even contribute to regeneration. In some cases the ependymal glial cells proliferate and help to replace lost neurons and glia (Michel and Reier, 1979; Gaete *et al.*, 2012; Munoz *et al.*, 2015), and have also been reported to produce 'tunnels' to guide axonal / neurite growth (Michel and Reier, 1979). The meninges are less reported on, however meningeal cells have been observed in close proximity to axons as they project into the lesion gap in the newt (Zukor *et al.*, 2011) and other studies have reported on a permissive extracellular matrix which may reflect that found in development (Caubit *et al.*, 1993; Caubit *et al.*, 1994)and may be aligned to guide axons across the injury (Butler and Ward, 1965).

Microglia and the inflammatory response in the non-mammalian models of SCI are reviewed in (Bloom, 2014) but information is lacking. The presence of inflammatory cells has been observed in the lesion following transection in *Xenopus laevis* (Sims, 1962) and crush injury in adult axolotl (Zammit *et al.*, 1993) but no comment has been made on how they behave or their influence on the regenerative process. Gene ontology analyses following transcriptomic or proteomic studies have shown the presence of an acute inflammatory response following transection or tail amputation in *Xenopus laevis* and *Xenopus tropicalis* (Tazaki *et al.*, 2005; Love *et al.*, 2011; Lee-Liu *et al.*, 2014; Lee-Liu *et al.*, 2018) and in axolotl tail regeneration (Monaghan *et al.*, 2007) however the details of this response were not reported. In *Xenopus laevis* a difference was observed between tadpole and froglet stages suggesting that specific inflammatory mechanisms may support while others impair regeneration (Lee-Liu *et al.*,

2014; Lee-Liu *et al.*, 2018). Presumably inflammation is involved in the acute 'clean up' following injury and then is quickly resolved.

In mammalian systems astrocytes are considered one of the main components of the glial scar. Very little literature refers to parenchymal astrocytes in the amphibian models, instead the focus is on the ependymal cells, which in newts are considered glial and express GFAP in their processes (Zukor *et al.*, 2011). In tadpole *Xenopus laevis* the ependymal cells are considered a NSPC population based on the shape of their nuclei and the expression of Sox2/3 (Gaete *et al.*, 2012; Munoz *et al.*, 2015).

Xenopus laevis glia in both tadpole and froglet have been recently characterised immunohistochemically by the Larrain group using a range of established astrocytic / radial glia markers (Edwards-Faret *et al.*, 2018). All are radial in nature with many processes extending to the pial surface, and all except those labelled with glutamine synthetase had their cell bodies in the ependymal zone and/or grey matter. BLBP was detected in both stages but was more strongly expressed in the tadpole, S100β was barely detectable in the tadpole but common in dorsal and ventral domains in the froglet, vimentin was confined to dorsal and ventral domains in both stages and peripherin was expressed in the glia of both developmental stages (Edwards-Faret *et al.*, 2018). Glutamine synthase, a marker of astrocytes in mature mice (Bayraktar *et al.*, 2014), was sparse in the tadpole but very widely expressed in froglet. In tadpole a small number of glutamine synthase positive cell bodies could be seen at the central canal and in the white matter, while in the froglet they were highly abundant and distributed throughout the ependymal zone, grey matter and white matter but were most abundant in the grey matter (Edwards-Faret *et al.*, 2018). GFAP expression, the most commonly used astrocyte marker in mammals, was studied in tadpole and froglet *Xenopus laevis* in another work. GFAP positive cells were found to be radial in nature extending as far as the pia matter. Signal intensity was much higher in the white matter but no cell bodies were observed there, they are likely present in the grey matter and/or ependymal zones. GFAP immunoreactivity was detectable as early as stage 44 (Maier and Miller, 1995).

The role of astrocytes has not been recognised in the context of *Xenopus laevis* SCI, however it has been observed that they became hypertrophic and phagocytic following injury to the optic nerve in *Xenopus laevis* and were thought to clean up myelin and axonal debris (Reier and Webster, 1974; Reier, 1979; Rungger-Brandle *et al.*, 1995). Following crush or transection injury the distal nerve degenerated but became populated by a cluster of astrocytes (Reier and Webster, 1974; Rungger-Brandle *et al.*, 1995). No scar was observed in tadpole injuries and astrocyte processes were actually observed to extend and possibly support axonal growth across the lesion (Reier and Webster, 1974) however a substantial glial scar composed of hypertrophic phagocytic astrocytes was formed in the

optic nerve following removal of the eye in adult *Xenopus.* Surprisingly transplantation of this scar tissue into tadpole optic nerve did not prevent axons from crossing the lesion (Reier, 1979).

1.5 Glycobiology

1.5.1 Basic glycochemistry

The building blocks for the glycan species discussed in this work consist of monosaccharides which are five or six membered cyclic structures mainly consisting of carbon, hydrogen and oxygen, with one of the oxygen atoms contributing to the ring, and the others present in the form of hydroxyl groups. Other functional groups may also be present, such as amine, acetyl and acidic groups. The carbon atoms in monosaccharides are numbered in a clockwise manner, with C1 being adjacent to the oxygen atom in the ring. The C1 carbon usually takes part in the glycosidic bond which occurs between two monosaccharides, or between a monosaccharide and the protein or lipid it is binding too. The exception is in sialic acid, where C2 links to the next sugar residue as C1 is occupied by the acidic carboxyl group.

Many glycans are epimers of each other, that is, they have the same molecular formula but they may differ in the orientation of the functional group around a particular carbon. For example glucose, galactose and mannose all have the molecular formula $C_6H_{12}O_6$, but differ from each other in the orientation of particular hydroxyl groups (Figure 1.2), and have different biological roles and activities. This close structural similarity between monosaccharides is one of the numerous reasons that the analysis of glycan samples can be challenging. For example, using mass spectrometric approaches it is impossible distinguish between epimers, and so unless additional experimental steps are incorporated, such as exoglycosidase digestions or tandem mass spectrometry with fragmentation, the investigator can only infer abundances of hexoses, deoxyhexoses and N-acetyl-hexosamines as in (Ohl *et al.*, 2003).

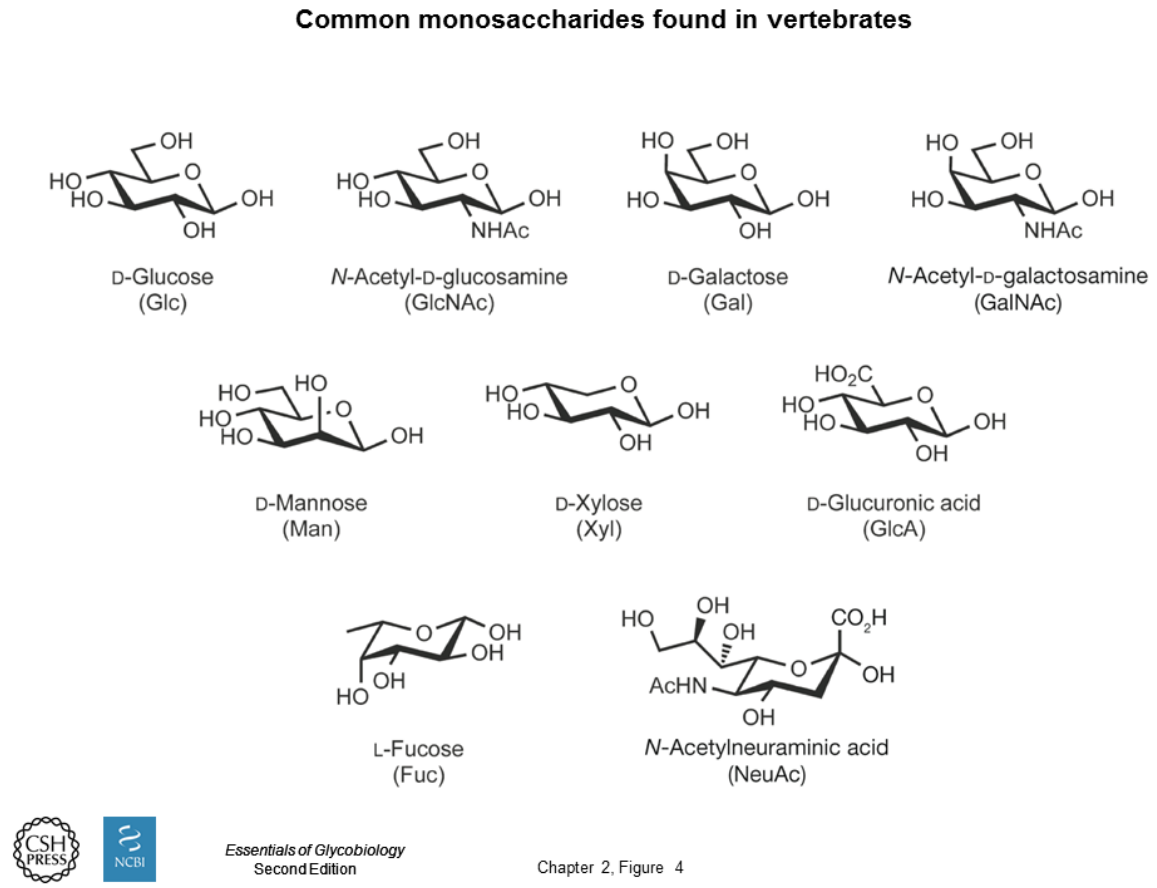

Figure 1.2 The common monosaccharides found in vertebrate glycans. Some are isomers of each other, for example galactose, glucose and mannose: each are 6 membered rings with 5 hydroxyl groups. They differ only in their stereochemistry. This figure is taken, with permission, from 'Essentials of Glycobiology' Chapter 2, (Bertozzi CR, 2009).

The glycosidic bond mentioned above allows monosaccharides to bind together in linear or branched chains. An individual monosaccharide can take part in one, two or three glycosidic linkages which allows for branching and substitution on the chain. The glycosidic bond occurs between C1 (or C2) of one monosaccharide and a hydroxyl group of another, releasing a water molecule and forming a very stable chemical species. It can also take place between C1 and the hydroxyl group of serine or threonine, or between C1 and the amide nitrogen in arginine. The glycosidic bond can exist in one of two conformations, α or β, and influences the biological activity of the glycan. The α conformation is considered to be when the linkage lies below the plane of C1, β conformation is when the linkage lies above the C1 plane. The location of the hydroxyl groups determines which carbons can take place in the glycosidic bond.

1.5.2 Glycans found in tissue

Glycans can exist in many different forms in tissue, they may be present as free sugars, but are more commonly found chemically linked to proteins or lipids forming glycoproteins, proteoglycans or glycolipids (Figure 1.3).

Glycolipids are important constituents of the cell membrane, in most cell types, and comprise the majority of glycosylated species in the mammalian brain (Norton W.T., 1984). Glycosphingolipids are the major class of glycolipids in animals. Another type, the glycosylphosphatidylinositols (GPIs) are frequently covalently attached to proteins (Schnaar RL, 2017). The glycosphingolipids galactosylceramide (GalCer) and sulfatide are important components of myelin, comprising 27% of total myelin lipid (Norton W.T., 1984; Coetzee *et al.*, 1996). Sialylated glycolipids known as gangliosides are common in neuronal membranes (Ledeen *et al.*, 1992; Sandhoff and Kolter, 2003).

In proteoglycans, the sugars are present as a long linear chain of repeating mono- or di-saccharides (the glycosaminoglycan or GAG chain) attached to a protein core. The glycans in these structures are often further modified by chemical moieties such as sulphate groups, and the protein component can be modified by *N*-or *O*-linked glycosylation. Proteoglycans are commonly found in the ECM and cell membrane. The major GAG chain families include the chondroitin sulphates, heparan sulphates, keratin sulphates, dermatan sulphates and hyaluronic acid. These families differ in monosaccharide composition and level of sulphation. Proteoglycans are important constituents of the ECM in the CNS (De Luca and Papa, 2017). The CSPGs are thought to be major contributors to the glial scar and failure of axonal regrowth and have been well studied in relation to SCI (Bradbury *et al.*, 2002; Morgenstern *et al.*, 2002).

Glycoproteins are very common across all tissues, with glycosylation considered to be the most frequent post-translational modification (Apweiler *et al.*, 1999). Protein glycosylation falls under two major categories, *N*-linked and *O*-linked. *C*-linked mannosylation may also occur, although it is uncommon, and the GPI molecule mentioned above links a phospholipid and a protein via the glycan. *N*-linked and *O*-linked glycans differ in their linkage to protein and in their structural patterns. Some proteins have only *N*-glycan modifications, some have only *O*-glycan and some have both. *O*-glycans are linked to the –OH group of a serine or threonine of the protein through a glycosidic bond, they are generally small, branched or linear oligosaccharides. The core monosaccharide is most commonly GalNAc, however *O*-glycans with fucose, mannose, GlcNAc, glucose, galactose or xylose can also be found (Brockhausen I, 2017; Stanley P, 2017).

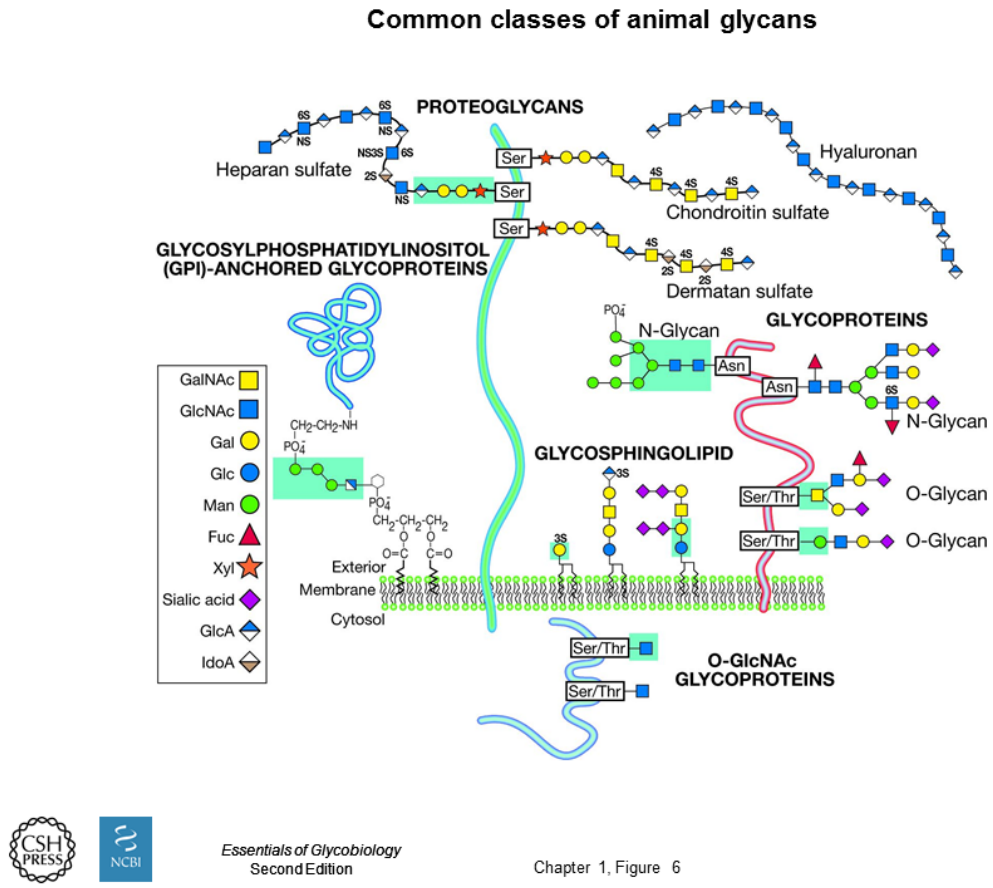

Figure 1.3 The main types of glycoconjugate found in vertebrates. Many are membrane associated including glycosphingolipids, glycosylphosphatidylinositol-anchored proteins and both *N*- and *O*-linked glycoproteins. Proteoglycans may be membrane associated or free in the extracellular matrix. *O*-GlcNAc decorated glycoproteins are more commonly found in the cytoplasm. This figure is taken from 'Essentials of Glycobiology', Chapter 1, (Varki A, 2009b), adapted from (Fuster and Esko, 2005), with permission.

N-glycans are linked to the nitrogen of an asparagine in protein, also through a glycosidic bond, but the asparagine must be part of a particular consensus sequence required for *N*-glycosylation: asparagine-[any amino acid except proline]-serine/threonine. *N*-glycans tend to be bigger than their *O*-linked counterparts and have a conserved core pentasaccharide consisting of two GlcNAcs and three mannoses, where one of the GlcNAcs links to the asparagine residue. This core is then elongated and elaborated in a sequential manner described below, with branching being common. The finished glycan product can be categorised as being complex (i.e. bi-, tri-, or tetra-antennary), high- or oligo-mannose, or hybrid (see Section 1.5.4, Table 1.1 for glycan naming).

N-glycans can be analysed as complete structures as the entire glycan can be removed enzymatically using PNGaseF (peptide N-glycosidase F). This enzyme breaks the glycosidic bond between the inner

GlcNAc residue and the asparagine of the protein, leaving the glycan itself intact. As a result *N*-glycans are the most commonly studied biological glycans and are the main focus of this work.

1.5.3 N-glycan biosynthesis

The *N*-glycosylation biosynthetic pathway for eukaryotic cells has been extensively characterised and is well described in the chapter on *N*-glycans in 'Essentials of Glycobiology' (Stanley P, 2017). *N*-glycan biosynthesis is a sequential, enzyme dependent process which begins in the endoplasmic reticulum with monosaccharide addition and removal occurring as the glycan and later the glycoprotein moves along the membrane of the endoplasmic reticulum (ER) and later the Golgi. Some of the earlier steps occur in tandem with protein elongation and folding, and it is believed that the glycosylation process can influence protein folding. There are many steps involved in producing a mature *N*-glycan with many intermediate species along the way. Interestingly some of these intermediates are as large or even larger than the final product, particularly the extensively mannosylated precursor produced in the endoplasmic reticulum, which is then cut down and remodelled to produce the final conformation (Stanley P, 2017).

The earliest sugar chain is attached to a phosphorylated lipid called dolichol. The very first step is the transfer of a phosphorylated GlcNAc residue to the phosphorylated dolichol. The two phosphate groups form the link. GlcNAc is transferred from UDP-GlcNAc by GlcNAc-1-phosphotransferase yielding UMP and dolichol-P-P-GlcNAc. All sugars of the biosynthetic pathway are nucleotide sugars, and the availability of these species as well as the enzymes present and active determines what glycans can be produced by any cell at any given time. The second GlcNAc residue is then added, from UDP-GlcNAc, followed by sequential addition of the mannose residues from GDP-man until the structure of Man5GlcNAc2-P-P-dolichol has been formed. These initial steps occur on the cytoplasmic side of the endoplasmic reticulum membrane, and after this the glycan precursor, still linked to the lipid dolichol, is transferred to the lumenal side of the endoplasmic reticulum membrane. This change of location is carried out by the enzyme flippase. A further four mannose residues are added here. Three glucose residues are then attached forming a chain on one of the outer mannose residues. The glucose residues also are transferred from the nucleotide sugar, UDP-Glc. This sugar Glc3Man9GlcNAc2-P-P-dolichol is the first major precursor and is ready to lose the dolichol and phosphate groups and to be attached via glycosidic bond to the asparagine residue of the growing protein. This attachment is mediated by the enzyme complex oligosaccharyltransferase (Stanley P,

2017). More detail on the components of oligosaccharyltransferase is given in the review by (Mohorko *et al.*, 2011).

Before leaving the ER the glucose residues are removed, and one of the mannose residues is cleaved off. First, α-glucosidase-I removes the terminal α(1-2) glucose and then α-glucosidase-II removes the inner α(1-3) glucose residues one after the other. On some glycoproteins, the ER α-mannosidase-I cleaves off the outer α(1-2)-linked mannose before transfer of the resulting Man8GlcNAc2 to the Golgi apparatus. These earliest steps of *N*-glycan biosynthesis are summarised in a simplified manner in Figure 1.4. The glycan attached to its protein is transferred to the Golgi for further processing. Key steps of this activity are summarised in Figure 1.5. In the *cis*-Golgi a further three mannose residues are removed by α-mannosidases IA, IB and IC. As the immature glycoprotein leaves the *cis*-Golgi it has a glycan structure of Man5GlcNAc2, another important intermediate. Oligomannose type *N*-glycans do not undergo any further processing in the *medial*- or *trans*-Golgi (Stanley P, 2017).

The development into hybrid or complex type glycans begins as the glycoprotein makes its way through the *medial*-Golgi. GlcNAc-transferase-I (GnT-I) is the first enzyme responsible for the formation of hybrid or complex sugars. It transfers a single GlcNAc, again from the nucleotide donor, to the α(1-3)-linked mannose. After this α-mannosidase-II is free to remove the remaining outer mannose residues, if this enzyme acts at this stage then complex glycans are formed, if it does not then a hybrid structure results. The second GlcNAc beginning the complex glycan is added by GnT-II, onto the α(1-6)-linked mannose. GnT-III is responsible for the introduction of a bisecting GlcNAc residue (Stanley P, 2017).

If the sugar is to be tri- or tetra- antennary then the activity of GnT-IV and GnT-V are engaged. These two enzymes can work in either order, with GnT-IV always adding a β(1-4) linked GlcNAc to the α(1-3) Mannose arm, and GnT-V always adding a β(1-6) GlcNAc to the α(1-6)-linked mannose arm (Stanley P, 2017). Another enzyme, known as GnT-IX or GnT-Vb, is an unusual enzyme found almost exclusively in the brain both in humans (Inamori *et al.*, 2003) and in mice (Inamori *et al.*, 2006). The activity of GnT-IX is similar to GnT-V, adding a β(1-6) linked GlcNAc to a di- or tri-antennary glycan, and it can produce the same reaction product as GnT-V, but it also has other distinct activity. GnT-IX can add a β(1-6)GlcNAc to the α(1-3)-linked mannose, in place of the β(1-4) linked GlcNAc normally added by GnT-IV. This unusual structure can be added to either a di- antennary substrate, or a tri-antennary substrate which has already been acted on by GnT-V, forming tri- and tetra-antennary products with unusual β(1-6) branch patterns. In the absence of GnT-V, GnT-IX can add β(1-6) branches to both arms. Such a structure has been identified by HPLC and mass spectrometry, with nuclear magnetic resonance (NMR) to investigate linkage information (Inamori *et al.*, 2003).

The final modifications of complex and hybrid glycans are added in the *medial*- and *trans*-Golgi (Figure 1.4, Figure 1.5). Core fucose is linked via α(1-6) bond to the innermost GlcNAc by a fucosyltransferase, coming from a GDP-Fucose donor. Galactose comes from a UDP-Gal donor. Short repeating units of galactose and GlcNAc can be added being linked together usually by a β(1-4) linkage but sometimes by β(1-3). Branches can also be "capped" with sialic acid, fucose, GalNAc or sulphate, which is important for the spatial conformation, and glycan-protein interactions later on. Finally, once all the appropriate monosaccharides have been attached, the mature glycoprotein is secreted or is transported to the cell membrane (Stanley P, 2017).

Glycoproteins are of course broken down and their constitutent sugars reactivated for incorporation into fresh glycoconjugates. This generally involves endocytosis before lysosomal degradation, and activation of released monosaccharides takes place in the cytoplasm (Colley KJ, 2017).

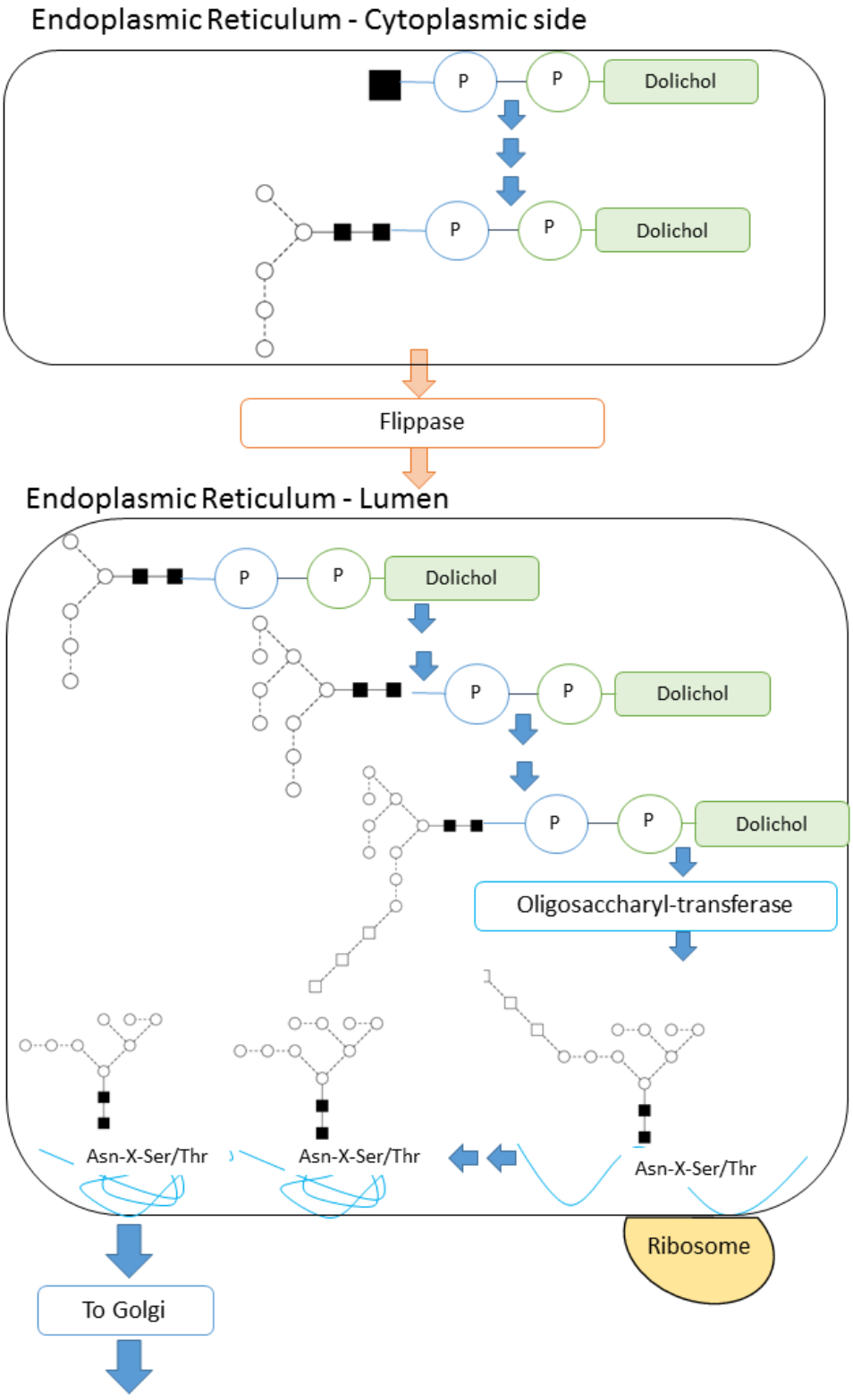
Endoplasmic Reticulum - Cytoplasmic side
P
P
Dolichol
P
P
Dolichol
Flippase
Endoplasmic Reticulum - Lumen
P
P
Dolichol
P
P
Dolichol
P
P
Dolichol
Oligosaccharyl-transferase
Asn-X-Ser/Thr
Asn-X-Ser/Thr
Asn-X-Ser/Thr
Ribosome
To Golgi

Figure 1.4 *N*-glycan biosynthesis begins at the endoplasmic reticulum, on the cytoplasmic side with the attachment of a single phosphorylated GlcNAc residue to a phosphorylated lipid, dolichol. The lipid is linked to GlcNAc by the two phosphate groups. Dolichol anchors or carries the sugar as it grows into a large oligosaccharide precursor. It grows to M5-P-P-Dolichol on the cytoplasmic side of the ER until it is transferred across the membrane onto the lumenal side by the enzyme flippase. Here more mannose residues are added sequentially to give an M9 intermediate, and to this 3 glucose residues are added to form M9Glc3-P-P-Dolichol. This large intermediate is then transferred from the dolichol anchor to a growing polypeptide by the enzyme oligosaccharyltransferase, at the N-glycan consensus sequence Asparagine-X-Serine/Threonine. The glucose residues and one of the mannoses are cleaved off in tandem with folding of the protein. The folded protein with M8 attached is then transferred to the Golgi apparatus for further processing. Each monosaccharide is added in a sequential manner by a series of glycosylatransferases. GlcNAc residues are attached from UDP-GlcNAc precursors, mannose residues from GDP-Mannose and Glucose from UDP-Glucose. Black filled squares, GlcNAc; empty circles, mannose; empty squares, glucose.For more detail and the enzyme responsible for each intermediate steps see Chapter 9 of 'Essentials of Glycobiology' (Stanley P, 2017).

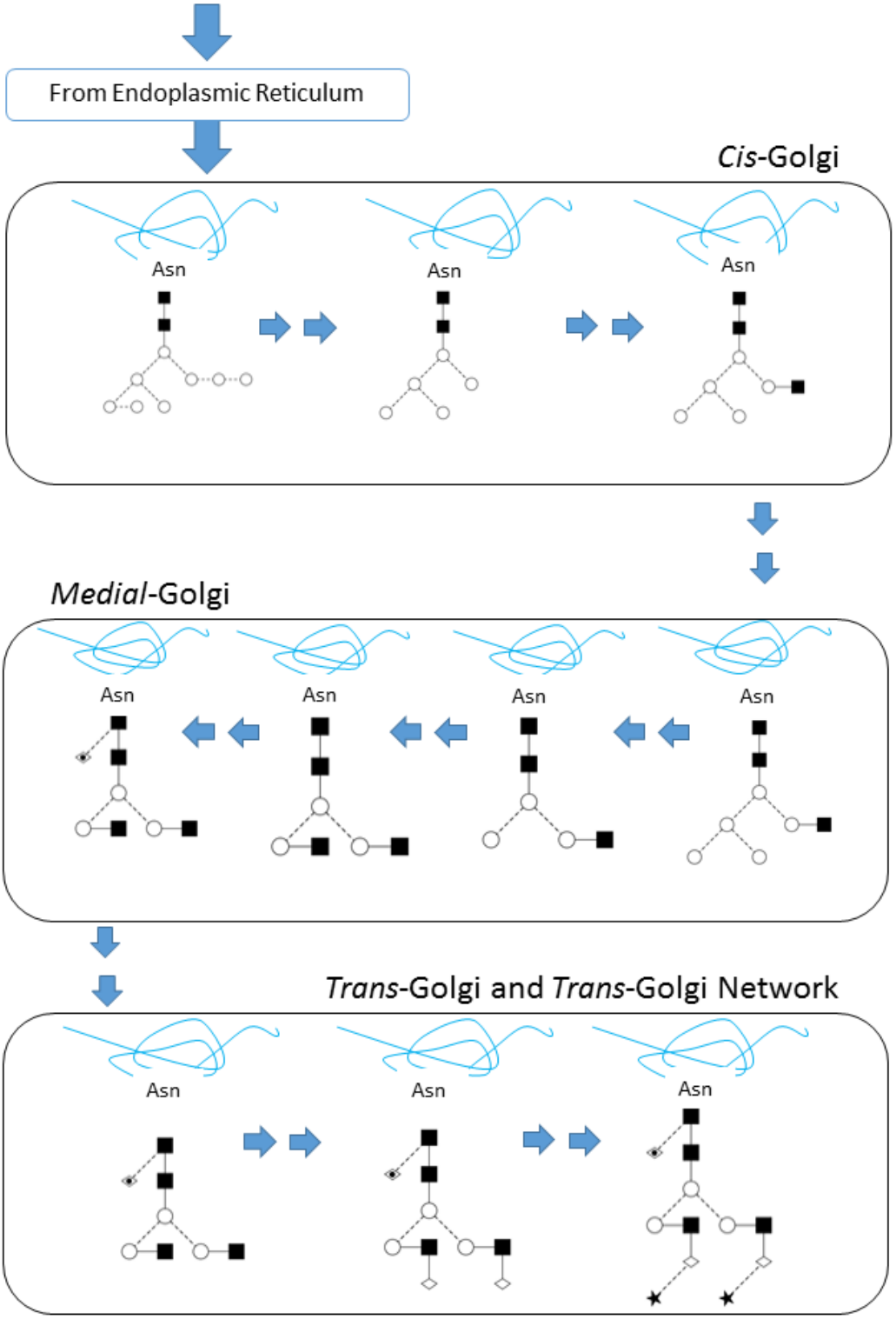
From Endoplasmic Reticulum
Cis-Golgi
Asn
Asn
Asn
Medial-Golgi
Asn
Asn
Asn
Asn
Trans-Golgi and *Trans*-Golgi Network
Asn
Asn
Asn

Figure 1.5 *N*-glycan biosynthesis in the Golgi. The large glycan precursor is then carried to the Golgi for trimming down and remodelling. In the *cis*-Golgi a series of α-mannosidases remove each mannose residue sequentially to produce M5 and then another GlcNAc is added to create M5A1. M5A1 and the protein then moves into the *medial*-Golgi where additional mannose residues are removed and antennae are formed in their place. The core fucose modification is also placed in the *medial* Golgi. Galactose and sialic acid decoration are added in the *trans*-Golgi. GlcNAc are supplied from UDP-GlcNAc, fucose from GDP-fucose, galactose from UDP-galactose and sialic acid from CMP-sialic acid. Black filled squares, GlcNAc; empty circles, mannose; empty diamonds, galactose; black stars, sialic acid. For more detail and the enzyme responsible for each intermediate steps see Chapter 9 of 'Essentials of Glycobiology' (Stanley P, 2017).

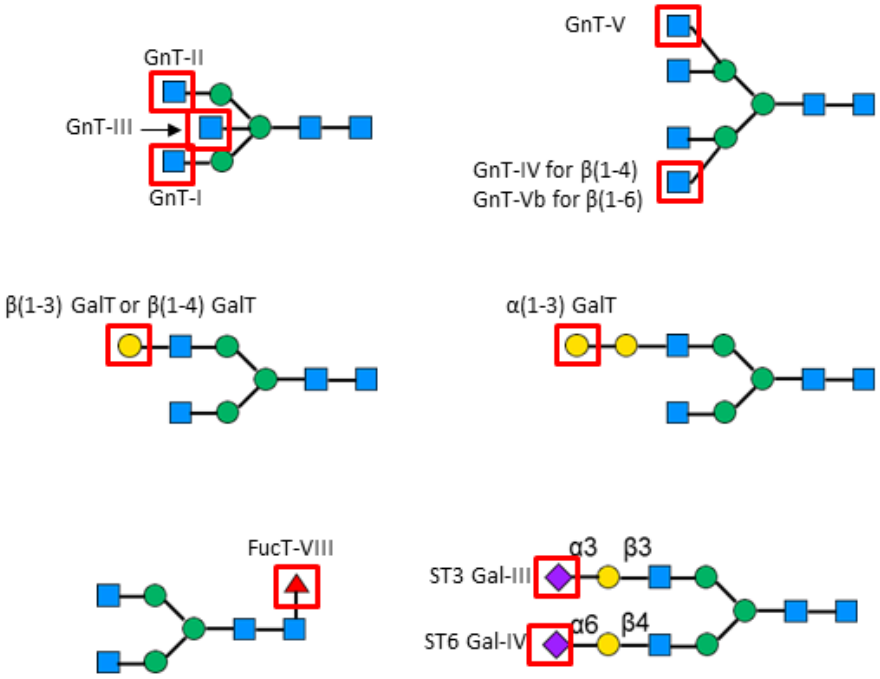

Figure 1.6 Key enzymes in the biosynthesis of complex *N*-glycans. GnT, GlcNAc-transferase; FucT, fucosyltransferase; GalT, galactosyltransferase, ST, sialyltransferase.

1.5.4 Glycan nomenclature

There are two major systems of nomenclature used in the field of glycobiology, Oxford nomenclature and CFG (Consortium for Functional Glycomics) nomenclature. Each utilises a variety of geometrical shapes to represent individual monosaccharides which are then linked together as the entire *N*-glycan. Oxford nomenclature also includes a simple lettering system which can be utilised when discussing glycans in a text. In this system the presence of the core pentasaccharide (see Table 1.1) is not directly mentioned but must always be assumed. The name describes the modifications added to the core. To denote the GlcNAc antennae the letter 'A' is used, followed by a number to indicate how many antennae are present. For example if there are two GlcNAc residues on the core pentasaccharide the structure is simply represented as A2, A3 represents a structure with three GlcNAc residues, and A4 has 4. Bisecting GlcNAc is indicated with the letter B, e.g. A3B has four GlcNAc's, three of which are present as antennae and one of which is β(1-4)-linked to the central mannose residue. Galactose residues are represented by the letter G and are again followed by a number to indicate how many residues there are, e.g. A3G2. If desired, the linkage between the galactose residue and the antenna can be indicated by another number in brackets, for example two β(1-4)-linked galactose resides on a di-antennary glycan would be represented as A2G(4)2. Sialic acid is represented by the letter S and again the linkage is indicated by a number in brackets followed by another number to indicate how many sialic acids are present, e.g. A2G(4)2S(3)2 has two sialic acids, each in α(2-3) linkage. Fucose may be present on the core GlcNAc residue attached to the protein, in this case it is indicated before the rest of the glycan, and in mammals this residue is always (1-6) linked, e.g. F(6)A2G(4)2S(3)2. Outer-arm fucose is also indicated by the letter F, but it is notated after the antenna it is attached to. For example the glycan A2G(4)2 with fucose on the antenna would be written as A2F(3)1G(4)2. In the case of the high mannose species, only the two core GlcNAc residues of the core pentasaccharide are assumed, here the total number of mannose residues are included in the name. Table 1.1 below gives examples of some simple glycans using Oxford text based nomenclature, and CFG schematic nomenclature.

Core pentasaccharaide			M3	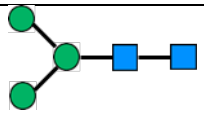
GlcNAc, forms antennae	GlcNAc		A1	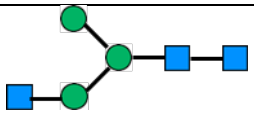

			A2	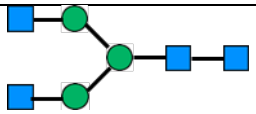
			A3	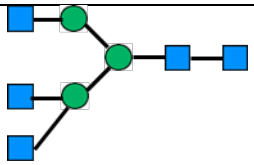
			A4	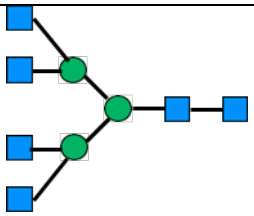
GlcNAc, as bisect	B		A2B	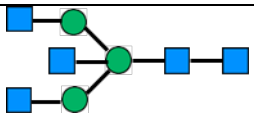
Galactose, β-linked	G		A2G1	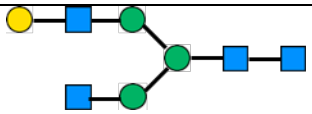
Galactose, α-linked	Ga		A2G2Ga1	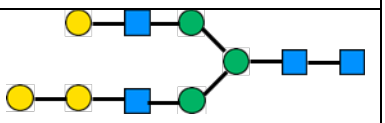
GlcNAc, as extension	GlcNAc		A2G1GlcNAc1	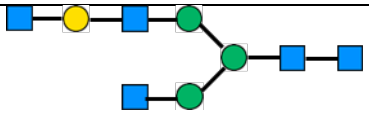
Fucose, core	F		FM3	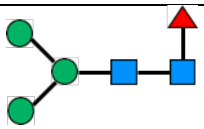
			FA2	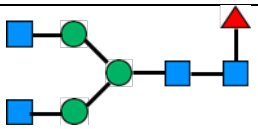
Fucose, outer arm	F		A2F	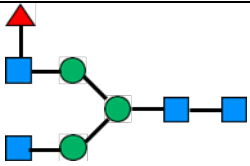

			A2F1G1	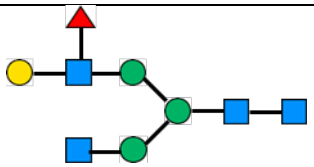
Sialic acid, Neu5Ac	S		FA2G1S1	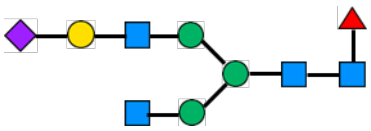
Sialic acid, Neu5Gc	Sg		FA2G1Sg1	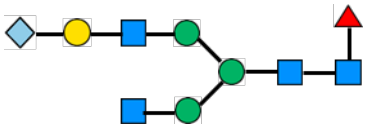
Mannose, High mannose type glycans	M		M9	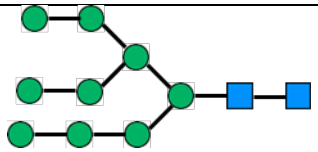
Mannose, Hybrid type glycans			M4A1G1	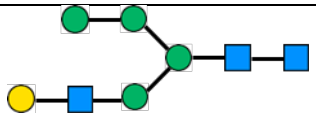

Table 1.1 Glycan naming systems used in this work. For in text glycan naming the Oxford system is used, for schematics CFG system is used. Examples of simple sugars are given with each monosaccharide type.

1.5.5 Glycobiology of the healthy CNS

Few studies have attempted to profile the glycans present in the rodent CNS. The two most comprehensive studies were of whole rat brain (Chen *et al.*, 1998; Zamze *et al.*, 1998) and there are no reports of characterisation of specific brain regions or of the spinal cord. Some other studies reporting on changes in glycosylation with degenerative disease (Gizaw *et al.*, 2015; Gizaw *et al.*, 2016), injury (Abou-Abbass *et al.*, 2016) or development (Ishii *et al.*, 2007) of the CNS, described in Section 1.5.6 below, appear to agree with the general structures proposed in these two characterisation studies.

(Zamze *et al.*, 1998) profiled the sialylated fraction and (Chen *et al.*, 1998) characterised neutral fractions of *N*-glycans present in the adult rat brain using a variety of liquid chromatography separation techniques in combination with mass spectrometry and exoglycosidase digestions. In these two studies the three major types of *N*-glycan were identified: high mannose, hybrid and complex.

In the neutral fraction high mannose species were common making up 15% of total brain *N*-glycans, and occurred with 5, 6, 7, 8 or 9 mannose residues attached to the two core GlcNAcs, without any other modifications. Hybrid *N*-glycans were seen in both neutral and charged groups. The single antenna was always in β(1-2) linkage. Complex structures were di- or tri-antennary in the neutral fraction, and in the sialylated fraction di-, tri- and tetra-antennary species were all common. In the neutral fraction many of the di-antennary glycans were truncated, i.e. lacking decoration on one or more of the antennae.

On both complex and hybrid *N*-glycans a range of structural features were identified. Both core and outer arm fucosylation were widespread on both sialylated and neutral *N*-glycans, with outer arm fucose occurring in multiples up to 2, depending on how many antennae were present. Bisecting GlcNAc, which was always β(1-4) linked to the central mannose of the trimannosyl core, was another common feature. In both sialylated and neutral fractions, multiple galactose residues could be found: in sialylated glycans it could be found linked to GlcNAc in either a β(1-4) or β(1-3) linkage. In the neutral fraction, galactose was only reported in the β(1-4) linkage.

Sialic acid residues were always of the Neu5Ac (*N*-acetyl neuraminic acid) type and were more commonly found in the α(2-3) than the α(2-6) conformation. It has been reported that no Neu5Gc (*N*-glycolyl neuraminic acid) is found in the vertebrate nervous system (Davies and Varki, 2015). Weak anion exchange high performance liquid chromatography (WAX-HPLC) indicated that approximately 12% of *N*-glycans were monosialylated, with 10%, 7% and 7% being di-, tri- or tetra-sialylated

respectively. Enzymatic removal of sialic acid residues removed the charge from approximately 40% of the species examined.

An additional feature which could be found in sialylated glycans was the presence of one or two repeat lactosamine units (Gal-(β1-4)-GlcNAc or Gal-(β1-3)-GlcNAc). This feature was found on glycans which were quite highly charged, having several sialic acid residues. Terminal galactose in β(1-3) linkage was present on every structure, and core and outer fucosylation was common. The authors concluded that lactosamine repeats were predominantly found on the tetra-antennary glycans, with some also occurring on triantennary species.

Polysialylation could also be found on some *N*-glycans. Polysialylation was suggested from the presence of later eluting species in the WAX-HPLC profile beyond the region for four sialic acid residues. Since only one NeuAc can be attached directly to each antenna, thus allowing a maximum of four, it was concluded that these additional charged species were existing as chains of polysialic acid, which occur linked together in α(2-8) conformation. These glycans did not carry any outer arm fucose residues, but core fucose was sometimes present, and could be found on glycans with lactosamine repeats, again being more common on tri- and tetra-antennary sugars. Regarding charged species other studies have reported the presence of glucuronic acid residues, which tend to be on *N*-acetyl lactosamine extensions and preferentially on the α(1-3) Mannose arm (Oka *et al.*, 2000) and both sulphate and glucuronic groups for example on polysialylated glycans of mouse brain derived neural cell adhesion molecule (NCAM) (Geyer *et al.*, 2001). Oka et al. also observed highly charged species on the WAX-HPLC profile, which were not removed following sialidase treatment.

Some studies of the mouse brain have been carried out, particularly in the development of mass spectrometry techniques for tissue sections. Matrix assisted laser desorption/ionisation (MALDI) mass spectrometry imaging was carried out on adult mouse brain cryosections by (Powers *et al.*, 2013) who identified a range of PNGaseF released *N*-glycans. The results are reported in the format Hex*X* dHex*X* NeuAc*X* HexNAc*X*, where X is an integer from 1 to 8. However with hexoses most likely to be mannoses and galactoses, HexNAc's most likely to be GlcNAc, dHex (deoxy-hexoses) being fucose and following the known standard assembly of *N*-glycans, we can estimate structure from the reported compositions, and say that there are some oligomannose species, a few hybrids, complex glycans are common, and that they are often fucosylated, either terminally or on the core. Not much sialylation was observed. Normal phase HPLC was included as a supporting experiment here which strengthens some of the results from the mass spectrometry analysis: complex and oligomannose species were also observed in this analysis, including the major structures A2, A2B, A2G2, F(6)A2G1, F(6)A2BG2,

M7, M8, and M9 as well as a small number of sialylated glycans eluting later in the run (Powers *et al.*, 2013).

Another mass spectrometry study of mouse brain tissue identified 43 glycans, including high-mannose, hybrid and complex. M5, M6, M7 and M9 high mannose species were identified as well as a fucosylated M5 hybrid. Again, the majority were complex being di-, tri- or tetra-antennary. Most structures were core fucosylated, many carried terminal galactose, outer arm fucose was also present on some but sialylation was quite low. Some were isomers of each other (Hu *et al.*, 2013).

Human CSF *N*-glycans were profiled using MALDI time of flight mass spectrometry. Glycans obtained from CSF consisted predominantly of complex glycans, mainly di-antennary with much core fucose, terminal galactose and some outer arm fucose and sialic acid. Bisecting GlcNAc was mentioned as a feature of these glycans, however is not shown in any of the figures, and one high-mannose species was mentioned, M5 (Goyallon *et al.*, 2015). This suggests that the glycans present in brain tissue itself and CSF are shared, which could potentially be a useful diagnostic tool.

Interestingly, it appears from the above studies that the CNS *N*-glycans are conserved between rats, mice and humans. The same was concluded in the review conducted by (Albach *et al.*, 2001), and is highly useful from a translational point of view. CNS glycosylation patterns are quite different from other tissues within the same species however, with features such as bisecting GlcNAc, a preference for α(2-3) sialylation, high levels of fucosylation and undecorated antennae distinguishing these glycans from those found elsewhere in the body.

1.5.6 Glycobiology of the injured or diseased CNS

In the traumatic brain injury (TBI) study conducted by (Abou-Abbass *et al.*, 2016) LC-ESI-MS (liquid chromatography coupled electrospray ionisation mass spectrometry) was used to investigate proteomic and glycomic changes in response to injury and to pharmacological treatment in the rat. A total of 58 *N*-glycan structures were identified and are divided into high mannose structures, with each structure contributing between 1 and 35% of the total *N*-glycan pool, high abundant complex structures (1 to 14%), medium abundant complex structures (0 to 2%), and low abundant complex structures (<0.5% of total). Of the high mannose species M5 and M6 were the most abundant and were found to be reduced following injury. No glycan species containing a bisecting GlcNAc was reported in any group in this study and no linkage information was given (Abou-Abbass *et al.*, 2016).

Most of the glycans reported in this study were differentially regulated in response to TBI, although it is unclear whether these changes were statistically significant or not. For a list of structures observed to change in abundance following TBI see Table 1.2.

Grouping	**Glycan**	**Direction of change**
High mannose structures	M5	Decrease
	M6	Decrease
Highly abundant complex and hybrid structures	A2G2S2	Increase
	FA2G2S2	Increase
	FM4A2G2S1 (hybrid)	Increase
Medium abundant complex and hybrid structures	A2G1S1	Decrease
	FA1G1S1	Increase
	FA2G1	Increase
	FA2G1S1	Increase
	A2G2	Increase
	FA2G2S1	Increase
	FA3G1S1	Increase
	FA3G3S3	Increase
	FA4	Increase
	FA4G1	Increase
	FA4G1S1	Increase
	M5A1G1S1 (hybrid)	Increase
	FM5A1G1S1 (hybrid)	Increase
Low abundant complex and hybrid structures	FA2G2	Increase
	FA3G2	Increase
	FA3G1S1	Increase
	A3G3S3	Increase
	FA3G3S1	Increase
	FA3F1G3S3	Increase
	FA4G1S1	Increase
	FA4G4S4	Increase
	FA4F1G4S1	Increase
	FA4F1G4S4	Increase
	FM4A2G2S2 (hybrid)	Increase

Table 1.2 *N*-glycans which change in abundance in response to TBI in the rat (Abou-Abbass et al., 2016).

Changes in *N*-glycosylation have also been investigated in the neurodegenerative diseases. In a mouse model of Huntington's disease (HD) a decrease in the high mannose species and an increase in core fucose and bisecting GlcNAc were identified in the cortex and striatum compared to wild-type controls. Serum *N*-glycans were more highly sialylated in the diseased mice (Gizaw *et al.*, 2015). The same group performed similar analysis in human Alzheimer's brain and found the opposite pattern: high mannose species were slightly increased while core fucose and bisecting GlcNAc were decreased. However these changes were not statistically significant (Gizaw *et al.*, 2016). This suggests that changes in glycosylation may be specific to the pathology and not a general feature of neurodegeneration. Other groups have identified changes in the glycosylation specifically of the pathological proteins involved in these diseases. Tau glycosylation was seen to be altered in Alzheimer's brain compared to healthy controls and to contribute to its altered secondary structure (Wang *et al.*, 1996). Specifically, pathological tau was found to be decorated with a variety of *N*-glycans including FM3, FA1, FA2B, A2G2, FA2G2, A3G3 and the high mannose species M4, M5, M6, M7, M8 and M9 (Sato *et al.*, 2001). Glycosylation of BACE (β-site APP cleaving enzyme) was found to influence its folding and secretion rates (Vanoni *et al.*, 2008) and sialylation of APP was also proposed to increase its secretion (Nakagawa *et al.*, 2006). A relationship between bisecting GlcNAc and amyloid-β production has also been proposed by the Endo group: Alzheimer's brains were found to express more GnT-III, and GnT-III expression in cultured neuroblastoma cells altered the activity of some of the secretase enzymes leading to decreased amyloid-β production (Akasaka-Manya *et al.*, 2010). Mutant amyloid protein associated with inherited Alzheimer's disease (AD) displayed more bisecting GlcNAc and more core fucose than protein from healthy controls (Akasaka-Manya *et al.*, 2008).

In multiple sclerosis*, N*-glycan branching may contribue to disease pathogenesis by controlling the growth of T cells. In mice, insufficient activity of the enzymes responsible for branching of *N*-glycans, GnT-I, GnT-II, and GnT-V, can lead to spontaneous neurodegeneration reminiscent of multiple sclerosis pathology. This is particularly severe for mice lacking GnT-V. In human, mutations in the genes for IL-2 and IL-7 are associated with increased risk for multiple sclerosis, and these cytokines have been proposed to regulate transcription of the above branching enzymes. In cultured human T cell blasts exhibiting the risk alleles there is reduced activity of GnT-I and subsequent reduction in branched *N*-glycans. For reviews see (Grigorian *et al.*, 2012a; Grigorian *et al.*, 2012b; Chien *et al.*, 2018).

1.5.7 Glycans and inflammation

The importance of glycan-lectin interactions has been well established in the systemic immune system (Marth and Grewal, 2008; van Kooyk and Rabinovich, 2008; Sperandio *et al.*, 2009; Rabinovich and Croci, 2012) and evidence is beginning to accumulate to support similar activity in the CNS.

Changes in expression patterns of many of the endogenous lectins in association with inflammatory processes suggest that these lectins, and glycans by association, may be involved in regulation of inflammation in the CNS. In particular there is evidence that lectin glycan interactions may be involved in the recruitment and proliferation of inflammatory cells, their activation and polarisation and regulation of phagocytic activity.

There are three main families of lectins found in vertebrates, the galectins, the siglecs and the selectins. Both selectins and siglecs are sialic acid binding lectins, but they differ slightly in their binding preferences and differ greatly in their functional properties. The siglecs are of the immunoglobulin type and most have extensive intracellular signalling capabilities. These features are reviewed by (Crocker *et al.*, 2007; Linnartz-Gerlach *et al.*, 2014). The selectins are calcium dependent lectins which are found mainly on circulating white blood cells and on endothelial cells, and so seem to be primarily involved in immune cell migration out of the vasculature. Galectins bind to a variety of carbohydrate residues, most simply those containing disaccharides of *N*-acetyl-lactosamine (Rabinovich and Toscano, 2009). Galectins have a variety of functions in the nervous and immune systems, some of which are described below.

Numerous studies have identified an alteration in galectin expression following traumatic CNS injury. Galectin-3 (Gal-3) upregulation has been identified following spinal cord contusion (Pajoohesh-Ganji *et al.*, 2012). Following transient middle cerebral artery occlusion (MCAO) there was an acute increase from almost undetectable levels of Gal-3 to a high level of expression in the location of injury (Lalancette-Hebert *et al.*, 2012; Young *et al.*, 2014). In the healthy spinal cord galectin-1 (gal-1) expression was found in neurons (McGraw *et al.*, 2005; Kurihara *et al.*, 2010; Gaudet *et al.*, 2015), however following SCI there was a switch from neuronal to glial expression. In both hemisection and contusion models of SCI gal-1 was found to be associated with neutrophils, microglia or macrophages and astrocytes (Kurihara *et al.*, 2010; Gaudet *et al.*, 2015). From 1 week post-injury to the final 28 day time-point almost half of astrocytes in the glial scar were expressing gal-1 (Gaudet *et al.*, 2015).

Whether gal-3 expression is beneficial or detrimental remains to be seen, and most likely depends on specific characteristics of the injury in question. Microglial gal-3 production was seen to negatively affect outcome in neonatal hypoxic-ischaemia. Hypoxic-ischaemic injury was more severe in gal-3(+/+)

mouse pups than gal-3(-/-) pups. The mechanism for this was briefly investigated: there was no difference in IL-1 production, while gal-3(-/-) animals produced significantly less MMP-9 (matrix metalloproteinase-1) and nitrotyrosine, a marker of oxidative stress. These results suggest that gal-3 positive activated microglia may play a role in the pathogenesis of hypoxic-ischaemic injury and that microglial gal-3 expression is related to phenotype (Doverhag *et al.*, 2010). In contrast, MCAO resulted in a significantly larger number of apoptotic neurons and an increase in the total size of injured area in gal-3 knockout animals, while *in vitro* cells lacking gal-3 showed reduced activation in response to glutamate insult (Lalancette-Hebert *et al.*, 2012). When proliferation of gal-3 positive microglia was prevented following MCAO there was an upregulation of proinflammatory cytokines and more apoptosis of both neurons and microglia (Lalancette-Hebert *et al.*, 2007).

The sialic acid binding siglecs have also been found to be differentially expressed in response to injury. Siglec-1, also known as sialoadhesin, expression is specific to macrophages and microglia and in the healthy brain expression is only seen in a small subpopulation of microglia in regions where the blood brain barrier is leaky (Perry *et al.*, 1992). Following injury however siglec-1 expression has been shown to be upregulated in a variety of situations. Traumatic injury involving blood-brain-barrier disruption was found to induce siglec-1 expression in a subset of microglia local to the injury (Perry *et al.*, 1992). Genetic modelling of myelin degeneration induced expression of siglec-1 in up to 90% of microglia / macrophages, with this lectin being undetectable in healthy CNS (Kobsar *et al.*, 2006; Ip *et al.*, 2007). Knockout of siglec-1 in genetic models of myelin degeneration resulted in a less severe disruption of myelin integrity and electrophysiological function (Kobsar *et al.*, 2006; Ip *et al.*, 2007). In genetically induced degeneration of retinal photoreceptors in the *rds* mouse, siglec-1 appearance was again associated with the injury process. Healthy WT mice expressed no siglec-1 in the retina, however in the *rds* mouse, siglec-1 appeared in approximately 20% of microglia coinciding with the time of maximal photoreceptor cell death. The level of expression peaked at the same time as total microglia numbers. The absence of iNOS or nitrotyrosine led the authors to conclude that these microglia are not playing a neurotoxic role but may be phagocytic (Hughes *et al.*, 2003). It has been suggested that siglec-1 is actually a sialic acid dependent adhesion molecule specific for macrophages (Crocker and Gordon, 1986; Crocker *et al.*, 2007) as it lacks the intracellular signal transduction machinery commonly associated with this lectin family (Crocker *et al.*, 1994).

1.5.7.1 Glycans in recruitment and proliferation of inflammatory cells

The sialic acid binding selectins are found expressed both on circulating white blood cells and on the surface of endothelial cells, and have been shown to be very important for the recruitment of peripheral immune cells. (Lee and Benveniste, 1999) review the expression of adhesion molecules, including selectins, on glial cells of the CNS and their relation to the migration of immune cells from the blood to the brain. In particular, the selectins are thought to facilitate the first steps of this process, i.e. the targeting of circulating immune cells to vessel walls and the characteristic rolling along the endothelium. The selectin ligands present on immune cells likely influence the target tissue: (Angiari *et al.*, 2014) found that the reduction in accumulation of T cells in inflamed skin was more pronounced with a deletion of P-selectin glycoprotein ligand (PSGL-1), which is considered the 'traditional' P-selectin ligand, than with T-cell immunoglobulin and mucin domain-1 (TIM-1) mucin domain deletion, while the opposite was seen in inflamed brain tissue. Another class of sialic acid binding lectins, the siglecs, may also be involved in recruitment. As mentioned above Siglec-1 expression peaked at the same time as microglial numbers during retinal photoreceptor degeneration (Hughes *et al.*, 2003), and Siglec-1 deletion prevented the increase in macrophage and CD8+ T cell numbers in genetic models of myelin degeneration in central and peripheral nervous systems (Kobsar *et al.*, 2006; Ip *et al.*, 2007).

The galectins may also play a role in inflammatory cell recruitment: following sciatic nerve transection it was found that endogenous gal-1 production is necessary to target sufficient numbers of macrophages to the injury in a timely manner (Gaudet *et al.*, 2009). gal-3 however has an ambiguous role in microglial proliferation: gal-3-KO mice subjected to MCAO had significantly fewer microglia than WT counterparts due to a reduction in proliferation (Lalancette-Hebert *et al.*, 2012). However in response to MCAO in a different mouse strain there was no reduction in microglial numbers compared to WT (Young *et al.*, 2014), and in response to neonatal hypoxic-ischaemia there were more microglia in the affected region in gal-3-KO mice (Doverhag *et al.*, 2010). Thus the involvement of gal-3 in the injury-induced proliferative response of microglia may be dependent on the age and strain of the animal and of course on the type and severity of the injury. *In vitro* studies were carried out using microglia isolated from WT and gal-3-KO mice to determine the mechanism of altered proliferation. The proliferative response to IGF-1 (insulin like growth factor-1), a microglial mitogen, was lacking in gal-3 deficient cells (Lalancette-Hebert *et al.*, 2012). The authors hypothesised that this abnormal response may be glycan mediated as *N*-glycosylation is known to be necessary for membrane localisation of IGF-R1 (Carlberg *et al.*, 1996), and glycosylation is widely known to affect growth factor binding and function in general. This was found to be true, as tunicamycin inhibition of *N*-glycsoylation

in WT (wild-type) cells also abolished the proliferative influence of IGF-1, and Gal-3 was shown to bind IGF-1 receptor (Lalancette-Hebert *et al.*, 2012).

1.5.7.2 Glycans and polarisation of immune cells

Siglec-9, particularly the secreted ectodomain (ED-Siglec-9) has been shown to have a beneficial role following contusive SCI, through modulation of microglia/macrophage phenotype. The results suggest that ED-Siglec-9, MCP-1 and the MCP-1 receptor CCR2 form a complex on the surface of microglia/macrophages, where the ED-Siglec-9 binding is dependent on CCR2 α(2-3) sialylation. Following complex formation CCR2 signalling was modulated to induce these cells to a more anti-inflammatory, M2 type phenotype (Matsubara *et al.*, 2015).

The role of siglecs in polarisation has been more extensively studied in relation to peripheral B cells. Siglec-2 (also known as CD22) can be found on B lymphocytes and is thought to be involved in the modulation of B cell functional phenotype. Siglec-2 binds α(2-6) linked sialic acids monovalently, in particular the α(2-6) sialyllactosaminyl oligosaccharide which can be found on a variety of cell types with

proteins such as the CD45 tyrosine phosphatase. *In vitro* examination of the function of siglec-2 suggested a role in regulation of B cell activity. A number of results support this hypothesis: firstly, artificial activation of B cells allows ligand binding by Siglec-2; secondly, B lymphocytes, which do show cell surface sialylation, could not bind Siglec-2's preferred oligosaccharide unless the cells were treated with sialidase or the glycan side chains were disrupted using periodate treatment. These results also suggest that changes in activation status are accompanied by a change in cell surface glycosylation. The precise mechanism of the changes in siglec-2 activity is not defined here, although the authors suggest that it may be due to conformational changes in the siglec itself, or removal of 'cis-masking' sialic acid residues by an endogenous sialidase (Razi and Varki, 1998).

There is also some evidence that galectins influence microglial phenotype: as mentioned, microglia expressing Gal-3 were found following hypoxic-ischaemic insults in neonatal rat. These Gal-3 positive microglia had a morphology typical to the activated state (Doverhag *et al.*, 2010).

Gal-1 and its glycan binding activity was studied in detail with regard to an EAE mouse model of MS (Starossom *et al.*, 2012). Similar to T cells in the periphery (Earl *et al.*, 2010), they found that Gal-1 binds to the CD45 tyrosine phosphatase complex on the surface of microglia. This repressed the pro-

inflammatory 'M1' phenotype characterised by iNOS, TNF and CCL2 production and promoted the reparative 'M2' phenotype characterised by arginase production. The selective binding of M1 reactive microglia is due to the characteristic glycan expression on the cell surface, as determined by histochemistry with a number of plant lectins and coimmunoprecipitation experiments. Gal-1 – CD45 interaction was suggested to be mediated by O-glycans, most likely by core 1 O-glycans (Galβ(1-3)GalNAc) recognised by the peanut agglutinin (PNA) lectin. Gal-1 binding to CD45 functionally translates to the ability of Gal-1 to 'hold' CD45 on the outer membrane of microglia, thus maintaining its activity for a longer period of time; this is likely to be responsible for the observed phenotypic changes in the affected microglia. *In vitro* and *in vivo* work in EAE mice with and without endogenous Gal-1 production shows that endogenous Gal-1, produced by astrocytes, has essential roles in the modulation of microglial activation during autoimmune disease progression, and confers neuroprotection by reducing M1 microglial activation. For example, gal-1(-/-) mice subjected to EAE display increased pro-inflammatory microglia and GFAP immunoreactivity, with a decrease in axonal growth and myelination and reduced neuronal immunoreactivity (Starossom *et al.*, 2012).

1.5.7.3 Glycans and phagocytosis

Siglec-5 is found on macrophages in the periphery, and has been suggested to play a role in phagocytosis. Cultured macrophages were shown to phagocytose UV treated, apoptotic, cancer cells and this activity was deemed to be dependent on siglec-5 interaction with sialic acids on the cell surface. In support of the sialic acid dependence of this interaction apoptotic cells were also shown to bind the sialic acid-binding plant lectins SNA and MAA which target α(2-6) and α(2-3) linked sialic acids respectively (Rapoport *et al.*, 2005).

Siglec-11 is a human specific CD33 related siglec with a specific affinity for α(2-8)-linked sialic acids and multiple immunoreceptor tyrosine-based inhibitory motif (ITIM) domains in the intracellular portion. It is approximately 80kDa in size and has been shown to be located on the cell surface of all human microglia (Wang and Neumann, 2010; Wang *et al.*, 2012). Engineering mouse primary microglia to express human siglec-11 significantly lowered the phagocytic capacity of these cells. The authors suggest that the sialic acid chains on neural NCAM interact with microglial siglec-11 to act in a neuroprotective manner (Wang and Neumann, 2010).

A later study by the same group examined whether mouse siglec E, which binds a wide range of sialic acids but also has a preference for α(2-8) linkages, has a similar function to the human siglec-11 (Claude *et al.*, 2013). Similarly to siglec-11, siglec E prevented phagocytosis of neural debris. Siglec E

senses the intact glycocalyx which is enriched in sialic acid residues to inhibit immunoreceptor tyrosine-based activatory motif (ITAM) mediated apoptosis (Graham *et al.*, 2007; Claude *et al.*, 2013).

Galectins may also play a role in phagocytosis. As mentioned above, (Young *et al.*, 2014) observed Gal-3 positive microglia at the epicentre of ischaemic injury and expression of Gal-1 by lesion macrophages was also seen following contusive SCI (Gaudet *et al.*, 2015). These results suggest a role in phagocytosis for both Gal-3 and Gal-1 from both the localisation of the microglia and the expression of ED1, which is associated with phagocytic activity. One day following an impact injury to the head in rat Gal-3 expression appeared in microglia in the corpus callosum, and expression remained high throughout the 28 day study period. These microglia were seen to be involved in clearing injured axons but it was not shown directly whether Gal-3 is directly involved in the act of phagocytosis (Venkatesan *et al.*, 2010). (Gaudet *et al.*, 2015) suggested that Gal-1 is involved in phagocytosis and that this is most likely dependent on its carbohydrate binding activity as the dimeric carbohydrate-binding Gal-1 is increased from 3 to 28 days following injury, significantly so at 7 days, although monomeric Gal-1 which is oxidised and displays no lectin-like properties is also increased in a similar manner.

Glycosylation possibly also influences the functional phenotype of astrocytes. Astrocytes in the glial scar can be observed to express Gal-1 following SCI (Kurihara *et al.*, 2010; Gaudet *et al.*, 2015). (Sasaki and Endo, 2000) observed that DSA, a plant lectin, could alter the phenotype of astrocytes in culture. Gal-1 was isolated from rat brain using its glycan binding ability. Treatment of immature astrocyte cultures with this isolated protein resulted in increased GFAP immunoreactivity. This work also indicated that Gal-1's influence on astrocytes is dependent on its carbohydrate-binding properties – kinetically, the effective doses indicate that Gal-1 has the greatest effect in its dimeric form which is where the lectin activity comes to the fore. The effect is also eliminated by co-incubation with lactose, further supporting the necessity of glycan binding.

This important publication prompted others to examine the potential of Gal-1 to play a role in the astrocytic response to traumatic injury. The Wang group performed two studies of photochemically induced focal ischaemia, one focussed on the hippocampus, the other on the neocortex (Qu *et al.*, 2010; Qu *et al.*, 2011). In both cases Gal-1 expression increased in response to the injury and was predominantly seen in astrocytes at the edge of the injured region. In the cortex, a small amount of Gal-1 reactivity was observed in neurons undergoing programmed cell death (Qu *et al.*, 2010; Qu *et al.*, 2011). In kainate induced hippocampal injury upregulation of astrocytic Gal-1 was observed in the affected area. These astrocytes were also positive for nestin, a marker of neural progenitors (Kajitani *et al.*, 2009).

1.5.7.4 Glycan based experimental treatments

Based on some of the findings described above a number of groups have tested the benefit of manipulating glycan activity to provide therapy in a variety of experimental injuries and diseases.

Considering the role of selectins in immune cell infiltration, antibodies targeting E- and P-selectins have been administered intravenously in an attempt to limit the severity of EAE in mice. Surprisingly this had no impact on the progression of EAE or on the microscopic pathological characteristics (Engelhardt *et al.*, 1997). Galectin based treatments show more promise however: given that Gal-1 can be secreted by astrocytes (Kajitani *et al.*, 2009), the therapeutic potential of exogenously applied Gal-1 has been investigated. Again, the Wang group have investigated this in focal ischaemia of both hippocampus and neocortex. A daily intrathecal dose of recombinant Gal-1 resulted in decreased neuronal apoptosis supported by improved functional outcome following ischaemia localised to the hippocampus (Qu *et al.*, 2010). Daily Gal-1 delivery to the brain conferred a statistically significant decrease in neuronal apoptosis, smaller total lesion volume and improved neurological severity score after cortical injury. Astrocyte proliferation at the lesion border was also reduced (Qu *et al.*, 2011). An investigation into the role of gal-3 following spinal cord contusion injury suggested that inhibition of gal-3 activity may be protective as assessed by a subtle improvement in hindlimb motor function and a larger proportion of white matter remaining intact (Pajoohesh-Ganji *et al.*, 2012).

There are a number of explanations as to the neuroprotective benefits of Gal-1. As astrocytes are well known to produce trophic factors supporting neuronal survival and function the influence of Gal-1 on trophic factor production by astrocytes has been investigated. (Sasaki *et al.*, 2004) reported a dramatic production of BDNF occurring shortly after Gal-1 administration to cultured immature astrocytes, and (Qu *et al.*, 2010) saw that BDNF was increased 7 days after ischaemic injury mirroring the appearance of Gal-1, both mainly in reactive astrocytes. Gal-1 treatment was also found to limit astrocytic production of iNOS and IL-1β (Qu *et al.*, 2011). *In vitro* treatment of astrocytes with anti-inflammatory stimulators such as IL-4 or TGF-β1 lead to increased Gal-1 secretion (Starossom *et al.*, 2012). The importance of Gal-1's lectin activity to its biological effects is supported by the findings that all benefit is eliminated when the lectin is mixed with 100mM lactose before administration (Qu *et al.*, 2011).

1.6 Phases and rationale for the project

The primary aim of this work was to improve our understanding of the pathology of SCI, and how the injured mammalian spinal cord responds to a biomaterial treatment. We also investigate the mechanism of how the injured spinal cord may be regenerated spontaneously in an amphibian model. In both cases, we have focussed primarily at the molecular level, examining *N*-glycosylation changes (in this thesis) and proteomic changes (Aniket Kshirsagar's thesis). Neuronal outgrowth and astrocytosis were also examined, this is split between the two theses. We would like to bring all of this knowledge together to improve the design of future biomaterial therapies so that they can be functionalised in a more informed manner.

This work described in this thesis was broken into a number of phases. The first was to characterise the rate of repair following transection of the spinal cord of *Xenopus laevis* tadpoles. The next phase was a comparison of the astrocytic response to injury between tadpoles and froglets, followed by a comparison of the glycosylation response to injury between tadpoles and froglets. For the next phases we turned to a rat model of SCI to investigate in detail the *N*-glycosylation response: first a comprehensive characterisation of the *N*-glycome of the healthy spinal cord was carried out followed by an investigation into the changes in *N*-glycosylation following spinal cord transection and with biomaterial treatment. In parallel with this, inflammatory changes following injury and biomaterial treatment were investigated. A pilot time-course study with inflammatory markers as the main readout was performed in order to determine the most appropriate time points to perform detailed analysis.

This entire study was carried out alongside Aniket Kshirsagar's thesis project, which used the same animal models, experimental groups and time-points. This work is described in a separate thesis and examines neuronal outgrowth across the lesion, astrocytosis with GFAP and CSPG deposition in the rat model, as well as a comprehensive proteomic investigation into injury, repair and treatment in both *Xenopus laevis* and rat models. For a more complete picture of the molecular, neuronal and glial response to injury and treatment across these models these two theses should be considered together.

2 Chapter 2 - Materials and Methods

2.1 *In vivo* modelling of SCI in *Xenopus laevis*

All *Xenopus laevis* experiments were carried out in accordance with the Council Directive 2010/63/EU of the European Parliament and with the related Irish legislation S.I. No. 543/2012 - European Union (Protection of Animals used for Scientific Purposes) Regulations 2012. All housing and surgical procedures carried out in this study were approved by the Animal Care Research Ethics Committee at the National University of Ireland, Galway, and the Health Products Regulatory Authority. All individuals in contact with living *Xenopus laevis* held valid individual authorisations. At all times *Xenopus laevis* embryos were kept in 0.1X modified Barth solution (MBS, Appendix VIII). Animals had sufficient space to allow for movement and growth at an adequate rate, and were maintained at room temperature on a 12-hour light-dark cycle. Reagents and consumables for these experiments are listed in Appendix III.

2.1.1 Growth of Xenopus laevis

Embryos were obtained following *in vitro* fertilisation of oocytes and grown in petri dishes on a cold plate cooled to 17˚C until reaching approximately Nieuwkoop and Faber (NF) stage 35 (Nieuwkoop *et al.*, 1956). At NF stage 35 and thereafter embryos were transferred to plastic containers of approximately three litre capacity and maintained at room temperature, 18 - 22˚C. Once the yolk sac had been resorbed, at NF stage 40, feeding with a solution of finely ground nettle tea began. During metamorphosis pelleted frog food was also provided. For the first week of life 0.1X MBS solution was changed daily, thereafter three times weekly was sufficient.

2.1.2 Spinal cord injury stage 50 tadpole

Work area and all instruments were cleaned thoroughly with 70% ethanol. Tadpoles were anaesthetised by immersion in 0.1% tricaine methanesulfonate (MS222, Fisher Scientific, Ireland) diluted in 0.1X MBS for approximately 30 seconds or until loss of reflex responses. Excess MS222 was washed off in 0.1X MBS before immobilisation in plasticine. At the level of the sixth to seventh myotome the skin, muscle and dura were opened individually with a pair of fine forceps (Dumont #5, Fine Science Tools, Germany) to expose the spinal cord (Figure 2.1 A, B). The tip of a 25G needle (BD, UK) was inserted ventrally to the spinal cord (Figure 2.1 C) and pulled dorsally in one smooth movement, separating the spinal cord into two separate pieces (Figure 2.1 D). Complete transection

was confirmed at the time of surgery by passing the tips of of the Dumont #5 forceps through the gap in the spinal tissue, and only those tadpoles with complete separation and an absence of movement on the following day were included in the following studies.

For sham injury, tadpoles were anaesthetised and immobilised in plasticine. Skin and muscle were opened at myotome six to seven as above, but spinal cord and dura mater were left intact. For inclusion in the following studies sham injured animals needed to display normal swimming movement on recovery from anaesthesia.

Immediately following sham and transection injuries tadpoles were transferred to transplantation buffer, a solution high in calcium and sodium, for thirty minutes. Tadpoles were then individually housed in separate wells of a six-well plate containing 0.1X MBS solution supplemented with penicillin (10,000 units per ml) streptomycin (10 mg/ml) and gentamycin (2.5 mg/ml) (Sigma Aldrich, Ireland) until the desired time-point. Feeding with a solution of finely ground nettle tea was re-introduced two days post-injury. Solutions were changed and health monitoring was carried out twice daily.

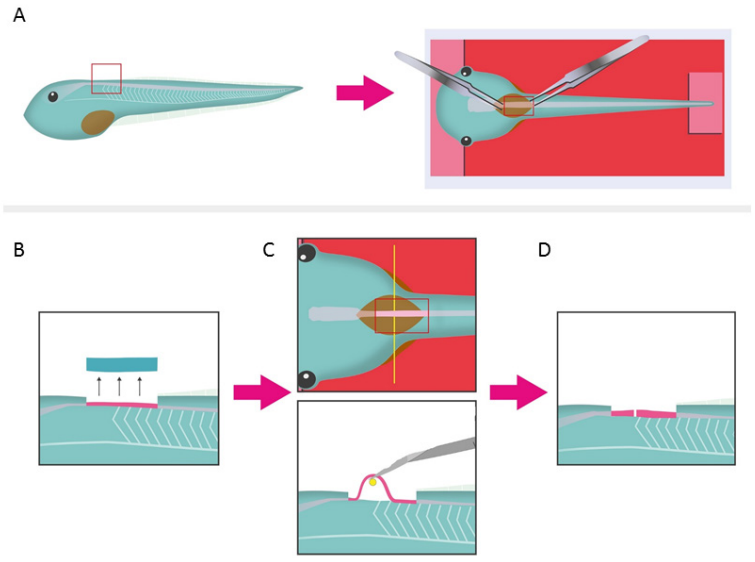

Figure 2.1 Schematic of spinal cord transection procedure for NF stage 50 *Xenopus laevis* tadpole

2.1.3 Spinal cord injury stage 66 froglet

Work area and all instruments were cleaned thoroughly with 70% ethanol. Froglets were anaesthetised by immersion in 0.5% MS222 for approximately 30 seconds or until loss of reflex

responses. Excess MS222 was washed off in 0.1X MBS before immobilisation in plasticine. An incision through the skin and underlying connective tissue was made along the length of the spine using a #11 scalpel (Swann Morton, England). A laminectomy was performed at the sixth vertebra using a Dumont #5 forceps (Fine Science Tools, Germany). Bleeding was minimised by compression with gauze and by flushing with transplantation solution (Appendix VIII). When sufficient bone had been cleared away the spinal cord was loosened from the surrounding vertebra by inserting one side of the forceps between the cord and the bone. A fine scissors (Fine Science Tools, Germany) was inserted into the vertebral canal perpendicularly to the spine to transect the spinal cord. Complete transection was confirmed by passing the tip of the forceps through the resulting gap in the tissue. Only those froglets displaying complete paralysis in the days following transection were included for further study.

To perform sham injury, froglets were anesthetised and an incision made in the skin and connective tissue along the length of the spine as above. A laminectomy of the sixth vertebra was performed without touching the spinal cord. For inclusion in the study, normal movement must have been displayed following recovery from anaesthesia.

For the first thirty minutes following injury froglets were kept in transplantation solution. They were then moved to 0.1X MBS supplemented with antibiotics as described above. Froglets were housed in pairs or in threes in plastic tanks containing a volume of liquid sufficient to cover the back of the animal, preventing dehydration, while still allowing them to raise their head to breathe. (This was approximately 100 ml in a 600 ml container). Solutions were changed and health was monitored twice daily. Food was re-introduced 2 days post-injury.

2.1.4 Euthanasia: Xenopus laevis

At the desired timepoint (see Table 2.1), euthanasia was carried out for both tadpoles and froglets by anaesthetic overdose. Animals were immersed in 1% MS222 until cessation of heartbeat, approximately twenty minutes, and death was confirmed by destruction of the brainstem region. In the case of froglets, the vertebral column was removed using forceps and a #11 scalpel.

Developmental stage	**Injury**	**Time point (dpi)**				
Tadpole	Sham	1	3	5	7	10
	Transection	1	3	5	7	10
Froglet	Sham	1			7	
	Transection	1			7	

Table 2.1 Experimental treatment and time-points for Xenopus laevis experiments. n=5 per group

2.1.5 Processing of Xenopus laevis *tissue*

Following euthanasia the entire tadpole or the isolated vertebral column of froglets was fixed by immersion in 1.5 ml 4% paraformaldehyde (PFA, Sigma Aldrich, Ireland) in 1X phosphate buffered saline (1X PBS, Appendix VIII) at 4^{o}C for 24 hours in the case of tadpoles, or 48 hours in the case of froglet spinal column. PFA was washed away with two 10 minute washes in PBS followed by cryoprotection in 30% sucrose dissolved in PBS. Tadpoles were left in sucrose solution for 24 hours at 4^{o}C, while froglet vertebral column remained in sucrose for 48 hours.

In an effort to stabilise the froglet spinal cord in position, and to find any cells which may be present in the lesion gap, a 10g per 100 ml solution of gelatin (type A from porcine skin, Sigma Aldrich, Ireland) was placed on the dorsal side of the cord, having removed dorsal laminae. Once set (less than 10 minutes at 4^{o}C) excess gelatin and remaining vertebral bone was removed with a pair of fine forceps.

To freeze, tissue was placed in a small agarose mould and surrounded by optimal cutting temperature (OCT) medium (Sakura, Netherlands), before immersing in 2-methylbutane which had been cooled to freezing point in liquid nitrogen. Tissue was then stored at -80^{o}C before cryosectioning with the chamber temperature set to -24^{o}C. 20µm cryosections were cut and mounted on charged Superfrost Ultra Plus slides (Thermo Fisher Scientific, Ireland). For tadpoles, serial sections were collected across a series of six slides so that adjacent sections were mounted on separate slides and there was a distance of 120 µm between sections on the same slide, as shown in Figure 2.2. Froglet tissue was similarly collected across a series of twelve slides so that there was a distance of 240 µm between sections on the same slide. Approximately sixty sections were collected per froglet. All cryosections were stored at -20^{o}C until histochemistry was performed.

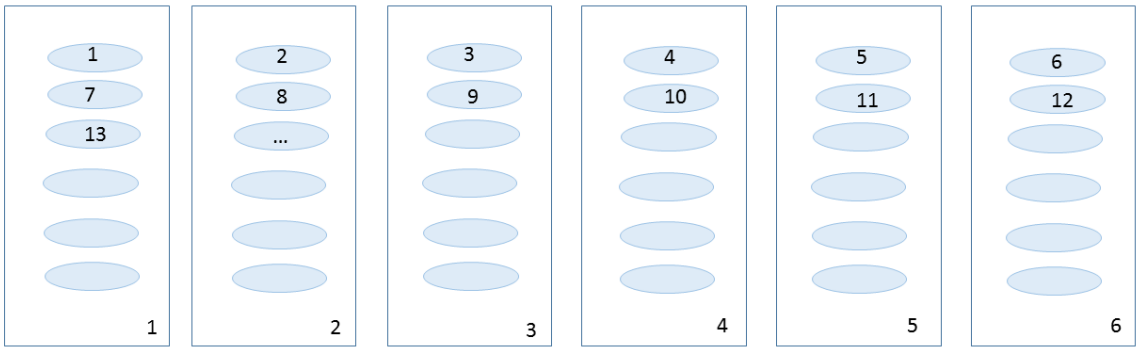

Figure 2.2 Distribution of tissue sections across slides for tadpole tissue.

2.2 *In vivo* modelling of SCI in the rat

All rat experiments were carried out in accordance with the Council Directive 2010/63EU of the European Parliament Parliament and with the related Irish legislation S.I. No. 543/2012 - European Union (Protection of Animals used for Scientific Purposes) Regulations 2012. All housing and surgical procedures carried out in this study were approved by the Animal Care Research Ethics Committee at the National University of Ireland, Galway and the Health Products Regulatory Authority. All individuals in contact with living animals held valid individual authorisations. Reagents and consumables for surgery, care and tissue processing for rat experiments are given in Appendix IV.

2.2.1 Spinal cord transection injury, collagen hydrogel implantation and sham injury in the rat

Adult female Sprague-Dawley rats of weight 250 – 300 g, (Charles River, UK) were anaesthetised with isofluorane (Iso-vet, Chanelle group, Ireland) delivered at 5% in 0.8% oxygen, anaesthesia was maintained with 2% isofluorane in 0.8% oxygen delivered via a facemask. Buprenorphine (Bupaq, Chanelle group, Ireland) was administered at a dose of 0.05 mg/kg subcutaneously a minimum of one hour before surgery. Vidisic 0.2% w/w eye gel (Bausch & Lomb, UK) was applied to the eyes and 5 ml of normal saline (0.9% (w/v) sodium chloride, Braun Medical, Ireland) was given subcutaneously to maintain hydration. The back of the animal was shaved and cleaned with chlorhexidine (Hibiscrub). Surgery was performed on a heated table using aseptic technique.

An incision was made in the skin above the lower thoracic vertebrae using blunt-tipped surgical scissors (World Precision Instruments, UK). Muscle was cleared from the eighth to tenth thoracic vertebrae (T8 – T10). The prominent spinous process of T2 was used as a landmark. Using a Friedman-Pearson rongeur (Fine Science Tools, Germany) a laminectomy of T9 was carried out to expose the spinal cord. At this stage the wound was closed for animals designated as sham. To transect the spinal cord a 0.5mm cup curette (Fine Science Tools, Germany) was inserted into the vertebral column

underneath the spinal cord lifting it up slightly. To transect, a # 15 scalpel (Swann-Morton, England) was passed through the entire thickness of the spinal cord adjacent to the curette. A successful transection was determined by the immediate and obvious retraction of the cord leaving a gap of approximately 2 mm between the two cut ends. Bleeding was controlled with sterile gauze. Lignocaine and adrenaline were applied topically to minimise bleeding during laminectomy and cord transection. For those animals receiving collagen hydrogel treatment, it was implanted immediately following transection of the cord. Once the injury site was relatively cleared of blood the hydrogel was carefully placed into the resulting gap, ensuring that the alignment of collagen fibres was running parallel to the spinal cord. The wound was closed by suturing the muscle and skin in separate layers using 4-0 Vicryl sutures (Ethicon, Belgium) and/or skin staples.

Following surgery oxygen was delivered to animals at 0.8% until recovery from anaesthesia. All animals were kept on heated blankets for approximately two hours following surgery. Animals were housed singly on 'VetBed' (Pet Life, UK) bedding for the first 3 days and in twos and threes with regular bedding thereafter. Drinking water was supplemented with Dioralyte to prevent dehydration for the first three days. Buprenorphine was administered for analgesia at 0.05 mg/kg every 12 hours for the first 3 days and every 24 hours until 7 days post injury. Animals were monitored twice daily for signs of general infection, health and distress. These signs included but were not limited to skin turgor as an indication of dehydration, the grimace scale as an indication of pain, hair loss as a sign of distress, evidence of autophagia. The wound was also monitored for possible infection. Manual bladder expression was performed twice daily and animals were monitored for signs of urinary infection, including a bloody or cloudy appearance or proteinuria. In the event of urinary infection enrofloxacine (Baytril, Bayer, Germany) was administered at 10 mg / kg as required.

Following spinal cord transection complete hindlimb and tail paralysis was observed with minimal improvement seen over the duration of the study. Animals remained mobile through the use of the forelimbs.

2.2.2 Euthanasia: rat

At the appropriate timepoint (see Table 2.2) animals were euthanised by overdose of anaesthetic. Sodium pentobarbitone was given intraperitoneally at a dose of 140 mg/kg delivered in sterile saline. Once a surgical plane of anaesthesia had been reached the thorax was opened to expose the heart. A butterfly needle was inserted into the apex of the left ventricle and a small opening was made in the right atrium. Vasculature was cleared of blood by flushing with approximately 200 ml of 1X PBS via syringe.

	Time-point	Experimental group	n (histochemistry)	n (*N*-glycomics)
Pilot study	3 dpi	Transection only	3	-
		Transection + aligned hydrogel	3	-
	7 dpi	Transection only	3	-
		Transection + aligned hydrogel	3	-
	14 dpi	Transection only	3	-
		Transection + aligned hydrogel	3	-
	21 dpi	Transection only	3	-
		Transection + aligned hydrogel	3	-
	28 dpi	Transection only	3	-
		Transection + aligned hydrogel	3	-
Main study	7 dpi	Sham	10	3
		Transection only	10	3
		Transection + random hydrogel	10	3
		Transection + aligned hydrogel	10	3
	14 dpi	Sham	10	3
		Transection only	10	3
		Transection + random hydrogel	10	3
		Transection + aligned hydrogel	10	3

Table 2.2 Experimental groups, time-points and n numbers for rat experiments

2.2.3 Tissue harvesting and processing of rat tissue

For those animals designated for immunohistochemistry (see Table 2.2) transcardial perfusion fixation with 4% PFA diluted in 1X PBS was performed following perfusion with PBS. PFA perfusion was considered complete when perfusion tremors ceased and muscle was rigid to touch.

The vertebral column was dissected out immediately and post-fixed in 4% PFA for up to 48 hours at 4^{o}C. Following fixation the injured segment of spinal cord, including the injury site and approximately two vertebral levels either side, was removed and incubated in 30% sucrose in PBS overnight at 4^{o}C for cryoprotection. Tissue was embedded in OCT and frozen in 2-methylbutane cooled in liquid nitrogen and stored at -80^{o}C until cryosectioning. Sections were cut to a thickness of 20 µm at a temperature of approximately -22^{o}C on a Leica CM1900 cryostat and stored at -20^{o}C until staining.

Sections were distributed across slides in a similar manner as outlined above for *Xenopus laevis* cryosections (Figure 2.2): tissue was collected onto 40 slides per animal with serial sections being placed on adjacent slides, for example the first section was placed on slide 1, the second on slide 2, the third on slide 3 etc., the 41st section was placed on slide 1, the 42nd on slide 2, the 43rd on slide 3 etc. Approximately 160 sections were cut per animal.

For those animals designated for glycomic analysis (see Table 2.2) the tissue harvesting procedure differed slightly. These animals also received an overdose of sodium pentobarbitone and were transcardially perfused with PBS only, in order to flush out the vasculature, but no fixation was performed. Instead, the injured portion of the spinal cord was then immediately dissected out and snap frozen on dry ice, before being stored at -80^{o}C.

2.2.4 Collagen hydrogel preparation

The collagen solution used for synthesis of hydrogels was bovine type I collagen, dissolved in acetic acid at a concentration of 4 mg/ml. The solution was dialysed before using to form hydrogels.

Aligned collagen fibres were formed by placing 300 µl collagen solution on a hydrophobic Teflon surface, connecting two wires which in turn were connected to the cathode and anode of a bench top power supply. The collagen solution allowed for the flow of current throughout the circuit. The power supply was run for 15 minutes at 6V. This process resulted in the creation of a pH gradient across the solution, which encouraged collagen fibrils to migrate to their isoelectric point, forming one continuous fibre of approximately 350 µm diameter. The collagen fibre was placed in PBS overnight.

Approximately 12-14 such fibres were arranged together to form the aligned collagen hydrogel for implantation into the transected rat spinal cord.

The random collagen hydrogel was prepared from the same dialysed solution. A drop of 1 ml was incubated overnight in PBS, and was then ready for implantation into the spinal cord.

2.3 Immunohistochemistry

Reagents and consumables for all immunohistochemistry experiments are listed in Appendix V. Recipes for buffers etc. are in Appendix VIII.

2.3.1 Immunohistochemistry: Xenopus laevis

Slides were allowed to come to room temperature and washed three times in 0.2% Triton X-100 in 1X PBS (PBS-T). Blocking of non-specific binding was ensured with a thirty minute incubation in 3% bovine serum albumin (BSA, Sigma Aldrich, Ireland) in 1X PBS. Blocking solution was removed, primary antibodies diluted in PBS-T (Table 2.3) were applied directly and left to incubate for ninety minutes at room temperature. Slides were washed three times in PBS-T before incubating for sixty minutes with secondary antibodies in PBS-T (Table 2.3). Two washes in PBS were performed before nuclear staining with Hoechst (Invitrogen, California) for ten minutes at a dilution of 1:2000 in PBS. Two final washes in PBS were carried out before applying Fluoromount (Sigma Aldrich, Ireland) and coverslipping. Slides were left to dry at room temperature overnight, then sealed with nail polish and stored at 4^{o}C until imaging. Images were acquired within two days of staining. For all stains a negative control was performed by carrying out the protocol as above but omitting the primary antibody, and incubating with PBS only for 60 minutes at room temperature. No signal was observed for negative controls.

Primary antibody	**Catalogue number**	**Dilution**	**Secondary antibody**	**Catalogue number**	**Dilution**
Anti-acetylated α-tubulin	Sigma, T6793	1:1000	Alexa Fluor 488	Invitrogen, A21202	1:1000
			Alexa Fluor 647	Life Technologies A21236	1:1000
Anti-GAP43	Abcam, ab12274	1:100	Alexa Fluor 546	Invitrogen, A11035	1:1000
Anti-GFAP	Dako, Z0334	1:200	Alexa Fluor 546	Invitrogen, A11035	1:1000

Table 2.3 Primary and secondary antibodies used in *Xenopus laevis* experiments.

2.3.2 Immunohistochemistry: rat

Cryosections were brought to room temperature and OCT washed away with three washes in 0.1% triton X-100 in PBS (PBS-T). Non-specific binding was blocked by incubating with 10% normal donkey serum (Sigma Aldrich, Ireland) in PBS for 30 minutes at room temperature. The primary antibody (Table 2.4) was incubated for 60 minutes at room temperature. Excess antibody solution was removed by 3 washes in PBS-T. Secondary antibodies (Table 2.4) were applied to slides and also incubated for

60 minutes at room temperature. Two washes with PBS-T were performed to remove excess secondary antibody before incubating with Hoechst nuclear counterstain (Invitrogen, California, USA), diluted 1:2000 in PBS, for 10 minutes at room temperature. Two final PBS washes were performed before applying Fluoromount mounting media (Sigma Aldrich, Ireland) and coverslips. Slides were left to dry in the dark at room temperature for 12-24 hours before sealing with nail polish and storing at 4^{o}C. For all stains a negative control was performed by carrying out the protocol as above but omitting the primary antibody, and incubating with PBS only for 60 minutes at room temperature. No signal was observed for negative controls.

Primary antibody	**Catalogue number**	**Dilution**	**Secondary antibody**	**Catalogue number**	**Dilution**
CD11b	EMD Millipore, CBL1512	1:200	- Donkey anti-mouse AF647 Or AF555	Jackson Immuno, 715-605-151 Biosciences, A-31570	1:1000 1:500
Arginase-1	Santa Cruz Biotechnology sc-18351	1:100	Donkey anti-goat AF488	Invitrogen, A11055	1:1000
iNOS	Pierce, PA3-030A	1:500	Donkey anti-rabbit AF594	Invitrogen, A21207	1:1000

Table 2.4 Primary and secondary antibodies for rat tissue immunohistochemistry. CD11b was used as a global microglia/macrophage marker; iNOS as the 'pro-inflammatory' type microglia/macrophage marker; Arginase-1 as the 'anti-inflammatory', 'tissue repair' type microglia/macrophage marker.

2.4 Lectin histochemistry

Reagents and consumables for all immunohistochemistry experiments are listed in Appendix V. Recipes for buffers etc. are in Appenidix VIII. Sections were allowed to return to room temperature and rehydrated with three x three minute washes of tris buffered saline (TBS) containing 0.05% triton-X-100 (TBS-T) (Appendix VIII). Non-specific binding was blocked with a 2% solution of periodate treated BSA in TBS for one hour at room temperature. Periodate treatment disrupts the carbohydrate structures found on serum proteins. Following three washes in TBS-T a solution of FITC-conjugated lectin diluted in TBS-T (see Table 2.5) was applied for ninety minutes at room temperature. Sections were washed twice in TBS followed by a ten minute incubation with Hoechst (Invitrogen, California) diluted in TBS at 1:2000. Two more washes with TBS were carried out before application of Fluoromount (Sigma Aldrich, Ireland) and coverslips. Slides were left to dry at room temperature overnight, then sealed with nail polish and stored at 4^{o}C until imaging. Images were acquired within two days of staining. As a negative control a solution of lectin pre-saturated by incubation with a 100mM solution of the relevant haptenic sugar (Table 2.5) was applied to a tissue section. This was deemed to be successful with a reduction of 50% in fluorescence signal intensity.

Lectin	**Catalogue Number**	**Specificity**	**Concentration**	**Haptenic sugar control**
SNA-I	EY Labs, F-6802-1	α(2-6) sialic acid	10 µg/ml	D-lactose
DSA	EY Labs, F-5701-2	β(1-4) N-acetyl glucosamine (GlcNAc)	5 µg/ml	D-GlcNAc
AIA	EY Labs, F-6301-2	α-Galactose	10 µg/ml	D-Galactose
WFA	EY Labs, F-3101-2	N-acetyl galactosamine (GalNAc)	10 µg/ml	N-Acetyl-D-galactosamine

Table 2.5 Lectins used in this study with corresponding dilutions and haptenic controls. All lectins were purchased pre-conjugated to FITC. All haptenic sugars for inhibitory controls were purchased from Sigma Aldrich, Ireland and were used at a concentration of 100mM.

2.5 Combined lectin- and immuno-histochemistry

To examine the relative distribution of glycans relative to various cell types, dual and triple staining with lectins and antibodies was performed on tissue from *Xenopus laevis* and rat. In this case washes and blocking were performed as for lectin histochemistry (Section 2.4). Following the initial blocking and washing steps, lectins diluted in TBS-T were incubated on the tissue for 60 minutes, followed by primary and secondary antibodies, also diluted in TBS-T, with each incubation carried out for 60 minutes at room temperature. Excess of each solution was removed with TBS washes in between each step. Hoescht nuclear stain was applied after the secondary antibodies, before application of Fluoromount and coverslipping as described above.

2.6 Histology

Two histological stains were used to study extracellular matrix and scar composition following SCI and treatment. To investigate collagen composition of the injured spinal cord Masson's trichrome was performed, while alcian blue was used to examine proteoglycan deposition. Recipes for histological stains are given in Appendix VIII. Before beginning the staining procedures cryosections were brought to room temperature and excess OCT was cleared by three washes in tap water.

2.6.1 Alcian blue

Slides were immersed in alcian blue solution (pH 2.5) for 30 minutes. Excess stain was rinsed away in running tap water for 5 minutes before counterstaining in nuclear fast red for 5 minutes. Excess fast red was rinsed away in running tap water for 1 minute before dehydrating sections through a series of ascending alcohol concentrations (50% to 100%) and coverslipping with distyrene, plasticiser and xylene (DPX) mounting medium. A full protocol for this staining procedure is given in Appendix VI.

2.6.2 Masson's trichrome

Sections were immersed in a series of solutions as follows: potassium permanganate dissolved in sulphuric acid, sodium metabisulphate, water, Gomori's aldehyde fuchsin, water, 95% ethanol, water, Celestine blue, water, Mayer's haemalum, water, acid alcohol, water, Masson's cytoplasmic stain, water, 1% dodeca-molybdophosphoric acid, water, fast green dissolved in acetic acid and 1% acetic acid. Excess stain was removed by very briefly immersing sections into water before dehydrating across an ascending series of alcohols (50% to 100%) and coverslipping with DPX mounting medium. A full protocol for this staining procedure is given in Appendix VI.

2.7 Image acquisition and analysis

Images were acquired using three different approaches. The Andor Revolution spinning disk confocal microscope (Andor Technology Ltd, UK) was used when high magnification and elimination of background signal was required. The Olympus VS120 digital slide scanner was used in order to get a more global view of the injury and surrounding tissue using wide-field fluorescence. For histological staining in the rat the digital slide scanner was also used but in bright-field mode.

Images acquired with the Andor spinning disk were captured at 40x magnification and viewed and analysed in the Fiji program (Fiji version 1.50d, National Institute of Health, USA. Java 1.60_24 (64-bit)). Images acquired using the Olympus VS120 digital slide scanner (Olympus, UK) were captured using the 20x objective lens. VS-ASW software was used for image acquisition, OlyVIA software (version 2.8) for image viewing and Fiji for analysis.

Where possible the analyst was blinded to treatment group. However due to differences in tissue structure between sham and transected tissue, and between ROIs within the transected tissue complete blinding was not possible.

2.7.1 High magnification image acquisition for **Xenopus laevis** *experiments*

Images were acquired from five regions of interest (ROIs) in tadpoles and four ROIs in froglets. Two to four images were acquired per ROI per section, Figure 2.3. In tadpole sections these ROIs were defined as being in the lesion epicentre, the borders of the lesion both rostral and caudal (rostral border, caudal corder), and in intact tissue far from the lesion (rostral intact, caudal intact; see Figure 2.3 A). The border ROIs were each defined as beginning directly at the border of the lesion. The field of view of acquisition of the Andor system at 40x magnification covers a square of side length 170 µm approximately. To acquire two images within these regions one image was taken directly at the lesion edge, with the second 170 µm away from the border. Where the spinal cord was wider an extra image adjacent to the first, but still against the lesion border, was acquired. Thus the border zones as defined here extended 340 µm from the edge of the lesion. Images from intact tissue were acquired at a region approximately 510 µm from the edge of the lesion and again images were acquired adjacent to each other. In the tadpoles, at later survival time points such as 7 dpi the 'lesion' appeared much smaller than at earlier time points and so it became difficult to exclude the rostral and caudal borders. In this case one image of the lesion itself was acquired which unavoidably included some of the newly repaired tissue from rostral and caudal stumps, with border regions being defined as immediately adjacent to the edges of this field of view. At 10 dpi the cord appeared to be healed completely and

so a general lesion environment was defined using the gut as a landmark. Here the lesion and border ROIs were combined.

Images from similar ROIs were acquired from froglet tissue, with some small changes, Figure 2.3 B. No cells or tissue could be identified in the lesion site of the froglet spinal cord. This may be an artefact of tissue processing as during the isolation of the spinal cord form the surrounding tissue in froglets the lesion site could not be stabilised. Regardless, no images were acquired from this area in stage 66 animals. Images were acquired from the remaining four ROIs at the lesion borders (rostral border, caudal border) and in intact tissue far from the lesion (rostral intact, caudal intact; Figure 2.3 B). Due to the larger size of the spinal cord at this stage images were taken so as to be distributed across the width of the section and to include both white matter and grey matter areas. The regions 'far' from the lesion were acquired at a distance of 640 µm from the borders of the lesion. In both developmental stages images for sham animals were acquired from an area at an equivalent level to that for injured animals, i.e. at approximately the sixth to seventh myotome for tadpoles, and at approximately the sixth vertebra for froglets.

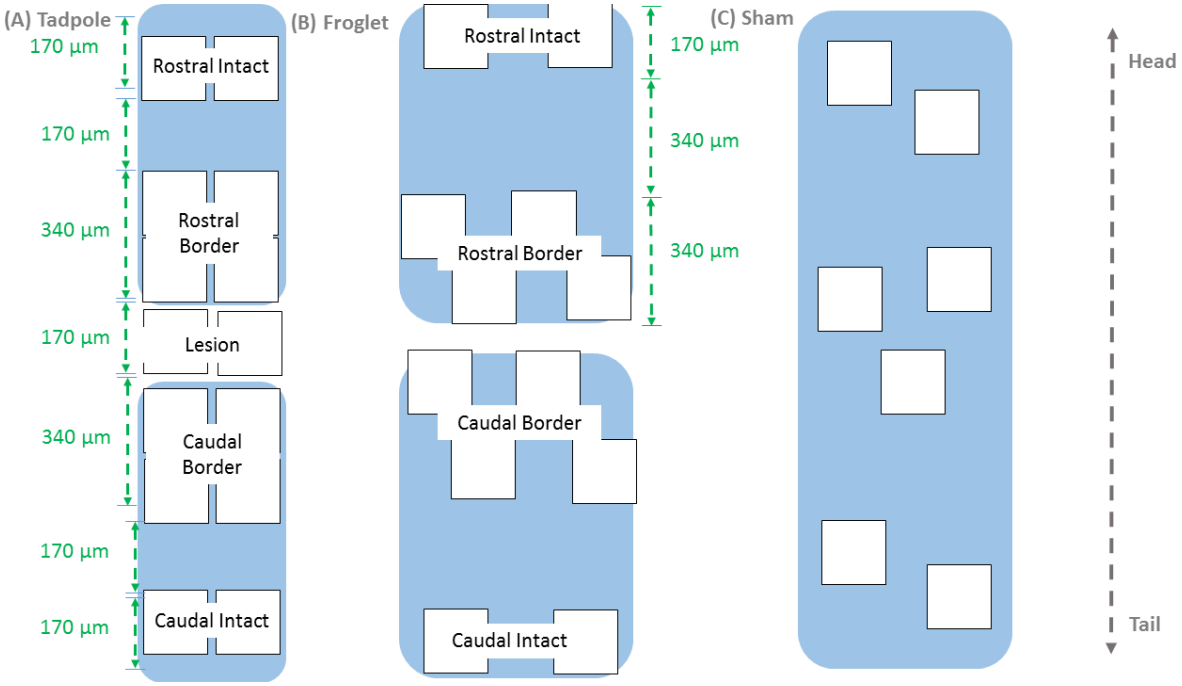

Figure 2.3 Five ROIs were defined for tadpoles (A) and four for froglets (B). White boxes represent where images were captured. Images at 40x magnification captured a region within a square with side 170 µm.

2.7.2 Analysis of timeline of neuronal growth in tadpole Xenopus laevis

Tissue was immunostained with GAP43 and acetylated alpha-tubulin. Images were acquired using the Andor spinning disk confocal at 40x magnification comprising multiple Z-planes. GAP43 signal was analysed from a maximum projection image, taken across 12 to 15 z planes, each 1 µm apart. Images were processed and analysed in Fiji. Optimal brightness and contrast values were obtained from calculating the median values for each channel from a selection of 4-5 images each for 20 random tadpoles from various groups. A macro (see Appendix IX) was used to apply identical processing parameters to each individual image, prior to analysis. Analysis was carried out on 8-bit grayscale images. Total tissue area and area of positive GAP43 signal were measured using Fiji's threshold and analyse particle functions. Total tissue area was measured in the merged image of GAP43, tubulin and Hoechst nuclear staining. The channels were then split so that positive GAP43 signal could be measured alone. GAP43 area was then expressed as a fraction of the total tissue area.

2.7.3 Analysis of astrocyte response to SCI in Xenopus laevis

A single optical slice from each image was analysed. The image was inverted and the brightness and contrast adjusted to distinguish positive signal: the minimum and maximum displayed values were at either tail of the histogram. A grid with square of side 112 pixels, or 18 µm, was applied to the image using Fiji. The number of points (intersections of the squares) which lay on positive astrocyte signal were counted and recorded using the Cell Counter plugin. The brightness and contrast was then adjusted so that total tissue could be seen and the number of points falling on tissue was counted and recorded. The area fraction of astrocytes was then expressed as (number of points falling on positive astrocyte signal) / (number of points falling on tissue) *100).

2.7.4 Analysis of lectin histochemistry in Xenopus laevis

Xenopus laevis tissue was stained with both lectins and antibodies. Images were acquired using the Andor spinning disk confocal microscope at 40x magnification across multiple Z-planes. Image analysis was performed in Fiji employing a stereological approach together with Fiji's threshold and integrated density functions. Integrated density was chosen to incorporate both area and intensity of staining. Thresholding the image allowed for distinguishing between positive signal and background fluorescence. A uniform threshold was used for all images for any given lectin, and the threshold was chosen based on a selection of images from each experimental group.

One optical slice was analysed per image. A grid of square size 128 by 128 pixels was applied to the image resulting in the image being divided into 64 areas, each sized to 21.3 µm by 21.3 µm. Starting in the top left corner of the image the integrated density value for every other square was taken, so 16 squares making up ¼ of the image were included. Any square which contained no tissue above threshold was excluded from analysis. The average of all squares was taken per image, and the average per animal for each region was used for statistical analysis.

A macro was used to apply the grid to the image, apply the threshold and collect integrated density information from the designated areas. Macro codes are included in Appendix IX.

2.7.5 Histological analysis of scar tissue in the rat

Spinal cord tissue was stained with Masson's trichrome to identify collagen, and with Alcian blue to distinguish proteoglycans. Images of the entire tissue section were acquired using the VS120 digital slide scanner in brightfield mode. The tissue was divided into three zones for analysis: lesion, scar zone and tissue far from the lesion which appeared intact (see Figure 2.4). A 4x image for each zone was exported from OlyVIA to Fiji and saved as a tiff for analysis. These images were approximately 1mm in width, with a gap of 1mm between scar zone and tissue far from the scar zone**.** The stereology point-counting method was used to determine the volume fraction (Vv) of collagen or proteoglycans in relation to total tissue. A grid was applied within the Fiji program, with each square having an area of 13683 pixels^2). Vv was then calculated as ((points on collagen or proteoglycan)/ (points on total tissue)).

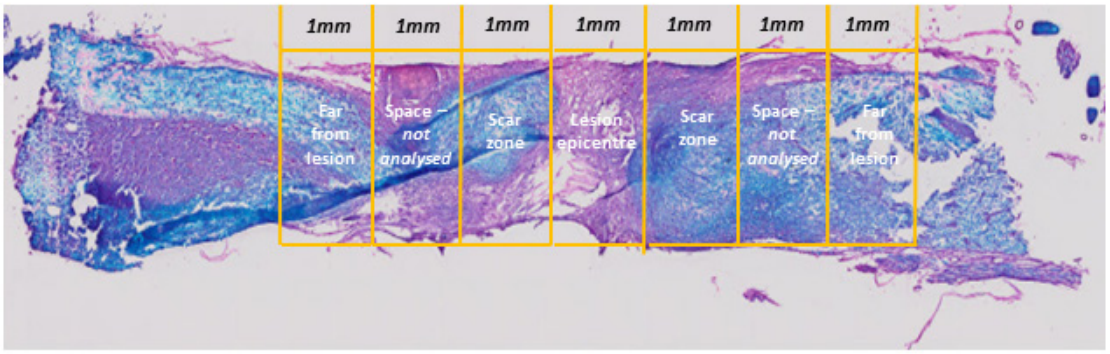

Figure 2.4 Definition of regions of interest for histological study of collagen and proteoglycan deposition.

2.7.6 Analysis of microglia / macrophage phenotype in the rat

Images were stained with three antibodies so that a 4-channel image was obtained. Images were acquired using the VS120 digital slide scanner at 20x magnification. Modification of brightness and contrast settings were made in OlyVIA before exporting to Fiji for analysis. This was necessary as a default auto-contrast setting is applied on acquisition, and brightness must be uniform on all images for accurate pixel based quantification. Before exporting both red and green channels were set to have a minimum value of 0 and a maximum value of 4000. Red and green channels were exported in one image (iNOS and Arginase-1 markers respectively) while the CD11b and Hoechst markers were exported in separate images. No quantification was performed on CD11b or Hoechst markers.

For image analysis the tissue was divided up into ROIs based on some general observations from the Masson's trichrome stained images, regarding the extension and structure of scar tissue. The scar

could be divided into three regions based on the tissue composition, see Figure 2.5. A 'cap' of fibrous tissue was seen sealing the lesion site, this was quite high in collagen and fibres were quite ordered in nature. Zone A was largely made up of this type of tissue. Beyond this the tissue was highly cellular – the cell density appeared higher than in healthy spinal cord tissue. This is seen in Zone B. In Zone C tissue was beginning to return to the normal structure but was somewhat disrupted by small cavities. Inflammatory cell phenotype was analysed for each of these three scar zones, as well as the lesion epicentre.

Three to four 10x images were exported to Fiji and saved as tiffs for analysis of the lesion epicentre. One to two 10x images were saved for analysis of each of the three scar zones. 10x images corresponded to areas approximately 450 x 650 µm.

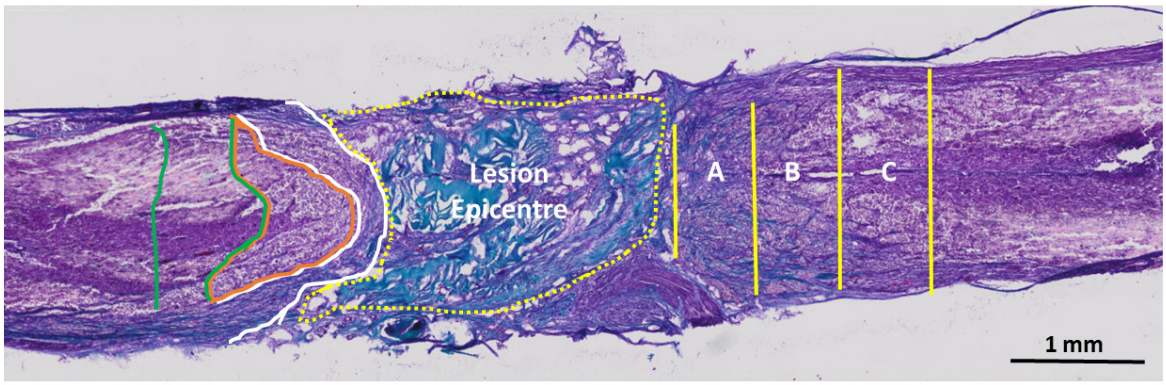

Figure 2.5 ROIs for microglial phenotype analysis. Region A is fibrous in structure and high in collagen, white outline, Region B is densely populated with a variety of cells, orange outline and Region C is less densely cellular with some cyst formation, green outline.

The ratio of iNOS expressing cells (red) to Arginase-1 expressing cells (green) was quantified using the thresholding function in Fiji, details in Table 2.6. Brightness threshold was set individually for each image to eliminate background and non-specific fluorescence. Hue threshold was used to distinguish between cells which were iNOS positive only, Arginase-1 positive only or positive for both markers, termed 'transitional'. The area of each was measured using the Analyse Particles function, having set calibration in µm before beginning. For each phenotype, the area was expressed as a percentage of the total area of positive staining for either marker, i.e. within the entire range of hue values.

	Total	**iNOS (Red)**	**Transitional (Yellow)**	**Arginase-1 (Green)**
Hue	0, 250	0,30	31, 49	50,80
Saturation	0, 250	0, 250	0, 250	0, 250
Brightness	x, 250	58, 250	58, 250	58, 250

Table 2.6 Threshold values used for analysis of inflammatory cell phenotype.

2.8 *N*-glycan analysis of the rat spinal cord

N-glycan analysis was carried out in the Glycoscience group at the National Institute for Bioprocessing Research and Training, Dublin. A schematic illustrating the workflow for spinal cord *N*-glycome analysis of the intact and injured spinal cord is shown in Figure 2.6. Reagents and consumables for this work are shown in Appendix VII. Recipes for buffers etc. are in Appendix VIII.

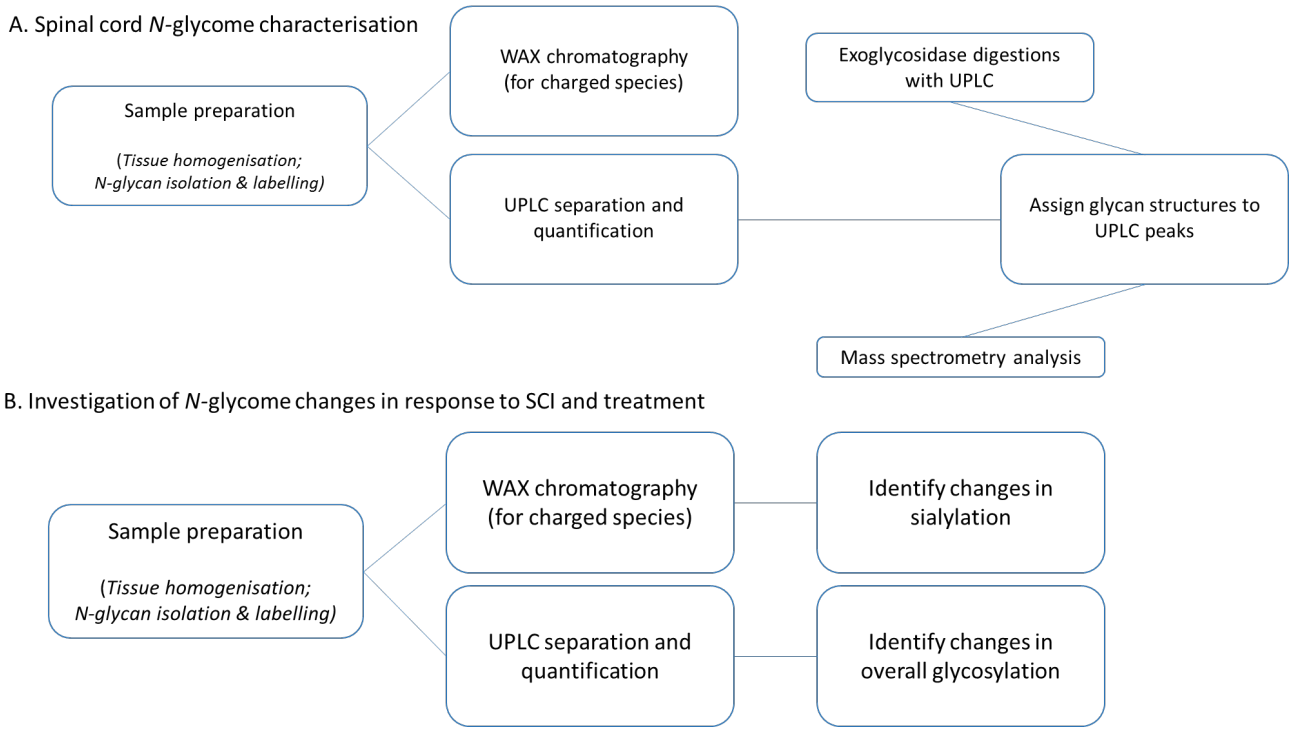

Figure 2.6 Workflow for *N*-glycosylation studies. (A) characterisation of the normal N-glycome of the healthy adult rat spinal cord (B) investigation into changes in N-glycosylation following SCI. UPLC, ultra-performance liquid chromatography, WAX, weak anion exchange.

2.8.1 Sample preparation

2.8.1.1 Tissue homogenisation

Frozen tissue was allowed to defrost on ice. It was weighed before being homogenised using mechanical and chemical disruption: tissue was placed in a round bottom 2 ml microtube tube with 500 µl of homogenisation buffer (Appenix VII, VIII) before placing in the Qiagen Tissue Lyser II with one bead at a speed of 40/s. Disruption of uninjured tissue was complete within 8 minutes, while transected spinal cords needed up to 24 minutes to be completely disrupted. The homogenate was centrifuged at a speed of 13,400 rpm for 20 minutes at 4^{o}C. Supernatant was collected and stored at -80^{o}C.

2.8.1.2 N-*glycan release, isolation and labelling*

Spinal cord homogenate was dried completely in a vacuum centrifuge before being redissolved and an acrylamide gel (Appendix VII, VIII) formed around it using Protogel (National Diagnostics, UK), tetramethylethylenediamine (TEMED) (Sigma Aldrich, Ireland) and ammonium peroxisulphate (Sigma Aldrich, Ireland). The gel was removed from the tube, chopped into approx. 1mm^3 pieces using a scalpel and placed in individual wells of a 96-well glass fibre filter plate with 1 µm pore size (Pall Life Sciences, UK). Gels were then reduced and alkylated: 200 µl of 50mM dithiothreitol (DTT, Sigma Aldrich, Ireland) was added to each well and incubated for 15 minutes at 65^{o}C, followed by 200µl 100mM iodoacetamide (IAA, Sigma Aldrich, Ireland) to give a final concentration of 10mM and incubated for 30 minutes at room temperature in the dark. Gels were then washed, with alternating acetonitrile and 20mM $NaHCO_3$, pH 7.0, before incubating in 1:400 solution of PNGaseF (New England Biolabs, through Brennan and Co., Ireland) in 20mM $NaHCO_3$ overnight at 37^{o}C to release *N*-linked glycans. Released glycans were collected by washing with both water and acetonitrile followed by vacuuming through the filter plate to a collection block underneath. The resulting glycan solution was dried completely in a vacuum centrifuge.

Released glycans were labelled with 2AB (2-aminobenzamide): glycans were first converted to their free reducing form by incubation in 1% formic acid (Sigma Aldrich, Ireland) and were then incubated in 2AB labelling solution (Appendix VIII) for 2 hours at 65^{o}C. The labelling solution was a mixture of 2AB dissolved in acetic acid (Sigma Aldrich, Ireland), sodium cyanoborohydride (Sigma Aldrich, Ireland) and DMSO (dimethyl sulfoxide) (Sigma Aldrich, Ireland). Excess label was removed by applying glycan labelling solution to chromatography paper and subjecting to a series of acetonitrile washes. Clean labelled glycans were eluted in water before being dried completely in a vacuum centrifuge.

2.8.2 Weak anion exchange high performance liquid chromatography (WAX-HPLC)

WAX-HPLC was performed on a Waters Acquity UPLC separations module with Waters DEAE anion exchange column, 75 x 7.5 mm internal diameter, 10 µm particle size (Waters, Ireland). Solvent A was 20% acetonitrile, solvent B was 0.1 M ammonium acetate buffer pH 7.0 in 20% v/v acetonitrile. The starting gradient was 100% A, changing to 100% B at 40 minutes and returning to 100% A at 43 minutes. Total run time was 50 minutes per sample, and the flow rate was 0.75 ml per minute. The column was kept at room temperature. Fetuin-*N* in aqueous solution was included as a control. Fetuin-*N* is a commonly used standard for WAX-HPLC analysis of biological samples as it is highly sialylated and has been well characterised. Samples were prepared as above, dried down and resuspended in 50 µl ultra-pure water, for a completely aqueous solution. 49 µl of sample was injected.

2.8.3 ***Exoglycosidase digestions***

Dry glycan samples were diluted in buffer and enzyme solutions as shown in Table 2.7. Solutions were vortexed and briefly centrifuged before being incubated overnight at 37^{o}C. Enzymes were inactivated by heating to 65^{o}C for 15 minutes. Digested sugars were then filtered through 10 kDa molecular weight cut off microcentrifuge filtration devices (Pall Life Sciences, UK) by centrifugation at 13,000 rpm. Digests were dried completely in a vacuum centrifuge.

Enzyme	Full name	Specificity	Supplier	Cat No.	Volume
ABS	*Arthrobacter ureafaciens* sialidase	α(2-3, -6, -8) linked sialic acid	NEB	P0722	1 µl
NAN-1	Recombinant sialidase	α(2-3) linked sialic acid	NEB	P0734	1 µl
BTG	Bovine testes β-galactosidase	β(1-3, -4) linked galactose	Prozyme	GKX-5013	2 µl
SPG	*Streptococcus pneumoniae* β-galactosidase	β(1-4) linked galactose	Prozyme	GKX-5014	2 µl
CBG	Coffee bean α-galactosidase	α(1-3, -4) linked galactose	Prozyme	GKX-5007	2.5 µl
AMF	Almond meal α-fucosidase	α(1-3) linked fucose (outer arm fucose)	NEB	P0769	1 µl
BKF	Bovine kidney α-fucosidase	α(1-6) linked fucose (core fucose), some α(1-2) outer arm fucose	NEB	P0749	1 µl
GUH	*Streptococcus pneumonia* hexosamindase	β-linked GlcNAc	Prozyme	GK800050	1 µl
JBH	Jack bean β-N-acetylhexoaminidase	β-linked GlcNAc and GalNAc residues	Prozyme	GKX-5003	2 µl
JBM	Jack bean mannosidase	α(1-2, -6, -3) linked mannose	NEB	P0768	2 µl

Table 2.7 Details of exoglycosidase enzymes. Digestions were performed in a total of 10 µl and in the presence of 0.05M sodium acetate buffer (1 µl). Digestion with JBM was performed independently, in the presence of zinc, following an ABS+BTG+BKF+GUH digestion on the previous day. NEB, New England Biolabs.

2.8.4 Hydrophilic interaction liquid chromatography-ultra-performance liquid chromatography (HILIC-UPLC) separation and quantification of released, labelled N-glycans

HILIC-UPLC was performed on a Waters Acquity H-class system with an Acquity UPLC Glycan BEH amide column, 1.7 µm particle size, 2.1mm x 150mm internal diameter. Solvent A was 50mM ammounium formate, solvent B was 100% acetonitrile. The starting gradient was 30% A, 70% B, changing briefly to 70% A, 30% B at towards the end of the 30 minute run. The starting flow rate was 0.561 ml/min but was briefly reduced to 0.3 ml/min while the aqueous solvent was dominant, details in Table 2.8. Column temperature was maintained at 40^{o}C throughout. Two controls were included on every run: a water blank and a dextran calibration ladder (Waters, Ireland) as a standard, diluted to give a 30% aqueous, 70% organic solution. All samples were also diluted to give a 30% aqueous, 70% organic solution with a 19 µl injection volume. A Waters Acquity UPLC fluorescence detector, with excitation wavelength 350 nm and emission wavelength 397 nm, was used to quantitatively detect fluorescently labelled glycans.

Time (mins)	% A	% B	Flow rate (ml/min)
0.00	30	70	0.561
24.81	47	53	0.561
25.50	70	30	0.561
26.25	70	30	0.3
26.55	30	70	0.3
28.50	30	70	0.4
30.00	30	70	0.561

Table 2.8 Solvent gradients and solvent flow rate over each 30 minute HILIC-UPLC run. Solvent A, 50 mM ammonium formate pH 4.4, Solvent B, 100% acetonitrile.

2.8.5 Integration, assignments and analysis of UPLC data

Using Empower 3 chromatography software, all peaks were integrated and assigned GU (glucose unit) values based on the dextran ladder used as an internal standard. Dextran is a glucose homopolymer consisting of chains of glucose of variable length, up to 150,000 units. The GU unit replaced the retention time in the labelling of the peak. This accounts for any changes in retention time due to column life, slight inconsistencies in buffers, etc, and so allows for clearer comparison between chromatograms.

2.8.6 Liquid chromatography coupled mass spectrometry (LC-MS)

2.8.6.1 Sample preparation

N-glycans were released and labelled as in Section 2.8.1. Further clean up of excess label was required prior to the LC-MS experiment. PhyTips (PhyNexus, California, USA) were used for clean-up. These are pipette tips loaded with 10µl of normal phase-1 resin. The hydrophilic glycan sample binds tightly to the resin while the non-hydrophilic 2-AB label is washed off in organic solvent. 'Clean' glycans can then be eluted out of the resin in aqueous solvent.

Dry sample was resuspended in 95 µl water, and 900 µl acetonitrile was added. This sample solution was loaded by repeated aspiration and expiration onto the PhyTips which had been primed with both aqueous and organic washes. Excess 2AB label was removed by repeated aspiration and expiration of 1 ml batches of acetonitrile. Glycans were eluted by aspiration and expiration with 20% acetonitrile in water. Samples were dried completely and stored at -80^{o}C until LC-MS analysis.

2.8.6.2 LC-MS analysis

LC-MS was performed using a Waters Xevo G2 QToF spectrometer coupled to a Waters Acquity UPLC system for pre-separation. MassLynx software was used for both instrument control and subsequent analysis. Spinal cord glycan samples were resuspended in 3 µl water and 9 µl acetonitrile for LC-MS analysis for an 8 µl injection onto the column.

Sample infusion rate was 5 µl per minute and samples were ionised by electrospray ionisation. The experiment was run in negative and sensitivity modes for optimal detection of 2AB-labelled glycans. Leucine enkephalin (Waters, Ireland) was used as the reference compound and was sampled at regular intervals during sample acquisition for 'lock mass correction', i.e. to account for any drift during the run. The UPLC system here was run under similar conditions to the UPLC used for exoglycosidase experiments and profiling of SCI experimental samples. The column chemistry was the same (Waters Acquity UPLC BEH amide 1.7 µm), but a lower flow rate and slightly different solvent gradients were used to achieve appropriate flow rate into the mass spectrometer, Table 2.9. The fluorescent trace obtained from this system was comparable to that obtained for the undigested sample run on HILIC-UPLC, and so individual peaks could be related to the corresponding peak from the HILIC-UPLC run.

Time (mins)	% A	% B	Flow rate (ml/min)
0.00	28	72	0.15
31.00	43	57	0.15
32.00	45	55	0.15
36.00	28	72	0.15
40.00	30	70	0.15

Table 2.9 Details of solvent gradients and solvent flow rate over each 30 minute run on LC-MS. Solvent A, 50 mM ammonium formate pH 4.4; solvent B, 100% acetonitrile

2.8.7 DMB assay

Chemical analysis of sialic acid subtype was performed using the LudgerTag™ DMB sialic acid release and labelling kit (Ludger, UK). Spinal cord homogenate (Section 2.8.1.1) was incubated for 1 hour in 0.1M HCl at 80°C to release sialic acids by hydrolysis. The labelling reagent was prepared according to kit instructions, added to hydrolysed sample and standards and incubated for 3 hours at 50°C in darkness. The reaction was terminated by addition of water. Sialic acid subtypes were analysed by HILIC-UPLC using a Waters Acquity UPLC system with fluorescent detection and a LudgerSep UR2 HPLC column. Solvent A was acetonitrile:methanol:water 9:7:84 (v/v), solvent B was 100% acetonitrile. Flow and gradient details are given in Table 2.10. Column temperature was maintained at 30°C. Identity analysis of the sialic aicd subtypes was performed by comparing retention times of peaks in spinal cord sample to the retention times of the reference standards.

Time (min)	Flow (mL/min)	%A	%B
0.0	0.25	100	0
7.0	0.25	100	0
7.5	0.25	10	90
8.0	0.25	10	90
8.5	0.25	100	0
15.0	0.25	100	0

Table 2.10 Solvent gradients and flow rate for DMB analysis. Solvent A, acetonitrile:methanol:water 9:7:84 (v/v); solvent B, acetonitrile.

2.9 Statistical analysis

All immunohistochemical and histological results were analysed using GraphPad Prism software version 5.0 (Prism 7, USA). All the results were presented as mean ± standard error of the mean (SEM).

The timeline of repair and GAP43 expression was analysed by one-way analysis of variance (ANOVA) followed by Tukey's post-hoc test, with a probability value (p) < 0.05 considered statistically significant.

Astrocyte and lectin experiments in *Xenopus laevis* were analysed by two-way ANOVA followed by Bonferroni's post-hoc test, with $p<0.05$ considered statistically significant. These were analysed two ways:

1. with time-point as the row factor and developmental stage as the column factor
2. with developmental stage as the row factor and time-point as the column factor

Both of these results were taken into account.

Alcian blue and Masson's trichrome staining were analysed by two-way ANOVA, followed by Bonferroni's post-hoc test. $p<0.05$ was considered statistically significant.

Microglia / macrophage phenotype results were analysed by two-way ANOVA, followed by Bonferroni's post-hoc test. $p<0.05$ was considered statistically significant.

N-glycan results were analysed in Minitab 17 using the general linear model analysis of variance, and Tukey's multiple comparisons test with $p<0.05$ considered statistically significant.

3 Chapter 3 - The cellular response to spinal cord transection in regenerative and non-regenerative stages of *Xenopus laevis*

3.1 Introduction

It has been established that the level of repair after SCI in *Xenopus laevis* depends on the developmental stage, with pre-metamorphic tadpoles exhibiting full structural and functional repair and post-metamorphic froglets unable to regenerate at all (Sims, 1962; Beattie *et al.*, 1990; Lee-Liu *et al.*, 2014). Reconnection between the two injured edges of the spinal cord has been reported to occur anywhere between 7 and 20 dpi in *Xenopus laevis* (Sims, 1962; Beattie *et al.*, 1990; Lee-Liu *et al.*, 2014; Munoz *et al.*, 2015). There are a variety of surgical procedures used to model SCI in *Xenopus laevis*, including isolated transection of the spinal cord or amputation of the entire tail, and this together with the variety of developmental stages SCI has been studied at are likely reasons for this wide window in the observed time for the spinal cord to repair.

Following injury to the spinal cord it has been observed that repair occurs due to proliferation of the ependymal layer and migration of these ependymal layer cells to the lesion epicentre (Michel and Reier, 1979; Gaete *et al.*, 2012; Munoz *et al.*, 2015). This cell proliferation and migration is accompanied by outgrowth from the cut axons of the white matter (Sims, 1962; Michel and Reier, 1979; Gibbs and Szaro, 2006; Lee-Liu *et al.*, 2014). While the cut axons have an overall forward oriented growth which can be observed as early as 3 dpi, some evidence of retraction has been observed (Sims, 1962). It has also been suggested that axonal growth from the cut white matter is supported and guided by channels or processes formed from the cells that have migrated into the lesion epicentre (Michel and Reier, 1979) or from aligned fibrous matrix elements (Munoz *et al.*, 2015). The proliferative ependymal cells have been identified as expressing Sox2/3 and this, together with their location and their nuclear morphology has suggested that they are a population of neural progenitors (Gaete *et al.*, 2012; Munoz *et al.*, 2015). These cells have been reported to become highly proliferative in a rapid and transient manner (Gaete *et al.*, 2012; Munoz *et al.*, 2015) migrating into the lesion centre where they form organised structures and possibly differentiate into neurons, thus replacing some of the cells lost to the injury (Munoz *et al.*, 2015). Morpholino knockdown has shown that it is Sox2/3 and not some other characteristic of these cells which is important for this response and for regeneration (Munoz *et al.*, 2015). In the post-metamorphic froglet these cells are much fewer and more dispersed and do not undergo the same proliferative response following injury (Munoz *et al.*, 2015) reinforcing their importance in the regenerative process.

There has been no study of the astrocytic response to SCI either in transection or in tail amputation models in *Xenopus laevis*. However, it appears that in either pre- or post-metamorphic uninjured animals the glia are different from those seen in mammalian systems. Glia have been studied using a range of known markers of either astrocytes or radial glia in *Xenopus laevis* and almost all markers examined stain in a radial pattern (Maier and Miller, 1995; Edwards-Faret *et al.*, 2018). GFAP, the most commonly used astrocyte marker in mammalian tissue, is only expressed in white matter areas of radially arranged cells, close to the pial surface. There was no cell body immunoreactivity observed (Maier and Miller, 1995) which is the same as what was observed here. The strongest cell body labelling and greatest distribution throughout all the grey and white matter of the spinal cord was seen with glutamine synthase, however even these cells did not exhibit the characteristic morphology of mammalian astrocytes (Edwards-Faret *et al.*, 2018). Despite these differences a glial reaction to injury has still been observed following injury to the optic nerve which is somewhat reminiscent of the mammalian astrocytic response to injury. Cells identified as astrocytes have been observed to become hypertrophic and to phagocytose myelin debris (Reier and Webster, 1974; Reier, 1979; Rungger-Brandle *et al.*, 1995). These cells cluster together at the degenerating distal end of the cut or crushed nerve (Reier and Webster, 1974; Rungger-Brandle *et al.*, 1995) in a manner which could be considered similar to the accumulation seen around the edges of an SCI. A difference in response was observed between the tadpole and froglet stages: in tadpoles these glia were seen to extend their processes along the length of the optic nerve, apparently guiding regrowing axons across the injury (Reier and Webster, 1974) while a substantial glial scar composed of hypertrophic phagocytic astrocytes was formed in the optic nerve following removal of the eye in adult *Xenopus laevis.* These scar-forming astrocytes did not impede axonal regrowth when transplanted into a transected tadpole optic nerve (Reier, 1979). It is unclear whether this is due to a lack of inhibitory factors associated with this particular glial scar, or whether tadpole axons are just resistant to this type of inhibition.

From this we can say that despite the difference in morphology and characteristic markers between glia of *Xenopus laevis* and rat or human that these cells still respond to CNS injury and still have the potential to form scar tissue. Therefore it is important to study their response to SCI in both regenerative and non-regenerative stages.

In this study, we examined the neuronal and astroglial response to SCI in *Xenopus laevis*. The timeline of repair was established following SCI in stage 50 tadpoles induced by an improved surgical procedure developed in our group. The astrocyte response was also compared between regenerative tadpole and non-regenerative froglets to try to understand the cellular basis of regeneration.

3.2 Hypotheses

1. The spinal cord of regenerating tadpole *Xenopus laevis* repairs rapidly following injury and axonal repair is concentrated at particular time-points following injury
2. There is a greater astrocyte response to injury in non-regenerating froglet than in regenerating tadpole

3.3 Objectives

1. Establish the time-line of repair following injury in tadpole *Xenopus laevis*
2. Compare the astrocyte response to injury in tadpole and froglet *Xenopus laevis*

3.4 Experimental design

These experiments aim to establish the neuronal and astrocyte response to spinal cord transection in the regenerative tadpole and the non-regenerative froglet. The first part of this study was a time-course study to establish the timeline of growth activity in the regenerative tadpole, using the surgical procedure developed in our group (Section 2.1.2). This method involved gently opening a minimal region of muscle to expose the spinal cord, which was then loosened from the underlying notochord using a fine forceps, before using a fine needle to transect the cord. This method differs from those described in the literature (Sims, 1962; Gaete *et al.*, 2012; Lee-Liu *et al.*, 2014; Lee-Liu *et al.*, 2018) which use a scissors to cut through skin, muscle and spinal cord in one movement, increasing the risk of damaging more tissue, in particular the notochord.

The second part of the study was a comparative study to understand whether astrocytes may play a role in promoting or supressing repair of the spinal cord.

To investigate the timeline of repair, pre-metamorphic tadpoles were subjected to spinal cord transection or sham injury as described in Section 2.1.2, and kept until the appropriate time-point post injury when they were euthanized and tissue prepared for immunohistochemistry (Section 2.1.4 and 2.1.5). Tissue was stained with the neuronal marker acetylated tubulin and the neuronal growth marker GAP43 as described in Section 2.3.1. Images were acquired using both the Andor Revolution spinning disk confocal (as described in Section 2.7.1) and the Olympus VS120 digital slide scanner (Section 2.7). Slide scanner images were purely for overview and overall visualisation of sections while all analysis was performed using high magnification, high resolution confocal micrographs. Images were analysed in Fiji using the 'analyse particles' function after first thresholding to define positive signal, as described in Section 2.7.2. The proportion of positive GAP43 signal was expressed as a

percentage of total tissue area per image. Details of experimental groups are given in Table 3.1, n=5 tadpoles per group.

Injury	**Timepoint (dpi)**				
Sham	1	3	5	7	10
Transection	1	3	5	7	10

Table 3.1 Details of experimental groups for the study of timeline of repair in the tadpole. n=5 per group.

For comparison of the astrocytic response to injury in tadpoles and froglets days 1 and 7 post injury were chosen based on the results of the tadpole time course study mentioned above. Tadpoles were treated in the same way as described above for the time course study. Froglets were subjected to spinal cord transection or sham injury as described in Section 2.1.3 and tissue was harvested and processed as in Section 2.1.4 and 2.1.5. In order to reduce the amount of tissue and therefore animals required sections were stained using a combined immuno- and lectin-histochemistry protocol as described in Section 2.5. High magnification images were acquired using the Andor Revolution spinning disk confocal (as described in Section 2.7.1). The stereology point-counting method was employed to quantify the area of tissue composed of astrocytes, Section 2.7.3. Details of experimental groups are given in Table 3.2, n=5 tadpoles per group, n=4 froglets per group.

Developmental stage	**Injury**	**Time point (dpi)**	
Tadpole	Sham	1	7
	Transection	1	7
Froglet	Sham	1	7
	Transection	1	7

Table 3.2 Details of experimental groups for the study of astrocyte response to transection in regenerative and non-regenerative stages of *Xenopus laevis*. n=5 tadpoles per group, n=4 froglets per group

3.5 Results

3.5.1 Timeline of regeneration following spinal cord transection in stage 50 tadpole

The duration of time required for complete repair following SCI induced with the new surgical procedure was studied using immunohistochemistry. Repair was assessed visually using the neuronal marker acetylated tubulin and measured quantitatively using the neuronal growth marker GAP43.

Using the acetylated tubulin neuronal marker an acute repair response was observed as early as 1 dpi with small acetylated tubulin positive projections seen extending into the lesion area from the borders (white arrow in Figure 3.1 E, I). There was also some positive signal observed in the lesion epicentre, in the form of thin rings, however it is not clear whether these were new neurons migrating to the site of injury, or dying cells. At 3, 5 and 7 dpi axons at the borders of the injury continued to project into the lesion site in an ordered directed manner. Tubulin was increased in these regions as evidenced by the stronger fluorescent signal. There was not much change in the amount or appearance of tubulin signal in the lesion epicentre between 1 and 3 dpi, but by 5 dpi extensive neurite outgrowth was observed although this appeared highly unorganised. There were no clear associations between tubulin and Hoechst signals and so it is difficult to interpret the source of these neurites. By 7 dpi a thin tissue bridge had formed linking both sides of the injured spinal cord. This bridge was highly organised with neurites lying parallel to each other and neuronal cell bodies identifiable (yellow arrow in Figure 3.1 L). By 10 dpi (Figure 3.1 O) the normal architecture of the spinal cord had been restored with grey and white matter regions clearly identifiable (compare to the sham image in Figure 3.1 P). Lesion epicentre or lesion borders could no longer be distinguished. When capturing images it was impossible to distinguish the lesion epicentre or lesion borders as ROIs at this stage and so 3 images were taken from the expected region of the injury using the gut as a landmark.

Since the most significant phases of repair were considered to be the initiation of neurite outgrowth, the formation of the tissue bridge and the return to the normal architecture of the spinal cord, occurring at 1, 7 and 10 dpi respectively, further representative images (from different animals) for each of these time-points have been included in Figure 3.2.

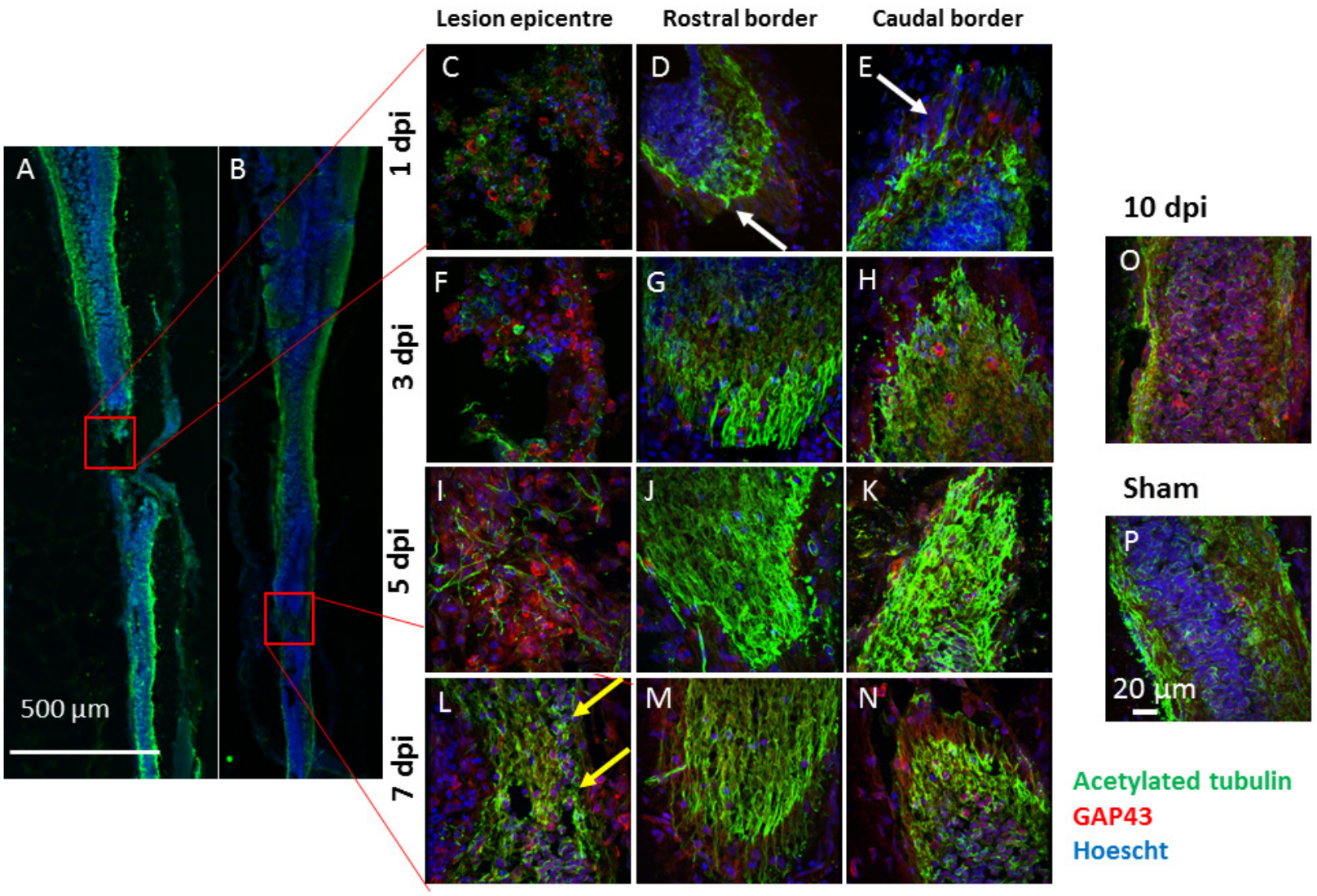
Lesion epicentre
Rostral border
Caudal border
A
B
C
D
E
F
G
H
I
J
K
L
M
N
O
P
1 dpi
3 dpi
5 dpi
7 dpi
10 dpi
Sham
500 µm
20 µm
Acetylated tubulin
GAP43
Hoescht

Figure 3.1 The stages of repair following spinal cord transection in stage 50 tadpole *Xenopus laevis*. (A, B) low magnification slide scanner images of the injured spinal cord of stage 50 *Xenopus laevis*, with the injured region marked with a red box. (A) 1 dpi, (B) 7 dpi. (C –P) confocal images showing acetylated tubulin expression (green), GAP43 (red) and Hoechst stained nuclei (blue) at the lesion site (C, F, I, L), rostral border of lesion site (D, G, J, M), and caudal border of lesion site (E, H, K, N) at 1, 3, 5 and 7 dpi respectively. The injured region at 10 dpi is shown in (O). A representative image of sham tissue is shown in (P). Small acetylated tubulin positive projections extending into lesion area from borders at 1 dpi are indicated with white arrows in (D, E). Cell bodies positively stained for acetylated tubulin are indicated with yellow arrows in (L). Scalebar in (A, B) = 500 µm, in (C-P) = 20 µm.

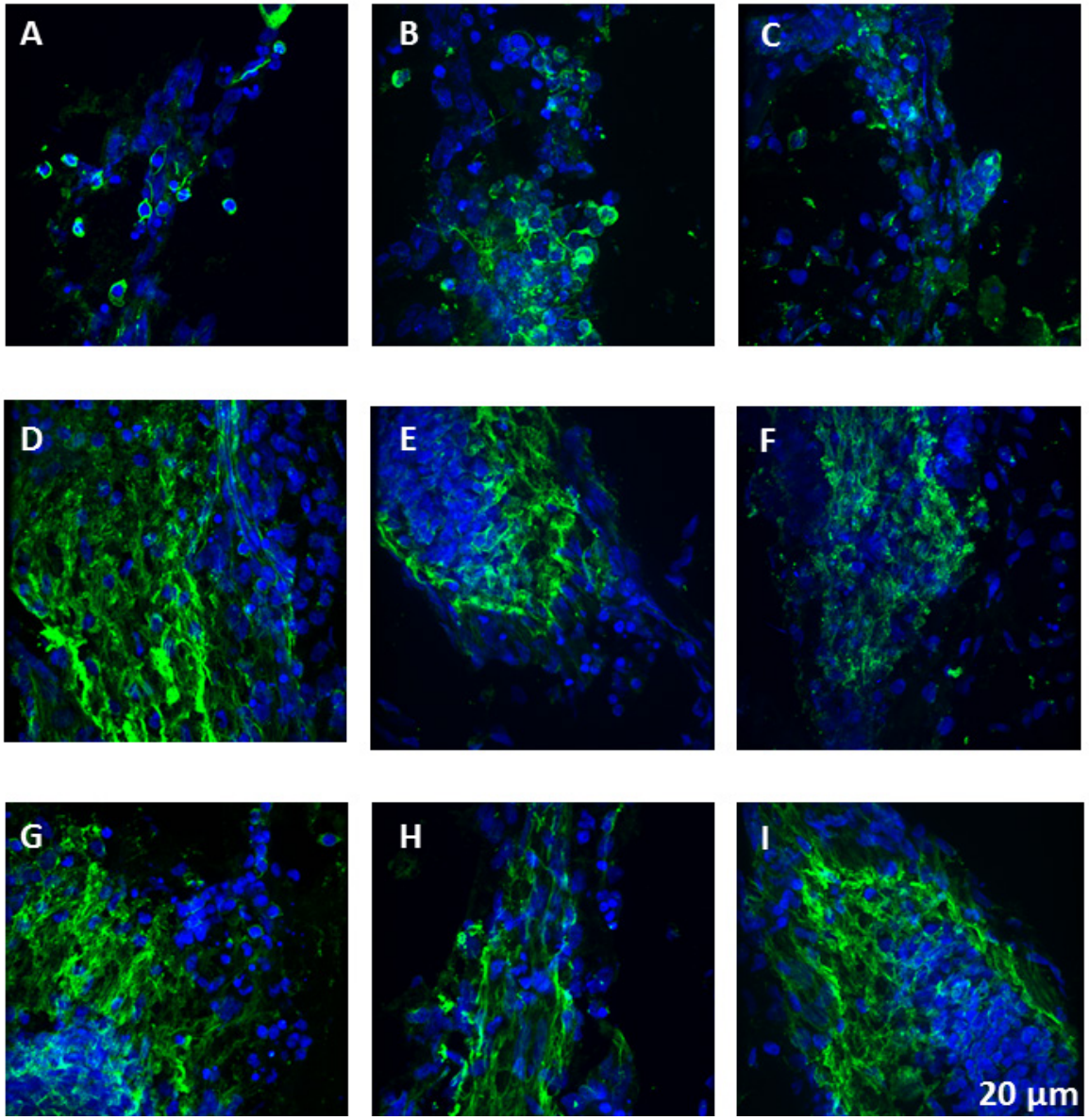

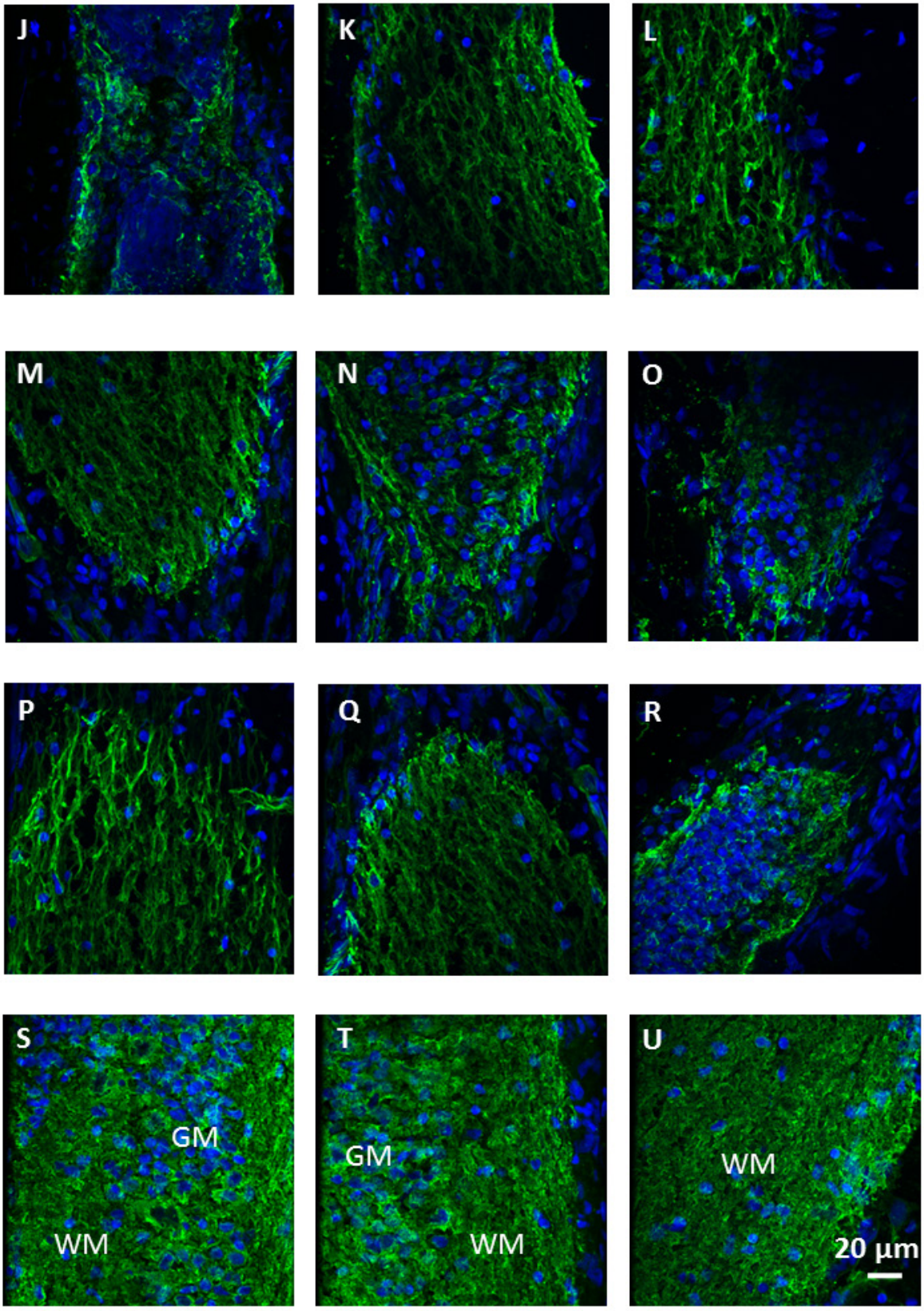
J
K
L
M
N
O
P
Q
R
S
GM
WM
T
GM
WM
U
WM
20 µm

Figure 3.2 Additional representative images of the neurongal repair response to spinal cord transection in tadpole *Xenopus laevis*. Images A-C show the disrupted tissue of the lesion epicentre at 1 dpi, and the early neuronal sprouting response at the borders of the injury at 1 dpi are shown in D-F (rostral) and G-I (caudal). At 7 dpi a thin tissue bridge has formed across the epicentre of the injury (images J-L), while axonal extension continued from the edges which had not yet reconnected on both rostral (M-O) and caudal (P-R) sides. By 10 dpi the normal white matter (WM) and grey matter (GM) structure had returned. The images in each row (i.e. A, B and C; J, K and L etc.) were captured from different animals.

Following transection of the spinal cord the ability of the tadpoles to swim in response to a vibration stimulus was significantly reduced and almost completely abolished. By 7 dpi, the stage of tissue bridge formation, tadpoles moved significantly more than at 1 dpi demonstrating that the structural repair allowed for some functional recovery, Figure 3.3.

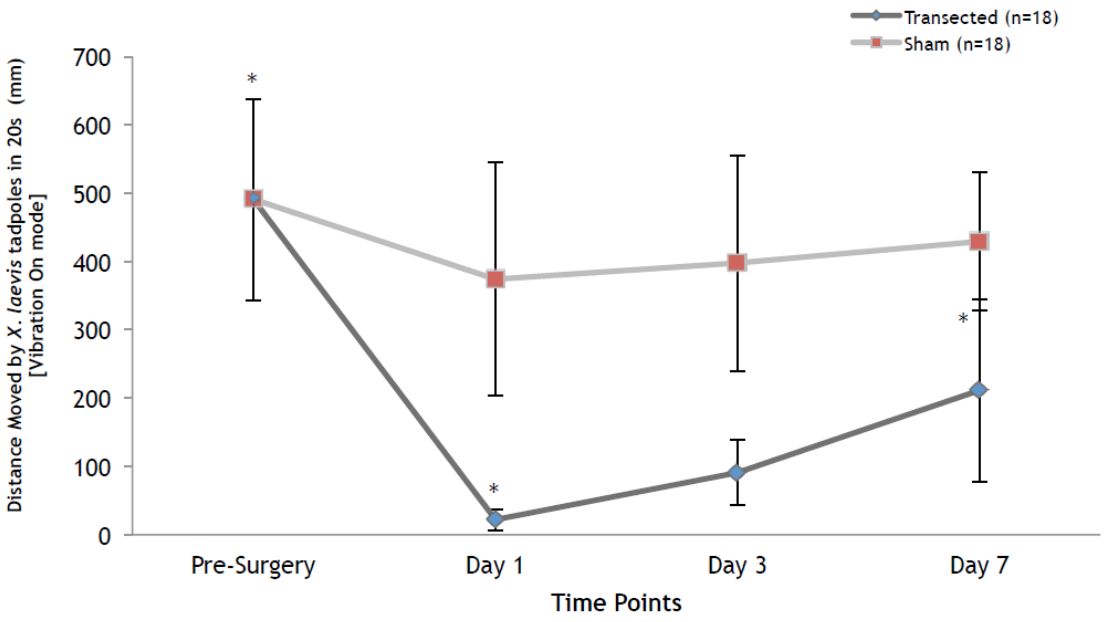

Figure 3.3 Distance moved by tadpoles in response to vibration. Tadpoles were exposed to a vibration stimulus for a total of of 20 seconds per trial. Tadpoles were tested before surgery and at 1, 3 and 7 dpi post spinal cord transection or sham injury (n=18 in each group). Data is shown as mean ± S.D. Asterisks (*) indicate that there are statistically significant differences between transected animals at pre-surgery and those at 1 dpi. Similarly the difference between animals at 1 and 7 dpi are also statistically significant using the paired Kruskal-Wallis test, $p<0.05$. At 1, 3 and 7 dpi there are also significant differences between the sham and the corresponding transected groups according to the Kruskal-Wallis test ($p<0.05$). This data was collected and analysed by Ms Ana Lúcia Rebelo as part of her MSc thesis, using the Daniovision equipment designed for recording the movement of zebrafish, and modified to incorporate a vibration stimulus for tadpoles.

Growth activity was examined using GAP43 and was quantified using Fiji. Results are represented as the percentage of tissue area positive for GAP43 protein. GAP43 expression was measured across five ROIs: the lesion epicentre, the lesion borders (rostral and caudal) and portions of intact tissue far from the lesion (rostral and caudal), see Figure 3.4.

In terms of GAP43 distribution there was minimal colocalisation seen between GAP43 and the neuronal marker at the earlier time-points of 1, 3 and 5 dpi, suggesting that perhaps there are other pathfinding glial cells which are the drivers of growth and that axons follow these. At 7 and 10 dpi however GAP43 signal was much more widespread and there was lots of colocalisation. At 7 dpi in the lesion epicentre there was both neuronal and non-neuronal GAP43 expression (Figure 3.1). In sham injured spinal cord GAP43 was expressed at a similar level as in the transected spinal cord.

The pattern of change in GAP43 expression was reasonably consistent across these ROIs. No differences were observed at individual time-points between ROIs. Within each ROI however some small non-significant changes were observed over time. In most cases GAP43 was present across approximately 50% of the tissue area at 1 dpi, dipped slightly at 3 dpi and then rose gradually to peak at approximately 70% by 7 dpi. GAP43 then fell to approximately 55% by 10 dpi (see Figure 3.4). None of these changes were found to be statistically significant using one way ANOVA with Tukey's post hoc test ($n=4\text{-}6$, $p<0.05$). The expression of GAP43 also changed in sham injured tissue, and followed the same trends as that observed in the transected tissue, being approximately equal at all time-points except at 3 dpi. At this time-point there was significantly less GAP43 expression in the sham tissue than in the transected in all ROIs except the caudal border (Figure 3.4 A-E).

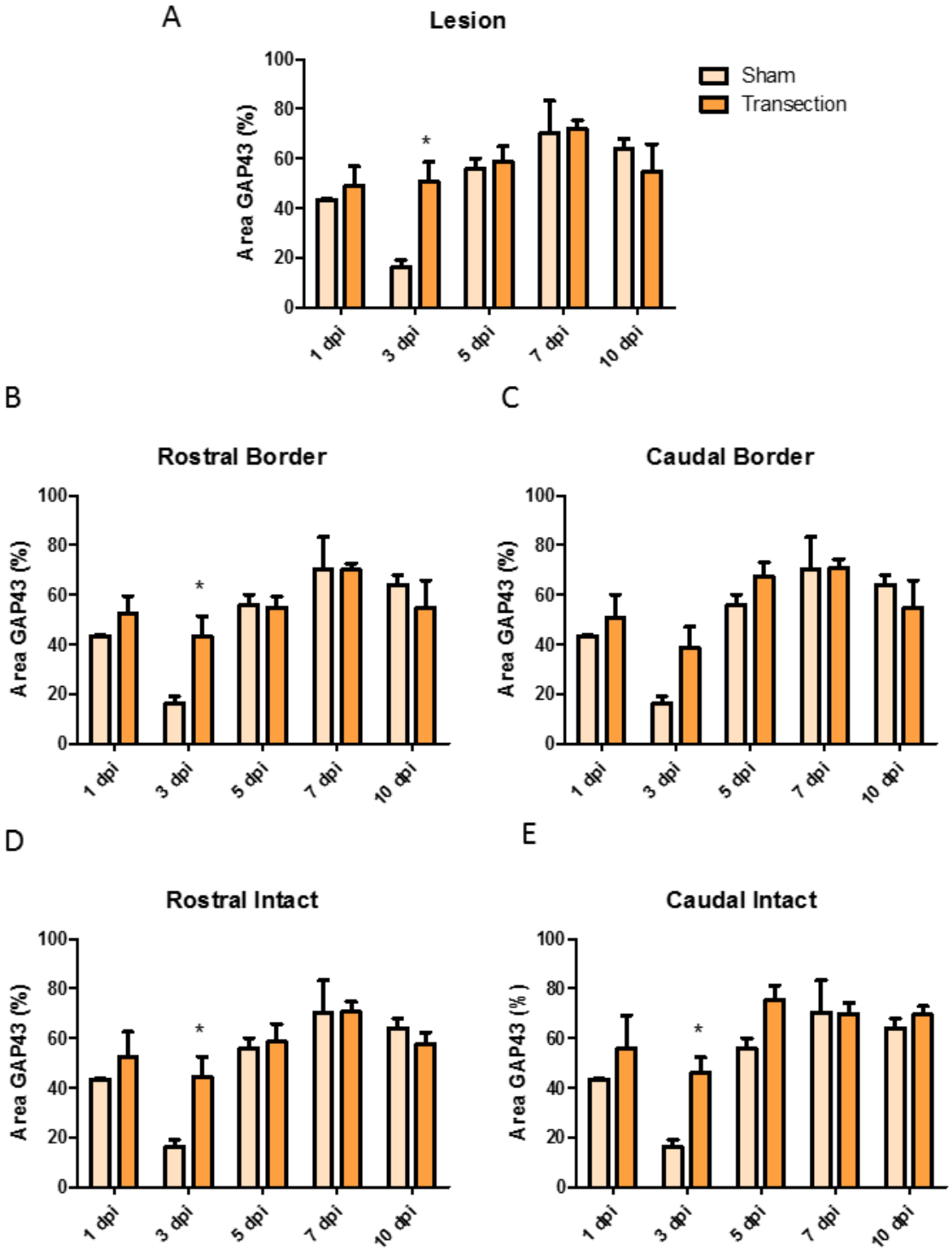
A
Lesion
Sham
Transection
Area GAP43 (%)
100
80
60
40
20
0
*
1 dpi
3 dpi
5 dpi
7 dpi
10 dpi
B
Rostral Border
C
Caudal Border
D
Rostral Intact
E
Caudal Intact

Figure 3.4 Changes in GAP43 expression following transection or sham injury in tadpole *Xenopus laevis*. Graphs show GAP43 immunohistochemical staining expressed as a fraction of total tissue area at the lesion site (A), rostral border (B), caudal border (C), rostral intact tissue (D) and caudal intact tissue (E). Dpi; days post injury. Mean ± SEM. *p ≤ 0.05. Mean differences were analysed using one way ANOVA with Tukey's post hoc test (n=4-6).

3.5.2 Astrocytes increase following spinal cord transection in stage 66 froglet

Immunohistochemical staining for the astrocytic marker GFAP revealed a differential astrocytic response to spinal cord transection between regenerative tadpoles and non-regenerating froglets. Comparing tadpole to froglet at both 1 and 7 dpi there was an increase in the area fraction of the tissue composed of astrocytes in injured froglet spinal cord versus injured tadpole spinal cord after normalising to the relevant sham group (see Figure 3.5). In the rostral intact tissue developmental stage was found to significantly influence variance based on the results of the two way ANOVA test, however Bonferroni's post hoc analysis did not reveal significant differences between groups (Figure 3.5 C). No significant differences were found for the caudal intact ROI (Figure 3.5 D). At both rostral and caudal borders of the injury, the area fraction of positive GFAP signal was significantly higher in froglet than in tadpole at both timepoints (Figure 3.5 A, B). Two-way ANOVA found that developmental stage had a significant influence on the variance and this was confirmed with the Bonferroni post hoc analysis for both ROIs, Figure 3.5.

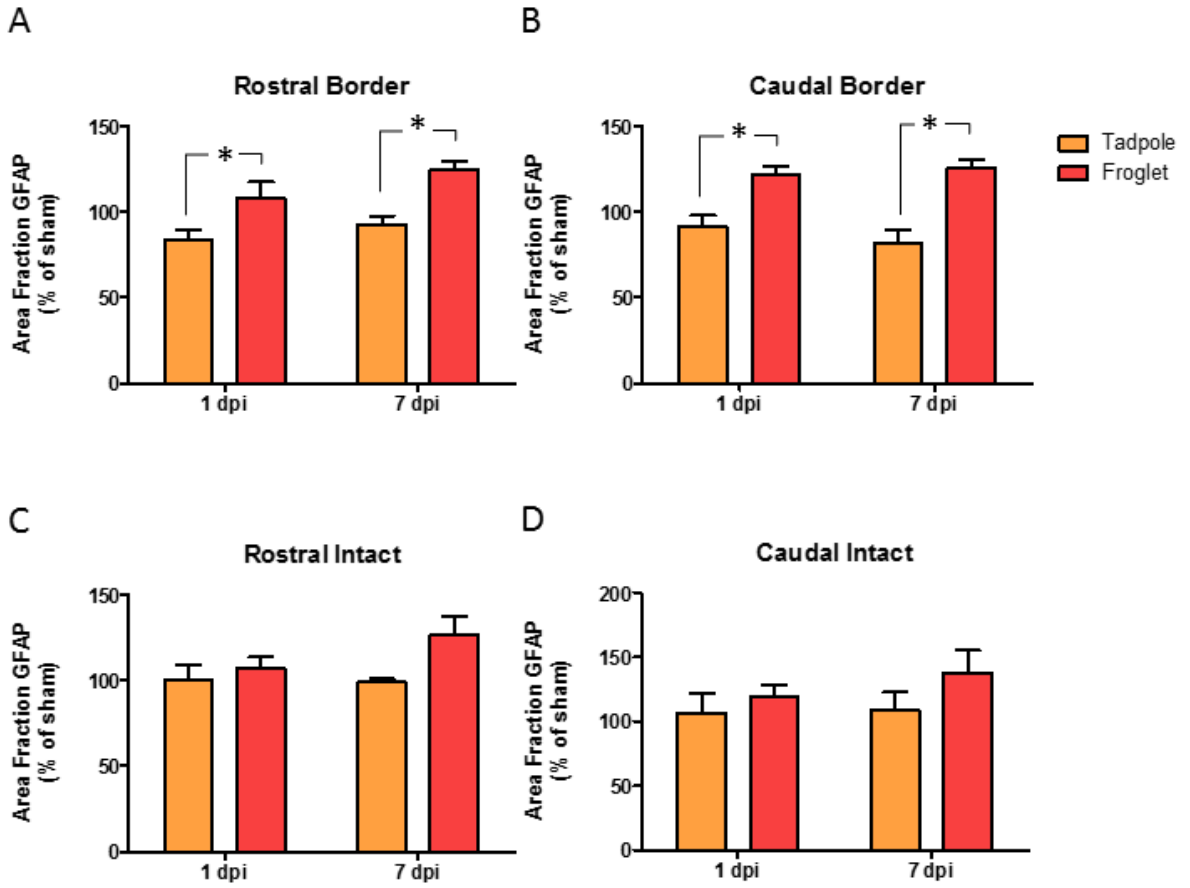

Figure 3.5 Changes in astrocyte composition in the spinal cord following injury in tadpole and froglet at 1 and 7 dpi. Graphs show GFAP immunohistochemical staining expressed as a fraction of total tissue area at the rostral border (A), caudal border (B), rostral intact tissue (C) and caudal intact tissue (D). Mean ± SEM. *$p \leq 0.05$. Mean differences were analysed using two way ANOVA with Bonferroni's post hoc test (n=4-6).

It was only possible to analyse astrocyte area at the lesion epicentre in tadpole spinal cord tissue and not in the lesion site in froglet spinal cord tissue, so no comparison could be made between tadpoles and froglets for this region. At the lesion epicentre in tadpole there was a significant increase in the proportion of tissue composed of astrocytes at 7 dpi as compared to 1 dpi (Figure 3.6). At the lesion borders or in intact tissue the change in astrocyte area over time within developmental stage was minimal and did not reach statistical significance (Figure 3.5).

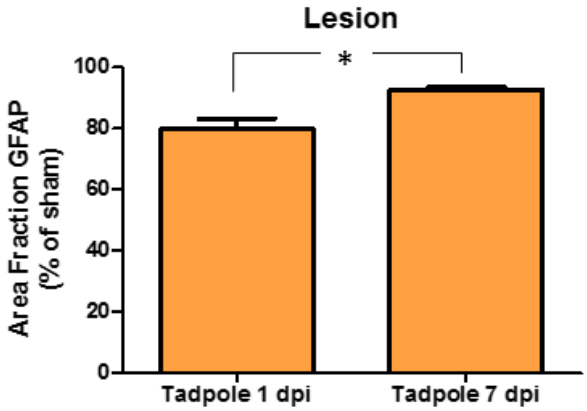

Figure 3.6 Changes in astrocyte composition of the tissue at the lesion epicentre over time in the tadpole. Graph shows GFAP immunohistochemical staining expressed as a fraction of total tissue area at the lesion site. Mean ± SEM. *p ≤ 0.05. Mean differences were analysed using t-test (n=4-6).

A key difference to note is that in tadpoles the amount of astrocytes present decreased following injury in comparison to sham, while in froglets there was an increase at 1 dpi compared to sham. These differences were not found to be statistically significant for either developmental stage at either time-point, using Dunnett's post hoc test to compare all groups to the appropriate sham group, Figure 3.7. Representative images for all groups in tadpole spinal cord are shown in Figure 3.8 and for all groups in froglet spinal cord are shown in Figure 3.9.

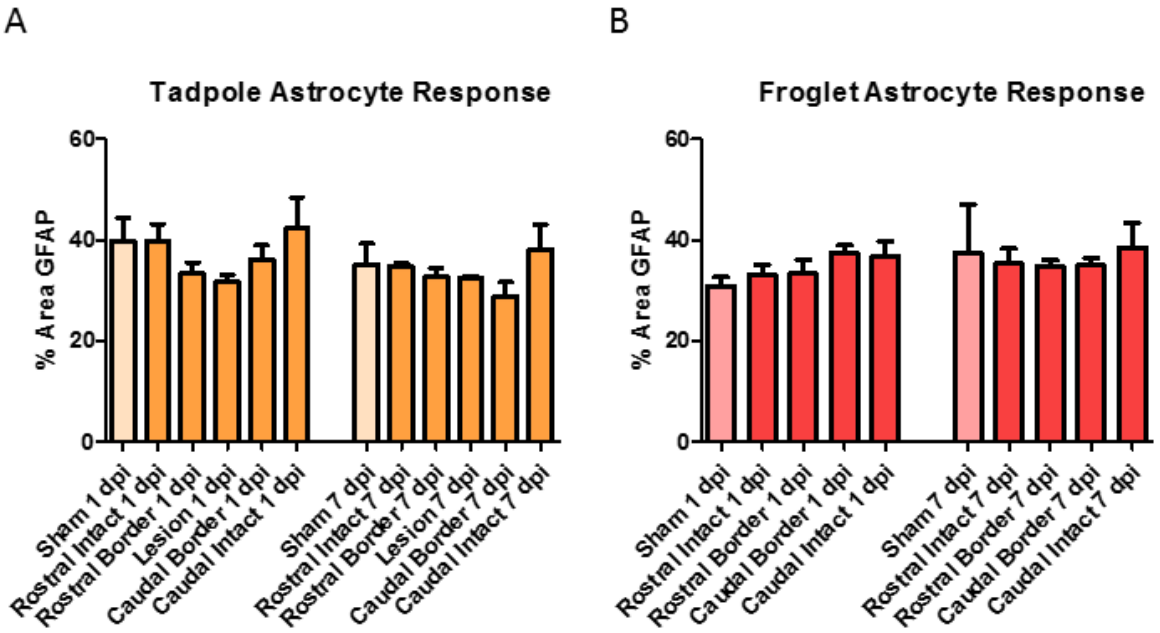

Figure 3.7 A comparison of astrocyte response to injury in tadpole and in froglet across all ROIs. Graphs show GFAP immunohistochemical staining expressed as the percentage area of the total tissue in tadpole (A) and froglet (B). Mean ± SEM. No significant differences, one way ANOVA with Dunnett's post hoc test, $p<0.05$, n=4-5

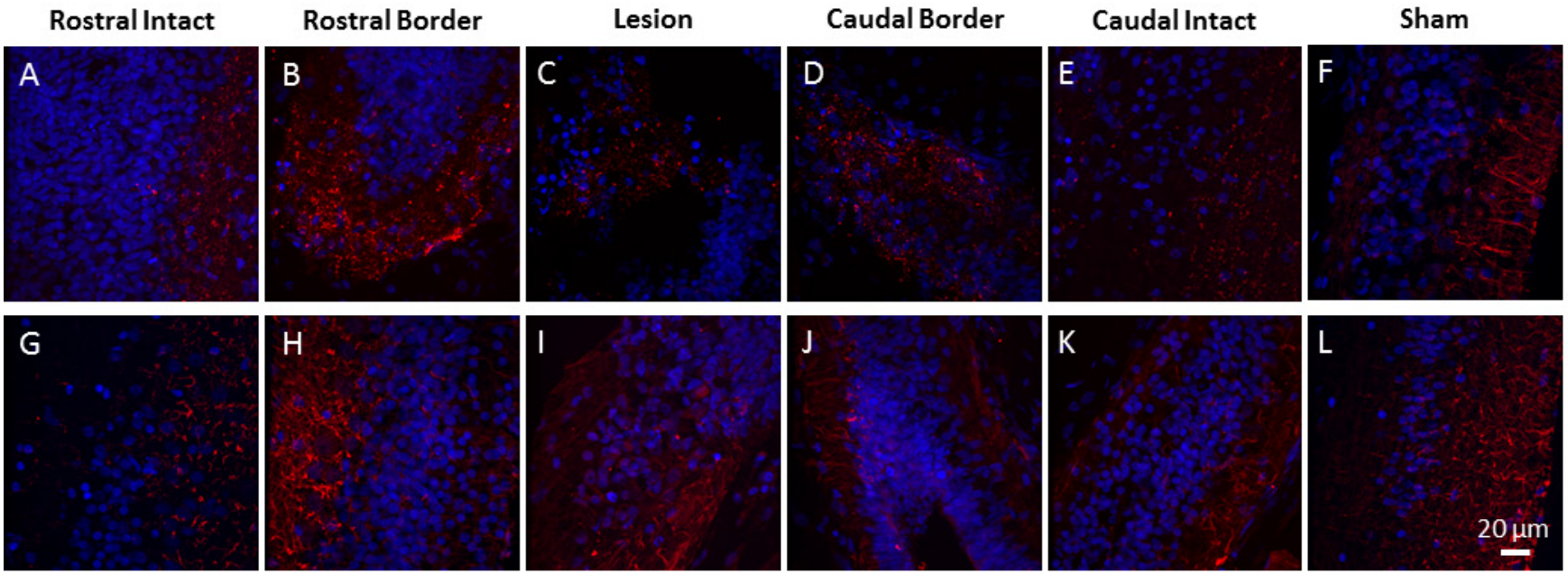

Figure 3.8 Astrocytes in spinal cord tissue visualised with GFAP immunohistochemistry in tadpole *Xenopus laevis*. Confocal images show GFAP (red) and Hoechst stained nuclei (blue) in sham animals (F, L) and in transected animals at the rostral lesion border (B, H), lesion epicentre (C, I) caudal lesion border(D, J), rostral intact tissue (A, G) and caudal intact tissue (E, K) at 1 dpi (A-F) and 7 dpi (G-L). Scalebar = 20µm

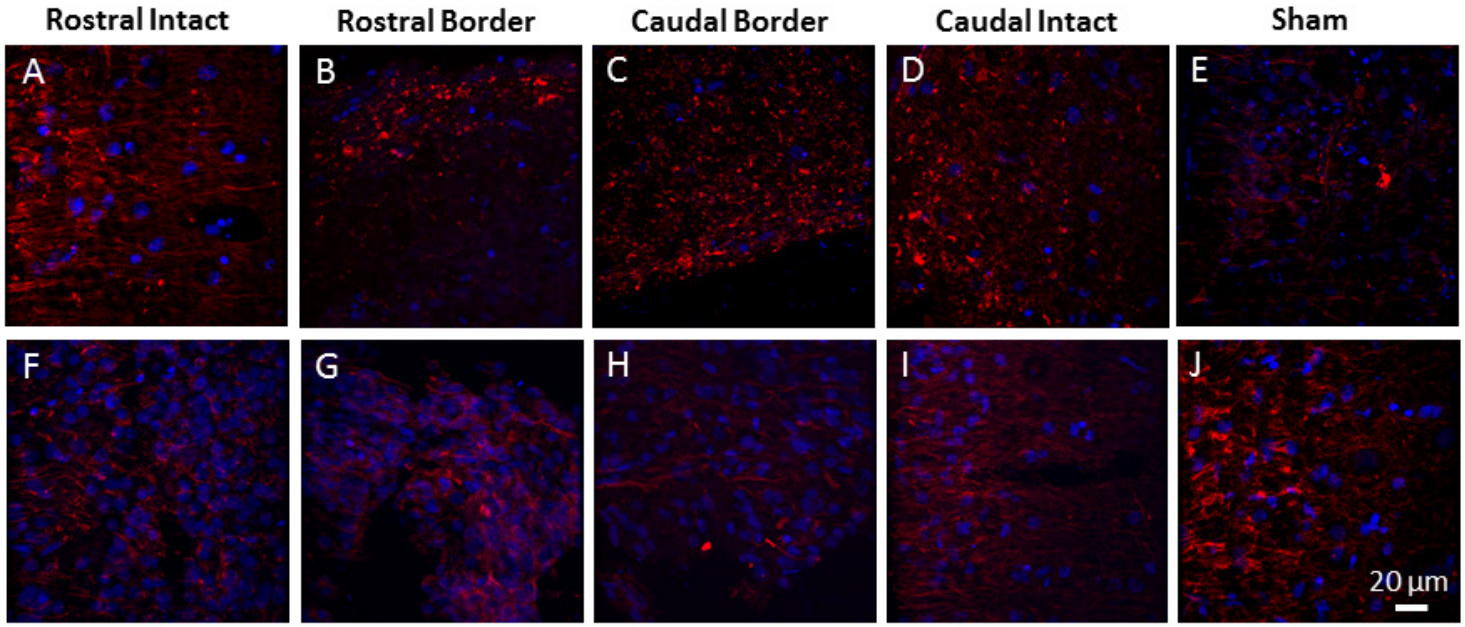

Figure 3.9 Astrocytes in spinal cord tissue visualised with GFAP immunohistochemistry in froglet *Xenopus laevis*. Confocal images show GFAP (red) and Hoechst stained nuclei (blue) in sham animals (E, J) and in transected animals at the rostral lesion border (B, G), caudal lesion border(C, H), rostral intact tissue (A, F) and caudal intact tissue (D, I) at 1 dpi (A-E) and 7 dpi (F-J). Scalebar = 20µm

Another important difference in the response to injury between the two developmental stages is in the morphology of astrocytes. This is most noticeable at the borders of the lesion at 7 dpi. In tadpole, GFAP positive processes did not seem to be arranged in any particular direction, while in froglet the majority of these appeared to be aligned parallel to the cut surface of the spinal cord (see Figure 3.10). Dual staining for GFAP and the neuronal marker acetylated tubulin revealed that, in some cases, the processes of each cell type were closely associated and appeared to form a network in the injured froglet spinal cord (see Figure 3.10).

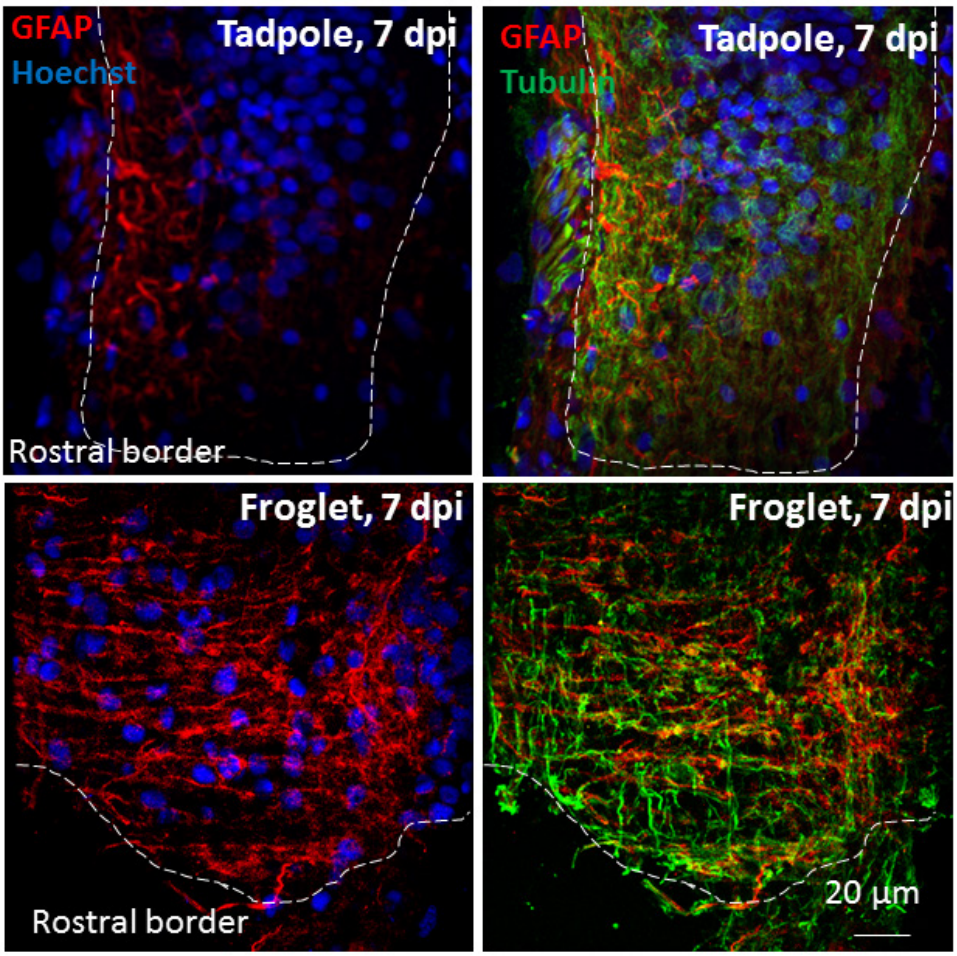

Figure 3.10 Morphology of astrocytes at the lesion border in tadpole and froglet spinal cord. Confocal images showing GFAP expression (red) and Hoechst stained nuclei (blue) in the tadpole and froglet at 7 dpi and acetylated tubulin expression (green) in the froglet at 7 dpi. Astrocyte processes were arranged parallel to the edge of the injury (white dashed line) in froglet while there was no obvious arrangement of GFAP positive astrocyte processes in the tadpole. Neurons were seen in close proximity to these astrocyte processes in the froglet. Images from each developmental stage were from the same section but have different channels displayed. Scalebar = 20µm.

3.6 Discussion

Spinal cord regeneration following the surgical procedure developed in our group compares well with other transection models previously employed in tadpole *Xenopus laevis*. Complete repair was observed far earlier than in other reports. By 10 dpi in our model the lesion site was no longer identifiable, whereas in other studies this level of regeneration has not been reported until 20 - 28 dpi (Gaete *et al.*, 2012; Lee-Liu *et al.*, 2014; Munoz *et al.*, 2015).This would allow for a higher throughput for future research with less time to wait from day of surgery to whichever stage of repair is of interest.

A reconnection or tissue bridge between the two cut ends of the spinal cord was observed at 7 dpi here. This was the same as reported by (Sims, 1962) but earlier than in the model employed by the Larrain group despite their using tadpoles at the same stage as we have (Gaete *et al.*, 2012; Lee-Liu *et al.*, 2014; Munoz *et al.*, 2015). We observed the first evidence of neuronal outgrowth as early as 1 dpi. This is two days earlier than that reported by (Sims, 1962), who also examined spinal cords fixed at the 1 dpi time-point, and 4 days earlier than in the work of (Lee-Liu *et al.*, 2014) who looked at tissue as early as 2 dpi. This difference in timing for each stage of repair may be due to a difference in housing temperature for the tadpoles, as housing at a higher temperature accelerates their development and so it is likely that this would also influence the rate of repair. Sims reports housing tadpoles at 20^{o}C, which is similar to our conditions however the housing temperature was not reported in the study of Lee Liu and colleagues and so this possibility cannot be ruled out. It is just as likely that the rapid repair seen in our work is due to the nature of the surgical procedure we have employed. This procedure limits the damage to surrounding tissues including muscles and eliminates any injury to the notochord, a structure which may potentially be important for the repair of the spinal cord (Chernoff *et al.*, 2003; Taniguchi *et al.*, 2014).

In agreement with the publications discussed above regrowth in this model occurs as a combination of axonal regeneration from the severed axons and migration of cells to the lesion site, some of which at least differentiate into new neurons. Of note, in our model growth efforts appear to be comparable from both rostral and caudal axons with no difference in GAP43 expression between the two sides. Regarding the cells in the lesion gap, it is possible that some of the cells observed have remained there after the injury, and indeed some show signs of being in distress as evidenced by the condensed appearance of the nuclei at 1 and 3 dpi, but by 5 dpi their appearance is healthier and there is plenty of GAP43 expression suggesting that these cells are ready to contribute to the repair effort (Figure 3.1 I). Tubulin positive outgrowths are also visible at this time-point and although they are apparently randomly orientated at this stage, they presumably rapidly align and contribute to the highly ordered tissue bridge observed at 7 dpi (Figure 3.1 L). We could assume that these cells migrate from the

ependymal canal however we cannot be sure unless examined with the Sox2/3 marker used by the Larrain group (Gaete *et al.*, 2012; Munoz *et al.*, 2015).

In this study we have measured the growth activity in the regenerating spinal cord using the marker GAP43. This marker is commonly associated with the axonal growth cone and so should directly relate to neuronal extension. In this work however, we observed the strange result that GAP43 was also increased in sham injured tissue in a similar pattern to transected spinal cord, except at 3 dpi. It is possible that this increase in growth marker is a result of efforts to regenerate any peripheral nerve segments which have been ablated during the exposure of the spinal cord. It is also possible that this is due to the repair of the muscle which was cut through to access the spinal cord. A number of studies of tail regeneration have suggested that the spinal cord is necessary for proper repair of the other tail tissues including notochord either by release of soluble mediators into the surrounding tissues (Lin *et al.*, 2012) or by other mechanisms. Laser ablation (Mondia *et al.*, 2011) or physical removal (Schnapp *et al.*, 2005; Taniguchi *et al.*, 2008) of all or part of the spinal cord impeded correct tail regeneration in *Xenopus laevis* tadpoles and removal of the spinal cord glial cells have also been observed to aid muscle repair (Echeverri and Tanaka, 2002).

In support of this result GAP43 was observed to be one of the most differentially regulated proteins in tadpole following SCI in a large quantitative proteomic study of spinal cord regeneration (Lee-Liu *et al.*, 2018).

The astrocyte response to injury seen here was interesting as there was a noticeable difference morphologically between tadpole and froglet but the dense 'wall' of astrocytes commonly observed following mammalian SCI was not seen in the non-regenerative froglet. Instead of the large, hypertrophic, densely accumulated cells seen in mammals, here in the froglet we observed instead a meshwork of GFAP positive processes. The majority of these processes appeared to align parallel to the cut surface of the injury. It would be interesting to study the expression of adhesion molecules on the astrocyte and neuron processes to better understand how astrocytes may influence neuronal growth and arrangement in this context. It is possible that the arrangement of these cellular extensions is actually a secondary effect of a similar organisation of the ECM. This would also warrant further study. The earliest morphological change was an apparent shrinking or withdrawal of processes giving the staining pattern a somewhat punctate appearance at the earlier time-point. Perhaps this is an indication of an early stress response in these cells.

There was only a slight increase in the area of tissue positively labelled with GFAP after injury in the froglet which didn't reach statistical significance. This was somewhat unexpected based on the known

reaction of astroyctes in mammalian SCI (Sofroniew and Vinters, 2010; O'Shea *et al.*, 2017), and the reports of the glial scarring reaction seen following optic nerve injury in post-metamorphic frogs (Reier, 1979). In both cases they have been reported to become hypertrophic and this should lead to an increased area fraction of the tissue greater than that which was observed here. Perhaps the time-point examined is too early to detect this kind of reaction: in rats the glial scar begins to form at around the first week after injury, and in the study of optic nerve above the scarred tissue was harvested between 25 and 40 dpi (Reier, 1979). There is also no indication here of whether astrocytes become phagocytic and contribute to the cleaning up of the lesion as GFAP does not label cell bodies in *Xenopus laevis*. Glutamine synthase may be a better marker to investigate this aspect and to see more evidence of hypertrophy (Edwards-Faret *et al.*, 2018).

The work outlined above serves to characterise the timeline of regeneration following spinal cord transection in pre-metamorphic *Xenopus laevis*, and to investigate at a basic cellular level how this regeneration occurs pre-metamorphically but fails post-metamorphically. The following chapter will investigate at a deeper molecular level the differences in regenerative ability between the two developmental stages of *Xenopus laevis*.

4 Chapter 4 - The Glycosylation Response to Spinal Cord Transection in Pre- and Post-Metamorphic *Xenopus Laevis*

4.1 Introduction

The differences between regeneration competent tadpoles and regeneration incompetent froglets presented in the previous chapter will be probed more deeply here. In this chapter we attempt to investigate the molecular differences between the two developmental stages with a focus on glycosylation. Very little is known in general about glycosylation in *Xenopus laevis*, and nothing at all has been studied in relation to CNS glycosylation.

It can be assumed that glycans exist in all the major forms as outlined in Section 1.5.2, including the compact *N*- and *O*-glycans attached to protein, the long linear chains on proteoglycans, the glycolipids and the free monosaccharides, as these are all found throughout the plant and animal kingdoms (Varki *et al.*, 2009). Since glycosylation changes have been identified in traumatic brain injury (Abou-Abbass *et al.*, 2016), in multiple sclerosis (Grigorian *et al.*, 2012a; Grigorian *et al.*, 2012b; Chien *et al.*, 2018) and brain degenerative diseases including Alzheimer's disease (Wang *et al.*, 1996; Gizaw *et al.*, 2016) and Huntington's disease (Gizaw *et al.*, 2015), as well as being an established regulator of peripheral inflammation (Rabinovich and Croci, 2012) it is logical to assume that a traumatic injury to the spinal cord may affect the glycosylation profile.

Here we employ lectin histochemistry to establish glycosylation patterns in the injured spinal cord of pre- and post-metamorphic *Xenopus laevis*, using four lectins to label common monosaccharides, namely DSA to label GlcNAc, AIA to label galactose, WFA for GalNAc and SNA-I for sialic acid.

4.2 Hypothesis

The glycosylation response to spinal cord transection in regenerative stage *Xenopus laevis* is different from the glycosylation response to transection in non-regenerative stage *Xenopus laevis.*

4.3 Objectives

1. Compare the amount of galactose following injury between the two developmental stages of *Xenopus laevis*
2. Compare the amount of β(1-4)-GlcNAc following injury between the two developmental stages of *Xenopus laevis*

3. Compare the amount of α(2-6)-sialic acid following injury between the two developmental stages of *Xenopus laevis*
4. Compare the amount of GalNAc following injury between the two developmental stages of *Xenopus laevis*

4.4 Experimental design

In order to investigate the changes in glycosylation resulting from SCI, injured tissue at 1 and 7 dpi from pre- and post-metamorphic *Xenopus laevis* was stained with lectins which bind to particular monosaccharide residues, including galactose, GlcNAc, GalNAc and sialic acid.

SCI was induced in tadpole and froglet *Xenopus laevis* as described in Sections 2.1.2 and 2.1.3. Tissue was collected and processed as in Sections 2.1.4 and 2.1.5. Sections were then stained histochemically with both lectins and antibodies using the combined protocol described in Section 2.5. The lectins AIA, DSA, WFA and SNA-I were used to stain for galactose, GlcNAc, GalNAc and sialic acid respectively. Antibodies against GFAP and acetylated tubulin were used to label astrocytes and neurons.

This combined protocol was advantageous in that it reduced the amount of tissue, and therefore animals, required to complete all experiments. The combined protocol could also be used to investigate which cell types were producing sugars of interest, by searching for colocalisation between positive lectin staining and the antibody marker. High magnification confocal images were acquired as described in Section 2.7.1 and analysed as in Section 2.7.4. Statistical analysis was performed using GraphPad Prism, see Section 2.9. Details of experimental groups are given in Table 4.1, n=3-6 per group, details in results section.

Developmental stage	**Injury**	**Time point (dpi)**	
Tadpole	Sham	1	7
	Transection	1	7
Froglet	Sham	1	7
	Transection	1	7

Table 4.1 Details of experimental groups for investigation into the glycosylation response to SCI in regenerative and non-regenerative stages of *Xenopus laevis*. n=3-6 per group.

Taking each monosaccharide individually, the differences in transection were compared to sham, i.e. the direct response to the injury, was compared at each time-point for each developmental stage. For this analysis, data from the lesion borders both rostral and caudal were averaged for each animal before comparing to the sham (Figure 4.1, Figure 4.5, Figure 4.9, Figure 4.13). Next the differences in ROIs were examined for each time-point and developmental stage (Figure 4.2, Figure 4.6, Figure 4.10, Figure 4.14) followed by the main comparison: how the regenerative tadpoles and non-regenerative froglets differ in their response to the injury (Figure 4.3, Figure 4.7, Figure 4.11, Figure 4.15). For both of these tests, data for injured spinal cord was normalised to sham controls. No comparison could be made between tadpole and froglet for the lesion epicentre due to problems with stabilising this area during tissue processing of froglet spinal cord. Data is included for tadpole lesion epicentre only. Finally, for each sugar the sham groups for each developmental stage were compared, to account for any baseline differences in the level of glycoylsation between the two developmental stages which may be responsible for the differential response to the injury (Figure 4.17).

4.5 Results

Changes in abundance of each of the four sugars, galactose, GlcNAc, sialic acid and GalNAc, were examined in pre-metamorphic tadpoles at 1 and 7 dpi, and in post-metamorphic froglets at 1 and 7 dpi to understand the changes in glycosylation associated with injury and regeneration. These changes were investigated across a number of ROIs: the lesion epicentre, the borders of the lesion rostral and caudal, and in intact tissue adjacent to the lesion, both rostral and caudal.

4.5.1 Galactose in and around the lesion increases following SCI but decreases as regeneration proceeds in tadpole

Comparing transected to sham injured tissue at 1 and 7 dpi in tadpole and froglet it can be seen that spinal cord transection results in increased galactose at 1 dpi, with a reduction compared to sham at 7 dpi. The differences between transection and sham were more pronounced in tadpole spinal cord than in froglet, however no statistical significance was observed, Figure 4.1.

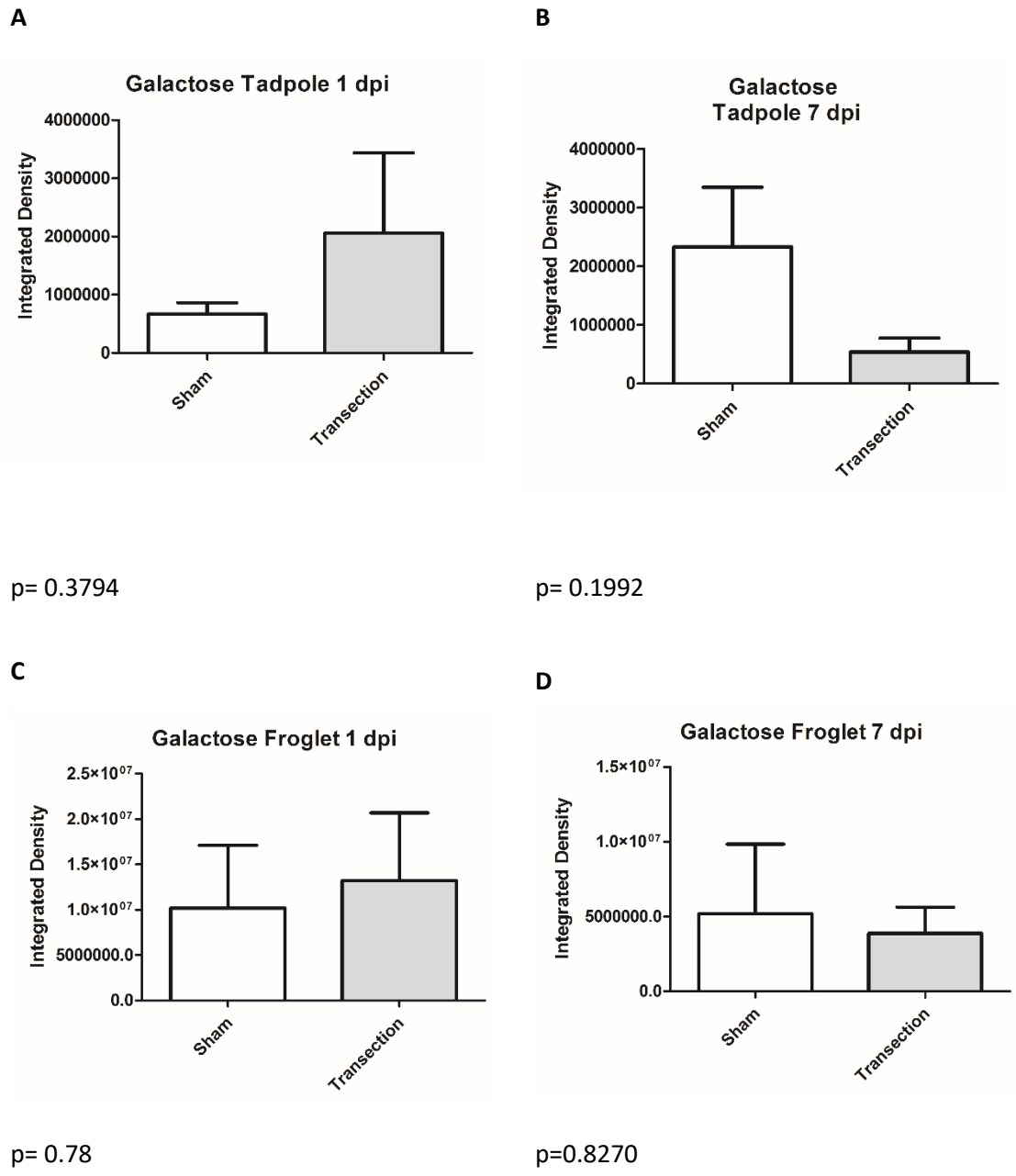

Figure 4.1 Comparison of galactose changes in sham and transected animals following SCI in pre- and post-metamorphic *Xenopus laevis*. Graphs show AIA lectin staining in spinal cord tissue in tadpole at 1 dpi (A) and 7 dpi (B) and in froglet at 1 dpi (C) and 7 dpi (D). For transected animals, data from the lesion borders rostral and caudal were pooled. Data was analysed using the t-test. No statistical significance was observed. p values for each analysis are given under the relevant graph. A value of $p<0.05$ was considered significant.

Each individual ROI showed an increase in comparison to sham at 1 dpi but a reduction at 7 dpi in tadpole spinal cord (Figure 4.2 A, B) in keeping with the indication from the pooled lesion borders, suggesting that a similar response was exhibited throughout the spinal cord. The amount of galactose detected following injury was much less homogenous in the froglet than in the tadpole (Figure 4.2 C, D). In the froglet, the intact tissue rostral to the injury had lower levels of galactose than sham at 1 dpi while all other regions produced more galactose. At 7 dpi there were slight elevations compared to sham for all ROIs except for the caudal border which showed a much greater increase. Despite the apparently large changes in the amount of galactose across the ROIs in froglet spinal cord, no statistical significance was observed (Figure 4.2 C, D).

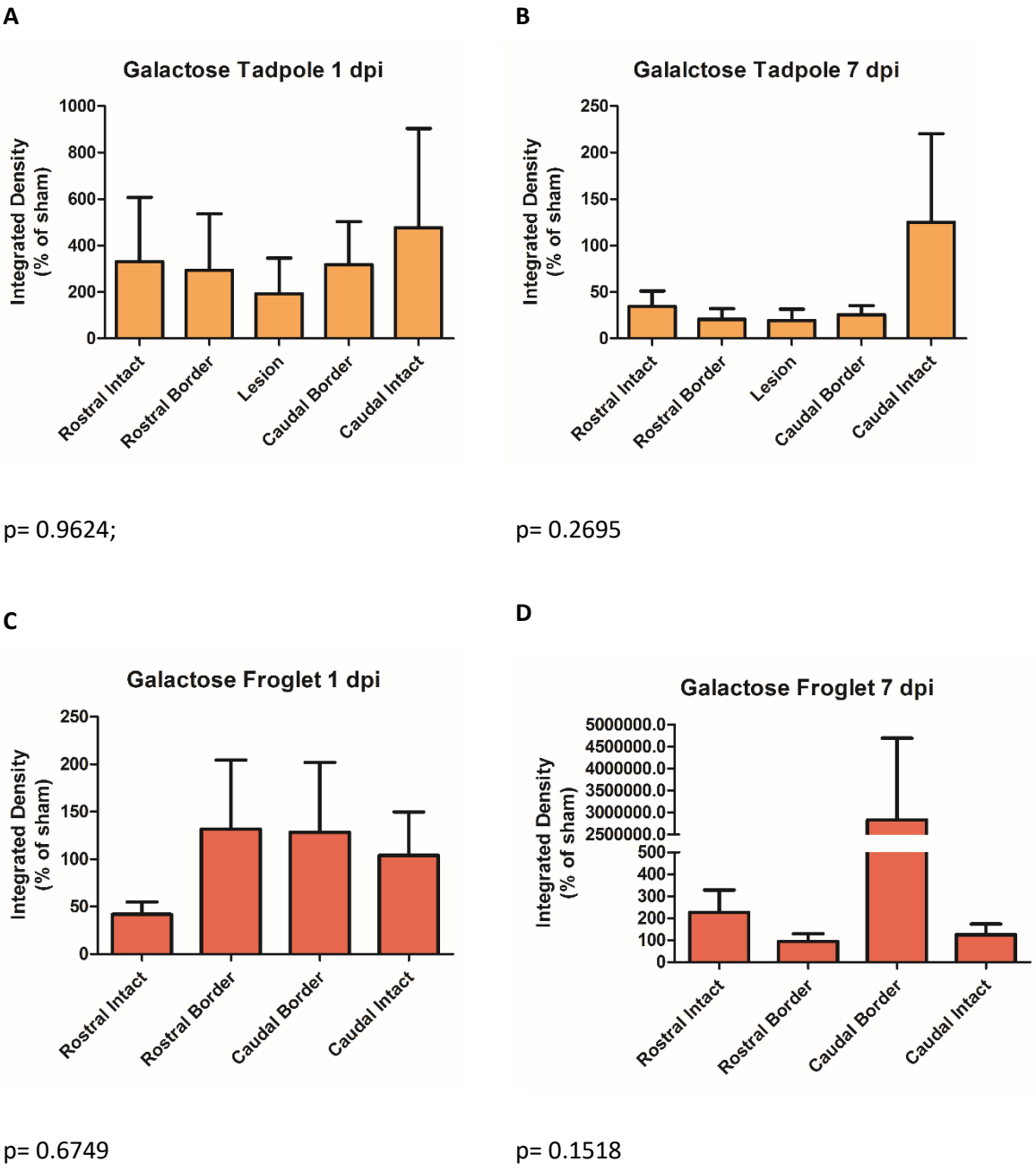

p= 0.9624;

p= 0.2695

p= 0.6749

p= 0.1518

Figure 4.2 Comparison of galactose abundance throughout the regions of the spinal cord. Graphs show AIA lectin staining in spinal cord tissue in tadpole at 1 dpi (A) and 7 dpi (B) and in froglet at 1 dpi (C) and 7 dpi (D). Data was normalised to the relevant sham group and analysed using a one way ANOVA with Tukey's post hoc test. No statistical significance was observed. p values for each analysis are given under the relevant graph. A value of $p<0.05$ was considered significant.

No significant differences between time-point or developmental stage were found for galactose (Figure 4.3). However some trends could be seen: at the lesion borders both rostral and caudal there was an increase relative to sham in both developmental stages at 1 dpi (Figure 4.3 B, C). There was more galactose present in the regenerating tadpole than in the non-regenerating froglet at 1 dpi, although it decreased again by 7 dpi, at which stage there was more galactose present in the froglet tissue (Figure 4.3 B, C). In the intact tissue distant from the lesion there were no similarities between rostral and caudal tissue (Figure 4.3 D, E): galactose was detected in rostral tissue in a similar manner to the lesion borders, with an immediate elevation in galactose at 1 dpi in the tadpole and a delayed elevation at 7 dpi in the froglet. In caudal intact tissue galactose levels at 1 dpi in froglet remained unchanged compared to sham while in the tadpole they were reduced. By 7 dpi both tadpole and froglet had increased the amount of galactose relative to sham to a similar extent (Figure 4.3 D, E).

At the lesion epicentre in the tadpole, a similar pattern was seen as at the lesion borders. There was an increase in galactose immediately following injury, which dropped to well below sham levels by 7 dpi (Figure 4.3 A).

Representative images for all groups and all ROIs are shown in Figure 4.4.

A

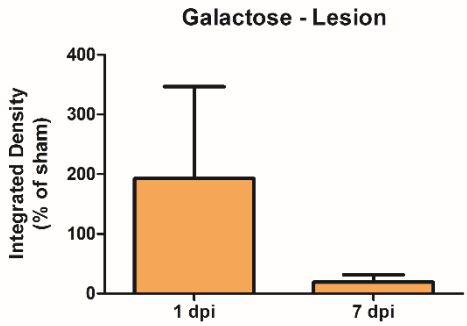

p= 0.4282

B

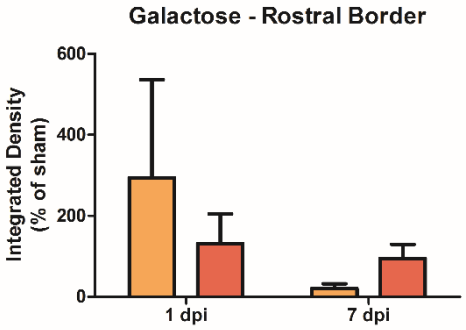

	p
Interaction	0.6100
Developmental Stage	0.8475
Time post injury	0.5046

C

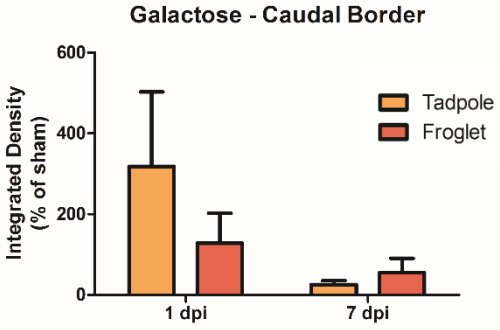

	p
Interaction	0.5382
Developmental Stage	0.6508
Time post injury	0.3104

D

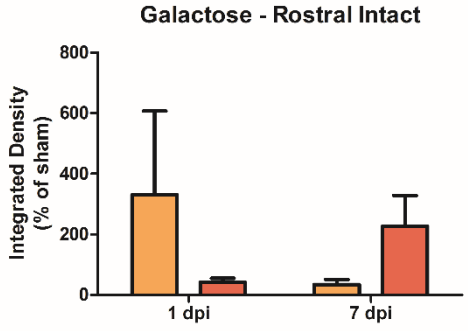

	p
Interaction	0.3183
Developmental Stage	0.8375
Time post injury	0.8134

E

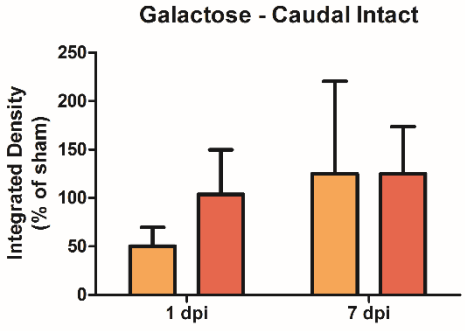

	p
Interaction	0.6617
Developmental Stage	0.6647
Time post injury	0.4411

Figure 4.3 Comparison of galactose abundance between pre- and post-metamorphic *Xenopus laevis* at 1 and 7 dpi. Graphs show AIA lectin staining in spinal cord tissue, comparing tadpole at 1 and 7 dpi (A), and comparing tadpole and froglet at 1 and 7 dpi (B-E). Data was normalised to sham before

analysis with two way ANOVA and Bonferroni's post hoc test. No statistical significance was observed. A value of $p<0.05$ was considered significant.

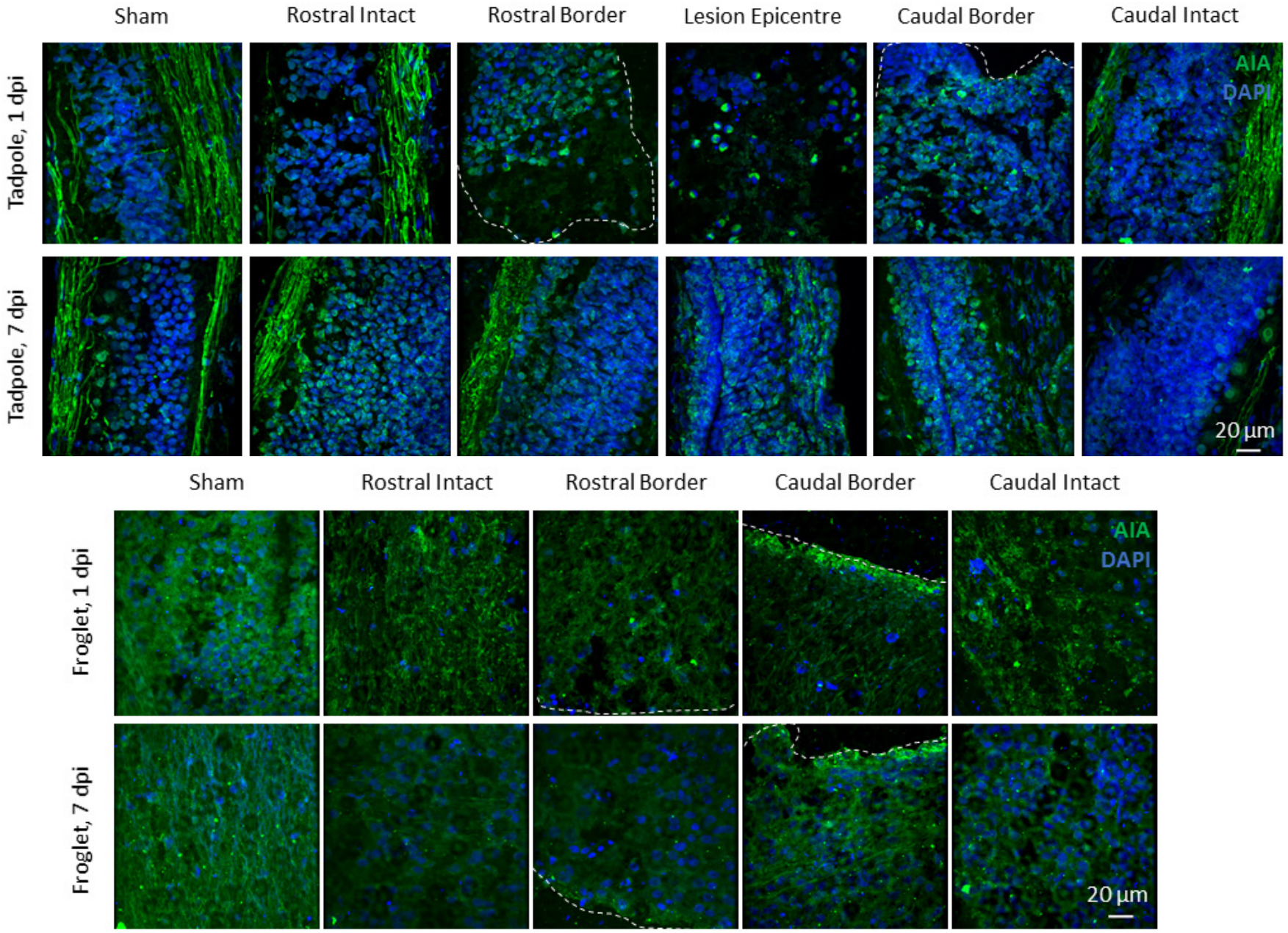
Sham
Rostral Intact
Rostral Border
Lesion Epicentre
Caudal Border
Caudal Intact
Tadpole, 1 dpi
Tadpole, 7 dpi
AIA
DAPI
20 µm
Sham
Rostral Intact
Rostral Border
Caudal Border
Caudal Intact
Froglet, 1 dpi
Froglet, 7 dpi
AIA
DAPI
20 µm

Figure 4.4 Representative images of galactose distribution in the spinal cord of pre- and post-metamorphic *Xenopus laevis* at 1 and 7 days following SCI. FITC-conjugated AIA lectin was used to label galactose. Nuclei were stained with Hoechst (blue). The edge of the lesion is outlined with a white dashed line. Scale bar for all images = 20 μm.

4.5.2 β(1-4) GlcNAc in and around the lesion increases following SCI but decreases over time in both tadpole and froglet

At the lesion borders the pattern of β(1-4)-linked GlcNAc expression was similar to that of galactose comparing transected to sham tissue at each time-point and at each developmental stage. At 1 dpi in both the tadpole and the froglet GlcNAc was increased relative to sham, while at 7 dpi the opposite was seen. The difference between injury and control was statistically significant only in tadpole at 1 dpi, Figure 4.5.

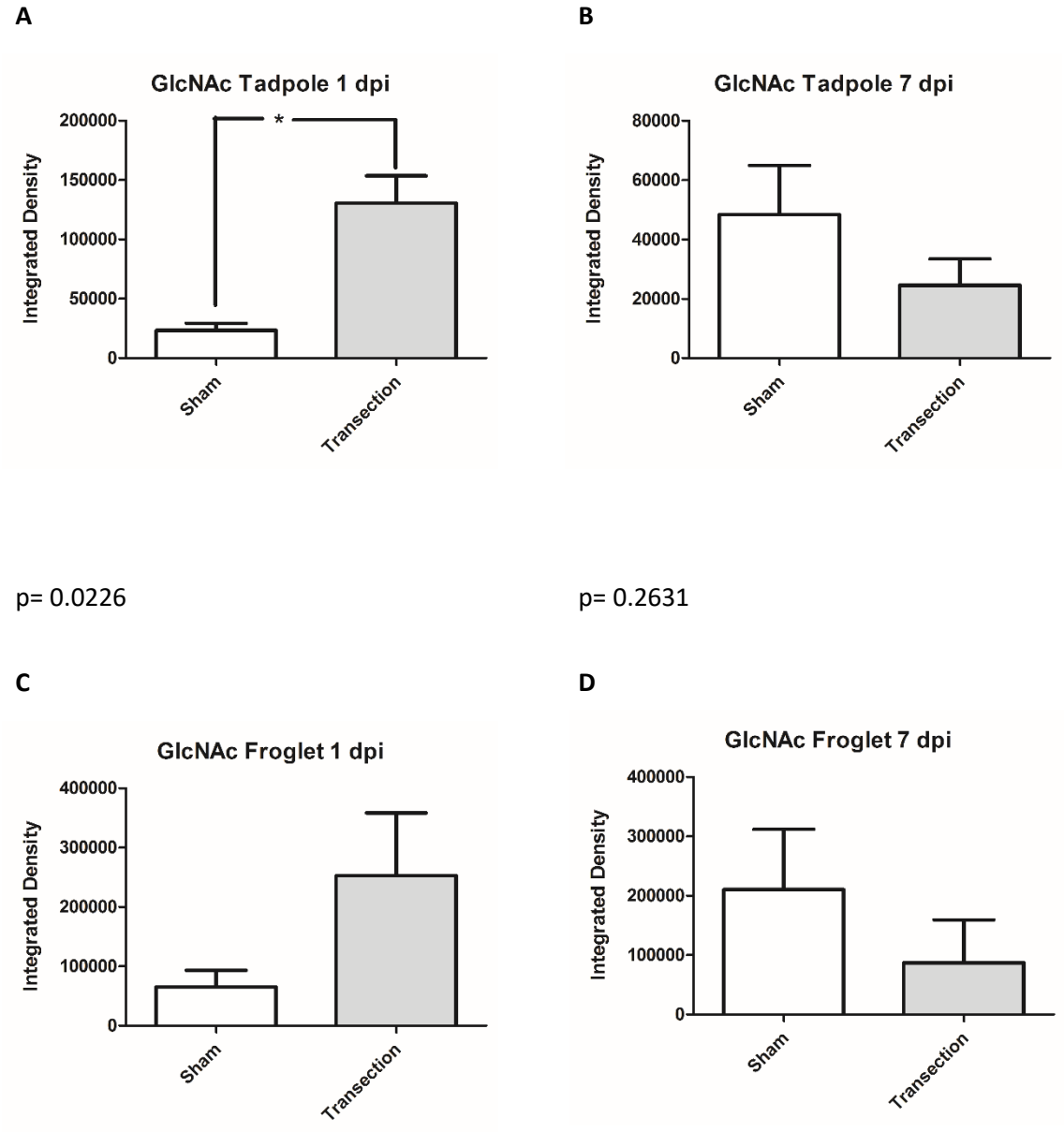

p= 0.0226

p= 0.2631

p= 0.1374

p= 0.3538

Figure 4.5 Comparison of GlcNAc changes in sham and transected animals following SCI in pre-and post-metamorphic *Xenopus laevis*. Graphs show DSA lectin staining in spinal cord tissue in tadpole at 1 dpi (A) and 7 dpi (B) and in froglet at 1 dpi (C) and 7 dpi (D). For transected animals, data from the lesion borders rostral and caudal were pooled. Data was analysed using the t-test. p values for each analysis are given under the relevant graph. A value of $p<0.05$ was considered significant. Groups which differ significantly are indicated with an asterisk.

The increase in GlcNAc production was similar across all ROIs at 1 dpi in the tadpole (Figure 4.6 A) and at both at 1 and 7 dpi in the froglet (Figure 4.6 C, D) with no significant differences between any regions. At 7 dpi in the tadpole however a much greater response was seen in the intact tissue far from the lesion compared to the tissue at the borders and in the lesion epicentre itself. In fact while GlcNAc production in the lesion epicentre and at the lesion borders was reduced relative to sham at this time-point the amount of GlcNAc produced far from the lesion was much higher, although it did not reach statistical significance (Figure 4.6 B).

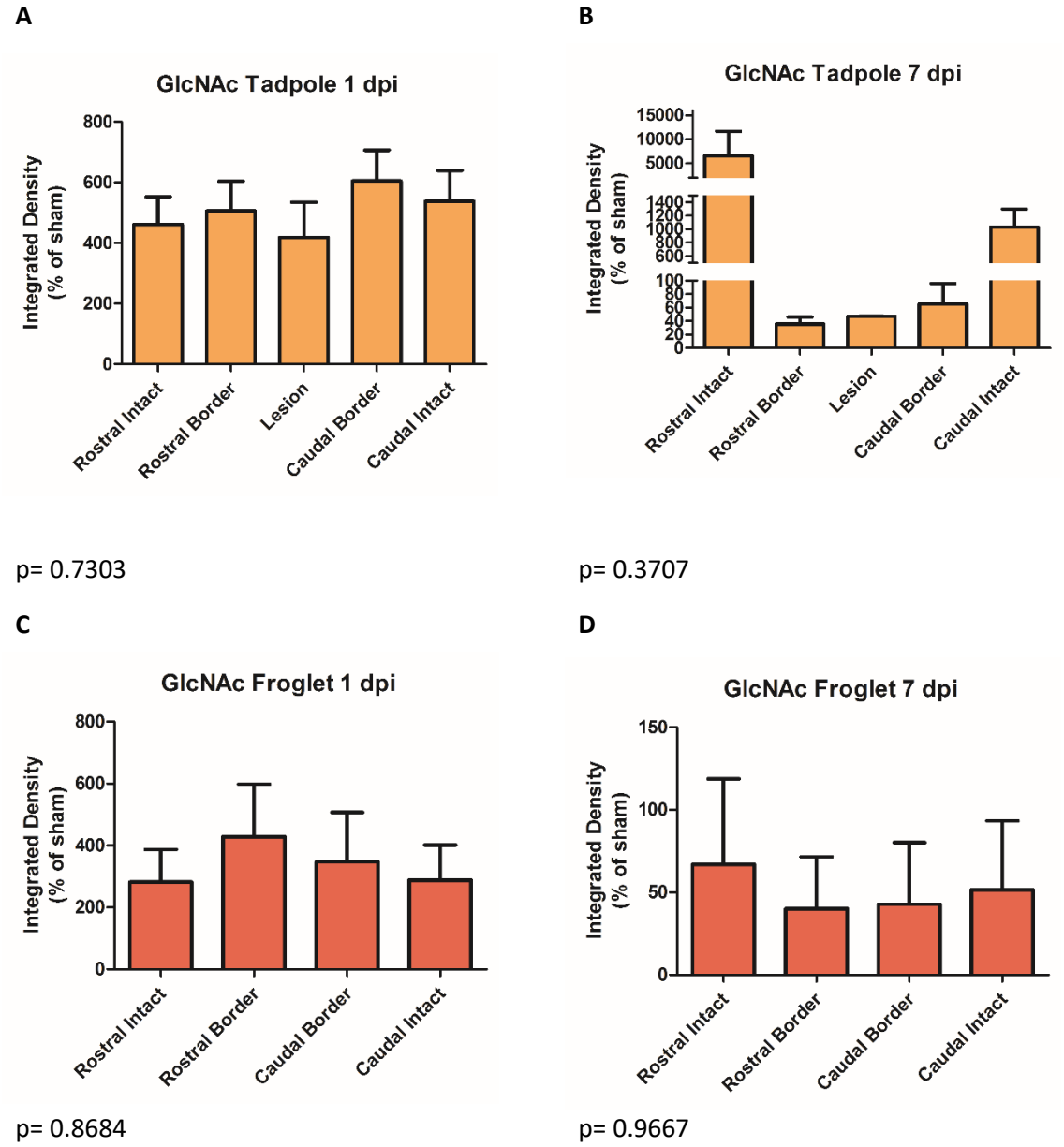

Figure 4.6 Comparison of GlcNAc abundance throughout the regions of the spinal cord. Graphs show DSA lectin staining in spinal cord tissue in tadpole at 1 dpi (A) and 7 dpi (B) and in froglet at 1 dpi (C) and 7 dpi (D). Data was normalised to the relevant sham group and analysed using a one way ANOVA with Tukey's post hoc test. No statistical significance was observed. p values for each analysis are given under the relevant graph. A value of $p<0.05$ was considered significant.

Comparing normalised data across time-point and developmental stage a significant difference could be seen with time for GlcNAc production in the tadpole in the vicinity of the injury (Figure 4.7 A, B, C). Both tadpole and froglet increased the amount of GlcNAc present at the lesion borders at 1 dpi and reduced GlcNAc below sham levels by 7 dpi to a similar extent, however the differences only reached statistical significance for tadpole tissue (Figure 4.7 B, C). In the froglet the intact tissue distant from the lesion produced GlcNAc in a similar manner to the lesion borders: GlcNAc increased above sham levels at 1 dpi and reduced by 7 dpi (Figure 4.7 D, E). In the tadpole however GlcNAc increased at 1 dpi in keeping with the other regions, but had increased even further by 7 dpi. The amount of GlcNAc detected in the tadpole spinal cord at 7 dpi in the intact caudal region was significantly higher than the amount present at 1 dpi in tadpole, and the amount present at 7 dpi in the froglet cord (Figure 4.7 D, E).

At the tadpole lesion epicentre, there was also an increase compared to sham at 1 dpi and a reduction compared to sham at 7 dpi, with the differences between the two time-points being statistically significant, and following the same pattern of change as the lesion borders (Figure 4.7 A).

Representative images for all groups and all ROIs are shown in Figure 4.8.

A

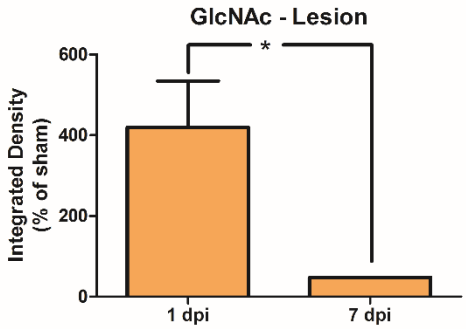

p= 0.0294

B

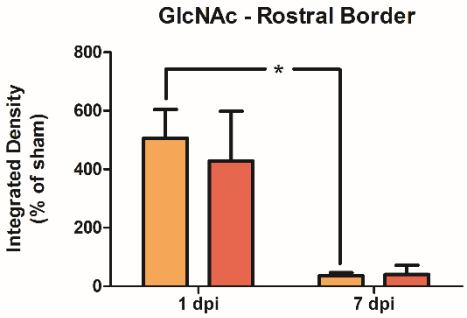

	p
Interaction	0.6972
Developmental Stage	0.7282
Time post injury	0.0007

C

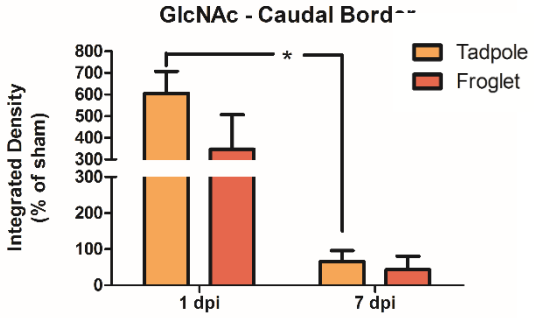

	p
Interaction	0.2796
Developmental Stage	0.1996
Time post injury	0.0009

D

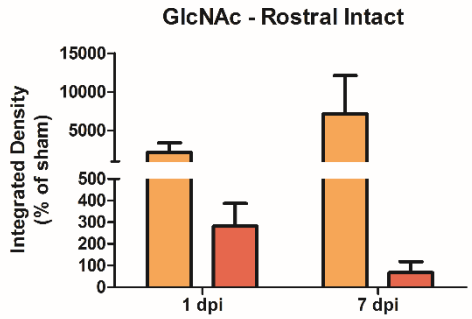

	p
Interaction	0.3797
Developmental Stage	0.1382
Time post injury	0.4195

E

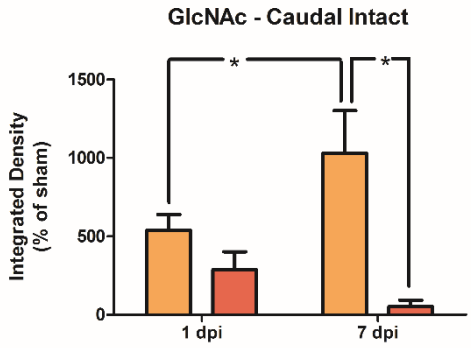

	p
Interaction	0.0174
Developmental Stage	0.0005
Time post injury	0.3561

Figure 4.7 Comparison of GlcNAc abundance between pre- and post-metamorphic *Xenopus laevis* at 1 and 7 dpi. Graphs show DSA lectin staining in spinal cord tissue, comparing tadpole at 1 and 7 dpi (A), and comparing tadpole and froglet at 1 and 7 dpi (B-E). Data was normalised to sham before

analysis with two way ANOVA and Bonferroni's post hoc test. P values are shown beneath the graphs. A value of $p<0.05$ was considered significant. Groups which differ significantly are indicated with an asterisk.

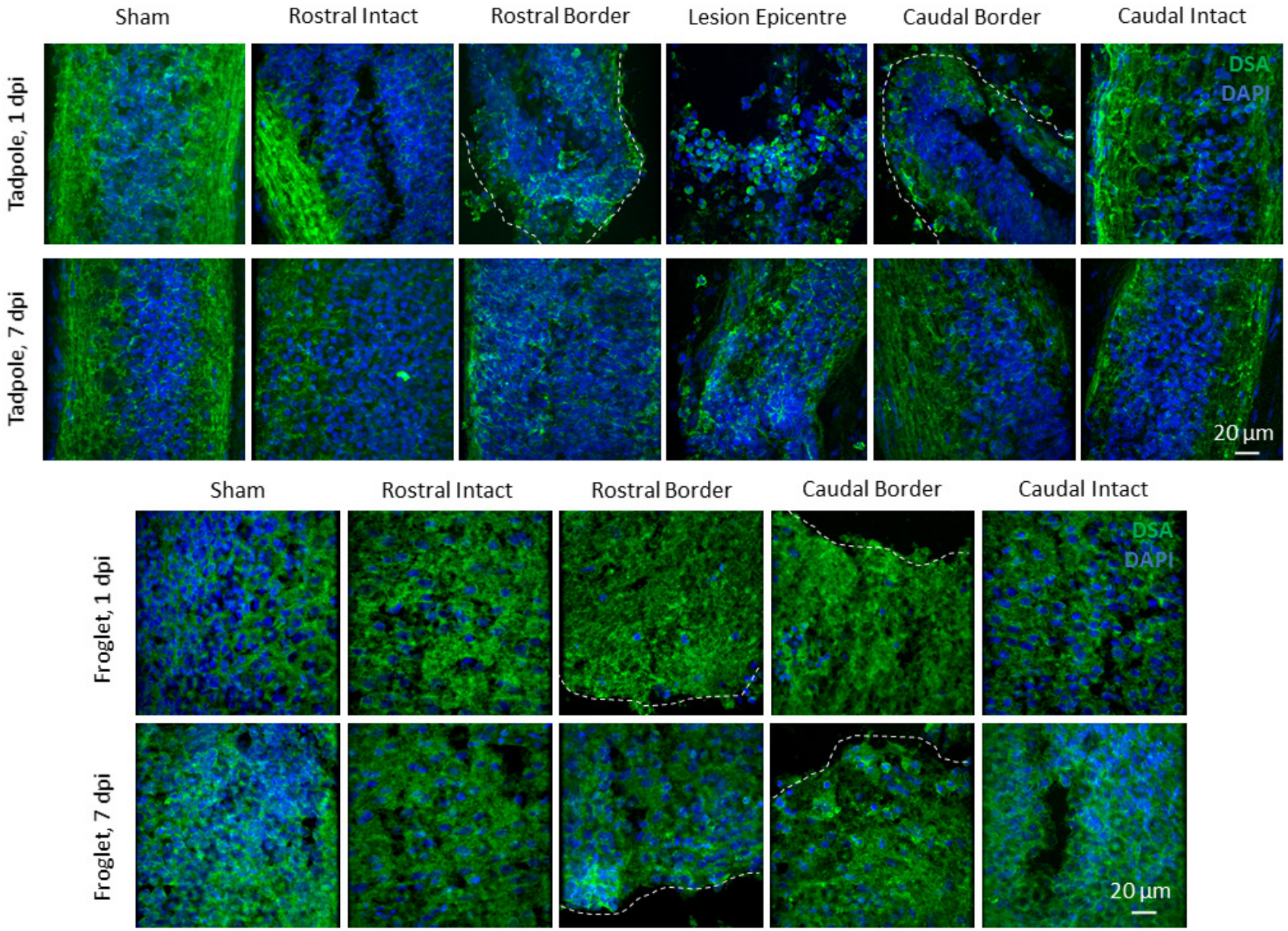
Sham
Rostral Intact
Rostral Border
Lesion Epicentre
Caudal Border
Caudal Intact
Tadpole, 1 dpi
Tadpole, 7 dpi
DSA
DAPI
20 µm
Sham
Rostral Intact
Rostral Border
Caudal Border
Caudal Intact
Froglet, 1 dpi
Froglet, 7 dpi
DSA
DAPI
20 µm

Figure 4.8 Representative images of GlcNAc distribution in the spinal cord of pre- and post-metamorphic *Xenopus laevis* at 1 and 7 days following SCI. FITC-conjugated DSA lectin was used to label GlcNAc (green). Nuclei were labelled with Hoechst (blue). The edge of the lesion is outlined with a white dashed line.

4.5.3 α(2-6) sialic acid increases in and around the lesion following SCI in tadpole and to a greater extent in froglet

Comparing sialic acid production at 1 dpi in the tadpole an increase was observed between transected spinal cord (lesion borders) and sham injured spinal cord (Figure 4.9 A). By 7 dpi this appeared to have normalised, but this was due to an increase in positive SNA-I signal in the sham injured cord, while the amount in the transected cord stayed approximately the same (Figure 4.9 B). In the froglet, the amount of sialic acid in the transected spinal cord was much higher than in the sham at 1 dpi, and was still higher than sham at 7 dpi (Figure 4.9 C, D).

A

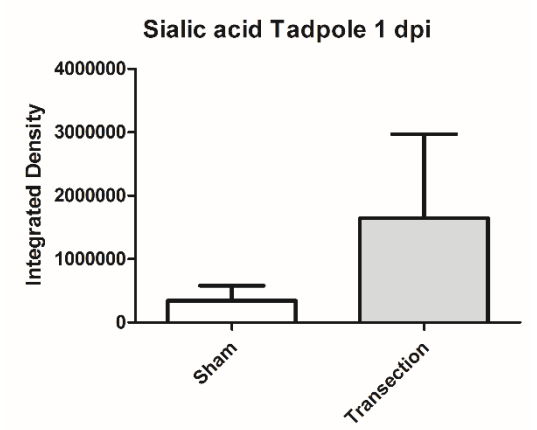

p= 0.4205;

B

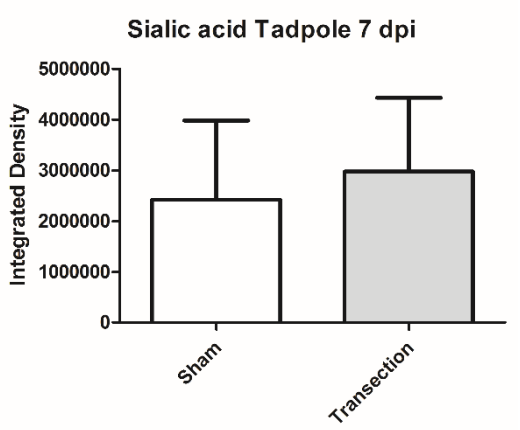

p= 0.8046

C

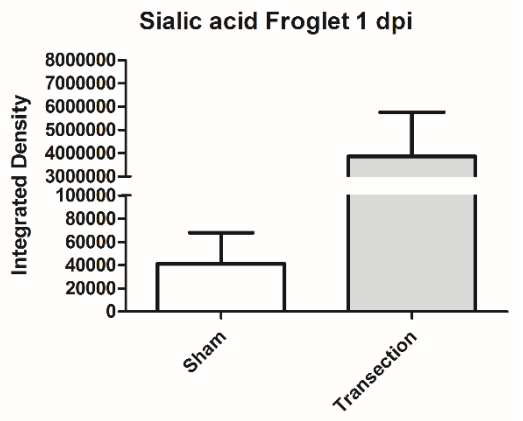

p= 0.0615;

D

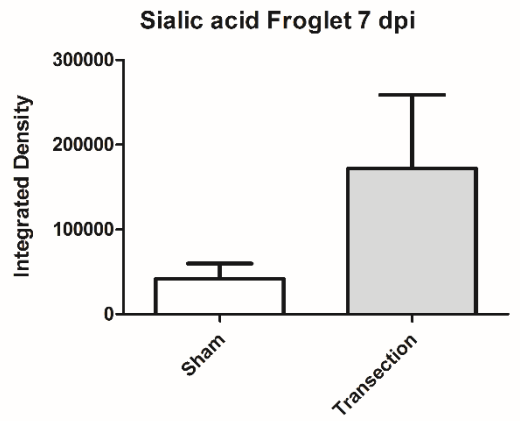

p= 0.2162

Figure 4.9 Comparison of sialic acid changes in sham and transected animals following SCI in pre- and post-metamorphic *Xenopus laevis*. Graphs show SNA-I lectin staining in spinal cord tissue in tadpole at 1 dpi (A) and 7 dpi (B) and in froglet at 1 dpi (C) and 7 dpi (D). For transected animals, data from the lesion borders rostral and caudal were pooled. Data was analysed using the t-test. No statistical significance was observed. p values for each analysis are given under the relevant graph. A value of $p<0.05$ was considered significant.

Examining the ROIs for tadpole and froglet, it was observed that at 1 dpi in the tadpole, the lesion epicentre had the lowest level of sialic acid , with the caudal regions slightly higher, and the rostral regions highest in the amount of α(2-6)-sialic acid detected (Figure 4.10 A). At 7 dpi the intact tissue both rostral and caudal looked quite similar, and the rostral lesion border had a similar amount of sialic acid to the intact tissue, but the lesion epicentre and the caudal lesion border had slightly lower amounts of sialic acid, while still being elevated compared to sham (Figure 4.10 B). At 1 dpi in the froglet the rostral had higher amounts of sialic acid than the caudal for the lesion borders and in the intact tissue, and the lesion borders expressed more sialic acid than the intact tissue (Figure 4.10 C). At 7 dpi, all regions had similar amounts of sialic acid except for the caudal border which was slightly higher (Figure 4.10 D). For all ROIs in tadpole and froglet at both time-points the amount of sialic acid was higher than that seen in the sham, and there were no significant differences between the regions (Figure 4.10 A-D).

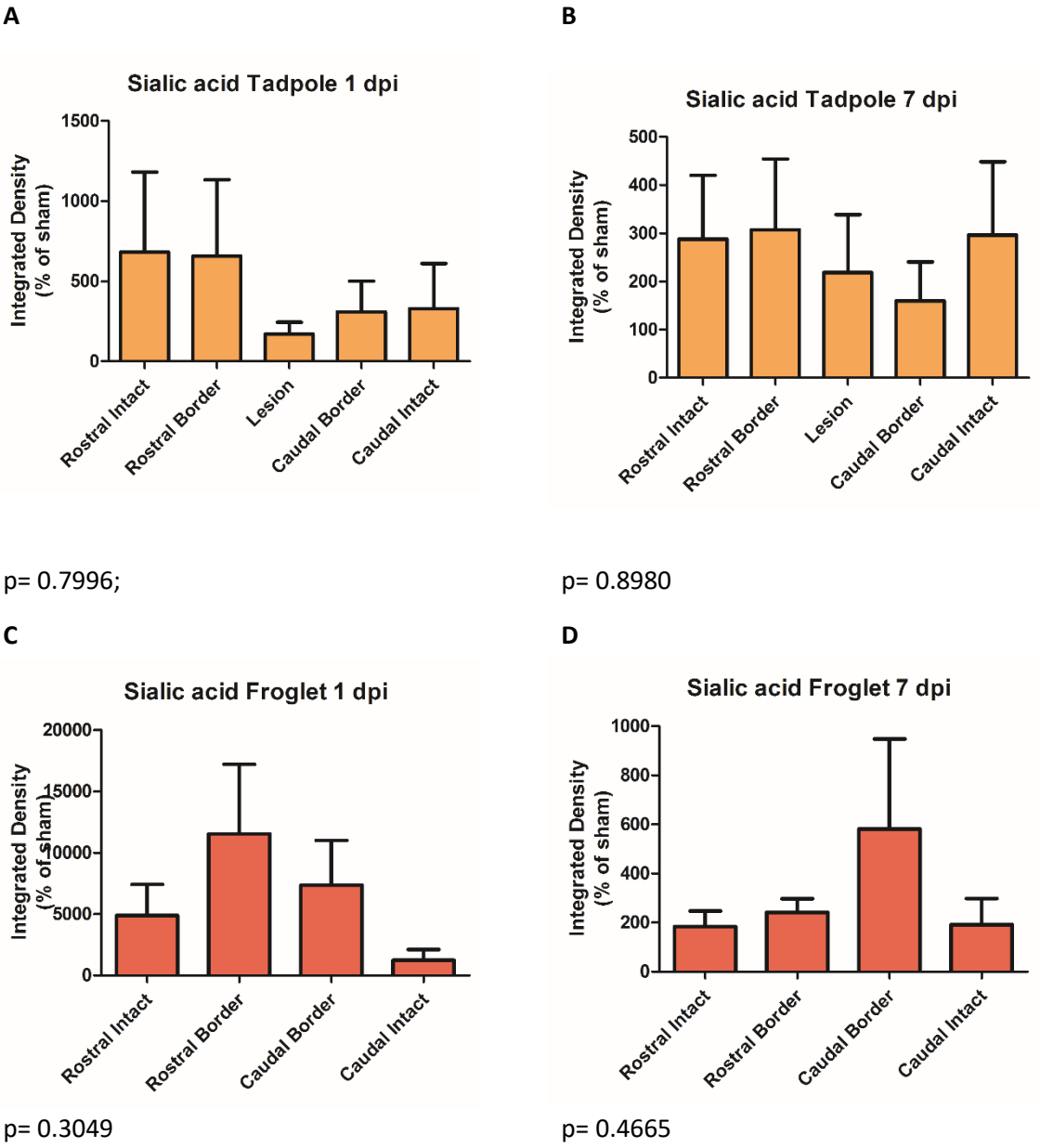

Figure 4.10 Comparison of sialic acid abundance throughout the regions of the spinal cord. Graphs show SNA-I lectin staining in spinal cord tissue in tadpole at 1 dpi (A) and 7 dpi (B) and in froglet at 1 dpi (C) and 7 dpi (D). Data was normalised to the relevant sham group and analysed using a one way ANOVA with Tukey's post hoc test. No statistical significance was observed. p values for each analysis are given under the relevant graph. A value of $p<0.05$ was considered significant.

Normalising to sham tissue the amount of sialic acid present in tadpole can be compared to froglet at each time-point. At the lesion borders both rostral and caudal the amount of sialic acid present in froglet spinal cord at 1 dpi was seen to be significantly higher than in the tadpole spinal cord at 1 dpi, and the froglet spinal cord at 7 dpi (Figure 4.11 B, C). This same pattern was seen in the intact tissue far from the lesion, but the difference was only significant on the rostral side (Figure 4.11 D, E). Rostral to the lesion both at the borders and far from the lesion there was a slight reduction in sialic acid in the tadpole spinal cord between 1 and 7 dpi (Figure 4.11 B, D). Caudal to the lesion at both the borders and in the intact tissue there was no noticeable change between the two time-points. At 7 dpi the difference between tadpole and froglet spinal cord had greatly reduced (Figure 4.11 C, E).

At the tadpole lesion epicentre, a very slight increase in sialylation was seen between 1 and 7 dpi (Figure 4.11 A).

Representative images for all groups and all ROIs are shown in Figure 4.12.

A

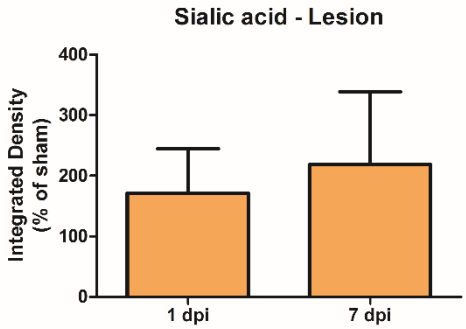

p= 0.7296;

B

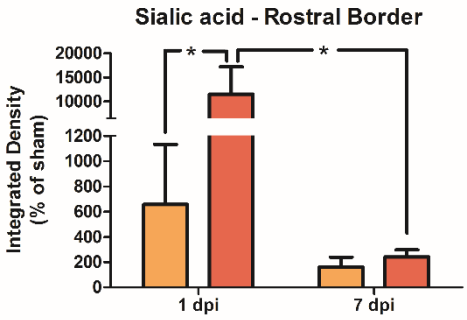

	p
Interaction	0.0257
Developmental Stage	0.0239
Time post injury	0.0167

C

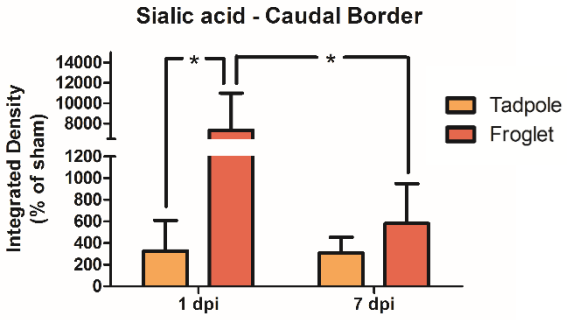

	p
Interaction	0.0540
Developmental Stage	0.0400
Time post injury	0.0527

D

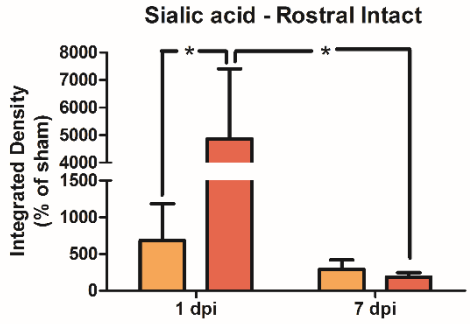

	p
Interaction	0.0785
Developmental Stage	0.0921
Time post injury	0.0424

E

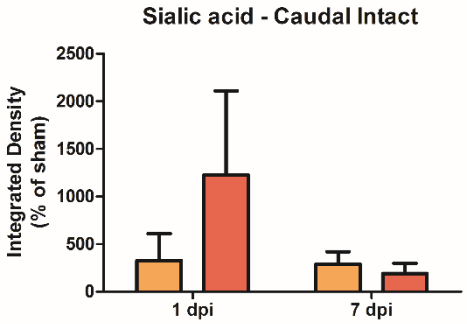

	p
Interaction	0.2985
Developmental Stage	0.3975
Time post injury	0.2634

Figure 4.11 Comparison of sialic acid abundance between pre- and post-metamorphic *Xenopus laevis* at 1 and 7 dpi. Graphs show SNA-I lectin staining in spinal cord tissue, comparing tadpole at 1 and 7 dpi (A), and comparing tadpole and froglet at 1 and 7 dpi (B-E). Data was normalised to sham

before analysis with two way ANOVA and Bonferroni's post hoc test. A value of $p<0.05$ was considered significant. Groups which differ significantly are indicated with an asterisk.

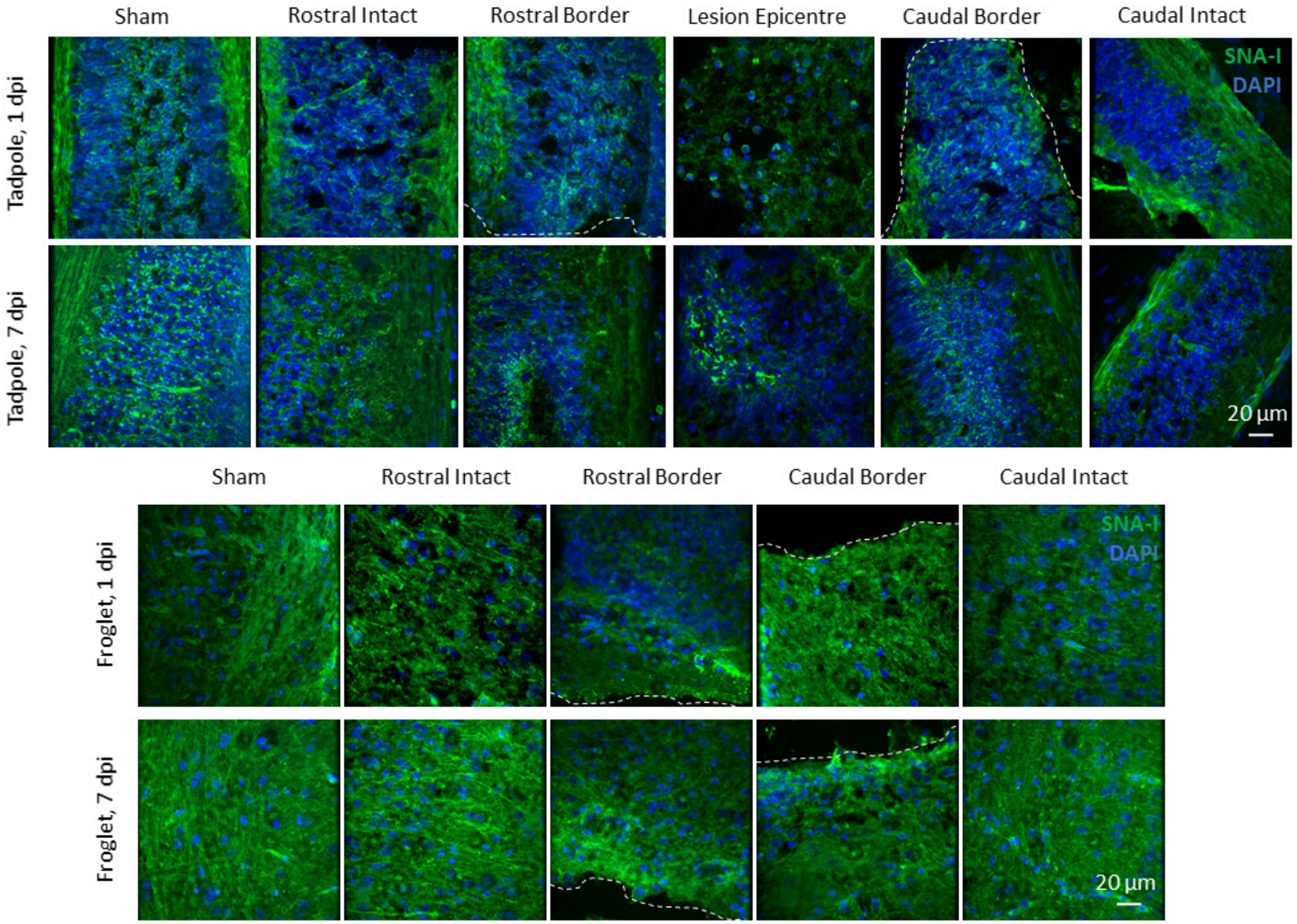
Sham
Rostral Intact
Rostral Border
Lesion Epicentre
Caudal Border
Caudal Intact
Tadpole, 1 dpi
Tadpole, 7 dpi
SNA-I
DAPI
20 µm
Sham
Rostral Intact
Rostral Border
Caudal Border
Caudal Intact
Froglet, 1 dpi
Froglet, 7 dpi
SNA-I
DAPI
20 µm

Figure 4.12 Representative images of sialic acid distribution in the spinal cord of pre- and post-metamorphic *Xenopus laevis* at 1 and 7 days following SCI. FITC-conjugated SNA-I lectin was used to label sialic acid. Nuclei were labelled with Hoechst (blue). The edge of the lesion is outlined with a white dashed line.

4.5.4 GalNAc is increased following SCI in tadpole, but decreased following SCI in froglet

Transection injury increased the amount of GalNAc at the lesion borders compared to sham at both time-points in the tadpole although these changes were not statistically significant (Figure 4.13 A, B). In the froglet levels of GalNAc fell following spinal cord transection at both 1 and 7 dpi, but again no significance was observed (Figure 4.13 C, D).

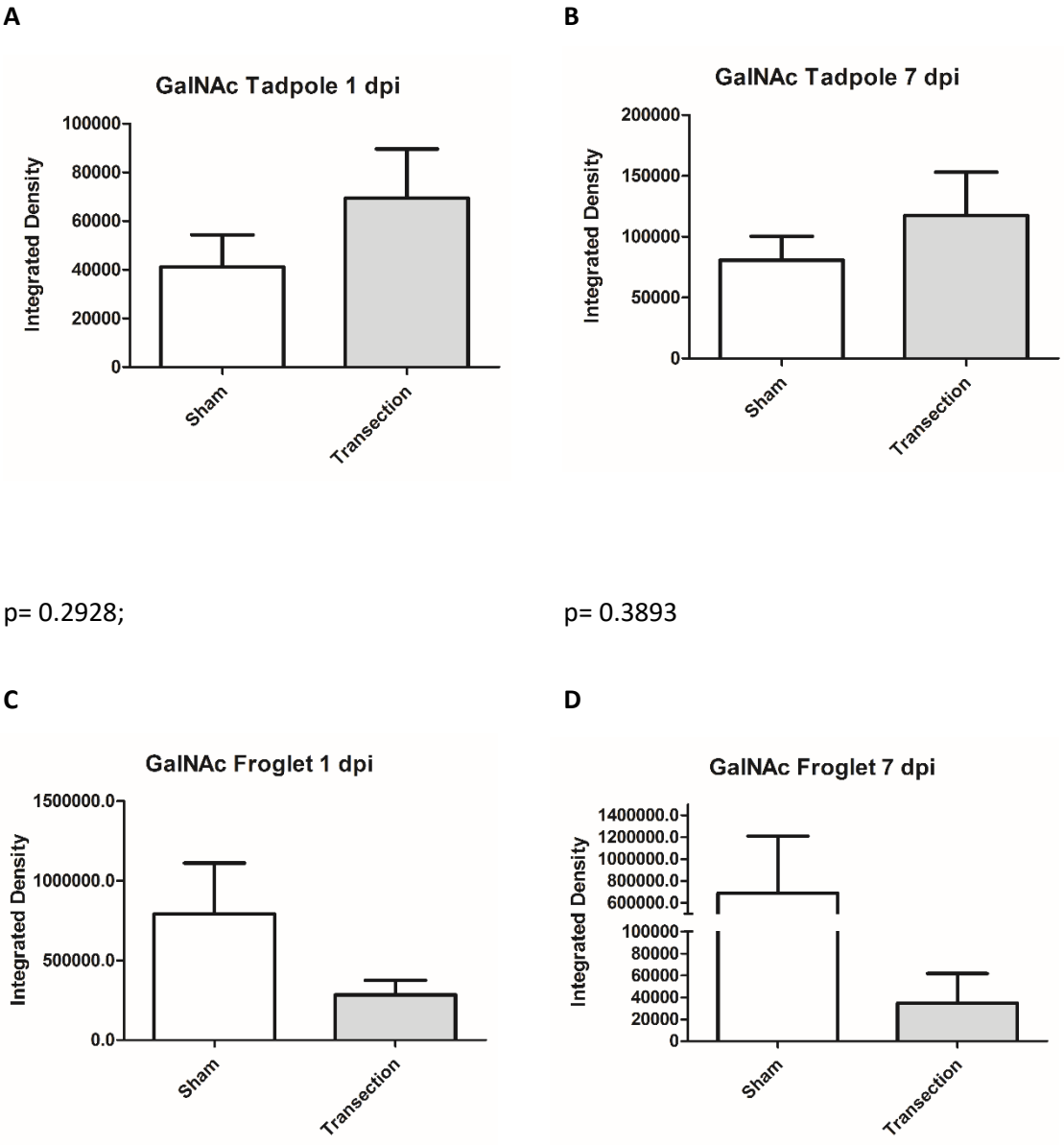

Figure 4.13 Comparison of GalNAc changes in sham and transected animals following SCI in pre-and post-metamorphic *Xenopus laevis*. Graphs show WFA lectin staining in spinal cord tissue in tadpole at 1 dpi (A) and 7 dpi (B) and in froglet at 1 dpi (C) and 7 dpi (D). For transected animals, data from the lesion borders rostral and caudal were pooled. Data was analysed using the t-test. No statistical significance was observed. p values for each analysis are given under the relevant graph. A value of $p<0.05$ was considered significant.

Some subtle differences in GalNAc expression between different ROIs were observed for the tadpole. At 1 dpi the amount of GalNAc present rostral to the lesion, both at the borders and in intact tissue, was lower than in the lesion epicentre and in caudal regions (Figure 4.14 A). At 7 dpi the amount of GalNAc did not differ greatly between ROIs except for in the caudal intact tissue which produced more GalNAc than any of the other regions (Figure 4.14 B). In all ROIs at both time-points in the tadpole GalNAc expression was increased compared to sham (Figure 4.14 A, B). In the froglet there was less GalNAc in all the ROIs compared to sham. At 1 dpi there was slightly more GalNAc rostral to the injury than caudal, and at 7 dpi there were very little differences between ROIs (Figure 4.14 C, D).

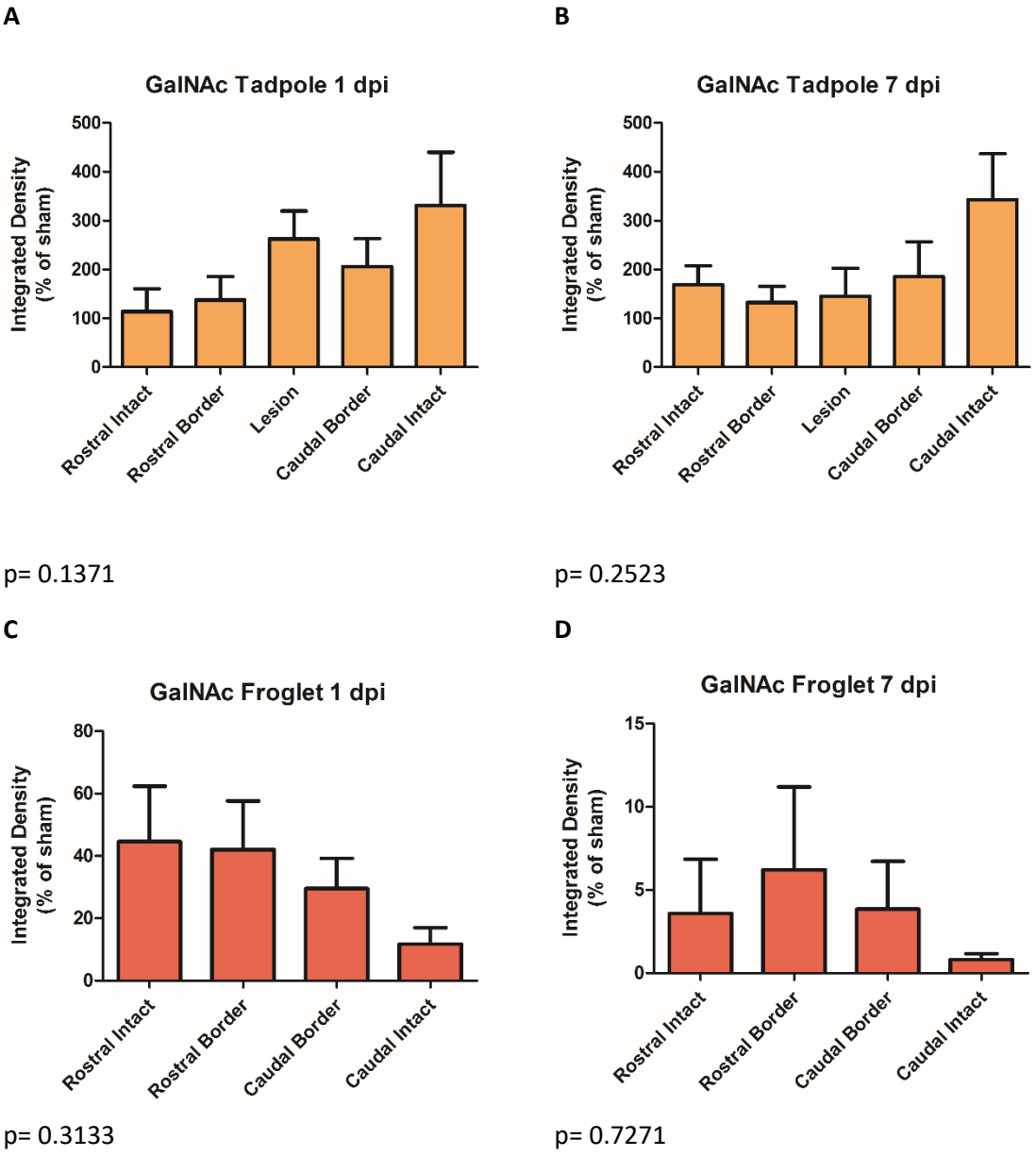

Figure 4.14 Comparison of sialic acid abundance throughout the regions of the spinal cord. Graphs show WFA lectin staining in spinal cord tissue in tadpole at 1 dpi (A) and 7 dpi (B) and in froglet at 1 dpi (C) and 7 dpi (D). Data was normalised to the relevant sham group and analysed using a one way ANOVA with Tukey's post hoc test. No statistical significance was observed. p values for each analysis are given under the relevant graph. A value of $p<0.05$ was considered significant.

Comparing tadpole and froglet across each time-point using data normalised to the sham it can be seen that the regenerative tadpoles increased the amount of GalNAc in response to transection and that there was very little change over the first seven days following the injury. This was true for both lesion borders and the intact tissue at the caudal end (Figure 4.15 B, C, E). The rostral intact tissue had an increased amount of GalNAc present between 1 and 7 dpi (Figure 4.15 D). While tadpole spinal cord increased GalNAc production, froglet spinal cord decreased GalNAc at both time-points following transection (Figure 4.15 B-E). There appeared to be a large difference between tadpole and froglet but no statistical significance was seen at the lesion borders (Figure 4.15 B, C). In the intact tissue however the amount of GalNAc present was significantly lower in froglet spinal cord than in tadpole for rostral tissue at 7 dpi, and for caudal tissue at both 1 and 7 dpi (Figure 4.15 D, E).

GalNAc expression in the lesion epicentre of tadpoles reduced from 1 to 7 dpi but remained above sham levels of expression, and no significant difference was detected (Figure 4.15 A).

Representative images for all groups and all ROIs are shown in Figure 4.16.

A

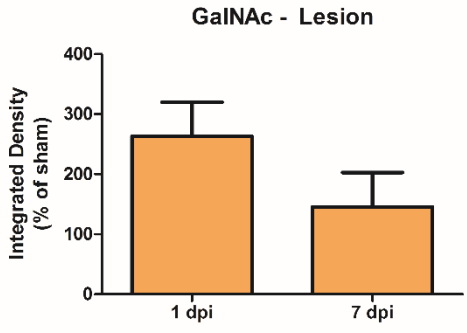

p= 0.1846;

B

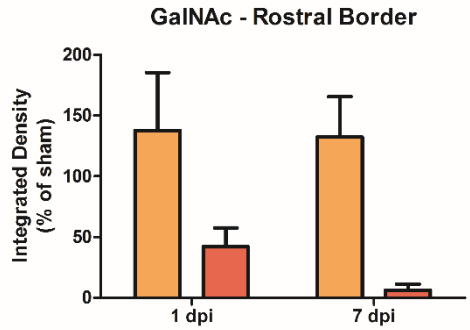

	p
Interaction	0.7082
Developmental Stage	0.0145
Row Factor	0.6164

C

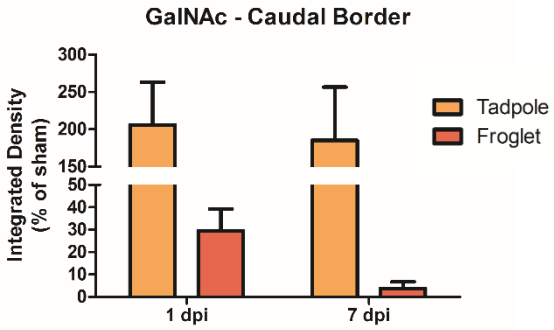

	p
Interaction	0.9689
Developmental Stage	0.0113
Row Factor	0.7136

D

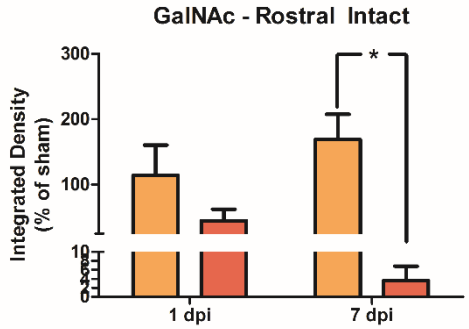

	p
Interaction	0.2700
Developmental Stage	0.0132
Time post injury	0.8718

E

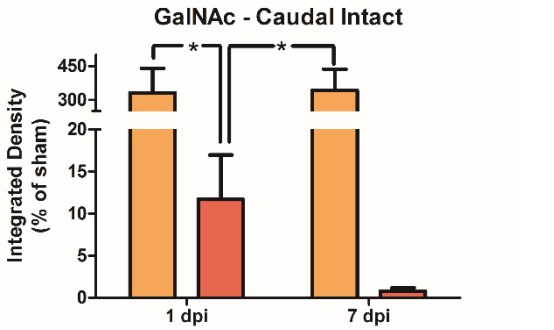

	p
Interaction	0.8854
Developmental Stage	0.0014
Time post injury	0.9966

Figure 4.15 Comparison of GalNAc abundance between pre- and post-metamorphic *Xenopus laevis* at 1 and 7 dpi. Graphs show WFA lectin staining in spinal cord tissue, comparing tadpole at 1 and 7 dpi (A), and comparing tadpole and froglet at 1 and 7 dpi (B-E). Data was normalised to sham before

analysis with two way ANOVA and Bonferroni's post hoc test. A value of $p<0.05$ was considered significant. Groups which differ significantly are indicated with an asterisk.

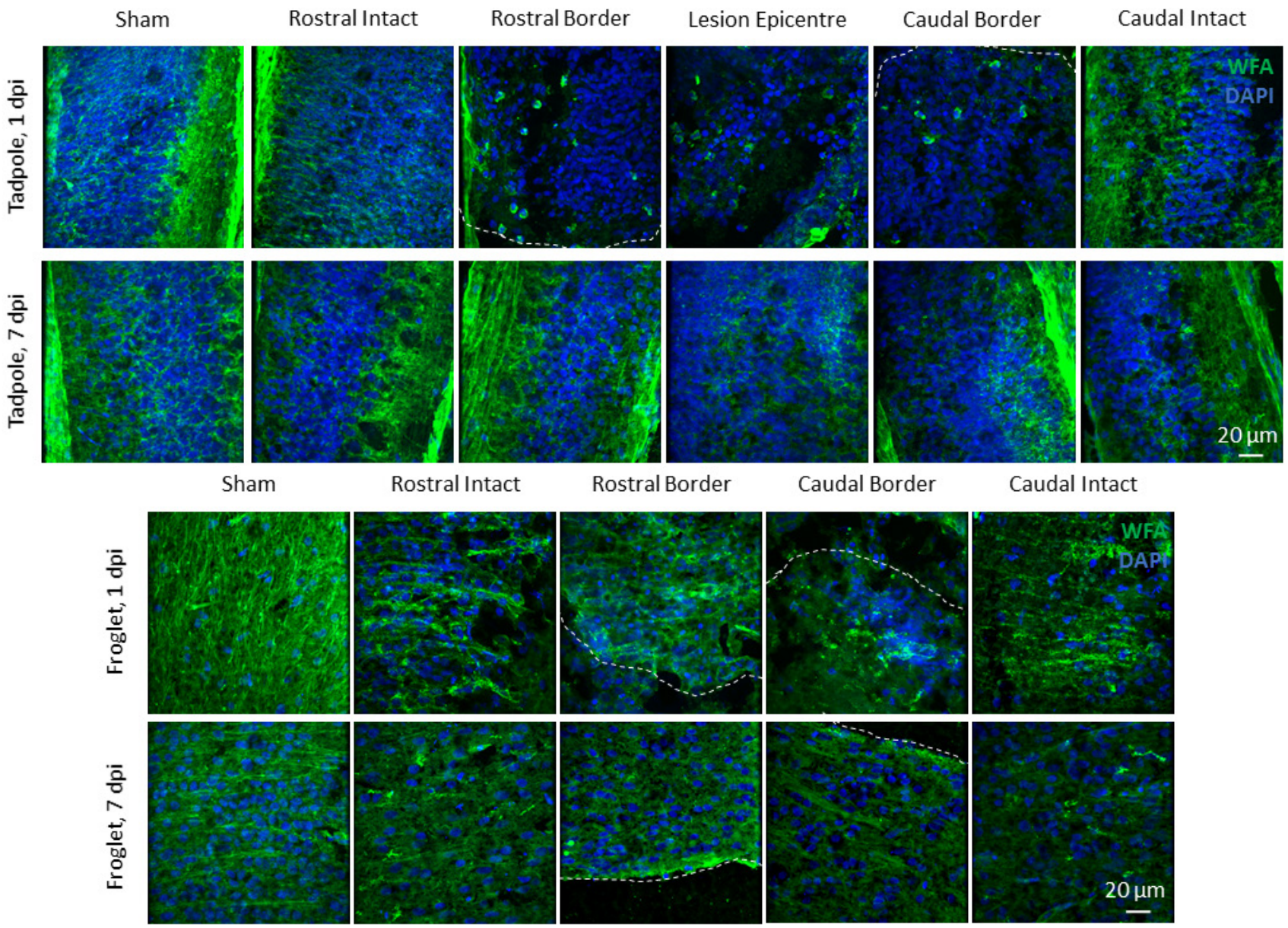
Sham
Rostral Intact
Rostral Border
Lesion Epicentre
Caudal Border
Caudal Intact
Tadpole, 1 dpi
Tadpole, 7 dpi
WFA
DAPI
20 µm
Sham
Rostral Intact
Rostral Border
Caudal Border
Caudal Intact
Froglet, 1 dpi
Froglet, 7 dpi
WFA
DAPI
20 µm

Figure 4.16 Representative images of GalNAc distribution in the spinal cord of pre- and post-metamorphic *Xenopus laevis* at 1 and 7 days following SCI. FITC-conjugated WFA lectin was used to label GalNAc. Nuclei were labelled with Hoechst (blue). The edge of the lesion is outlined with a white dashed line

4.5.5 Sugar abundance in sham injured tissue

To investigate whether the differential response to the injury may be due to baseline differences in the sugar expression at each developmental stage the sham data was compared for each monosaccharide in tadpole and froglets at 1 and 7 dpi using a two way ANOVA.

Staining for galactose with AIA a noticeable difference was seen between tadpole and froglet, both in the amount of galactose present and also in how this changes over time following exposure of the spinal cord to the external environment. The amount of galactose present in the tadpole sham injured spinal cord was much lower than in the froglet sham injured spinal cord at either time-point. In the tadpole galactose levels increased over the 7 day period, while in the froglet they declined. None of these differences reached statistical significance, Figure 4.17 A. Representative images can be seen in Figure 4.4.

With DSA lectin staining for β(1-4) GlcNAc a difference between tadpole and froglet was seen also. Similarly to the galactose result more GlcNAc was detected for froglets than for tadpoles and in both developmental stages there was an increase in GlcNAc levels over time. Two way ANOVA found developmental stage to be a significant contributor to GlcNAc level, and Bonferroni's post hoc test revealed a significant difference between tadpole and froglet sham groups at 7 dpi, Figure 4.17 B. Representative images can be seen in Figure 4.8.

Using SNA-I to investigate the amount of sialic acid in α(2-6) linkage there was again a difference between tadpole and froglet but for this sugar tadpole tissue produced more sialic acid than froglet. Tadpole spinal cord produced more sialic acid at 7 dpi than at 1 dpi whereas sialylation in the froglet spinal cord remained approximately the same over time. The differences between developmental stage were large but did not reach statistical significance, neither did the change over time in the tadpole spinal cord, Figure 4.17 C. Representative images can be seen in Figure 4.12.

Investigating GalNAc levels in sham tissue with WFA showed that froglet tissue produced more GalNAc than tadpole tissue. Two way ANOVA found developmental stage to significantly contribute to the

variance but Bonferroni post hoc testing did not find differences between any individual pairs of groups. With time, tadpole spinal cord increased the amount of GalNAc produced and froglet tissue slightly decreased GalNAc. Changes with time were not significant here, Figure 4.17 D. Representative images can be seen in Figure 4.16.

A

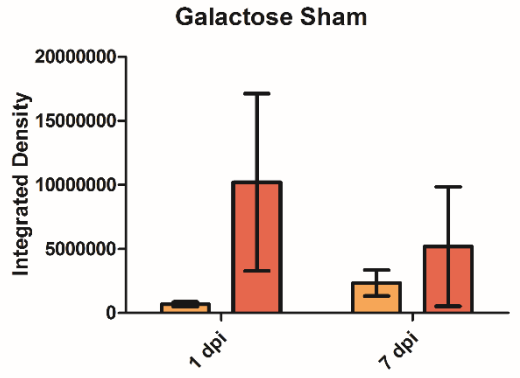

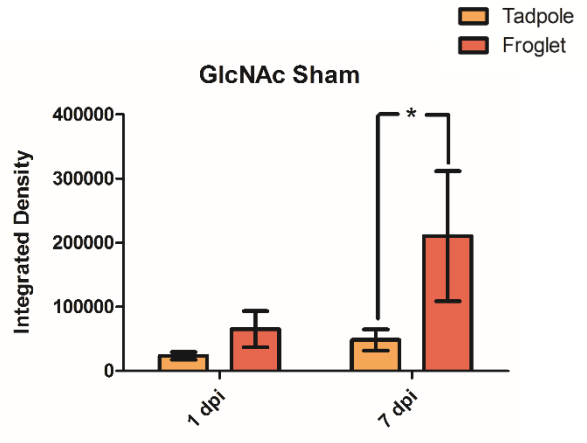

B

	p
Interaction	0.3353
Developmental Stage	0.0844
Time post injury	0.6246

	p
Interaction	0.1820
Developmental Stage	0.0335
Time post injury	0.0682

C

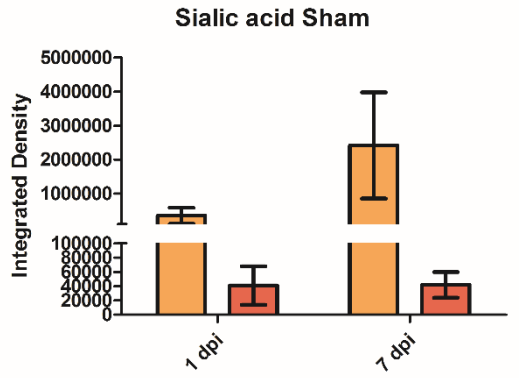

D

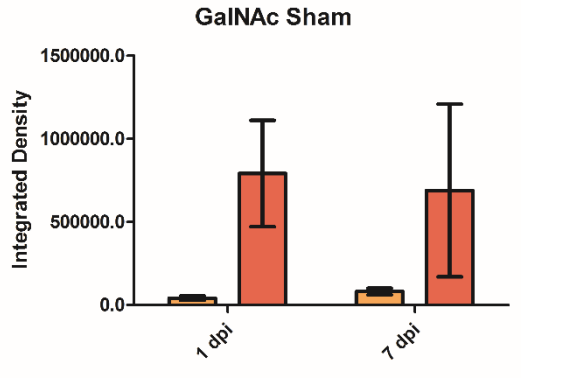

	p
Interaction	0.3360
Developmental Stage	0.2188
Time post injury	0.3356

	p
Interaction	0.7851
Developmental Stage	0.0176
Time post injury	0.9043

Figure 4.17 Changes in sugar abundance following spinal cord transection in pre- and post-metamorphic *Xenopus laevis* at 1 and 7 dpi. Graphs show lectin staining in sham injured tissue at 1 and 7 dpi. (A) Galactose, (B) GlcNAc, (C) sialic acid, (D) GalNAc. Data was analysed with a two way ANOVA and Bonferroni's post hoc test. For all tests a value of $p<0.05$ was considered significant. Groups which differ significantly are indicated with an asterisk.

4.5.6 Lectin signal does not co-localise with tubulin positive neurons or GFAP positive astroglia

In an attempt to identify the cell types producing each of these sugars dual staining was performed with the lectin together with either a neuronal marker or a glial marker. Acetylated-tubulin was chosen to label neurons, GFAP to label astrocytes. Surprisingly, no colocalisation was seen with either marker for any of the four lectins studied, in any region of interest, in either tadpole or froglet tissue. Representative images from the tadpole lesion site at 1 dpi are shown here to illustrate the lack of colocalisation (Figure 4.18).

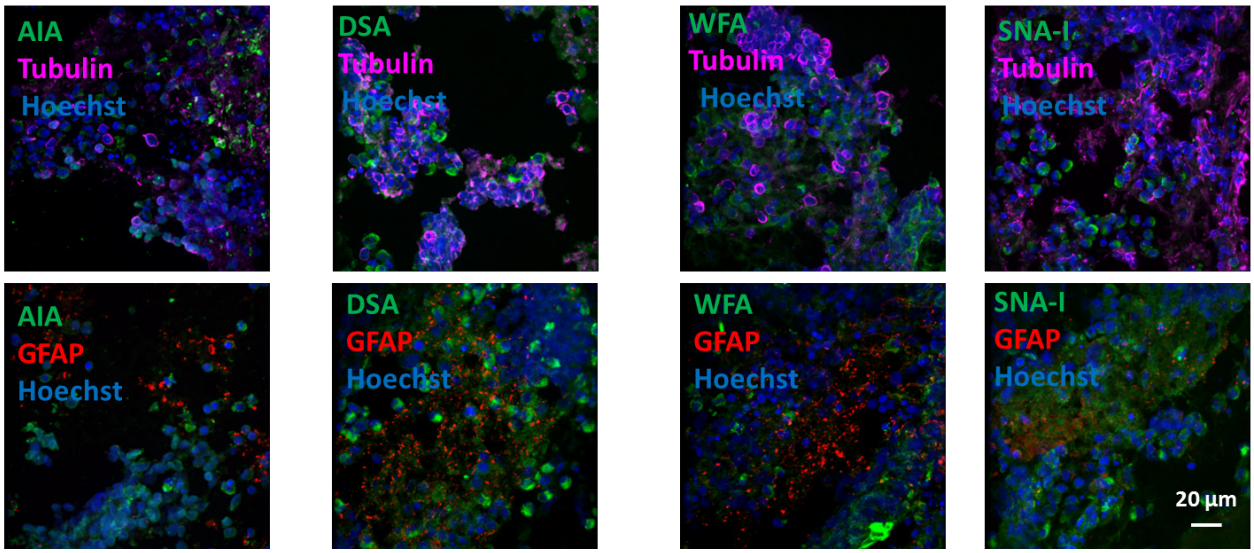

Figure 4.18 Representative images of the lesion epicentre of injured tadpole spinal cord at 1 dpi. All lectins are FITC conjugated and shown in green, AIA labels galactose, DSA labels GlcNAc, WFA labels GalNAc and SNA-I labels sialic acid. Tubulin was used as a neuronal marker and is shown in magenta, GFAP was used as an astrocytic marker and is shown in red. All nuclei were stained with Hoechst (blue). Scale bar for all images = 20 µm.

4.6 Discussion

The work outlined above is the first attempt to uncover the glycosylation changes which accompany SCI in a regenerative organism such as *Xenopus laevis.* Very little is known regarding glycosylation changes which occur alongside traumatic CNS injury in general, and nothing at all in terms of the difference in glycosylation changes between regeneration competent or non-competent species. The work outlined in this chapter is by no means comprehensive but serves as a first step in investigating the role of glycosylation specifically and post-translational modifications in general, in the context of regenerative success and failure.

A point to note with the data presented here is the high variance associated with each group for each sugar, represented by standard error of the mean on the graphs. There are a number of possible reasons for this, including the natural variance which occurs with most biological samples and investigations, as well as some limitations of the technique. The technique used here employed fluorescently labelled lectins which were applied to fixed tissue sections and imaged using confocal microscopy. Lectins are glycan binding proteins which occur naturally in all species, the ones used here were isolated from plants. Each lectin has an affinity for a particular monosaccharide, usually binding when this monosaccharide occurs as a terminal residue, and some have a preference for the linkage of this monosaccharide to the next in the chain, for example SNA-I used here has a preference for α(2-6) linked sialic acid over α(2-3) linked sialic acid. However the affinities and specificity for the indicated sugars may be reduced in the context of more complex glycoconjugates, or altered by the presence of other monosaccharides in close proximity (Wu *et al.*, 2008; Cummings RD, 2009), and it is recognised that many lectins also possess protein binding capabilities (Barondes, 1988). For this reason all results presented here should be treated as preliminary data, and warrant further investigation with more sophisticated techniques such as HILIC-UPLC or mass spectrometry which are techniques that are employed in later chapters.

The lectins used here were purchased directly conjugated to FITC (which fluoresces green). *Xenopus laevis* spinal cord tissue fixed in PFA was found to have a reasonably high level of background autofluorescence, which was picked up with the same microscope filter sets as those used for FITC fluorescence. Effort was made to reduce this, by exposing the tissue to light prior to staining but this did not improve the signal to background ratio. Further effort was made to account for this at the stage of image analysis, by thresholding for positive signal and only measuring within a specified range deemed to be higher than the background. This was found to be reliable for those groups in which there was a high degree of binding and a clear difference between positive signal and background autofluorescence, but in those groups with a lower level of positive staining it was difficult to distinguish between positive signal and background noise. For future lectin histochemistry work it may be preferable to use a chromogenic detection method as opposed to fluorescent. The use of a biotinylated lectin which can then be targeted with the detection method of choice may allow for signal amplification and clearer identification of positive signal above background. If fluorescence is necessary, for example to allow for double staining with antibodies and identification of cell types as above, then a TRITC labelled lectin may be more practical, since red autofluorescence was far less pronounced in the tissue than green.

The lack of statistical significance between groups in these studies was surprising considering the apparently large differences between the means for many treatment groups, for example with galactose (Figure 4.3 A-D) and GlcNAc (Figure 4.6 B). The large standard errors are likely to account for this, as discussed above, as well as the differences in n numbers between groups. The mismatch in n numbers was not ideal and were due to technical difficulties in obtaining tissue of sufficient quality to determine the lesion itself and the surrounding ROIs. The spinal cord of tadpole *Xenopus laevis* is very narrow in diameter and so while cryosectioning it was difficult to obtain the tissue in the correct orientation to collect lesion area and the tissue both rostral and caudal on each section. Froglet tissue was also particularly scarce as it took a long time to grow animals through all the developmental stages.

All of the factors above make it hard to interpret the results reliably. However we can make some general conclusions, the most important of which is that there are clear changes in glycosylation associated with the response to spinal cord transection, and that these changes differ between regeneration competent and regeneration incompetent stages. The features of the glycans present also change over time following injury in both developmental stages. This suggests that there are active changes in the glycosylation pathway which plays a role in determining the success or failure of spinal cord regeneration. Unravelling these specific motifs and the proteins or lipids that they decorate may be key to understanding the response to injury and later manipulating it in terms of treatment.

The lectins chosen for this study were picked to examine some key features of *N*-glycans, which are considered one of the most widespread post-translational modification on proteins (Khoury *et al.*, 2011), and also to give an indication of the level of CSPGs present in the tissue, which have been established as important inhibitors of regeneration in mammalian SCI (Morgenstern *et al.*, 2002). The likely binding interactions of the chosen lectins with *N*-glycans is demonstrated in Figure 4.19. DSA lectin binds GlcNAc (Section 4.5.2) which is key to establishing the degree of branching of an *N*-glycan, as opposed to its being high mannose type. AIA lectin binds galactose (section 4.5.1) which is the most commonly found decoration on a GlcNAc residue. SNA-I lectin binds sialic acid (Section 4.5.3) which may be attached to galactose to terminate a branch of a complex *N*-glycan. As sialic acid is a charged residue it may possibly influence the activity of a protein to a greater extent than any other sugar residue and so may be a key influencer of biological activity. Galactosylation (Ercan *et al.*, 2010) and sialylation (Saldova *et al.*, 2013; Chrostek *et al.*, 2014) changes have been linked with inflammatory diseases (as introduced in Section 1.5.7), and were considered here (Sections 4.5.1 and 4.5.3 respectively) as being particularly interesting candidates in investigation of SCI as an injury with unresolved inflammation as part of its characteristic pathology.

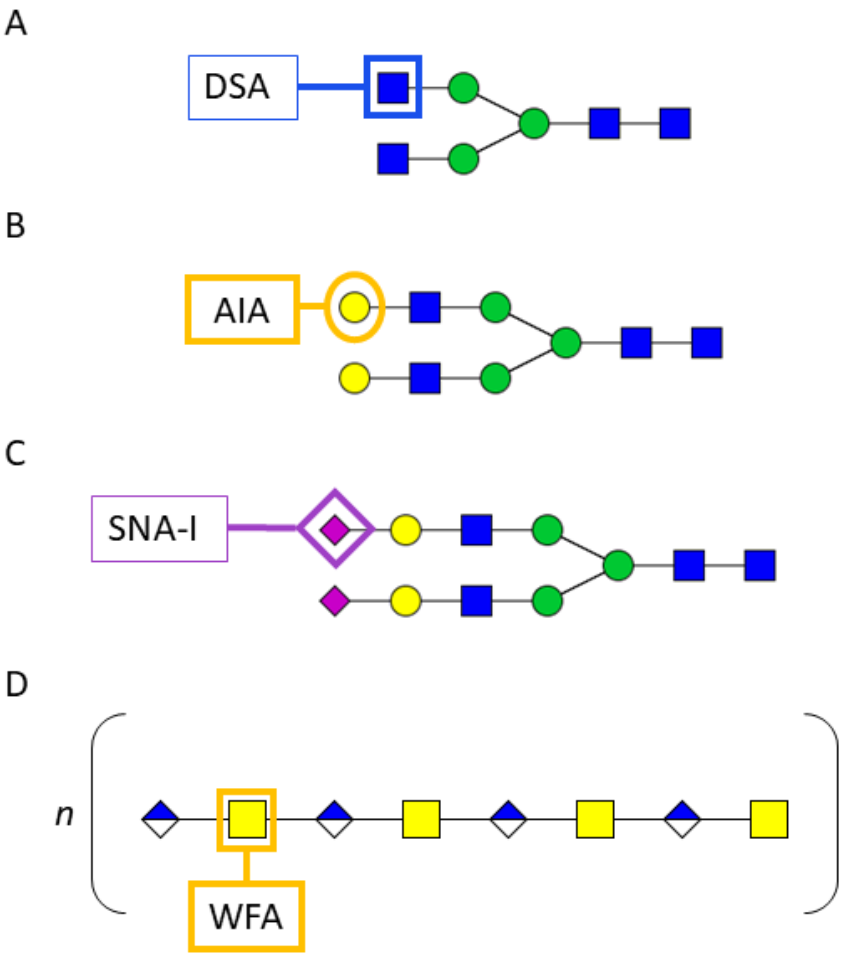

Figure 4.19 The likely binding interactions of the lectins used in this study with *N*-linked glycans: GlcNAc (A), galactose (B), sialic acid (C) and proteoglycan chains of CSPGs: GalNAc (D). Monosaccharide residues are most accessible to lectin binding when in a terminal position. Blue squares, GlcNAc; green circles, mannose; yellow circles, galactose; magenta diamond, sialic acid; blue and white diamond, glucuronic acid.

The initial increase in GlcNAc in the vicinity of the injury (Figure 4.7 A, B, C) may be interpreted in one of two ways: there may be an increase in *N*-glycan branching or a decrease in substitution on the antennae with galactose and/or fucose and/or sialic acid. An increase in branching may mean a reduction in high mannose species with a resulting preference towards complex glycans, or it may mean the complex glycans themselves are becoming more highly branched, i.e. tri- and tetra-antennary glycans are becoming more abundant than mono- and di-antennary glycans. A schematic

to explain this idea is shown in Figure 4.20 A-C. From this analysis it is impossible to determine which of these phenomena are occurring, and a more detailed technique such as HILIC-UPLC would yield far more information. Whichever has occurred is clearly a transient phenomenon as the amount of detectable GlcNAc was reduced by 7 dpi in both tadpole and froglet in the vicinity of the lesion (Figure 4.7).

Examining the GlcNAc result in isolation would also suggest the possibility that antennae which were decorated with galactose residues are now losing galactose and the branches are becoming shorter, for example in Figure 4.20 B. However the AIA result reveals the same pattern as the DSA result, i.e. galactose is increased in parallel with GlcNAc at the early time-point (Figure 4.3), showing that a loss of terminal galactosylation is not the case. Of course there may be a combination of the two: there may be an increase in *N*-glycan branching accompanied by an increase in galactosylsation, with many GlcNAc residues remaining undecorated, and so accessible to the DSA lectin, for example in Figure 4.20 A.

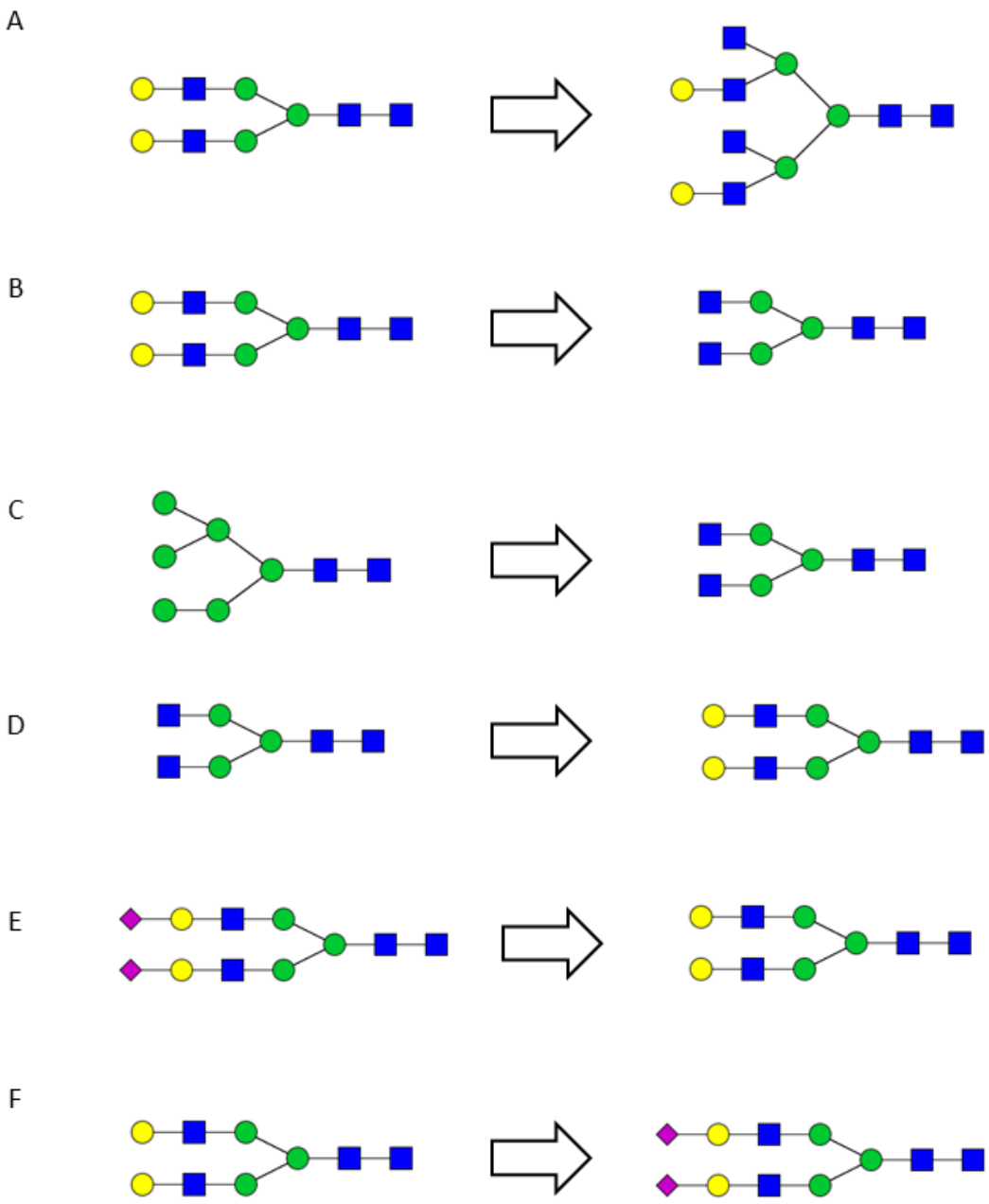

Figure 4.20 Potential changes in *N*-glycan structures indicated by the observed changes in lectin binding. (A, B, C) indicate potential changes in structure which would result in increased GlcNAc binding. (D, E) indicate potential changes which would increase AIA binding. (F) indicates potential changes which would increase SNA-I binding. All structures in this figure are simplistic glycans included to illustrate the idea, and should not be interpreted as defined structures detected in the tissue. Blue squares, GlcNAc; green circles, mannose; yellow circles, galactose; magenta diamond, sialic acid.

Sialic acid decoration increased compared to sham at 1 dpi in the tadpole also (Figure 4.11). This together with the increase in GlcNAc and galactose suggests an overall increase in the complexity and branch elongation of glycans following transection injury in the tadpole spinal cord. Figure 4.21 attempts to demonstrate this increased glycan complexity. This effect occurs transiently within the first day post injury. For all three lectins, signal was reduced in intensity by 7 dpi in the tadpole which is the time-point when a tissue bridge was observed connecting the severed ends of the spinal cord. Perhaps this increase in glycan complexity is necessary to drive neuronal growth. This idea is supported by the widespread neurodevelopmental and neurological deficits seen in the congenital disorders of glycosylation, where one or more enzymes are impaired, leading to a loss in glycan complexity (Freeze *et al.*, 2015). In particular, *N*-glycosylation has been shown to be essential for neuronal growth and migration in the cerebellum, in a mouse model deficient for the enzyme responsible for the first step in *N*-glycan synthesis (Medina-Cano *et al.*, 2018).

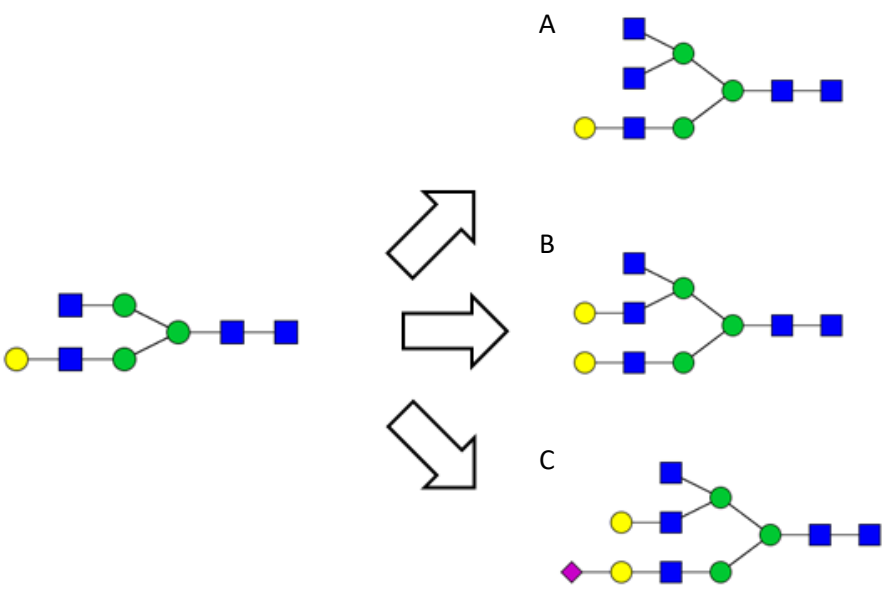

Figure 4.21 An example of possible structures which can be interpreted from the combined result of increased binding with DSA, AIA, and SNA-I. (A) Increased DSA binding (B) increased DSA and AIA binding (C) increased DSA, AIA and SNA-I binding. The glycans shown in the diagram are greatly simplified and serve only to illustrate a possible interpretation, they are not to be interpreted as specific glycans identified. Blue squares, GlcNAc; green circles, mannose; yellow circles, galactose; magenta diamond, sialic acid.

The increase in GlcNAc after injury occurred in the tadpole to a larger extent than in the froglet (Figure 4.7), while the increase in galactose was quite similar between the two (Figure 4.3). The increase in sialylation on the other hand was much more pronounced in the froglet than in the tadpole (Figure 4.11). These fine differences in the glycosylation response suggest that there is a specific signature required for regeneration, and not just a general increase in complexity and elongation of glycan branches (such as that illustrated in Figure 4.21). The sialic acid response in particular was significantly higher in the froglet than in the tadpole, although both were increased relative to the relevant sham group (Figure 4.11). Perhaps an increase in sialic acid is necessary for repair but within a certain range: too much sialylation may be detrimental. This is interesting in the context of inflammation and the lack of resolution of inflammation in the non-regenerating mammalian spinal cord.

WFA was used to investigate GalNAc which is a major component of the GAG chains found on CSPGs. CSPGs have been proposed to contribute some of the neurite inhibitory properties of the glial scar which forms after mammalian SCI, and the inhibitory properties have been attributed to the GAG portion by chondroitinase experiments (Bradbury *et al.*, 2002; Bartus *et al.*, 2014). The result for GalNAc here was surprising, as there was an increase in the amount of GalNAc detected in the tadpole spinal cord after transection. In addition there was less GalNAc detected in the non-regenerating froglet spinal cord (Figure 4.15). GalNAc in the froglet spinal cord even decreased with time after injury. Even more surprisingly there was no reduction in GalNAc at the later time-point in the tadpole spinal cord (Figure 4.15). This result contradicts the established idea of CSPG GAG chains inhibiting neuronal growth and further investigation in this model may be of use. It is also possible that the sugar components of CSPGs influence the repair process differently depending on the temporal stage post injury (Rolls *et al.*, 2008; Carter *et al.*, 2011; Bartus *et al.*, 2014) . Perhaps proteoglycan deposition at early time-points is beneficial, for example in containing the injury, one of the proposed benefits of the glial scar (Adams and Gallo, 2018), with the negative effect coming into play with sustained presence of CSPGs.

Very few differences were seen across the various ROIs (Figure 4.2, Figure 4.6, Figure 4.10, Figure 4.14) suggesting that glycosylation responses are widespread throughout the injured tissue and not just confined to the immediate lesion area. One exception however is the amount of detectable GlcNAc present in the tadpole at 7 dpi where the response was greater in the intact tissue at 7 dpi (Figure 4.6 B). This may be interesting from an intervention point of view as it informs which part of the tissue should be targeted with a particular therapeutic.

The finding that there are differences in glycosylation between the sham groups comparing both time-point and developmental stage was particularly interesting. This may be due to differences in the glycans present at each developmental stage regardless of injury, or may be a result of removing the protective tissue surrounding the spinal cord and exposing it to the external environment. The changes in glycosylation in sham tissue between 1 and 7 dpi suggest that it was primarily the latter. This result reinforces the importance of using sham injury as the negative control in SCI studies as opposed to using naïve spinal cord. For statistical analysis the response to transection was normalised to the sham to ensure that any findings were due to the transection of the spinal cord itself and not simply to exposing the cord to the surrounding environment.

Of course all of the above interpretations of results are limited by the inability to be sure where the detected monosaccharides are located, whether they are part of *N*-glycans or proteoglycans as discussed, or whether they are actually contributing to *O*-glycans or glycosphingolipids, which are very

prominent in the nervous system, or even occurring as free glycans. This could be further investigated with the use of enzymes to release different types of glycans from the glycoconjugate, followed by a lectin blot for example. The enzyme PNGaseF releases *N*-glycans from the protein, ceramidase releases glycans from many glycolipids. *O*-glycans are more difficult to release and are generally released by hydrazinolysis. Following the release of the various glycan types from their associated molecule, the lectin histochemistry experiment could be repeated to try to establish the source of the monosaccharides identified above.

Changes in glycosylation in the lesion epicentre could only be detected in the tadpole as this region could not be stabilised during tissue processing of the froglet spinal cord. DSA and AIA were seen to label a population of cells which infiltrated this area at 1 dpi. They appeared as small round cells, and were not immuno-reactive for alpha-tubulin or GFAP, making them difficult to identify. However from the literature it can be proposed that these may be the Sox2/3 positive neuronal precursor cells and these cells have been shown to populate a similar area in the model studied by the Larrain group (Gaete *et al.*, 2012; Munoz *et al.*, 2015). Perhaps a high degree of GlcNAcylation and galactosylation are characteristics of immature neural precursor cells, which is lost as they differentiate into neurons and/or glia. Neural stem cells in the mouse can be isolated from a mix of cell types using the E-PHA lectin, suggesting that they have a distinct surface glycosylation signature (Hamanoue *et al.*, 2009). Colocalisation between lectins and alpha-tubulin or GFAP could not be found in other ROIs either. This is surprising as all cells carry a dense glycocalyx on their outer surface, and so theoretically these lectins should label all cell types. Possible explanations are that these lectins are labelling immature cells which do not yet express these established markers; it has been revealed that GFAP expression is generally localised in the processes of glia and is not seen close to the cell body (Edwards-Faret *et al.*, 2018), although acetylated tubulin can be observed throughout development (Chu and Klymkowsky, 1989). The lectins may also be labelling other glia such as microglia or oligodendrocytes or potentially sugar residues on matrix proteins.

5 Chapter 5 - Inflammation and Scar Deposition following SCI and Collagen Hydrogel Implantation in a Rat Transection Model

5.1 Introduction

This chapter is concerned with establishing how treatment of a spinal cord transection injury with a collagen hydrogel, in which the collagen fibres are highly aligned, may influence inflammation and scarring within the first month post-injury. This was investigated using a pilot study in the rat, from which time-points for a second, more in depth molecular study were chosen (the second study is described in Chapter 6). Chronic inflammation is major hallmark of SCI, as is the formation of glial and fibrotic scars, all of which contribute to the failure of regeneration in mammalian species. We believe that understanding and manipulating the inflammatory and scarring processes in the acute and sub-acute phases may reduce their impact at later stages, and so influence the spinal cord regenerative potential. Here we use collagen in the form of an aligned hydrogel. Collagen hydrogels have been successfully used in the CNS without any excessive inflammatory response (Hoban *et al.*, 2013; Moriarty *et al.*, 2017) and have even been shown to alleviate inflammation in the injured spinal cord (Breen *et al.*, 2016). As outlined in the Introduction (Section 1.3.1) the fibrillar nature of collagen allows for the creation of aligned structures. This property was used here with the aim of providing a substrate for directed axonal outgrowth or cell migration across the injury (examined in the thesis of Aniket Kshirsagar). This chapter examines the influence of the aligned collagen hydrogel on the scarring and inflammatory processes following spinal cord transection.

There are two classes of scar which develop after an SCI in mammals, namely the glial scar and the fibrotic scar. The fibrotic scar is more commonly a consequence of transection type injuries where the meninges have been disrupted and there is an invasion of meningeal cells into the spinal cord parenchyma. These cells, together with the spinal cord glia, then produce a dense ECM rich in collagens, proteoglycans and other ECM proteins. Due the density and often the alignment of this ECM scar it can act as a barrier to regrowing axons attempting to cross the injury site. This inhibition has been proposed to result from the presence of semaphorin III A and the ephrins with their receptors (Hermanns *et al.*, 2001). The glial scar, as the name suggests, is composed mainly of reactive glia, most noticeably astrocytes but also other cells including microglia, oligodendrocyte precursor cells, endothelial cells and others. These reactive glia form a wall composed of their tightly interconnected processes together with CSPGs which have been shown to be mainly growth inhibitory in nature, although growth permissive CSPG species have also been identified (Morgenstern *et al.*, 2002; Miller

and Hsieh-Wilson, 2015). Overcoming the inhibition resulting from these two types of scar may be key to achieving repair after SCI.

Inflammatory activity typically begins within hours of the initial injury but fails to resolve over time. The first stage of inflammation after SCI is the transient invasion of neutrophils which arrive at approximately 24 hours post injury but which are no longer detectable by 3 dpi (Norenberg *et al.*, 2004). Microglia and macrophage response becomes important at this stage: microglial activation occurs around 1 dpi, and infiltration of peripheral macrophages occurs over the following days and weeks (Popovich *et al.*, 1997). Macrophages have been seen to persist in the injured spinal cord over long periods of time, and a second wave of infiltration has even been detected at 60 dpi (Kjell and Olson, 2016). T-cells have been identified in the injured spinal cord (Brennan and Popovich, 2018), but not much is known about the timeline of their arrival and departure, or what roles they may play. Microglia and macrophage response is the main focus for this chapter.

5.2 Hypothesis

Scarring and inflammation resulting from spinal cord transection can be alleviated with aligned collagen hydrogel treatment.

5.3 Objectives

1. Examine proteoglycan deposition over time in response to transection and aligned collagen treatment
2. Examine endogenous collagen deposition over time in response to transection and aligned collagen treatment
3. Determine the inflammatory phenotype of microglia / macrophages over time in response to transection and aligned collagen treatment

5.4 Experimental design

This chapter describes a pilot time-course study in the rat to determine the time-points following injury where an aligned collagen hydrogel makes the greatest impact following transection SCI. For this study small n numbers were used (n=3) and only two experimental groups: transection only and transection with aligned hydrogel treatment, full details are shown in Table 5.1. The surgical procedure, post-procedural care and tissue collection were performed as in Sections 2.2.1, 2.2.2 and 2.2.3.

Time-point	**Experimental group**	**n**
3 dpi	Transection only	3
	Transection + aligned hydrogel	3
7 dpi	Transection only	3
	Transection + aligned hydrogel	3
14 dpi	Transection only	3
	Transection + aligned hydrogel	3
21 dpi	Transection only	3
	Transection + aligned hydrogel	3
28 dpi	Transection only	3
	Transection + aligned hydrogel	3

Table 5.1 Experimental design for pilot study of spinal cord transection in the rat.

Proteoglycan deposition was measured using the alcian blue stain (Section 2.6.1) as an indication of the ECM component of the glial scar. Collagen deposition was measured using the Masson's trichrome stain (Section 2.6.2) as an indication of fibrotic scarring. Images were acquired using the Olympus VS120 digital slide scanner, at 20x magnification in brightfield mode and analysed using the stereology point counting method as described in Section 2.7.5. Proteoglycan and collagen deposition were measured in the lesion epicentre, scar zone and in intact tissue.

Triple antibody staining was used to attempt to determine the functional phenotype of resident microglia and infiltrating macrophages following spinal cord transection. Each slide was stained with three antibody markers: CD11b to label all microglia and macrophages, iNOS to label those behaving as pro-inflammatory, tissue damaging cells (M1 type), and Arginase-1 to label those cells with an anti-inflammatory, tissue repair phenotype (M2 type).

Immunohistochemistry for these markers was performed as described in Section 2.3.2. Images were acquired using the digital slide scanner, at 20x magnification in fluorescent mode (Section 2.7.6) and exported to Fiji for analysis. Quantification was performed using the hue threshold function in Fiji so that red cells (iNOS positive only) green cells (Arginase-1 positive only) or yellow 'transitional' cells (double positive for both markers) could be counted in an unbiased manner, see Section 2.7.6. The CD11b marker was used as a visual aid to ensure all iNOS or Arginase cells being analysed were in fact microglia or macrophages. No quantitative analysis was performed on the CD11b labelled cells.

5.5 Results

5.5.1 Scar deposition and extracellular matrix composition

5.5.1.1 Effect of collagen hydrogel on proteoglycan deposition in transected rat spinal cord

Within the lesion epicentre there was little change in alcian blue staining between groups and over time, while this was decreased in the scar zone, and remained reasonably constant far from the lesion, Figure 5.1.

No differences in proteoglycan deposition were seen between transection only and hydrogel treated groups in the lesion epicentre (Figure 5.1B) except at 3 dpi. At this early time-point there was significantly more proteoglycan present in the transection only group (Vv approximately 0.4) compared to hydrogel treated (Vv <0.05, $p<0.05$). From 7 dpi onwards similar amounts of proteoglycan were observed in each group and there was no change between 7 and 28 dpi.

In the scar zone proteoglycan decreased over time (Figure 5.1C). At 3 dpi there was a high proportion of proteoglycans in the tissue, (Vv approximately 0.7), with no difference between experimental groups. Proteoglycan gradually reduced over time in this region with Vv at 28 dpi approximately 0.2 for transection and 0.25 for hydrogel treated.

In the area far from the lesion the amount of proteoglycan changed minimally with regards to time and treatment, Figure 5.1.

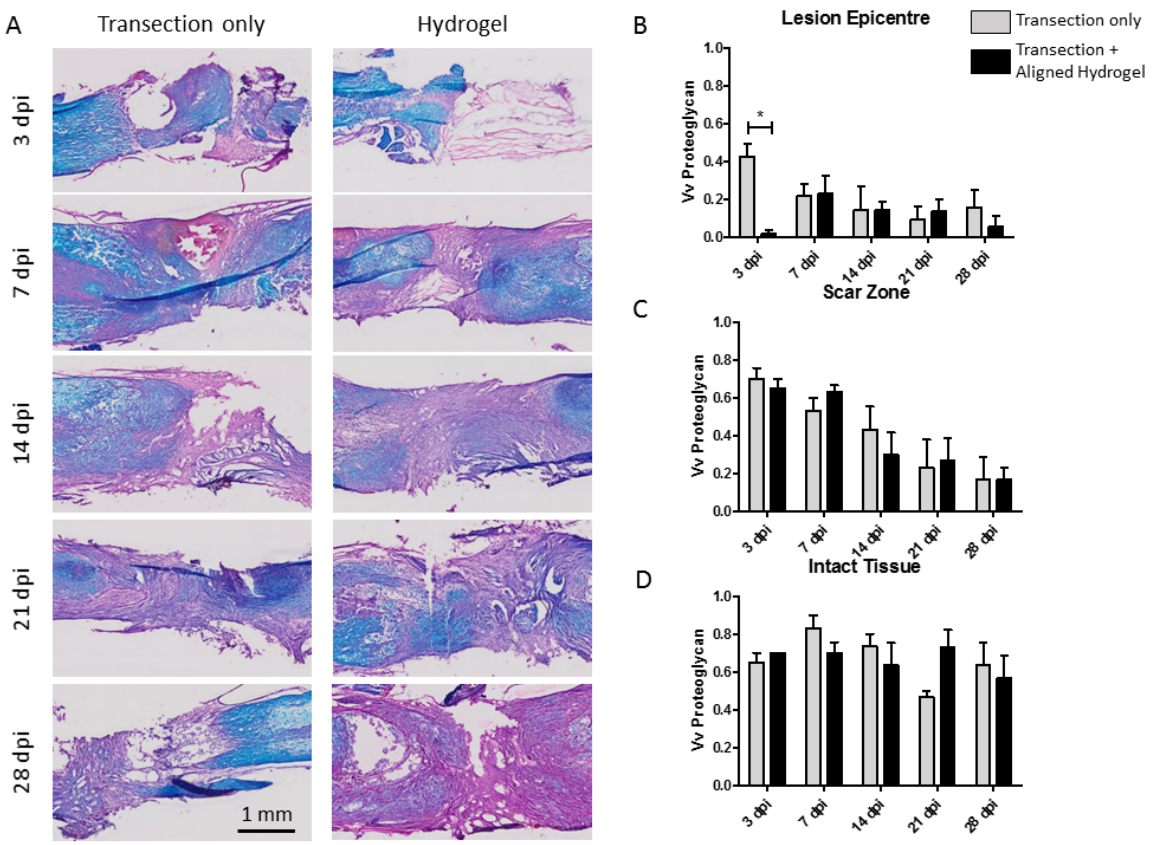

Figure 5.1 Alcian blue demonstrates the change in proteoglycans in the ECM over time and in response to treatment following transection injury. Photomicrographs show alcian blue staining in the transection only and transection + aligned hydrogel treated rat spinal cord at 3, 7, 14, 21 and 28 dpi (A). Scalebar = 1 mm. Proteoglycans are stained in bright blue. Graphs show Vv alcian blue staining in the lesion epicentre (B), scar zone (C) and intact spinal cord tissue (C). Data is shown as mean ± SEM. Data was analysed by one way ANOVA with Bonferroni's post hoc test, $p<0.05$, $n=3$. Significant differences between groups are indicated with an asterisk, *.

5.5.1.2 Effect of collagen hydrogel on collagen deposition in transected rat spinal cord

Masson's trichrome staining showed very small changes in collagen composition in the injured spinal cord for all regions examined. In general, the hydrogel treated group had a slightly higher proportion of collagen, but this difference was small and not found to be statistically significant, Figure 5.2.

In the lesion epicentre the amount of collagen present was much higher in the hydrogel treated group at 3 dpi, this is likely due to the histological stain marking the hydrogel itself. There was a reduction in collagen for both experimental groups at 7 dpi before increasing again at 14 dpi. Between 14 and 28 dpi the amount of collagen remained stable in both experimental groups. The proportion of collagen was much lower at 7 dpi compared to 3, 14, 21 and 28 dpi in both experimental groups, Figure 5.2 B.

There were no significant differences in collagen deposition between groups in the scar zone. Very low amounts of collagen were present in the two groups at 3 and 7 dpi. From 14 to 28 dpi there was a small increase in collagen deposition for both groups compared to the earlier time-poionts. At all time-points there was slightly more collagen in the aligned hydrogel treated group, but this was not significant, Figure 5.2 C. The alignment of Masson's trichrome stained collagen fibres in the tissue of the scar zone appeared to be highly ordered and aligned, not only in the hydrogel treated group, but in the transection only group also (Figure 5.3).

In intact appearing tissue far from the lesion there was a slight increase in the amount of collagen present over time, with similar amounts present in the transection only and hydrogel treated groups, Figure 5.2 D.

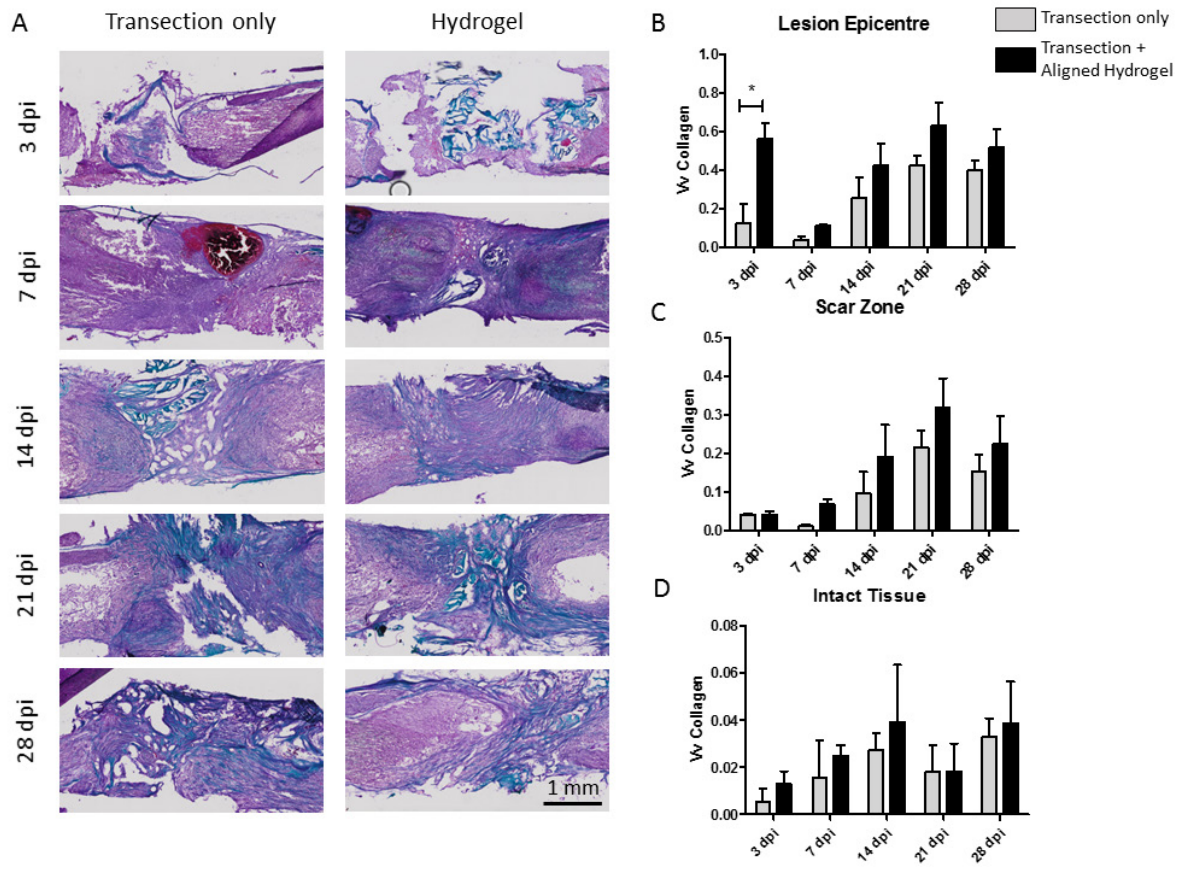

Figure 5.2 Masson's trichrome for the study of collagen deposition in the transected spinal cord. Photomicrographs show Masson's trichrome staining in the transection only and transection + aligned hydrogel treated rat spinal cord at 3, 7, 14, 21 and 28 dpi (A). Scalebar = 1 mm. Collagen is stained a blue/turquoise colour. Graphs show Vv Masson's trichrome staining in the lesion epicentre (B), scar zone (C) and intact spinal cord tissue (D). Data is presented as mean ± SEM. Two-way ANOVA with Bonferroni's post hoc test, $p<0.05$, n=3. Statistical difference is indicated with an asterisk, *.

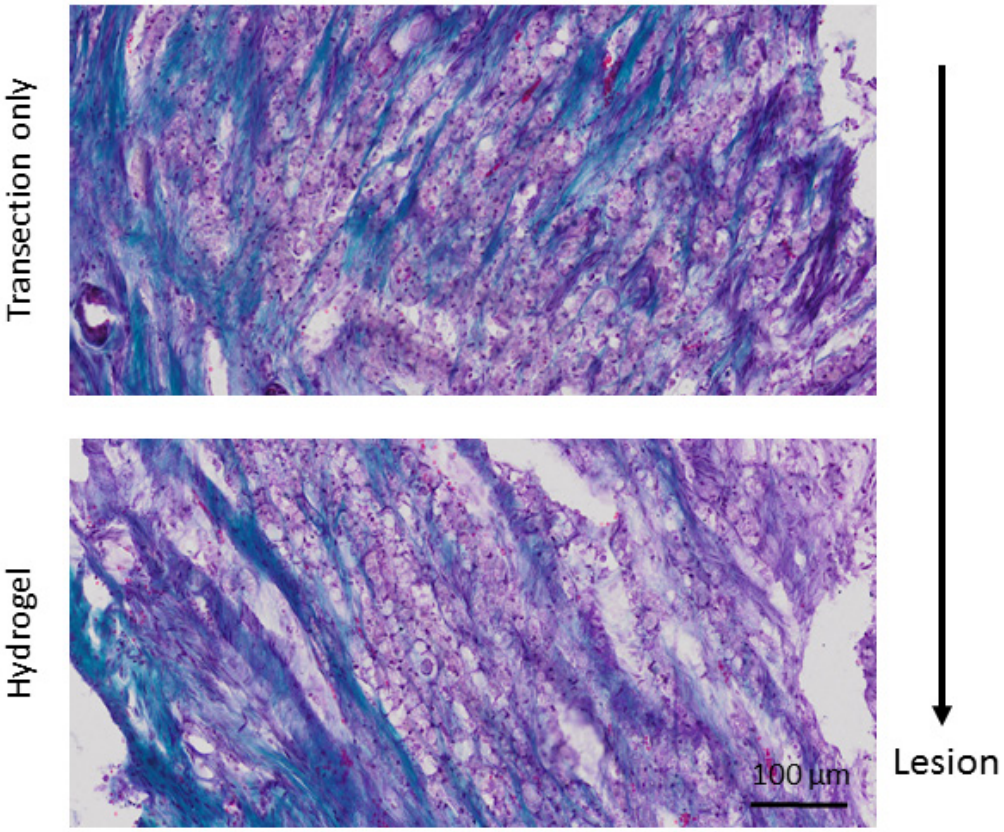

Figure 5.3 Photomicrographs show collagen deposition in the injured and collagen hydrogel treated spinal cord in the scar zone at 28 dpi. Endogenous collagen is laid down in an organised manner. Scalebar = 100 µm. Collagen is stained a blue/turquoise colour. The arrow indicates the region of the lesion in relation to the location within the tissue that both these images were acquired. Images were captured immediately adjacent to the lesion.

5.5.2 Time-course of microglia and macrophage polarisation in injured rat spinal cord

To study microglia/macrophage phenotype over time the injured cord was divided into four regions of interest (lesion epicentre and scar zones A, B and C) as described in Section 2.7.6. The phenotype was determined based on expression of either of two enzymes, iNOS or Arginase-1. iNOS expression was indicative of a pro-inflammatory phenotype, Arginase-1 expression suggested an anti-inflammatory phenotype. In reality many cells expressed both markers, these were considered to have a 'transitional' phenotype. Examination of microglia/macrophages within each ROI with respect to time and treatment group revealed some changes: the two-way ANOVA test revealed that time-point was a significant contributor to variance for Arginase-1 positive cells, iNOS positive cells and transitional cells for all ROIs, but there were no significant differences observed between groups using Bonferroni's post hoc test (Figure 5.4, Figure 5.5). In terms of morphology most positively stained cells were large and round with many vacuoles to be seen, this was particularly evident at the earlier time-point of 7 dpi (Figure 5.6 A-F). This was less prominent from 14 dpi onwards (Figure 5.6 G-L).

In the lesion epicentre there were no significant differences between experimental groups in Arginase-1 positive cells, iNOS positive cells or transitional cells. At 3 and 7 dpi the vast majority of microglia and macrophages were Arginase-1 positive only (Figure 5.4 A, B). Cells expressing iNOS alone were rare, while transitional cells expressing both markers made up a small proportion (less than 20%) in hydrogel treated animals at 3 dpi. At 7 dpi transitional cells disappeared from hydrogel treated animals but were seen in the transection only group (Figure 5.4 B). A change in phenotype was seen in the lesion epicentre at 14 dpi. Cells expressing only Arginase-1 were greatly reduced in number. This was most pronounced in the transection only group where Arginase-1 area fell from 80% at 7 dpi to 25% at 14 dpi. Transitional microglia/macrophages were most frequent in this group making up 65% of the total, and single iNOS expression was seen in 10% of microglia and macrophages (Figure 5.4B). In the hydrogel treated group the expression solely of Arginase-1 remained dominant at 62%, with transitional type cells making up 36% and iNOS expressing cells accounting for only 2%, 5-fold lower than in the untreated group (Figure 5.4 B). At the later time-points of 21 and 28 dpi the differences between treatment groups had evened out with similar numbers of each cell type present in each, Figure 5.4.

A

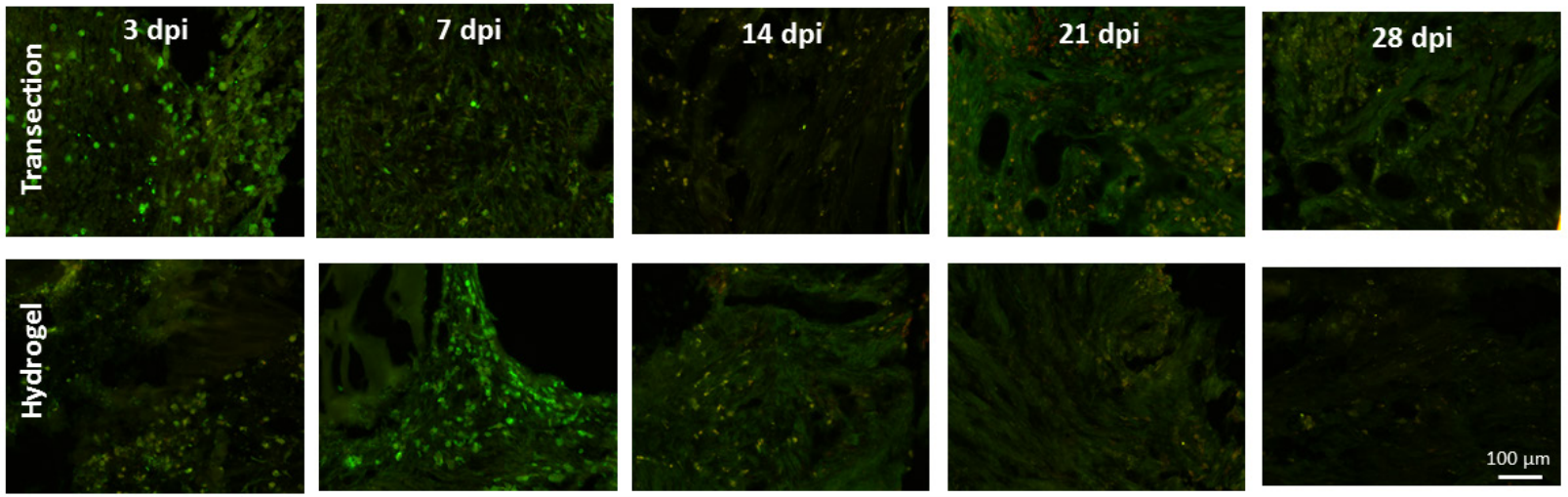
3 dpi
7 dpi
14 dpi
21 dpi
28 dpi
Transection
Hydrogel
100 µm

B

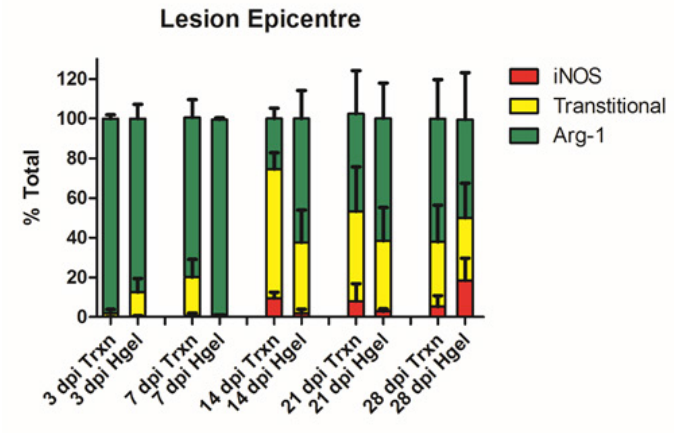
Lesion Epicentre
% Total
120
100
80
60
40
20
0
iNOS
Transtitional
Arg-1
3 dpi Trxn
3 dpi Hgel
7 dpi Trxn
7 dpi Hgel
14 dpi Trxn
14 dpi Hgel
21 dpi Trxn
21 dpi Hgel
28 dpi Trxn
28 dpi Hgel

Figure 5.4 Phenotype of microglia and macrophages at the lesion epicentre. (A) Photomicrographs show iNOS positive staining in red, Arginase-1 positive staining in green, transitional cells expressing both markers appear yellow. Scalebar = 100 μm. (B) Graph shows % of positive staining for iNOS, Arginase-1 and transitional cells at the lesion epicentre, the same colour scheme is used as for immunohistochemistry. Trxn = transection only, Hgel = aligned hydrogel. Data is shown as mean ± SEM. Data was analysed using two-way ANOVA followed by Bonferroni's post hoc test. Each cell type (iNOS positive, Arginase-1 positive or transitional) were analysed separately. Time-point was a significant contributor to variance for all cell types, however there were no significant differences between individual treatment groups.

In all three zones of the scar microglia/macrophages expressing Arginase-1 only were most abundant (Figure 5.5). There were no significant differences in the types of microglia/macrophages between the two treatment groups at any time-point. The area of Arginase-1 staining was highest at 3 and 7 dpi, after which there was a slight reduction of 20-30% in all ROIs and all groups from 14 to 28 dpi (Figure 5.5 A, B, C). Microglia/macrophages expressing only iNOS were very low in the scar zones also, only beginning to appear from 14 dpi and in general making up less than 7% of the total microglia/macrophage area. Only in the hydrogel treated group at 21 dpi in Zone C did these cells rise to 15% of total area (Figure 5.5 C).

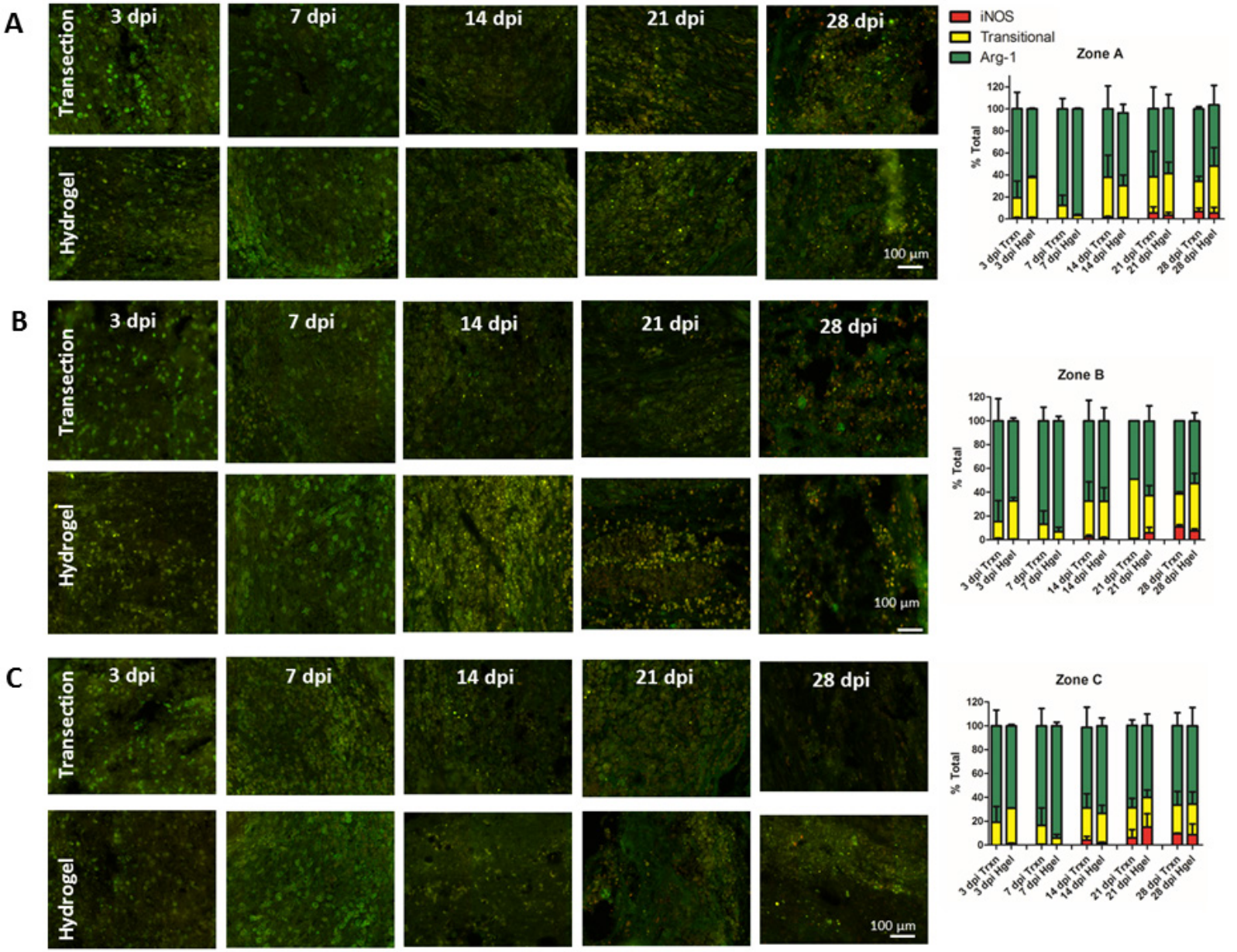
A
Transection
Hydrogel
3 dpi
7 dpi
14 dpi
21 dpi
28 dpi
100 µm
iNOS
Transitional
Arg-1
Zone A
% Total
3 dpi Trxn
3 dpi Hgel
7 dpi Trxn
7 dpi Hgel
14 dpi Trxn
14 dpi Hgel
21 dpi Trxn
21 dpi Hgel
28 dpi Trxn
28 dpi Hgel
B
Zone B
C
Zone C

Figure 5.5 Microglia/macrophage phenotype within the scar zone. Photomicrographs and graphs show iNOS positive staining in red, Arginase-1 positive staining in green and transitional cells expressing both markers in yellow. (A) Zone A ROI extends to 450 µm beyond the edge of the lesion. (B) Zone B ROI extends from 450 – 900 µm beyond the edge of the lesion. (C) Zone C ROI extends from 900 to 1350 µm beyond the edge of the lesion. Trxn = transection only, Hgel = aligned hydrogel. Data is shown as mean ± SEM. Data was analysed with two-way ANOVA followed by Bonferroni's post hoc test. Each cell type (iNOS positive, Arginase-1 positive or transitional) were analysed separately. Time-point was a significant contributor to variance for all ROIs for all cell types (except in Zone C for transitional type cells). There were no significant differences between individual treatment groups.

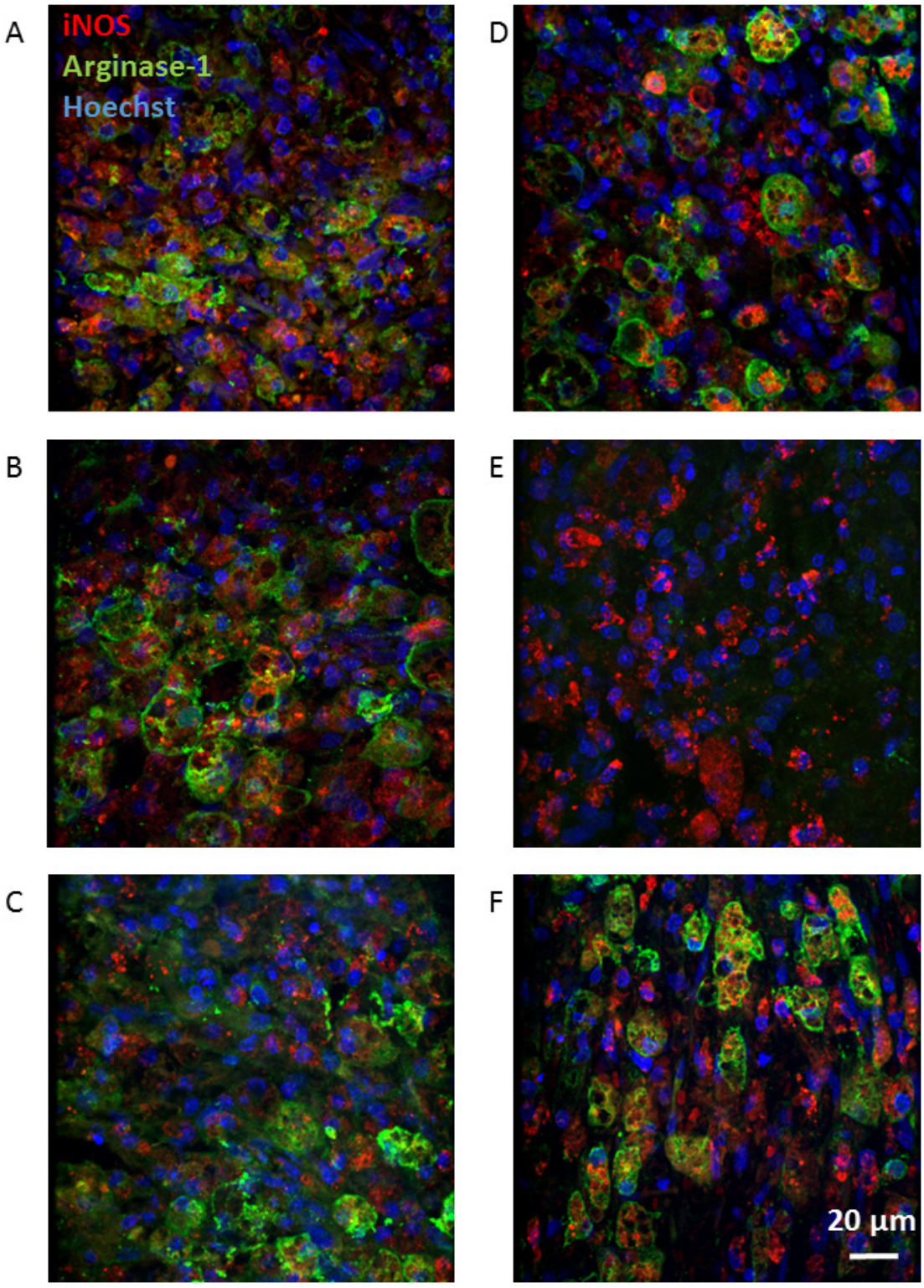
A
iNOS
Arginase-1
Hoechst
D
B
E
C
F
20 µm

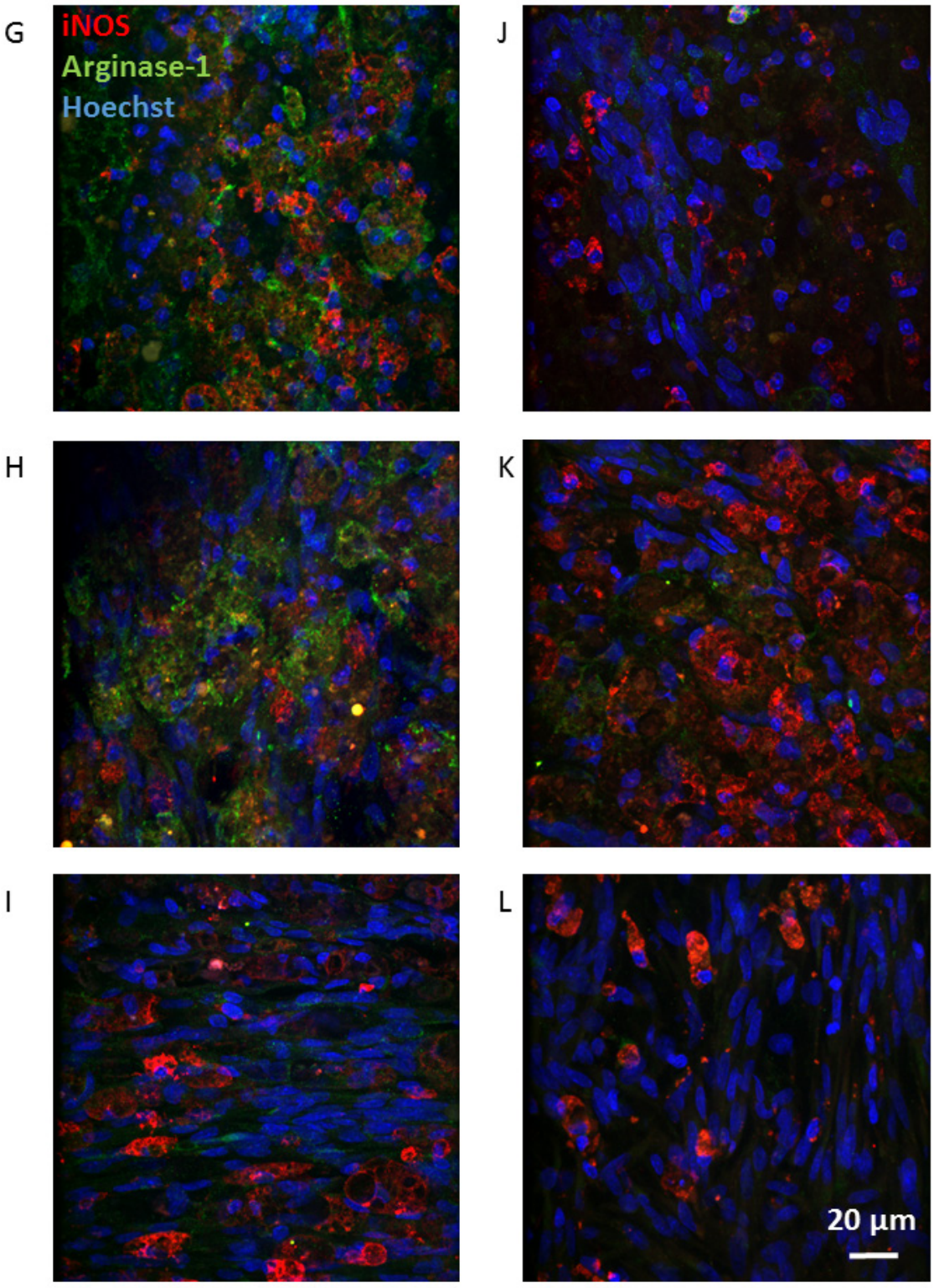

Figure 5.6 High magnification confocal images of microglia/macrophages at the borders of the injury. (A-C) Transection only group at 7 dpi (D-F) transection with aligned collagen hydrogel group at 7 dpi. (G-I) Transection only group at 14 dpi (J-L) transection with aligned collagen hydrogel group at 14 dpi Scale bar 20 µm.

5.5.3 Collagen hydrogel reduced bleeding at the site of injury

Implantation of the collagen hydrogel appeared to reduce bleeding at the site of injury, this was observed during surgery at the time of implantation, and during tissue dissection blood clots were observed to be much smaller and less frequent in the collagen hydrogel group (Figure 5.7 E-H) compared to the transection only group (Figure 5.7 A-D).

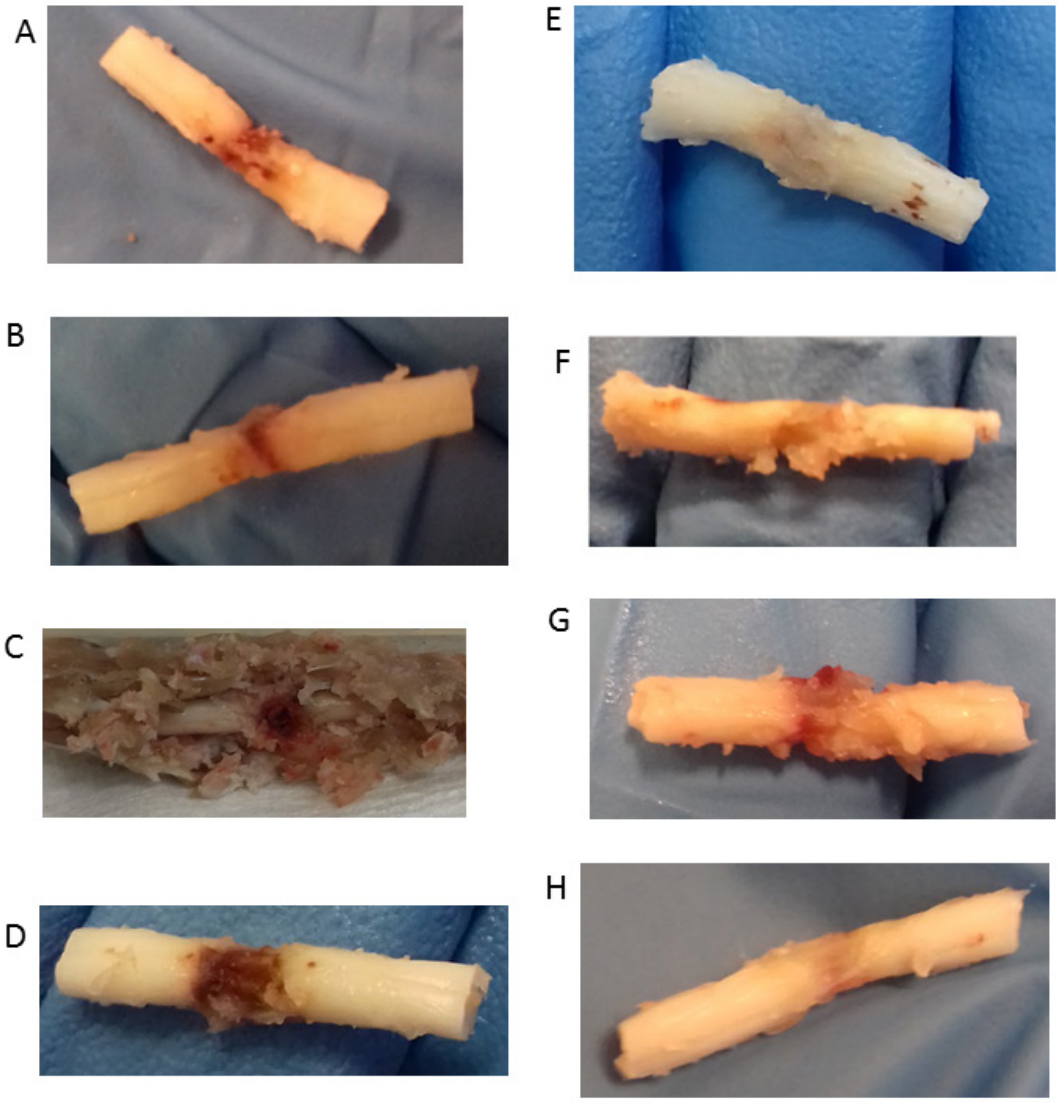

Figure 5.7 Treatment with collagen hydrogel reduces bleeding at the site of injury. Images were captured at the time of tissue dissection, post fixation in 4% PFA. In the transection only group (A-D) there appeared to be a large blood clot at the site of injury. In those animals treated with aligned collagen hydrogel (E-H) there was much less evidence of bleeding.

5.6 Discussion

In this study, the effect of a hydrogel scaffold in transected spinal cord was examined in terms of scar formation, specifically proteoglycan and collagenous scar, and the polarisation of microglia and macrophages. Proteoglycan deposition was examined in this study using alcian blue as a method of investigating differences in the inhibitory scar, specifically the CSPG component, which surrounds the lesion following SCI. CSPGs are thought to be major contributors to the failure of neurite outgrowth across the injury, as degradation of their GAG chains greatly improves axonal regeneration and functional recovery (Bradbury *et al.*, 2002). The expected result would be to see an increase in proteoglycans up to two weeks (Jones *et al.*, 2003), however in this data we see an initially high proportion of proteoglycan which falls until 28 dpi in both experimental groups at the lesion borders (Figure 5.1 B). It is difficult to tell from these results whether the presence of the collagen hydrogel provides any real benefit. There was no difference between the untreated or the collagen hydrogel treated group in the amount of positive staining.

Assuming that the tissue far from the lesion reflects the normal amount of proteoglycan in intact healthy tissue (Vv approximately 0.7) it appears that there is a reduction in proteoglycans in response to the injury. Again this is unexpected. However, a confounding factor in the interpretation of this result is that normal CNS ECM is rich in a variety of proteoglycans (Zimmermann and Dours-Zimmermann, 2008). It is possible that the results here reflect a breakdown in the normal spinal cord ECM, and that the CSPG element of the scar would appear at a later time-point. Antibody staining for particular proteoglycan species would yield more information.

Again, it is possibly too early to say for certain whether the presence of the collagen hydrogel provided any real benefit based on our results of Masson's trichrome stained spinal cord. In the lesion epicentre the amount of collagen present was higher at 3 dpi in the hydrogel treated group (Figure 5.2 B). This was as expected due to the hydrogel itself being composed of collagen. There was little difference between the transection only and the collagen hydrogel treated group at later time-points. Collagen, a component of the fibrotic scar, has been suggested to contribute to axonal growth failure following transection of the postcommissural fornix (Stichel *et al.*, 1999), however in the injured spinal cord preventing collagen deposition did not promote axonal outgrowth (Weidner *et al.*, 1999). It is unlikely that the collagenous scar alone acts as a primary inhibitor of axonal regeneration, and that many other factors contribute such as inflammation and other scar components (Weidner *et al.*, 1999; Orr and Gensel, 2018). In this case it is important to note the orientation of the collagen fibres – if they run in a favourable direction they could potentially contribute a substrate on which axons could grow and cells migrate, in a similar manner to the way in which collagen scaffolds can act as a substrate to bridge

the lesion (Han *et al.*, 2014; Li *et al.*, 2015; Breen *et al.*, 2016; Chen *et al.*, 2017). In both experimental groups the collagen fibres appeared to be highly aligned in the tissue adjacent to the injury (Figure 5.3). The amount of collagen present in the tissue far from the lesion gradually increased over time. It is interesting to note this spread of pathology into seemingly intact tissue and should be borne in mind for future therapeutic approaches.

The main focus for this pilot study was on the investigation into the inflammatory status of the cells in the transected spinal cord in the presence or absence of aligned collagen hydrogel. Two antibody markers were chosen for this investigation, iNOS to label the classically activated, pro-inflammatory macrophages and microglia, and arginase-1 to label alternatively activated, more anti-inflammatory macrophages and microglia. These two markers were chosen as they are widely used in the literature, although not the most commonly used, and as they are both intracellular. But the main reason for choosing this pair of markers is that they are both enzymes which compete for the same substrate, L-arginine. iNOS utilises L-arginine to produce nitric oxide which is largely damaging to surrounding tissue, while arginase-1 uses L-arginine in the first step of collagen biosynthesis, promoting tissue remodelling (Campbell *et al.*, 2013). In this way the aim was to examine the balance of tissue damage versus tissue remodelling activity. Of course the inflammatory status of a cell is not a black and white, all or nothing phenomenon and so many cells were identified as expressing both markers, these are the 'transitional' cells described in the results section. These type of dual expressing cells have not been reported in many studies, usually single labelling is used, however cells expressing both pro- and anti-inflammatory markers have been reported in (Bermudez *et al.*, 2016).

It is generally accepted that to reduce inflammation an anti-inflammatory drug must be introduced, however it has been seen in a small number of studies (Breen *et al.*, 2016; Ham and Leipzig, 2018) that the presence of a biomaterial may slightly reduce inflammation after injury. It is possible that implantation of a biomaterial into the site of injury immediately after the injury has been created helps to reduce bleeding at the site of injury, and thus reduce the influx of blood borne immune cells, and the other blood components which the CNS is usually isolated from. At the stage of post-mortem tissue dissection it was observed in this work that those animals treated with the collagen hydrogel had much smaller volumes of clotted blood at the site of injury (Figure 5.7) A haemostatic effect of the hydrogel was also observed at the time of transection injury.

The primary role for microglia and macrophages following SCI is to clear the debris from dead and dying cells, and to restore homeostasis (David and Kroner, 2011). To carry out these important functions, the microglia and macrophages need to become activated, and this may occur in one direction or another. The polarisation of macrophages has been widely discussed with regard to the

peripheral immune system (Liu *et al.*, 2014; Gensel and Zhang, 2015), and is proposed to occur along a spectrum with the extremes being the so-called 'M1' type cells, which are pro-inflammatory in nature and often referred to as classically activated, or the 'M2' type cells, which are proposed to respond to and release anti-inflammatory mediators for the promotion of tissue repair and remodelling, and may be referred to as alternatively activated (Gensel and Zhang, 2015). Each polarisation state is important for recovery after a traumatic SCI but the balance of these states is important and appears to be dysregulated in many instances (David and Kroner, 2011; Gensel and Zhang, 2015). In this study the iNOS-positive cells are considered the pro-inflammatory type cells and the arginase-1-poitive cells are considered the anti-inflammatory type cells.

The review by Gensel and Zhang puts into context the inflammatory profile seen in SCI against the profile seen in a tissue such as muscle which is capable of successful wound repair. Both begin in the same manner generally speaking but over time a divergence occurs, where in the muscle the inflammation switches from a pro-inflammatory to a tissue repair type and then gradually resolves. In contrast the injured spinal cord maintains the pro-inflammatory environment and the switch to tissue repair and resolution of inflammation doesn't occur (Gensel and Zhang, 2015). In other tissues, the transition from starting inflammatory conditions to resolving inflammatory conditions seems to be important. In our study, although we have what seems to be a response favourable to tissue repair, this profile was largely maintained over the study period and there was no switching or transitioning. Perhaps the switching and transitioning itself is important to the repair process more so than the phenotype of the inflammatory cells.

The results here demonstrate a predominantly M2 type response following injury in both the transection only group, and the group treated with the aligned collagen hydrogel. A similar response has been shown in many studies of rat SCI (Hakim *et al.*, 2015; Dyck *et al.*, 2018; Wang *et al.*, 2018) while the opposite has also been shown (Song *et al.*, 2017; Cornelison *et al.*, 2018; Riemann *et al.*, 2018). These inconsistencies between studies make it difficult to interpret a 'normal' response. However the only study using transection injury in the rat and examining the M1/M2 ratio does agree with our overall results (Hakim *et al.*, 2015).

It is interesting to note the low level of iNOS-positive microglia and macrophages, and that many cells are double positive for both M1 and M2 markers. This reinforces the idea of macrophages existing on a continuum or spectrum (Gensel and Zhang, 2015) instead of being definitively polarised in one or other direction, and shows how delicate the fine-tuning of these responses will need to be. It is difficult however to pinpoint how these transitional type cells affect the surrounding cells and tissue; is there a net release of pro-inflammatory cytokines or anti-inflammatory cytokines? What are the levels of

free radicals and oxidative species in this environment? All of these questions require further work to be answered, and should be considered when defining any potential treatment to interfere with this fine balance.

One limitation of this study is the use of only one marker for the M1 type and one marker for the M2 type. It is not possible to gain an overall picture of what is happening in the injured environment in terms of inflammation with this single snap shot. As noted in the work of Kigerl *et al.* (2009) inflammation following SCI is a highly dynamic process, with many different players with distinct functional roles and temporal profiles. For this reason, it may be more sensible to use a technique such as flow cytometry or to perform a gene or protein array to investigate a variety of markers simultaneously in order to determine a more reliable overall picture of the inflammatory environment post-injury. This study was part of a larger body of work, for which much of the analysis required visualisation of the tissue in its native structure and so the tissue was prepared for immunohistochemistry. In this study double immunohistochemistry for both M1 and M2 markers simultaneously was used. This adds an advantage by allowing identification of the transitional phenotype. Many publications report only single staining (see table in Appendix I) and so are likely misrepresenting the balance of pro- and anti-inflammatory activity. In our work we can see that purely pro-inflammatory activity (iNOS-positive cells, M1 type cells) is reasonably low in comparison to purely anti-inflammatory activity (arginase-1-positive cells, M2 type cells), and that a substantial proportion of cells exhibit both together (double stained, transitional type cells).

6 Chapter 6 - *N*-glycosylation of the healthy, injured and collagen treated rat spinal cord

6.1 Introduction

N-glycosylation is an important post-translational modification, present on a large proportion of proteins, especially secreted proteins (Stanley P, 2017). The addition of *N*-glycans to a protein is an enzymatic process and is not template driven. The complement of *N*-glycans on a protein depends on the enzymes present and their activity, as well as the availability of monosaccharide precursors. Therefore there is huge variation in the potential *N*-glycans present in a sample and their characterisation may be somewhat difficult. *N*-glycans are built onto a protein as it moves through the endoplasmic reticulum and Golgi apparatus in a sequential manner as described in the Introduction, Section 1.5.3.

As an abundant post-translational modification, *N*-glycosylation potentially acts as a fine tuning mechanism for a wide range of biological processes, and so may be very important in controlling the response to injury and disease. Indeed, the *N*-glycans have been recognised as having an important role in cancer, (Taniguchi and Kizuka, 2015) and inflammation, (van Kooyk and Rabinovich, 2008; Rabinovich and Croci, 2012). In the CNS specifically not much is known about their role and even less in the context of traumatic CNS injury. One study examined changes in *N*-glycans following a controlled cortical impact in a rat model. Here changes in a variety of glycans were seen as a result of injury, see Introduction, Section 1.5.6, (Abou-Abbass *et al.*, 2016). Alterations in *N*-glycosylation have also been seen in some of the neurodegenerative diseases such as AD (Wang *et al.*, 1996; Akasaka-Manya *et al.*, 2010; Gizaw *et al.*, 2015; Gizaw *et al.*, 2016) and multiple sclerosis, for reviews see (Grigorian *et al.*, 2012a; Grigorian *et al.*, 2012b; Chien *et al.*, 2018). However it is difficult to say whether these are cause or consequence of the disease.

The only extensive characterisation of CNS *N*-glycans performed to date was carried out in the 1990s using HPLC technology and exoglycosidase digestion (Chen *et al.*, 1998; Zamze *et al.*, 1998). The *N*-glycan profile of the entire brain was studied, and a similar selection of structures were found to what has been found in the spinal cord in this study. The sialylated and the neutral fractions were studied separately and high mannose structures and hybrid structures were identified, as well as complex structures which occurred as di-, tri- or tetra-antennary and were decorated with bisecting GlcNAc, core and outer arm fucose, galactose and sialic acid. Some structures with lactosamine repeats were also found, as well as occasional poly-sialylation. (Chen *et al.*, 1998; Zamze *et al.*, 1998).

This work uses liquid chromatography to separate and profile the *N*-glycans released from glycoproteins of the spinal cord. Spinal cord homogenate was prepared using the procedure optimised by the Rudd group, (Royle *et al.*, 2008), with some modifications. This procedure involves denaturation of the protein followed by enzymatic release of *N*-linked glycans with PNGaseF. Released glycans are then fluorescently labelled with 2-aminobenzamide (2AB) (Bigge *et al.*, 1995), with extensive washing steps included throughout the protocol. Released labelled glycans are then suitable for profiling using UPLC or HPLC technology. This method has been used to extensively characterise the *N*-glycoprofile of human serum both in healthy controls and in breast cancer patients (Saldova *et al.*, 2014). For this project, the preparation protocol was modified to be appropriate for tissue samples as described in Section 6.5.1.

6.2 Hypotheses

1. The *N*-linked glycome of the spinal cord can be characterised using HILIC-UPLC *N*-glycoprofiling
2. Traumatic SCI results in changes in spinal cord *N*-glycosylation, and collagen hydrogel treatment can modify this response

6.3 Objectives

1. Optimise tissue homogenisation and *N*-glycan release and labelling from spinal cord
2. Characterise *N*-glycans of healthy spinal cord
3. Investigate changes in *N*-glycosylation with injury and treatment

6.4 Experimental design

Optimisation of the sample preparation was required before beginning with the characterisation of the spinal cord *N*-linked glycome. As a part of this optimisation, three different homogenisation buffers were tested: homogenisation buffer (62.5mM Tris with 2% SDS, pH 6.6), homogenisation buffer with Proteinase K (20mg / ml), 1% Triton X-100 and 5mM $CaCl_2$, and RIPA buffer with 1% protease inhibitor cocktail. A mechanical disruption step and centrifugation steps to separate debris from protein rich supernatant were consistent for all. The final optimised protocol is detailed in Materials and Methods, Section 2.8.1.

Each of the three homogenisation methods were then compared for glycan yield, resolution and reproducibility of the HILIC-UPLC chromatograms. Each homogenate was divided into three and subjected to the in gel block protocol established and commonly used in the NIBRT Glycoscience group

(Royle *et al.*, 2008). Briefly, homogenate was dried in a vacuum centrifuge and resuspended a mixture of water and homogenisation buffer. Reduction and alkylation was performed directly following resuspension. The acrylamide gel was formed entrapping the sample and transferred to the filter plate. Washing of gels, PNGase release of *N*-glycans, labelling and clean up were then performed as in Section 2.8.1.2. The initial steps of reduction, alkylation and gel formation were altered slightly during the optimisation process in order to improve ease of handling and glycan yield, see Section 6.5.1. All characterisation of *N*-glycans in healthy and injured spinal cord was carried out using the final optimised method in Section 2.8.1. This work completed Objective 1.

A large portion of this work is to characterise the *N*-linked glycome of the healthy adult rat spinal cord, Objective 2. For all characterisation experiments healthy uninjured tissue isolated from the thoracic spinal cord of adult female rats was used. To obtain enough tissue for all experiments tissue samples from the thoracic spinal cord of thirteen rats was collected. Euthanasia and tissue harvesting were performed in the same manner as for the subsequent analysis of *N*-glycans in spinal cord injured tissue (Sections 2.2.2 and 2.2.3). Extraction and fluorescent labelling of *N*-glycans was performed as described in Section 2.8.1, after which the released labelled *N*-glycans were pooled and later split into appropriate amounts for each experiment. Pooling was essential to allow for direct comparison between the various analytical techniques.

The primary method to investigate the healthy spinal cord *N*-glycome (Objective 2) was using exoglycosidase digestions (Section 2.8.3, Table 6.1) together with HILIC-UPLC profiling (Sections 2.8.4 and 2.8.5). The principle of this technique is that the HILIC-UPLC profile changes when glycans are digested with enzymes removing particular monosaccharides, i.e. peaks change in area and/or elute at a different time. Exoglycosidase enzymes are specific for the monosaccharide they remove and the linkage in which it is attached, but not for the underlying monosaccharide the target sugar is linked to. Certain combinations of sugars sterically prevent access to an enzyme's active site, preventing it from digesting its target sugar. For example the enzyme AMF generally cannot remove outer arm fucose attached to a GlcNAc residue if a galactose residue is also attached to the same GlcNAc. For this reason, AMF is often used in combination with BTG, to remove the outer galactose residues.

Samples from the pooled rat spinal cord *N*-glycans were treated with each of the enzyme combinations shown in Table 6.1 and the resulting digested sample run on HILIC-UPLC. The percentage area and GU value of each peak in the resulting profiles was obtained from the Empower workstation. The movement of each peak was then followed throughout each exoglycosidase treated HILIC-UPLC profile, and also compared to known structures associated with a particular GU value obtained from the Glycostore database.

To support the HILIC-UPLC and exoglycosidase experiments, WAX-HPLC (Section 2.8.2) was used to establish the amount of sialic acid and other charged species present, and a DMB assay (Section 2.8.7) was performed to investigate the proportion of Neu5Ac vs Neu5Gc sialic acid present. LC-MS (Section 2.8.6) was used to confirm the structures proposed from the HILIC and WAX-HPLC, and DMB experiments. The results from these four experiments were interpreted in relation to each other to build a comprehensive *N*-glycoprofile of the spinal cord as seen in Section 6.5.2.

Enzyme	**Combination applied to tissue**	**Monosaccharide removed**	**Linkage specification**
UND	undigested, no enzyme		
NAN-1	NAN-1	Sialic acid	α(2-3) linkage
ABS	ABS	Sialic acid	all linkages α(2-3, -6, -8)
BTG	ABS+BTG	Galactose	β(1-3, -4) linkage
BKF	ABS+BTG+BKF	Core fucose (and outer arm)	α(1-2, -6), partially α(1-3, -4)
AMF	ABS+AMF	Outer arm fucose on galactose	α(1-3, -4)
	ABS+BTG+AMF	Outer arm fucose on GlcNAc	
BKF+AMF	ABS+BTG+BKF+AMF	All fucose, core and outer	α(1-2, -6), α(1-3, -4)
GUH	ABS+BTG+BKF+AMF+GUH	GlcNAc	β-linked, but not bisected
JBM	ABS+BTG+BKF+AMF+GUH+JBM	Mannose	α(1-2, -3, -6)
CBG	ABS+CBG	Galactose	α(1-3, -4)
	ABS+BTG+BKF+AMF+GUH+CBG		
SPG	ABS+SPG	Galactose	β(1-4) linkage
JBH	ABS+JBH	GlcNAc and GalNAc	β-linked

Table 6.1 Exoglycosidase enzymes used to investigate the *N*-glycan composition of the rat spinal cord and their specificities. Enzymes were used in sequential combinations to gradually cleave off monosaccharides so that only the core structure remained.

To fulfil Objective 3 and understand the changes in *N*-glycosylation following traumatic SCI with and without collagen hydrogel treatment each experimental sample was collected as in Section 2.2.2 and 2.2.3. Tissue from three regions of interest were collected from each animal: the lesion epicentre (Region A), and two regions of tissue rostral and caudal to the injury (Regions B and C respectively), Figure 6.1. The experimental groups are described in Table 6.2. *N*-glycans were released and labelled from the tissue according to Section 2.8.1. The main readout for this experiment was HILIC-UPLC

profiling (as in Section 2.8.4). 70% of each tissue sample was profiled using HILIC-UPLC, the remaining 30% was examined using WAX-HPLC (Section 2.8.2) to understand sialylation changes.

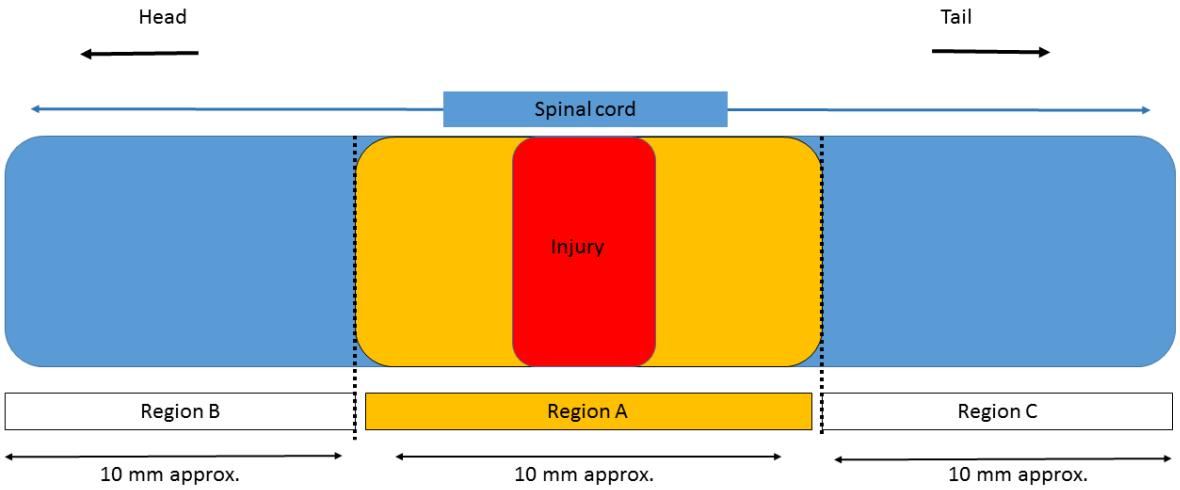

Figure 6.1 Tissue harvesting for SCI experiment. Region A is the injury epicentre and immediately surrounding tissue including the scar area. Region B is an uninjured region rostral to the injury. Region C is an uninjured region caudal to the injury. Each region spans approximately 10 mm in length.

Timepoint	Experimental group	n	Regions
7 dpi	Sham	3	A, B, C
	Transection only	3	A, B, C
	Transection + Random collagen	3	A, B, C
	Transection + Aligned collagen	3	A, B, C
14 dpi	Sham	3	A, B, C
	Transection only	3	A, B, C
	Transection + Random collagen	3	A, B, C
	Transection + Aligned collagen	3	A, B, C

Table 6.2 Experimental design for SCI experiment.

6.5 Results

6.5.1 Method development to analyse spinal cord N-*glycosylation*

6.5.1.1 A homogenisation buffer of tris and SDS is optimal for tissue homogenisation for glycan analysis

Glycan yield was tested with three potential lysis buffers for tissue homogenisation: RIPA buffer together with a protease inhibitor cocktail (PIC), homogenisation buffer composed of tris and SDS, and homogenisation buffer with added Proteinase K, Triton X-100 and $CaCl_2$. A tissue sample was homogenised in each of the three before using the in gel block method for *N*-glycan release and labelling, and testing the result by HILIC-UPLC. Homogenisation buffer alone was found to be most efficient based on the number and resolution of individual peaks and on the yield of glycans (Figure 6.2 C), i.e. the emission unit on the y-axis of the chromatogram. Successful isolation of *N*-glycans was also obtained using RIPA buffer with PIC (Figure 6.2 B) but the yield and resolution were slightly poorer. No glycans were obtained using homogenisation buffer with added proteinase K (Figure 6.2 A).

There was also advantage to using homogenisation buffer only, over the other two methods in terms of ease of handling: at the step of resuspension of dried sample, before gel formation, samples homogenised in homogenisation buffer were much easier to dissolve and to mix the next reagents. Samples homogenised in RIPA buffer were viscous and gel like, the dry sample was bigger in volume than the samples from either of the other two methods. Samples homogenised in buffer with Proteinase K were very difficult to dissolve, these required a larger volume of solution and remained in a jelly.

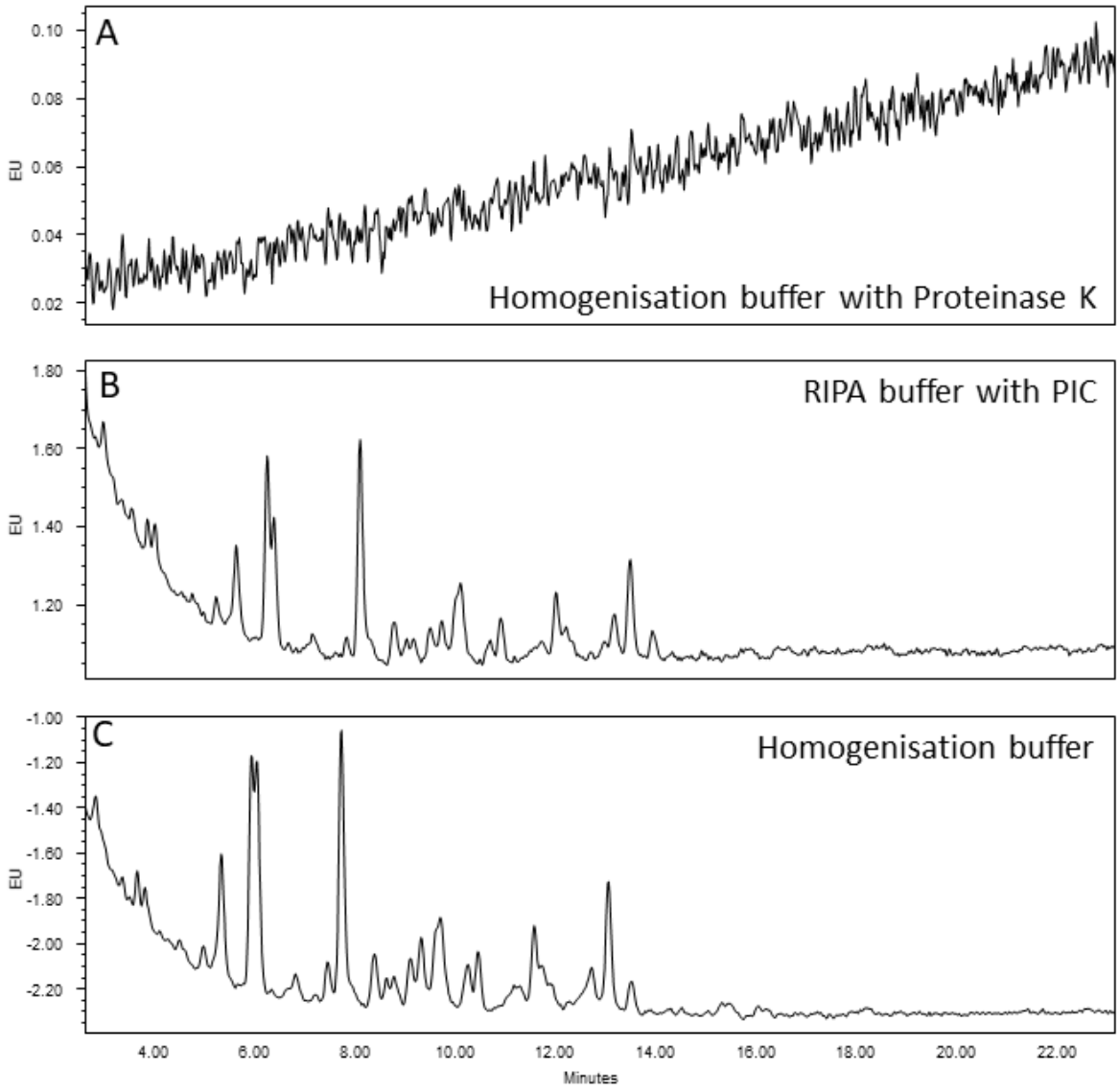

Figure 6.2 Homogenisation buffer composed of Tris and SDS is optimal for *N*-glycan analysis. No *N*-glycans were obtained from tissue homogenised in the presence of proteinase K (A). RIPA buffer and PIC allowed for successful HILIC-UPLC profiling of *N*-glycans (B) but the yield was slightly lower than that obtained with homogenisation buffer alone (C).PIC, protease inhibitor cocktail; EU, emission units. Recipes for buffers are given in Appendix VIII.

6.5.1.2 Optimised sample preparation procedure is technically reproducible for spinal cord tissue

To test the reproducibility of the optimised tissue preparation, i.e. homogenisation, glycan release and labelling with 2AB, thoracic spinal cord tissue from a number of animals was pooled together, split into seven identical replicates and processed according to the optimised procedure. Labelled glycans were run on HILIC-UPLC and integrated to give 25 peaks (Figure 6.3 A). The protocol was deemed technically reproducible since the coefficient of variation (% CV) of the percentage area of individual peaks between replicates was sufficiently low: 16 of the 25 peaks had CV less than 10%, 6 were below 20% and 2 were between 20 and 25%. The only peak exceeding accepted CV values was the fifth peak with a CV of 33%. This peak was especially small, and may even fall below baseline in some chromatograms (Figure 6.3 B).

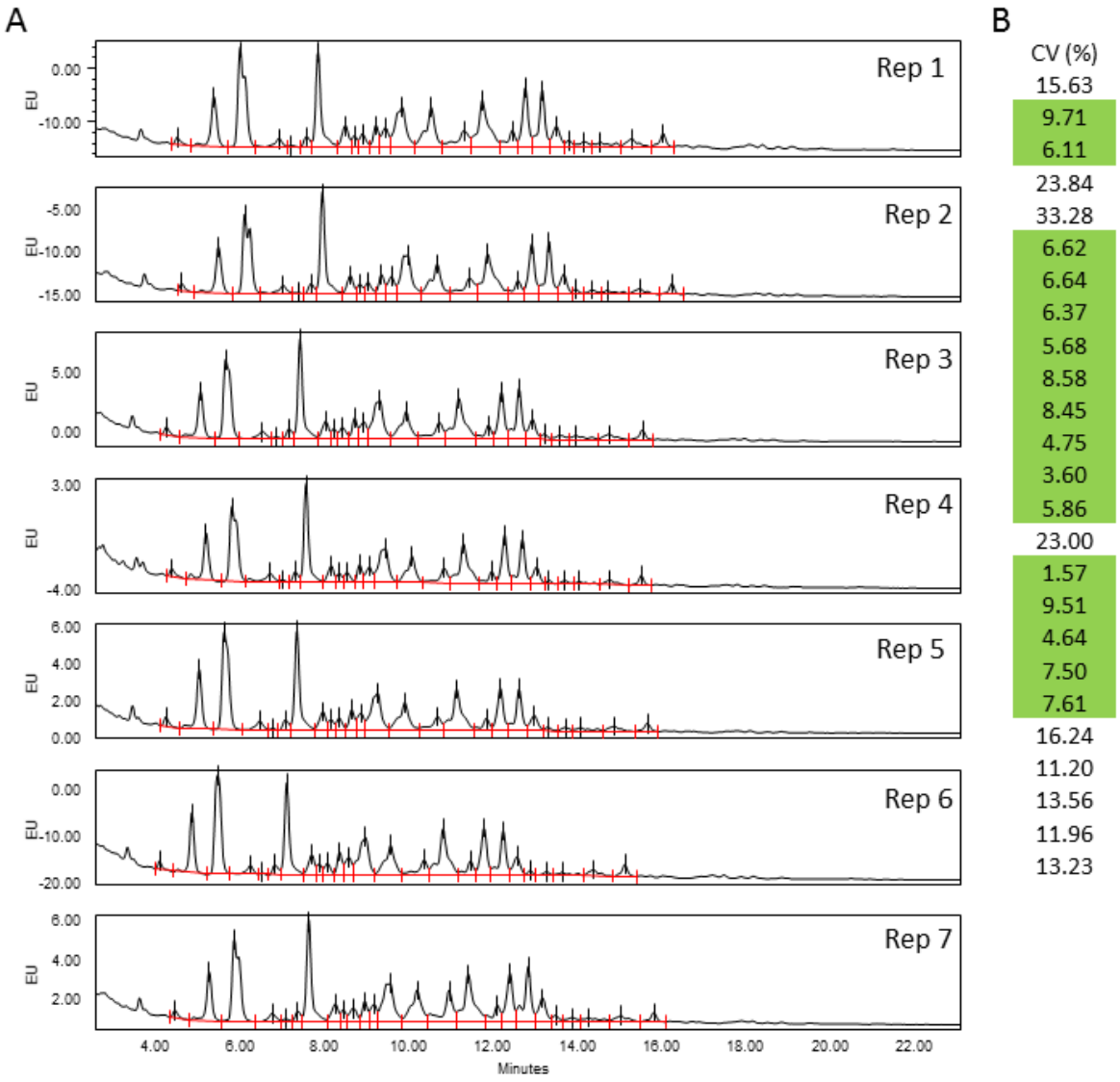

Figure 6.3 HILIC-UPLC profiling of spinal cord *N*-glycans is technically reproducible. (A) The HILIC-UPLC profile from seven identical replicates is shown. (B) Peaks were integrated and the coefficient of variation (%CV) for percentage area obtained for each peak. The majority of peaks had CV values of less than 10%, indicated in green. Almost all remaining peaks had a CV of below 20%.

6.5.2 Characterisation of spinal cord of the healthy adult female rat

The *N*-glycoprofile of rat spinal cord glycans is shown in Figure 6.4. A total of 54 individual peaks were integrated across the entire range of the profile, demonstrating the wide complexity of *N*-glycans present. The individual glycan species identified will be presented in the coming sections.

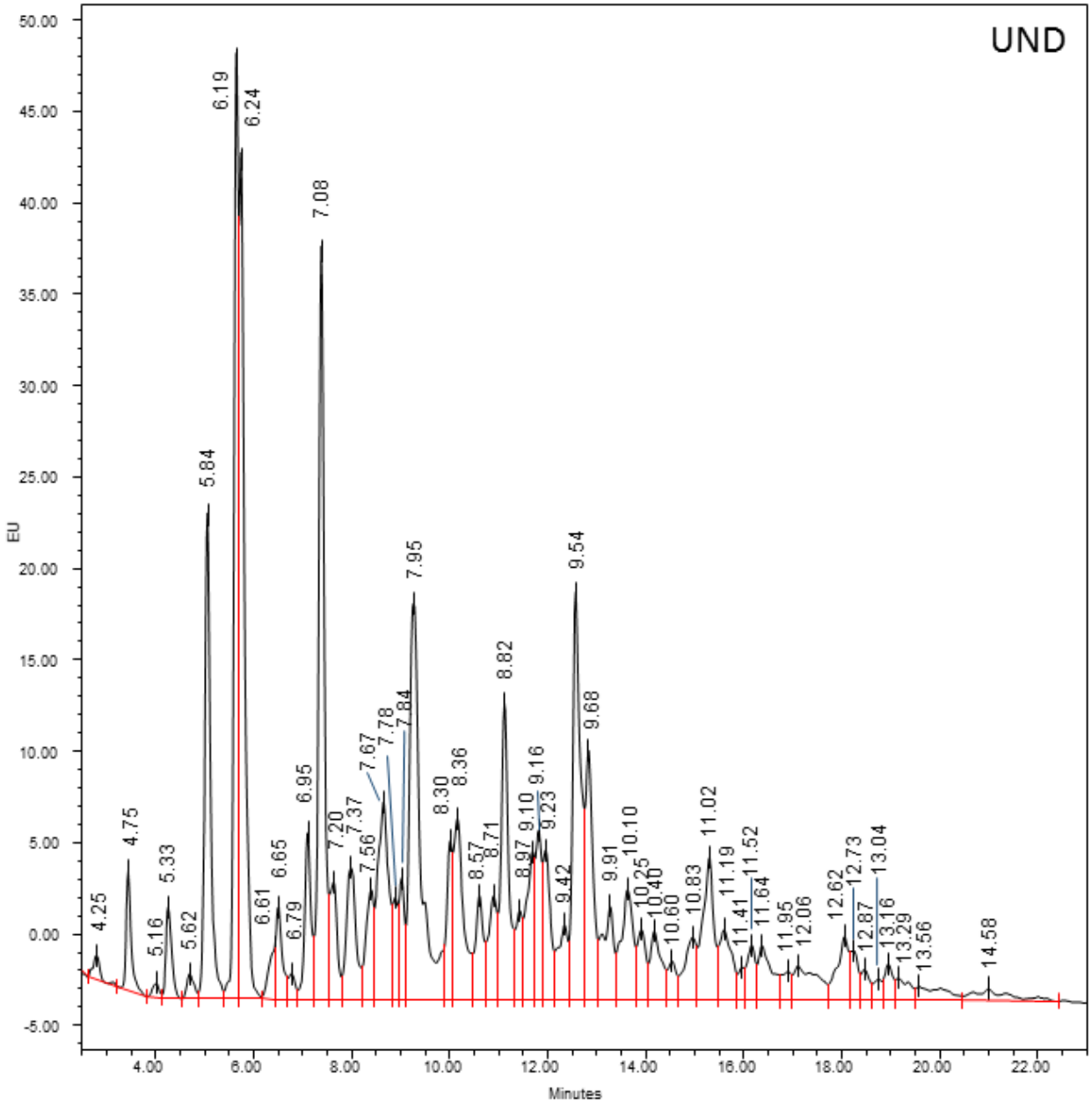

Figure 6.4 Undigested HILIC-UPLC profile of the *N*-glycans of the adult female rat spinal cord. Peaks are labelled with the GU (glucose unit) value. UND, undigested; EU, emission units.

6.5.2.1 The majority of spinal cord N-*glycans are neutral and the sialic acids are of Neu5Ac type*

WAX-HPLC was used to separate the *N*-glycans of the spinal cord based on charge. In general, sialic acid is the main donor of charge to any *N*-glycan. The major peaks of the WAX-HPLC profile consist of neutral (S0), mono-sialylated (S1), di-sialylated (S2), tri-sialylated (S3) and tetra-sialylated (S4) fractions. Peaks eluting beyond the tetra-sialylated region (>S4) were also seen. These may be particularly highly charged species, such as those carrying polysialic acid chains or other charged groups such as glucuronic acid, sulphate or phosphate groups, or sialic acid which itself has been modified by sulphation or phosphorylation. Such modification of sialic acid makes it resistant to enzymatic removal. Sulphate groups have been identified in spinal cord glycans, as well as sialic acid carrying extra acetyl groups, see following sections, however phosphate groups or glucuronic acid were not detected.

The vast majority (77%) of *N*-glycans present were neutral, i.e. without sialic acid. There were small proportions of mono-sialylated (12%) and di-sialylated (4%) species present also, with a very small amount of tri- (1%) and tetra-sialylated glycans identified (<1%), Figure 6.5. Digestion with ABS, a sialidase which digests α(2-3, -6, -8)-linked sialic acids reduced the charged region (S1-S4) however did not eliminate it completely Figure 6.5. ABS digestion increased the area of the neutral peak (S0) to 86%, indicating that 10% of charged species were due to unmodified sialic acid. Peaks S1, S2 and S4 were obviously reduced indicating that unmodified sialic acid contributes to these peaks. The changes in the S3 peak are harder to interpret, this area actually increased following ABS digestion. Some of the tetra-sialylated glycans may have partially digested to move into this position, but it is not possible to tell whether glycans from the S3 region have been digested in parallel. The highly charged region at the end of the profile (>S4) was unaffected by ABS digestion and so does not contain unmodified sialic acids, Figure 6.5.

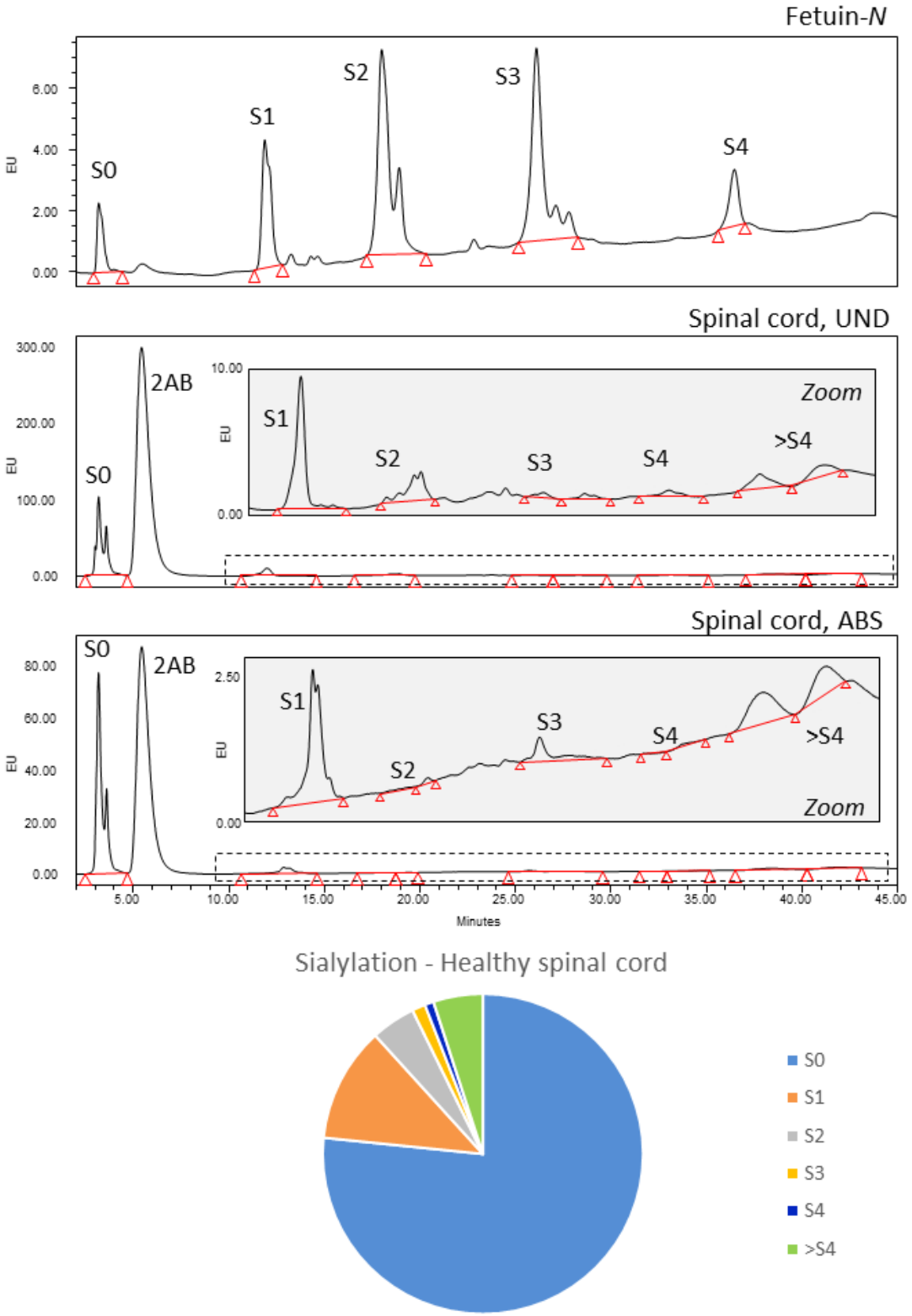

Figure 6.5 Sialic acids of rat spinal cord *N*-glycans. WAX-HPLC separates glycans on the basis of charge, fetuin-*N* was used as a reference standard. S0, neutral glycans (77%); S1, mono-sialylated (12%); S2, di-sialylated (4%); S3, tri-sialylated (1%); S4, tetra-sialylated (0.9%); >S4, unidentified highly charged species (5%); 2AB, excess 2AB label; UND, undigested; ABS; ABS (sialidase) digested. Dashed line indicates the zoomed region. The pie chart indicates the abundance of each species relative to the total.

DMB assay demonstrated that the majority of spinal cord sialic acids were present as Neu5Ac type, peak 2 in Figure 6.6, with minor amounts of NGNA, peak 1 in Figure 6.6, and also minor amounts of NANA with one extra acetyl group, peaks 3-6, or two extra acetyl groups, peak 7 in Figure 6.6. Peak 4 contains sialic acids with both acetyl and glycolyl groups. In the spinal cord this is almost undetectable (Figure 6.6), and no sialic acids of this variety were assigned for the final result. It should be noted that the DMB assay is performed on total spinal cord sialic acids, not just those present on *N*-glycans.

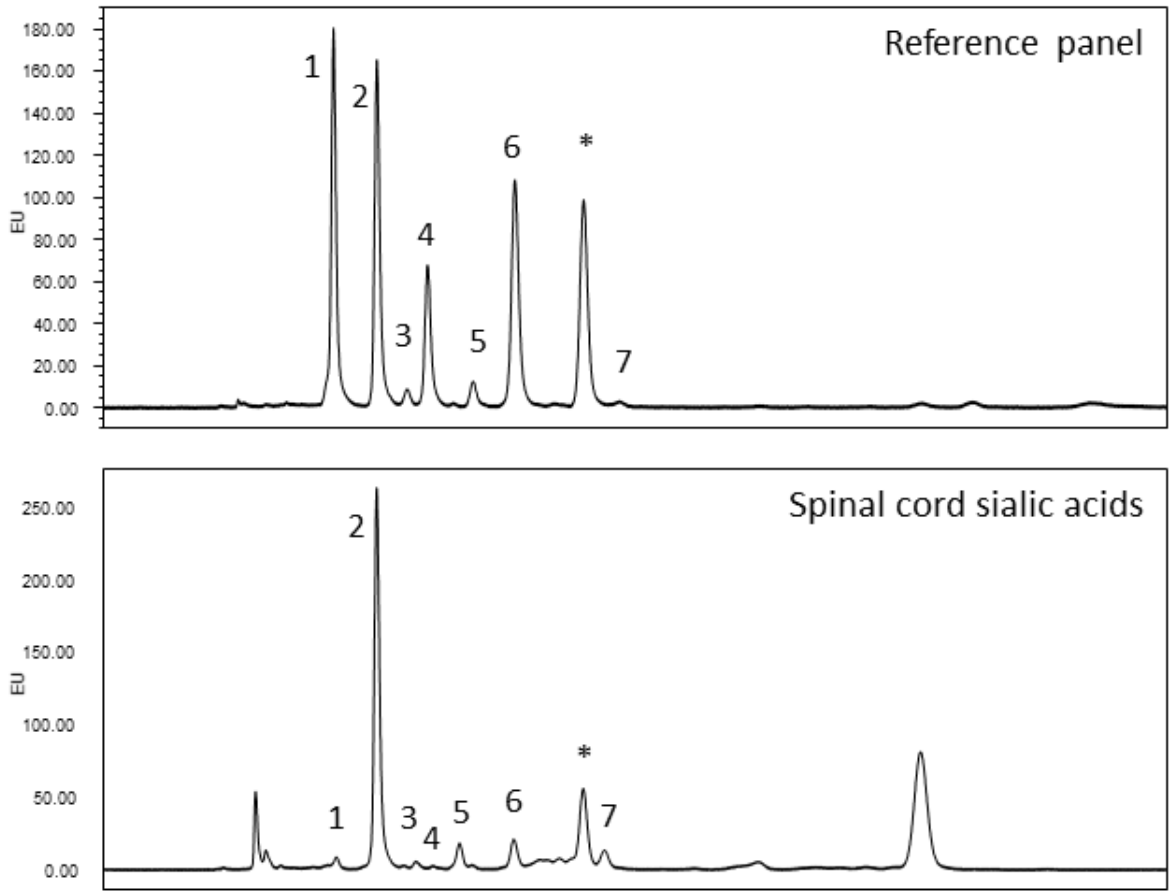

Figure 6.6 Neu5Ac is the most common type of sialic acid in the rat spinal cord. Sialic acids were released from spinal cord *N*-glycans by hydrolysis and separated on the basis of chemical structure. Reference panel was supplied with the assay kit. Peak 1, Neu5Gc; peak 2, Neu5Ac; peak 3, Neu5,7Ac2; peak 4, Neu5Gc9Ac; peak 5, Neu5,8Ac2; peak 6, Neu5,9Ac2; peak 7, Neu5,x,xAc3, where x is an unknown position; * contaminant peak.

6.5.2.2 Spinal cord N-*glycan composition*

HILIC-UPLC with exoglycosidase digestions was used to identify the *N*-glycan species present in the rat spinal cord. A HILIC-UPLC profile of the undigested healthy spinal cord was obtained for each combination of exoglycosidase enzymes, Table 6.1, and compared back to the UND profile to identify the glycans present (Figure 6.7).

From the panel shown below in Figure 6.7 clear shifts can be seen with ABS (sialidase), BTG (galactosidase), BKF and AMF (fucosidases) and GUH (hexosaminidase) indicating that sialic acids, galactose and fucose decorate multi-antennary glycans. Digestion of the glycans with JBM (mannosidase) indicates a large abundance of mannose species also. The full complement of all structures identified in the undigested sample, and for each enzyme digest is given as a table in Appendix X. Further detail on how linkages and locations of each sugar were identified are described in the following sections. A table with the major structures for each peak is given at the end of this section (Table 6.3). Mass data for those structures confirmed by LC-MS are given in Appendix XI.

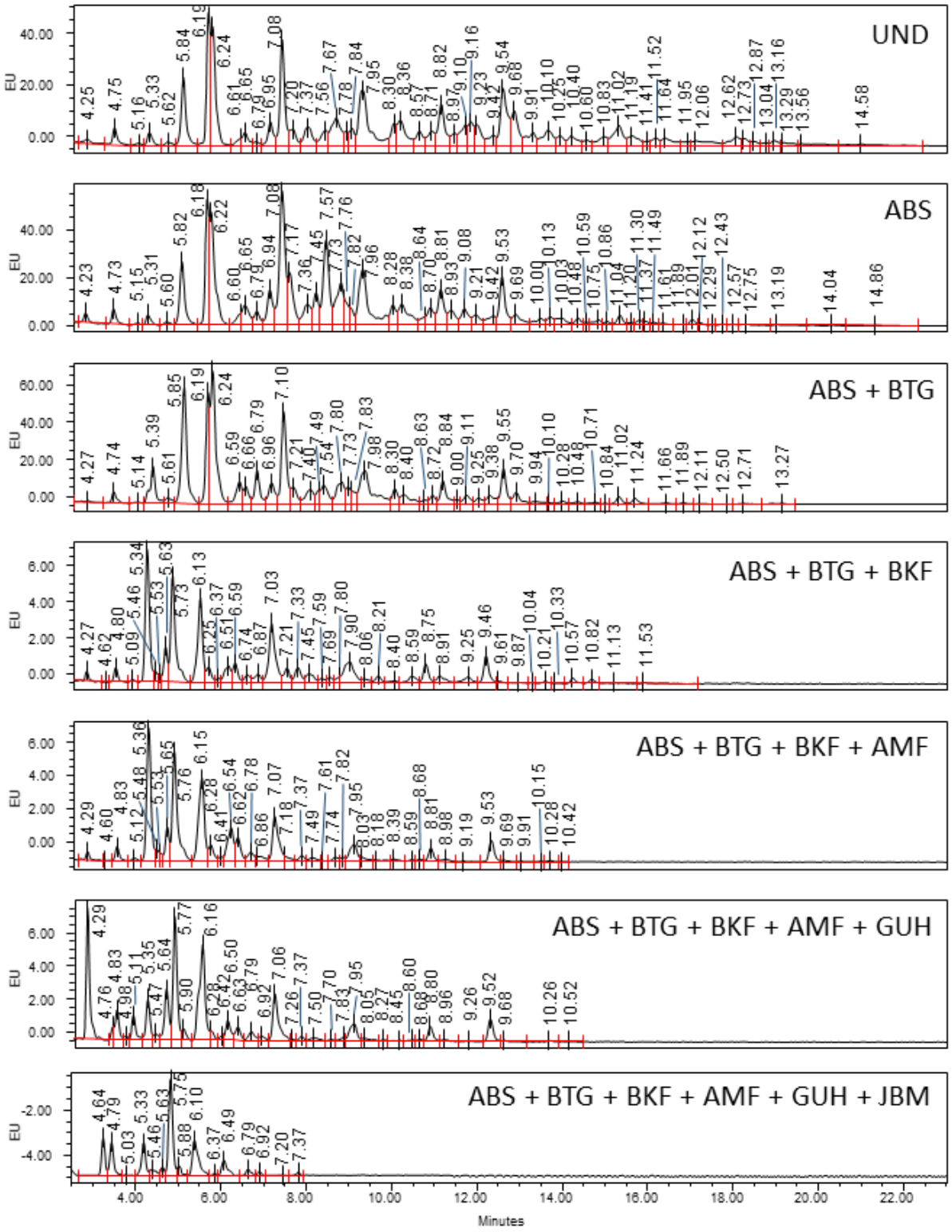

Figure 6.7 Main panel of exoglycosidase digestions profiled using HILIC-UPLC. NAN-1 removes α(2-3)-sialic acids, ABS removes α(2-3, 6, 8)-sialic acids. BTG removes β(1-3, 4) galactose, BKF removes core α(1-6)-fucose and outer arm α(1-2)-fucose, AMF removes α(1-3, 4)-fucose and GUH removes β-GlcNAc. Peaks are labelled with GU values. EU, emission units.

The majority of *N*-glycans identified were found to be complex (36%), being mono-, di- , tri- or tetra-antennary. Complex glycans containing a bisecting GlcNAc contributed a further 7%. A range of oligo-mannose species were also highly abundant, having from 3 to 9 mannose residues and making up approximately 26% of all *N*-glycans (Figure 6.8 A). Large high-mannose structures, M6, M7, M8, M9 and M10 were far more abundant than the smaller M4 and M5 species. M4 and M5 were more commonly found as hybrid glycans, i.e. oligo-mannose structures with a single antenna. These constituted 8% of all *N*-glycans (Figure 6.8 A). The remaining 23% were made up of more unusual glycan species including sulphated glycans (9%), those terminating in sialic acids modified with extra acetyl groups (8%), and alpha-galactose containing glycans (6%) (Figure 6.8 B). Of the complex glycans di- and tri-antennary were most common (A2 and A3) each making up 17% of total *N*-glycans. Tetra-antennary glycans (A4) made up approximately 7% of total *N*-glycans with mono-antennary (A1) glycans present as a minor species at 2% (Figure 6.8 C).

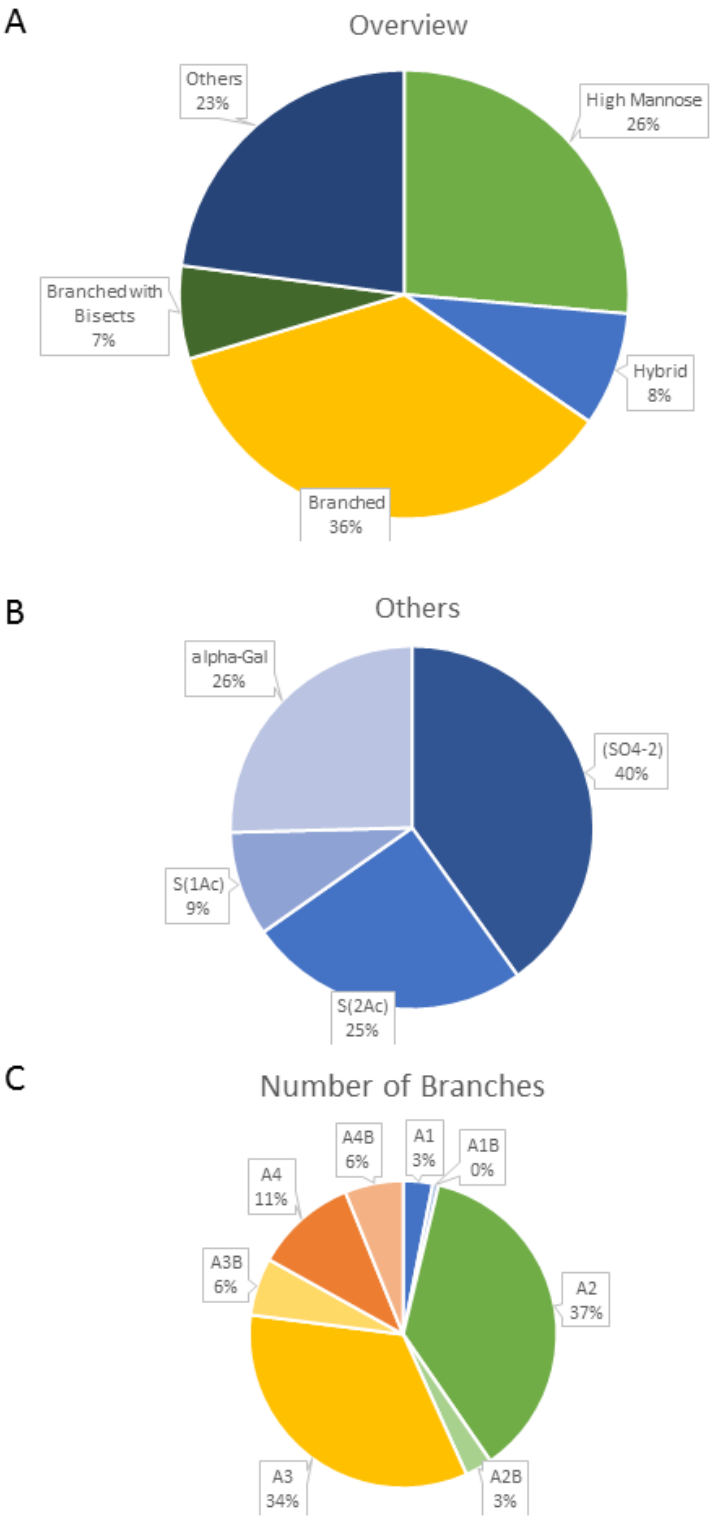

Figure 6.8 Summary of the types of *N*-glycan identified in the adult rat spinal cord. (A) All of the major classes of *N*-glycan can be found in the spinal cord, high-mannose, hybrid and branched. Branched glycans also occur with a bisecting GlcNAc β(1-4) linked to the central mannose. (B) In the group shown as 'others' in (A) are glycans decorated with some more unusual modifications. These modifications occur on all of the main classes of glycan. (C) A breakdown of the number of branches and their relative abundance found on branched and bisected glycans. A2 and A3 structures are most common.

On complex glycans extension of the branch with galactose residues is very common. 79% of hybrid glycans, 74% of complex glycans and 89% of complex glycans with bisects had their antennae further decorated with galactose residues. Galactose was found to be present mainly in β(1-4) linkage to the underlying GlcNAc. β(1-3) linkage was ruled out based on the similarity between BTG and SPG digests (see Figure 6.9). Minor amounts of α-linked galactose were identified (on approximately 6% of total *N*-glycan species) on complex glycans including A1, A2, A3, A4 (see table in Appendix X). CBG digestion confirmed the presence of galactose in this linkage (Figure 6.10). No α-linked galactose was found on hybrid structures or on complex glycans with bisects (see table in Appendix X).

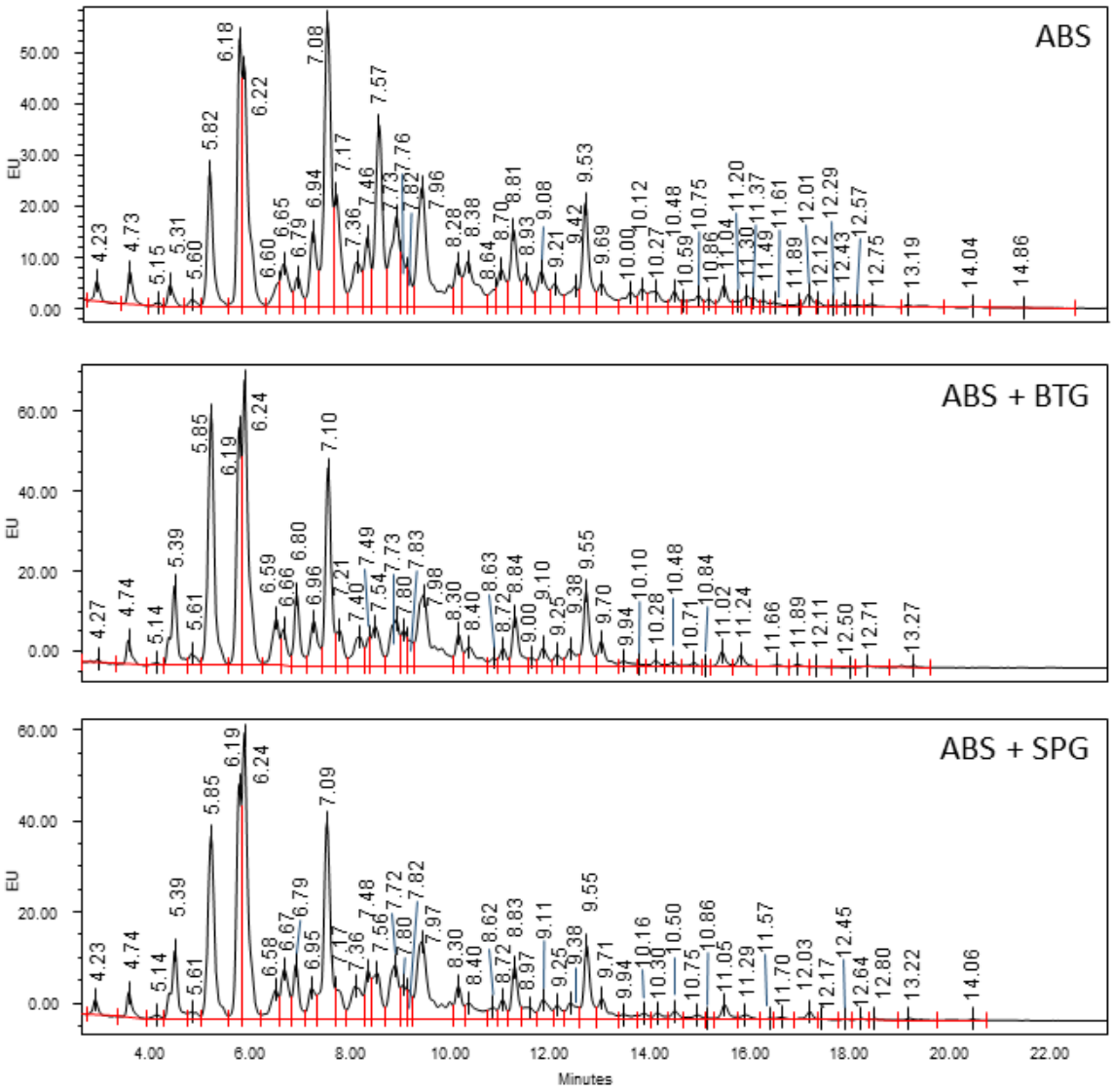

Figure 6.9 Galactose is generally linked to GlcNAc in β(1-4) linkage. BTG removes β(1-3) and (1-4) linked galactose while SPG removes only β(1-4)-galactose. The two digests are highly similar indicating that galactose is present in β(1-4) linkage to GlcNAc. Peaks are labelled with GU values. EU, emission unit.

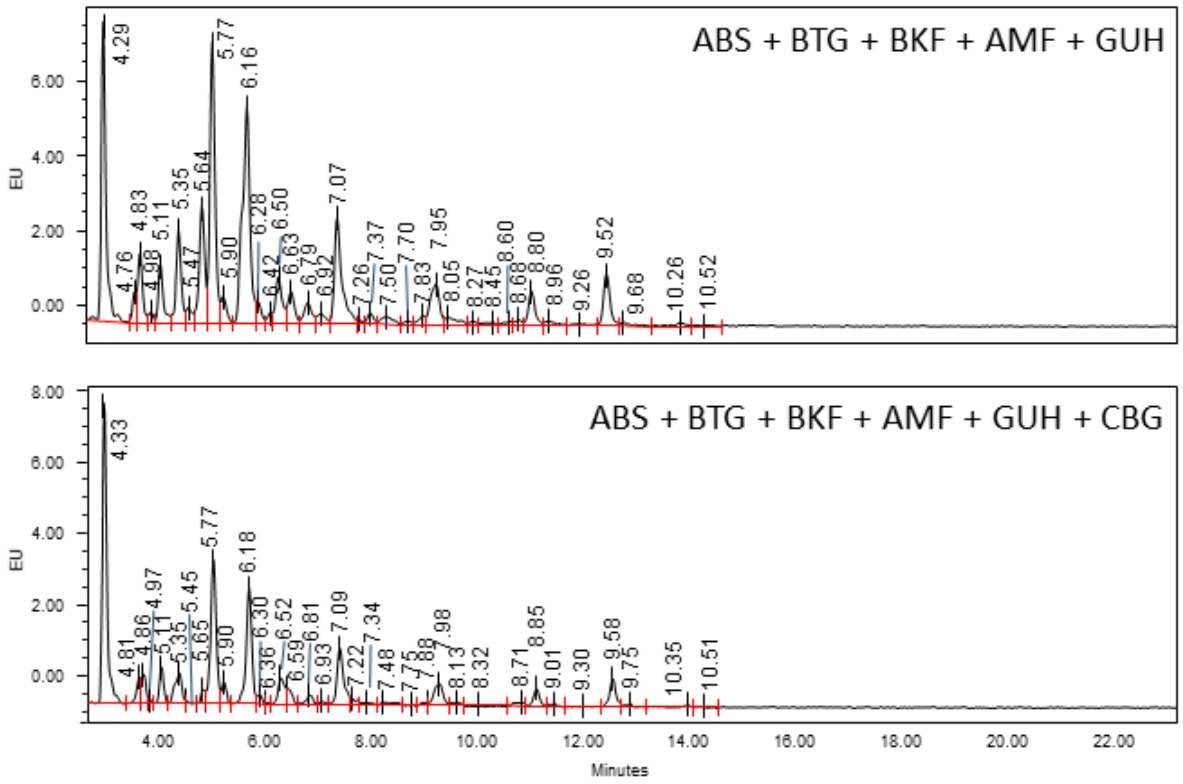

Figure 6.10 Small amounts of α-linked galactose are present in the rat spinal cord. α-linked galactose prevents digestion of the antennae it is attached to. CBG removes α(1-3) and α(1-4) linked galactose. Digestion with a full panel of enzymes including GUH and CBG allows complete digestion of these α-galactose decorated antennae. Major peaks at 5.64 and 6.16 can be seen to digest with CBG, as well as a number of other smaller peaks. Peaks are labelled with GU values. EU, emission unit.

In agreement with the WAX-HPLC result only minor changes were seen with ABS digestion, confirming a low level of sialylation. Sialic acid was deemed present in both α(2,3) and α(2,6) linkage due to the differential digestion with NAN-1 and ABS enzymes, Figure 6.11. Terminal sialic acid was seen in small amounts on all glycan types: hybrid glycans, complex glycans, and complex glycans with bisects, and on structures decorated with core and/or outer arm fucose (table in Appendix X). Sulphated and α-galactose containing glycans also carry sialic acid. Small amounts (<3%) of a form of poly-sialylation were also seen in the rat spinal cord. Poly sialic acid usually occurs as long chains of α(2-8)-sialic acid. This was not seen here, however there were a number of glycans carrying only a single galactose which exhibited two sialic acid residues present in either α(2-3) or α(2-6) linkage, with α(2-8) linkage also possible (table in Appendix X). Galactose is generally accepted as only being capable of binding a single sialic acid residue so the precise structure of these unusual poly-sialylated glycans is unclear. Perhaps it is possible for the sialic acid to attach to the GlcNAc branch, as suggested in (Saldova *et al.*, 2013).

The various sialic acid species identified with DMB assay, Neu5Ac, Neu5Gc and Neu5Ac with additional acetyl groups, could be assigned in similar proportions using HILIC-UPLC and exoglycosidase digestions. Neu5Gc type sialic acid has a larger GU shift on digestion with sialidase. LC-MS data confirmed the presence of glycans terminating in this Neu5Gc type sialic acid (tables in Appendix X, Appendix XI). Neu5Ac sialic acid with additional acetyl groups was more difficult to assign, and many of these species could not be confirmed by LC-MS. However, acetylation of sialic acid makes it resistant to digestion with sialidase, and so the whole branch decorated with this sialic acid will remain intact in the presence of any combination of exoglycosidase enzymes. Undigested glycans at a GU of 5.35 and 5.47 in the ABS+BTG+BKF+AMF+GUH digest (Table in Appendix X) were identified as A1G1S1-2Ac and A1G1S1-1Ac following discussion with the NIBRT Contract Research group (confidential client data, exoglycosidase digestion, HILIC-UPLC and LC-MS). Further extension of this 'core' structure was then followed through the range of exoglycosidase digestions to build the final structures shown.

This acetylated sialic acid was only present on complex glycans (A1, A2, A3, A4), some of which were further decorated with core and/or outer arm fucose (Figure 6.7 and table in Appendix X).

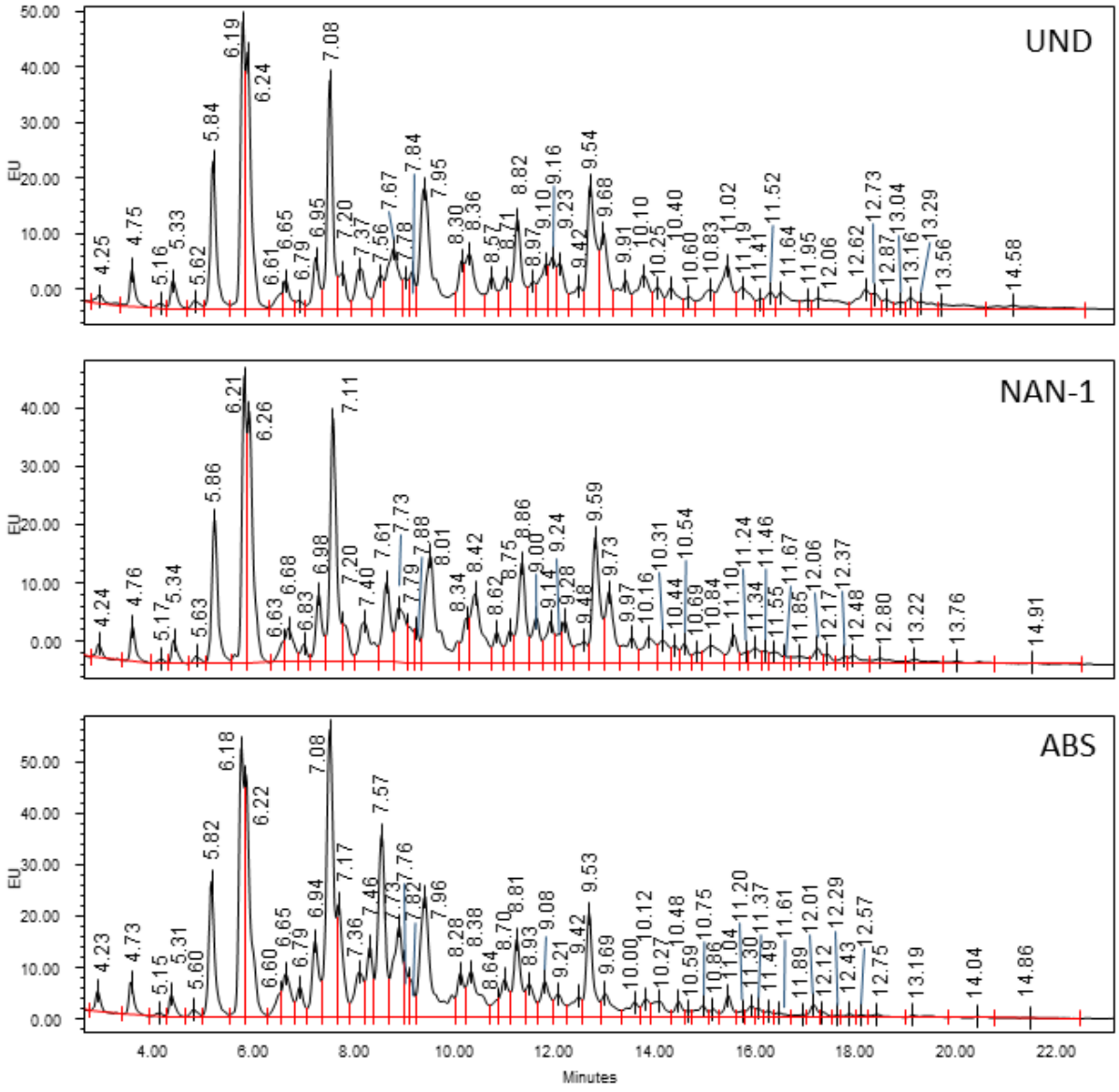

Figure 6.11 Spinal cord *N*-glycan sialic acids are found in both α(2-3) and α(2-6) linkage. NAN-1 digests α(2-3) linked sialic acids only, ABS removes α(2-3, 6, 8) linked sialic acids. Some digestion was seen on treatment of glycans with NAN-1, with further digestion seen with ABS indicating both α(2-3) and α(2-6) or α(2-8) linkages .

Fucosylation was found to be very common on rat spinal cord *N*-glycans. Core fucose was present on 24% of all *N*-glycans (Figure 6.12 A), outer arm fucose was seen on 8% of all *N*-glycans (Figure 6.12 B) and 11% of all *N*-glycans were decorated with both core and outer arm fucose residues (Figure 6.12 C). The bar chart in (Figure 6.12 D) illustrates where substitution with fucose is most common. The majority of complex glycans (hybrid, complex and complex with a bisect) were decorated with fucose: 75%, 87% and 63% respectively. Following the general trend, fucose was most commonly found as a core fucose residue on hybrids (35% of all hybrids), complex glycans (50% of all complex) and complex glycans with a bisect (26% of all bisected). The presence of both core and outer arm fucose was more common than solely outer arm fucose for all three glycan types: 25% vs 15% for hybrid, 22% vs 15% for complex, and 21% vs 16% for bisected (Figure 6.12 D).

Of the high mannose species, the majority were non-fucosylated with only 8% decorated with a core fucose (Figure 6.12 D). Outer arm fucosylation is not possible on high mannose glycans.

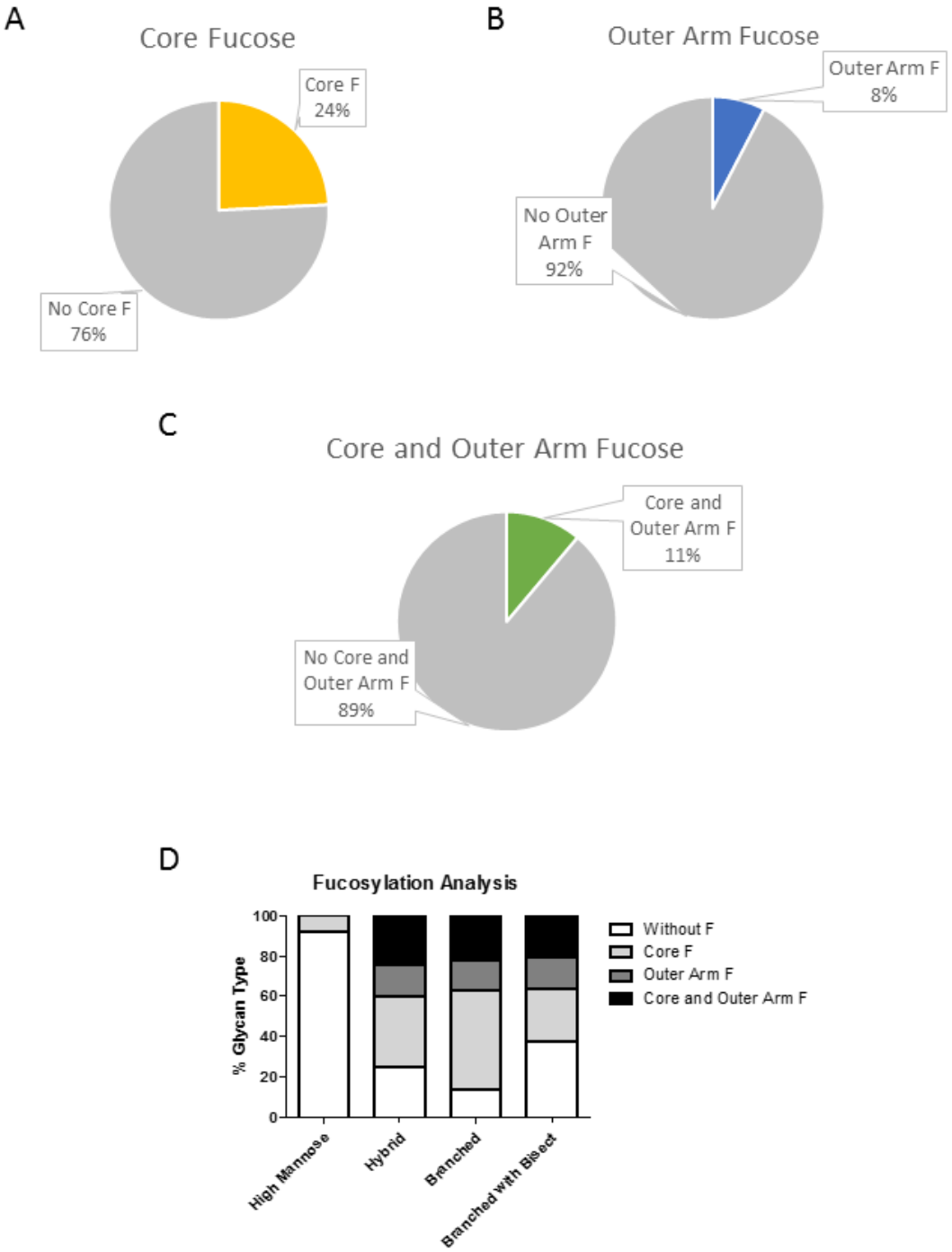

Figure 6.12 Frequency of fucose decoration on *N*-glycans of the rat spinal cord. (A) Proportion of total glycans decorated with core fucose. (B) Proportion of total glycans decorated with outer arm fucose. (C) Proportion of total glycans decorated with both core and outer arm fucose (D) distribution of fucosylation across the main *N*-glycan classes.

Core fucose on mammalian *N*-glycans is always present in α(1-6) linkage to the GlcNAc residue involved in the *N*-glycosidic bond to the protein's asparagine residue (Stanley P, 2017). Outer arm fucose can occur in a variety of positions and linkages. Outer arm fucose can be found on galactose or GlcNAc residues on *N*-glycan branches. In the rat spinal cord, the majority of fucose was deemed to be present on GlcNAc residues due to the absence of digestion seen with ABS+AMF digest. Only when galactose residues were removed could AMF successfully digest fucose (compare ABS+AMF digest to ABS+BTG+AMF, Figure 6.13). The linkage of outer arm fucose in rat spinal cord was determined to be α(1-3) in most cases: AMF is capable of digesting α(1-3) and α(1-4), but since the galactose is present in α(1-4) conformation, it is not possible to also have fucose in this same conformation side by side. Therefore fucose was assigned as being in the α(1-3) linkage in most cases. A small number of glycans were found to have α(1-2) linked fucose due to their digestion with BKF only (Figure 6.14). This was distinguished from digestion of core fucose due to the difference in GU shift observed: a shift of 0.4 to 0.5 is typical of core fucose, with a shift of approximately 0.7 seen with the removal of outer arm fucose.

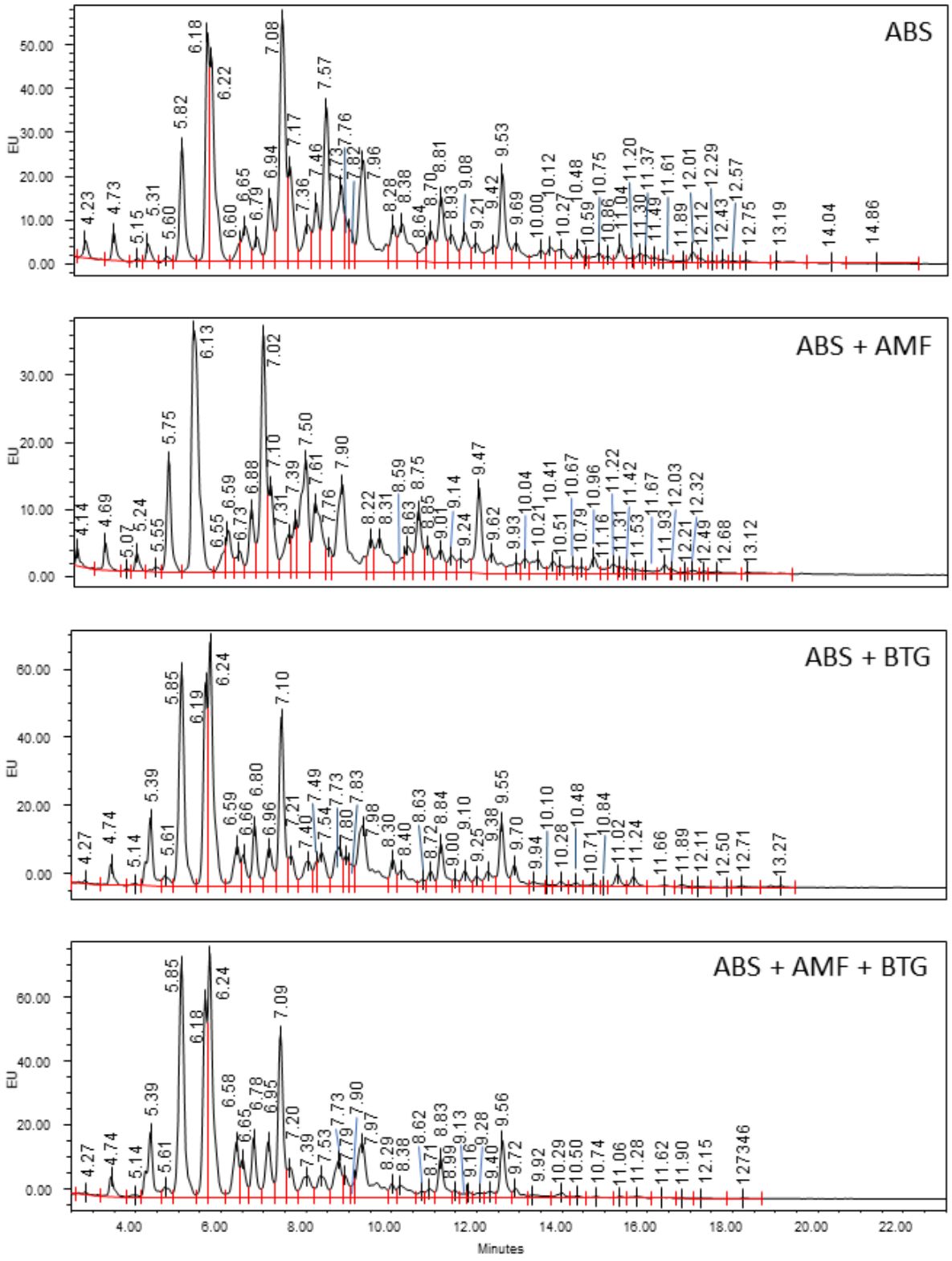

Figure 6.13 Outer arm fucose is attached to GlcNAc on *N*-glycan branches. The presence of galactose attached to the same GlcNAc residues sterically prevents digestion of α(1-3)-fucose by AMF. When glycans are digested with a combination of AMF and BTG the galactose is removed, making it possible for AMF to access the underlying fucose and cleave.

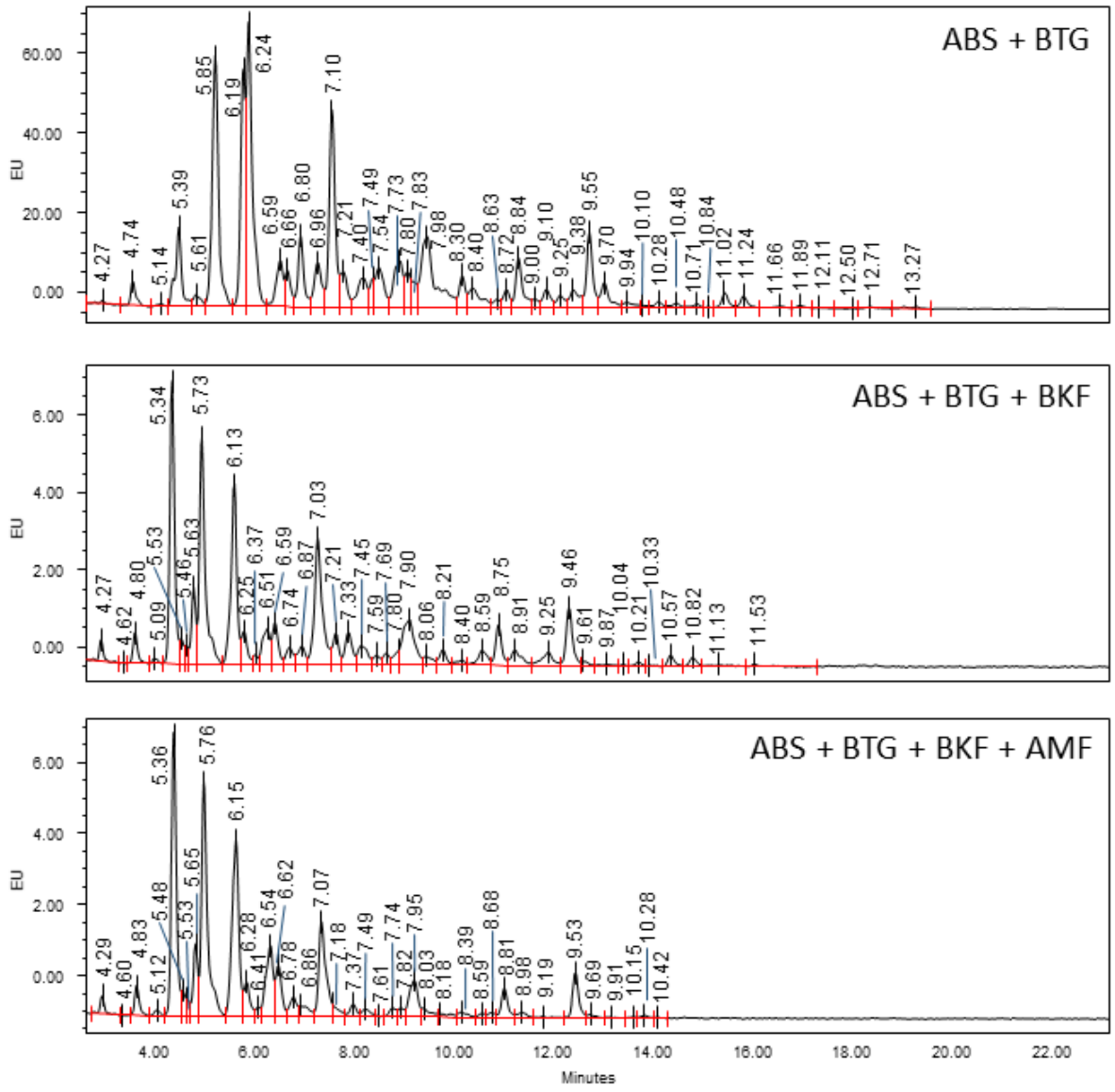

Figure 6.14 Core and outer arm fucose are widespread on rat spinal cord *N*-glycans. Many peaks shift to the left on digestion with BKF indicating widespread core fucosylation of spinal cord *N*-glycans. Some outer arm α(1-2)-fucose also digests with this enzyme. Further digestion is achieved on addition of AMF indicating a large amount of outer arm α(1-3)-fucose.

The presence of branch extension by GalNAc was investigated with the enzyme JBH. No additional digestion was seen with ABS + JBH compared to ABS alone, suggesting an absence of GalNAc residues, Figure 6.15.

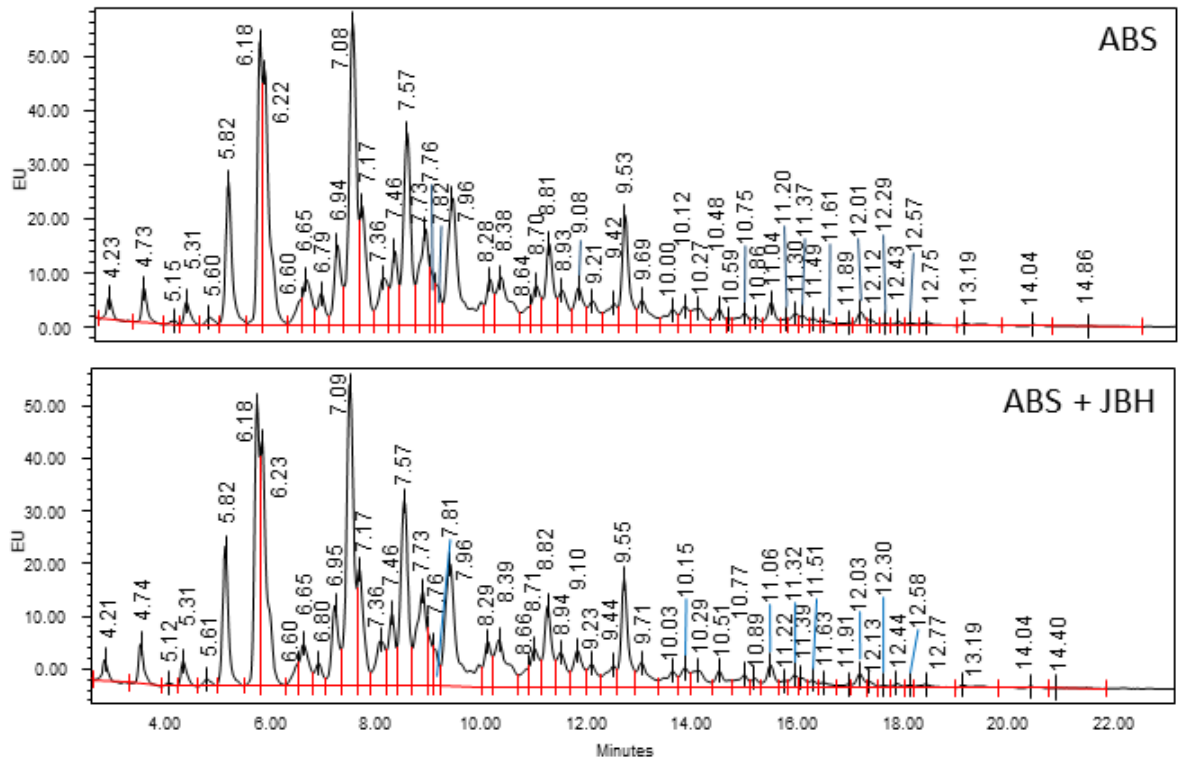

Figure 6.15 No GalNAc is present on rat spinal cord *N*-glycans. JBH is a hexosaminidase which digests both GlcNAc and GalNAc. However the majority of GlcNAc residues here are further decorated with galactose, fucose and sialic acids, making them resistant to digestion. The absence of digestion with JBH indicates an absence of branch extension by GalNAc.

In order to consider changes in glycosylation which may occur in the context of SCI and its treatment it is necessary to determine the major structure for each glycan peak. Table 6.3 below indicates the major structures seen in the characterisation study, and relates it to the corresponding glycan peak seen in the SCI study (Section 6.5.3). In cases where more than one peak in the characterisation experiment relates to a single peak in the SCI experiment, the glycan which is more abundant was chosen. Abundance of individual glycans is shown in the table in Appendix X. A brief legend is included at the end of the table, for a full explanation of glycan nomenclature, see Introduction Section 1.5.4.

Glycan Peak (GU), Characterisation	**Peak %Area, Characterisation**	**Glycan Peak (Average GU), SCI**	**Structure**	
1 (4.25)	0.31	**1 (4.25)**	M3	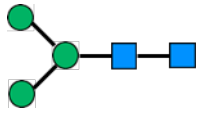
2 (4.75)	1.02	**2 (4.72)**	FM3	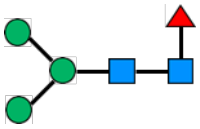
3 (5.16)	0.16	**3 (5.26)**	M4	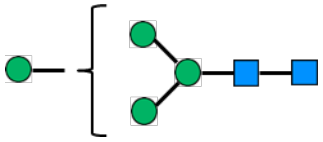
4 (5.33)	0.89		FA1*	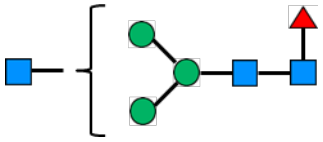 *

5 (5.62)	0.31	**4 (5.63)**	M4A1	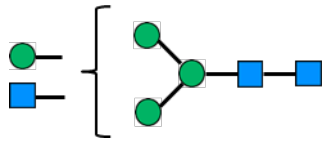
			FM4	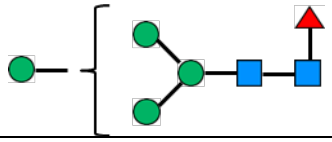
6 (5.84)	4.71	**5 (5.80)**	FA2	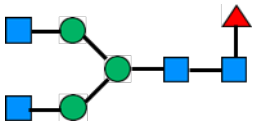
7 (6.19)	6.45	**6 (6.17)**	M5	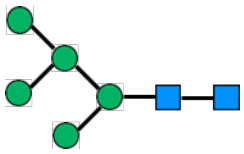
8 (6.24)	8.05		FA3*	* 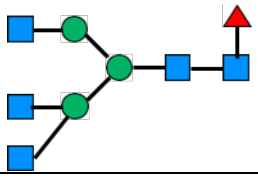
9 (6.61)	0.50	**7 (6.57)**	A4	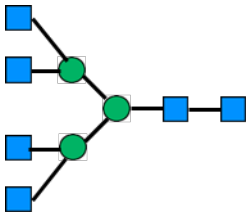
10 (6.65)	1.03	**8 (6.63)**	FM5	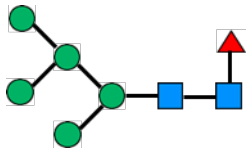
11 (6.79)	0.29	**9 (6.77)**	A2G2	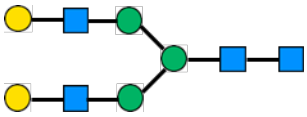
12 (6.95)	1.75	**10 (6.94)**	A3F(2)1G1S(2Ac)1	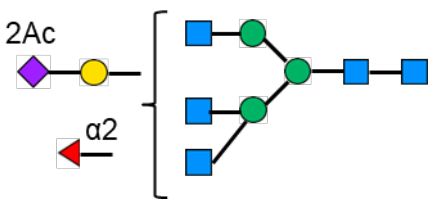

13 (7.08)	7.10	**11 (7.08)**	M6	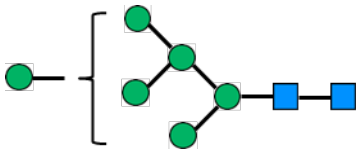
14 (7.20)	1.41	**12 (7.19)**	FA3G1	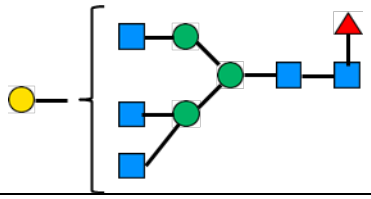
15 (7.37)	2.14	**13 (7.38)**	M6	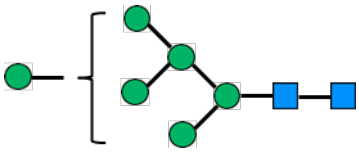
16 (7.56)	1.44	**14 (7.55)**	M6A1	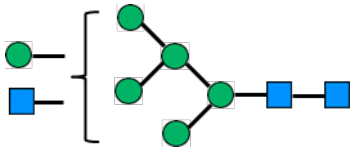
17 (7.67)	3.66	**15 (7.69)**	FM4A1F(2)1G1	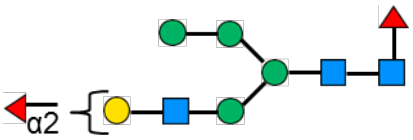
18 (7.78)	0.81	**16 (7.85)**	M7*	* 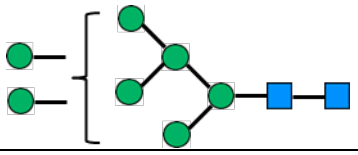
19 (7.84)	1.20		FA2F2G1 (both isomers with outer arm fucose F(2) and F(3) linked)	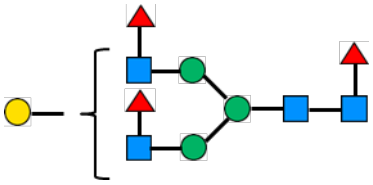
			FA2F2G(SO_4^{2-})1	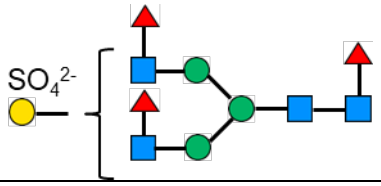
20 (7.95)	7.64	**17 (7.97)**	M7*	* 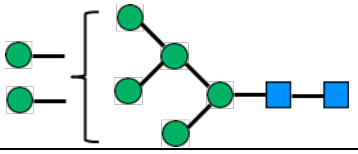

21 (8.30)	1.45		FA3F(2)3G1S(2Ac)1	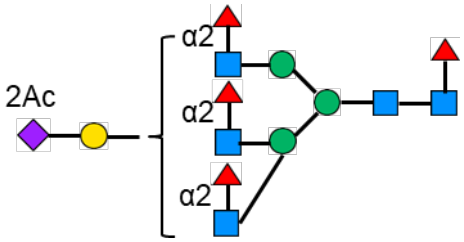
			A4G2	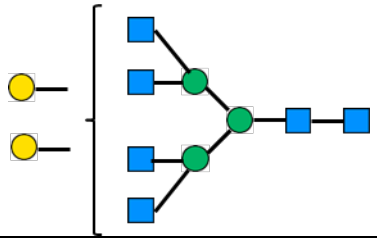
22 (8.36)	3.00	**18 (8.27)**	FA3G1S(6)1	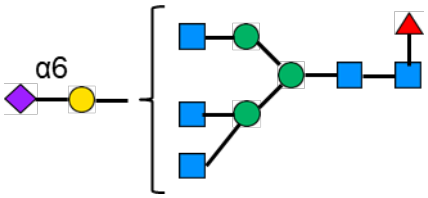
23 (8.57)	1.44	**19 (8.42)**	A3F2G(SO_4^{-2})1G1	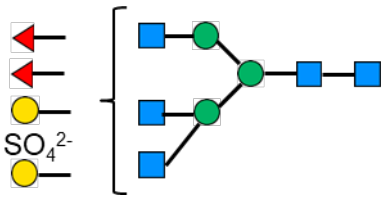
			FA3G1S(3)2	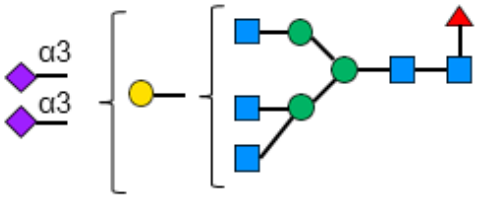
24 (8.71)	1.40	**20 (8.70)**	A3BG3	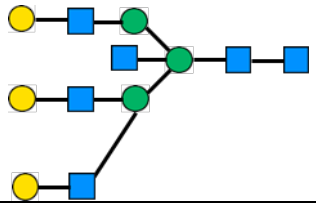
25 (8.82)	3.79	**21 (8.82)**	M8	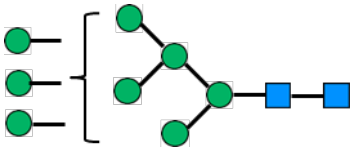

26 (8.97)	0.96	**22 (8.95)**	M8	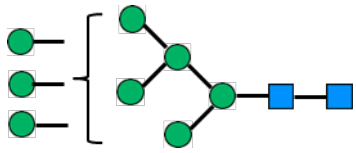
27 (9.10)	1.93	**23 (9.02)**	FA2G2Ga2	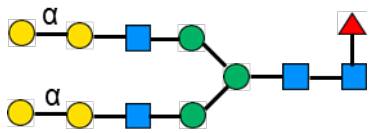
28 (9.16)	1.81	**24 (9.09)**	FA2G2S(3)2	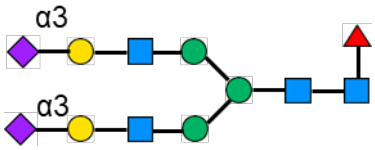
29 (9.23)	1.86	**25 (9.26)**	FA3F1G3S(2Ac)1	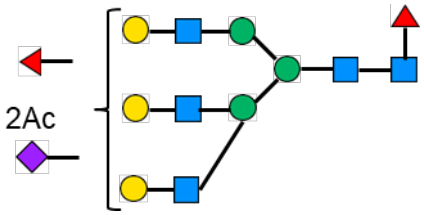
			FM5A1G1S(6)1	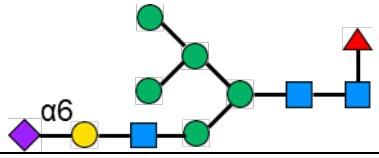
30 (9.42)	1.22	**26 (9.46)**	A2F(2)2G1Ga1S(6)1	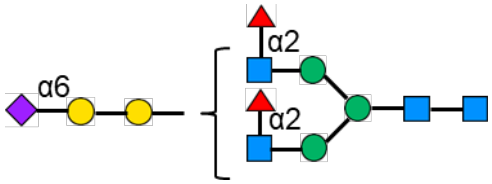
31 (9.54)	5.54	**27 (9.54)**	M9	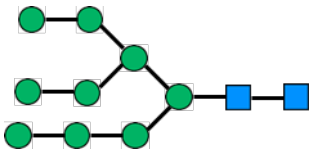

32 (9.68)	3.23	**28 (9.71)**	M9 A3G2S(6)2	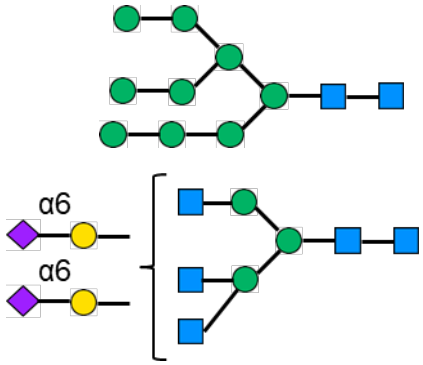
33 (9.91)	1.71	**29 (9.93)**	FA3F3G(SO_4^{-2})1G1 A3F(2)1G(*)1G1Ga1	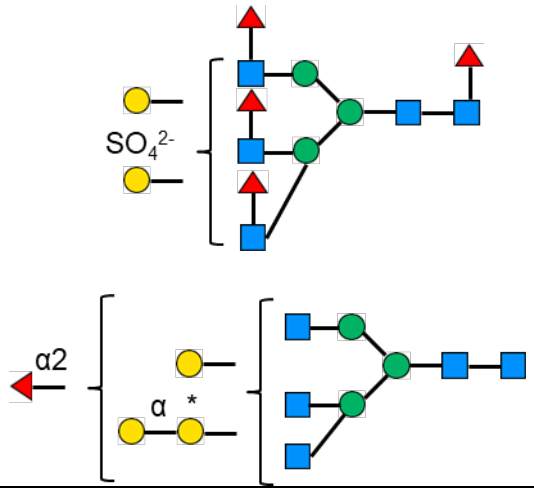
34 (10.10)	2.23	**30 (10.10)**	FA2G2Sg(3)1S(6)1	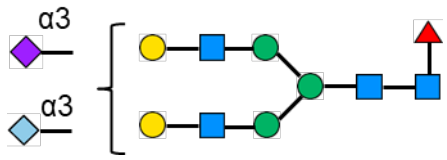
35 (10.25)	1.01	**31 (10.32)**	M9Glc1	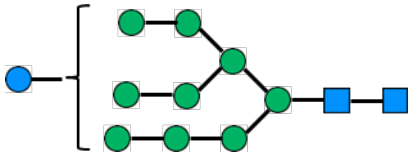

36 (10.40)	1.25	**32 (10.54)**	FA2F1G1Sg(6)1S(8)1 or FA2F1G1S(6)1Sg(8)1 or FA2F1G1Sg(6)1S(6)1	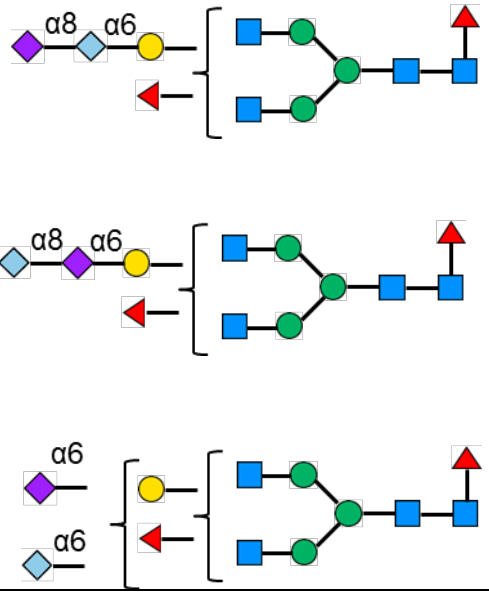
37 (10.60)	0.58	**33 (10.71)**	FA3F(2)3G3	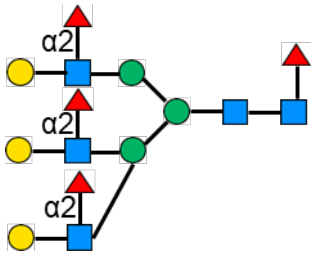
38 (10.83)	1.25	**34 (10.91)**	FA3G(SO_4^{-2})1G2Lac2 FA2F2G2S(6)2	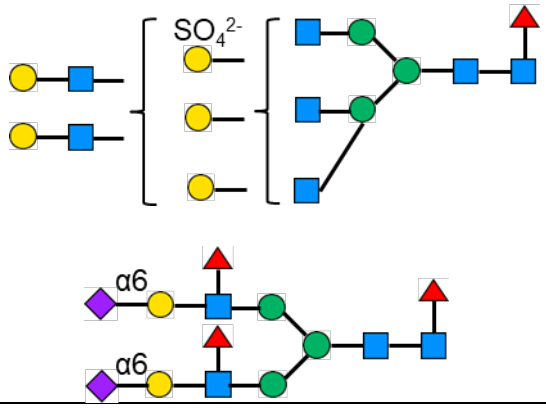

39 (11.02)	2.65	**35 (11.03)**	A2F(2)2G1Ga1Sg(3)2 FA3BF3G3 FA3F2G3S(2Ac)1	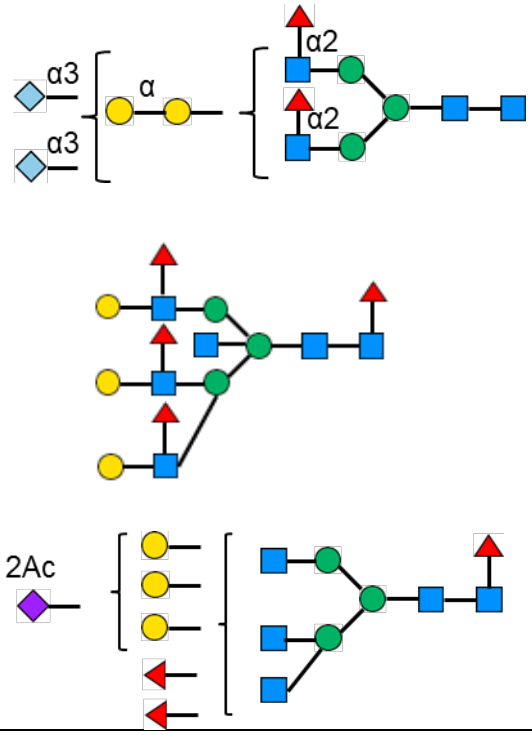
40 (11.19)	1.51	**36 (11.34)**	FA4F3G3	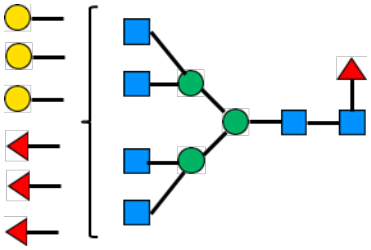
41 (11.41)	0.33	**37 (11.44)**	Sialylated A3 structures with or without fucose in core or outer arm positions	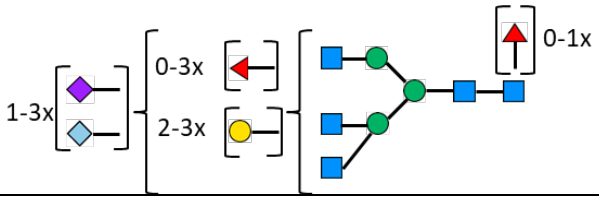
42 (11.52)	0.78		FA2G2S(6)2S(8)2 or FA2G2S(6)4*	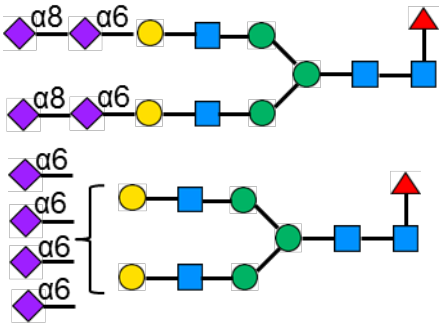 *

43 (11.64)	1.26	**38 (11.80)**	A3F(2)2F(3)1G1G(*)1Ga1	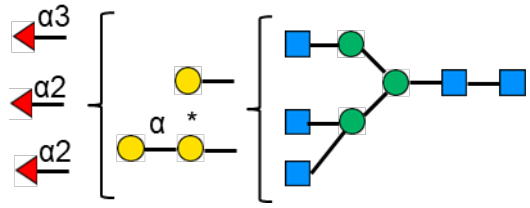
44 (11.95)	0.45		FA4F1G(SO_4^{-2})1G2Lac2	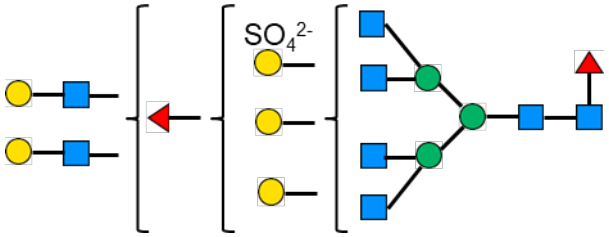
45 (12.06)	1.36	**39 (12.03)**	A4BG3Sg(3)1Sg(6)1	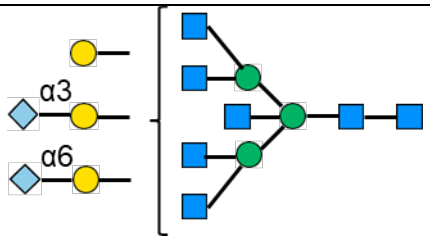
			FA3F2G2Sg(6)1S(3)1	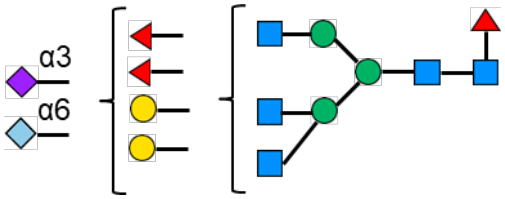
			A4BF1G4Sg(3)1	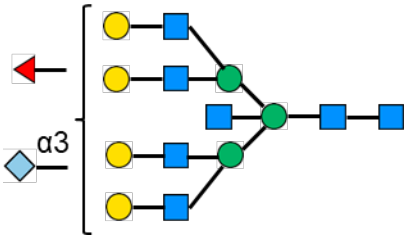
46 (12.62)	1.34	**40 (12.55)**	FA4F2G(SO_4^{-2})1G2Lac2	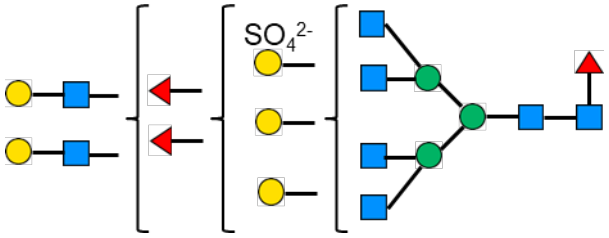

47 (12.73)	0.55	**41 (12.61)**	FA4F4G(SO_4^{-2})1G2GlcNAc3	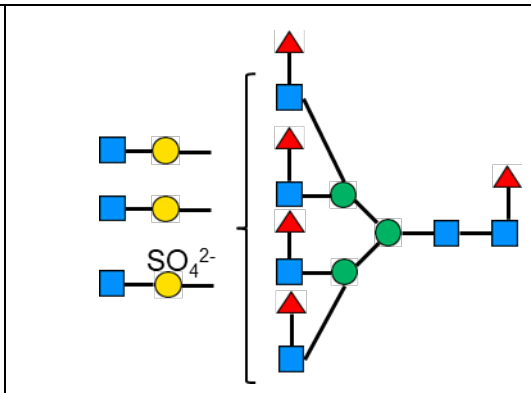
48 (12.87)	0.45	**42 (12.85)**	FA3F(2)3G1G(*)1Ga1Sg(3)1	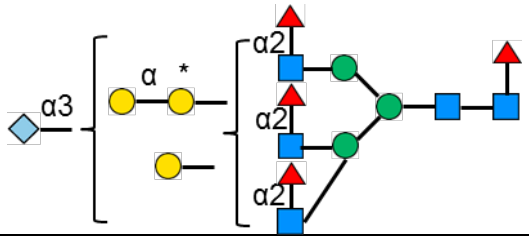
49 (13.04)	0.31	**43 (13.03)**	FA3F(2)3G1G(*)1Ga1Sg(3)1 (isomer of previous peak)	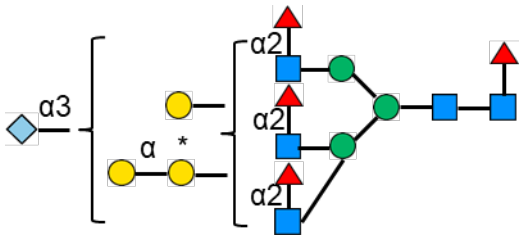
50 (13.16)	0.51	**44 (13.19)**	FA4F3G(SO_4^{-2})1G3GlcNAc4*	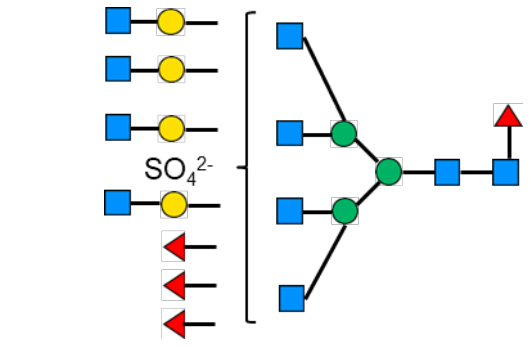 *
51 (13.29)	0.53		FA4F4G4S(6)1	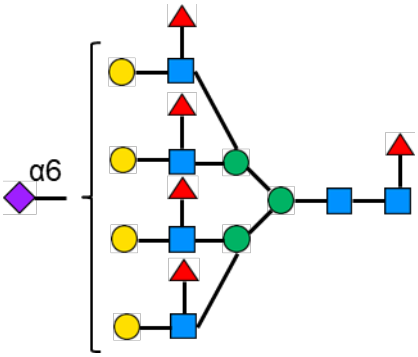

52 (13.56)	0.70	**45 (13.59)**	A3F(2)2G1G(*)1Ga1Sg(6)2	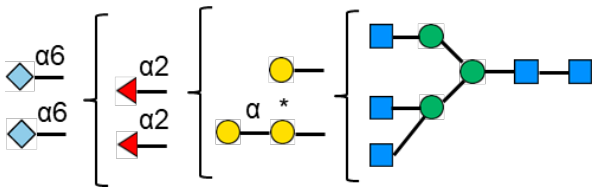
53 (14.58)	0.74	**46 (14.48)**	A4F1G4S(6)4	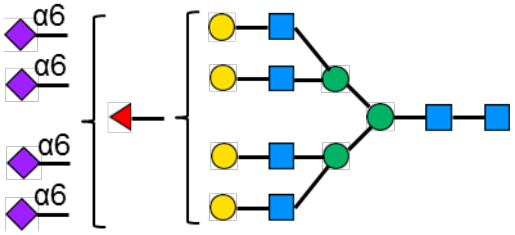

Monosaccharide symbols			
GlcNAc	Mannose	Galactose	Fucose
Sialic acid (Neu5Ac)	Sialic acid (Neu5Gc)	Sulphate (on galactose)	Acetyl (on sialic acid)
		SO_4^{2-}	Ac

Conventional linkage			
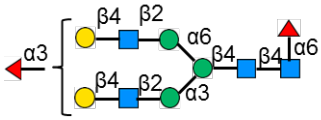	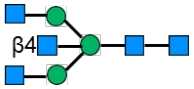	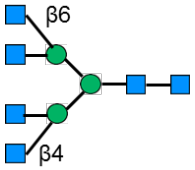

Table 6.3 The major glycans of each peak determined in the characterisation study, and translation of these structures to the *N*-glycoprofile obtained in the SCI study. The *N*-glycoprofile for the SCI study can be seen in the following section (6.5.3). In the case where one glycan peak in the SCI study translates to multiple peaks from the characterisation study the glycan with the highest overall abundance was chosen and is marked with an asterisk (*).The GU values shown for the SCI study are an average for the peak across all experimental animals. Changes in glycan peaks with SCI will be described in greater detail in the following sections. Dark blue squares, GlcNAc; green circles, mannose; yellow circles, galactose; red triangles, fucose; magenta diamonds, Neu5Ac type sialic acid; light blue diamonds, Neu5Gc type sialic acid. Unless otherwise stated, all galactose residues are in β(1-4) linkage, all outer arm fucose are in α(1-3) linkage, core fucose residues are in α(1-6) linkage and the branching of the core pentasaccharide and antennae follow the conventional linkage rules. Bisecting GlcNAc is β(1-4) linked to the central mannose. G(*) indicates a galactose residue which has been modified with an unidentified group causing the A1G(*)1Ga1 structure in the GUH digest to elute earlier than expected. For the complete list of all structures and how they digest with exoglycosidase

enzymes, see Appendix X. For mass data for these structures, see Appendix XI. For explanation of the glycan naming systems see Introduction, Section 1.5.4.

6.5.3 Changes in N*-glycosylation as a result of transection and treatment with aligned collagen hydrogel at the lesion epicentre*

Changes in *N*-glycosylation associated with spinal cord transection and treatment with collagen hydrogel composed of either randomly orientated or aligned collagen fibres were investigated using HILIC-UPLC *N*-glycoprofiling. Changes in *N*-glycosylation was investigated across three ROIs: Region A the lesion epicentre, Region B an area of intact tissue rostral to the injury and Region C an area of intact tissue caudal to the injury (Figure 6.1). Representative HILIC-UPLC chromatograms for Region A, the lesion epicentre of each treatment group at 7 dpi are shown in Figure 6.16 and representative chromatograms for each group at 14 dpi are shown in Figure 6.17. Chromatograms for regions B and C are highly similar to those of Region A and are not shown. The data is presented in the form of heat maps which illustrate the percentage change for each individual glycan peak as compared to the sham group for the relevant time-point. The heat map for Region A can be seen in Figure 6.18, for Region B in Figure 6.21 and for Region C in Figure 6.23.

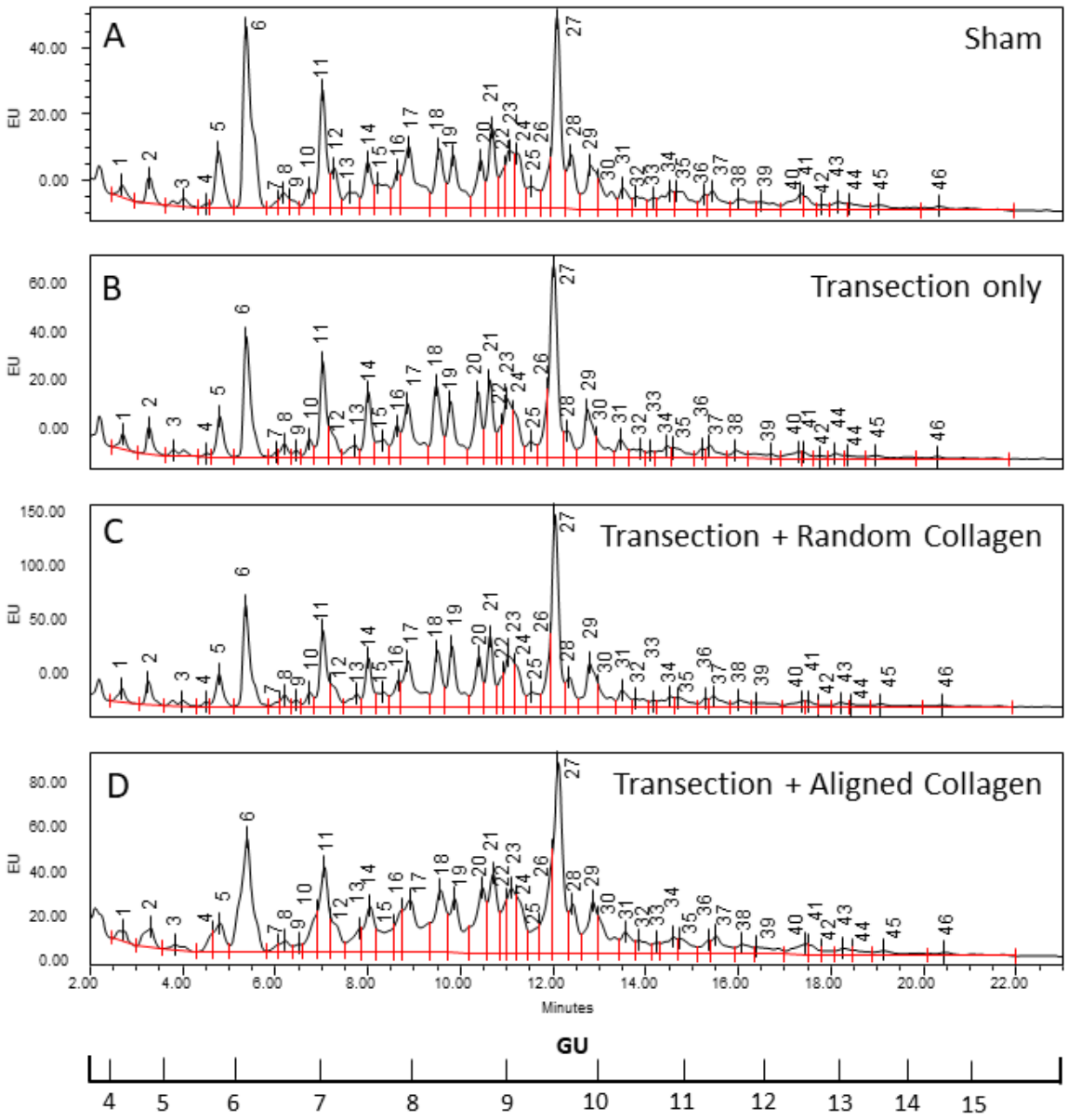

Figure 6.16 Representative HILIC-UPLC chromatograms for *N*-glycans released from the lesion epicentre of injured spinal cord at 7 dpi. (A) Sham injured, (B) transected, (C) transected and treated with random collagen hydrogel, (D) transected and treated with aligned collagen hydrogel. All peaks are labelled with the glycan peak (GP) number. GU, glucose units shown as a scale. EU, emission units.

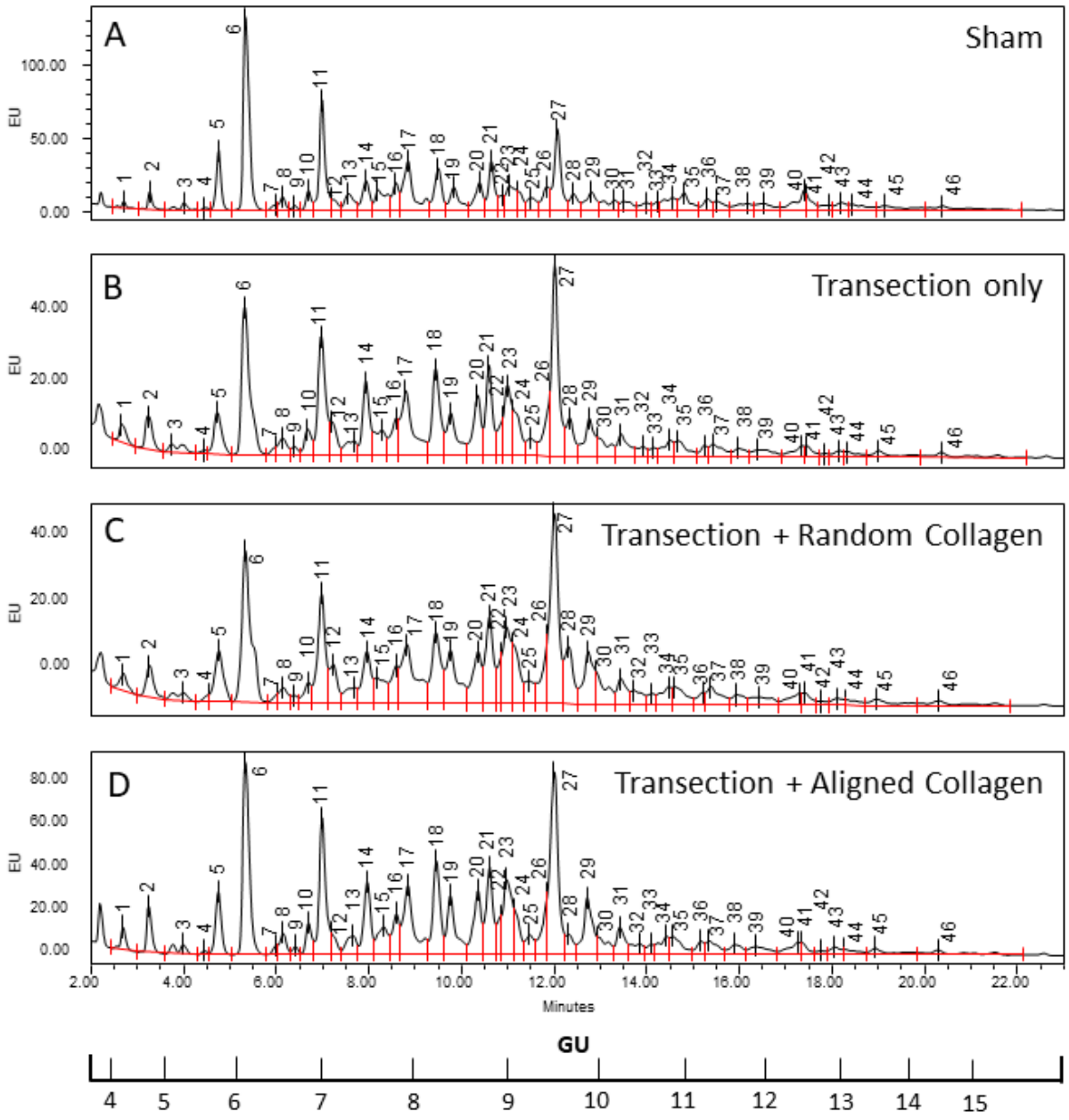

Figure 6.17 Representative HILIC-UPLC chromatograms for *N*-glycans released from the lesion epicentre of injured spinal cord at 14 dpi. (A) Sham injured, (B) transected, (C) transected and treated with random collagen hydrogel, (D) transected and treated with aligned collagen hydrogel. All peaks are labelled with the glycan peak (GP) number. GU, glucose units shown as a scale. EU, emission units.

6.5.3.1 There are widespread changes in protein N-*glycosylation in response to SCI in the lesion epicentre*

It can clearly be seen from the heat map in Figure 6.18 that there is a large response to injury in almost all of the 46 glycan peaks. For many of these peaks the response was almost uniform across the three injury groups, transection only, random collagen hydrogel and aligned collagen hydrogel, suggesting that the largest influence was from the injury and not from the presence of biomaterial treatment. However in a number of peaks small differences can be seen in the presence of the hydrogel. At 7 dpi for GP17 there was a decrease compared to sham in the transection only group while both of the collagen hydrogel groups remained unchanged. In GP26 all three groups were increased in comparison to sham, but this was more pronounced in the two collagen hydrogel treated groups. GP37 was unchanged in the transection only group, but decreased with the biomaterial treatment. In GP3 and GP30 there was a difference between the randomly oriented collagen hydrogel and the aligned collagen hydrogel: GP3 was increased in the random collagen hydrogel group and decreased in the aligned collagen hydrogel group and GP30 was decreased in random collagen hydrogel but unchanged in the aligned collagen hydrogel group (Figure 6.18).

At 14 dpi more changes began to emerge as being related to the treatment. GP3 was unchanged from sham in the transection only group at 14 dpi while there was an increase in the random and aligned collagen hydrogel groups. The random and aligned collagen groups were no different from sham in GP8 and GP26 but the transection only group was decreased in GP8 and increased in GP26. In GP10, GP28 and GP32 all three injury groups were different from each other. GP10 was increased in the transection only group, there was a smaller increase in the aligned collagen hydrogel group, and the random collagen hydrogel group was decreased. GP28 was very slightly increased in the transection only group, strongly increased in the random collagen hydrogel group and strongly decreased in the aligned collagen hydrogel group. GP32 was decreased in the transection only group, slightly increased in the random collagen hydrogel group and more strongly increased in the aligned collagen hydrogel group. In other peaks the aligned collagen hydrogel group behaved differently than the random collagen hydrogel and the transection only groups. GP4 was decreased in the aligned collagen hydrogel group but increased in the random collagen hydrogel and the transection only groups. GP24 was increased in all three groups but to a smaller extent in the aligned collagen hydrogel group than in the other two. GP30 was much more decreased in the aligned collagen hydrogel group than in either of the other two groups, and GP39 was unchanged in the aligned collagen hydrogel group while there was a decrease in the random collagen hydrogel and the transection only groups (Figure 6.18).

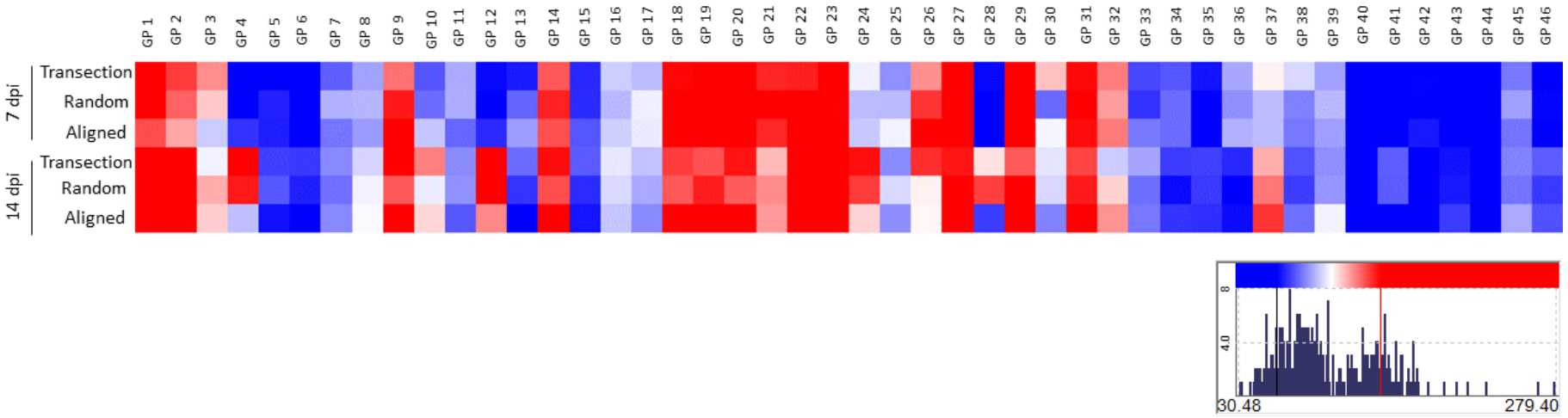

Figure 6.18 Heat map demonstrating the changes in glycan peak (GP) 1 to 46 in response to spinal cord transection with or without treatment with random or aligned collagen hydrogel in Region A, the lesion epicentre. Data is shown as the percentage of sham, i.e. the % area for each peak for each animal in the injury groups were expressed as a percentage of the mean peak % area for the corresponding sham group at 7 or 14 dpi. Blue squares indicate a decrease in comparison to sham, with the maximum decrease shown in darkest blue at 30.48%. Red squares indicate an increase in peak area in comparison to sham, with the maximum increase shown in darkest red at 279.4%.

Treatment was not found to be a significant contributor to any glycan peaks in region A when data was normalised to the sham groups, using the ANOVA general linear model. This is another indication that it is the transection injury itself which is majorly responsible for any changes in *N*-glycosylation in this region. Time-point on the other hand was found to significantly contribute to variance for many peaks, and there were some significant differences between experimental groups with regard to time-point, as seen with Tukey's multiple comparisons test. There was a significant difference in GP1 between 7 and 14 dpi for both the random ($p=0.006$) and aligned ($p=0.001$) collagen hydrogel groups, GP2 was significantly higher at 14 dpi for the random collagen hydrogel group ($p=0.032$), GP21 was significantly higher at 7 dpi for the random collagen hydrogel group ($p=0.033$) and GP36 was significantly lower at 14 dpi for both the random ($p=0.037$) and aligned ($p=0.020$) collagen hydrogel groups.

To investigate whether the response to transection injury and/or biomaterial treatment was significant as compared to sham, the ANOVA general linear model and Tukey's multiple comparisons test were performed on non-normalised data. Here the ANOVA found both time-point and treatment to be significant contributors to variance for most glycan peaks, and ignoring time-point all three injury groups were significantly different from sham. All three injury groups were different from the corresponding sham group at both 7 and 14 dpi in glycan peaks GP6, GP34, GP35, GP40, GP43, GP44 and GP46, at 7 dpi only in GP5, GP20 and GP21, and at 14 dpi only in GP1, GP15, GP36 and GP42. For p values see Table 6.4. There were significant differences from sham in just a subset of groups in: GP1 at 7 dpi (transection only and random collagen hydrogel) GP2 at 14 dpi (random and aligned collagen hydrogel groups), GP5 at 14 dpi (transection only and aligned collagen hydrogel), GP13 at 14 dpi (random and aligned collagen hydrogel groups), GP14 at 14 dpi (aligned collagen hydrogel), GP15 at 7 dpi (transection and random collagen hydrogel only), GP17 and GP18 at 14 dpi (aligned collagen hydrogel), GP19 at 7 dpi (random and aligned collagen hydrogel groups), GP23 at 14 dpi (aligned collagen hydrogel), GP27 at 7 dpi (transection only and random collagen hydrogel) and at 14 dpi (aligned collagen hydrogel only), GP29 at 14 dpi (aligned collagen hydrogel), GP31 at 7 dpi (random collagen hydrogel) and at 14 dpi (aligned collagen hydrogel only), GP33 at 7 dpi (transection only and random collagen hydrogel) and GP41 at 7 dpi (random collagen hydrogel). For p values see Table 6.4.

Glycan Peak	Time-point	Grouping	p value
GP1	7 dpi	Sham vs transection only	p=0.018
		Sham vs random collagen hydrogel	p=0.018
		Sham vs aligned collagen hydrogel	ns
	14 dpi	Sham vs transection only	p=0.004
		Sham vs random collagen hydrogel	p=0.000
		Sham vs aligned collagen hydrogel	p=0.000
GP2	7 dpi	Sham vs transection only	ns
		Sham vs random collagen hydrogel	ns
		Sham vs aligned collagen hydrogel	ns
	14 dpi	Sham vs transection only	ns
		Sham vs random collagen hydrogel	p=0.004
		Sham vs aligned collagen hydrogel	p=0.029
GP5	7 dpi	Sham vs transection only	p=0.004
		Sham vs random collagen hydrogel	p=0.020
		Sham vs aligned collagen hydrogel	p=0.018
	14 dpi	Sham vs transection only	p=0.026
		Sham vs random collagen hydrogel	ns
		Sham vs aligned collagen hydrogel	p=0.003
GP6	7 dpi	Sham vs transection only	p=0.001
		Sham vs random collagen hydrogel	p=0.000
		Sham vs aligned collagen hydrogel	p=0.000
	14 dpi	Sham vs transection only	p=0.016
		Sham vs random collagen hydrogel	p=0.006
		Sham vs aligned collagen hydrogel	p=0.000
GP13	7 dpi	Sham vs transection only	ns
		Sham vs random collagen hydrogel	ns
		Sham vs aligned collagen hydrogel	ns
	14 dpi	Sham vs transection only	ns
		Sham vs random collagen hydrogel	p=0.048
		Sham vs aligned collagen hydrogel	p=0.006
GP14	7 dpi	Sham vs transection only	ns
		Sham vs random collagen hydrogel	ns
		Sham vs aligned collagen hydrogel	ns
	14 dpi	Sham vs transection only	ns
		Sham vs random collagen hydrogel	ns
		Sham vs aligned collagen hydrogel	p=0.024
GP15	7 dpi	Sham vs transection only	p=0.021

		Sham vs random collagen hydrogel	p=0.024
		Sham vs aligned collagen hydrogel	ns
	14 dpi	Sham vs transection only	p=0.033
		Sham vs random collagen hydrogel	p=0.003
		Sham vs aligned collagen hydrogel	p=0.001
GP17	7 dpi	Sham vs transection only	ns
		Sham vs random collagen hydrogel	ns
		Sham vs aligned collagen hydrogel	ns
	14 dpi	Sham vs transection only	ns
		Sham vs random collagen hydrogel	ns
		Sham vs aligned collagen hydrogel	p=0.025
GP18	7 dpi	Sham vs transection only	ns
		Sham vs random collagen hydrogel	ns
		Sham vs aligned collagen hydrogel	ns
	14 dpi	Sham vs transection only	ns
		Sham vs random collagen hydrogel	ns
		Sham vs aligned collagen hydrogel	p=0.013
GP19	7 dpi	Sham vs transection only	ns
		Sham vs random collagen hydrogel	p=0.004
		Sham vs aligned collagen hydrogel	p=0.005
	14 dpi	Sham vs transection only	ns
		Sham vs random collagen hydrogel	ns
		Sham vs aligned collagen hydrogel	ns
GP20	7 dpi	Sham vs transection only	p=0.002
		Sham vs random collagen hydrogel	p=0.001
		Sham vs aligned collagen hydrogel	p=0.000
	14 dpi	Sham vs transection only	ns
		Sham vs random collagen hydrogel	ns
		Sham vs aligned collagen hydrogel	ns
GP21	7 dpi	Sham vs transection only	p=0.023
		Sham vs random collagen hydrogel	p=0.003
		Sham vs aligned collagen hydrogel	p=0.024
	14 dpi	Sham vs transection only	ns
		Sham vs random collagen hydrogel	ns
		Sham vs aligned collagen hydrogel	ns
GP23	7 dpi	Sham vs transection only	ns
		Sham vs random collagen hydrogel	ns
		Sham vs aligned collagen hydrogel	ns

	14 dpi	Sham vs transection only	ns
		Sham vs random collagen hydrogel	ns
		Sham vs aligned collagen hydrogel	p=0.002
GP27	7 dpi	Sham vs transection only	p=0.003
		Sham vs random collagen hydrogel	p=0.020
		Sham vs aligned collagen hydrogel	ns
	14 dpi	Sham vs transection only	ns
		Sham vs random collagen hydrogel	ns
		Sham vs aligned collagen hydrogel	p=0.033
GP29	7 dpi	Sham vs transection only	ns
		Sham vs random collagen hydrogel	ns
		Sham vs aligned collagen hydrogel	ns
	14 dpi	Sham vs transection only	ns
		Sham vs random collagen hydrogel	ns
		Sham vs aligned collagen hydrogel	p=0.025
GP31	7 dpi	Sham vs transection only	ns
		Sham vs random collagen hydrogel	p=0.040
		Sham vs aligned collagen hydrogel	ns
	14 dpi	Sham vs transection only	ns
		Sham vs random collagen hydrogel	ns
		Sham vs aligned collagen hydrogel	p=0.002
GP33	7 dpi	Sham vs transection only	p=0.023
		Sham vs random collagen hydrogel	p=0.010
		Sham vs aligned collagen hydrogel	ns
	14 dpi	Sham vs transection only	ns
		Sham vs random collagen hydrogel	ns
		Sham vs aligned collagen hydrogel	ns
GP34	7 dpi	Sham vs transection only	p=0.010
		Sham vs random collagen hydrogel	p=0.031
		Sham vs aligned collagen hydrogel	p=0.030
	14 dpi	Sham vs transection only	p=0.000
		Sham vs random collagen hydrogel	p=0.000
		Sham vs aligned collagen hydrogel	p=0.000
GP35	7 dpi	Sham vs transection only	p=0.000
		Sham vs random collagen hydrogel	p=0.000
		Sham vs aligned collagen hydrogel	p=0.000
	14 dpi	Sham vs transection only	p=0.001
		Sham vs random collagen hydrogel	p=0.001

		Sham vs aligned collagen hydrogel	p=0.000
GP36	7 dpi	Sham vs transection only	ns
		Sham vs random collagen hydrogel	ns
		Sham vs aligned collagen hydrogel	ns
	14 dpi	Sham vs transection only	p=0.002
		Sham vs random collagen hydrogel	p=0.000
		Sham vs aligned collagen hydrogel	p=0.001
GP40	7 dpi	Sham vs transection only	p=0.001
		Sham vs random collagen hydrogel	p=0002
		Sham vs aligned collagen hydrogel	p=0.001
	14 dpi	Sham vs transection only	p=0.000
		Sham vs random collagen hydrogel	p=0.000
		Sham vs aligned collagen hydrogel	p=0.000
GP41	7 dpi	Sham vs transection only	ns
		Sham vs random collagen hydrogel	p=0.025
		Sham vs aligned collagen hydrogel	ns
	14 dpi	Sham vs transection only	ns
		Sham vs random collagen hydrogel	ns
		Sham vs aligned collagen hydrogel	ns
GP42	7 dpi	Sham vs transection only	ns
		Sham vs random collagen hydrogel	ns
		Sham vs aligned collagen hydrogel	ns
	14 dpi	Sham vs transection only	p=0.001
		Sham vs random collagen hydrogel	p=0.000
		Sham vs aligned collagen hydrogel	p=0.000
GP43	7 dpi	Sham vs transection only	p=0.001
		Sham vs random collagen hydrogel	p=0.001
		Sham vs aligned collagen hydrogel	p=0.001
	14 dpi	Sham vs transection only	p=0.002
		Sham vs random collagen hydrogel	p=0.002
		Sham vs aligned collagen hydrogel	p=0.012
GP44	7 dpi	Sham vs transection only	p=0.006
		Sham vs random collagen hydrogel	p=0.009
		Sham vs aligned collagen hydrogel	p=0.005
	14 dpi	Sham vs transection only	p=0.001
		Sham vs random collagen hydrogel	p=0.000
		Sham vs aligned collagen hydrogel	p=0.000
GP46	7 dpi	Sham vs transection only	p=0.001

		Sham vs random collagen hydrogel	p=0.005
		Sham vs aligned collagen hydrogel	p=0.001
	14 dpi	Sham vs transection only	p=0.032
		Sham vs random collagen hydrogel	p=0.006
		Sham vs aligned collagen hydrogel	p=0.019

Table 6.4 GPs which changed significantly following SCI and/or treatment in Region A, the lesion epicentre. P-values for these peaks are indicated in this table. Text in red indicates a significant increase, text in blue indicates a significant decrease. Data was analysed in Minitab 17 using the ANOVA general linear model and Tukey's multiple comparisons test. A p-value <0.05 was considered significant.

Grouping individual GPs by feature can reveal more information about the types of changes seen with injury and with treatment. GPs were grouped according to the main features of the major glycan (Table 6.3) i.e. whether they were high mannose, hybrid, complex or complex with a bisect, and whether they were decorated with core fucose, outer arm fucose, both core and outer arm fucose or no fucose at all. The sulphated glycans (including those with Lac repeats) and alpha-gal containing glycans were considered as separate families. Sialylation was investigated independently using WAX-HPLC and is discussed in Section 6.5.3.3 below. The heat map in Figure 6.20 demonstrates the feature changes seen in response to the injury in Region A. From this feature analysis we can see that there were changes in high mannose type, hybrid and complex (particularly those with a bisect) *N*-glycans. Specifically, in relation to both hybrid and bisected type *N*-glycans, there was a decrease in those glycans carrying both core and outer arm fucose, with a corresponding increase in the non-fucosylated versions. This could be seen across all injured groups at both time-points and so can be considered a result of the transection injury. On complex glycans there was a reduction in those carrying only outer arm fucose and in those without any fucose at 7 dpi, and a reduction in those decorated with both core and outer arm fucose at 14 dpi across all three injured groups, Figure 6.20 A. There were no differences in the degree of branching on complex glycans between the treatment groups, Figure 6.20 B. Decoration of high mannose structures with core fucose was increased in all three injury groups at 14 dpi, but there was little change in the undecorated high mannose type glycans, Figure 6.20 A.

As the main changes in gycan type were a direct response to the injury, and not greatly influenced by the presence of the collagen hydrogel, features analysis the sham and transection only groups are shown independently on a bar graph in Figure 6.19. Using the t-test to compare sham injured to transected tissue at both 7 and 14 dpi significant differences were found for bisects without fucose, bisects with core and outer fucose, complex glycans carrying both core and outer fucose and hybrid

glycans carrying both core and outer fucose. At 14 dpi only there were additional differences in response to the injury for hybrid glycans with core fucose only or with no fucose, and for high mannose structures decorated with core fucose, Figure 6.19.

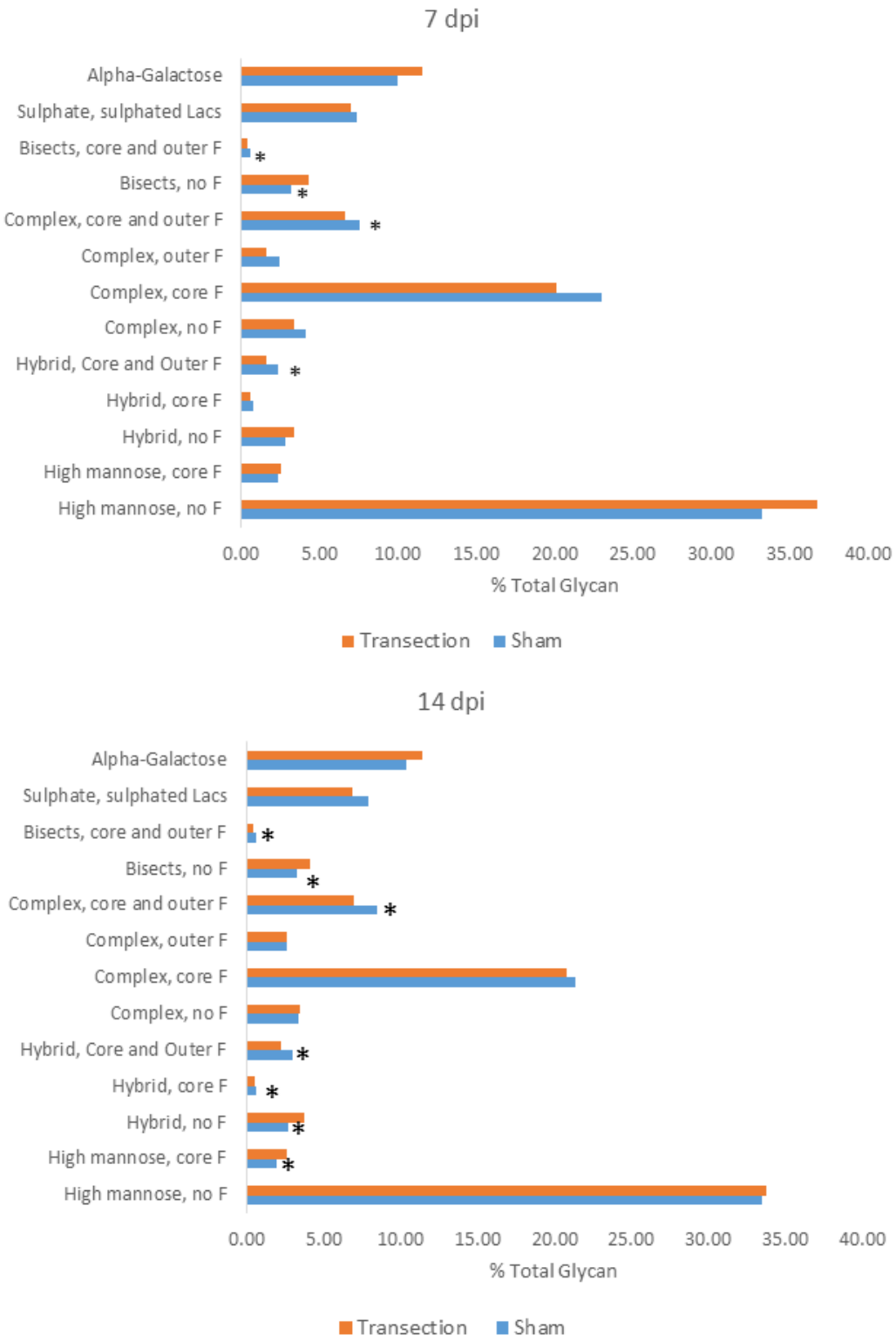

Figure 6.19 Differences in glycan features between sham and transection only groups, at 7 and 14 dpi. Asterisks indicate a difference between sham and transected groups, using the T-test, n=3, $p<0.05$.

Some subtle differences could be seen in those groups treated with a collagen hydrogel. At 7 dpi sulphated and sulphated glycans with Lac repeats were slightly decreased in the transection only group, but were slightly increased in the two collagen hydrogel treated groups. At 14 dpi, complex glycans decorated with outer arm fucose were unchanged in the transection only group, but were slightly decreased in both collagen hydrogel treated groups. Some small differences could also be seen depending on whether the collagen fibres were in a random or aligned orientation. Hybrid glycans decorated with core fucose were decreased in the transection only and random collagen hydrogel treated groups, but slightly increased in the aligned collagen hydrogel treated group at 7 dpi. These glycans were decreased in the transection only and the aligned collagen hydrogel treated groups at 14 dpi, but were unchanged in the random collagen hydrogel group at this time-point, Figure 6.20 A.

Complex glycans without fucose, and those carrying core fucose were only slightly changed from sham in the transection only and the random collagen hydrogel groups at 14 dpi, with a decrease seen in the aligned collagen hydrogel group. Sulphated glycans (including those with Lac repeats) were increased at 7 dpi and decreased at 14 dpi in both collagen hydrogel treated groups, however the change was less pronounced in the aligned collagen hydrogel treated group at each time-point. Alpha-galactose carrying glycans were more strongly increased at 14 dpi in the aligned collagen hydrogel treated group than in either the transection only or the random collagen hydrogel treated group, Figure 6.20 A. It should be noted that the alpha-galactose carrying glycans also carry core and/or outer arm fucose.

Statistically, time-point was the only significant contributor to variance for this data, using the ANOVA general linear model with a p-value of less than 0.05 considered significant. No significant differences were observed between individual treatment groups. Examining non-normalised data however treatment was a significant contributor to variance for fucosylated mannose structures ($p=0.020$); for hybrids without fucose ($p=0.003$) and hybrids with both core and outer arm fucose ($p=0.000$); for complex structures carrying core fucose ($p=0.019$), outer arm fucose ($p=0.001$) and both core and outer arm fucose ($p=0.000$); for bisected structures without fucose ($p=0.000$) and bisected structures carrying both core and outer arm fucose ($p=0.000$) and for alpha-galactose decorated structures ($p=0.002$). Time-point was still a significant contributor for many glycan types. Performing Tukey's post hoc analysis on the non-normalised data and ignoring time-point, the sham group was significantly different from all injured groups for hybrid glycans ($p=0.018$ for transection only, $p=0.023$ for random collagen hydrogel and $p=0.003$ for aligned collagen hydrogel), hybrid glycans with both core and outer fucose ($p=0.000$ for all three groups), complex glycans with both core and outer arm fucose ($p=0.000$ for all three groups), bisected glycans ($p=0.000$ for all three groups) and bisected glycans with both

core and outer arm fucose (p=0.000 for all three groups). This reinforces the observation that there is a loss of fucosylation in response to the injury.

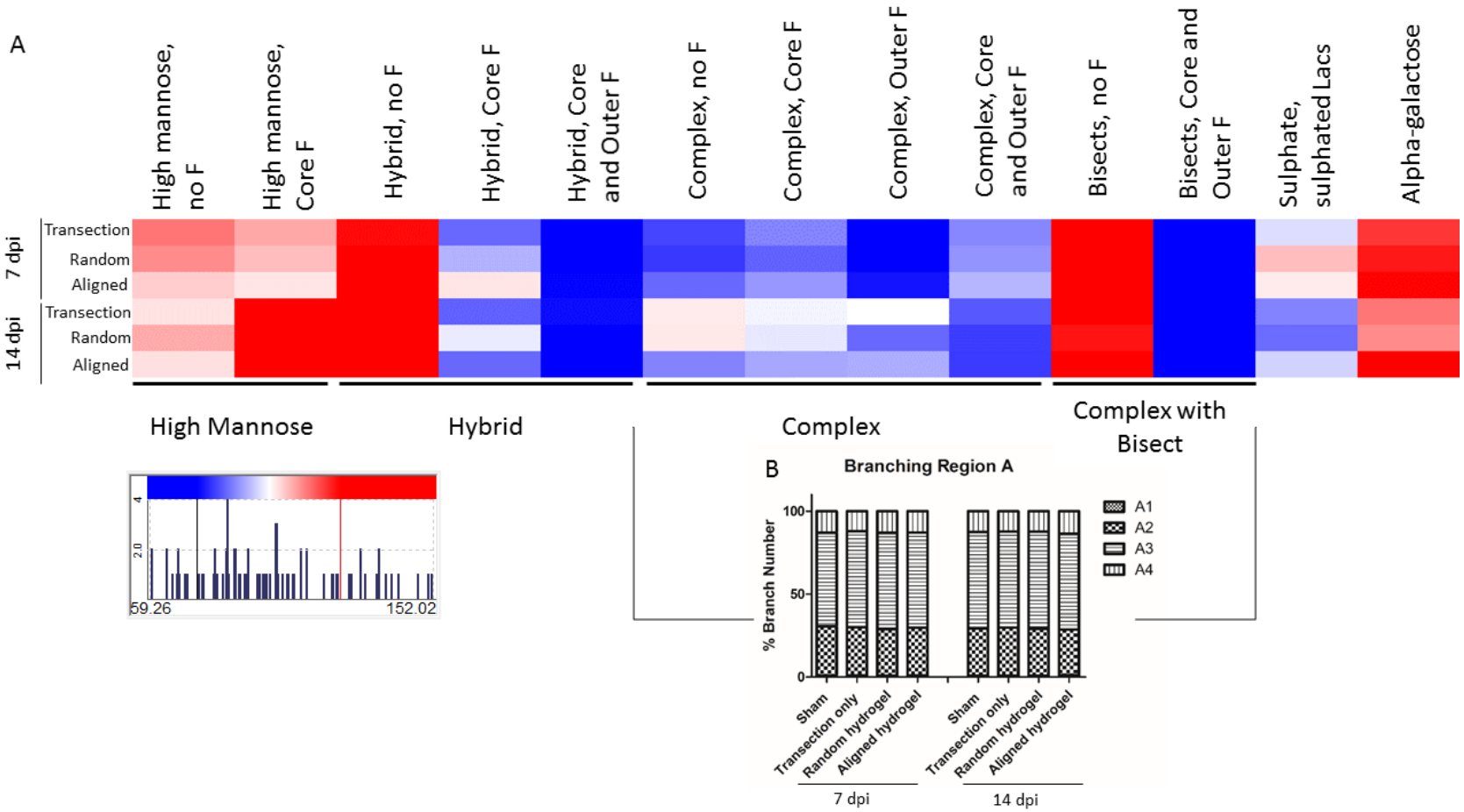

Figure 6.20 Changes in *N*-glycans in Region A the lesion epicentre grouped by feature. Individual GPs were grouped according to whether they were high-mannose, hybrid, branched or branched with bisect, and the type of fucose (F) they were decorated with. (A) Heat map of major features. Data presented here is expressed as the percentage of the sham group for the appropriate time-point. Blue squares indicate a reduction compared to sham, with the greatest reduction shown in darkest blue at 59.26%. Red squares indicate an increase compared to sham with the greatest increase shown in darkest red at 152.02%. (B) Bar chart showing the degree of branching of the complex and bisected complex glycans. A1 branching is <1%.

6.5.3.2 Alteration in protein N-*glycosylation is not confined to the lesion epicentre*

Changes to *N*-glycosylation following SCI is not a local response confined to the lesion epicentre. Tissue portions 10 mm in length taken 5 mm from the lesion epicentre on both the rostral and caudal side (Figure 6.1, Regions B and C) showed widespread alteration of the *N*-glycan profile as compared to sham (Figure 6.21, Figure 6.23). The patterns of change are far more varied than those seen in Region A (Figure 6.18) and there appears to be a more evident response to the biomaterial. The response is different between rostral (Region B, Figure 6.21) and caudal (Region C, Figure 6.23) suggesting a possible influence from descending signals.

In Region B rostral to the injury, a differential response between the collagen treated groups and the transection only groups could be seen. At 7 dpi, in peaks GP1, GP2, GP3, GP16 and GP32 both random and aligned collagen hydrogel groups were greatly increased while the transection only group was either decreased or only slightly increased relative to sham (Figure 6.21). In GP 7 and GP18 the collagen hydrogel groups were strongly decreased while the transection only group was increased (GP7) or only slightly decreased (GP18) (Figure 6.21). In an even greater number of peaks, the glycosylation response was different depending on whether the collagen hydrogel had random or aligned fibres. This effect was seen in glycan peaks GP5, GP6, GP11, GP13, GP14, GP16, GP27, GP31, GP41, GP42 and GP44 (Figure 6.21).

At 14 dpi the same types of changes were seen but in different glycan peaks. In GP1, GP3, GP8, GP11, GP31, GP38 and GP44 both random and aligned hydrogel groups were strongly increased compared to sham while the transection only group was decreased or only slightly increased. GP12, GP26 and GP28 were decreased in both hydrogel groups while there was an increase in the transection only group. The change in glycosylation was different between random and aligned collagen hydrogel treated groups in glycan peaks GP7, GP10, GP14, GP16, GP19, GP20, GP23, GP24, GP25, GP27 and GP41 (Figure 6.21).

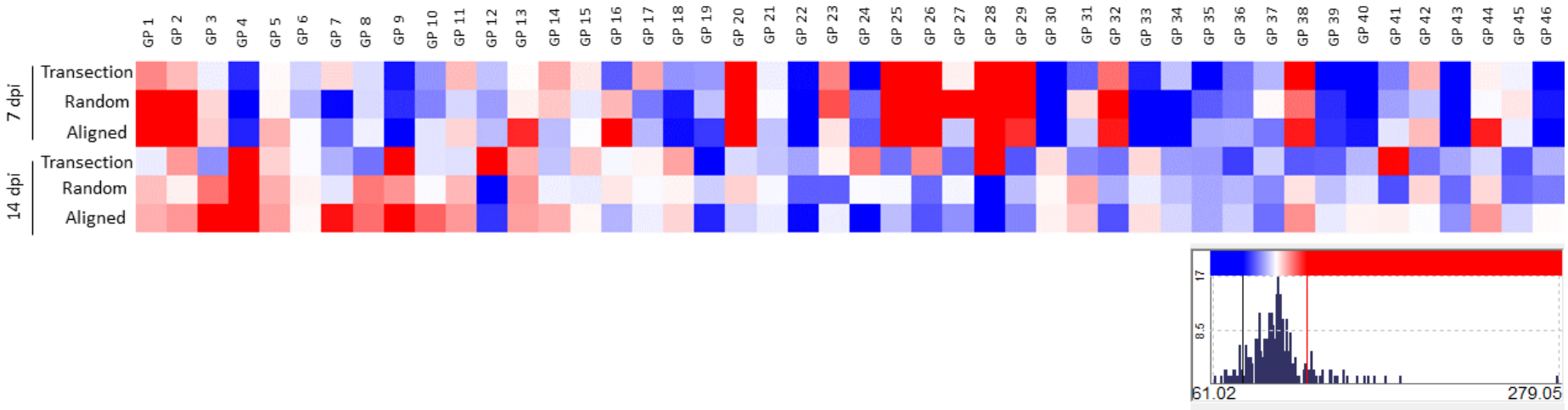

Figure 6.21 Heat map demonstrating the changes in glycan peak (GP) 1 to 46 in response to spinal cord transection with or without treatment with random or aligned collagen hydrogel in Region B, rostral to the injury. Data is shown as the percentage of sham, i.e. the % area for each peak for each animal in the injury groups were expressed as a percentage of the mean peak % area for the corresponding sham group at 7 or 14 dpi. Blue squares indicate a decrease in comparison to sham, with the maximum decrease shown in darkest blue at 61.02%. Red squares indicate an increase in peak area in comparison to sham, with the maximum increase shown in darkest red at 279.05%.

Interestingly, for most peaks there was a change in response to injury and/or treatment between 7 and 14 dpi, (Figure 6.21) and time-point was found to be a significant contributor to variance for many peaks by the ANOVA general linear model.

Treatment was a significant contributor to variance for a much smaller number of peaks, including GP17 (p=0.032), GP27 (p=0.023), GP29 (p=0.049), GP31 (p=0.044) and GP41 (p=0.008). For GP41 the interaction between time-point and treatment was also significant (p=0.002). Using Tukey's multiple comparisons test with data normalised to the sham group, the specific changes between experimental groups were investigated. The random collagen hydrogel treatment significantly lowered the amount of GP41 glycan compared to the transection only group at 14 dpi (p=0.001). Ignoring time-point, the random collagen hydrogel group was significantly different than the transection only group for GP17 (p=0.032) and GP31 (p=0.041), and for GP27 (p=0.048) the random collagen hydrogel group was significantly different from the transection only group and the aligned collagen hydrogel group (p=0.033). All other statistically significant results lay in the difference between 7 and 14 dpi for a particular treatment group: for GP9 the transection only group was significantly higher at 14 dpi than at 7 dpi (p=0.041), and for GP20, GP25 and GP26 the aligned hydrogel group was significantly lower at 14 dpi than at 7 dpi (p=0.016, p=0.007 and p=0.012 respectively). Both the aligned and random collagen hydrogel groups were significantly lower at 7 dpi than at 14 dpi for GP30 (p=0.044 for random, p=0.033 for aligned) and GP33 (p=0.024 for random, p=0.006 for aligned). All three injury groups were significantly higher at 7 dpi for GP29 (p=0.001 for random, p=0.030 for aligned, p=0.004 for transection only) and GP32 (p=0.005 for random, p=0.002 for aligned, p=0.022 for transection only).

To investigate any significant differences from the sham group Tukey's multiple comparison test was performed on non-normalised data. For a number of peaks there were significant differences between the sham groups at 7 and 14 dpi. These included GP20 (p=0.010), GP25 (p=0.050), GP26 (p=0.016), GP29 (p=0.004), GP30 (p=0.010) and GP33 (p=0.010). For GP30 both of the collagen hydrogel treated groups were significantly lower than the sham group at 7 dpi only (p=0.024 for random, p=0.018 for aligned).

Features analysis was also performed for Region B, see Figure 6.22.

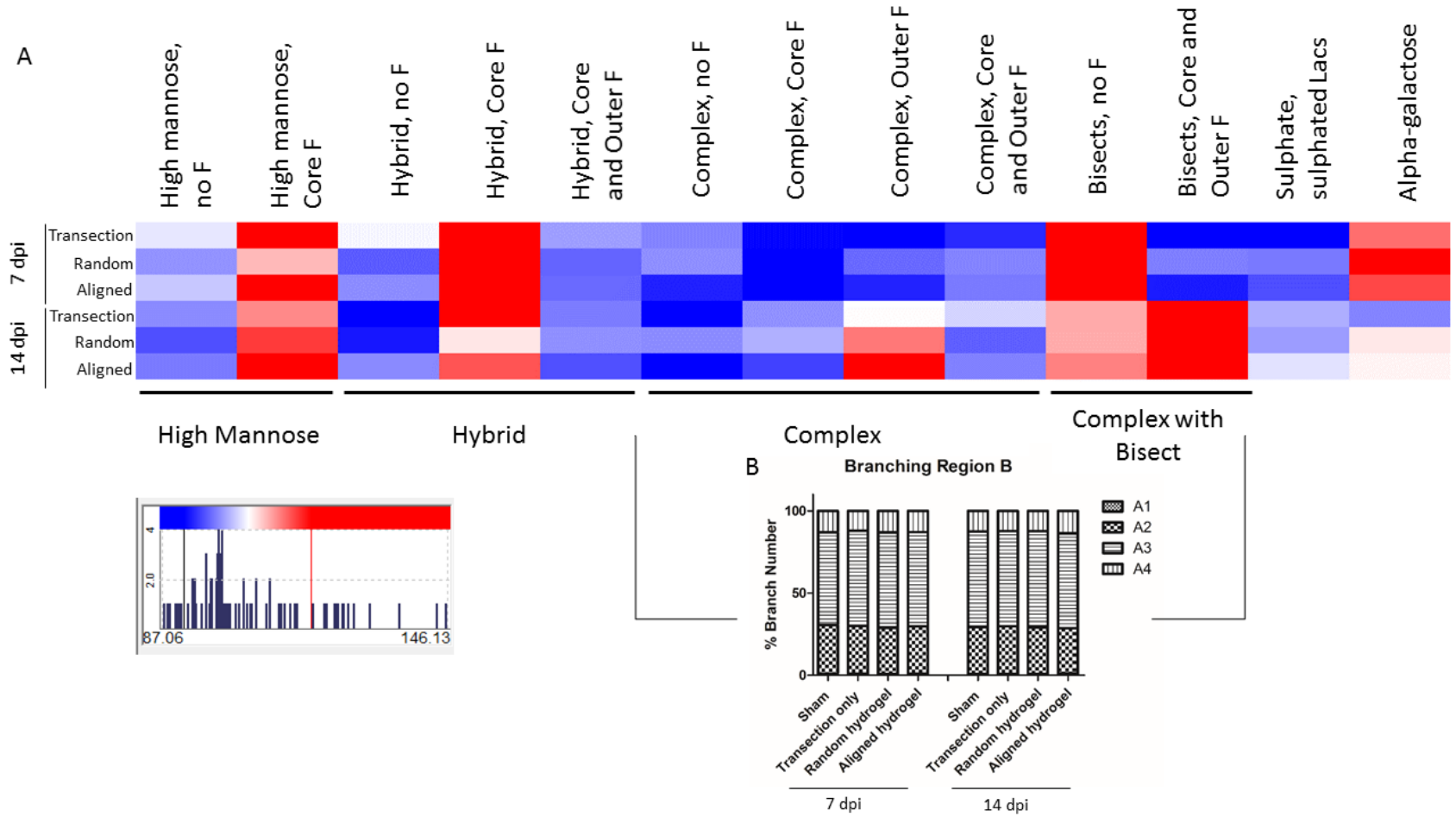

Figure 6.22 Changes in *N*-glycans in Region B, rostral to the injury, grouped by feature. Individual GPs were grouped according to whether they were high-mannose, hybrid, branched or branched with bisect, and the type of fucose (F) they were decorated with. (A) Heat map of the major features. Data presented here is expressed as the percentage of the sham group for the appropriate time-point. Blue squares indicate a reduction compared to sham, with the greatest reduction shown in darkest blue at 87.06%. Red squares indicate an increase compared to sham with the greatest increase shown in darkest red at 146.13%. (B) Bar chart showing the degree of branching of the complex and bisected complex glycans. A1 branching is <1%.

In region B, there was an increase in core fucosylation of both high mannose and hybrid type glycans at both 7 and 14 dpi. Hybrids carrying core and outer arm fucose were reduced. There was a general reduction in complex type glycans, likely in favour of the core fucosylated high mannose and hybrid structures. An exception to this was in the complex glycans carrying only outer arm fucose. At 14 dpi this glycan family was unchanged in the transection only group but increased in both collagen hydrogel treated groups, and more so in the aligned collagen hydrogel group than in the random collagen hydrogel group, Figure 6.22 A. The increase in core fucosylated hybrid glycans was less pronounced at 14 dpi in the collagen treated groups and this may be related to the increase in outer arm fucosylated complex glycans seen in these groups at this time-point. There were distinct changes in the complex and bisected glycans with time-point but not with treatment group. At 7 dpi there was a decrease in bisected glycans with both core and outer arm fucose, with a corresponding increase in the bisected glycans without any fucose. By 14 dpi bisected glycans with both core and outer arm fucose were strongly increased in all three injured groups and the non-fucosylated bisected glycans were also increased but to a lesser extent, Figure 6.22 A. There were no differences in the degree of branching of the complex and bisected complex glycans between treatment groups, Figure 6.22 B. The amount of alpha-galactose carrying glycans changed between 7 and 14 dpi: at 7 dpi there was an increase in these glycans compared to sham, but by 14 dpi there was a decrease in the transection only group and the collagen hydrogel groups were almost unchanged, Figure 6.22 A.

This normalised data was investigated using the ANOVA general linear model. Time-point was found to be a significant contributor to variance for many peaks, however treatment was only a significant contributor to variance for complex glycans without any fucose. Specifically, there was a significant difference between the random collagen hydrogel group and the aligned collagen hydrogel group ($p=0.024$). Performing similar analysis on the non-normalised data treatment was found to significantly contribute to variance for hybrids with core fucose ($p=0.006$), complex glycans with core fucose ($p=0.036$), bisected glycans ($p=0.003$) and glycans carrying alpha-galactose ($p=0.005$). Pooling data for both time-points Tukey's multiple comparisons test found a significant difference between sham group and all injured groups for bisected glycans ($p=0.030$ for transection only, $p=0.013$ for the random collagen hydrogel and $p=0.003$ for aligned collagen hydrogel) and for hybrid glycans with a core fucose ($p=0.009$ for transection only, $p=0.048$ for the random collagen hydrogel and $p=0.014$ for aligned collagen hydrogel).

In Region C caudal to the injury (Figure 6.23), the response was different from both the lesion epicentre (Region A, Figure 6.18) and from rostral to the injury (Region B, Figure 6.21). Many of the changes in glycosylation appeared to be related to the injury itself but there were still some

differences between transection only and random or aligned collagen hydrogel groups. A response specific to the two collagen hydrogel treated groups was seen in a number of peaks. In GP1 and GP2, there was an increase compared to sham in both random and aligned collagen hydrogel groups at 7 and 14 dpi, while in the transection only group there was a decrease compared to sham. At 7 dpi, GP23 was decreased in the transection only group but remained unchanged in both collagen hydrogel treated groups, and there was an increase in GP30 at 7 dpi in the transection only group and no change in either collagen hydrogel treated group, Figure 6.23.

Some differences could be seen between the random and aligned collagen hydrogel groups in Region C. At 7 dpi for GP9 and GP12 the increase in peak % area was less pronounced in the aligned than in the random collagen hydrogel group. At 7 dpi in glycan peaks GP3, GP7, GP10, GP12, GP22, GP26, GP28, GP38, GP39, GP40 and GP44 the direction of change was opposite between the two collagen hydrogel groups, i.e. where one group was increased, the other was decreased in comparison to sham. There were differences between random and aligned collagen hydrogel in many glycan peaks at 14 dpi: in GP11, GP19, GP20, GP22, GP23, GP24, GP25, GP26, GP27, GP29 and GP30 the direction of change in comparison to sham was opposite for the random and aligned collagen hydrogel groups. In GP13 the random collagen hydrogel group was unchanged while the aligned collagen hydrogel group was increased compared to sham, and in GP25 the aligned collagen hydrogel group was unchanged compared to sham while the random group was increased. In many other peaks both collagen hydrogel groups were increased or decreased compared to sham, but the change was more pronounced in one group or the other, Figure 6.23.

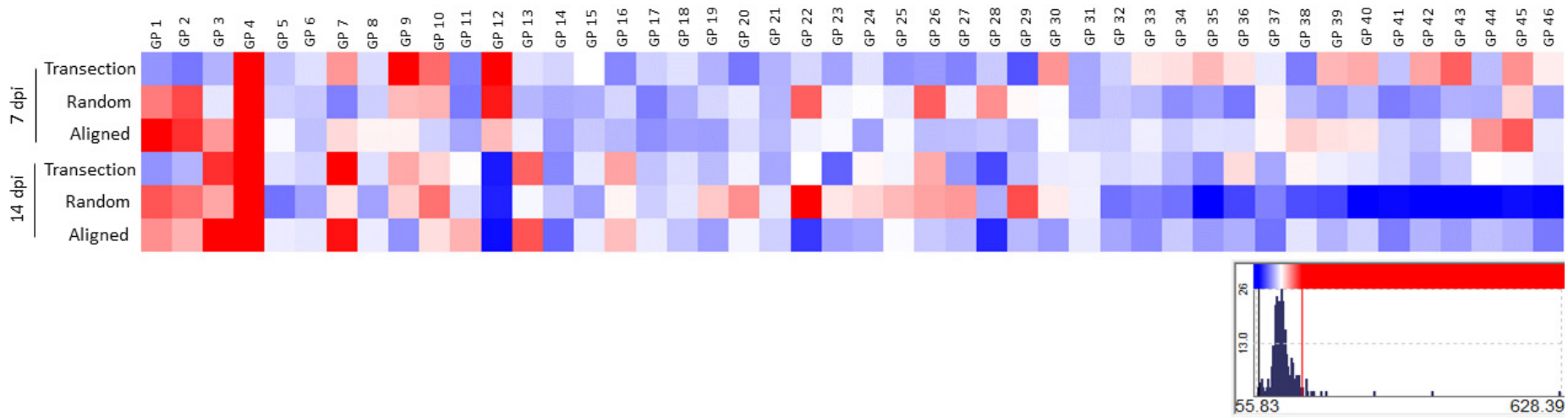

Figure 6.23 Heat map demonstrating the changes in glycan peak (GP) 1 to 46 in response to spinal cord transection with or without treatment with random or aligned collagen hydrogel in Region C, caudal to the injury. Data is shown as the percentage of sham, i.e. the % area for each peak for each animal in the injury groups were expressed as a percentage of the mean peak % area for the corresponding sham group at 7 or 14 dpi. Blue squares indicate a decrease in comparison to sham, with the maximum decrease shown in darkest blue at 55.83%. Red squares indicate an increase in peak area in comparison to sham, with the maximum increase shown in darkest red at 628.39%.

Similarly to regions A and B, time-point was a significant contributor to variance by the ANOVA general linear model, indicating changes in *N*-glycosylation following injury are not stable. Treatment was also found to be a significant contributor to variance for a number of peaks in this region: GP2 (p=0.039), GP15 (p=0.034) GP20 (=0.015), GP22 (p=0.025), GP23 (p=0.003), GP27 (p=0.003), GP29 (P=0.041), GP33 (p=0.043), GP34 (p=0.015), GP35 (p=0.004), GP36 (p=0.042), GP41 (p=0.034), GP43 (p=0.037) and GP46 (p=0.023). Tukey's multiple comparisons test revealed that at 14 dpi GP23 and GP27 were significantly higher in the random collagen hydrogel than in the transection only group (p=0.010 and p=0.018 respectively). In the aligned hydrogel group GP11 and GP17 were significantly lower at 7 dpi than at 14 dpi (p= 0.026 and p=0.024 respectively).

Ignoring time-point, there was a significant difference between transection only and random collagen hydrogel groups for glycan peaks GP46 (p=0.018), GP43 (p=0.030), GP42 (p=0.047), GP41 (p=0.033), GP36 (p=0.034), GP34 (p=0.014), GP33 (p=0.038), GP29 (p=0.042), GP27 (p=0.002), GP23 (p=0.002), GP20 (p=0.012) and GP15 (p=0.030). The difference between random and aligned collagen hydrogels were significantly different for GP22 (p=0.023) and GP13 (p=0.036). Random collagen hydrogel was significantly different from both aligned collagen hydrogel and transection only groups for GP35 (p=0.004).

To investigate whether the response to injury was significant in this region, i.e. whether the change from the sham group was significantly different, Tukey's multiple comparison test was performed on non-normalised data. The random collagen hydrogel group was significantly lower than the sham group at 7 dpi for GP 17 (p=0.026) and at 14 dpi for GP35 (p=0.014). The aligned collagen hydrogel group was significantly higher than the sham group at 14 dpi only for GP13 (p=0.038). There was also a significant difference between the sham groups at 7 and 14 dpi for GP17 (p=0.046).

Feature analysis for Region C is shown in Figure 6.24. The increase in high-mannose species carrying core fucose and alpha-galactose decorated glycans, and the decrease in hybrids with core and outer fucose, complex glycans with core and outer fucose and the sulphated (including sulphated with Lac repeats) glycans were consistent between treatment groups and time-points. At 7 dpi a response to collagen hydrogel can be seen in the complex glycans and complex glycans with outer arm fucose. In the transection only group there was an increase in outer arm fucosylated complex glycans and a corresponding decrease in the complex glycans without fucose, while in both cases the opposite was seen in both collagen hydrogel groups: in these groups there was a decrease in complex glycans with outer arm fucose and an increase in complex glycans without any fucose, Figure 6.24 A. There were

no differences between the treatment groups in the degree of branching on the complex and bisected complex glycans, Figure 6.24 B.

For many of the glycan families a difference between random and aligned collagen hydrogel groups could be seen in this region. At both time-points there was less high mannose type glycans in the random collagen hydrogel than in the aligned collagen hydrogel group. For both non-fucosylated hybrids and core-fucosylated hybrids at 7 dpi there was a stronger increase in the aligned collagen hydrogel group than in the random collagen hydrogel group. There were less complex glycans with core fucose in the aligned hydrogel groups than in the random collagen hydrogel groups at both 7 and 14 dpi. At 7 dpi bisected glycans with both core and outer arm fucose were increased in the random collagen hydrogel group with a corresponding decrease in bisected glycans without any fucose, while the opposite response was seen with the aligned collagen hydrogel group: there was a decrease in bisected glycans with both core and outer arm fucose at 7 dpi with a corresponding increase in the non-fucosylated bisected glycans. Sulphated glycans (including those with Lac repeats) were decreased at both time-points in all treatment groups but this was more pronounced in the aligned collagen hydrogel group than in any of the others, Figure 6.24 A.

Statistically time-point was found to be the major contributor to variance for this data, and treatment was found to contribute to variance in bisected glycans carrying core and outer arm fucose. Specifically, the difference between random and aligned collagen hydrogel was significantly different at 7 dpi for this type of glycan ($p=0.048$). Performing the ANOVA on non-normalised data, treatment was found to be a significant contributor to variance for high mannose glycans carrying core fucose ($p=0.030$), for complex glycans carrying core and outer arm fucose ($p=0.024$) and bisected glycans carrying core and outer arm fucose ($p=0.029$). Pooling data from both time-points Tukey's multiple comparisons revealed a significant difference between sham and aligned collagen hydrogel groups for core-fucosylated high mannose glycans ($p=0.032$) , core-fucosylated hybrid glycans ($p=0.049$), complex glycans with both core and outer arm fucose ($p=0.015$) and bisected glycans with both core and outer arm fucose ($p=0.031$). The difference in high mannose type glycans between random and aligned collagen hydrogels was also found to be significant ($p=0.040$).

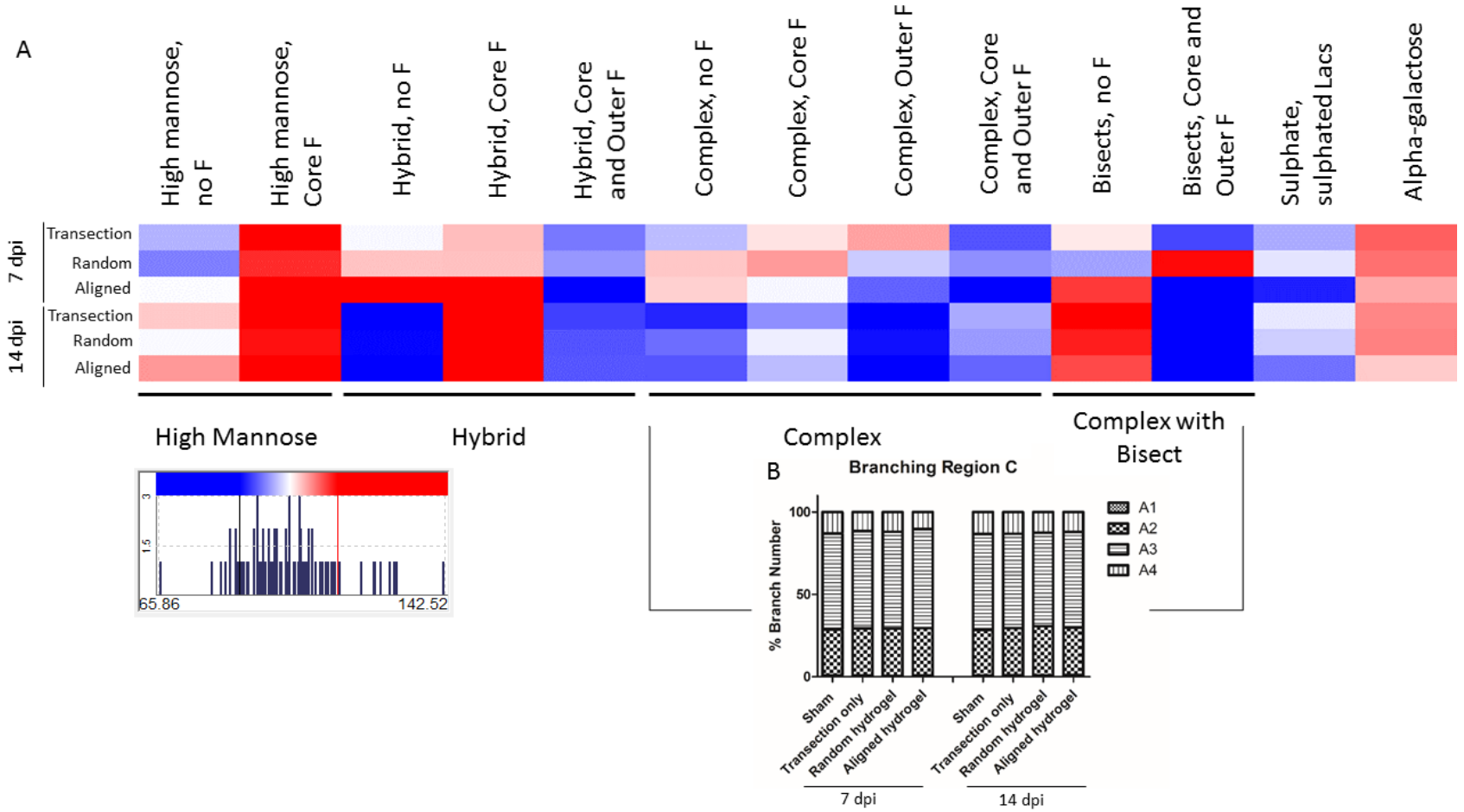

Figure 6.24 Changes in *N*-glycans in Region C, caudal to the injury, grouped by feature. Individual GPs were grouped according to whether they were high-mannose, hybrid, branched or branched with bisect, and the type of fucose (F) they were decorated with. (A) Heat map of the major features. Data presented here is expressed as the percentage of the sham group for the appropriate time-point. Blue squares indicate a reduction compared to sham, with the greatest reduction shown in darkest blue at 65.86%. Red squares indicate an increase compared to sham with the greatest increase shown in darkest red at 142.52%. (B) Bar chart showing the degree of branching of the complex and bisected complex glycans. A1 branching is <1%.

6.5.3.3 Changes in charged N-*glycan species with SCI and collagen hydrogel treatment*

Since sialylated structures are relatively minor components of the *N*-glycome of the intact spinal cord, changes in these potentially important species may be masked by more abundant structures. WAX-HPLC was performed on *N*-glycan samples from the lesion epicentre of each experimental group to provide a more in depth analysis of changes in charged structures. A representative undigested WAX-HPLC profile for each experimental group at 7 and 14 dpi are shown in Figure 6.25 and Figure 6.26 respectively. The graph in Figure 6.27 indicates the changes in charged species as a stacked bar graph. From here it is clear that at 7 dpi in all injured groups there is an increase in charged species in the spinal cord. Di-sialylated and tri-sialylated (S2 and S3) were particularly increased in comparison to sham. At 14 dpi, the aligned collagen hydrogel group also seemed to have increased charged structures, in particular S1, S2 and S3, Figure 6.26. No statistics were performed on this data due to low n numbers.

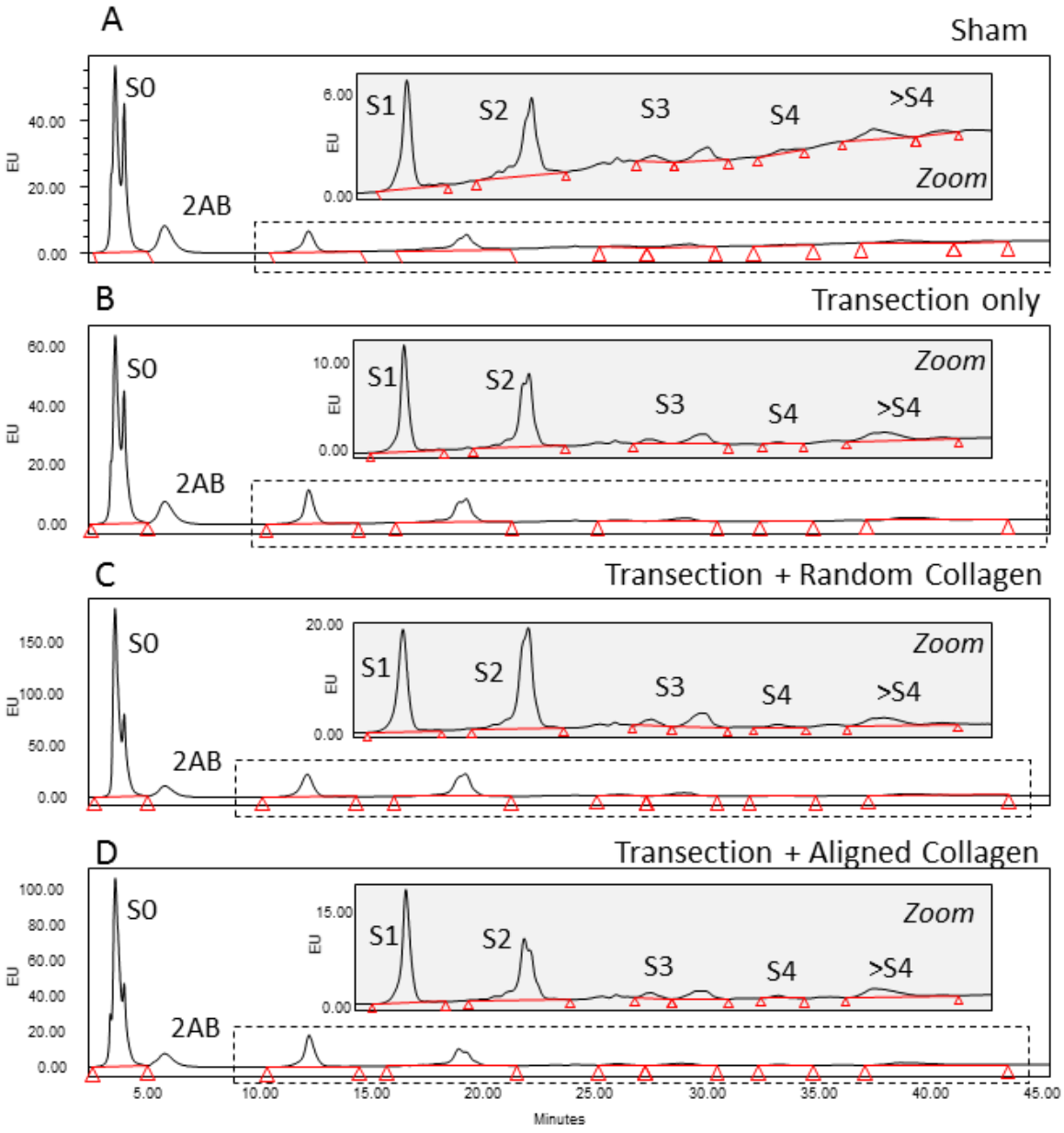

Figure 6.25 WAX-HPLC profile of undigested *N*-glycans from the lesion epicentre at 7 dpi. (A) Sham injured, (B) transected, (C) transected and treated with random collagen hydrogel, (D) transected and treated with aligned collagen hydrogel. The charged region S1- >S4 is shown highlighted in grey, inset into the full view chromatogram, with dashed line indicating the zoomed region. S0, neutral glycans; S1, mono-sialylated; S2, di-sialylated; S3, tri-sialylated; S4, tetra-sialylated; >S4, unidentified highly charged species.

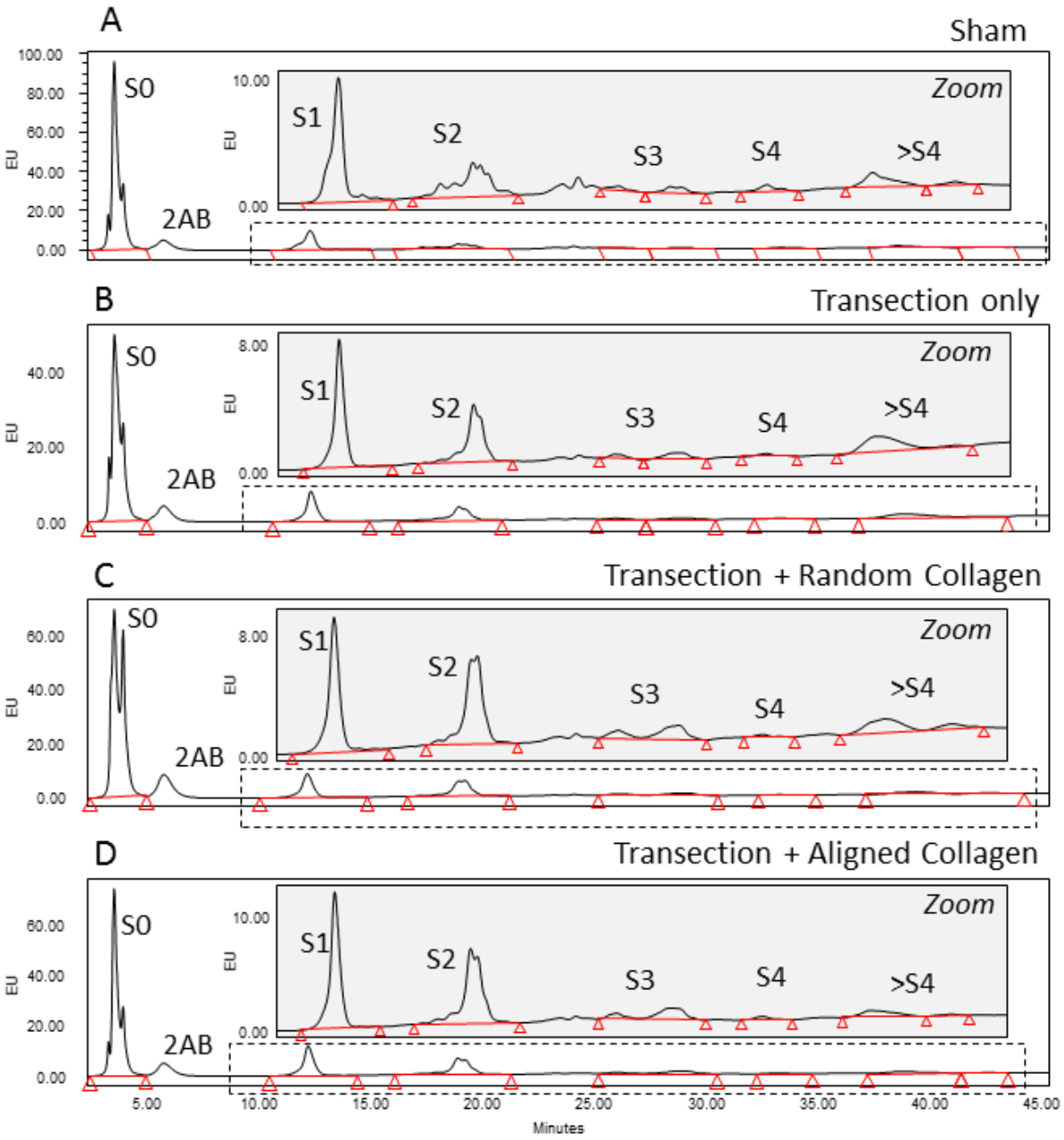

Figure 6.26 WAX-HPLC profile of undigested *N*-glycans from the lesion epicentre at 14 dpi. (A) Sham injured, (B) transected, (C) transected and treated with random collagen hydrogel, (D) transected and treated with aligned collagen hydrogel. The charged region S1- >S4 is shown highlighted in grey, inset into the full view chromatogram, with dashed line indicating the zoomed region. S0, neutral glycans; S1, mono-sialylated; S2, di-sialylated; S3, tri-sialylated; S4, tetra-sialylated; >S4, unidentified highly charged species.

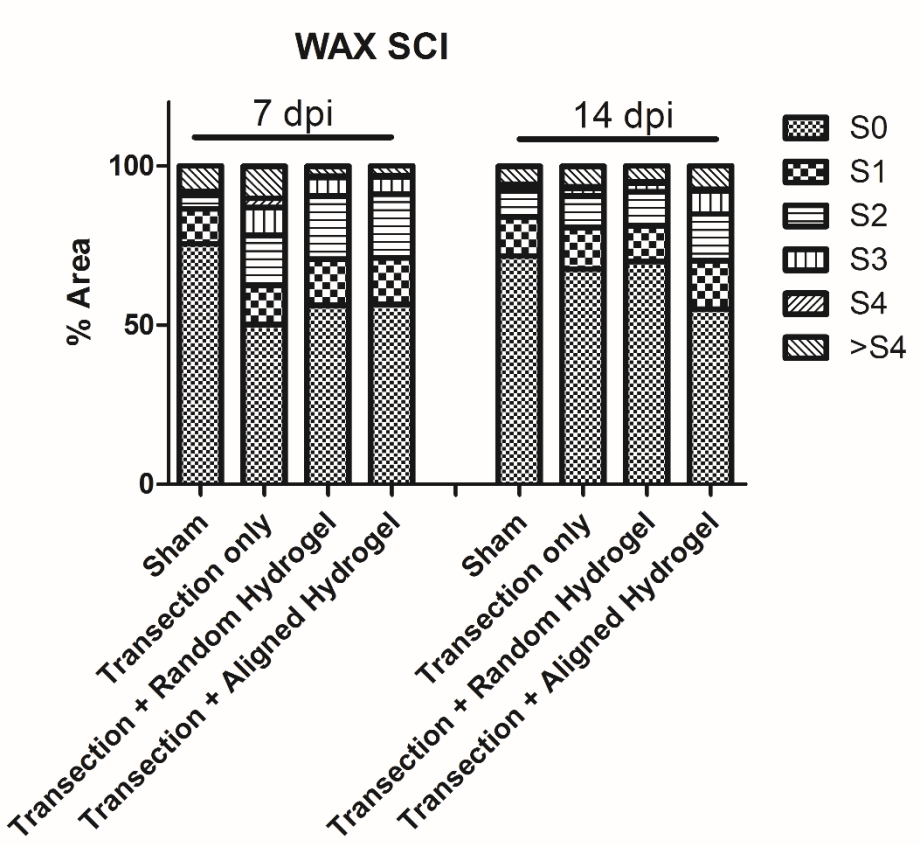

Figure 6.27 Changes in charged *N*-glycan species at the lesion epicentre investigated with WAX HPLC. S0, neutral glycans; S1, mono-sialylated; S2, di-sialylated; S3, tri-sialylated; S4, tetra-sialylated; >S4, unidentified highly charged species.

6.5.3.4 Sialic acid is found on the surface of inflammatory cells in the injured spinal cord

Since sialic acid has been implicated in the regulation of inflammation (see Introduction Section 1.5.7), lectin histochemistry with the SNA-I lectin which binds α(2-6)-sialic acid was performed in conjunction with immunohistochemistry against CD11b, a marker of macrophages and microglia, at 7 dpi. In sham tissue SNA-I bound what appeared to be blood vessels, and the small number of CD11b positive microglia did not co-localise with positive SNA-I signal at all (Figure 6.28 A). However, in the transected spinal cord, large numbers of CD11b positive macrophages and microglia were evident at the lesion border, and almost all of them were also positively stained with the SNA-I lectin (Figure 6.28 B). A similar result was seen in the random collagen hydrogel treated group (Figure 6.28 D). In the aligned hydrogel group there were still many cells with positive SNA-I binding on their surface, however the

level of positive CD11b staining was lower and did not seem to co-localise with the lectin (Figure 6.28 F). In the lesion epicentre of the transected and collagen treated groups there were far fewer CD11b positive cells, and there was no co-localisation between them and the SNA-I lectin. SNA-I staining could be seen in a fibrous pattern. It is unclear what exactly this fibrous SNA-I binding structure is, it may be extracellular matrix components.

SNA-I lectin did not co-localise with astroglial (Figure 6.29 A-D), or neuronal markers (Figure 6.30 A-D) at the borders of the injury or in the sham injured spinal cord. No GFAP positive or β III tubulin positive cells could be detected in the lesion epicentre.

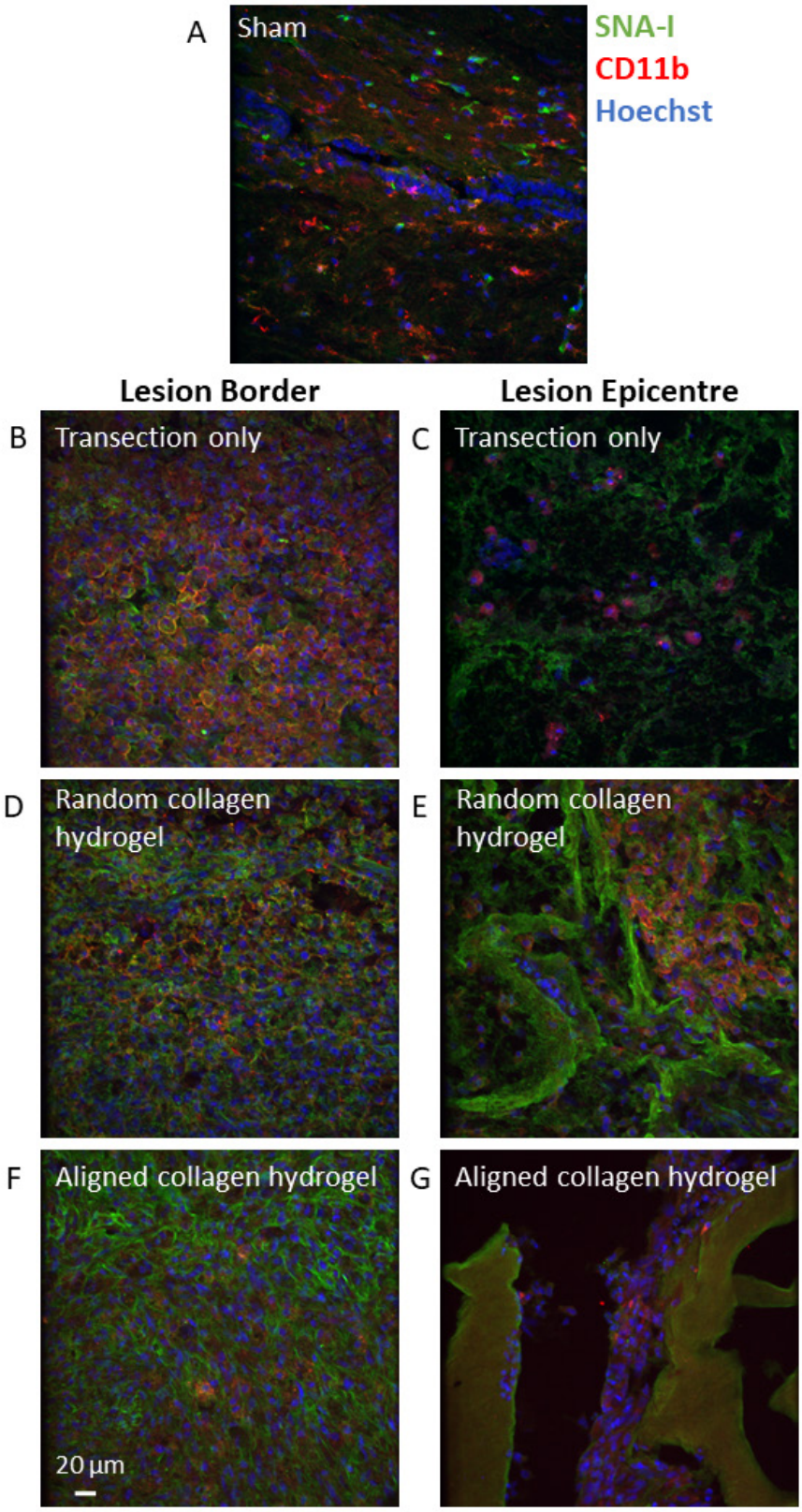

Figure 6.28 Distribution of sialic acid labelled with SNA-I lectin and its relationship to CD11b positive microglia and macrophages. (A) Sham (B and C) transection only, (D and E) random collagen hydrogel treated, (E and F) aligned collagen hydrogel treated. Images B,D, F were captured at the borders of the injury, images C,E, G were captured in the lesion epicentre. Aligned hydrogel can be seen auto-fluorescing in G. All images are from spinal cord at 7 dpi. Scale bar 20 µm.

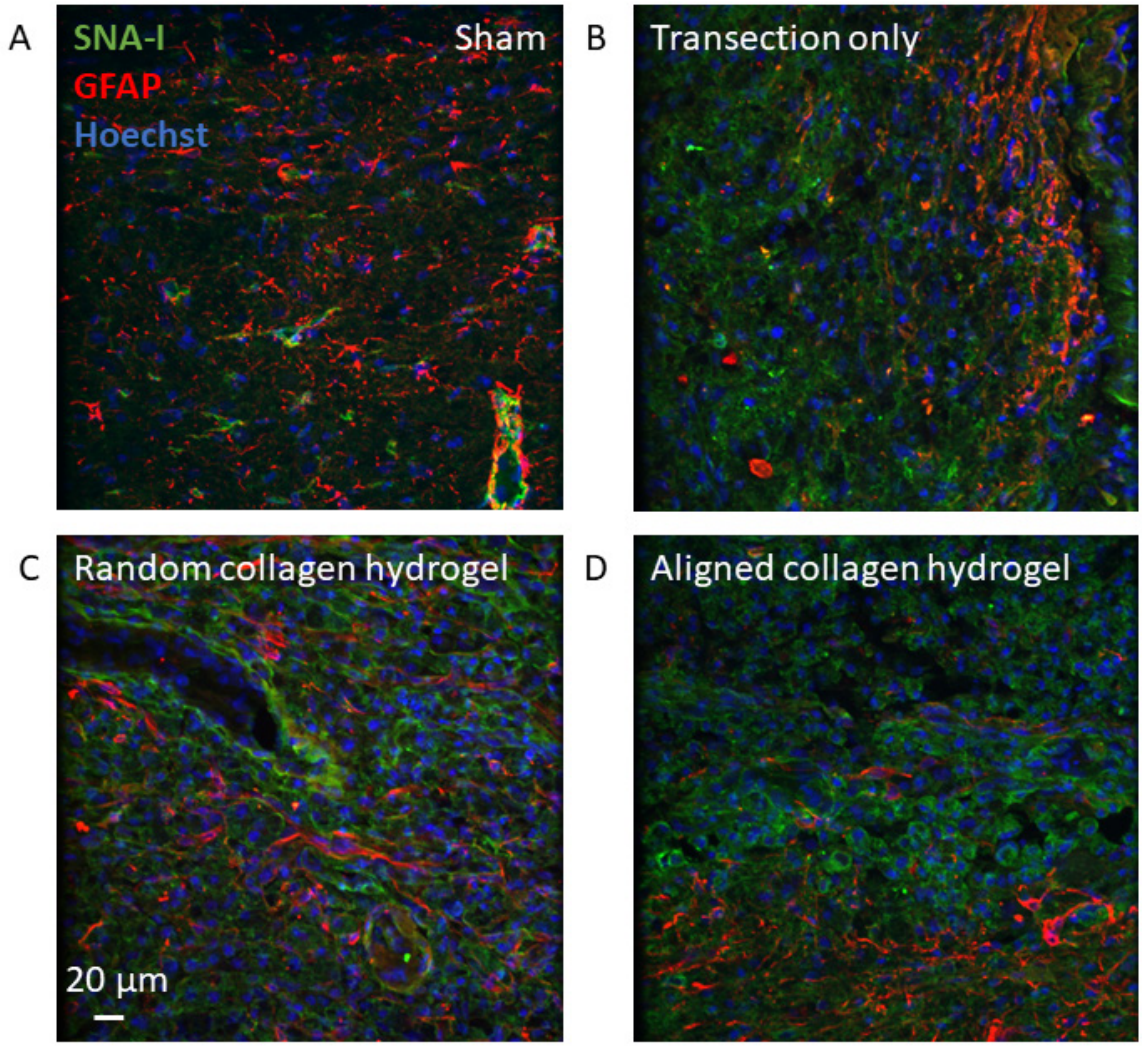

Figure 6.29 Distribution of sialic acid labelled with SNA-I lectin and its relationship to GFAP positive astrocytes. (A) Sham (B) transection only, (C) random collagen hydrogel treated, (D) aligned collagen hydrogel treated. Images B, C, D were captured at the borders of the injury. No positively stained astrocytes were seen in the lesion epicentre. No co-localisation was observed between SNA-I and GFAP. All images are from spinal cord at 7 dpi. Scale bar 20 µm.

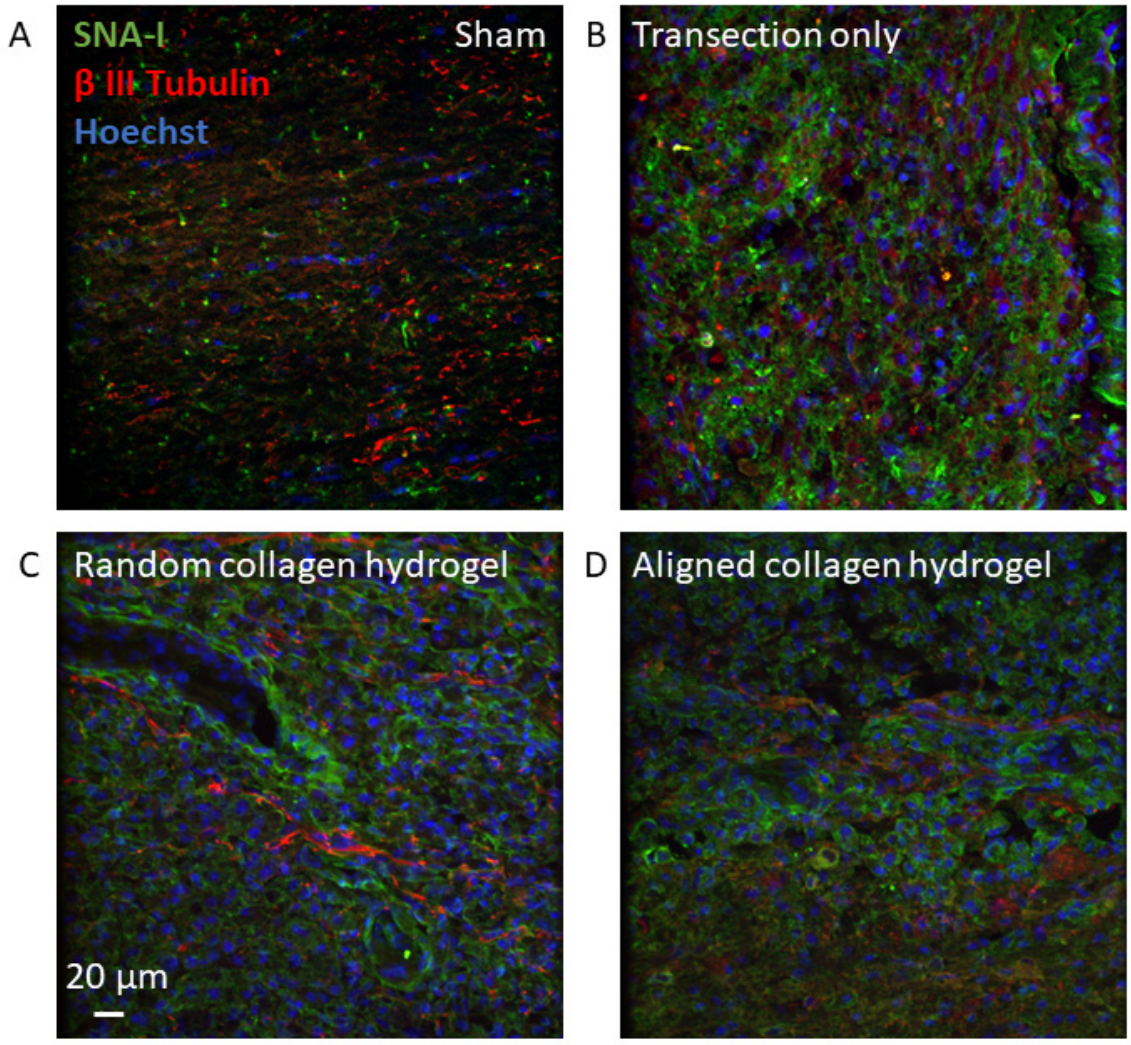

Figure 6.30 Distribution of sialic acid labelled with SNA-I lectin and its relationship to β III tubulin positive neurons. (A) Sham (B) transection only, (C) random collagen hydrogel treated, (D) aligned collagen hydrogel treated. Images B, C, D were captured at the borders of the injury. No positively stained neurons were observed in the lesion epicentre. No co-localisation was observed between SNA-I and β III tubulin. All images are from spinal cord at 7 dpi. Scale bar 20 µm.

6.6 Discussion

This chapter describes the complete *N*-linked glycome of the rat spinal cord. No other reports of the spinal cord *N*-glycome in any species has been published to date. The closest reference for CNS *N*-glycosylation characterisation is that published in the late 1990s, where the neutral fraction (Chen *et al.*, 1998) and the sialylated fraction (Zamze *et al.*, 1998) of the whole rat brain were characterised extensively, using a similar approach to that employed here. The *N*-glycan species identified in the spinal cord in this study largely agree with the structures published in the two studies above. In the whole rat brain, high mannose species, hybrid species and complex structures were identified. The

complex structures were decorated with galactose, fucose in both core and outer arm positions, bisecting GlcNAcs, lactosamine repeats, and sialic acid (Chen *et al.*, 1998; Zamze *et al.*, 1998). All of these features were also identified in the rat spinal cord in this study. The main difference between these older studies of the brain and our current findings in the spinal cord is in the level of sialylation. We have found a reasonably low level of sialic acid (~10% unmodified, with a further 14% being charged as a result of sialic acid modified with acetyl groups or the presence of a sulphate group) whereas (Zamze *et al.*, 1998) reports up to 40% of *N*-glycans carrying sialic acid. There are a number of possible explanations for this. One is that this is simply a difference between brain and spinal cord, although *N*-glycoprofiling of the rat substantia nigra and striatum revealed a low level of sialylation, comparable to that seen in the spinal cord (reported in the thesis of Juhi Samal, manuscript in preparation) suggesting that this is unlikely to be the case. Another explanation may lie in the difference in tissue processing. There is no mention of tissue perfusion at the time of euthanasia in either of the older papers, and so it is likely that there was blood still present during the sample preparation. Spinal cord tissue on the other hand was perfused with 1X PBS at the time of euthanasia to remove all blood from the tissue before freezing. It is widely known that serum proteins are quite highly sialylated, (Stanta *et al.*, 2010; Saldova *et al.*, 2013; Saldova *et al.*, 2014) and this may be the reason a much higher amount of sialic acid was found in the brain than in the spinal cord.

An increase in sialic acid was seen in the lesion epicentre (Region A) following injury to the spinal cord using WAX-HPLC, particularly at the earlier time-point of 7 dpi (Figure 6.25). A possible explanation for this is the influx of blood into the tissue following spinal cord transection. This is supported by the observation that the increase in sialylation is slightly lower in the two collagen hydrogel treated groups. At the time of surgery, a clear haemostatic effect was seen with the implantation of collagen hydrogel either in the random or aligned form. Again, at the time of tissue harvesting in the transection only group large accumulations of what appeared to be clotted blood could be seen macroscopically, making up a large portion of this tissue region. In both collagen hydrogel treated groups the apparent clot was much smaller, with this portion of tissue largely being filled by the material itself. By 14 dpi the increase in sialylation in the injured groups was smaller, this may be due to the clearing of the clot and associated debris. The increase in sialic acid may also have been due to the influx of peripheral macrophages and/or the activation and proliferation of resident microglia. Since sialic acid is widely known to play a role in regulation of the immune system and inflammation (Marth and Grewal, 2008; van Kooyk and Rabinovich, 2008) double labelling with lectin- and immuno-histochemistry was used to investigate whether sialic acid could be seen on activated microglia and macrophages. In the sham tissue microglia were present in low numbers in the spinal cord but did not show any co-localisation with the SNA-I lectin which binds α(2-6) sialic acid. No peripheral macrophages were seen in these

tissue sections. Following SCI however there was a large increase in the amount of macrophages and/or activated microglia present, and at the lesion borders almost all of these cells were also stained positively with the SNA-I lectin in the transection only and random collagen hydrogel groups (Figure 6.28 B, D). Surprisingly the injury epicentre was largely devoid of CD11b positive microglia or macrophages. There was not a large amount of cell infiltration in general into the clot/fibrous scar in the transection only group, or into the collagen hydrogel in the random or aligned hydrogel groups. There appeared to be some SNA-I binding to the fibrous structures in the transection only group however this was of a low intensity, and it is difficult to say whether this is specific staining or background (Figure 6.28 C, E, G). In the aligned collagen hydrogel group there appeared to be less CD11b staining in general.

Considering the overall changes in the *N*-glycoprofile, time-point had a statistically significant influence on the size of individual glycan peaks in all groups in the three ROIs examined. In some cases the difference between the two time-points reached statistical significance for individual treatment groups. This highlights the dynamic nature of the *N*-glycosylation response, and if any of these glycans were to be utilised for a therapeutic in the future then the timing of delivery would require careful consideration.

From the heat map of Region A (Figure 6.18) it can be seen that the changes in response to the injury seem to cluster in blocks. Many of the smaller and middle sized glycans have been increased (GPs 1, 2, 9, 14, 18-23) with those peaks at the end of the profile which contain large highly substituted glycans being decreased (GPs 33-46). This suggests that proteins are undergoing an early exit from the *N*-glycosylation pathway. This is supported by an increase in high mannose and hybrid glycans in the feature analysis (Figure 6.20 A). These are the first structures to be formed in the synthesis of any *N*-glycan (see the section on *N*-glycan biosynthesis in Introduction, Section 1.5.3). This may be evidence of cellular stress and particularly stress in the endoplasmic reticulum (ER) and Golgi apparatus as a result of the injury. This was also observed in Regions B and C and will be discussed further below.

The changes observed in Regions B and C do not occur in such general patterns, and these seem to be more directed alterations in specific glycan species. This may be evidence of the tissue attempting to repair itself, or may be associated with the widely studied scar formation or inflammatory responses characteristic of mammalian SCI (Norenberg *et al.*, 2004; Fitch and Silver, 2008). It is impossible to tell from this work which of these, if any, are responsible for the observed changes, and further functional studies will be necessary to more deeply understand the role of these specific glycans.

A common theme in these regions is the increase of some of the smaller mannose species, including M3 (GP1), M6 (GP11) and M7 (GP16) and some of their core-fucosylated variants, FM3 (GP2) and FM5 (GP8) in Regions B and C). Another small simple glycan, FA1 (GP3), was also increased at both time-points in Region B. The peaks which decreased were some of the more highly complex (A4, GP7) or highly complex and substituted glycans, (FA3G1S(6)1, GP18; FA3G1, GP12; A2F2G1Ga1S(6)1, GP26; A3G2S(6)2, GP28). These observations are confirmed with feature analysis (Figure 6.22 A, Figure 6.24 A). At both time-points in Regions B and C there was an increase in core fucosylated high mannose and hybrid structures, and an overall decrease in complex glycans with and without fucose. These changes can be considered a direct result of traumatic SCI as they could be seen in all three injured groups, and can be generalised as evidence as a loss of complexity in the *N*-glycome. The observation that the degree of branching remains consistent on the complex and bisected glycans (Figure 6.22 B, Figure 6.24 B) supports the idea that the loss in complexity is due to a switch from complex to high mannose and hybrid type glycans. This switch suggests a failure of the *N*-glycosylation machinery in the Golgi apparatus in response to SCI. In short, spinal cord *N*-glycans lost their complexity following injury. In normal conditions, the Golgi takes in a protein decorated with a high mannose glycan precursor from the ER, then trims it down and remodels it to form the final glycan structure. If the enzymes in the Golgi apparatus are not functioning as they should then we would expect to see an increase in high mannose species and a decrease in the more highly branched and decorated complex species as seen here. It is also possible that the Golgi is functioning as normal and the increase of high mannose species and small glycan structures is a biological response to tissue disruption, cell death and inflammation, or that there is simply a shortage of nucleotide sugars to act as building blocks for the more complex glycans. Considering the proximity of these time-points to the time of injury, it is likely that all of the cells are under stress, and that there may be a shortage of sugar precursors (possibly due to failure of the normal cellular metabolic pathways) as well as sub-optimal Golgi and ER function. High mannose species have been reported as being associated with the formation and maintenance of the synapse (Matus *et al.*, 1973; Kleene and Schachner, 2004) and so alterations in the abundance of these species may also be a result in breakdown of the synaptic machinery in the vicinity of the injury, or attempts to re-establish connections between neurons and engage mechanisms of plasticity.

In Regions B and C the mannose and hybrid glycans which increased also carried core-fucose (Figure 6.22 A, Figure 6.24 A). Complex structures with a bisecting GlcNAc were also increased in all three regions (Figure 6.20 A, Figure 6.22 A, Figure 6.24 A). This may be related to death of neurons and/or glia as changes in these features have been observed in the context of neurodegenerative disease. Increased bisected *N*-glycans have been associated with increased amyloid-β production and the

production of mutant amyloid in AD models(Akasaka-Manya *et al.*, 2008; Akasaka-Manya *et al.*, 2010) and human CSF exhibited altered levels of bisected glycans in AD patients (Palmigiano *et al.*, 2016). Increased core fucose was also seen on the mutant amyloid (Akasaka-Manya *et al.*, 2008) and there were alterations in core fucosylated glycans in the CSF of AD patients (Palmigiano *et al.*, 2016). Increases in core fucose and bisects have also been observed in a mouse model of HD (Gizaw *et al.*, 2015). It is difficult to interpret the results of all these studies in relation to each other, and in relation to this work as the direction of change for a particular glycan type is often conflicting even within studies, for example in the CSF glycan profiling of AD patients the patients could be divided into two groups with distinct glycosylation changes (Palmigiano *et al.*, 2016). Additionally in the context of neurodegenerative diseases, it is impossible to distinguish changes which may be secondary to the neuronal death or be a cause of it. However, we can conclude that in general alterations in *N*-glycans carrying bisects and core fucose resdiues are associated with injury and disease in the CNS.

N-glycans carrying sulphate groups and alpha linked galactose also changed in response to injury in all three regions (Figure 6.20 A, Figure 6.22 A, Figure 6.24 A). Sulphated *N*-glycans may play a similar role to the HNK-1 epitope (human natural killer cell epitope) commonly found on glycolipids and *O*-glycans. The HNK-1 epitope consists of a sulphated glucuronic acid bound to galactose and has been associated with plasticity and the synapse (Strekalova *et al.*, 2001; Kleene and Schachner, 2004). Changes in sulphation may therefore reflect either a breakdown or remodelling of the synaptic machinery, as mentioned above in relation to the high mannose structures. In most experimental groups sulphated structures were decreased after SCI (Figure 6.20 A, Figure 6.22 A, Figure 6.24 A). Glycolipids carrying the HNK-1 epitope have been shown to interact with the lectican family of proteoglycans to promote cell adhesion and neuronal growth (Miura *et al.*, 1999; Miura *et al.*, 2001). It is possible that sulphated *N*-glycans may also interact with these proteoglycans. Considering that manipulation of the proteoglycan scar has been shown to improve the response to injury (Bradbury *et al.*, 2002; Bartus *et al.*, 2014), targeting these sulphated *N*-glycans may lead to improved results in combination with therapies such as chondroitinase. The significance of alpha-galactose is difficult to interpret and would be difficult to clinically translate, as it is immunogenic to humans (Galili, 2013).

In region A, the lesion epicentre, the changes in glycosylation seem to be mainly a direct result of the injury. In Regions B and C however we begin to see more glycans which are influenced by the presence of the collagen hydrogel, and even more interestingly which are influenced by the orientation of the collagen fibres within the hydrogel. In Region B a number of peaks showed a response which was similar between the random and aligned collagen hydrogel groups but different from the transection only group. In Region C fewer peaks were changed in both the random and aligned collagen hydrogel

treated groups: GP1 and GP2 were increased at both 7 and 14 dpi while the transection only group decreased, and GP23 and GP30 were unchanged in the collagen treated groups while there was a decrease or an increase respectively in the transection only group. Surprisingly, the few peaks where the response was statistically significant were those where the random collagen hydrogel had the greatest effect. Pooling the data from the 7 and 14 dpi groups Tukey's test found that the random collagen hydrogel group was significantly different from the transection only group for a large number of glycan peaks in Region C. It is unclear why there was such a difference between the two treatments differing only in the orientation of the collagen fibres, and there is no way of knowing from this study whether these effects are beneficial or detrimental to the injured tissue. These changes may be considered either as an indication that collagen hydrogel can modify the injury response, or they may simply represent a host response to the introduction of a foreign object, the collagen hydrogel.

There were some distinct differences between the ROIs. Different *N*-glycosylation responses were seen between the lesion epicentre and the intact tissue either side (Figure 6.18, Figure 6.21, Figure 6.23) and further differences between the intact tissue rostral and caudal to the injury (regions B and C, Figure 6.21, Figure 6.23). High mannose structures were generally increased in Region A but decreased in Region B at both time-points (Figure 6.20, Figure 6.22), and in Region C there was an early decrease in high mannose species at 7 dpi with an increase at 14 dpi (Figure 6.24). There were noticeable differences in the hybrid structures depending on the region examined. In Region A, the lesion epicentre, non-fucosylated hybrids were strongly increased at both time-points across all injury groups, while those carrying core fucose were decreased in most of the groups (Figure 6.20). In contrast, in Regions B and C it was the core fucosylated hybrids which were increased (Figure 6.22, Figure 6.24). There were further differences between Regions B and C in the non-fucosylated hybrids and a collagen hydrogel response could also be seen here. At 7 dpi there was a decrease in non-fucosylated hybrids in the collagen hydrogel groups in Region B and an increase in Region C. In both regions there was no change seen in these glycans in the transection only group at 7 dpi.

A difference could also be seen between regions and treatment group for the level of fucosylation on complex glycans and on complex, bisected glycans. In Region C opposite responses could be seen between the random and aligned collagen hydrogel groups at 7 dpi in relation to fucosylation of bisected glycans. Fucose was increased on bisected glycans in the random collagen hydrogel group but decreased in the aligned hydrogel group (Figure 6.24). In Region B complex glycans carrying outer arm fucose were increased at 14 dpi only in the collagen hydrogel treated groups. The transection only group was unchanged from sham at this time-point (Figure 6.22). It is possible that this is related to local neuronal repair efforts, as axon sprouting could be observed in this region by this time-point,

particularly in the aligned hydrogel group where the greater increase was seen (reported in the thesis of Aniket Kshirsagar, manuscript in preparation). Outer arm fucose has also been associated with axonal growth and synapse formation during development (Murrey *et al.*, 2006; Hayes and Melrose, 2018).

The difference seen between the three ROIs was interesting and is another factor which would require consideration regarding delivery of a glycan based therapeutic. It is possible that region B rostral to the injury received descending signals which do not reach the other regions due to the disruption of the tissue. Perhaps then Region C can be considered a true local response to the injury in adjacent, largely undamaged cells, with the profile seen in Region A being a general response to large scale tissue destruction.

To more deeply understand the observed changes in the *N*-glycome it would be helpful to know more about the cell type, organelle and proteins carrying and affected by these changes. From this work all we can say is that phagocytic macrophages and microglia display high amounts of sialic acid on their surface. On macrophages at least this is possibly related to the mechanism by which immune cells extravasate from the vasculature. Selectins, sialic acid binding lectins, are expressed on the surface of the blood vessel endothelial cells, and facilitate the classic tethering and rolling of immune cells before they pass into the tissue (reviewed in (Lee and Benveniste, 1999). Fucosylated glycans have also been implicated in this process (Becker and Lowe, 1999; Hayes and Melrose, 2018). We do not know for certain where the high mannose species are localised, although they are likely associated with the synapses (Matus *et al.*, 1973; Kleene and Schachner, 2004), or any of the other more complex glycans which have been decreased. We also cannot say whether the changes seen here are beneficial or detrimental to tissue repair, which glycan species would be best chosen as a target, or whether their presence should be encouraged or prevented. Deeper investigation will be necessary to know the cells and proteins where glycosylation has been altered and to understand the most appropriate way to influence this.

7 Chapter 7 – Conclusions

The overall aim of this work was to determine how we can develop and improve future biomaterial based therapies for SCI. Biomaterials, and collagen in particular show promise in pre-clinical models when used alone or in combination with other therapeutic factors (Kim *et al.*, 2014; Haggerty *et al.*, 2017), and a collagen scaffold combination treatment with human MSCs has even been brought to clinical trial (Xiao *et al.*, 2016; Zhao *et al.*, 2017; Xiao *et al.*, 2018). However there is still vast room for improvement in their efficacy (Ham and Leipzig, 2018). In previous work, we have seen improvement in axonal sprouting with NT-3 functionalised collagen, while motor function was improved in the group without NT-3 (Breen *et al.*, 2016). From this it is clear that collagen does provide some benefit for repair after SCI but there is much room for improvement.

In order to properly design and functionalise more successful collagen based therapies it is necessary to first understand how regeneration can occur spontaneously, and secondly to understand the host response to the implanted biomaterial, in the injured environment. The aim of this thesis work was to investigate these two questions with a focus on the glycosylation response, using *Xenopus laevis* to study unaided successful regeneration after SCI, and using the rat to understand how a collagen hydrogel modulates the SCI response in the non-regenerative mammalian spinal cord. In both cases, the main focus was on glycosylation.

Glycosylation, particularly *N*-glycosylation, is considered to be one of the most widespread post-translational modifications, and influences proteins' subcellular localisation, their stability, secretion and interaction with ligands or receptors (Varki A, 2009a). Glycans can also be important mediators of cell-cell or cell-matrix interaction (Varki A, 2009a), and so understanding their expression and behaviour can give deeper insight into the pathogenesis and cellular behaviour underlying injury and disease.

The tadpole *Xenopus laevis* SCI model used here used surgical procedure modified from that reported in the literature, and so before investigating glycosylation changes, it was necessary to examine regeneration at the cellular level, and to establish the time-line of repair following this injury. Chapter 3 outlined some of the cellular bases for successful regeneration in tadpole *Xenopus laevis* and differences between these and froglet *Xenopus laevis* which are known not to regenerate (Sims, 1962; Beattie *et al.*, 1990; Lee-Liu *et al.*, 2014). The timeline of regeneration in this transection model was established using immunohistochemistry to follow the growth of neurons across the lesion. Following transection in the tadpole, axonal sprouting could be observed as early as 1 dpi. A thin tissue bridge

was evident by 7 dpi reconnecting each end of the cut spinal cord. Functional recovery could also be observed at this stage. In agreement with other studies (Sims, 1962; Michel and Reier, 1979; Gaete *et al.*, 2012; Lee-Liu *et al.*, 2014) repair appeared to be a combined result of sprouting from cut axons either side of the injury and also from a population of cells which migrated into the lesion epicentre. Since reactive astrocytosis and the formation of the glial scar is proposed to contribute to the failure of regeneration in mammalian SCI (Fawcett and Asher, 1999) the astrocytic response was briefly investigated in this model. In the regenerating tadpole spinal cord GFAP immunoreactivity was low, and the processes did not appear to align in any one direction. In contrast, froglet astrocytes extended long processes which often seemed to run parallel to the cut surface of the cord. It seems possible from this study that the glial response could be contributor to whether repair is successful or not after an injury, and warrants further study.

Following from the observation that repair begins as early as 1 dpi and that there is a reconnection of the spinal cord by 7 dpi, these time-points were chosen for a deeper examination of the difference in response to SCI between regenerative tadpole and non-regenerative froglet, using lectin histochemistry to focus on the glycosylation response. This work is outlined in Chapter 4. Transection injury resulted in clear changes in glycosylation which were distinct between tadpole and froglet. The greatest difference was in the sialylation response to SCI: in the tadpole there was an increase in response to transection at 1 dpi, but at 7 dpi the amount of sialic acid was very similar in transected and sham injured animals. In the froglet there was an increase in comparison to sham at both time-points, however there was a much larger increase at 1 dpi, which was significantly higher than the tadpole at 1 dpi and the froglet at 7 dpi. This suggests that an early and sustained increase in sialic acid is a negative influencer of regeneration. The change in GlcNAc was quite similar between tadpoles and froglets in the vicinity of the region, but was quite different in the intact tissue far from the injury, being much higher in the tadpole. Maybe this is related to repair efforts initiated further along the injured axons, or to control of glial behaviour distant from the injury. For both tadpole and froglet galactose increased initially and then was decreased compared to sham by 7 dpi. The increase was much more pronounced in the tadpole and there was more of a decrease over time. Careful temporal regulation of galactose may be important for the regenerative response. GalNAc may be very important in influencing the regenerative response: in the tadpole at both 1 and 7 dpi there was an increase compared to sham, but in the froglet GalNAc was decreased at both time-points. The increase was maintained in the tadpole between the two time-points and in the froglet, there was a decrease between 1 and 7 dpi. Therefore a sustained increase in GalNAc may be required to encourage spinal cord regeneration. There may be a specific glycosylation signature required for regeneration to proceed which encompasses these changes in sialic acid, GlcNAc, galactose and GalNAc.

In Chapter 5 the focus moved to examining SCI in a non-regenerative mammalian environment in the presence of a biomaterial therapy, namely an aligned collagen hydrogel. This study examined changes in the inflammatory profile of the injured spinal cord over time, from 3 dpi to 28 dpi comparing two groups: transection only and transection with aligned collagen hydrogel. The balance between pro-inflammatory, M1 type microglia and macrophages and the anti-inflammatory M2 type microglia and macrophages was investigated using dual immunohistochemistry. In all regions examined, there was a largely M2, anti-inflammatory type response at the earlier time-point of 3 dpi. From 7 dpi a pro-inflammatory response began to increase. However this was mainly seen as a population of cells positive for both the pro-inflammatory marker (iNOS) and the anti-inflammatory marker (Arginase-1) and throughout all time-points examined cells positive for iNOS only were very low in number (<20% of total labelled cells). The dual labelled cells were termed transitional cells and were considered as having both pro- and anti-inflammatory effects on the surrounding tissue. Treatment with aligned collagen hydrogel alone resulted only in very small, non-significant changes in the inflammatory profile, and so combinatorial therapy of aligned collagen hydrogel with an anti-inflammatory therapeutic may be useful, but the timing of delivery of the anti-inflammatory would be important.

Chapter 6 first established the normal *N*-glycoprofile of the intact adult female rat spinal cord, and then investigated the response to transection injury and to treatment with aligned collagen hydrogel at the *N*-glycosylation level using HILIC-UPLC *N*-glycoprofiling. In the uninjured spinal cord, high-mannose type *N*-glycans were very common, some hybrid glycans were present and complex *N*-glycans were abundant being mostly di- or tri-antennary. Some of the complex glycans carried a bisecting GlcNAc residue. Core fucose residues were a common feature of all three glycan types and hybrid and complex glycans were commonly decorated with outer arm fucose residues and galactose in both beta and alpha linkage. A low level of sialylation was seen but other charged species such as sulphate groups were identified, as well as acetylated sialic acids.

Injury to the spinal cord resulted in many changes to the *N*-glycan species present, both in the lesion epicentre and in the intact tissue either side. An overall loss of complexity in *N*-glycan species was observed in response to the transection injury with only subtle differences in the presence of collagen hydrogel. This was seen in the increase in high mannose species, particularly those carrying core fucose, and the increase in hybrid structures (those without fucose in Region A, and those with core fucose in Region B) and the general reduction in complex structures across both regions. There was however an increase in bisected complex glycans in the three regions in most experimental groups. This may be related to neuronal and/or glial death, as increased bisecting GlcNAc has been observed in relation to AD and HD (Akasaka-Manya *et al.*, 2008; Akasaka-Manya *et al.*, 2010; Gizaw *et al.*, 2015).

Increased core fucosylation has also been observed in these neurodegenerative diseases (Akasaka-Manya *et al.*, 2008; Gizaw *et al.*, 2015; Palmigiano *et al.*, 2016). Increased sialylation was another feature of the injury, particularly at 7 dpi, and this affect did appear to be reduced in the presence of the hydrogels. The inability of either of the collagen hydrogels to prevent the loss of glycan complexity reinforces the idea that a combinatorial therapy will be necessary. Perhaps interfering with the production of bisected or alpha-galactosylated *N*-glycans would be helpful, or encouraging branching and substitution to restore some of the complexity.

It is possible that the increase in high mannose and hybrid structures exacerbates and sustains the inflammatory response after SCI. Many macrophage receptors, such as the CD206 receptor, have mannose binding activity for recognition of pathogens. Normally macrophages are not exposed to the high mannose structures typical of CNS glycans, with these glycans being a relatively minor component of serum glycans (Saldova *et al.*, 2014), but in SCI the BSCB is disrupted and there is a large influx of peripheral macrophages (Popovich *et al.*, 1997) bringing these cells into contact with the 'apparently foreign' high mannose glycans, and likely exacerbating the inflammatory response (Green *et al.*, 2007).

Linking the glycosylation studies performed on *Xenopus laevis* in Chapter 4 with the glycosylation studies performed on the rat in Chapter 6 some general conclusions can be made regarding glycan species which are associated with injury and which may be beneficial or detrimental to the regenerative response. The most striking is the sialic acid response to injury. In all cases, tadpole and froglet, rat with and without collagen hydrogel, there was an early increase in sialic acid following injury. The extent of this increase and the length of time it was maintained for seems to be important. In the regenerative tadpole, the increase was seen only at 1 dpi, by 7 dpi it was there was no difference between transection and sham groups. In the non-regenerative froglet the increase at 1 dpi was much greater, and although the amount of sialic acid reduced by 7 dpi it was still well above sham levels. In the rat sialic acid was increased in response to injury in all groups at both 7 and 14 dpi. Double labelling by lectin- and immuno-histochemistry revealed that this increase in sialic acid in the rat is associated with the increased activated macrophages and microglia present in the injured cord. Attempts were made to perform similar experiments in the injured *Xenopus laevis* spinal cord but satisfactory immuno-labelling of microglia/macrophages could not be achieved. However, double labelling with astrocyte and neuronal markers showed that these cells did not carry the sialic acid. If it is the inflammatory cells which carry sialic acid in the tadpole, the resolution of this sialylation response may be an indication of resolution of inflammation as the cord reconnects at 7 dpi.

If pursued as a therapeutic target sialic acid could be utilised in one of two ways. One option could be to use the surface sialic acid to target a therapeutic, such as an anti-inflammatory, to microglia and

macrophages, while avoiding astrocytes and neurons. Another would be to try to mimic the pattern of expression seen in the regenerative tadpole. Delivery of a sialidase to the injured spinal cord at later time-points could cleave the terminal sialic acid residues from the glycan, or inhibiting the activity of the sialyltransferase enzymes in the Golgi would prevent the production of sialylated glycans in the first place.

Trends could also be seen relating *Xenopus laevis* and rat response to SCI in terms of glycan branching and complexity. In the injured rat spinal cord there was an overall decrease in complex glycans and the level of their fucosylation in favour of the high mannose species and the hybrids. In *Xenopus laevis* there seemed to be an increase in branching (increased DSA binding to GlcNAc) coupled with an increase in galactose (AIA binding) indicating more complexity in the glycans present. This was apparent in both tadpole and froglet but the response was slightly greater in the tadpole, and these increases were only seen at the earlier time-point. This suggests that a transient increase in *N*-glycan complexity is necessary for the repair of the spinal cord. The requirement for this effect to be present so early after injury could make it difficult to exploit therapeutically.

Throughout all the studies described in this thesis changes with time were evident: there were slight increases in astrocyte area in the froglet between 1 and 7 dpi, the polarisation of microglia and macrophages shifted over the 28 day time-period studied, and glycosylation was seen to be a dynamic process in both *Xenopus laevis* and the rat. These temporal changes are important to consider in the development of any therapeutic: some therapies will need administration immediately following injury, while others may require a more delayed delivery, for example in the case of sialic acid outlined above, the early increase in the tadpole may be important, but this needs to be reduced soon after. Differential responses depending on the ROI studied were also present. These differences are not often reported in other studies, but could be just as important as timing in terms of delivery of a therapeutic, especially in a tissue such as the spinal cord where many cells have their soma far from the injury, for example the large motor neurons. It is also likely that many microglia travel towards the site of injury from elsewhere in the cord, and perhaps preventing this migration could help to reduce the inflammatory response in the locality of the injury.

Glycans in other forms have been tested as experimental therapies for injury and diseases of the nervous system, including targeting the proteoglycan component of the scar in SCI (Bradbury *et al.*, 2002; Bartus *et al.*, 2014) and galectins have been used in models of focal ischaemia (Qu *et al.*, 2010; Qu *et al.*, 2011) and SCI (Pajoohesh-Ganji *et al.*, 2012). The positive results seen in these studies highlights the importance of investigating glycan based therapies.

7.1 Future directions

Extensive further study will be necessary before any of the findings of this thesis work could be incorporated into a biomaterial therapy for the injured spinal cord. Greater detail on the glycosylation response in tadpole and froglet *Xenopus laevis* will be necessary in order to know whether the changes observed here were actually due to changes in *N*-glycans as assumed here, or whether the detected monosaccharides were actually components of *O*-glycans, glycolipids or others. Ideally HILIC-UPLC *N*-glycoprofiling should be employed to study the *N*-glycans of the tadpole and froglet spinal cord and how they change in response to injury. A stronger comparison between this model and the rat model could then be made, and a more specific glycan signature could be associated to the regenerative response for combinatorial treatment with a biomaterial such as the aligned collagen hydrogel used here.

Since the major change in the *N*-glycoprofile was the loss of complexity of *N*-glycan species and the increase in high mannose and hybrid species it is first important to understand whether this is a result of damage or stress to the ER and Golgi apparatus. Some simple ultrastructural study of the tissue may indicate whether this is the case.

In order to properly interpret the observed changes in *N*-glycosylation seen in the transected rat spinal cord some functional work will be necessary. From the current results it is not possible to say which glycan species may be beneficial and which may be detrimental in terms of repair of the injured tissue. Glyco-engineering could be employed to attach glycans to the collagen hydrogel. A neuronal differentiation affect has been observed in the presence of collagen with glucose molecules chemically attached (Russo *et al.*, 2014). It would be interesting to see if this effect could be seen *in vivo* in the injured spinal cord with simple glycans such as these, or with the more complex branched species. Obtaining complex glycans for such work may be challenging, simpler glycans such as those found on IgGs are available commercially as standards, however the highly complex, CNS-specific glycans identified here may be difficult to purchase and/or synthesise chemically. In this case, it may be more effective to target the *N*-glycosylation pathway itself, by transfecting cells to express more of a particular glycotransferase enzyme or by knocking down the glycotransferase. If increasing the activity of a particular enzyme, it may also be necessary to supply the nucleotide sugars which act as substrates. A selection of glycans should be targeted, with a representative of each of the major glycan features, high mannose, hybrid, complex and bisected complex. The hybrid and complex glycans should be tested with various degrees of galactose, outer fucose and sialic acid decoration. The role of core fucose, alpha-galactose and glycan sulphation should also be examined.

Understanding where in the tissue a particular glycan species is located could be very useful in understanding its role in the injury process. Further lectin- and immuno-histochemistry studies, similar to those outlined in Chapter 6, could be used to understand the cellular location of other glycan types. Since *N*-glycosylation occurs as a post-translational modification of proteins it may be necessary to find out which protein(s) a glycan is present on in order to properly exploit it as a therapeutic. Affinity chromatography with a lectin or other glycan-binding substance could be performed on a spinal cord homogenate in order to isolate the glycoprotein to which a particular glycan is attached. A technique such as mass spectrometry could then be employed to identify the glycoprotein of interest. This could then form the basis for a more focussed therapeutic target.

8 Chapter 8 - Bibliography

ABOU-ABBASS, H., BAHMAD, H., ABOU-EL-HASSAN, H., ZHU, R., ZHOU, S., DONG, X., HAMADE, E., MALLAH, K., ZEBIAN, A., RAMADAN, N., MONDELLO, S., FARES, J., COMAIR, Y., ATWEH, S., DARWISH, H., ZIBARA, K., MECHREF, Y. & KOBEISSY, F. 2016. Deciphering glycomics and neuroproteomic alterations in experimental traumatic brain injury: Comparative analysis of aspirin and clopidogrel treatment. *Electrophoresis,* 37**,** 1562-76.

ADAMS, K. L. & GALLO, V. 2018. The diversity and disparity of the glial scar. *Nature neuroscience,* 21**,** 9-15.

AHUJA, C. S., NORI, S., TETREAULT, L., WILSON, J., KWON, B., HARROP, J., CHOI, D. & FEHLINGS, M. G. 2017. Traumatic Spinal Cord Injury—Repair and Regeneration. *Neurosurgery,* 80**,** S9-S22.

AKASAKA-MANYA, K., MANYA, H., SAKURAI, Y., WOJCZYK, B. S., KOZUTSUMI, Y., SAITO, Y., TANIGUCHI, N., MURAYAMA, S., SPITALNIK, S. L. & ENDO, T. 2010. Protective effect of N -glycan bisecting GlcNAc residues on β-amyloid production in Alzheimer's disease. *Glycobiology,* 20**,** 99-106.

AKASAKA-MANYA, K., MANYA, H., SAKURAI, Y., WOJCZYK, B. S., SPITALNIK, S. L. & ENDO, T. 2008. Increased bisecting and core-fucosylated N-glycans on mutant human amyloid precursor proteins. *Glycoconjugate Journal,* 25**,** 775-786.

ALBACH, C., KLEIN, R. A. & SCHMITZ, B. 2001. Do rodent and human brains have different N-glycosylation patterns? *Biol Chem,* 382**,** 187-94.

ALTINOVA, H., MOLLERS, S., FUHRMANN, T., DEUMENS, R., BOZKURT, A., HESCHEL, I., DAMINK, L. H., SCHUGNER, F., WEIS, J. & BROOK, G. A. 2014. Functional improvement following implantation of a microstructured, type-I collagen scaffold into experimental injuries of the adult rat spinal cord. *Brain Res,* 1585**,** 37-50.

ANDERSON, M. A., BURDA, J. E., REN, Y., AO, Y., O'SHEA, T. M., KAWAGUCHI, R., COPPOLA, G., KHAKH, B. S., DEMING, T. J. & SOFRONIEW, M. V. 2016. Astrocyte scar formation aids central nervous system axon regeneration. *Nature,* 532**,** 195-200.

ANGIARI, S., DONNARUMMA, T., ROSSI, B., DUSI, S., PIETRONIGRO, E., ZENARO, E., DELLA BIANCA, V., TOFFALI, L., PIACENTINO, G., BUDUI, S., RENNERT, P., XIAO, S., LAUDANNA, C., CASASNOVAS, J. M., KUCHROO, V. K. & CONSTANTIN, G. 2014. TIM-1 glycoprotein binds the adhesion receptor P-selectin and mediates T cell trafficking during inflammation and autoimmunity. *Immunity,* 40**,** 542-53.

APWEILER, R., HERMJAKOB, H. & SHARON, N. 1999. On the frequency of protein glycosylation, as deduced from analysis of the SWISS-PROT database. *Biochim Biophys Acta,* 1473**,** 4-8.

BAIYILA, B., HE, B., HE, G. & LONG, T. 2018. Anti-inflammatory effect of Mongolian drug Naru-3 on traumatic spinal cord injury and its mechanism of action. *J Int Med Res,* 46**,** 2346-2358.

BARONDES, S. H. 1988. Bifunctional properties of lectins: lectins redefined. *Trends in Biochemical Sciences,* 13**,** 480-482.

BARTUS, K., JAMES, N. D., DIDANGELOS, A., BOSCH, K. D., VERHAAGEN, J., YÁÑEZ-MUÑOZ, R. J., ROGERS, J. H., SCHNEIDER, B. L., MUIR, E. M. & BRADBURY, E. J. 2014. Large-Scale Chondroitin Sulfate Proteoglycan Digestion with Chondroitinase Gene Therapy Leads to Reduced Pathology and Modulates Macrophage Phenotype following Spinal Cord Contusion Injury. *The Journal of Neuroscience,* 34**,** 4822-4836.

BAYRAKTAR, O. A., FUENTEALBA, L. C., ALVAREZ-BUYLLA, A. & ROWITCH, D. H. 2014. Astrocyte development and heterogeneity. *Cold Spring Harb Perspect Biol,* 7**,** a020362.

BEATTIE, M. S., BRESNAHAN, J. C. & LOPATE, G. 1990. Metamorphosis alters the response to spinal cord transection in Xenopus laevis frogs. *J Neurobiol,* 21**,** 1108-22.

BECK, C. W., CHRISTEN, B. & SLACK, J. M. 2003. Molecular pathways needed for regeneration of spinal cord and muscle in a vertebrate. *Dev Cell,* 5**,** 429-39.

BECKER, D. J. & LOWE, J. B. 1999. Leukocyte adhesion deficiency type II. *Biochim Biophys Acta,* 1455**,** 193-204.

BERMUDEZ, S., KHAYRULLINA, G., ZHAO, Y. & BYRNES, K. R. 2016. NADPH oxidase isoform expression is temporally regulated and may contribute to microglial/macrophage polarization after spinal cord injury. *Molecular and Cellular Neuroscience,* 77**,** 53-64.

BERTOZZI CR, R. D. 2009. Structural Basis of Glycan Diversity. *In:* VARKI A, C. R., ESKO JD, ET AL., (ed.) *Essentials of Glycobiology.* 2nd edition ed. Cold Spring Harbor (NY): Cold Spring Harbor Laboratory Press.

BIGGE, J. C., PATEL, T. P., BRUCE, J. A., GOULDING, P. N., CHARLES, S. M. & PAREKH, R. B. 1995. Nonselective and efficient fluorescent labeling of glycans using 2-amino benzamide and anthranilic acid. *Anal Biochem,* 230**,** 229-38.

BLOOM, O. 2014. Non-mammalian model systems for studying neuro-immune interactions after spinal cord injury. *Experimental neurology,* 0**,** 130-140.

BRADBURY, E. J., MOON, L. D. F., POPAT, R. J., KING, V. R., BENNETT, G. S., PATEL, P. N., FAWCETT, J. W. & MCMAHON, S. B. 2002. Chondroitinase ABC promotes functional recovery after spinal cord injury. *Nature,* 416**,** 636-640.

BREEN, B. A., KRASKIEWICZ, H., RONAN, R., KSHIRAGAR, A., PATAR, A., SARGEANT, T., PANDIT, A. & MCMAHON, S. S. 2016. Therapeutic Effect of Neurotrophin-3 Treatment in an Injectable Collagen Scaffold Following Rat Spinal Cord Hemisection Injury. *ACS Biomaterials Science & Engineering*.

BRENNAN, F. H. & POPOVICH, P. G. 2018. Emerging targets for reprograming the immune response to promote repair and recovery of function after spinal cord injury. *Curr Opin Neurol*.

BROCKHAUSEN I, S. P. 2017. O-GalNAc Glycans. *In:* VARKI A, C. R., ESKO JD, ET AL. (ed.) *Essentials of Glycobiology [Internet].* Cold Spring Harbor (NY): Cold Spring Harbor Laboratory Press.

BUNGE, R. P., PUCKETT, W. R., BECERRA, J. L., MARCILLO, A. & QUENCER, R. M. 1993. Observations on the pathology of human spinal cord injury. A review and classification of 22 new cases with details from a case of chronic cord compression with extensive focal demyelination. *Adv Neurol,* 59**,** 75-89.

BUSH, T. G., PUVANACHANDRA, N., HORNER, C. H., POLITO, A., OSTENFELD, T., SVENDSEN, C. N., MUCKE, L., JOHNSON, M. H. & SOFRONIEW, M. V. 1999. Leukocyte infiltration, neuronal degeneration, and neurite outgrowth after ablation of scar-forming, reactive astrocytes in adult transgenic mice. *Neuron,* 23**,** 297-308.

BUTLER, E. G. & WARD, M. B. 1965. Reconstitution of the spinal cord following ablation in urodele larvae. *J Exp Zool,* 160**,** 47-65.

CAMPBELL, L., SAVILLE, C. R., MURRAY, P. J., CRUICKSHANK, S. M. & HARDMAN, M. J. 2013. Local Arginase 1 Activity Is Required for Cutaneous Wound Healing. *Journal of Investigative Dermatology,* 133**,** 2461-2470.

CARLBERG, M., DRICU, A., BLEGEN, H., WANG, M., HJERTMAN, M., ZICKERT, P., HOOG, A. & LARSSON, O. 1996. Mevalonic acid is limiting for N-linked glycosylation and translocation of the insulin-like growth factor-1 receptor to the cell surface. Evidence for a new link between 3-hydroxy-3-methylglutaryl-coenzyme a reductase and cell growth. *J Biol Chem,* 271**,** 17453-62.

CARTER, L. M., MCMAHON, S. B. & BRADBURY, E. J. 2011. Delayed treatment with chondroitinase ABC reverses chronic atrophy of rubrospinal neurons following spinal cord injury. *Exp Neurol,* 228**,** 149-56.

CAUBIT, X., ARSANTO, J. P., FIGARELLA-BRANGER, D. & THOUVENY, Y. 1993. Expression of polysialylated neural cell adhesion molecule (PSA-N-CAM) in developing, adult and regenerating caudal spinal cord of the urodele amphibians. *Int J Dev Biol,* 37**,** 327-36.

CAUBIT, X., RIOU, J. F., COULON, J., ARSANTO, J. P., BENRAISS, A., BOUCAUT, J. C. & THOUVENY, Y. 1994. Tenascin expression in developing, adult and regenerating caudal spinal cord in the urodele amphibians. *Int J Dev Biol,* 38**,** 661-72.

CHANG, J., BAKER, J. & WILLS, A. 2017. Transcriptional dynamics of tail regeneration in Xenopus tropicalis. *Genesis,* 55.

CHEN, C., ZHAO, M. L., ZHANG, R. K., LU, G., ZHAO, C. Y., FU, F., SUN, H. T., ZHANG, S., TU, Y. & LI, X. H. 2017. Collagen/heparin sulfate scaffolds fabricated by a 3D bioprinter improved mechanical

properties and neurological function after spinal cord injury in rats. *J Biomed Mater Res A,* 105**,** 1324-1332.

CHEN, S., YE, J., CHEN, X., SHI, J., WU, W., LIN, W., LIN, W., LI, Y., FU, H. & LI, S. 2018a. Valproic acid attenuates traumatic spinal cord injury-induced inflammation via STAT1 and NF-kappaB pathway dependent of HDAC3. *J Neuroinflammation,* 15**,** 150.

CHEN, X., ZHAO, Y., LI, X., XIAO, Z., YAO, Y., CHU, Y., FARKAS, B., ROMANO, I., BRANDI, F. & DAI, J. 2018b. Functional Multichannel Poly(Propylene Fumarate)-Collagen Scaffold with Collagen-Binding Neurotrophic Factor 3 Promotes Neural Regeneration After Transected Spinal Cord Injury. *Adv Healthc Mater,* 7**,** e1800315.

CHEN, Y. J., WING, D. R., GUILE, G. R., DWEK, R. A., HARVEY, D. J. & ZAMZE, S. 1998. Neutral N-glycans in adult rat brain tissue--complete characterisation reveals fucosylated hybrid and complex structures. *Eur J Biochem,* 251**,** 691-703.

CHEN, Y. J., ZHU, H., ZHANG, N., SHEN, L., WANG, R., ZHOU, J. S., HU, J. G. & LU, H. Z. 2015. Temporal kinetics of macrophage polarization in the injured rat spinal cord. *J Neurosci Res,* 93**,** 1526-33.

CHERNOFF, E. A., STOCUM, D. L., NYE, H. L. & CAMERON, J. A. 2003. Urodele spinal cord regeneration and related processes. *Dev Dyn,* 226**,** 295-307.

CHIEN, M. W., FU, S. H., HSU, C. Y., LIU, Y. W. & SYTWU, H. K. 2018. The Modulatory Roles of N-glycans in T-Cell-Mediated Autoimmune Diseases. *Int J Mol Sci,* 19.

CHOLAS, R., HSU, H. P. & SPECTOR, M. 2012a. Collagen scaffolds incorporating select therapeutic agents to facilitate a reparative response in a standardized hemiresection defect in the rat spinal cord. *Tissue Eng Part A,* 18**,** 2158-72.

CHOLAS, R. H., HSU, H. P. & SPECTOR, M. 2012b. The reparative response to cross-linked collagen-based scaffolds in a rat spinal cord gap model. *Biomaterials,* 33**,** 2050-9.

CHROSTEK, L., CYLWIK, B., GINDZIENSKA-SIESKIEWICZ, E., GRUSZEWSKA, E., SZMITKOWSKI, M. & SIERAKOWSKI, S. 2014. Sialic acid level reflects the disturbances of glycosylation and acute-phase reaction in rheumatic diseases. *Rheumatol Int,* 34**,** 393-9.

CHU, D. T. W. & KLYMKOWSKY, M. W. 1989. The appearance of acetylated α-tubulin during early development and cellular differentiation in Xenopus. *Developmental Biology,* 136**,** 104-117.

CLAUDE, J., LINNARTZ-GERLACH, B., KUDIN, A. P., KUNZ, W. S. & NEUMANN, H. 2013. Microglial CD33-related Siglec-E inhibits neurotoxicity by preventing the phagocytosis-associated oxidative burst. *J Neurosci,* 33**,** 18270-6.

COETZEE, T., FUJITA, N., DUPREE, J., SHI, R., BLIGHT, A., SUZUKI, K., SUZUKI, K. & POPKO, B. 1996. Myelination in the Absence of Galactocerebroside and Sulfatide: Normal Structure with Abnormal Function and Regional Instability. *Cell,* 86**,** 209-219.

COLLEY KJ, V. A., KINOSHITA T 2017. Cellular Organization of Glycosylation. *In:* VARKI A, C. R., ESKO JD, ET AL. (ed.) *Essentials of Glycobiology. 3rd edition.*: Cold Spring Harbor (NY): Cold Spring Harbor Laboratory Press;.

CORNELISON, R. C., GONZALEZ-ROTHI, E. J., PORVASNIK, S. L., WELLMAN, S. M., PARK, J. H., FULLER, D. D. & SCHMIDT, C. E. 2018. Injectable hydrogels of optimized acellular nerve for injection in the injured spinal cord. *Biomedical Materials,* 13**,** 034110.

CROCKER, P. R. & GORDON, S. 1986. Properties and distribution of a lectin-like hemagglutinin differentially expressed by murine stromal tissue macrophages. *J Exp Med,* 164**,** 1862-75.

CROCKER, P. R., MUCKLOW, S., BOUCKSON, V., MCWILLIAM, A., WILLIS, A. C., GORDON, S., MILON, G., KELM, S. & BRADFIELD, P. 1994. Sialoadhesin, a macrophage sialic acid binding receptor for haemopoietic cells with 17 immunoglobulin-like domains. *Embo j,* 13**,** 4490-503.

CROCKER, P. R., PAULSON, J. C. & VARKI, A. 2007. Siglecs and their roles in the immune system. *Nat Rev Immunol,* 7**,** 255-66.

CUMMINGS RD, E. M. 2009. Antibodies and Lectins in Glycan Analysis. *In:* VARKI A, C. R., ESKO JD, ET AL., (ed.) *Essentials of Glycobiology. 2nd edition.*: Cold Spring Harbor (NY): Cold Spring Harbor Laboratory Press.

CUSIMANO, M., BIZIATO, D., BRAMBILLA, E., DONEGÀ, M., ALFARO-CERVELLO, C., SNIDER, S., SALANI, G., PUCCI, F., COMI, G., GARCIA-VERDUGO, J. M., DE PALMA, M., MARTINO, G. & PLUCHINO,

S. 2012. Transplanted neural stem/precursor cells instruct phagocytes and reduce secondary tissue damage in the injured spinal cord. *Brain,* 135**,** 447-460.

DAVID, S. & KRONER, A. 2011. Repertoire of microglial and macrophage responses after spinal cord injury. *Nat Rev Neurosci,* 12**,** 388-99.

DAVIES, L. R. & VARKI, A. 2015. Why Is N-Glycolylneuraminic Acid Rare in the Vertebrate Brain? *Top Curr Chem,* 366**,** 31-54.

DE LA TORRE, J. C. 1982. Catecholamine fiber regeneration across a collagen bioimplant after spinal cord transection. *Brain Res Bull,* 9**,** 545-52.

DE LA TORRE, J. C., HILL, P. K., GONZALEZ-CARVAJAL, M. & PARKER, J. C., JR. 1984. Evaluation of transected spinal cord regeneration in the rat. *Exp Neurol,* 84**,** 188-206.

DE LUCA, C. & PAPA, M. 2017. Matrix Metalloproteinases, Neural Extracellular Matrix, and Central Nervous System Pathology. *Prog Mol Biol Transl Sci,* 148**,** 167-202.

DENNING, D., ABU-RUB, M. T., ZEUGOLIS, D. I., HABELITZ, S., PANDIT, A., FERTALA, A. & RODRIGUEZ, B. J. 2012. Electromechanical properties of dried tendon and isoelectrically focused collagen hydrogels. *Acta Biomaterialia,* 8**,** 3073-3079.

DIDANGELOS, A., IBERL, M., VINSLAND, E., BARTUS, K. & BRADBURY, E. J. 2014. Regulation of IL-10 by chondroitinase ABC promotes a distinct immune response following spinal cord injury. *J Neurosci,* 34**,** 16424-32.

DOVERHAG, C., HEDTJARN, M., POIRIER, F., MALLARD, C., HAGBERG, H., KARLSSON, A. & SAVMAN, K. 2010. Galectin-3 contributes to neonatal hypoxic-ischemic brain injury. *Neurobiol Dis,* 38**,** 36-46.

DUMONT, R. J., OKONKWO, D. O., VERMA, S., HURLBERT, R. J., BOULOS, P. T., ELLEGALA, D. B. & DUMONT, A. S. 2001. Acute spinal cord injury, part I: pathophysiologic mechanisms. *Clin Neuropharmacol,* 24**,** 254-64.

DYCK, S., KATARIA, H., ALIZADEH, A., SANTHOSH, K. T., LANG, B., SILVER, J. & KARIMI-ABDOLREZAEE, S. 2018. Perturbing chondroitin sulfate proteoglycan signaling through LAR and PTPsigma receptors promotes a beneficial inflammatory response following spinal cord injury. *J Neuroinflammation,* 15**,** 90.

EARL, L. A., BI, S. & BAUM, L. G. 2010. N- and O-glycans modulate galectin-1 binding, CD45 signaling, and T cell death. *J Biol Chem,* 285**,** 2232-44.

ECHEVERRI, K. & TANAKA, E. M. 2002. Ectoderm to mesoderm lineage switching during axolotl tail regeneration. *Science,* 298**,** 1993-6.

EDWARDS-FARET, G., CEBRIAN-SILLA, A., MENDEZ-OLIVOS, E. E., GONZALEZ-PINTO, K., GARCIA-VERDUGO, J. M. & LARRAIN, J. 2018. Cellular composition and organization of the spinal cord central canal during metamorphosis of the frog Xenopus laevis. *J Comp Neurol,* 526**,** 1712-1732.

EDWARDS-FARET, G., MUNOZ, R., MENDEZ-OLIVOS, E. E., LEE-LIU, D., TAPIA, V. S. & LARRAIN, J. 2017. Spinal cord regeneration in Xenopus laevis. *Nat Protoc,* 12**,** 372-389.

ENGELHARDT, B., VESTWEBER, D., HALLMANN, R. & SCHULZ, M. 1997. E- and P-selectin are not involved in the recruitment of inflammatory cells across the blood-brain barrier in experimental autoimmune encephalomyelitis. *Blood,* 90**,** 4459-72.

ERCAN, A., CUI, J., CHATTERTON, D. E., DEANE, K. D., HAZEN, M. M., BRINTNELL, W., O'DONNELL, C. I., DERBER, L. A., WEINBLATT, M. E., SHADICK, N. A., BELL, D. A., CAIRNS, E., SOLOMON, D. H., HOLERS, V. M., RUDD, P. M. & LEE, D. M. 2010. Aberrant IgG galactosylation precedes disease onset, correlates with disease activity, and is prevalent in autoantibodies in rheumatoid arthritis. *Arthritis Rheum,* 62**,** 2239-48.

FAN, C., LI, X., XIAO, Z., ZHAO, Y., LIANG, H., WANG, B., HAN, S., LI, X., XU, B., WANG, N., LIU, S., XUE, W. & DAI, J. 2017. A modified collagen scaffold facilitates endogenous neurogenesis for acute spinal cord injury repair. *Acta Biomater,* 51**,** 304-316.

FAN, J., XIAO, Z., ZHANG, H., CHEN, B., TANG, G., HOU, X., DING, W., WANG, B., ZHANG, P., DAI, J. & XU, R. 2010. Linear ordered collagen scaffolds loaded with collagen-binding neurotrophin-3

promote axonal regeneration and partial functional recovery after complete spinal cord transection. *J Neurotrauma,* 27**,** 1671-83.

FANG, P., LIN, J. F., PAN, H. C., SHEN, Y. Q. & SCHACHNER, M. 2012. A surgery protocol for adult zebrafish spinal cord injury. *J Genet Genomics,* 39**,** 481-7.

FAWCETT, J. W. 2006. The glial response to injury and its role in the inhibition of CNS repair. *Adv Exp Med Biol,* 557**,** 11-24.

FAWCETT, J. W. & ASHER, R. A. 1999. The glial scar and central nervous system repair. *Brain Res Bull,* 49**,** 377-91.

FITCH, M. T. & SILVER, J. 2008. CNS injury, glial scars, and inflammation: Inhibitory extracellular matrices and regeneration failure. *Experimental Neurology,* 209**,** 294-301.

FLEMING, J. C., NORENBERG, M. D., RAMSAY, D. A., DEKABAN, G. A., MARCILLO, A. E., SAENZ, A. D., PASQUALE-STYLES, M., DIETRICH, W. D. & WEAVER, L. C. 2006. The cellular inflammatory response in human spinal cords after injury. *Brain,* 129**,** 3249-3269.

FREEZE, H. H., EKLUND, E. A., NG, B. G. & PATTERSON, M. C. 2015. Neurological aspects of human glycosylation disorders. *Annu Rev Neurosci,* 38**,** 105-25.

FUKUSHIMA, K., ENOMOTO, M., TOMIZAWA, S., TAKAHASHI, M., WAKABAYASHI, Y., ITOH, S., KUBOKI, Y. & SHINOMIYA, K. 2008. The axonal regeneration across a honeycomb collagen sponge applied to the transected spinal cord. *J Med Dent Sci,* 55**,** 71-9.

FUSTER, M. M. & ESKO, J. D. 2005. The sweet and sour of cancer: glycans as novel therapeutic targets. *Nature Reviews Cancer,* 5**,** 526-542.

GAETE, M., MUNOZ, R., SANCHEZ, N., TAMPE, R., MORENO, M., CONTRERAS, E. G., LEE-LIU, D. & LARRAIN, J. 2012. Spinal cord regeneration in Xenopus tadpoles proceeds through activation of Sox2-positive cells. *Neural Dev,* 7**,** 13.

GALILI, U. 2013. Anti-Gal: an abundant human natural antibody of multiple pathogeneses and clinical benefits. *Immunology,* 140**,** 1-11.

GAUDET, A. D., LEUNG, M., POIRIER, F., KADOYA, T., HORIE, H. & RAMER, M. S. 2009. A role for galectin-1 in the immune response to peripheral nerve injury. *Exp Neurol,* 220**,** 320-7.

GAUDET, A. D., SWEET, D. R., POLINSKI, N. K., GUAN, Z. & POPOVICH, P. G. 2015. Galectin-1 in injured rat spinal cord: implications for macrophage phagocytosis and neural repair. *Mol Cell Neurosci,* 64**,** 84-94.

GELDERD, J. B. 1990. Evaluation of blood vessel and neurite growth into a collagen matrix placed within a surgically created gap in rat spinal cord. *Brain Res,* 511**,** 80-92.

GENSEL, J. C., KOPPER, T. J., ZHANG, B., ORR, M. B. & BAILEY, W. M. 2017. Predictive screening of M1 and M2 macrophages reveals the immunomodulatory effectiveness of post spinal cord injury azithromycin treatment. *Sci Rep,* 7**,** 40144.

GENSEL, J. C. & ZHANG, B. 2015. Macrophage activation and its role in repair and pathology after spinal cord injury. *Brain Res,* 1619**,** 1-11.

GEYER, H., BAHR, U., LIEDTKE, S., SCHACHNER, M. & GEYER, R. 2001. Core structures of polysialylated glycans present in neural cell adhesion molecule from newborn mouse brain. *Eur J Biochem,* 268**,** 6587-99.

GIBBS, K. M., CHITTUR, S. V. & SZARO, B. G. 2011. Metamorphosis and the regenerative capacity of spinal cord axons in Xenopus laevis. *Eur J Neurosci,* 33**,** 9-25.

GIBBS, K. M. & SZARO, B. G. 2006. Regeneration of descending projections in Xenopus laevis tadpole spinal cord demonstrated by retrograde double labeling. *Brain Res,* 1088**,** 68-72.

GIZAW, S. T., KODA, T., AMANO, M., KAMIMURA, K., OHASHI, T., HINOU, H. & NISHIMURA, S. 2015. A comprehensive glycome profiling of Huntington's disease transgenic mice. *Biochim Biophys Acta,* 1850**,** 1704-18.

GIZAW, S. T., OHASHI, T., TANAKA, M., HINOU, H. & NISHIMURA, S. 2016. Glycoblotting method allows for rapid and efficient glycome profiling of human Alzheimer's disease brain, serum and cerebrospinal fluid towards potential biomarker discovery. *Biochim Biophys Acta,* 1860**,** 1716-27.

GOYALLON, A., CHOLET, S., CHAPELLE, M., JUNOT, C. & FENAILLE, F. 2015. Evaluation of a combined glycomics and glycoproteomics approach for studying the major glycoproteins present in biofluids: Application to cerebrospinal fluid. *Rapid Commun Mass Spectrom,* 29**,** 461-73.

GRAHAM, D. B., STEPHENSON, L. M., LAM, S. K., BRIM, K., LEE, H. M., BAUTISTA, J., GILFILLAN, S., AKILESH, S., FUJIKAWA, K. & SWAT, W. 2007. An ITAM-signaling pathway controls cross-presentation of particulate but not soluble antigens in dendritic cells. *The Journal of Experimental Medicine,* 204**,** 2889-2897.

GREEN, R. S., STONE, E. L., TENNO, M., LEHTONEN, E., FARQUHAR, M. G. & MARTH, JAMEY D. 2007. Mammalian N-Glycan Branching Protects against Innate Immune Self-Recognition and Inflammation in Autoimmune Disease Pathogenesis. *Immunity,* 27**,** 308-320.

GRIGORIAN, A., MKHIKIAN, H. & DEMETRIOU, M. 2012a. Interleukin-2, Interleukin-7, T cell-mediated autoimmunity, and N-glycosylation. *Ann N Y Acad Sci,* 1253**,** 49-57.

GRIGORIAN, A., MKHIKIAN, H., LI, C. F., NEWTON, B. L., ZHOU, R. W. & DEMETRIOU, M. 2012b. Pathogenesis of multiple sclerosis via environmental and genetic dysregulation of N-glycosylation. *Semin Immunopathol,* 34**,** 415-24.

GUERRERO, A. R., UCHIDA, K., NAKAJIMA, H., WATANABE, S., NAKAMURA, M., JOHNSON, W. E. & BABA, H. 2012. Blockade of interleukin-6 signaling inhibits the classic pathway and promotes an alternative pathway of macrophage activation after spinal cord injury in mice. *J Neuroinflammation,* 9**,** 40.

HAAN, N., ZHU, B., WANG, J., WEI, X. & SONG, B. 2015. Crosstalk between macrophages and astrocytes affects proliferation, reactive phenotype and inflammatory response, suggesting a role during reactive gliosis following spinal cord injury. *J Neuroinflammation,* 12**,** 109.

HAGGERTY, A. E., MARLOW, M. M. & OUDEGA, M. 2017. Extracellular matrix components as therapeutics for spinal cord injury. *Neurosci Lett,* 652**,** 50-55.

HAKIM, J. S., ESMAEILI RAD, M., GRAHN, P. J., CHEN, B. K., KNIGHT, A. M., SCHMEICHEL, A. M., ISAQ, N. A., DADSETAN, M., YASZEMSKI, M. J. & WINDEBANK, A. J. 2015. Positively Charged Oligo[Poly(Ethylene Glycol) Fumarate] Scaffold Implantation Results in a Permissive Lesion Environment after Spinal Cord Injury in Rat. *Tissue Eng Part A*.

HAM, T. R. & LEIPZIG, N. D. 2018. Biomaterial strategies for limiting the impact of secondary events following spinal cord injury. *Biomed Mater,* 13**,** 024105.

HAMANOUE, M., MATSUZAKI, Y., SATO, K., OKANO, H. J., SHIBATA, S., SATO, I., SUZUKI, S., OGAWARA, M., TAKAMATSU, K. & OKANO, H. 2009. Cell surface N-glycans mediated isolation of mouse neural stem cells. *J Neurochem,* 110**,** 1575-84.

HAN, D., YU, Z., LIU, W., YIN, D., PU, Y., FENG, J., YUAN, Y., HUANG, A., CAO, L. & HE, C. 2018a. Plasma Hemopexin ameliorates murine spinal cord injury by switching microglia from the M1 state to the M2 state. *Cell Death Dis,* 9**,** 181.

HAN, Q., JIN, W., XIAO, Z., NI, H., WANG, J., KONG, J., WU, J., LIANG, W., CHEN, L., ZHAO, Y., CHEN, B. & DAI, J. 2010. The promotion of neural regeneration in an extreme rat spinal cord injury model using a collagen scaffold containing a collagen binding neuroprotective protein and an EGFR neutralizing antibody. *Biomaterials,* 31**,** 9212-20.

HAN, Q., SUN, W., LIN, H., ZHAO, W., GAO, Y., ZHAO, Y., CHEN, B., XIAO, Z., HU, W., LI, Y., YANG, B. & DAI, J. 2009. Linear ordered collagen scaffolds loaded with collagen-binding brain-derived neurotrophic factor improve the recovery of spinal cord injury in rats. *Tissue Eng Part A,* 15**,** 2927-35.

HAN, S., WANG, B., JIN, W., XIAO, Z., CHEN, B., XIAO, H., DING, W., CAO, J., MA, F., LI, X., YUAN, B., ZHU, T., HOU, X., WANG, J., KONG, J., LIANG, W. & DAI, J. 2014. The collagen scaffold with collagen binding BDNF enhances functional recovery by facilitating peripheral nerve infiltrating and ingrowth in canine complete spinal cord transection. *Spinal Cord,* 52**,** 867-73.

HAN, S., WANG, B., JIN, W., XIAO, Z., LI, X., DING, W., KAPUR, M., CHEN, B., YUAN, B., ZHU, T., WANG, H., WANG, J., DONG, Q., LIANG, W. & DAI, J. 2015. The linear-ordered collagen scaffold-BDNF complex significantly promotes functional recovery after completely transected spinal cord injury in canine. *Biomaterials,* 41**,** 89-96.

HAN, S., XIAO, Z., LI, X., ZHAO, H., WANG, B., QIU, Z., LI, Z., MEI, X., XU, B., FAN, C., CHEN, B., HAN, J., GU, Y., YANG, H., SHI, Q. & DAI, J. 2018b. Human placenta-derived mesenchymal stem cells loaded on linear ordered collagen scaffold improves functional recovery after completely transected spinal cord injury in canine. *Sci China Life Sci,* 61**,** 2-13.

HATAMI, M., MEHRJARDI, N. Z., KIANI, S., HEMMESI, K., AZIZI, H., SHAHVERDI, A. & BAHARVAND, H. 2009. Human embryonic stem cell-derived neural precursor transplants in collagen scaffolds promote recovery in injured rat spinal cord. *Cytotherapy,* 11**,** 618-30.

HAYAKAWA, K., OKAZAKI, R., MORIOKA, K., NAKAMURA, K., TANAKA, S. & OGATA, T. 2014. Lipopolysaccharide preconditioning facilitates M2 activation of resident microglia after spinal cord injury. *J Neurosci Res,* 92**,** 1647-58.

HAYES, A. J. & MELROSE, J. 2018. Glycans and glycosaminoglycans in neurobiology: key regulators of neuronal cell function and fate. *Biochemical Journal,* 475**,** 2511-2545.

HERMANNS, S., KLAPKA, N. & MÜLLER, H. W. 2001. The collagenous lesion scar - An obstacle for axonal regeneration in brain and spinal cord injury. *Restorative Neurology and Neuroscience,* 19**,** 139-148.

HOBAN, D. B., NEWLAND, B., MOLONEY, T. C., HOWARD, L., PANDIT, A. & DOWD, E. 2013. The reduction in immunogenicity of neurotrophin overexpressing stem cells after intra-striatal transplantation by encapsulation in an in situ gelling collagen hydrogel. *Biomaterials,* 34**,** 9420-9.

HOUWELING, D. A., LANKHORST, A. J., GISPEN, W. H., BAR, P. R. & JOOSTEN, E. A. 1998a. Collagen containing neurotrophin-3 (NT-3) attracts regrowing injured corticospinal axons in the adult rat spinal cord and promotes partial functional recovery. *Exp Neurol,* 153**,** 49-59.

HOUWELING, D. A., VAN ASSELDONK, J. T., LANKHORST, A. J., HAMERS, F. P., MARTIN, D., BAR, P. R. & JOOSTEN, E. A. 1998b. Local application of collagen containing brain-derived neurotrophic factor decreases the loss of function after spinal cord injury in the adult rat. *Neurosci Lett,* 251**,** 193-6.

HU, J.-G., SHI, L.-L., CHEN, Y.-J., XIE, X.-M., ZHANG, N., ZHU, A.-Y., JIANG, Z.-S., FENG, Y.-F., ZHANG, C., XI, J. & LÜ, H.-Z. 2016. Differential effects of myelin basic protein-activated Th1 and Th2 cells on the local immune microenvironment of injured spinal cord. *Experimental Neurology,* 277**,** 190-201.

HU, J. G., SHEN, L., WANG, R., WANG, Q. Y., ZHANG, C., XI, J., MA, S. F., ZHOU, J. S. & LU, H. Z. 2012. Effects of Olig2-overexpressing neural stem cells and myelin basic protein-activated T cells on recovery from spinal cord injury. *Neurotherapeutics,* 9**,** 422-45.

HU, Y., ZHOU, S., KHALIL, S. I., RENTERIA, C. L. & MECHREF, Y. 2013. Glycomic profiling of tissue sections by LC-MS. *Anal Chem,* 85**,** 4074-9.

HUANG, W., VODOVOTZ, Y., KUSTURISS, M. B., BARCLAY, D., GREENWALD, K., BONINGER, M. L., COEN, P. M., BRIENZA, D. & SOWA, G. 2014. Identification of Distinct Monocyte Phenotypes and Correlation With Circulating Cytokine Profiles in Acute Response to Spinal Cord Injury: A Pilot Study. *PM&R,* 6**,** 332-341.

HUGHES, E. H., SCHLICHTENBREDE, F. C., MURPHY, C. C., SARRA, G. M., LUTHERT, P. J., ALI, R. R. & DICK, A. D. 2003. Generation of activated sialoadhesin-positive microglia during retinal degeneration. *Invest Ophthalmol Vis Sci,* 44**,** 2229-34.

INAMORI, K., ENDO, T., IDE, Y., FUJII, S., GU, J., HONKE, K. & TANIGUCHI, N. 2003. Molecular cloning and characterization of human GnT-IX, a novel beta1,6-N-acetylglucosaminyltransferase that is specifically expressed in the brain. *J Biol Chem,* 278**,** 43102-9.

INAMORI, K., MITA, S., GU, J., MIZUNO-HORIKAWA, Y., MIYOSHI, E., DENNIS, J. W. & TANIGUCHI, N. 2006. Demonstration of the expression and the enzymatic activity of N-acetylglucosaminyltransferase IX in the mouse brain. *Biochim Biophys Acta,* 1760**,** 678-84.

IP, C. W., KRONER, A., CROCKER, P. R., NAVE, K. A. & MARTINI, R. 2007. Sialoadhesin deficiency ameliorates myelin degeneration and axonopathic changes in the CNS of PLP overexpressing mice. *Neurobiol Dis,* 25**,** 105-11.

ISHII, A., IKEDA, T., HITOSHI, S., FUJIMOTO, I., TORII, T., SAKUMA, K., NAKAKITA, S., HASE, S. & IKENAKA, K. 2007. Developmental changes in the expression of glycogenes and the content of N-glycans in the mouse cerebral cortex. *Glycobiology,* 17**,** 261-76.

ISHII, H., JIN, X., UENO, M., TANABE, S., KUBO, T., SERADA, S., NAKA, T. & YAMASHITA, T. 2012. Adoptive transfer of Th1-conditioned lymphocytes promotes axonal remodeling and functional recovery after spinal cord injury. *Cell Death Dis,* 3**,** e363.

JI, X. C., DANG, Y. Y., GAO, H. Y., WANG, Z. T., GAO, M., YANG, Y., ZHANG, H. T. & XU, R. X. 2015. Local Injection of Lenti-BDNF at the Lesion Site Promotes M2 Macrophage Polarization and Inhibits Inflammatory Response After Spinal Cord Injury in Mice. *Cell Mol Neurobiol,* 35**,** 881-90.

JO, M.-J., KUMAR, H., JOSHI, H. P., CHOI, H., KO, W.-K., KIM, J. M., HWANG, S. S. S., PARK, S. Y., SOHN, S., BELLO, A. B., KIM, K.-T., LEE, S.-H., ZENG, X. & HAN, I. 2018. Oral Administration of α-Asarone Promotes Functional Recovery in Rats With Spinal Cord Injury. *Frontiers in Pharmacology,* 9.

JONES, L. L., MARGOLIS, R. U. & TUSZYNSKI, M. H. 2003. The chondroitin sulfate proteoglycans neurocan, brevican, phosphacan, and versican are differentially regulated following spinal cord injury. *Experimental Neurology,* 182**,** 399-411.

KAJITANI, K., NOMARU, H., IFUKU, M., YUTSUDO, N., DAN, Y., MIURA, T., TSUCHIMOTO, D., SAKUMI, K., KADOYA, T., HORIE, H., POIRIER, F., NODA, M. & NAKABEPPU, Y. 2009. Galectin-1 promotes basal and kainate-induced proliferation of neural progenitors in the dentate gyrus of adult mouse hippocampus. *Cell Death Differ,* 16**,** 417-27.

KANEKO, A., MATSUSHITA, A. & SANKAI, Y. 2015. A 3D nanofibrous hydrogel and collagen sponge scaffold promotes locomotor functional recovery, spinal repair, and neuronal regeneration after complete transection of the spinal cord in adult rats. *Biomed Mater,* 10**,** 015008.

KATZENSTEIN, M. B. & BOHN, R. C. 1984. Regeneration of transected dorsal root ganglion cell axons into the spinal cord in adult frogs (Xenopus laevis). *Brain Res,* 300**,** 188-91.

KEHOE, S., ZHANG, X. F. & BOYD, D. 2012. FDA approved guidance conduits and wraps for peripheral nerve injury: a review of materials and efficacy. *Injury,* 43**,** 553-72.

KHATTAK, S., SCHUEZ, M., RICHTER, T., KNAPP, D., HAIGO, S. L., SANDOVAL-GUZMAN, T., HRADLIKOVA, K., DUEMMLER, A., KERNEY, R. & TANAKA, E. M. 2013. Germline transgenic methods for tracking cells and testing gene function during regeneration in the axolotl. *Stem Cell Reports,* 1**,** 90-103.

KHAYRULLINA, G., BERMUDEZ, S. & BYRNES, K. R. 2015. Inhibition of NOX2 reduces locomotor impairment, inflammation, and oxidative stress after spinal cord injury. *J Neuroinflammation,* 12**,** 172.

KHOURY, G. A., BALIBAN, R. C. & FLOUDAS, C. A. 2011. Proteome-wide post-translational modification statistics: frequency analysis and curation of the swiss-prot database. *Scientific Reports,* 1**,** 90.

KIGERL, K. A., GENSEL, J. C., ANKENY, D. P., ALEXANDER, J. K., DONNELLY, D. J. & POPOVICH, P. G. 2009. Identification of two distinct macrophage subsets with divergent effects causing either neurotoxicity or regeneration in the injured mouse spinal cord. *J Neurosci,* 29**,** 13435-44.

KIM, J. H., KIM, J. Y., MUN, C. H., SUH, M. & LEE, J. E. 2017. Agmatine Modulates the Phenotype of Macrophage Acute Phase after Spinal Cord Injury in Rats. *Exp Neurobiol,* 26**,** 278-286.

KIM, M., PARK, S. R. & CHOI, B. H. 2014. Biomaterial scaffolds used for the regeneration of spinal cord injury (SCI). *Histol Histopathol,* 29**,** 1395-408.

KJELL, J. & OLSON, L. 2016. Rat models of spinal cord injury: from pathology to potential therapies. *Dis Model Mech,* 9**,** 1125-1137.

KLEENE, R. & SCHACHNER, M. 2004. Glycans and neural cell interactions. *Nature Reviews Neuroscience,* 5**,** 195-208.

KOBSAR, I., OETKE, C., KRONER, A., WESSIG, C., CROCKER, P. & MARTINI, R. 2006. Attenuated demyelination in the absence of the macrophage-restricted adhesion molecule sialoadhesin (Siglec-1) in mice heterozygously deficient in P0. *Mol Cell Neurosci,* 31**,** 685-91.

KRONER, A., GREENHALGH, A. D., ZARRUK, J. G., PASSOS DOS SANTOS, R., GAESTEL, M. & DAVID, S. 2014. TNF and increased intracellular iron alter macrophage polarization to a detrimental M1 phenotype in the injured spinal cord. *Neuron,* 83**,** 1098-116.

KURIHARA, D., UENO, M., TANAKA, T. & YAMASHITA, T. 2010. Expression of galectin-1 in immune cells and glial cells after spinal cord injury. *Neurosci Res,* 66**,** 265-70.

KWON, B. K., TETZLAFF, W., GRAUER, J. N., BEINER, J. & VACCARO, A. R. 2004. Pathophysiology and pharmacologic treatment of acute spinal cord injury. *The Spine Journal,* 4**,** 451-464.

LALANCETTE-HEBERT, M., GOWING, G., SIMARD, A., WENG, Y. C. & KRIZ, J. 2007. Selective ablation of proliferating microglial cells exacerbates ischemic injury in the brain. *J Neurosci,* 27**,** 2596-605.

LALANCETTE-HEBERT, M., SWARUP, V., BEAULIEU, J. M., BOHACEK, I., ABDELHAMID, E., WENG, Y. C., SATO, S. & KRIZ, J. 2012. Galectin-3 is required for resident microglia activation and proliferation in response to ischemic injury. *J Neurosci,* 32**,** 10383-95.

LEDEEN, R. W., WU, G., AUTHOR_IN_JAPANESE & AUTHOR_IN_JAPANESE 1992. Ganglioside Function in the Neuron. *Trends in Glycoscience and Glycotechnology,* 4**,** 174-187.

LEE-LIU, D., MORENO, M., ALMONACID, L. I., TAPIA, V. S., MUNOZ, R., VON MAREES, J., GAETE, M., MELO, F. & LARRAIN, J. 2014. Genome-wide expression profile of the response to spinal cord injury in Xenopus laevis reveals extensive differences between regenerative and non-regenerative stages. *Neural Dev,* 9**,** 12.

LEE-LIU, D., SUN, L., DOVICHI, N. J. & LARRAIN, J. 2018. Quantitative Proteomics After Spinal Cord Injury (SCI) in a Regenerative and a Nonregenerative Stage in the Frog Xenopus laevis. *Mol Cell Proteomics,* 17**,** 592-606.

LEE, S. J. & BENVENISTE, E. N. 1999. Adhesion molecule expression and regulation on cells of the central nervous system. *J Neuroimmunol,* 98**,** 77-88.

LI, J., LIU, Y., XU, H. & FU, Q. 2016a. Nanoparticle-Delivered IRF5 siRNA Facilitates M1 to M2 Transition, Reduces Demyelination and Neurofilament Loss, and Promotes Functional Recovery After Spinal Cord Injury in Mice. *Inflammation,* 39**,** 1704-17.

LI, X., FAN, C., XIAO, Z., ZHAO, Y., ZHANG, H., SUN, J., ZHUANG, Y., WU, X., SHI, J., CHEN, Y. & DAI, J. 2018. A collagen microchannel scaffold carrying paclitaxel-liposomes induces neuronal differentiation of neural stem cells through Wnt/beta-catenin signaling for spinal cord injury repair. *Biomaterials,* 183**,** 114-127.

LI, X., HAN, J., ZHAO, Y., DING, W., WEI, J., HAN, S., SHANG, X., WANG, B., CHEN, B., XIAO, Z. & DAI, J. 2015. Functionalized Collagen Scaffold Neutralizing the Myelin-Inhibitory Molecules Promoted Neurites Outgrowth in Vitro and Facilitated Spinal Cord Regeneration in Vivo. *ACS Appl Mater Interfaces,* 7**,** 13960-71.

LI, X., HAN, J., ZHAO, Y., DING, W., WEI, J., LI, J., HAN, S., SHANG, X., WANG, B., CHEN, B., XIAO, Z. & DAI, J. 2016b. Functionalized collagen scaffold implantation and cAMP administration collectively facilitate spinal cord regeneration. *Acta Biomater,* 30**,** 233-245.

LI, X., TAN, J., XIAO, Z., ZHAO, Y., HAN, S., LIU, D., YIN, W., LI, J., LI, J., WANGGOU, S., CHEN, B., REN, C., JIANG, X. & DAI, J. 2017a. Transplantation of hUC-MSCs seeded collagen scaffolds reduces scar formation and promotes functional recovery in canines with chronic spinal cord injury. *Sci Rep,* 7**,** 43559.

LI, X., XIAO, Z., HAN, J., CHEN, L., XIAO, H., MA, F., HOU, X., LI, X., SUN, J., DING, W., ZHAO, Y., CHEN, B. & DAI, J. 2013. Promotion of neuronal differentiation of neural progenitor cells by using EGFR antibody functionalized collagen scaffolds for spinal cord injury repair. *Biomaterials,* 34**,** 5107-16.

LI, X., ZHAO, Y., CHENG, S., HAN, S., SHU, M., CHEN, B., CHEN, X., TANG, F., WANG, N., TU, Y., WANG, B., XIAO, Z., ZHANG, S. & DAI, J. 2017b. Cetuximab modified collagen scaffold directs neurogenesis of injury-activated endogenous neural stem cells for acute spinal cord injury repair. *Biomaterials,* 137**,** 73-86.

LIN, G., CHEN, Y. & SLACK, J. M. 2012. Transgenic analysis of signaling pathways required for Xenopus tadpole spinal cord and muscle regeneration. *Anat Rec (Hoboken),* 295**,** 1532-40.

LINNARTZ-GERLACH, B., KOPATZ, J. & NEUMANN, H. 2014. Siglec functions of microglia. *Glycobiology,* 24**,** 794-9.

LIU, S., SAID, G. & TADIE, M. 2001. Regrowth of the rostral spinal axons into the caudal ventral roots through a collagen tube implanted into hemisected adult rat spinal cord. *Neurosurgery,* 49**,** 143-50; discussion 150-1.

LIU, T., HOULE, J. D., XU, J., CHAN, B. P. & CHEW, S. Y. 2012. Nanofibrous collagen nerve conduits for spinal cord repair. *Tissue Eng Part A,* 18**,** 1057-66.

LIU, Y. C., ZOU, X. B., CHAI, Y. F. & YAO, Y. M. 2014. Macrophage polarization in inflammatory diseases. *Int J Biol Sci,* 10**,** 520-9.

LOVE, N. R., CHEN, Y., BONEV, B., GILCHRIST, M. J., FAIRCLOUGH, L., LEA, R., MOHUN, T. J., PAREDES, R., ZEEF, L. A. & AMAYA, E. 2011. Genome-wide analysis of gene expression during Xenopus tropicalis tadpole tail regeneration. *BMC Dev Biol,* 11**,** 70.

MA, S.-F., CHEN, Y.-J., ZHANG, J.-X., SHEN, L., WANG, R., ZHOU, J.-S., HU, J.-G. & LÜ, H.-Z. 2015. Adoptive transfer of M2 macrophages promotes locomotor recovery in adult rats after spinal cord injury. *Brain, Behavior, and Immunity,* 45**,** 157-170.

MADIGAN, N. N., MCMAHON, S., O'BRIEN, T., YASZEMSKI, M. J. & WINDEBANK, A. J. 2009. Current tissue engineering and novel therapeutic approaches to axonal regeneration following spinal cord injury using polymer scaffolds. *Respir Physiol Neurobiol,* 169**,** 183-99.

MAIER, C. E. & MILLER, R. H. 1995. Development of glial cytoarchitecture in the frog spinal cord. *Dev Neurosci,* 17**,** 149-59.

MARCHAND, R. & WOERLY, S. 1990. Transected spinal cords grafted with in situ self-assembled collagen matrices. *Neuroscience,* 36**,** 45-60.

MARCHAND, R., WOERLY, S., BERTRAND, L. & VALDES, N. 1993. Evaluation of two cross-linked collagen gels implanted in the transected spinal cord. *Brain Res Bull,* 30**,** 415-22.

MARTH, J. D. & GREWAL, P. K. 2008. Mammalian glycosylation in immunity. *Nat Rev Immunol,* 8**,** 874-87.

MATSUBARA, K., MATSUSHITA, Y., SAKAI, K., KANO, F., KONDO, M., NODA, M., HASHIMOTO, N., IMAGAMA, S., ISHIGURO, N., SUZUMURA, A., UEDA, M., FURUKAWA, K. & YAMAMOTO, A. 2015. Secreted ectodomain of sialic acid-binding Ig-like lectin-9 and monocyte chemoattractant protein-1 promote recovery after rat spinal cord injury by altering macrophage polarity. *J Neurosci,* 35**,** 2452-64.

MATUS, A., DE PETRIS, S. & RAFF, M. C. 1973. Mobility of concanavalin A receptors in myelin and synaptic membranes. *Nat New Biol,* 244**,** 278-80.

MCDONALD, J. W. & SADOWSKY, C. 2002. Spinal-cord injury. *The Lancet,* 359**,** 417-425.

MCGRAW, J., GAUDET, A. D., OSCHIPOK, L. W., KADOYA, T., HORIE, H., STEEVES, J. D., TETZLAFF, W. & RAMER, M. S. 2005. Regulation of neuronal and glial galectin-1 expression by peripheral and central axotomy of rat primary afferent neurons. *Exp Neurol,* 195**,** 103-14.

MEDINA-CANO, D., UCUNCU, E., NGUYEN, L. S., NICOULEAU, M., LIPECKA, J., BIZOT, J. C., THIEL, C., FOULQUIER, F., LEFORT, N., FAIVRE-SARRAILH, C., COLLEAUX, L., GUERRERA, I. C. & CANTAGREL, V. 2018. High N-glycan multiplicity is critical for neuronal adhesion and sensitizes the developing cerebellum to N-glycosylation defect. *Elife,* 7.

MENDEZ-OLIVOS, E. E., MUNOZ, R. & LARRAIN, J. 2017. Spinal Cord Cells from Pre-metamorphic Stages Differentiate into Neurons and Promote Axon Growth and Regeneration after Transplantation into the Injured Spinal Cord of Non-regenerative Xenopus laevis Froglets. *Front Cell Neurosci,* 11**,** 398.

MICHEL, M. E. & REIER, P. J. 1979. Axonal-ependymal associations during early regeneration of the transected spinal cord inXenopus laevis tadpoles. *Journal of Neurocytology,* 8**,** 529-548.

MILLER, G. M. & HSIEH-WILSON, L. C. 2015. Sugar-dependent modulation of neuronal development, regeneration, and plasticity by chondroitin sulfate proteoglycans. *Experimental Neurology,* 274**,** 115-125.

MIURA, R., ASPBERG, A., ETHELL, I. M., HAGIHARA, K., SCHNAAR, R. L., RUOSLAHTI, E. & YAMAGUCHI, Y. 1999. The proteoglycan lectin domain binds sulfated cell surface glycolipids and promotes cell adhesion. *J Biol Chem,* 274**,** 11431-8.

MIURA, R., ETHELL, I. M. & YAMAGUCHI, Y. 2001. Carbohydrate-protein interactions between HNK-1-reactive sulfoglucuronyl glycolipids and the proteoglycan lectin domain mediate neuronal cell adhesion and neurite outgrowth. *J Neurochem,* 76**,** 413-24.

MOHORKO, E., GLOCKSHUBER, R. & AEBI, M. 2011. Oligosaccharyltransferase: the central enzyme of N-linked protein glycosylation. *J Inherit Metab Dis,* 34**,** 869-78.

MONAGHAN, J. R., WALKER, J. A., PAGE, R. B., PUTTA, S., BEACHY, C. K. & VOSS, S. R. 2007. Early gene expression during natural spinal cord regeneration in the salamander Ambystoma mexicanum. *J Neurochem,* 101**,** 27-40.

MONDIA, J. P., LEVIN, M., OMENETTO, F. G., ORENDORFF, R. D., BRANCH, M. R. & ADAMS, D. S. 2011. Long-distance signals are required for morphogenesis of the regenerating Xenopus tadpole tail, as shown by femtosecond-laser ablation. *PLoS One,* 6**,** e24953.

MORGENSTERN, D. A., ASHER, R. A. & FAWCETT, J. W. 2002. Chondroitin sulphate proteoglycans in the CNS injury response. *Prog Brain Res,* 137**,** 313-32.

MORIARTY, N., PANDIT, A. & DOWD, E. 2017. Encapsulation of primary dopaminergic neurons in a GDNF-loaded collagen hydrogel increases their survival, re-innervation and function after intra-striatal transplantation. *Sci Rep,* 7**,** 16033.

MUNOZ, R., EDWARDS-FARET, G., MORENO, M., ZUNIGA, N., CLINE, H. & LARRAIN, J. 2015. Regeneration of Xenopus laevis spinal cord requires Sox2/3 expressing cells. *Dev Biol,* 408**,** 229-43.

MUNRO, K. M., PERREAU, V. M. & TURNLEY, A. M. 2012. Differential gene expression in the EphA4 knockout spinal cord and analysis of the inflammatory response following spinal cord injury. *PLoS One,* 7**,** e37635.

MURREY, H. E., GAMA, C. I., KALOVIDOURIS, S. A., LUO, W.-I., DRIGGERS, E. M., PORTON, B. & HSIEH-WILSON, L. C. 2006. Protein fucosylation regulates synapsin Ia/Ib expression and neuronal morphology in primary hippocampal neurons. *Proceedings of the National Academy of Sciences of the United States of America,* 103**,** 21-26.

NAKAGAWA, K., KITAZUME, S., OKA, R., MARUYAMA, K., SAIDO, T. C., SATO, Y., ENDO, T. & HASHIMOTO, Y. 2006. Sialylation enhances the secretion of neurotoxic amyloid-beta peptides. *J Neurochem,* 96**,** 924-33.

NAKAJIMA, H., UCHIDA, K., GUERRERO, A. R., WATANABE, S., SUGITA, D., TAKEURA, N., YOSHIDA, A., LONG, G., WRIGHT, K. T., JOHNSON, W. E. & BABA, H. 2012. Transplantation of mesenchymal stem cells promotes an alternative pathway of macrophage activation and functional recovery after spinal cord injury. *J Neurotrauma,* 29**,** 1614-25.

NIEUWKOOP, P., LABORATORY, H. & FABER, J. 1956. *Normal Table of Xenopus Laevis-Daudin. A Systematical and Chronological Survey of the Development from the Fertilized Egg Till the End of Metamorphosis. Edited by PD Nieuwkoop and J. Faber. Issued by the Hubrecht Laboratory, Utrecht.[With a Bibliography.]*, North-Holland Publishing Company.

NORENBERG, M. D., SMITH, J. & MARCILLO, A. 2004. The pathology of human spinal cord injury: defining the problems. *J Neurotrauma,* 21**,** 429-40.

NORTON W.T., C. W. 1984. Isolation and Characterization of Myelin. *In:* P, M. (ed.) *Myelin.* Springer, Boston, MA.

O'SHEA, T. M., BURDA, J. E. & SOFRONIEW, M. V. 2017. Cell biology of spinal cord injury and repair. *J Clin Invest,* 127**,** 3259-3270.

OHL, C., ALBACH, C., ALTEVOGT, P. & SCHMITZ, B. 2003. N-glycosylation patterns of HSA/CD24 from different cell lines and brain homogenates: a comparison. *Biochimie,* 85**,** 565-73.

OKA, S., TERAYAMA, K., IMIYA, K., YAMAMOTO, S., KONDO, A., KATO, I. & KAWASAKI, T. 2000. The N-glycan acceptor specificity of a glucuronyltransferase, GlcAT-P, associated with biosynthesis of the HNK-1 epitope. *Glycoconj J,* 17**,** 877-85.

ONUMA-UKEGAWA, M., BHATT, K., HIRAI, T., KABURAGI, H., SOTOME, S., WAKABAYASHI, Y., ICHINOSE, S., SHINOMIYA, K., OKAWA, A. & ENOMOTO, M. 2015. Bone Marrow Stromal Cells Combined With a Honeycomb Collagen Sponge Facilitate Neurite Elongation In Vitro and Neural Restoration in the Hemisected Rat Spinal Cord. *Cell Transplant,* 24**,** 1283-97.

ORR, M. B. & GENSEL, J. C. 2018. Spinal Cord Injury Scarring and Inflammation: Therapies Targeting Glial and Inflammatory Responses. *Neurotherapeutics,* 15**,** 541-553.

ORR, M. B., SIMKIN, J., BAILEY, W. M., KADAMBI, N. S., MCVICAR, A. L., VELDHORST, A. K. & GENSEL, J. C. 2017. Compression Decreases Anatomical and Functional Recovery and Alters Inflammation after Contusive Spinal Cord Injury. *J Neurotrauma,* 34**,** 2342-2352.

PAJOOHESH-GANJI, A., KNOBLACH, S. M., FADEN, A. I. & BYRNES, K. R. 2012. Characterization of inflammatory gene expression and galectin-3 function after spinal cord injury in mice. *Brain Res,* 1475**,** 96-105.

PALMIGIANO, A., BARONE, R., STURIALE, L., SANFILIPPO, C., BUA, R. O., ROMEO, D. A., MESSINA, A., CAPUANA, M. L., MACI, T., LE PIRA, F., ZAPPIA, M. & GAROZZO, D. 2016. CSF N-glycoproteomics for early diagnosis in Alzheimer's disease. *Journal of Proteomics,* 131**,** 29-37.

PAPA, S., CARON, I., ERBA, E., PANINI, N., DE PAOLA, M., MARIANI, A., COLOMBO, C., FERRARI, R., POZZER, D., ZANIER, E. R., PISCHIUTTA, F., LUCCHETTI, J., BASSI, A., VALENTINI, G., SIMONUTTI, G., ROSSI, F., MOSCATELLI, D., FORLONI, G. & VEGLIANESE, P. 2016. Early modulation of pro-inflammatory microglia by minocycline loaded nanoparticles confers long lasting protection after spinal cord injury. *Biomaterials,* 75**,** 13-24.

PERRY, V. H., CROCKER, P. R. & GORDON, S. 1992. The blood-brain barrier regulates the expression of a macrophage sialic acid-binding receptor on microglia. *J Cell Sci,* 101 (Pt 1)**,** 201-7.

PETTER-PUCHNER, A. H., FROETSCHER, W., KRAMETTER-FROETSCHER, R., LORINSON, D., REDL, H. & VAN GRIENSVEN, M. 2007. The long-term neurocompatibility of human fibrin sealant and equine collagen as biomatrices in experimental spinal cord injury. *Exp Toxicol Pathol,* 58**,** 237-45.

PIRES, L. R. & PEGO, A. P. 2015. Bridging the lesion-engineering a permissive substrate for nerve regeneration. *Regen Biomater,* 2**,** 203-14.

POPOVICH, P. G., WEI, P. & STOKES, B. T. 1997. Cellular inflammatory response after spinal cord injury in Sprague-Dawley and Lewis rats. *J Comp Neurol,* 377**,** 443-64.

POWERS, T. W., JONES, E. E., BETESH, L. R., ROMANO, P. R., GAO, P., COPLAND, J. A., MEHTA, A. S. & DRAKE, R. R. 2013. Matrix assisted laser desorption ionization imaging mass spectrometry workflow for spatial profiling analysis of N-linked glycan expression in tissues. *Anal Chem,* 85**,** 9799-806.

PRÜSS, H., KOPP, M. A., BROMMER, B., GATZEMEIER, N., LAGINHA, I., DIRNAGL, U. & SCHWAB, J. M. 2011. Non-Resolving Aspects of Acute Inflammation after Spinal Cord Injury (SCI): Indices and Resolution Plateau. *Brain Pathology,* 21**,** 652-660.

QU, W. S., WANG, Y. H., MA, J. F., TIAN, D. S., ZHANG, Q., PAN, D. J., YU, Z. Y., XIE, M. J., WANG, J. P. & WANG, W. 2011. Galectin-1 attenuates astrogliosis-associated injuries and improves recovery of rats following focal cerebral ischemia. *J Neurochem,* 116**,** 217-26.

QU, W. S., WANG, Y. H., WANG, J. P., TANG, Y. X., ZHANG, Q., TIAN, D. S., YU, Z. Y., XIE, M. J. & WANG, W. 2010. Galectin-1 enhances astrocytic BDNF production and improves functional outcome in rats following ischemia. *Neurochem Res,* 35**,** 1716-24.

RABINOVICH, G. A. & CROCI, D. O. 2012. Regulatory circuits mediated by lectin-glycan interactions in autoimmunity and cancer. *Immunity,* 36**,** 322-35.

RABINOVICH, G. A. & TOSCANO, M. A. 2009. Turning 'sweet' on immunity: galectin-glycan interactions in immune tolerance and inflammation. *Nat Rev Immunol,* 9**,** 338-52.

RAPOPORT, E. M., SAPOT'KO, Y. B., PAZYNINA, G. V., BOJENKO, V. K. & BOVIN, N. V. 2005. Sialoside-binding macrophage lectins in phagocytosis of apoptotic bodies. *Biochemistry (Mosc),* 70**,** 330-8.

RAZI, N. & VARKI, A. 1998. Masking and unmasking of the sialic acid-binding lectin activity of CD22 (Siglec-2) on B lymphocytes. *Proc Natl Acad Sci U S A,* 95**,** 7469-74.

REIER, P. J. 1979. Penetration of grafted astrocytic scars by regenerating optic nerve axons in Xenopus tadpoles. *Brain Res,* 164**,** 61-8.

REIER, P. J. & WEBSTER, H. F. 1974. Regeneration and remyelination of Xenopus tadpole optic nerve fibres following transection or crush. *J Neurocytol,* 3**,** 591-618.

RIEMANN, L., YOUNSI, A., SCHERER, M., ZHENG, G., SKUTELLA, T., UNTERBERG, A. W. & ZWECKBERGER, K. 2018. Transplantation of Neural Precursor Cells Attenuates Chronic Immune Environment in Cervical Spinal Cord Injury. *Frontiers in Neurology,* 9.

ROLLS, A., SHECHTER, R., LONDON, A., SEGEV, Y., JACOB-HIRSCH, J., AMARIGLIO, N., RECHAVI, G. & SCHWARTZ, M. 2008. Two faces of chondroitin sulfate proteoglycan in spinal cord repair: a role in microglia/macrophage activation. *PLoS Med,* 5**,** e171.

ROYLE, L., CAMPBELL, M. P., RADCLIFFE, C. M., WHITE, D. M., HARVEY, D. J., ABRAHAMS, J. L., KIM, Y. G., HENRY, G. W., SHADICK, N. A., WEINBLATT, M. E., LEE, D. M., RUDD, P. M. & DWEK, R. A. 2008. HPLC-based analysis of serum N-glycans on a 96-well plate platform with dedicated database software. *Anal Biochem,* 376**,** 1-12.

RUNGGER-BRANDLE, E., ALLIOD, C., FOUQUET, B. & MESSERLI, M. M. 1995. Behaviour of macroglial cells, as identified by their intermediate filament complement, during optic nerve regeneration of Xenopus tadpole. *Glia,* 13**,** 255-71.

RUOSLAHTI, E. 1996. Brain extracellular matrix. *Glycobiology,* 6**,** 489-92.

RUSSO, L., SGAMBATO, A., LECCHI, M., PASTORI, V., RASPANTI, M., NATALELLO, A., DOGLIA, S. M., NICOTRA, F. & CIPOLLA, L. 2014. Neoglucosylated collagen matrices drive neuronal cells to differentiate. *ACS Chem Neurosci,* 5**,** 261-5.

SALDOVA, R., ASADI SHEHNI, A., HAAKENSEN, V. D., STEINFELD, I., HILLIARD, M., KIFER, I., HELLAND, A., YAKHINI, Z., BORRESEN-DALE, A. L. & RUDD, P. M. 2014. Association of N-glycosylation with breast carcinoma and systemic features using high-resolution quantitative UPLC. *J Proteome Res,* 13**,** 2314-27.

SALDOVA, R., PICCARD, H., PEREZ-GARAY, M., HARVEY, D. J., STRUWE, W. B., GALLIGAN, M. C., BERGHMANS, N., MADDEN, S. F., PERACAULA, R., OPDENAKKER, G. & RUDD, P. M. 2013. Increase in sialylation and branching in the mouse serum N-glycome correlates with inflammation and ovarian tumour progression. *PLoS One,* 8**,** e71159.

SANDHOFF, K. & KOLTER, T. 2003. Biosynthesis and degradation of mammalian glycosphingolipids. *Philosophical Transactions of the Royal Society of London. Series B: Biological Sciences,* 358**,** 847-861.

SASAKI, T. & ENDO, T. 2000. Both cell-surface carbohydrates and protein tyrosine phosphatase are involved in the differentiation of astrocytes in vitro. *Glia,* 32**,** 60-70.

SASAKI, T., HIRABAYASHI, J., MANYA, H., KASAI, K. & ENDO, T. 2004. Galectin-1 induces astrocyte differentiation, which leads to production of brain-derived neurotrophic factor. *Glycobiology,* 14**,** 357-63.

SATO, A., OHTAKI, H., TSUMURAYA, T., SONG, D., OHARA, K., ASANO, M., IWAKURA, Y., ATSUMI, T. & SHIODA, S. 2012. Interleukin-1 participates in the classical and alternative activation of microglia/macrophages after spinal cord injury. *Journal of Neuroinflammation,* 9**,** 65.

SATO, Y., NAITO, Y., GRUNDKE-IQBAL, I., IQBAL, K. & ENDO, T. 2001. Analysis of N-glycans of pathological tau: possible occurrence of aberrant processing of tau in Alzheimer's disease. *FEBS Lett,* 496**,** 152-60.

SCHNAAR RL, K. T. 2017. Glycosphingolipids. *In:* VARKI A, C. R., ESKO JD, ET AL. (ed.) *Essentials of Glycobiology [Internet].* Cold Spring Harbor (NY): Cold Spring Harbor Laboratory Press.

SCHNAPP, E., KRAGL, M., RUBIN, L. & TANAKA, E. M. 2005. Hedgehog signaling controls dorsoventral patterning, blastema cell proliferation and cartilage induction during axolotl tail regeneration. *Development,* 132**,** 3243-53.

SHARIF-ALHOSEINI, M., KHORMALI, M., REZAEI, M., SAFDARIAN, M., HAJIGHADERY, A., KHALATBARI, M. M., SAFDARIAN, M., MEKNATKHAH, S., REZVAN, M., CHALANGARI, M., DERAKHSHAN, P. & RAHIMI-MOVAGHAR, V. 2017. Animal models of spinal cord injury: a systematic review. *Spinal Cord,* 55**,** 714.

SHI, Q., GAO, W., HAN, X., ZHU, X., SUN, J., XIE, F., HOU, X., YANG, H., DAI, J. & CHEN, L. 2014. Collagen scaffolds modified with collagen-binding bFGF promotes the neural regeneration in a rat hemisected spinal cord injury model. *Science China Life Sciences,* 57**,** 232-240.

SHRESTHA, B., COYKENDALL, K., LI, Y., MOON, A., PRIYADARSHANI, P. & YAO, L. 2014. Repair of injured spinal cord using biomaterial scaffolds and stem cells. *Stem Cell Res Ther,* 5**,** 91.

SIEBERT, J. R., EADE, A. M. & OSTERHOUT, D. J. 2015. Biomaterial Approaches to Enhancing Neurorestoration after Spinal Cord Injury: Strategies for Overcoming Inherent Biological Obstacles. *Biomed Res Int,* 2015**,** 752572.

SIMS, R. T. 1962. Transection of the spinal cord in developing Xenopus laevis. *J Embryol Exp Morphol,* 10**,** 115-26.

SNIDER, S., CAVALLI, A., COLOMBO, F., GALLOTTI, A. L., QUATTRINI, A., SALVATORE, L., MADAGHIELE, M., TERRENI, M. R., SANNINO, A. & MORTINI, P. 2017. A novel composite type I collagen scaffold with micropatterned porosity regulates the entrance of phagocytes in a severe model of spinal cord injury. *J Biomed Mater Res B Appl Biomater,* 105**,** 1040-1053.

SOFRONIEW, M. V. & VINTERS, H. V. 2010. Astrocytes: biology and pathology. *Acta Neuropathol,* 119**,** 7-35.

SONG, J. W., LI, K., LIANG, Z. W., DAI, C., SHEN, X. F., GONG, Y. Z., WANG, S., HU, X. Y. & WANG, Z. 2017. Low-level laser facilitates alternatively activated macrophage/microglia polarization and promotes functional recovery after crush spinal cord injury in rats. *Sci Rep,* 7**,** 620.

SPERANDIO, M., GLEISSNER, C. A. & LEY, K. 2009. Glycosylation in immune cell trafficking. *Immunological Reviews,* 230**,** 97-113.

STANLEY P, T. N., AEBI M 2017. N-Glycans. *Essentials of Glycobiology [Internet].* Cold Spring Harbor (NY): Cold Spring Harbor Laboratory Press.

STANTA, J. L., SALDOVA, R., STRUWE, W. B., BYRNE, J. C., LEWEKE, F. M., ROTHERMUND, M., RAHMOUNE, H., LEVIN, Y., GUEST, P. C., BAHN, S. & RUDD, P. M. 2010. Identification of N-glycosylation changes in the CSF and serum in patients with schizophrenia. *J Proteome Res,* 9**,** 4476-89.

STAROSSOM, S. C., MASCANFRONI, I. D., IMITOLA, J., CAO, L., RADDASSI, K., HERNANDEZ, S. F., BASSIL, R., CROCI, D. O., CERLIANI, J. P., DELACOUR, D., WANG, Y., ELYAMAN, W., KHOURY, S. J. & RABINOVICH, G. A. 2012. Galectin-1 deactivates classically activated microglia and protects from inflammation-induced neurodegeneration. *Immunity,* 37**,** 249-63.

STICHEL, C. C., HERMANNS, S., LUHMANN, H. J., LAUSBERG, F., NIERMANN, H., D'URSO, D., SERVOS, G., HARTWIG, H.-G. & MÜLLER, H. W. 1999. Inhibition of collagen IV deposition promotes regeneration of injured CNS axons. *European Journal of Neuroscience,* 11**,** 632-646.

STREKALOVA, T., WOTJAK, C. T. & SCHACHNER, M. 2001. Intrahippocampal administration of an antibody against the HNK-1 carbohydrate impairs memory consolidation in an inhibitory learning task in mice. *Mol Cell Neurosci,* 17**,** 1102-13.

SUN, G., LI, G., LI, D., HUANG, W., ZHANG, R., ZHANG, H., DUAN, Y. & WANG, B. 2018. hucMSC derived exosomes promote functional recovery in spinal cord injury mice via attenuating inflammation. *Materials Science and Engineering: C,* 89**,** 194-204.

TALAC, R., FRIEDMAN, J. A., MOORE, M. J., LU, L., JABBARI, E., WINDEBANK, A. J., CURRIER, B. L. & YASZEMSKI, M. J. 2004. Animal models of spinal cord injury for evaluation of tissue engineering treatment strategies. *Biomaterials,* 25**,** 1505-1510.

TAM, R. Y., FUEHRMANN, T., MITROUSIS, N. & SHOICHET, M. S. 2014. Regenerative therapies for central nervous system diseases: a biomaterials approach. *Neuropsychopharmacology,* 39**,** 169-88.

TANIGUCHI, N. & KIZUKA, Y. 2015. Glycans and cancer: role of N-glycans in cancer biomarker, progression and metastasis, and therapeutics. *Adv Cancer Res,* 126**,** 11-51.

TANIGUCHI, Y., SUGIURA, T., TAZAKI, A., WATANABE, K. & MOCHII, M. 2008. Spinal cord is required for proper regeneration of the tail in Xenopus tadpoles. *Dev Growth Differ,* 50**,** 109-20.

TANIGUCHI, Y., WATANABE, K. & MOCHII, M. 2014. Notochord-derived hedgehog is essential for tail regeneration in Xenopus tadpole. *BMC Dev Biol,* 14**,** 27.

TAZAKI, A., KITAYAMA, A., TERASAKA, C., WATANABE, K., UENO, N. & MOCHII, M. 2005. Macroarray-based analysis of tail regeneration in Xenopus laevis larvae. *Developmental Dynamics,* 233**,** 1394-1404.

VAN KOOYK, Y. & RABINOVICH, G. A. 2008. Protein-glycan interactions in the control of innate and adaptive immune responses. *Nat Immunol,* 9**,** 593-601.

VANONI, O., PAGANETTI, P. & MOLINARI, M. 2008. Consequences of individual N-glycan deletions and of proteasomal inhibition on secretion of active BACE. *Mol Biol Cell,* 19**,** 4086-98.

VARKI, A., FREEZE, H. H. & GAGNEUX, P. 2009. Evolution of Glycan Diversity. *In:* ND, VARKI, A., CUMMINGS, R. D., ESKO, J. D., FREEZE, H. H., STANLEY, P., BERTOZZI, C. R., HART, G. W. & ETZLER, M. E. (eds.) *Essentials of Glycobiology.* Cold Spring Harbor (NY): Cold Spring Harbor Laboratory Press

The Consortium of Glycobiology Editors, La Jolla, California.

VARKI A, L. J. 2009a. Biological Roles of Glycans. *In:* VARKI A, C. R., ESKO JD, ET AL. (ed.) *Essentials of Glycobiology. 2nd edition.*: Cold Spring Harbor (NY): Cold Spring Harbor Laboratory Press.

VARKI A, S. N. 2009b. Historical Background and Overview. *In:* VARKI A, C. R., ESKO JD, ET AL., (ed.) *Essentials of Glycobiology.* Cold Spring Harbor (NY): Cold Spring Harbor Laboratory Press.

VENKATESAN, C., CHRZASZCZ, M., CHOI, N. & WAINWRIGHT, M. S. 2010. Chronic upregulation of activated microglia immunoreactive for galectin-3/Mac-2 and nerve growth factor following diffuse axonal injury. *J Neuroinflammation,* 7**,** 32.

WANG, J. Z., GRUNDKE-IQBAL, I. & IQBAL, K. 1996. Glycosylation of microtubule-associated protein tau: an abnormal posttranslational modification in Alzheimer's disease. *Nat Med,* 2**,** 871-5.

WANG, T., FANG, X. & YIN, Z. S. 2018. Endothelial progenitor cell-conditioned medium promotes angiogenesis and is neuroprotective after spinal cord injury. *Neural Regen Res,* 13**,** 887-895.

WANG, X., MITRA, N., CRUZ, P., DENG, L., PROGRAM, N. C. S., VARKI, N., ANGATA, T., GREEN, E. D., MULLIKIN, J., HAYAKAWA, T. & VARKI, A. 2012. Evolution of siglec-11 and siglec-16 genes in hominins. *Mol Biol Evol,* 29**,** 2073-86.

WANG, Y. & NEUMANN, H. 2010. Alleviation of neurotoxicity by microglial human Siglec-11. *J Neurosci,* 30**,** 3482-8.

WANG, Z., NONG, J., SHULTZ, R. B., ZHANG, Z., KIM, T., TOM, V. J., PONNAPPAN, R. K. & ZHONG, Y. 2017. Local delivery of minocycline from metal ion-assisted self-assembled complexes promotes neuroprotection and functional recovery after spinal cord injury. *Biomaterials,* 112**,** 62-71.

WEIDNER, N., GRILL, R. J. & TUSZYNSKI, M. H. 1999. Elimination of basal lamina and the collagen "scar" after spinal cord injury fails to augment corticospinal tract regeneration. *Exp Neurol,* 160**,** 40-50.

WU, A. M., LISOWSKA, E., DUK, M. & YANG, Z. 2008. Lectins as tools in glycoconjugate research. *Glycoconjugate Journal,* 26**,** 899.

XIAO, Z., TANG, F., TANG, J., YANG, H., ZHAO, Y., CHEN, B., HAN, S., WANG, N., LI, X., CHENG, S., HAN, G., ZHAO, C., YANG, X., CHEN, Y., SHI, Q., HOU, S., ZHANG, S. & DAI, J. 2016. One-year clinical study of NeuroRegen scaffold implantation following scar resection in complete chronic spinal cord injury patients. *Science China Life Sciences,* 59**,** 647-655.

XIAO, Z., TANG, F., ZHAO, Y., HAN, G., YIN, N., LI, X., CHEN, B., HAN, S., JIANG, X., YUN, C., ZHAO, C., CHENG, S., ZHANG, S. & DAI, J. 2018. Significant Improvement of Acute Complete Spinal Cord Injury Patients Diagnosed by a Combined Criteria Implanted with NeuroRegen Scaffolds and Mesenchymal Stem Cells. *Cell Transplant***,** 963689718766279.

YAO, A., LIU, F., CHEN, K., TANG, L., LIU, L., ZHANG, K., YU, C., BIAN, G., GUO, H., ZHENG, J., CHENG, P., JU, G. & WANG, J. 2014. Programmed death 1 deficiency induces the polarization of macrophages/microglia to the M1 phenotype after spinal cord injury in mice. *Neurotherapeutics,* 11**,** 636-50.

YAO, L., DALY, W., NEWLAND, B., YAO, S., WANG, W., CHEN, B. K., MADIGAN, N., WINDEBANK, A. & PANDIT, A. 2013. Improved axonal regeneration of transected spinal cord mediated by

multichannel collagen conduits functionalized with neurotrophin-3 gene. *Gene Ther,* 20**,** 1149-57.

YOSHII, S., OKA, M., SHIMA, M., AKAGI, M. & TANIGUCHI, A. 2003. Bridging a spinal cord defect using collagen filament. *Spine (Phila Pa 1976),* 28**,** 2346-51.

YOSHII, S., OKA, M., SHIMA, M., TANIGUCHI, A., TAKI, Y. & AKAGI, M. 2004. Restoration of function after spinal cord transection using a collagen bridge. *J Biomed Mater Res A,* 70**,** 569-75.

YOUNG, C. C., AL-DALAHMAH, O., LEWIS, N. J., BROOKS, K. J., JENKINS, M. M., POIRIER, F., BUCHAN, A. M. & SZELE, F. G. 2014. Blocked angiogenesis in Galectin-3 null mice does not alter cellular and behavioral recovery after middle cerebral artery occlusion stroke. *Neurobiol Dis,* 63**,** 155-64.

ZAMMIT, P. S., CLARKE, J. D. W., GOLDING, J. P., GOODBRAND, I. A. & TONGE, D. A. 1993. Macrophage response during axonal regeneration in the axolotl central and peripheral nervous system. *Neuroscience,* 54**,** 781-789.

ZAMZE, S., HARVEY, D. J., CHEN, Y. J., GUILE, G. R., DWEK, R. A. & WING, D. R. 1998. Sialylated N-glycans in adult rat brain tissue--a widespread distribution of disialylated antennae in complex and hybrid structures. *Eur J Biochem,* 258**,** 243-70.

ZHANG, B., BAILEY, W. M., KOPPER, T. J., ORR, M. B., FEOLA, D. J. & GENSEL, J. C. 2015a. Azithromycin drives alternative macrophage activation and improves recovery and tissue sparing in contusion spinal cord injury. *J Neuroinflammation,* 12**,** 218.

ZHANG, K., ZHENG, J., BIAN, G., LIU, L., XUE, Q., LIU, F., YU, C., ZHANG, H., SONG, B., CHUNG, S. K., JU, G. & WANG, J. 2015b. Polarized Macrophages Have Distinct Roles in the Differentiation and Migration of Embryonic Spinal-cord-derived Neural Stem Cells After Grafting to Injured Sites of Spinal Cord. *Mol Ther,* 23**,** 1077-1091.

ZHANG, N., FANG, M., CHEN, H., GOU, F. & DING, M. 2014. Evaluation of spinal cord injury animal models. *Neural Regeneration Research,* 9**,** 2008-2012.

ZHANG, Q., BIAN, G., CHEN, P., LIU, L., YU, C., LIU, F., XUE, Q., CHUNG, S. K., SONG, B., JU, G. & WANG, J. 2016. Aldose Reductase Regulates Microglia/Macrophages Polarization Through the cAMP Response Element-Binding Protein After Spinal Cord Injury in Mice. *Mol Neurobiol,* 53**,** 662-676.

ZHANG, Y. K., WANG, J., LIU, L., CHANG, R. C., SO, K. F. & JU, G. 2013. The effect of Lycium barbarum on spinal cord injury, particularly its relationship with M1 and M2 macrophage in rats. *BMC Complement Altern Med,* 13**,** 67.

ZHAO, T., JING, Y., ZHOU, X., WANG, J., HUANG, X., GAO, L., ZHU, Y., WANG, L., GOU, Z., LIANG, C., XU, K., LI, F. & CHEN, Q. 2018. PHBV/PLA/Col-Based Nanofibrous Scaffolds Promote Recovery of Locomotor Function by Decreasing Reactive Astrogliosis in a Hemisection Spinal Cord Injury Rat Model. *J Biomed Nanotechnol,* 14**,** 1921-1933.

ZHAO, Y., TANG, F., XIAO, Z., HAN, G., WANG, N., YIN, N., CHEN, B., JIANG, X., YUN, C., HAN, W., ZHAO, C., CHENG, S., ZHANG, S. & DAI, J. 2017. Clinical Study of NeuroRegen Scaffold Combined With Human Mesenchymal Stem Cells for the Repair of Chronic Complete Spinal Cord Injury. *Cell Transplant,* 26**,** 891-900.

ZIEMBA, A. M. & GILBERT, R. J. 2017. Biomaterials for Local, Controlled Drug Delivery to the Injured Spinal Cord. *Front Pharmacol,* 8**,** 245.

ZIMMERMANN, D. R. & DOURS-ZIMMERMANN, M. T. 2008. Extracellular matrix of the central nervous system: from neglect to challenge. *Histochem Cell Biol,* 130**,** 635-53.

ZUKOR, K. A., KENT, D. T. & ODELBERG, S. J. 2011. Meningeal cells and glia establish a permissive environment for axon regeneration after spinal cord injury in newts. *Neural Dev,* 6**,** 1.

Appendices

Appendix I: Microglia and macrophage polarisation in rodent models of SCI

A summary of microglia / macrophage polarisation in rodent models of SCI, examined using immunohistochemistry and/or flow cytometry. Where possible a general conclusion as to the major polarisation state of these cells is given.

Model	Time-points	Marker	Most abundant?	Comment	Reference
Rat Clip compression C6/C7	8 weeks post injury	Iba-1 iNOS CD206	M1	iNOS abundant at 8 weeks but not CD206. No longer completely amoeboid at this time	(Riemann *et al.*, 2018)
Rat Compression T10	1, 7, 14 dpi	iNOS Arg-1 CD68	M1 at 7 Equal at 14	iNOS+/CD68+ far more abundant than Arg-1+/CD68+ at 7 dpi. Almost equal labelling of each marker at 14 dpi	(Jo *et al.*, 2018)
Rat Contusion T10	7 dpi	CD86 CD206	M2	CD206 cells far more abundant than CD86	(Wang *et al.*, 2018)
Rat Contusion T9-T10	?	CD86 CD163	M1	Majority of macrophages CD86+ (approx. 72%)	(Baiyila *et al.*, 2018)
Rat Clip compression T7/T8	1, 3, 5, 7, 14, 28 dpi	Iba-1/ CD45/ CD68 CD86 CD163	M2	No change in total numbers of microglia/ macrophages around lesion CD163+ cells were approximately twice the number of CD86+ cells	(Dyck *et al.*, 2018)
Rat Unilateral contusion C3/C4	14 dpi	CCR7 CD206	M1	M1:M2 ratio was 1.88 at 7 dpi	(Cornelison *et al.*, 2018)
Rat Contusion T9/T10	7 dpi	ED1 (all) iNOS CD206	Equal	Similar numbers of iNOS and CD206 cells dual positive with ED1	(Kim *et al.*, 2017)
Rat Forceps compression T8	1, 3, 7, 14 dpi	CD11b iNOS Arg-1 (IHC)	M1	iNOS+CD11b+ outnumber Arg-1+CD11b+ cells at all timepoints. Number of both cell types reduced by 14 dpi	(Song *et al.*, 2017)

Model	Time-points	Marker	Most abundant?	Comment	Reference
Rat Contusion C5	6 weeks post injury	CD68 iNOS Arg-1	M1	iNOS+/CD68+ cells were greater than Arg-1+/CD68+ cells	(Wang *et al.*, 2017)
Rat Transection T9/T10	28 dpi	CD86 CD206	M2	CD206+ far more abundant than CD86 +	(Hakim *et al.*, 2015)
Rat Contusion T10/11	7 dpi	Arg-1 CD206 iNOS	M2	Arg-1 is almost 3 times more than in control tissue CD206 almost double iNOS	(Didangelos *et al.*, 2014)
Rat Contusion T10/11	3, 14 dpi	CD68 CD206	?	CD206 increased at 3 and 14 dpi M1 not studied here	(Bartus *et al.*, 2014)
Rat Contusion T9/T10	7 dpi	iNOS & CD16/32 Arg-1 & CD206	M1	80% of Ox42+ cells were positive for M1 markers Almost none positive for M2	(Nakajima *et al.*, 2012)
Rat Contusion Level?	1, 3, 7, 14, 28 dpi	CD163 (M2) CD86 (Flow) CCR7 (M1) Arg-1 (IHC)	Equal at 1 dpi M1 thereafter	M1 markers increased from 1-7 dpi and remained elevated 14-28 dpi M2 markers were briefly increased at 3 & 7 dpi With both sets of markers M1:M2 was approximately 1 at 1 dpi, was just below 2 at 3-7 dpi, and was increased to 5 by 28 dpi	(Hu *et al.*, 2012)
Rat Lateral compression T8	7, 14 dpi	ED1 iNOS Arg-1	M2 at 7 Equal at 14	Arg-1 slightly above iNOS at 7 dpi, ratio is approximately 1 at 14 dpi	(Zhang *et al.*, 2013)
Rat Contusion T9	7 dpi	CD68 CCR7 Arg-1	M1	CCR7+CD68+ far more abundant than Arg-1+CD68+	(Hu *et al.*, 2016)
Rat Contusion T9/T10	7 dpi	Iba-1 CD16 CD206	M1	50% of Iba-1+ cells were CD16+, 30% were CD206+	(Chen *et al.*, 2018a)
Rat Contusion T9	1, 3, 5, 7, 14, 21, 28 dpi	CD68/CCR7	Equal from 1-5 dpi	CD68+ cells increased up to 5 dpi, were stable to 14 dpi then reduced. M1 were	(Chen *et al.*, 2015)

Model	Time-points	Marker	Most abundant?	Comment	Reference
		CD68/Arg-1 (IHC) CD68+CD163– (M1) CD68+CD163+ (M2) – flow and CD86	M1 thereafter	predominant, increased up to 14 dpi, also fell after 14 dpi. M2 increased up to 5 dpi then fell. M1/M2 ratio was around 1 for 1-5 dpi, then was approx. 3 at 7 dpi and increased significantly from 14-28 dpi (ratio approx. 9-11)	
Mouse Forceps compression T8/T9	4, 7 dpi	CD16/32 Arg-1	M1	CD16/32+ cells were more abundant than Arg-1+ cells. Arg-1 decreased from 4 – 7 dpi	(Han *et al.*, 2018a)
Mouse Contusion +/- maintained compression T9	14 dpi	CD86 & MARCO CD206 & Arg-1	M2	Arg-1+ and CD206+ cells outnumber CD86+ cells with or without compression	(Orr *et al.*, 2017)
Mouse Contusion T9	3, 7 dpi	MARCO CD86 Arg-1 CD206	M1 at 3 M2 at 7	Majority of M1 type (60-80%) at 3dpi Majority (70%) M2 type by 7 dpi (both markers in each case)	(Gensel *et al.*, 2017)
Mouse Contusion T9	1, 3, 7 dpi	CD86 CD206 Arg-1	M1	CD86 expression was higher than Arg-1 or CD206 at 3 and 7 dpi.	(Zhang *et al.*, 2015a)
Mouse Contusion Level?	1, 7, 28 dpi	CD86 iNOS CD206	M1	iNOS/CD86 increased at 1 and 7 dpi Decreased to almost normal levels at 28 dpi CD206 transiently increased at 1 dpi	(Khayrullina *et al.*, 2015)
Mouse Contusion T9/T10	6, 10, 14 dpi	CD206 Arg-1	No M1 studied here	CD206+ cells and Arg-1+ cells present at 6, 10 and 14 dpi. CD206 highest at 14 dpi, Arg-1 highest at 6 dpi	(Ishii *et al.*, 2012)
Mouse Hemisection T13/L1	2, 4 dpi	CD11b Arg-1	No M1 studied here	Almost 80% of CD11b+ cells were Arg-1+ at 2 dpi Fell to 55% at 14 dpi at lesion epicentre, and were almost gone at the border of the injury	(Munro *et al.*, 2012)
Mouse Contusion T9/T10	1, 4, 7, 28, 60 dpi	CD86 CD206	M1	CD86 significantly increased at all time-points except 7 dpi	(Bermudez *et al.*, 2016)

Model	Time-points	Marker	Most abundant?	Comment	Reference
				CD206 increased at 1 and 4 dpi Triple labelling shows intermediate state of cells	
Mouse Transection T9/T10	1, 3, 7, 14 dpi	Ym-1	No M1 studied here	Ym1 elevated at 1 and 3 dpi significantly increased at 7 and 14 dpi	(Sato *et al.*, 2012)
Mouse Contusion T10	3h, 1, 3, 7, 14 dpi	iNOS CD16/32 Arg-1 CD206	M1	iNOS greatly increased 1, 3, 7 dpi, fell but still elevated at 14 dpi Arg-1 also increased at these times but to a lesser extent CD16/32 increased at 3, 7, 14 dpi CD206 increased at 3, 7 dpi	(Guerrero *et al.*, 2012)
Mouse Contusion T12	14 dpi	M1 type: 7AAD-/CD11b+/CD11c+/GR1-/**CD206-** M2 type: 7AAD-/CD11b+/CD11c+/GR1-/**CD206+**	M1	More CD206- than CD206+	(Cusimano *et al.*, 2012)
Mouse Contusion T11	1, 4, 15 dpi	CD16/32 CD86 iNOS Arg-1 CD206 TGFβ	M1	All M1 markers increased steadily from 1-15 dpi, iNOS the lowest of the three, CD16/32 was significantly increased at all 3 time-points; Arg-1 was significantly higher at 1 dpi, CD206 at 4 and 15 dpi, TGFβ significantly lower at 15 dpi than at earlier time-points.	(Kroner *et al.*, 2014)
Mouse Contusion Thoracic	12h, 1, 3, 7, 14 dpi	Arg-1 CD206	M2	Arg-1 & CD206 increased to 3 dpi and then fell again. iNOS was highest at 1 dpi, CD16 was highest at 7 dpi, CD86 was highest 7- 14 dpi Arginase much higher than any M1 marker	(Hayakawa *et al.*, 2014)
Mouse Forceps crush T8/T9	14, 21 dpi	iNOS Arg-1	M2	Arg-1 much higher than iNOS at both time-points	(Yao *et al.*, 2014)

Model	**Time-points**	**Marker**	**Most abundant?**	**Comment**	**Reference**
Mouse Clip compression T9/T10	7, 14 dpi	CD16/32 iNOS Arg-1 CD206	M1	Number of M1 type cells higher than M2 type cells at 7 & 14 dpi. M1 numbers were stable, M2 numbers fell by 14 dpi but were still above sham.	(Ji *et al.*, 2015)
Mouse Contusion T9	0h, 6h, 1, 3, 7, 14 dpi	CD86 CD206 Arg-1	M1	Arg-1+ cells transiently increased at 1 dpi, returned to normal at 2 - 14 dpi. CD86+ increased from 1 - 14, but fell slightly from 7 - 14 dpi	(Li *et al.*, 2016a)
Mouse Forceps compression T8	0h, 4h, 1, 3, 7, 14 dpi	iNOS CD86 Arg-1 (mRNA)	M1	iNOS increased slightly at 4h, 10-fold higher at 1dpi, gradually reduced to normal level by 14 dpi. CD86 much slower increase, 4-fold higher at 7 dpi, 8-fold at 14 dpi Arg-1 was 4-fold increased at 4h, 8-fold at 1 dpi, 85-fold at 3dpi, 4-fold at 7 dpi and at 14 dpi had returned to normal	(Zhang *et al.*, 2016)
Mouse Clip compression T12	7 dpi	CD11b+/CX3CR1-GFPlow/Ly6Chigh (M1) CD11bpos/CX3CR1-GFPhigh/Ly6Clow (M2)	M2	M2 more abundant than M1	(Papa *et al.*, 2016)
Mouse Contusion T9	7 dpi	CD68 iNOS Arg-1	M2?	CD68+ cells increased approx. 12-fold iNOS+ CD68+ were significantly increased Arg-1+/CD68+ didn't increase vs sham, but were much more abundant than iNOS	(Haan *et al.*, 2015)
Mouse Contusion T11/T12	7 dpi	iNOS Arg-1	M1	iNOS+ F4/80+ almost twice Arg-1+/F4/80+	(Sun *et al.*, 2018)

Appendix II: Collagen biomaterials in pre-clinical models of SCI

Pre-clinical studies of collagen based biomaterial therapies for SCI. Unless otherwise stated collagen treatment was implanted at the time of injury inducing surgery. Citations shaded in grey all come from the Dai research group in China. BBB, Basso Beattie Bresnahan (locomotor scale); BDNF, brain derived neurotrophic factor; bFGF, basic fibroblast growth factor; BMSCs, bone marrow stromal cells; C-6-S, chondroitin-6-sulphate; CBD, collagen binding domain; chABC, chondroitinase ABC; CS-56, chondroitin-sulphate-56; EGFR, epidermal growth factor receptor; Fab, antigen binding fragment (of antibody); GDNF, glial-cell derived neurotrophic factor; GFAP, glial fibrillary acidic protein; hESC-NPCs, human embryonic stem cell derived neural precursor cells; IHC, immunohistochemistry; LBD, ligand binding domain; MSCs, mesenchymal stem cells; NEP1-40, nogo-66(1-40) antagonist peptide; NF, neurofilament; NG2, neural/glial antigen 2 (a chondroitin sulphate proteoglycan); NPCs, neural progenitor cells; NSCs, neural stem cells; NT-3, neurotrophin-3; PHBV, poly(hydroxybutyrate-cohydroxyvalerate); PLA, poly(lactic acid); PPF, poly(propylene fumarate); PTX, paclitaxel; SSER, somatosensory evoked responses.

Model	**Formulation**	**Other therapeutic**	**Time-point**	**Outcome**	**Reference**
Rat Lateral hemisection T8-T10	Collagen hydrogel with collagen microspheres	NT-3	1 and 6 weeks	Reduced Iba-1 Reduced NG2 No change in GFAP Increased βIIITubulin (NT3 group only) Improved motor function (Hydrogel only)	(Breen *et al.*, 2016)
Rat Lateral hemisection T13-L1	Collagen scaffold	Cetuximab NPCs	4 and 12 weeks	Difficult to interpret results, insufficient controls, but collagen+NPCs+/-cetuximab improved BBB score	(Li *et al.*, 2013)
Rat Hemisection T9	Collagen scaffold	bFGF attached via a CBD	4 and 8 weeks	No quantification of histology but apparently better tissue preservation, more neuronal growth, very little GFAP and improved motor function	(Shi *et al.*, 2014)

Model	Formulation	Other therapeutic	Time-point	Outcome	Reference
Rat Transection (2mm) T9/T10	Collagen scaffold	Ephrin-A4-LBD and/or PlexinB1-LBD attached via a CBD Combined group also received NEP1-40	12 weeks	Combined (triple) treatment resulted in increased axon growth into the lesion Very little difference in GFAP signal between groups Material alone was sufficient to improve myelination Combined treatment significantly improved motor function	(Li *et al.*, 2015)
Rat Transection (2mm) T9/T10	Collagen scaffold	EphA4-LBD PlexinB1-LBD BDNF NT-3 all attached via a CBD NEP1-40	12 weeks	Material alone improved tissue sparing, combined treatment greater effect Material alone slightly increased CD68, neutralising treatments and/or BDNF/NT-3 further reduced Material alone was sufficient to reduce CS-56 signal Combined treatments greatly improved axon growth into lesion and remyelination, and material alone offered slight but significant improvement in both	(Li *et al.*, 2016b)

Model	Formulation	Other therapeutic	Time-point	Outcome	Reference
				Combination treatment significantly improved motor function	
Dog Transection T12	Linear ordered collagen scaffold	BDNF attached via a CBD	12 weeks	Significant improvement in motor function, axonal growth, remyelination,	(Han *et al.*, 2014)
Dog 3mm complete resection T12	Linear ordered collagen scaffold	BDNF attached via a CBD	38 weeks	Early after injury scaffold +/- BDNF improved motor function. By 38 weeks scaffold+BDNF treated animals performed best. SSER response improved in scaffold group and scaffold+BDNF had an even higher score Better tissue organisation in both treated groups There was less GFAP in scaffold+BDNF (but not quantified) NF signal: scaffold was better than control, scaffold+BDNF better than scaffold only. NF signal was ordered in both. Improved remyelination in scaffold+BDNF group	(Han *et al.*, 2015)

Model	Formulation	Other therapeutic	Time-point	Outcome	Reference
Rat Transection (6mm resected) T8/T9	Linear ordered collagen scaffold	EGFR neutralising antibody (151IgG) and/or BDNF attached via a CBD	8 weeks	[Gelatine implanted control group] Incremental improvement in SSER with scaffold+IgG+BDNF performing best Same pattern for NF	(Han *et al.*, 2010)
Rat Transection (2mm) T8-T10	Linear ordered collagen scaffold	NT-3 attached via a CBD	4 months	Scaffold+NT3 had significantly improved motor function NF signal was significantly higher in this group	(Fan *et al.*, 2010)
Rat Lateral hemisection T8-T10	Linear ordered collagen scaffold	BDNF +/- CBD	15 weeks	No improvement in function with scaffold alone, , but significantly higher with BDNF +/- CBD Same pattern observed for NF signal	(Han *et al.*, 2009)
Rat Transection (3-4mm) T8	Linear ordered collagen scaffold	Cetuximab Fab (EGFR inhibiting antibody) attached via CBD	12 weeks	Scaffold alone slightly improved motor function, significant improvement when accompanied by Fab Lesion volume, GFAP signal, and remyelination all improved slightly with scaffold alone, all parameters further improved with Fab Scaffold+Fab improved axon growth through	(Fan *et al.*, 2017)

Model	Formulation	Other therapeutic	Time-point	Outcome	Reference
				lesion, in an aligned manner	
Dog Transection (5mm) T8	LOCS	Cetuximab	9 months	Scaffold + cetuximab significantly increased neuronal growth / migration into injury epicentre. Scaffold alone sufficient to reduce CS-56 signal Slight improvement in motor function with scaffold only, significant improvement with scaffold + cetuximab	(Li *et al.*, 2017b)
Rat Transection (1mm) T9	PPF multichannel scaffold, coated/channels filled with collagen	NT-3 attached via CBD	12 weeks	PPF +/- collagen +/- NT-3 reduced CS-56 signal at lesion epicentre PPF+collagen+NT-3 increased axonal growth, with scaffold alone there was little change. Slight improvement in motor function with PPF+collagen, significant improvement with PPF+collagen+NT-3	(Chen *et al.*, 2018b)
Rat Transection (4mm) T8	Collagen scaffold	PTX liposomes NSCs	8 weeks	Scaffold + PTX + NSCs showed best improvement in motor function and axonal growth into the lesion, collagen	(Li *et al.*, 2018)

Model	Formulation	Other therapeutic	Time-point	Outcome	Reference
				alone made no difference	
Rat Transection (3mm) T8/T9	Linear ordered collagen scaffold *At 12 weeks scar tissue was removed and scaffold implanted at this stage*	Human umbilical cord MSC	24 weeks (post scar resection, i.e. 36 weeks after initial injury)	Implantation of scaffold reduced GFAP and increased axonal growth, improved myelination in lesion centre	(Li *et al.*, 2016b)
Dog Transection (5mm) T8	Linear ordered collagen scaffold	Human placenta derived MSCs	36 weeks	Scaffold alone improved motor function, further improvement with scaffold+MSCs Scaffold +/- MSCs reduced cavity formation and CS-56 signal, and increased neuronal growth / migration through the lesion	(Han *et al.*, 2018b)
Dog	Linear ordered collagen scaffold	Human umbilical cord MSC	1 year	Scaffold+MSCs improved motor function, increased axon outgrowth and improved myelination in the lesion area. GFAP signal was increased with scaffold alone but scaffold+MSCs reduced GFAP Both treatments reduced CS56 signal	(Li *et al.*, 2017a)
Rat C3-C4 Partial transection	Orientated microstructured collagen scaffold	None	12 weeks	Scaffold significantly improved food pellet retrieval, GAP43 expression,	(Altinova *et al.*, 2014)

Model	Formulation	Other therapeutic	Time-point	Outcome	Reference
				and reduced astrocytosis	
Rat Transection T8-T10	Aligned collagen fibres, cross-linked and arranged into a multi-channel conduit	NT-3 gene (with transection vector)	4 weeks	[No injury only control] NT3 gene delivery significantly improved axon growth through lesion There was a non-significant increase in BBB score No difference in ED1+ cells	(Yao *et al.*, 2013)
Rat Lateral hemisection T8/T9	Honeycomb collagen sponge	BMSCs	4 weeks	[No injury only control] BMSCs improved neurite growth into the lesion	(Onuma-Ukegawa *et al.*, 2015)
Rat Lateral hemisection C3	Electrospun collagen nanofibers, photochemically cross-linked	none	10 dpi 30 dpi	[very low n number, nothing quantified, control is random collagen, no injury only control] GFAP appears to be reduced at 30 dpi and less ED1 signal at lesion border	(Liu *et al.*, 2012)
Rat Hemisection (3mm resection) T8/T9	Porous collagen scaffold with channels, with collagen membrane applied dorsally.	Soluble Nogo receptor ChABC MSCs	4 weeks	[no quantification of IHC] BBB score was higher for scaffolds alone Strongest NF signal in scaffold+ChABC Strongest GAP43 signal in ChABC+scaffold, only this group has	(Cholas *et al.*, 2012a)

Model	Formulation	Other therapeutic	Time-point	Outcome	Reference
				signal in the middle of the lesion CD68 was significantly reduced at lesion epicentre in scaffold only groups, and GFAP signal was slightly lower Combination treatment increased CD68 signal	
Rat Transection (5mm resected) T10	Collagen sponge with "honeycomb" pores filled with PuraMatrix	none	9 and 19 weeks	[no quantitation for IHC] Significant improvement in motor function with scaffold/PuraMatrix Strong neuronal signal throughout scaffold at 19 weeks, with GAP43, and signal appears ordered. Astrocytes were also present throughout lesion area but no evidence of scarring	(Kaneko *et al.*, 2015)
Rat Transection (5mm) T9/T9	Porous collagen scaffold with channels	Plasmid-GDNF NSCs	6 weeks	[No quantification of IHC] No recovery of motor function. Non-significant reduction in number of cysts in all scaffold groups. GDNF altered the organisation of tissue/collagen matrix in the lesion,	(Cholas *et al.*, 2012b)

Model	Formulation	Other therapeutic	Time-point	Outcome	Reference
				with a less intense collagen signal. Scaffold +/- NSCs group had much more aligned collagen	
Rat Contusion, with 5mm resection 10 days later T10	Collagen filaments	none	4 and 12 weeks post implant	[no graphs, incomplete panels of images] Axons passed through scaffold area between 4 and 12 weeks, not seen in control group. Functional recovery better in scaffold group	(Yoshii *et al.*, 2003)
Rat Contusion, with 5mm resection 10 days later T10	Collagen filaments arranged into scaffold	none	12 weeks	Improved function with collagen scaffold Much more axonal growth into the lesion area in scaffold group	(Yoshii *et al.*, 2004)
Rat Lateral hemisection T9	Collagen sponge	none	3, 7, 28 dpi	Collagen sponge improved motor function and increased NF signal Also increased ED-1+ cells	(Petter-Puchner *et al.*, 2007)
Rat Hemisection (5mm) T12	Collagen tube (to direct axons into the peripheral nerve)	none	9 months	Collagen tube promoted regrowth and myelination of axons, improved signal transduction (electrophysiology)	(Liu *et al.*, 2001)
Rat Lateral hemisection T10/T11	Collagen scaffold	hESC-NPCs	5 weeks	Small but significant improvement in motor function with scaffold+NPC only, sensory function	(Hatami *et al.*, 2009)

Model	Formulation	Other therapeutic	Time-point	Outcome	Reference
				improved with scaffold +/- NPCs	
Rat Contusion with resection (4mm) 10 days later T10	Collagen gel	none	1, 3, 7 days 3 months	[control rats had a single cut transection instead of resection] Collagen implant allowed axonal penetration into and across the implant, none in control group. Collagen promoted a very modest improvement in motor function	(de la Torre, 1982)
Rat Hemisection T8-T10	Collagen hydrogel	none	3 dpi, 1, 3, 6 months	[no injury only control] Axons grew through collagen implant	(Marchand *et al.*, 1993)
Rat Transection (1-1.5mm) T8-T10	Injectable collagen hydrogel	none	1, 2, 6, 8, 10, 12 dpi 2, 3, 4, 5 weeks 2, 3 months	Implants invaded by fibroblasts / meningeal cells, macrophages / microglia and some astrocytes. Astrocytes extended processes to connect either side of tissue. Axons grew through implant, appeared to follow collagen fibres	(Marchand and Woerly, 1990)
Rat Dorsal hemisection T8-T10	Injectable collagen	NT-3	4 weeks	Collagen supported axon ingrowth into lesion area, this was improved with scaffold+NT-3 Astrocytes did not invade collagen	(Houweling *et al.*, 1998a)

Model	Formulation	Other therapeutic	Time-point	Outcome	Reference
				Ox-42 microglia / macrophages were present at the edge	
Rat Dorsal hemisection T8-T10	Injectable collagen	BDNF	4 weeks	[no injury only controls] Collagen improved recovery of motor function, this was increased with collagen+BDNF	(Houweling *et al.*, 1998b)
Rat Transection (2mm) T8-T9	Honeycomb collagen	Coated with short laminin peptide	4 weeks	[randomly aligned collagen gel as control, no collagen without peptide coating] Scaffold with peptide greatly improved axonal growth, with continuous fibres observed to entirely cross the lesion/scaffold site. This was significantly greater than with random collagen	(Fukushima *et al.*, 2008)
Rats Transection (3-4mm) T8-T10	Collagen matrix	none	2-6 weeks	Macrophages and fibroblasts were in the implant area but not astrocytes. GFAP+ processes ran along the border between implanted collagen and host tissue. Implant area became vascularised. Axons grew into lesion area, but less	(Gelderd, 1990)

Model	Formulation	Other therapeutic	Time-point	Outcome	Reference
				so than in transected controls	
Rat Lateral hemisection (3mm) T10	Electrospun PHBV/PLA scaffolds +/- collagen (collagen blended into PHBV/PLA solution, 70:30 or 50:50)	none	4 and 8 weeks	All scaffolds reduced CD68+ cells and cavitation at the lesion Scaffolds with collagen increased NF signal in the lesion, reduced GFAP signal and improved motor function	(Zhao *et al.*, 2018)
Rat Contusion with transection 10 days later T10	Collagen matrix	None	90 dpi	More axonal processes growing into scar / lesion area in collagen group, and more myelination, with improved functional recovery. Collagen implant became vascularised	(de la Torre *et al.*, 1984)
Rat Transection (1.5mm) T10	Collagen scaffold with heparin sulphate	none	8 weeks	Scaffold significantly improved motor function and electrophysiological response Scaffold improved tissue integrity, more so with heparin sulphate included Scaffold improved axonal growth into lesion area	(Chen *et al.*, 2017)
Rat Transection (5mm)	Ordered collagen scaffold within conduit	none	9 weeks (7, 21 and 65 dpi for CD68)	Slight but significant improvement in motor function.	(Snider *et al.*, 2017)

Model	**Formulation**	**Other therapeutic**	**Time-point**	**Outcome**	**Reference**
T8-T10				Scaffold reduced lesion volume and improved tissue integrity. Demyelination was slightly reduced. Inflammatory cells were reduced at all time-points. Much greater neuronal growth through lesion with scaffold.	

Appendix III: Reagents, equipment and consumables required for *Xenopus laevis* growth and surgery

Reagent	Supplier	Cat. No.	Region
Sodium chloride (NaCl)	Sigma Aldrich	S7653	Wicklow, Ireland
Potassium chloride (KCl)	Sigma Aldrich	P9333	Wicklow, Ireland
Magnesium Sulphate heptahydrate ($MgSO_4.7H_2O$)	Sigma Aldrich	230391	Wicklow, Ireland
HEPES ($C_8H_{18}N_2O_4S$)	Sigma Aldrich	H3375	Wicklow, Ireland
Sodium bicarbonate ($NaHCO_{3)}$	Sigma Aldrich	S5761	Wicklow, Ireland
Calcium chloride ($CaCl_2$)	Sigma Aldrich	C1016	Wicklow, Ireland
Tricaine methanesulfonate (MS222)	Fisher Scientific	NC0342409	Ireland
Dumont #5 forceps, Inox	Fine Science Tools	11252-20	Germany
Needle, 25G	BD	305122	UK
Penicillin-Streptomycin solution	Sigma Aldrich	P4333	Wicklow, Ireland
Gentamycin	Sigma Aldrich	G1264	Wicklow, Ireland
Scalpel, #11	Swann Morton	0503	England
Fine scissors	Fine Science Tools	14060-09	Germany

Appendix IV: Reagents, equipment and consumables required for rat surgery and tissue processing

Reagent	Supplier	Cat. No.	Region
Isofluorane (Iso-vet)	Chanelle group		Loughrea, Ireland
Buprenorphine (Bupaq)	Chanelle group		Loughrea, Ireland
Lignocaine and Adrenaline	Chanelle group		Loughrea, Ireland
Enrofloxacine (Baytril)	Bayer		Germany
Saline (0.9% (w/v) sodium chloride)	B. Braun Medical		Dublin, Ireland
Vidisic 0.2% w/w eye gel	Bausch & Lomb		UK
Sodium pentobarbitone			
Chlorhexidine	Hibiscrub		
Friedman-Pearson rongeur, 0.5 mm cup	Fine Science Tools	16221-14	Germany
Curette, 0.5mm cup	Fine Science Tools	10080-05	Germany
Tissue forceps	Fine Science Tools	11023-12	Germany
Adson-Graefe forceps with teeth	Fine Science Tools	11030-12	Germany
Scissors, blunt tip	World Precision Instruments	503669	UK
Retractors	Fine Science Tools	17008-07	Germany
Scalpel, #15	Swann Morton	0505	England
4-0 Vicryl sutures	Ethicon	W9951	Belgium

Appendix V: Reagents and consumables for tissue processing, histology and lectin- and immuno-histochemistry

Sodium chloride (NaCl)	Sigma Aldrich	S7653	Ireland
Potassium chloride (KCl)	Sigma Aldrich	P9333	Ireland
Sodium phosphate dibasic (Na_2HPO_4)	Sigma Aldrich	S7907	Ireland
Potassium phosphate monobasic (KH_2PO_4)	Sigma Aldrich	P9791	Ireland
Tris-HCl	Sigma Aldrich	10812846001	Ireland
Paraformaldehyde (PFA)	Sigma Aldrich	158127	Wicklow, Ireland
Sucrose	Sigma Aldrich	S7903	Wicklow, Ireland
Gelatin, type A from porcine skin	Sigma Aldrich	G2500	Wicklow, Ireland
Optimal cutting temperature (OCT) medium	Sakura	4583	Netherlands
Superfrost Ultra Plus	Thermo Fisher Scientific	10149870	Ireland
Calcium chloride ($CaCl_2$)	Sigma Aldrich	C1016	Ireland
Magnesium chloride ($MgCl_2$)	Sigma Aldrich	M8266	Ireland
Hydrochloric acid (HCl; ~37% (vol/vol) or 11.7 M	Sigma Aldrich	258148	Ireland
Triton X-100	Sigma Aldrich	T8532	Ireland
Normal donkey serum	Sigma Aldrich	D9663	Ireland
Hoechst 33342	Invitrogen	H1399	California, USA
Fluoromount	Sigma Aldrich	F4680	Ireland
Periodic acid	Sigma-Aldrich	375810	Ireland
Bovine serum albumin	Sigma Aldrich	A7638	Ireland
D-lactose	Sigma Aldrich	61339	Ireland
D-GlcNAc	Sigma Aldrich	A3286	Ireland
D-Galactose	Sigma Aldrich	G0750	Ireland

N-Acetyl-D-galactosamine	Sigma Aldrich	A2795	Ireland
distyrene, plasticiser and xylene (DPX) mounting medium	Sigma Aldrich	06522	Ireland
Alcian blue 8GX	Sigma Aldrich	A5268	Ireland
Glacial acetic acid	Fisher Scientific	A/0360/PB17	Ireland
Aluminum sulphate $(Al_2(SO_4)_3).18H_2O$	Sigma Aldrich	A5268	Ireland
Nuclear fast red	Sigma Aldrich	N8002	Ireland
Potassium permanganate ($KMnO_4$)	Sigma Aldrich	223468	Ireland
Sulphuric acid	Sigma Aldrich	320501	Ireland
Sodium metabisulphate	Sigma Aldrich		Ireland
Gomori's aldehyde fuchsin	Sigma Aldrich		Ireland
Celestine blue	Sigma Aldrich	C7143	Ireland
Mayer's haemalum	Sigma Aldrich	R03060	Ireland
Masson's cytoplasmic stain	Sigma Aldrich		Ireland
Dodeca-molybdophosphoric	Fisher Scientific	M/5650/48	Ireland
Fast green	Sigma Aldrich	F7252	Ireland

Appendix VI: Protocols for histological stains

Alcian Blue

- Remove OCT in running tap water, 2 minutes.
- Stain in alcian blue solution for 30 minutes.
- Rinse in running tap water for 5 minutes
- Counterstain in nuclear fast red for 10 minutes.
- Wash in running tap water for 1 minute.
- Dehydrate through graded alcohols, 2 minutes each.
- Clear in xylene, 2 changes of 10 minutes.
- Cover sections with D.P.X. mounting medium and apply coverslip.
- Leave slides in fume hood overnight.

Masson's trichrome

- Bring sections to room temperature in tap water for 5 minutes
- Potassium permanganate (0.5%) – 2 minutes
- Water – brief rinse
- Sodium metabisulphite (2%) – 2 minutes
- Water – 30 seconds
- 70% ethanol – 1 minute
- Gomori's aldehyde fuchsin (see recipe below) – 1 minute
- Water – brief rinse
- 95% ethanol – 10 seconds
- Running water – 10 seconds
- Celestine blue – 4 minutes
- Running water – 30 seconds
- Mayer's haemalum – 4 minutes
- Water – 20 seconds
- Acid alcohol (247.5 ml of 70% absolute alcohol and 2.5 ml of HCL) – 20 seconds
- Running tap water – 4 minutes
- Masson's cytoplasmic stain (see recipe below) – 1 minute
- Water – brief rinse
- 1% dodeca-molybdophosphoric acid – 2 minutes
- Water – brief rinse
- Fast green (2%)– 1 minute
- 1% acetic acid – 1 minute
- Rinse excess off in running water
- Dehydrate through series of ethanol
- 50% - 10 seconds
- 70% - 10 seconds
- 95% - 2 minutes
- 100% - 2 x 2 minutes
- Xylene – 2 x 10 minutes
- Cover sections with DPX mounting medium, apply coverslip and leave in fume hood overnight

Appendix VII: Reagents and consumables required for *N*-glycosylation studies

Tris	Sigma Aldrich	10708976001	Ireland
SDS	Sigma Aldrich	L6026	Ireland
Tissue Lyser II	Qiagen	85300	UK
Protogel 30%	National Diagnostics	EC-890	UK
Tetramethylethylenediamine (TEMED)	Sigma Aldrich	T9281	Ireland
Ammonium peroxisulphate (APS)	VWR	100323W	Ireland
96 well filter plate, 1 µm pore size, 2ml depth	Pall Life Sciences	PN 8231	UK
Dithiothreitol (DTT)	Sigma Aldrich	D0632	Ireland
Iodoacetamide (IAA)	Sigma Aldrich	I1149	Ireland
$NaHCO_3$	Sigma Aldrich	S6014	Ireland
Acetonitrile, HPLC grade	Honeywell	34851	Romania
Formic acid	Sigma Aldrich	F0507	Ireland
PNGaseF	New England Biolabs,.	P0709	Ireland
10 kDa molecular weight cut off microcentrifuge filtration devices	Pall Life Sciences	516-8491	UK
2-aminobenzamide (2AB)	Sigma Aldrich	A89804	Ireland
Dimethyl sulfoxide (DMSO)	Sigma Aldrich	D2650	Ireland
Sodium cyanoborohidride	Sigma Aldrich	156159	Ireland
Acetic acid	Sigma Aldrich	695084	Ireland
Whatman 3MM Chromatography paper	Fisher Scientific	3030-917	Ireland
96 well blocks, 2ml depth	Fisher Scientific	11511963	Ireland
DEAE anion exchange column	Waters	186002180	Ireland
Ammonium hydroxide	Fluka	44273	Romania
Acetic acid	Sigma Aldrich	33209	Ireland
Acquity UPLC Glycan BEH amide column	Waters	186004742	Ireland
Dextran	Waters	186006841	Ireland
PhyTips, Normal Phase	PhyNexus	PTR-91-10-09	California, USA
Leucine encephalin standard	Waters	700003276	Ireland

Note: all water used in preparation and analysis of *N*-glycan samples was Type 1 ultra-pure water, 18.2 MΩ cm.

Appendix VIII: Recipes

10 X MBS Salts	
NaCl	51.3 g
KCl	0.75 g
$MgSO_4.7H_2O$	2.0 g
HEPES	23.8 g
$NaHCO_3$	2.0 g
pH	7.6
Final volume	1 l
1 X MBS	
10 X MBS Salts	100 ml
0.1M $CaCl_2$	7 ml
Final volume	1 l
0.1 X MBS	
1 X MBS	100 ml
dH_2O	900 ml
1 X MBSH	
10 X MBS Salts	100 ml
0.1M $CaCl_2$	7 ml
5M NaCl	4 ml
Final volume	1 l
Transplantation solution	
1 X MBSH	97 ml
0.1 M $CaCl_2$	2 ml
Penicillin (10,000 units/ml) plus Streptomycin (10 mg/ml)	1 ml
10 X PBS	
NaCl	80 g
KCl	2 g
Na_2HPO_4	14.4 g
KH_2PO_4	2.4 g
pH	7.4
Final volume (dH_2O)	1 l
1 X PBS	
10 X PBS	100 ml
dH_2O	900 ml
10 X TBS	
Tris-HCl	20 mM
NaCl	100 mM
$CaCl_2$	1 mM
$MgCl_2$	1 mM
pH	7.2
Final volume (dH_2O)	1 l
1 X TBS	

10 X TBS	100 ml
dH_2O	900 ml
Tris 100mM, pH6.6	
Tris	6 g
pH (with HCl)	6.6
Final volume	100 ml (Type I ultra-pure water)
3% acetic acid solution	
Glacial acetic acid	3 ml
Final volume	100 ml
Alcian blue solution	
Alcian blue 8GX	1 g
3% acetic acid solution	100 ml
Aldehyde-fuchsin (Gomori)	
Basic fuchsin	1.25 g
70% absolute	250 ml
Conc. HCL	2.5 ml
Paraldehyde	2.5 ml
Celestine Blue	
Celestine blue	1.25 g
Ferric Ammonium sulphate	12.5 g
Glycerin	35 ml
Distilled water 250 ml	250 ml
Cytoplasmic stain (Masson's Ponceau acid fuchsin)	
Solution A	
Ponceau 2R	2.0 g
Glacial acetic acid	2.0 ml
Distilled water	200 ml
Solution B	
Acid fuchsin	1.0gr
Distilled water	100ml
Combine solution A & B	
Homogenisation buffer (for *N*-glycan analysis)	
Tris 100mM, pH 6.6	12.5 ml
SDS	2 g
Final volume	100 ml (Type I ultra-pure water)
1.5 M Tris pH 8.8	
Tris	18.2 g
pH (with HCl)	8.8
Final volume	100 ml (Type I ultra-pure water)
10% SDS	
SDS	10 g
Final volume	100 ml (Type I ultra-pure water)
2 % APS (ammonium peroxisulphate)	1 g
Water	10 ml (Type I ultra-pure water)

Store at -20^{o} C	
Acrylamide gel	
Protogel	45µL
1.5 M Tris pH 8.8	22.5µL
10% SDS	2µL
APS	2µL
TEMED	2µL
90 mg/ml sodium cyanoborohydride in DMSO	
Sodium cyanoborohydride	483.84 mg
DMSO (dimethyl sulfoxide)	5.376 ml
160 mg/ml 2AB (2 aminobenzamide) in acetic acid	
2AB	368.64 mg
Acetic acid	2.304 ml
2 aminobenzamide (2AB) labelling solution	
90 mg/ml sodium cyanoborohydride in DMSO	5.376 ml
160 mg/ml 2AB in acetic acid	2.304 ml

Note: all water used in preparation and analysis of *N*-glycan samples was Type 1 ultra-pure water, 18.2 MΩ cm

Appendix IX: Macros

Macro to create maximum projection with desired brightness and contrast for analysis of time line of repair in* Xenopus laevis *tadpoles

```
name=getTitle();
prefix=substring(name, 0, lastIndexOf(name"f"));
newname=substring(name, 0, lastIndexOf(name".tif"));
run("Deinterleave", "how=3 keep");
run("Z Project...", "projection=[Max Intensity]");
run("Red");
//run("Brightness/Contrast...");
setMinAndMax(647, 3975);
selectWindow(""+prefix+"f #3");
close();
selectWindow(""+prefix+"f #2");
run("Z Project...", "projection=[Max Intensity]");
run("Green");
//run("Brightness/Contrast...");
setMinAndMax(495, 13496);
selectWindow(""+prefix+"f #2");
close();
selectWindow(""+prefix+"f #1");
run("Z Project...", "projection=[Max Intensity]");
selectWindow(""+prefix+"f #1");
close();
selectWindow("MAX_"+prefix+"f #1");
run("Merge Channels...", "c1=[MAX_"+prefix+"f #3] c2=[MAX_"+prefix+"f #2] c3=[MAX_"+prefix+"f
#1] create");
selectWindow("Composite");
run("RGB Color");
selectWindow("Composite");
close();
selectWindow("Composite (RGB)");
saveAs("Tiff", "D:\\Imaging\\Confocal\\Rachel\\TIMECOURSE\\GAP43 Tubu-lin\\07-12-
15\\TT114\\"+newname+"-comp.tif");
```

Macro for analysis of lectin histochemistry

```
//to set threshold on current slice, then sample squares of side 128 pixels, skipping every second square both across and down. Results in 25% of image being sampled. Ensure all parameters are checked under Analyse, Set measurements, i.e. area, area%, min, max, IntDen//
setThreshold(605, 65535)
//setTool("rectangle");
makeRectangle(0, 0, 128, 128);
run("Measure");
makeRectangle(256, 0, 128, 128);
run("Measure");
makeRectangle(512, 0, 128, 128);
run("Measure");
makeRectangle(768, 0, 128, 128);
run("Measure");
//2nd row//
makeRectangle(896, 256, 128, 128);
run("Measure");
makeRectangle(640, 256, 128, 128);
run("Measure");
makeRectangle(384, 256, 128, 128);
run("Measure");
makeRectangle(128, 256, 128, 128);
run("Measure");
//3rd row//
makeRectangle(0, 512, 128, 128);
run("Measure");
makeRectangle(256, 512, 128, 128);
run("Measure");
makeRectangle(512, 512, 128, 128);
run("Measure");
makeRectangle(768, 512, 128, 128);
run("Measure");
//4th row
makeRectangle(896, 768, 128, 128);
run("Measure");
makeRectangle(640, 768, 128, 128);
run("Measure");
makeRectangle(384, 768, 128, 128);
run("Measure");
makeRectangle(128, 768, 128, 128);
run("Measure");
```

Appendix X: Spinal cord *N*-glycome

Glycan structures identified in each peak of each exoglycosidase digest. The digests are arranged sequentially in adjacent columns. The peaks are arranged in rows, labelled with GU and the % area for the peak. The columns labelled (%) contain the proposed % area contributed by individual glycan species. Glycans are colour coded into groups based on their features. G(*) indicates galactose decorated with an unknown modification, which causes the A3G(*)1Ga1 structure to elute earlier than A1G1Ga1. (SO_4^{-2}) indicates a sulphate group, these are considered to be found on galactose. S(2Ac) and S(1Ac) indicate sialic acid which is modified with two or one extra acetyl group respectively. In GUH digest, some glycans are labelled 'und' - this indicates incomplete digestion. In UND digest, glycans marked in bold are those which have been confirmed by LC-MS. Mass data can be found in Appendix X. Those glycans in UND digest whose associated %area is in bold red text are considered to be the major glycan for that peak. The list of major glycans is given in Table 6.3. 'Junk' indicates non-glycan background signal. Numbers in brackets indicate monosaccharide linkages. All core fucose (F at the beginning of the glycan name) is α(1-6) linked to the core GlcNAc residue. All β-linked galactose is β-(1-4) linked. Ga indicates α-linked galactose and may be in α(1-3) or α(1-4). Outer-arm fucose is α(1-3) linked unless labelled F(2), which indicates α(1-2) linkage. It can be considered that outer-arm fucose is generally linked to the GlcNAc branches.Neu5Ac sialic acid is labelled as S, Neu5Gc sialic acid is labelled Sg.

UND (new)				NAN-1				ABS				ABS + BTG				ABS + BTG + BKF				ABS + BTG + BKF + AMF				ABS + BTG + BKF + AMF + GUH			
GU	% Area	%	Glycan	GU	% Area	%	Glycan	GU	% Area	%	Glycan	GU	% Area	%	Glycan	GU	% Area	%	Glycan	GU	% Area	%	Glycan	GU	% Area	%	Glycan
4.25	0.31	0.31	M3	4.24	0.43	0.43	M3	4.23	0.59	0.59	M3	4.27	0.22	0.22	M3	4.27	1.11	1.11	M3	4.29	1.07	1.07	M3	4.29	13.95	13.95	M3
4.75	1.02	0.05	M3B	4.76	0.98	0.04	M3B	4.73	0.96	0.04	M3B	4.74	1.01	0.04	M3B	4.62	0.04	0.04	M3B	4.60	0.04	0.04	M3B	4.76	1.00	1.00	M3B
		0.05	A1			0.04	A1			0.03	A1			0.08	A1	4.80	1.57	1.57	A1	4.83	1.72	1.72	A1	4.83	3.46	3.94	A1
		0.92	FM3			0.90	FM3			0.89	FM3			0.89	FM3									4.98	0.48		
5.16	0.16	0.08	A1B	5.17	0.15	0.07	A1B	5.15	0.15	0.07	A1B	5.14	0.17	0.09	A1B	5.09	0.33	0.16	A1B	5.12	0.38	0.19	A1B	5.11	2.98	2.13	A1B
		0.08	M4			0.08	M4			0.08	M4			0.09	M4			0.16	M4			0.19	M4			0.85	M4
5.33	0.89	0.06	A1G1S(2Ac)1	5.34	0.74	0.05	A1G1S(2Ac)1	5.31	0.70	0.05	A1G1S(2Ac)1	5.39	3.86	0.09	A1G1S(2Ac)1	5.34	14.37	0.60	A1G1S(2Ac)1	5.36	17.17	1.00	A1G1S(2Ac)1	5.35	4.80	1.36	A1G1S(2Ac)1
		0.05	A2			0.02	A2			0.01	A2			2.33	A2			13.60	A2			16.07	A2			3.34	A2 und
		0.17	M4			0.14	M4			0.12	M4			0.17	M4			0.17	M4			0.10	M4			0.10	M4
		0.05	A2B			0.03	A2B			0.02	A2B			0.07	A2B	5.46	0.99	0.99	A2B	5.48	1.16	1.16	A2B	5.47	0.94	0.34	A2B und
		0.56	FA1			0.50	FA1			0.50	FA1			1.20	FA1												
																5.53	0.66	0.66	A1G1S(1Ac)1	5.53	0.65	0.65	A1G1S(1Ac)1			0.60	A1G1S(1Ac)1
5.62	0.31	0.11	M4A1	5.63	0.29	0.10	M4A1	5.60	0.29	0.10	M4A1	5.61	0.73	0.35	M4A1	5.63	3.48	0.81	A1G(SO_4^{-2})1	5.65	3.81	0.81	A1G(SO_4^{-2})1	5.64	6.54	3.88	A1G(SO_4^{-2})1
		0.05	FA1B			0.05	FA1B			0.05	FA1B			0.19	FA1B			2.67	M4A1			3.00	M4A1			2.66	M4A1 und
		0.10	FM4			0.10	FM4			0.10	FM4			0.19	FM4												
		0.05	A1G1			0.04	A1G1			0.04	A1G1																
5.84	4.69	0.05	A1G(SO_4^{-2})1	5.86	4.63	0.05	A1G(SO_4^{-2})1	5.82	4.56	0.05	A1G(SO_4^{-2})1	5.85	12.06	0.05	A1G(SO_4^{-2})1	5.73	13.64	0.60	A1G(SO_4^{-2})1	5.76	17.03	0.60	A1G(SO_4^{-2})1	5.77	14.65	1.02	A1G(SO_4^{-2})1
		0.10	M4A1			0.10	M4A1			0.10	M4A1			0.30	M4A1			1.18	M4A1			1.50	M4A1			1.20	M4A1 und ?
																		0.40	A2G1S(2Ac)1			0.80	A2G1S(2Ac)1			2.14	A2G1S(2Ac)1
		0.20	A2G1S(1Ac)1			0.20	A2G1S(1Ac)1			0.20	A2G1S(1Ac)1			0.40	A2G1S(1Ac)1			0.55	A2G1S(1Ac)1			0.75	A2G1S(1Ac)1			1.24	A2G1S(1Ac)1
		0.11	A3			0.11	A3			0.11	A3			1.06	A3			10.41	A3			13.38	A3			10.55	A3 und
		0.35	A1F1G1S(2Ac)1			0.35	A1F1G1S(2Ac)1			0.35	A1F1G1S(2Ac)1			0.35	A1F1G1S(2Ac)1			0.50	A1F1G1S(2Ac)1								
		0.50	FA1G1S(2Ac)1			0.50	FA1G1S(2Ac)1			0.50	FA1G1S(2Ac)1			0.50	FA1G1S(2Ac)1												
		2.61	FA2			2.61	FA2			2.60	FA2			8.00	FA2									5.90	1.50		
		0.30	FA2B			0.28	FA2B			0.25	FA2B			0.90	FA2B												
		0.47	FA1G1S(1Ac)1			0.43	FA1G1S(1Ac)1			0.40	FA1G1S(1Ac)1			0.50	FA1G1S(1Ac)1												
6.19	6.43	4.40	M5	6.21	6.72	4.30	M5	6.18	6.97	4.25	M5	6.19	7.57	4.25	M5	6.13	10.78	5.35	M5	6.15	14.45	5.35	M5	6.16	16.61	5.35	M5
		0.11	A2G(SO_4^{-2})1			0.11	A2G(SO_4^{-2})1			0.11	A2G(SO_4^{-2})1			0.30	A2G(SO_4^{-2})1			1.55	A2G(SO_4^{-2})1			2.35	A2G(SO_4^{-2})1			0.99	A2G(SO_4^{-2})1 und
		0.06	A3G1S(2Ac)1			0.06	A3G1S(2Ac)1			0.06	A3G1S(2Ac)1			0.07	A3G1S(2Ac)1			1.65	A3G1S(2Ac)1			2.35	A3G1S(2Ac)1			1.99	A3G1S(2Ac)1 und
		0.20	FA1G(SO_4^{-2})1			0.20	FA1G(SO_4^{-2})1			0.20	FA1G(SO_4^{-2})1			0.20	FA1G(SO_4^{-2})1											3.84	A1F1G(SO_4^{-2})1
		0.30	FM4A1			0.30	FM4A1			0.30	FM4A1			0.90	FM4A1												
		0.15	A1F(2)1G1S(1Ac)1			0.15	A1F(2)1G1S(1Ac)1			0.15	A1F(2)1G1S(1Ac)1			0.15	A1F(2)1G1S(1Ac)1												
														0.90	A2(2)F1												
		1.10	A2G1			1.50	A2G1			1.50	A2G1																
		0.11	FA1G1			0.10	FA1G1			0.40	FA1G1			0.80	A1G(*)1Ga1			2.35	A1G(*)1Ga1			4.62	A1G(*)1Ga1			4.44	A1G(*)1Ga1

UND (new)				NAN-1				ABS				ABS + BTG				ABS + BTG + BKF				ABS + BTG + BKF + AMF				ABS + BTG + BKF + AMF + GUH			
GU	% Area	%	Glycan	GU	% Area	%	Glycan	GU	% Area		Glycan	GU	% Area	%	Glycan	GU	% Area	%	Glycan	GU	% Area	%	Glycan	GU	% Area	%	Glycan
6.24	8.03	0.25	A3B	6.26	7.97	0.25	A3B	6.22	7.87	0.18	A3B	6.24	13.85	1.85	A3B	6.25	2.08	1.93	A3B	6.28	2.52	2.40	A3B	6.28	0.99	1.25	A3B und
		0.05	A2G(SO_4^{-2})1			0.05	A2G(SO_4^{-2})1			0.05	A2G(SO_4^{-2})1			0.08	A2G(SO_4^{-2})1			0.30	A2G(SO_4^{-2})1			0.35	A2G(SO_4^{-2})1			0.08	A2G(SO_4^{-2})1
														0.08	A3G1S(1Ac)1			0.05	A3G1S(1Ac)1			0.10	A3G1S(1Ac)1			0.15	A3G1S(1Ac)1
		0.10	A1F1G1			0.10	A1F1G1			0.15	A1F1G1			0.05	A1F1G1			0.15	A1F1G1								
		0.50	FA1G(SO_4^{-2})1			0.50	FA1G(SO_4^{-2})1			0.50	FA1G(SO_4^{-2})1			0.55	FA1G(SO_4^{-2})1												
		0.15	FM4A1			0.15	FM4A1			0.10	FM4A1			0.35	FM4A1												
		0.20	FA2G1S(2Ac)1			0.20	FA2G1S(2Ac)1			0.20	FA2G1S(2Ac)1			0.49	FA2G1S(2Ac)1												
														0.20	FA2G1S(1Ac)1												
		5.50	FA3			5.50	FA3			5.50	FA3			9.20	FA3												
		0.15	FA1F1G1S(2Ac)1			0.15	FA1F1G1S(2Ac)1			0.15	FA1F1G1S(2Ac)1			0.15	FA1F1G1S(2Ac)1	6.37	0.47			6.41	0.55			6.42	0.49		
		0.80	A1F(2)1G(SO_4^{-2})1			0.80	A1F(2)1G(SO_4^{-2})1			0.75	A1F(2)1G(SO_4^{-2})1			0.85	A1F(2)1G(SO_4^{-2})1												
		0.14	FA1BG1			0.13	FA1BG1			0.14	FA1BG1																
		0.19	M4A1G1			0.14	M4A1G1			0.15	M4A1G1																
6.61	0.50	0.06	M5A1	6.63	0.54	0.10	M5A1	6.60	0.77	0.15	M5A1	6.58	2.48	0.85	M5A1	6.51	2.77	1.05	M5A1	6.54	6.24	1.80	M5A1	6.50	3.07		
		0.06	A3G(SO_4^{-2})1			0.04	A3G(SO_4^{-2})1			0.04	A3G(SO_4^{-2})1			0.08	A3G(SO_4^{-2})1			0.22	A3G(SO_4^{-2})1			1.20	A3G(SO_4^{-2})1			0.52	A3G(SO_4^{-2})1 und
		0.23	A4			0.20	A4			0.25	A4			1.55	A4			1.80	A4			3.24	A4			2.55	A4
		0.15	FA2G1			0.20	FA2G1			0.33	FA2G1																
6.65	1.02	0.02	M5A1	6.68	1.59	0.04	M5A1	6.65	1.94	0.03	M5A1	6.66	1.63	0.16	M5A1	6.59	2.60	1.10	M5A1	6.62	3.51	1.00	M5A1	6.63	2.13	0.85	M5A1 und?
		0.05	A3G(SO_4^{-2})1			0.10	A3G(SO_4^{-2})1			0.10	A3G(SO_4^{-2})1			0.16	A3G(SO_4^{-2})1			0.25	A3G(SO_4^{-2})1			0.80	A3G(SO_4^{-2})1			0.85	A3G(SO_4^{-2})1 und
														0.45	A4B			0.75	A4B			1.71	A4B			0.43	A4B und ?
		0.59	FM5			0.62	FM5			0.63	FM5			0.43	FM5												
		0.10	FA2G(SO_4^{-2})1			0.17	FA1G(SO_4^{-2})1			0.23	FA1G(SO_4^{-2})1			0.27	FA1G(SO_4^{-2})1												
														0.16	FA3G1S(2Ac)1												
		0.01	M4A1G1			0.12	M4A1G1			0.22	M4A1G1																
		0.08	A2G2S(1Ac)1			0.20	A2G2S(1Ac)1			0.22	A2G2S(1Ac)1																
		0.07	A3G1			0.12	A3G1			0.18	A3G1																
		0.10	FA2BG1			0.22	FA2BG1			0.33	FA2BG1																
6.79	0.29	0.05	A1G1Ga1	6.83	0.64	0.09	A1G1Ga1	6.79	1.15	0.07	A1G1Ga1	6.80	3.10	0.10	A1G1Ga1	6.74	1.17	0.15	A1G1Ga1	6.78	1.60	0.06	A1G1Ga1	6.79	1.68	1.68	A1G1Ga1
		0.09	A4G1S(2Ac)1			0.40	A4G1S(2Ac)1			0.45	A4G1S(2Ac)1			0.80	A4G1S(2Ac)1			1.22	A4G1S(2Ac)1			1.34	A4G1S(2Ac)1				
														0.30	FA3B												
		0.05	FA2G(SO_4^{-2})1			0.05	FA2G(SO_4^{-2})1			0.04	FA2G(SO_4^{-2})1			0.20	FA2G(SO_4^{-2})1												
														1.05	A2F(2)1G1												
										0.04	A2F(2)1G(SO_4^{-2})1			0.15	A2F(2)1G(SO_4^{-2})1							0.20	A2F1G(SO_4^{-2})1				
		0.10	A2G2			0.10	A2G2			0.55	A2G2																
														0.50	A3F(2)1G(*)1Ga1												

UND (new)				NAN-1				ABS				ABS + BTG				ABS + BTG + BKF				ABS + BTG + BKF + AMF				ABS + BTG + BKF + AMF + GUH			
GU	% Area	%	Glycan	GU	% Area	%	Glycan	GU	% Area		Glycan	GU	% Area	%	Glycan	GU	% Area	%	Glycan	GU	% Area	%	Glycan	GU	% Area	%	Glycan
7.37	2.13	0.50	M6	7.40	2.66	0.60	M6	7.36	2.31	0.70	M6	7.40	2.17	0.70	M6	7.33	2.42	0.69	M6	7.37	1.02	0.69	M6	7.37	0.69	0.69	M6
		0.20	A2G1Ga1			0.26	A2G1Ga1			0.30	A2G1Ga1			0.30	A2G1Ga1			0.33	A2G1Ga1			0.33	A2G1Ga1				
		0.10	M4A1F1G1			0.20	M4A1F1G1			0.20	M4A1F1G1			0.20	M4A1F1G1			0.40	M4A1F1G1								
		0.10	A3F1G1			0.10	A3F1G1			0.10	A3F1G1			0.55	A3F1G1			0.80	A3F1G1								
																		0.20	A2F1G2S(2Ac)1								
		0.19	FA2F1G1			0.20	FA2F1G1			0.80	FA2F1G1			0.85	FA2F1G1												
														0.01	FA2BF1G1												
		0.09	M4A1F(2)1G1			0.40	M4A1F(2)1G1			0.52	M4A1F(2)1G1			*0.50*	M4A1F(2)1G1												
		0.10	M5A1G1			0.10	M5A1G1			0.10	M5A1G1																
		0.05	A3G(SO_4^{-2})1G1			0.05	A3G(SO_4^{-2})1G1			0.05	A3G(SO_4^{-2})1G1																
		0.10	A4G1			0.10	A4G1	7.46	2.31	0.10	A4G1	7.49	0.94														
		0.10	FA3G2S(2Ac)1			0.10	FA3G2S(2Ac)1			0.10	FA3G2S(2Ac)1																
		0.10	A3G2			0.10	A3G2			0.60	A3G2																
		0.30	A2F(2)1G2			0.45	A2F(2)1G2			1.05	A2F(2)1G2																
		0.20	A2G1Sg(3)1																								
7.56	1.44	0.45	M6A1	7.61	3.37	0.60	M6A1	7.57	7.20	0.65	M6A1	7.54	2.57	0.70	M6A1	7.45	1.95	0.94	M6A1	7.49	0.85	0.94	M6A1	7.50	0.90	0.90	M6A1
		0.15	A2F2G1			0.25	A2F2G1			0.30	A2F2G1			0.30	A2F2G1			0.60	A2F2G1								
		0.05	A2F1G2S(1Ac)1			0.05	A2F1G2S(1Ac)1			0.05	A2F1G2S(1Ac)1			0.05	A2F1G2S(1Ac)1			0.10	A2F1G2S(1Ac)1								
														0.00	A2F2G1(SO_4^{-2})			0.31	A2F2G1(SO_4^{-2})								
		0.25	FM6D1,D3			0.38	FM6D1,D3			0.45	FM6D1,D3			0.51	FM6D1,D3												
														0.40	FA3F(2)1G1S(2Ac)1												
		0.35	FA2G2			1.70	FA2G2			4.80	FA2G2							0.00	*difference*								
		0.05	A2F2G1			0.05	A2F2G1			0.05	A2F2G1			0.05	A2F2G1	7.59	0.70	0.25	A2F2G1	7.61	0.09						
		0.05	A2F1G2S(1Ac)1			0.05	A2F1G2S(1Ac)1			0.05	A2F1G2S(1Ac)1			0.05	A2F1G2S(1Ac)1			0.10	A2F1G2S(1Ac)1								
										0.10	A2F1G(SO_4^{-2})1G1			0.10	A2F1G(SO_4^{-2})1G1			0.25	A2F1G(SO_4^{-2})1G1								
																		0.10	A3F1G2S(2Ac)1								
		0.05	A4G2S(2Ac)1			0.15	A4G2S(2Ac)1			0.20	A4G2S(2Ac)1																
		0.03	FA3BG1			0.08	FA3BG1			0.15	FA3BG1																
						0.05	FA2G(SO_4^{-2})1G1			0.10	FA2G(SO_4^{-2})1G1																
														0.41	A3F(2)2G(*)1Ga1												
		0.01	FA2BG2			0.01	FA2BG2			0.30	FA2BG2																

UND (new)				NAN-1				ABS				ABS + BTG				ABS + BTG + BKF				ABS + BTG + BKF + AMF				ABS + BTG + BKF + AMF + GUH			
GU	% Area	%	Glycan	GU	% Area	%	Glycan	GU	% Area	%	Glycan	GU	% Area	%	Glycan	GU	% Area	%	Glycan	GU	% Area	%	Glycan	GU	% Area	%	Glycan
		0.25	junk			0.25	junk			0.25	junk			0.25	junk			0.25	junk			0.25	junk			0.25	junk
		0.25	A3G1Ga1			0.20	A3G1Ga1			0.35	A3G1Ga1			0.44	A3G1Ga1			0.53	A3G1Ga1			0.54	A3G1Ga1				
		0.10	FA2G1Ga1			0.04	FA2G1Ga1			0.20	FA2G1Ga1			0.35	FA2G1Ga1												
		0.15	FM4A1F1G1			0.10	FM4A1F1G1			0.15	FM4A1F1G1			0.10	FM4A1F1G1												
		0.10	FA3F1G1			0.04	FA3F1G1			0.05	FA3F1G1			0.40	FA3F1G1												
		0.10	FA2F1G2S(2Ac)1			0.10	FA2F1G2S(2Ac)1			0.15	FA2F1G2S(2Ac)1			0.10	FA2F1G2S(2Ac)1												
														0.10	FA3F(2)1G1(SO_4^{-2})												
														0.05	FA4BF(2)1												
7.67	3.64	1.35	FM4A1F(2)1G1	7.73	2.85	1.15	FM4A1F(2)1G1	7.73	4.41	1.45	FM4A1F(2)1G1	7.73	3.19	1.40	FM4A1F(2)1G1	7.69	0.78			7.74	0.79			7.70	0.25		
		0.20	A4G(SO_4^{-2})1G1			0.20	A4G(SO_4^{-2})1G1			0.25	A4G(SO_4^{-2})1G1																
		0.20	A4G2S(1Ac)1			0.20	A4G2S(1Ac)1			0.25	A4G2S(1Ac)1																
		0.10	FM5A1G1			0.10	FM5A1G1			0.20	FM5A1G1																
		0.01	FA4G1			0.01	FA4G1			0.01	FA4G1																
		0.04	A3F1G2S(2Ac)1			0.04	A3F1G2S(2Ac)1			0.05	A3F1G2S(2Ac)1																
										0.05	A3G3S(1Ac)1																
		0.55	A2F(2)1G2			0.32	A2F(2)1G2			1.00	A2F(2)1G2																
		0.12	M4A1G1S(6)1			0.05	M4A1G1S(6)1																				
		0.12	FA2G1S(6)1			0.05	FA2G1S(6)1																				
		0.40	M7			0.60	M7			0.60	M7			0.57	M7			0.69	M7			0.63	M7			0.59	M7
		0.05	FA2G1Ga1			0.05	FA2G1Ga1			0.05	FA2G1Ga1			0.05	FA2G1Ga1												
		0.10	FM4A1F1G1			0.18	FM4A1F1G1			0.20	FM4A1F1G1			0.20	FM4A1F1G1												
7.78	0.81	0.00	FA3F1G1	7.79	1.20	0.12	FA3F1G1	7.76	1.27	0.22	FA3F1G1	7.80	1.42	0.30	FA3F1G1												
		0.11	FA2F1G2S(2Ac)1			0.20	FA2F1G2S(2Ac)1			0.20	FA2F1G2S(2Ac)1			0.30	FA2F1G2S(2Ac)1												
		0.05	A1F1G1S(6)1			0.05	A1F1G1S(6)1																				
		0.05	FA2BG1S(3)1																								
		0.05	FA3G1S(3)1																								
		0.25	FA2F2G1			0.25	FA2F2G1			0.31	FA2F2G1			0.30	FA2F2G1												
		0.05	FA2F1G2S(1Ac)1			0.04	FA2F1G2S(1Ac)1			0.05	FA2F1G2S(1Ac)1			0.05	FA2F1G2S(1Ac)1												
		0.25	FA2F2G(SO_4^{-2})1			0.25	FA2F2G(SO_4^{-2})1			0.30	FA2F2G(SO_4^{-2})1			0.30	FA2F2G(SO_4^{-2})1												
		0.25	FA2F(2)2G1			0.25	FA2F(2)2G1			0.30	FA2F(2)2G1			0.45	FA2F(2)2G1												
7.84	1.19	0.05	FA2G(SO_4^{-2})1S(6)1	7.88	0.91	0.04	FA2G(SO_4^{-2})1S(6)1	7.82	0.96			7.83	1.10			7.80	0.69			7.82	0.63			7.83	0.59		
		0.04	A3G1S(6)1			0.04	A3G1S(6)1																				
		0.05	FA2BG1S(6)1			0.04	FA2BG1S(6)1																				
		0.05	FA3G(SO_4^{-2})1S(3)1																								
		0.10	A2F1G1S(3)1																								
		0.10	FA3G1S(3)1																								

UND (new)				NAN-1				ABS				ABS + BTG				ABS + BTG + BKF				ABS + BTG + BKF + AMF				ABS + BTG + BKF + AMF + GUH			
GU	% Area	%	Glycan	GU	% Area	%	Glycan	GU	% Area		Glycan	GU	% Area	%	Glycan	GU	% Area	%	Glycan	GU	% Area	%	Glycan	GU	% Area	%	Glycan
7.95	7.62	3.43	**M7 /M7 D1**	8.01	7.20	3.22	M7 /M7 D1	7.96	7.67	3.23	M7 /M7 D1	7.98	7.52	3.25	M7 /M7 D1	7.90	5.70	3.50	M7 /M7 D1	7.95	3.85	3.85	M7 /M7 D1	7.95	3.73	3.73	M7 /M7 D1
		0.04	**A4F1G1**			0.04	A4F1G1			0.04	A4F1G1			0.15	A4F1G1			0.20	A4F1G1								
		0.05	**M5A1F1G1**			0.10	M5A1F1G1			0.30	M5A1F1G1			0.36	M5A1F1G1			0.80	M5A1F1G1								
														0.20	A3F1G(SO_4^{-2})1G1			0.40	A3F1G(SO_4^{-2})1G1								
		0.01	A4BF1G1			0.01	A4BF1G1			0.01	A4BF1G1			0.41	A4BF1G1			0.80	A4BF1G1								
		0.20	**FM6A1**			0.20	FM6A1			0.20	FM6A1			0.20	FM6A1												
		0.62	**M7**			0.62	M7			0.60	M7			0.76	M7			0.85	M7			0.93	M7			0.89	M7
						0.20	FA2F2G1			0.20	FA2F2G1			0.20	FA2F2G1												
		0.05	FA2F1G2S(1Ac)1			0.05	FA2F1G2S(1Ac)1			0.05	FA2F1G2S(1Ac)1			0.05	FA2F1G2S(1Ac)1												
						0.15	FA2F(2)1G(SO_4^{-2})1G1			0.15	FA2F(2)1G(SO_4^{-2})1G1			0.15	FA2F(2)1G(SO_4^{-2})1G1	8.06	0.85			8.03	0.93			8.05	0.89		
														0.10	FA3F1G2S(2Ac)1												
		0.22	junk			0.22	junk			0.22	junk			0.22	junk			0.20	junk			0.22	junk			0.22	junk
														0.30	A4G1Ga1			0.30	A4G1Ga1			0.35	A4G1Ga1				
		0.05	**A2F2G2**			0.05	A2F2G2			0.40	A2F2G2			0.40	A2F2G2			0.65	A2F2G2								
		0.65	FA2F(2)2G(SO_4^{-2})1G1			0.65	FA2F(2)2G(SO_4^{-2})1G1			0.72	FA2F(2)2G(SO_4^{-2})1G1			*0.77*	FA2F(2)2G(SO_4^{-2})1G1												
		0.05	A4G(SO_4^{-2})1G1			0.05	A4G(SO_4^{-2})1G1			0.05	A4G(SO_4^{-2})1G1																
										0.05	A2F1G2																
		0.15	**FM5A1G1**			0.18	FM5A1G1			0.75	FM5A1G1																
		0.05	**A2G2Ga1**			0.05	A2G2Ga1			0.05	A2G2Ga1																
		0.04	**A3F1G2**			0.10	A3F1G2			0.25	A3F1G2																
		0.10	FA4G2S(2Ac)1			0.10	FA4G2S(2Ac)1			0.10	FA4G2S(2Ac)1																
		0.04	A3BG2			0.08	A3BG2			0.10	A3BG2					8.21	1.16			8.18	0.57			8.27	0.22		
						0.08	FA3G2			0.20	FA3G2																
		0.10	**A1F(2)1G(SO_4^{-2})1S(6)1**			0.10	A1F(2)1G(SO_4^{-2})1S(6)1																				
		0.10	**FA2G1Sg(3)1**																								
		0.05	**A2F1G(SO_4^{-2})1S(6)1**			0.05	A2F1G(SO_4^{-2})1S(6)1																				
		0.20	**A2G2S(6)1**			0.20	A2G2S(6)1																				
		0.40	**FM4A1G1S(6)1**			0.40	FM4A1G1S(6)1																				
		0.41	**M4A1F(2)1G1S(3)1**																								
		0.31	**FA3G1S(3)1**																								
		0.30	**FA1G1Sg(6)1**			0.30	FA1G1Sg(6)1																				

UND (new)				NAN-1				ABS				ABS + BTG				ABS + BTG + BKF				ABS + BTG + BKF + AMF				ABS + BTG + BKF + AMF + GUH			
GU	% Area	%	Glycan	GU	% Area	%	Glycan	GU	% Area	%	Glycan	GU	% Area	%	Glycan	GU	% Area	%	Glycan	GU	% Area	%	Glycan	GU	% Area	%	Glycan
8.30	1.45	0.30	junk	8.34	1.44	0.30	junk	8.28	1.60	0.30	junk	8.30	1.49	0.40	junk	8.40	0.56	0.30	junk	8.39	0.60	0.31	junk	8.45	0.31	0.31	junk
		0.10	A4G1Ga1			0.10	A4G1Ga1			0.10	A4G1Ga1			0.20	A4G1Ga1			0.25	A4G1Ga1			0.29	A4G1Ga1				
														0.05	A4F1G2S(2Ac)1			0.01	A4F1G2S(2Ac)1								
		0.20	**FA2F(2)2G1**			0.25	FA2F(2)2G1			0.27	FA2F(2)2G1			0.30	FA2F(2)2G1												
		0.39	FA3F(2)3G1S(2Ac)1			0.35	FA3F(2)3G1S(2Ac)1			0.40	FA3F(2)3G1S(2Ac)1			0.54	FA3F(2)3G1S(2Ac)1												
		0.01	A3G(SO_4^{-2})1G2			0.01	A3G(SO_4^{-2})1G2			0.01	A3G(SO_4^{-2})1G2																
		0.39	A4G2			0.41	A4G2			0.50	A4G2																
		0.01	A4BG2			0.01	A4BG2			0.01	A4BG2																
		0.05	**FA3BG1S(3)1**																								
8.36	2.99	0.05	**FA4F1G1**	8.42	4.23	0.05	FA4F1G1	8.38	3.10	0.05	FA4F1G1	8.40	1.84	0.05	FA4F1G1												
		0.25	**FM5A1F1G1**			0.42	FM5A1F1G1			0.42	FM5A1F1G1			0.41	FM5A1F1G1												
														0.21	FA3F1G(SO_4^{-2})1G1												
		0.15	FA4BF1G1			0.21	FA4BF1G1			0.22	FA4BF1G1			0.41	FA4BF1G1												
														0.30	FA3F(2)3												
		0.20	A4G3S(2Ac)1			0.20	A4G3S(2Ac)1			0.20	A4G3S(2Ac)1																
						0.05	FA3BG2			0.05	FA3BG2																
		0.05	A3G2Ga1			0.05	A3G2Ga1			0.10	A3G2Ga1																
		0.03	**FA2G2Ga1**			0.08	FA2G2Ga1			0.20	FA2G2Ga1																
		0.05	**FA3F1G2**			0.10	FA3F1G2			0.30	FA3F1G2																
		0.10	FA3F(2)1G(SO_4^{-2})1G1			0.10	FA3F(2)1G(SO_4^{-2})1G1			0.10	FA3F(2)1G(SO_4^{-2})1G1																
		0.05	FA4BF(2)1G1			0.05	FA4BF(2)1G1			0.05	FA4BF(2)1G1																
		0.05	A3G3			0.10	A3G3			0.20	A3G3																
		0.10	**FA1F1G1Sg(3)1**																								
		0.60	**FA3G1S(6)1**			0.90	FA3G1S(6)1																				
		0.10	**A2G1Ga1S(6)1**			0.10	A2G1Ga1S(6)1																				
		0.10	**M4A1F1G1S(6)1**			0.10	M4A1F1G1S(6)1																				
		0.45	**M5A1G1S(6)1**			0.60	M5A1G1S(6)1																				
		0.20	**FA2G2S(3)1**																								
		0.05	**FA3BG1S(3)1**			0.32	A3G2G(*)1Ga1			0.45	A3G2G(*)1Ga1																
		0.41	**A2F(2)1G2S(6)1**			0.60	A2F(2)1G2S(6)1																				
						0.20	A2F(2)2G1Ga1			0.36	A2F(2)2G1Ga1			0.46	A2F(2)2G1Ga1												

UND (new)				NAN-1				ABS				ABS + BTG				ABS + BTG + BKF				ABS + BTG + BKF + AMF				ABS + BTG + BKF + AMF + GUH			
GU	% Area	%	Glycan	GU	% Area	%	Glycan	GU	% Area	%	Glycan	GU	% Area	%	Glycan	GU	% Area	%	Glycan	GU	% Area	%	Glycan	GU	% Area	%	Glycan
8.57	1.44	0.10	A2G2Ga2	8.62	1.30	0.10	A2G2Ga2	8.64	0.65	0.10	A2G2Ga2	8.63	0.46	0.04	A2G2Ga2	8.59	1.58	0.30	A2G2Ga2	8.59	0.34	0.34	A2G2Ga2	8.60	0.28	0.28	A2G2Ga2
																		0.20	A4F2G1								
		0.40	A3F2G(SO_4^{-2})1G1			0.45	A3F2G(SO_4^{-2})1G1			0.45	A3F2G(SO_4^{-2})1G1			0.42	A3F2G(SO_4^{-2})1G1			0.70	A3F2G(SO_4^{-2})1G1								
		0.05	A4G(SO_4^{-2})1G2			0.05	A4G(SO_4^{-2})1G2			0.05	A4G(SO_4^{-2})1G2																
		0.05	A4G3S(1Ac)1			0.05	A4G3S(1Ac)1			0.05	A4G3S(1Ac)1																
		0.05	**FA4G2**			0.10	FA4G2			0.10	FA4G2																
		0.05	A3F1G3S(2Ac)1			0.05	A3F1G3S(2Ac)1			0.05	A3F1G3S(2Ac)1																
		0.05	**FA2G2Ga1**			0.05	FA2G2Ga1			0.05	FA2G2Ga1																
		0.05	**FA3F1G2**			0.10	FA3F1G2			0.05	FA3F1G2																
		0.14	**FA2F(2)2G2**			0.15	FA2F(2)2G2			0.15	FA2F(2)2G2																
		0.30	**FA3G1S(3)2**																								
		0.20	**FA2BG2S(6)1**			0.20	FA2BG2S(6)1																				
8.71	1.40	0.30	**M8**	8.75	1.20	0.28	M8	8.70	1.63	0.31	M8	8.72	0.89	0.29	M8	8.59	1.58	0.38	M8	8.68	0.41	0.38	M8	8.68	0.38	0.38	M8
														0.10	FA4G1Ga1												
		0.06	**FA2F2G2**			0.05	FA2F2G2			0.50	FA2F2G2			0.50	FA2F2G2												
		0.21	A3F1G(SO_4^{-2})1G2			0.20	A3F1G(SO_4^{-2})1G2			0.20	A3F1G(SO_4^{-2})1G2																
		0.11	FA3F1G3S(2Ac)1			0.10	FA3F1G3S(2Ac)1			0.10	FA3F1G3S(2Ac)1																
		0.02	**A4G(SO_4^{-2})1G2**			0.01	A4G(SO_4^{-2})1G2			0.01	A4G(SO_4^{-2})1G2																
		0.42	**A3BG3**			0.46	A3BG3			0.50	A3BG3																
		0.11	**A2G2S(3)1S(1Ac)1**																								
		0.06	**FA3F1G1S(6)1**			0.05	FA3F1G1S(6)1																				
		0.06	**FM5A1G1S(6)1**			0.05	FM5A1G1S(6)1																				
		0.05	**M5A1F1G1S(3)1**																								
8.82	3.77	2.26	**M8**	8.86	4.17	2.26	M8	8.81	3.13	2.26	M8	8.84	2.61	2.30	M8	8.75	2.68	2.30	M8	8.81	2.26	2.26	M8	8.80	2.31	2.31	M8
														0.04	A4F2G1			0.05	A4F2G1								
		0.20	A3F2G(SO_4^{-2})1G1			0.20	A3F2G(SO_4^{-2})1G1			0.27	A3F2G(SO_4^{-2})1G1			0.27	A3F2G(SO_4^{-2})1G1			0.33	A3F2G(SO_4^{-2})1G1								
		0.01	FA3G3			0.01	FA3G3			0.50	FA3G3																
		0.10	A4G2Ga1			0.10	A4G2Ga1			0.10	A4G2Ga1																
		0.10	**M4A1F1G1Sg(3)1**																								
		0.45	**A2F(2)1G2S(6)1**			0.40	A2F(2)1G2S(6)1																				
		0.45	**FA2G2S(6)1**			1.20	FA2G2S(6)1																				
		0.05	**A2F1G1G(SO_4^{-2})1S(3)1**																								
		0.10	**FA2G1Ga1S(3)1**																								
		0.05	**FM5A1G1S(3)1**																								

UND (new)				NAN-1				ABS				ABS + BTG				ABS + BTG + BKF				ABS + BTG + BKF + AMF				ABS + BTG + BKF + AMF + GUH			
GU	% Area	%	Glycan	GU	% Area	%	Glycan	GU	% Area	%	Glycan	GU	% Area	%	Glycan	GU	% Area	%	Glycan	GU	% Area	%	Glycan	GU	% Area	%	Glycan
8.97	0.96	0.35	**M8**	9.00	1.95	0.60	M8	8.93	1.57	0.50	M8	9.00	0.43	0.38	M8	8.91	1.78	0.46	M8	8.98	0.66	0.46	M8	8.96	0.46	0.46	M8
		0.20	A4BF1G2			0.40	A4BF1G2			0.30	A4BF1G2							0.20	$A3G(SO_4^{-2})1G2GlcNAc2$			0.20	$A3G(SO_4^{-2})1G2GlcNAc2$				
		0.08	A3F2G2			0.10	A3F2G2			0.08	A3F2G2			0.05	A3F2G2			1.12	A3F2G2								
		0.05	A4G2Ga1			0.07	A4G2Ga1			0.05	A4G2Ga1																
						0.05	A3F1G3			0.12	A3F1G3																
		0.12	FA4G3S(2Ac)1			0.12	FA4G3S(2Ac)1			0.12	FA4G3S(2Ac)1																
		0.10	A4G3			0.50	A4G3			0.40	A4G3																
		0.06	**A2F2G2S(6)1**			0.07	A2F2G2S(6)1																				
						0.04	A3BG2S(6)1																				
9.10	1.93	0.37	**FA2G2Ga2**	9.14	1.85	0.36	FA2G2Ga2	9.08	1.74	0.30	FA2G2Ga2	9.11	1.14	0.30	FA2G2Ga2												
		0.32	FA4F2G1			0.32	FA4F2G1			0.25	FA4F2G1			0.25	FA4F2G1												
		0.32	$FA3F2G(SO_4^{-2})1G1$			0.32	$FA3F2G(SO_4^{-2})1G1$			0.25	$FA3F2G(SO_4^{-2})1G1$			0.25	$FA3F2G(SO_4^{-2})1G1$												
		0.03	A4F1G3S(2Ac)1			0.02	A4F1G3S(2Ac)1			0.01	A4F1G3S(2Ac)1																
		0.06	A3F1G3			0.03	A3F1G3			0.15	A3F1G3																
		0.06	**A4BG3**			0.38	A4BG3			0.48	A4BG3																
		0.12	**A2F2G2S(6)1**			0.10	A2F2G2S(6)1																				
		0.35	A3G2G(*)1Ga1S(6)1			0.32	A3G2G(*)1Ga1S(6)1																				
		0.30	A3G2G(*)1Ga1S(3)1																								
														0.34	FA3F(2)3G(*)1Ga1												

UND (new)				NAN-1				ABS				ABS + BTG				ABS + BTG + BKF				ABS + BTG + BKF + AMF				ABS + BTG + BKF + AMF + GUH			
GU	% Area	%	Glycan	GU	% Area	%	Glycan	GU	% Area		Glycan	GU	% Area	%	Glycan	GU	% Area	%	Glycan	GU	% Area	%	Glycan	GU	% Area	%	Glycan
9.16	1.80	0.20	M9	9.24	0.77	0.20	M9	9.21	1.17	0.10	M9	9.25	0.76	0.20	M9	9.25	1.68	0.23	M9	9.19	0.20	0.20	M9	9.26	0.26	0.26	M9
		0.20	A3F3G2			0.20	A3F3G2			0.35	A3F3G2			0.18	A3F3G2			0.45	A3F3G2								
		0.10	A4F2G2			0.10	A4F2G2			0.05	A4F2G2			0.05	A4F2G2			0.10	A4F2G2								
		0.10	A3F3G(SO_4^{-2})1G1			0.10	A3F3G(SO_4^{-2})1G1			0.05	A3F3G(SO_4^{-2})1G1			0.05	A3F3G(SO_4^{-2})1G1			0.10	A3F3G(SO_4^{-2})1G1								
		0.20	A4BF2G2			0.20	A4BF2G2			0.11	A4BF2G2			0.14	A4BF2G2			0.40	A4BF2G2								
		0.20	A4F2G2S(2Ac)1			0.20	A4F2G2S(2Ac)1			0.11	A4F2G2S(2Ac)1			0.14	A4F2G2S(2Ac)1			0.40	A4F2G2S(2Ac)1								
		0.90	FA2G2S(3)2																								
		0.10	A2F1G(SO_4^{-2})1G1S(6)1			0.10	A2F1G(SO_4^{-2})1G1S(6)1																				
		0.10	FA3F1G1Sg(3)1																								
		0.15	FA2F(2)1G(SO_4^{-2})1G1Sg(3)1																								
		0.10	A3F1G2S(6)1			0.10	A3F1G2S(6)1																				
		0.10	FA3G2S(6)1			0.10	FA3G2S(6)1																				
		0.05	FA2G2Ga1S(3)1																								
9.23	1.86	0.20	FA3F1G(SO_4^{-2})1G2	9.28	1.76	0.20	FA3F1G(SO_4^{-2})1G2			0.15	FA3F1G(SO_4^{-2})1G2																
		0.30	FA3F1G3S(2Ac)1			0.30	FA3F1G3S(2Ac)1			0.30	FA3F1G3S(2Ac)1																
		0.10	A3G3Ga1			0.10	A3G3Ga1			0.05	A3G3Ga1																
		0.05	FA3F1G3			0.10	FA3F1G3			0.12	FA3F1G3																
						0.05	FA3BG3			0.08	FA3BG3																
		0.28	FM5A1G1S(6)1			0.30	FM5A1G1S(6)1																				
		0.18	M5A1F1G1S(6)1			0.18	M5A1F1G1S(6)1																				
		0.05	FA3F1G2S(3)1																								
9.42	1.21	0.05	FA4F2G1	9.48	1.32	0.05	FA4F2G1	9.42	1.15	0.07	FA4F2G1	9.38	1.35	0.01	FA4F2G1												
		0.20	FA3F2G(SO_4^{-2})1G1			0.20	FA3F2G(SO_4^{-2})1G1			0.20	FA3F2G(SO_4^{-2})1G1			0.05	FA3F2G(SO_4^{-2})1G1												
		0.06	FA3G(SO_4^{-2})1G2GlcNAc2			0.07	FA3G(SO_4^{-2})1G2GlcNAc2			0.08	FA3G(SO_4^{-2})1G2GlcNAc2			0.25	FA3G(SO_4^{-2})1G2GlcNAc2										
		0.40	FA3F2G2			0.45	FA3F2G2			0.80	FA3F2G2			1.04	FA3F2G2												
						0.05	A2F2G2S(6)1																				
		0.50	A2F(2)2G1Ga1S(6)1			0.50	A2F(2)2G1Ga1S(6)1																				
9.54	5.53	3.51	M9	9.59	4.98	3.41	M9	9.53	3.95	3.45	M9	9.55	3.63	3.46	M9	9.46	3.92	3.45	M9	9.53	3.44	3.44	M9	9.52	3.44	3.44	M9
		0.04	A4F2G2			0.04	A4F2G2			0.05	A4F2G2			0.00	A4F2G2			0.05	A4F2G2								
		0.05	A3F3G(SO_4^{-2})1G1			0.05	A3F3G(SO_4^{-2})1G1			0.05	A3F3G(SO_4^{-2})1G1			0.06	A3F3G(SO_4^{-2})1G1			0.12	A3F3G(SO_4^{-2})1G1								
		0.10	A4BF2G2			0.10	A4BF2G2			0.10	A4BF2G2			0.11	A4BF2G2			0.30	A4BF2G2								
		0.05	A4F1G3			0.05	A4F1G3			0.05	A4F1G3																
										0.20	FA4BG3																
		0.05	A4G3Ga1			0.05	A4G3Ga1			0.05	A4G3Ga1																
		1.25	FA2G2S(6)2			1.18	FA2G2S(6)2																				
		0.20	FA2F2G1Sg(3)1																								
		0.06	A3F1G2S(3)2																								
		0.11	FA3G2S(3)2																								
		0.11	FA3F1G2S(6)1			0.10	FA3F1G2S(6)1																				

UND (new)				NAN-1				ABS				ABS + BTG				ABS + BTG + BKF				ABS + BTG + BKF + AMF				ABS + BTG + BKF + AMF + GUH			
GU	% Area	%	Glycan	GU	% Area	%	Glycan	GU	% Area	%	Glycan	GU	% Area	%	Glycan	GU	% Area	%	Glycan	GU	% Area	%	Glycan	GU	% Area	%	Glycan
9.68	3.21	0.60	**M9**	9.73	3.28	0.60	M9	9.69	1.43	0.43	M9	9.70	1.62	0.42	M9	9.61	0.40	0.40	M9	9.69	0.37	0.37	M9	9.68	0.35	0.35	M9
		0.05	FA3F3G2			0.12	FA3F3G2			0.28	FA3F3G2			0.27	FA3F3G2												
		0.10	**FA4F2G2**			0.10	FA4F2G2			0.10	FA4F2G2			0.05	FA4F2G2												
		0.06	FA3F3G(SO_4^{-2})1G1			0.06	FA3F3G(SO_4^{-2})1G1			0.06	FA3F3G(SO_4^{-2})1G1			0.05	FA3F3G(SO_4^{-2})1G1												
		0.35	FA4BF2G2			0.35	FA4BF2G2			0.28	FA4BF2G2			0.27	FA4BF2G2												
		0.35	FA4F2G2S(2Ac)1			0.35	FA4F2G2S(2Ac)1			0.28	FA4F2G2S(2Ac)1			0.27	FA4F2G2S(2Ac)1												
		0.05	**FA2G(SO_4^{-2})1G1S(3)2**											0.29	A3F(2)2F(3)1G1G(*)1Ga1												
						0.05	FA3F1G1Sg(6)1																				
		0.35	**FM5A1G1S(6)2**			0.40	FM5A1G1S(6)2																				
		0.05	**A3G3S(6)1S(1Ac)1**			0.05	A3G3S(6)1S(1Ac)1																				
		0.05	**FA2F(2)2G1Sg(3)1**																								
		0.15	**M5A1F1G1S(6)2**			0.15	M5A1F1G1S(6)2																				
		0.10	**FA2G2Ga1S(6)1**			0.10	FA2G2Ga1S(6)1																				
		0.35	**FA2F2G2S(6)1**			0.35	FA2F2G2S(6)1																				
		0.60	A3G2S(6)2			0.60	A3G2S(6)2																				
9.91	1.70			9.97	1.70			10.00	0.91			9.94	0.51			9.87	0.30	0.20	A4F1G(SO_4^{-2})1G2GlcNAc2	9.91	0.16	0.16	A4F1G(SO_4^{-2})1G2GlcNAc2	9.68	0.35		
		0.10	A4F3G2			0.10	A4F3G2			0.07	A4F3G2			0.07	A4F3G2			0.10	A4F3G2								
		0.10	FA4F2G2			0.10	FA4F2G2			0.08	FA4F2G2			0.18	FA4F2G2												
		0.35	FA3F3G(SO_4^{-2})1G1			0.40	FA3F3G(SO_4^{-2})1G1			0.28	FA3F3G(SO_4^{-2})1G1			0.18	FA3F3G(SO_4^{-2})1G1												
		0.10	FA4BF2G2			0.10	FA4BF2G2			0.08	FA4BF2G2			0.08	FA4BF2G2												
		0.15	FA4BF1G3			0.15	FA4BF1G3			0.10	FA4BF1G3																
		0.05	**A2F1G1Sg(6)1S(6)1**			0.05	A2F1G1Sg(6)1S(6)1																				
		0.05	**FA3F1G1S(3)1Sg(3)1**																								
		0.05	**A3F1G2S(6)2**			0.05	A3F1G2S(6)2																				
						0.05	A3F1G2Sg(6)1																				
						0.02	FA3G2Sg(6)1																				
		0.05	**FA3G2S(6)2**			0.05	FA3G2S(6)2																				
		0.05	**FA3BG2S(3)2**																								
		0.05	**FA4G2S(3)2**																								
		0.05	**A3BG3Sg(3)1**																								
		0.15	**FA3G3S(6)1**			0.18	FA3G3S(6)1																				
		0.05	**A3F1G3S(3)1**																								
		0.35	A3F(2)1G2G(*)1Ga1			0.45	A3F(2)1G2G(*)1Ga1			0.30	A3F(2)1G2G(*)1Ga1																

UND (new)				NAN-1				ABS				ABS + BTG				ABS + BTG + BKF				ABS + BTG + BKF + AMF				ABS + BTG + BKF + AMF + GUH			
GU	% Area	%	Glycan	GU	% Area	%	Glycan	GU	% Area		Glycan	GU	% Area	%	Glycan	GU	% Area	%	Glycan	GU	% Area	%	Glycan	GU	% Area	%	Glycan
10.10	2.22			10.16	1.71			10.13	0.77			10.10	0.14	0.14	A4F1G(SO_4^{-2})1G2GlcNAc2	10.04	0.11	0.11	A4F1G(SO_4^{-2})1G2GlcNAc2	10.15	0.13	0.13	A4F1G(SO_4^{-2})1G2GlcNAc2	10.26	0.41		
		0.15	**FA3F2G3**			0.63	FA3F2G3			0.62	FA3F2G3																
		0.10	FA4BF1G3			0.25	FA4BF1G3			0.15	FA4BF1G3																
		0.51	**A2G2S(6)3**			0.70	A2G2S(6)3																				
		0.05	**FA2G(SO_4^{-2})1G1S(6)2**			0.08	FA2G(SO_4^{-2})1G1S(6)2																				
		0.20	**A4G3Sg(3)1**																								
						0.05	FA2G2Ga1Sg(6)1																				
		0.20	**FA2G2S(3)1S(2Ac)1**																								
		0.20	**FA2G2S(3)1S(1Ac)1**																								
		0.81	**FA2G2Sg(3)1S(6)1**																								
10.25	1.01	**0.41**	**M9Glc1**	10.31	1.24	0.48	M9Glc1	10.27	1.10	0.35	M9Glc1	10.28	0.43	0.43	M9Glc1	10.21	0.35	0.25	M9Glc1	10.28	0.33	0.23	M9Glc1			0.41	M9Glc1
		0.10	**FA4G3Ga1**			0.10	FA4G3Ga1			0.10	FA4G3Ga1							0.10	A4F2G(SO_4^{-2})1G2GlcNAc2			0.10	A4F2G(SO_4^{-2})1G2GlcNAc2				
										0.25	A4F1G4																
		0.15	A4G4Ga1			0.16	A4G4Ga1			0.15	A4G4Ga1																
						0.02	A3F3G2S(6)1																				
						0.02	FA3F2G2S(6)1																				
		0.35	A3F(2)2G2G(*)1Ga1			0.46	A3F(2)2G2G(*)1Ga1			0.25	A3F(2)2G2G(*)1Ga1																
10.40	1.25	0.09	**M9Glc1**	10.44	0.68	0.10	M9Glc	10.48	0.66	0.10	M9Glc1	10.48	0.35	0.10	M9Glc1	10.33	0.12	0.12	M9Glc1	10.42	0.11	0.11	M9Glc1	10.52	0.21	0.21	M9Glc1
														0.20	FA4F1G(SO_4^{-2})1G2GlcNAc2												
		0.04	FA4F3G2			0.05	FA4F3G2			0.05	FA4F3G2			0.05	FA4F3G2												
										0.10	FA4F2G3																
		0.04	A4BF1G4			0.20	A4BF1G4			0.20	A4BF1G4																
		0.40	**FA2F1G1Sg(6)1S(6)1**			0.52	FA2F1G1Sg(6)1S(6)1																				
		0.04	**A2F1G2S(6)2**	10.54	0.78	0.05	A2F1G2S(6)2	10.59	0.18																		
		0.25	**FA2G2S(6)3**			0.29	FA2G2S(6)3																				
		0.04	**A2F1G(SO_4^{-2})1G1S(6)2**			0.05	A2F1G(SO_4^{-2})1G1S(6)2																				
		0.05	**FA3F1G1S(3)1Sg(6)1**																								
		0.05	**A3BG2Sg(3)2**																								
		0.05	**A3G2Ga1S(6)2**			0.05	A3G2Ga1S(6)2																				
		0.05	**A3G3S(6)2**			0.05	A3G3S(6)2																				
		0.05	**FA3F1G3S(6)1**			0.05	FA3F1G3S(6)1																				
		0.05	**FA3BG3Sg(3)1**																								
		0.05	**FA3F2G2S(6)1**			0.05	FA3F2G2S(6)1																				
										0.39	A3F(2)2G2G(*)1Ga1																

UND (new)				NAN-1				ABS				ABS + BTG				ABS + BTG + BKF				ABS + BTG + BKF + AMF				ABS + BTG + BKF + AMF + GUH			
GU	% Area	%	Glycan	GU	% Area	%	Glycan	GU	% Area	%	Glycan	GU	% Area	%	Glycan	GU	% Area	%	Glycan	GU	% Area	%	Glycan	GU	% Area	%	Glycan
10.60	0.58	0.06	A3BF3G3	10.69	0.53	0.05	A3BF3G3	10.75	0.64	0.05	A3BF3G3	10.71	0.28	0.07	A3BF3G3	10.57	0.84	0.42	A3BF3G3								
		0.06	A3F2G3S1-2Ac			0.05	A3F2G3S1-2Ac			0.05	A3F2G3S1-2Ac			0.06	A3F2G3S1-2Ac			0.42	A3F2G3S1-2Ac								
														0.15	FA4F2G(SO_4^{-2})1G2GlcNAc2												
		0.34	**FA3F(2)3G3**			0.38	FA3F(2)3G3			0.54	FA3F(2)3G3																
		0.06	**A2F2G2S(6)1Sg(3)1**																								
		0.06	**FA3F1G2S(3)2**																								
						0.05	FA3F3G2S(6)1																				
10.83	1.24			10.84	1.48	0.12	A4F3G3	10.86	0.34	0.07	A4F3G3	10.84	0.07	0.07	A4F3G3	10.82	0.73	0.73	A4F3G3								
		0.40	FA3G(SO_4^{-2})1G2Lac2			0.35	FA3G(SO_4^{-2})1G2Lac2			0.27	FA3G(SO_4^{-2})1G2Lac2																
		0.05	**A4G2Sg(3)2**																								
		0.14	**FA3F1G2S(6)2**			0.13	FA3F1G2S(6)2																				
		0.35	**FA2F2G2S(6)2**			0.30	FA2F2G2S(6)2																				
		0.20	**FA3G3S(6)2**			0.18	FA3G3S(6)2																				
		0.10	**A3F1G3S(6)2**			0.10	A3F1G3S(6)2																				
						0.30	A4BG3Sg(6)1																				
11.02	2.64	0.01	A4F4G3	11.10	1.20	0.12	A4F4G3	11.04	0.88	0.12	A4F4G3	11.02	0.87	0.11	A4F4G3	11.13	0.51	0.51	A4F4G3								
		0.70	FA3BF3G3			0.38	FA3BF3G3			0.38	FA3BF3G3			0.38	FA3BF3G3												
		0.70	FA3F2G3S(2Ac)1			0.38	FA3F2G3S(2Ac)1			0.38	FA3F2G3S(2Ac)1			0.38	FA3F2G3S(2Ac)1												
		0.11	**A3F3G2Sg(6)1**			0.11	A3F3G2Sg(6)1																				
		0.10	**FA3F2G2Sg(6)1**			0.10	FA3F2G2Sg(6)1																				
		0.26	**FA3F3G2Sg(3)1**																								
		0.11	**FA3F2G3S(6)1**			0.11	FA3F2G3S(6)1																				
		0.65	**A2F(2)2G1Ga1Sg(3)2**																								
11.19	1.50	1.50	FA4F3G3	11.2	0.36	0.43	FA4BG3Sg(6)1	11.20	0.23																		
				11.34	0.87	0.80	FA4F3G3	11.30	0.43	0.66	FA4F3G3			0.76	FA4F3G3												
11.41	0.33	0.06	**A3F1G2S(3)2Sg(6)1**	11.46	0.42			11.37	0.32			11.24	0.76														
		0.03	**FA3G2S(3)2Sg(6)1**																								
		0.06	**A3G3S(6)3**			0.05	A3G3S(6)3																				
		0.06	**FA3F1G3S(6)2**			0.05	FA3F1G3S(6)2																				
		0.06	**FA3F2G2S(3)1Sg(3)1**																								
		0.06	**FA3F(2)3G3S(3)1**																								
						0.32	FA3F(2)3G2G(*)1Ga1			0.32	FA3F(2)3G2G(*)1Ga1																

UND (new)				NAN-1				ABS				ABS + BTG				ABS + BTG + BKF				ABS + BTG + BKF + AMF				ABS + BTG + BKF + AMF + GUH			
GU	% Area	%	Glycan	GU	% Area	%	Glycan	GU	% Area	%	Glycan	GU	% Area	%	Glycan	GU	% Area	%	Glycan	GU	% Area	%	Glycan	GU	% Area	%	Glycan
11.52	0.78	0.05	A4F4G4	11.55	0.66	0.05	A4F4G4	11.49	0.25	0.10	A4F4G4	11.66	0.26	0.11	A4F4G4	11.53	0.58	0.35	A4F4G4								
		0.15	**FA4F4G3**			0.15	FA4F4G3			0.15	FA4F4G3			0.15	FA4F4G3			0.23	A4F3G(SO$_4^{-2}$)1G2GlcNAc3				A4F3G(SO$_4^{-2}$)1G2GlcNAc3				
		0.23	**FA2G2S(6)4**			0.21	FA2G2S(6)4																*this glycan is present but peak has not been integrated*				
		0.02	**A3BG2Sg(3)2S(6)1**																								
		0.02	**A4G2Sg(3)2S(3)1**																								
		0.02	**FA2G2Ga1Sg(3)1Sg(6)1**																								
		0.10	**FA2F2G2S(6)3**			0.10	FA2F2G2S(6)3																				
		0.02	**A3F3G2Sg(3)1S(6)1**																								
		0.02	**FA3F2G2Sg(3)1S(6)1**																								
		0.10	**A4F1G3Sg(6)1**			0.10	A4F1G3Sg(6)1																				
		0.05	**FA4F2G3S(6)1**			0.05	FA4F2G3S(6)1																				
11.64	1.26	0.22	A4F1G(SO$_4^{-2}$)1G2Lac2	11.67	0.21	0.20	A4F1G(SO$_4^{-2}$)1G2Lac2	11.61	0.26	0.14	A4F1G(SO$_4^{-2}$)1G2Lac2																
		0.15	**FA3G3S(6)3**			0.13	FA3G3S(6)3																				
		0.05	**A3F1G3S(3)3**																								
		0.18	**A4BG3Sg(3)2**																								
		0.15	**FA3F3G2Sg(6)1**	11.85	0.58	0.13	FA3F3G2Sg(6)1	11.89	0.16																		
		0.18	**FA3F2G3S(3)2**																								
		0.33	A3F(2)2F(3)1G2G(*)1Ga1			0.33	A3F(2)2F(3)1G2G(*)1Ga1			0.28	A3F(2)2F(3)1G2G(*)1Ga1																
11.95	0.45	0.15	FA4F4G4	12.06	0.66	0.20	FA4F4G4	12.01	0.51	0.25	FA4F4G4	11.89	0.20	0.20	FA4F4G4												
		0.20	FA4F1G(SO$_4^{-2}$)1G2Lac2			0.35	FA4F1G(SO$_4^{-2}$)1G2Lac2			0.26	FA4F1G(SO$_4^{-2}$)1G2Lac2																
		0.05	**FA3BG3S(6)3**			0.11	FA3BG3S(6)3																				
		0.05	**FA3F3G2Sg(3)1S(6)1**																								

UND (new)				NAN-1				ABS				ABS + BTG				ABS + BTG + BKF				ABS + BTG + BKF + AMF				ABS + BTG + BKF + AMF + GUH			
GU	% Area	%	Glycan	GU	% Area	%	Glycan	GU	% Area	%	Glycan	GU	% Area	%	Glycan	GU	% Area	%	Glycan	GU	% Area	%	Glycan	GU	% Area	%	Glycan
12.06	1.36	0.07	junk	12.17	0.40	0.07	junk	12.12	0.18	0.05	junk	12.11	0.08	0.08	junk				*junk present, not integrated*				*junk present, not integrated*				*junk present, not integrated*
		0.17	**FA2BG2Sg(6)2S(6)1**			0.17	FA2BG2Sg(6)2S(6)1																				
		0.12	**A3F1G3S(6)3**			0.12	A3F1G3S(6)3																				
		0.22	**A4BG3Sg(3)1Sg(6)1**																								
		0.17	**A3F3G2Sg(6)1S(6)1**	12.37	0.31	0.17	A3F3G2Sg(6)1S(6)1	12.29	0.06																		
		0.22	**FA3F2G2Sg(6)1S(3)1**																								
		0.17	**FA3F2G3S(6)2**			0.18	FA3F2G3S(6)2																				
		0.22	**A4BF1G4Sg(3)1**																								
12.62	1.33	0.69	FA4F2G(SO_4^{-2})1G2Lac2	12.48	0.57	0.44	FA4F2G(SO_4^{-2})1G2Lac2	12.43	0.14	0.44	FA4F2G(SO_4^{-2})1G2Lac2	12.50	0.02														
		0.39	**FA4BG3Sg(6)1Sg(3)1**																								
		0.25	**FA3F(2)3G3S(6)2**			0.13	FA3F(2)3G3S(6)2	12.57	0.11																		
12.73	0.55	0.55	FA4F4G(SO_4^{-2})1G2GlcNAc3	12.80	0.60	0.60	FA4F4G(SO_4^{-2})1G2GlcNAc3	12.75	0.19	0.19	FA4F4G(SO_4^{-2})1G2GlcNAc3	12.71	0.17	0.17	FA4F4G(SO_4^{-2})1G2GlcNAc3				A4F3G(SO_4^{-2})1G3GlcNAc4								
																			this glycan is present but peak has not been integrated								
12.87	0.45	0.45	FA3F(2)3G2G(*)1Ga1Sg(3)1																								
13.04	0.30	0.30	FA3F(2)3G2G(*)1Ga1Sg(3)1																								
13.16	0.51	0.34	FA4F3G(SO_4^{-2})1G3GlcNAc4	13.22	0.50	0.28	FA4F3G(SO_4^{-2})1G3GlcNAc4	13.19	0.17	0.26	FA4F3G(SO_4^{-2})1G3GlcNAc4	13.27	0.24	0.24	FA4F3G(SO_4^{-2})1G3GlcNAc4												
		0.17	**A4F4G3Sg(3)1S(3)1**																								
13.29	0.53	0.10	**FA4F4G4S(6)1**			0.05	FA4F4G4S(6)1																				
13.56	0.69	0.05	**FA4F2G3S(6)3**	13.76	0.42	0.05	FA4F2G3S(6)3	14.04	0.09																		
		0.15	**A4F3G3S(3)3**																								
		0.15	**A4F4G4S(6)2**			0.12	A4F4G4S(6)2																				
		0.77	A3F(2)2G2G(*)1Ga1Sg(6)2			0.42	A3'F(2)2G2G(*)1Ga1Sg(6)2																				
14.58	0.74	0.20	junk	14.91	0.25	0.10	junk	14.86	0.05	0.05	junk				*junk present, not integrated*				*junk present, not integrated*				*junk present, not integrated*				*junk present, not integrated*
		0.54	**A4F1G4S(6)4**			0.15	A4F1G4S(6)4																				

Appendix XI: Mass data for spinal cord *N*-glycans

Undigested *N*-glycans were analysed using a Waters Xevo G2 Q-TOF mass spectrometer in negative mode. For most glycans, the double-charged ion $[M-2H]^{-2}$ was the most abundant and is what is reported here. In some cases the mono-charged $[M-H]^{-1}$ or triple-charged $[M-3H]^{-3}$ ion was more abundant. The theoretical mass for the glycan with 2AB attached to the reducing end was obtained from the GlycoWorkbench 2 program. The theoretical mass was then searched for in the spinal cord glycan data using MassLynx software. To accept a glycan structure as being present, an error of < 20ppm comparing experimental to theoretical m/z value was necessary, as well as the characteristic ladder formation of spectal peaks. m/z, mass/charge; ppm, parts per million; nd, not detected. Structures marked with * indicates the presence of isomers for that mass value.

GU	% Area	Glycan	Experimental m/z	Theoretical m/z	Error (ppm)	Ion	
4.25	0.31	**M3**	1029.3994	1029.3893	9.81	$[M-H]^{-1}$	
4.75	1.02	**M3B**	615.7351	615.7307	7.15	$[M-2H]^{-2}$	*
		A1	615.7351	615.7307	7.15	$[M-2H]^{-2}$	*
		FM3	1175.4475	1175.4472	0.26	$[M-H]^{-1}$	
5.16	0.16	A1B	nd	-	-	-	
		M4	1191.4563	1191.4421	11.92	$[M-H]^{-1}$	*
5.33	0.89	A1G1S(2Ac)1	nd	-	-	-	
		A2	nd	-	-	-	
		M4	1191.4563	1191.4421	11.92	$[M-H]^{-1}$	*
		A2B	818.8066	818.8100	4.15	$[M-2H]^{-2}$	*
		FA1	1378.5193	1378.5265	5.22	$[M-H]^{-1}$	
5.62	0.31	**M4A1**	696.7487	696.7571	12.06	$[M-2H]^{-2}$	*
		FA1B	1581.5890	1581.6059	10.69	$[M-H]^{-1}$	*
		FM4	1337.5261	1337.5000	19.51	$[M-H]^{-1}$	
		A1G1	696.7487	696.7571	12.06	$[M-2H]^{-2}$	*
5.84	4.69	A1G(SO_4^{-2})1	nd	-	-	-	
		M4A1	696.7487	696.7571	12.06	$[M-2H]^{-2}$	*
		A2G1S(1Ac)1	nd	-	-	-	
		A3	818.8066	818.8100	4.15	$[M-2H]^{-2}$	*
		A1F1G1S(2Ac)1	nd	-	-	-	
		FA1G1S(2Ac)1	nd	-	-	-	
		FA2	1581.5890	1581.6059	10.69	$[M-H]^{-1}$	*
		FA2B	1784.6901	1784.6853	2.69	$[M-H]^{-1}$	*
		FA1G1S(1Ac)1	nd	-	-	-	
6.19	6.43	**M5**	676.2433	676.2438	0.74	$[M-2H]^{-2}$	
		A2G(SO_4^{-2})1	nd	-	-	-	
		A3G1S(2Ac)1	nd	-	-	-	
		FA1G(SO_4^{-2})1	809.7762	809.7644	14.57	$[M-2H]^{-2}$	*
		FM4A1	769.7905	769.7860	5.85	$[M-2H]^{-2}$	*
		A1F(2)1G1S(1Ac)1	nd	-	-	-	
		A2G1	798.2964	798.2968	0.50	$[M-2H]^{-2}$	
		FA1G1	769.7905	769.7860	5.85	$[M-2H]^{-2}$	*
6.24	8.03	**A3B**	920.3376	920.3497	13.15	$[M-2H]^{-2}$	*
		A2G(SO_4^{-2})1	nd	-	-	-	
		A1F1G1	769.7905	769.7860	5.85	$[M-2H]^{-2}$	*
		FA1G(SO_4^{-2})1	809.7762	809.7644	14.57	$[M-2H]^{-2}$	*
		FM4A1	769.7905	769.7860	5.85	$[M-2H]^{-2}$	*
		FA2G1S(2Ac)1	nd	-	-	-	
		FA3	1784.6901	1784.6853	2.69	$[M-H]^{-1}$	*
		FA1F1G1S(2Ac)1	nd	-	-	-	
		A1F(2)1G(SO_4^{-2})1	809.7762	809.7644	14.57	$[M-2H]^{-2}$	*
		FA1BG1	871.3260	871.3257	0.34	$[M-2H]^{-2}$	*
		M4A1G1	777.7891	777.7835	7.20	$[M-2H]^{-2}$	*

GU	% Area	Glycan	Experimental m/z	Theoretical m/z	Error (ppm)	Ion	
6.61	0.50	**M5A1**	777.7891	777.7835	7.20	$[M-2H]^{-2}$	*
		A3G(SO_4^{-2})1	nd	-	-	-	
		A4	920.3376	920.3497	13.15	$[M-2H]^{-2}$	*
		FA2G1	871.3260	871.3257	0.34	$[M-2H]^{-2}$	*
6.65	1.02	**M5A1**	777.7891	777.7835	7.20	$[M-2H]^{-2}$	*
		A3G(SO_4^{-2})1	nd	-	-	-	
		FM5	749.2676	749.2728	6.94	$[M-2H]^{-2}$	
		FA2G(SO_4^{-2})1	911.2883	911.3041	17.34	$[M-2H]^{-2}$	*
		M4A1G1	777.7891	777.7835	7.20	$[M-2H]^{-2}$	*
		A2G2S(1Ac)1	nd	-	-	-	
		A3G1	899.8459	899.8365	10.45	$[M-2H]^{-2}$	
		FA2BG1	972.8575	972.8654	8.12	$[M-2H]^{-2}$	*
6.79	0.29	**A1G1Ga1**	777.7891	777.7835	7.20	$[M-2H]^{-2}$	*
		A4G1S(2Ac)1	nd	-	-	-	
		FA2G(SO_4^{-2})1	911.2883	911.3041	17.34	$[M-2H]^{-2}$	*
		A2G2	879.3173	879.3232	6.71	$[M-2H]^{-2}$	*
6.95	1.75	**M6**	1515.5414	1515.5477	4.16	$[M-H]^{-1}$	*
		A1G1Ga1	777.7891	777.7835	7.20	$[M-2H]^{-2}$	*
		A4G(SO_4^{-2})1	nd	-	-	-	
		A4G1S(1Ac)1	nd	-	-	-	
		A2F1G1	871.3139	871.3257	13.54	$[M-2H]^{-2}$	*
		FM5A1	1702.6091	1702.6322	13.57	$[M-H]^{-1}$	*
		FA4	993.3903	993.3787	11.68	$[M-2H]^{-2}$	
		A3F(2)1G1S(2Ac)1	1160.4202	1160.4237	3.02	$[M-2H]^{-2}$	
		A2G(SO_4^{-2})1G1	nd	-	-	-	
		FM4A1G1	1702.6091	1702.6322	13.57	$[M-H]^{-1}$	*
		A2BG2	980.8702	980.8629	7.44	$[M-2H]^{-2}$	*
7.08	7.07	**M6D1,D3**	1515.5414	1515.5477	4.16	$[M-H]^{-1}$	*
		A4G(SO_4^{-2})1	nd	-	-	-	
		A2F1G1	871.3139	871.3257	13.54	$[M-2H]^{-2}$	*
		A2BF1G1	972.8639	972.8654	1.54	$[M-2H]^{-2}$	*
		FM5A1	1702.6091	1702.6322	13.57	$[M-H]^{-1}$	*
		FA4B	nd	-	-	-	
		A3BG1	1001.3831	1001.3761	6.99	$[M-2H]^{-2}$	*
		FM4A1G1	1702.6091	1702.6322	13.57	$[M-H]^{-1}$	*
		FA3G1	972.8575	972.8654	8.12	$[M-2H]^{-2}$	*

GU	% Area	Glycan	Experimental m/z	Theoretical m/z	Error (ppm)	Ion	
7.20	1.41	**M6**	1515.5414	1515.5477	4.16	$[M-H]^{-1}$	*
		A2G1Ga1	879.3173	879.3232	6.71	$[M-2H]^{-2}$	*
		M4A1F1G1	1702.6345	1702.6322	1.35	$[M-H]^{-1}$	*
		A3F1G1	972.8639	972.8654	1.54	$[M-2H]^{-2}$	*
		A2F1G2S(2Ac)1	nd	-	-	-	
		FA1G1Ga1	1702.6091	1702.6322	13.57	$[M-H]^{-1}$	*
		FA4G1S(2Ac)1	nd	-	-	-	
		A3BG1	1001.3831	1001.3761	6.99	$[M-2H]^{-2}$	*
		FA3G1	972.8575	972.8654	8.12	$[M-2H]^{-2}$	*
		M5A1G1	858.7972	858.8099	14.79	$[M-2H]^{-2}$	*
		A4G1	1001.3831	1001.3761	6.99	$[M-2H]^{-2}$	*
7.37	2.13	**M6**	1515.5414	1515.5477	4.16	$[M-H]^{-1}$	*
		A2G1Ga1	879.3173	879.3232	6.71	$[M-2H]^{-2}$	*
		M4A1F1G1	1702.6345	1702.6322	1.35	$[M-H]^{-1}$	*
		A3F1G1	972.8639	972.8654	1.54	$[M-2H]^{-2}$	*
			-	-	-	-	
		FA2F1G1	944.3533	944.3547	1.48	$[M-2H]^{-2}$	*
			-	-	-	-	
		M4A1F(2)1G1	1702.6345	1702.6322	1.35	$[M-H]^{-1}$	*
		M5A1G1	858.7972	858.8099	14.79	$[M-2H]^{-2}$	*
		A3G(SO_4^{-2})1G1	nd	-	-	-	
		A4G1	1001.3831	1001.3761	6.99	$[M-2H]^{-2}$	*
		FA3G2S(2Ac)1	nd	-	-	-	
		A3G2	980.8702	980.8629	7.44	$[M-2H]^{-2}$	*
		A2F(2)1G2	952.3492	952.3521	3.05	$[M-2H]^{-2}$	*
		A2G1Sg(3)1	951.8430	951.8419	1.16	$[M-2H]^{-2}$	
7.56	1.44	**M6A1**	858.7972	858.8099	14.79	$[M-2H]^{-2}$	*
		A2F2G1	944.3533	944.3547	1.48	$[M-2H]^{-2}$	*
		A2F1G2S(1Ac)1	nd	-	-	-	
		FM6D1,D3	830.2964	830.2992	3.37	$[M-2H]^{-2}$	
		FA2G2	952.3429	952.3521	9.66	$[M-2H]^{-2}$	*
		A2F2G1	944.3533	944.3547	1.48	$[M-2H]^{-2}$	*
		A2F1G2S(1Ac)1	nd	-	-	-	
		A4G2S(2Ac)1	nd	-	-	-	
		FA3BG1	1074.4230	1074.4051	16.66	$[M-2H]^{-2}$	*
		FA2BG2	1053.8770	1053.8918	14.04	$[M-2H]^{-2}$	*

GU	% Area	Glycan	Experimental m/z	Theoretical m/z	Error (ppm)	Ion	
7.67	3.64	**A3G1Ga1**	980.8573	980.8629	5.71	$[M-2H]^{-2}$	*
		FA2G1Ga1	952.3492	952.3521	3.05	$[M-2H]^{-2}$	*
		FM4A1F1G1	923.8314	923.8414	10.82	$[M-2H]^{-2}$	*
		FA3F1G1	1045.8892	1045.8944	4.97	$[M-2H]^{-2}$	
		FA2F1G2S(2Ac)1	nd	-	-	-	
		FM4A1F(2)1G1	923.8314	923.8414	10.82	$[M-2H]^{-2}$	*
		A4G(SO_4^{-2})1G1	nd	-	-	-	
		A4G2S(1Ac)1	nd	-	-	-	
		FM5A1G1	931.8528	931.8389	14.92	$[M-2H]^{-2}$	*
		FA4G1	1074.4230	1074.4051	16.66	$[M-2H]^{-2}$	*
		A3F1G2S(2Ac)1	nd	-	-	-	
		A2F(2)1G2	944.3533	944.3547	1.48	$[M-2H]^{-2}$	*
		M4A1G1S(6)1	923.3203	923.3312	10.13	$[M-2H]^{-2}$	*
		FA2G1S(6)1	1016.8694	1016.8734	3.93	$[M-2H]^{-2}$	*
7.78	0.81	**M7**	838.2878	838.2966	10.50	$[M-2H]^{-2}$	*
		FA2G1Ga1	952.3492	952.3521	3.05	$[M-2H]^{-2}$	*
		FM4A1F1G1	923.8314	923.8414	10.82	$[M-2H]^{-2}$	*
		FA3F1G1	923.8314	923.8414	10.82	$[M-2H]^{-2}$	*
		FA2F1G2S(2Ac)1	nd	-	-	-	
		A1F1G1S(6)1	915.3171	915.3337	18.14	$[M-2H]^{-2}$	
		FA2BG1S(3)1	1118.4135	1118.4131	0.36	$[M-2H]^{-2}$	*
		FA3G1S(3)1	1118.3997	1118.4131	11.98	$[M-2H]^{-2}$	*
7.84	1.19	**FA2F2G1**	1017.3992	1017.3836	15.33	$[M-2H]^{-2}$	*
		FA2F1G2S(1Ac)1	nd	-	-	-	
		FA2F2G(SO_4^{-2})1	1057.3687	1057.362	6.34	$[M-2H]^{-2}$	
		FA2F(2)2G1	1017.3992	1017.3836	15.33	$[M-2H]^{-2}$	*
		FA2G(SO_4^{-2})1S(6)1	1056.8419	1056.8518	9.37	$[M-2H]^{-2}$	*
		A3G1S(6)1	1045.3719	1045.3842	11.77	$[M-2H]^{-2}$	
		FA2BG1S(6)1	1118.3997	1118.4131	11.98	$[M-2H]^{-2}$	*
		FA3G(SO_4^{-2})1S(3)1	1158.3950	1158.3915	3.02	$[M-2H]^{-2}$	
		A2F1G1S(3)1	1016.8890	1016.8734	15.34	$[M-2H]^{-2}$	*
		FA3G1S(3)1	1118.3997	1118.4131	11.98	$[M-2H]^{-2}$	*

GU	% Area	Glycan	Experimental m/z	Theoretical m/z	Error (ppm)	Ion	
7.95	7.62	**M7 /M7 D1**	838.2878	838.2966	10.50	$[M-2H]^{-2}$	*
		A4F1G1	1074.4095	1074.4051	4.10	$[M-2H]^{-2}$	*
		M5A1F1G1	931.8528	931.8389	14.92	$[M-2H]^{-2}$	*
		A4BF1G1	-	-	-	-	
		FM6A1	931.8528	931.8389	14.92	$[M-2H]^{-2}$	*
		M7	838.2878	838.2966	10.50	$[M-2H]^{-2}$	*
		FA2F1G2S(1Ac)1	nd	-	-	-	
		A2F2G2	1025.3696	1025.3811	11.22	$[M-2H]^{-2}$	
		FA2F(2)2G(SO_4^{-2})1G1	nd	-	-	-	
		A4G(SO_4^{-2})1G1	nd	-	-	-	
		FM5A1G1	931.8528	931.8389	14.92	$[M-2H]^{-2}$	*
		A2G2Ga1	960.3344	960.3496	15.83	$[M-2H]^{-2}$	
		A3F1G2	1053.8770	1053.8918	14.04	$[M-2H]^{-2}$	*
		FA4G2S(2Ac)1	nd	-	-	-	
		A3BG2	nd	-	-	-	
		A1F(2)1G(SO_4^{-2})1S(6)1	955.3136	955.3122	1.47	$[M-2H]^{-2}$	
		FA2G1Sg(3)1	1024.8640	1024.8709	6.73	$[M-H]^{-2}$	*
		A2F1G(SO_4^{-2})1S(6)1	1056.8352	1056.8518	15.71	$[M-2H]^{-2}$	*
		A2G2S(6)1	1024.8640	1024.8709	6.73	$[M-H]^{-2}$	*
		FM4A1G1S(6)1	996.3596	996.3602	0.60	$[M-2H]^{-2}$	*
		M4A1F(2)1G1S(3)1	996.3596	996.3602	0.60	$[M-2H]^{-2}$	*
		FA3G1S(3)1	1118.4135	1118.4131	0.36	$[M-2H]^{-2}$	*
		FA1G1Sg(6)1	923.3203	923.3312	10.13	$[M-2H]^{-2}$	*
8.30	1.45	A4G1Ga1	nd	-	-	-	
		FA2F(2)2G1	1017.3992	1017.3836	15.33	$[M-2H]^{-2}$	*
		FA3F(2)3G1S(2Ac)1	nd	-	-	-	
		A3G(SO_4^{-2})1G2	nd	-	-	-	
		A4G2	nd	-	-	-	
		A4BG2	nd	-	-	-	
		FA3BG1S(3)1	1219.9418	1219.9528	9.02	$[M-2H]^{-2}$	*

GU	% Area	Glycan	Experimental m/z	Theoretical m/z	Error (ppm)	Ion	
8.36	2.99	**FA4F1G1**	1147.4131	1147.4341	18.30	$[M-2H]^{-2}$	
		FM5A1F1G1	1004.8713	1004.8678	3.48	$[M-2H]^{-2}$	
		FA4BF1G1	nd	-	-	-	
		A4G3S(2Ac)1	nd	-	-	-	
		A3G2Ga1	nd	-	-	-	
		FA2G2Ga1	1033.3843	1033.3785	5.61	$[M-H]^{-2}$	*
		FA3F1G2	1126.9001	1126.9208	18.37	$[M-H]^{-2}$	*
		FA3F(2)1G(SO_4^{-2})1G1	nd	-	-	-	
		FA4BF(2)1G1	nd	-	-	-	
		A3G3	nd	-	-	-	
		FA1F1G1Sg(3)1	996.3596	996.3602	0.60	$[M-H]^{-2}$	*
		FA3G1S(6)1	1118.4135	1118.4131	0.36	$[M-H]^{-2}$	*
		A2G1Ga1S(6)1	1024.8640	1024.8709	6.73	$[M-H]^{-2}$	*
		M4A1F1G1S(6)1	996.3596	996.3602	0.60	$[M-H]^{-2}$	*
		M5A1G1S(6)1	1004.3383	1004.3576	19.22	$[M-H]^{-2}$	*
		FA2G2S(3)1	1097.8975	1097.8998	2.09	$[M-H]^{-2}$	*
		FA3BG1S(3)1	1219.9633	1219.9528	8.61	$[M-H]^{-2}$	*
		A2F(2)1G2S(6)1	1097.8975	1097.8998	2.09	$[M-H]^{-2}$	*
8.57	1.44	A2G2Ga2	nd	-	-	-	
		A3F2G(SO_4^{-2})1G1	nd	-	-	-	
		A4G(SO_4^{-2})1G2	nd	-	-	-	
		A4G3S(1Ac)1	nd	-	-	-	
		FA4G2	1155.4303	1155.4315	1.04	$[M-2H]^{-2}$	
		A3F1G3S(2Ac)1	nd	-	-	-	
		FA2G2Ga1	1033.3843	1033.3785	5.61	$[M-H]^{-2}$	*
		FA3F1G2	1126.9001	1126.9208	18.37	$[M-H]^{-2}$	*
		FA2F(2)2G2	1098.3937	1098.4100	14.84	$[M-H]^{-2}$	*
		FA3G1S(3)2	1263.9497	1263.9608	8.78	$[M-2H]^{-2}$	
		FA2BG2S(6)1	1199.4409	1199.4395	1.17	$[M-2H]^{-2}$	
8.71	1.40	**M8**	919.3174	919.3230	6.09	$[M-2H]^{-2}$	*
		FA2F2G2	1098.3937	1098.4100	14.84	$[M-H]^{-2}$	*
		A3F1G(SO_4^{-2})1G2	nd	-	-	-	
		FA3F1G3S(2Ac)1	nd	-	-	-	
		A4G(SO_4^{-2})1G2	1203.3934	1203.4074	11.63	$[M-2H]^{-2}$	
		A3BG3	1163.4124	1163.4290	14.27	$[M-2H]^{-2}$	
		A2G2S(3)1S(1Ac)1	1191.4280	1191.4239	3.44	$[M-2H]^{-2}$	
		FA3F1G1S(6)1	1191.4280	1191.4421	14.54	$[M-2H]^{-2}$	*
		FM5A1G1S(6)1	1077.3762	1077.3866	9.65	$[M-2H]^{-2}$	*
		M5A1F1G1S(3)1	1077.3762	1077.3866	9.65	$[M-2H]^{-2}$	*

GU	% Area	Glycan	Experimental m/z	Theoretical m/z	Error (ppm)	Ion	
8.82	3.77	**M8**	919.3174	919.3230	6.09	$[M-2H]^{-2}$	*
		A3F2G(SO_4^{-2})1G1	nd	-	-	-	
		FA3G3	nd	-	-	-	
		A4G2Ga1	nd	-	-	-	
		M4A1F1G1Sg(3)1	1004.3447	1004.3576	12.84	$[M-2H]^{-2}$	*
		A2F(2)1G2S(6)1	1097.8839	1097.8998	14.48	$[M-2H]^{-2}$	*
		FA2G2S(6)1	1097.8839	1097.8998	14.48	$[M-2H]^{-2}$	*
		A2F1G1G(SO_4^{-2})1S(3)1	1137.8737	1137.8783	4.04	$[M-2H]^{-2}$	*
		FA2G1Ga1S(3)1	1097.8839	1097.8998	14.48	$[M-2H]^{-2}$	*
		FM5A1G1S(3)1	1077.3762	1077.3866	9.65	$[M-2H]^{-2}$	*
8.97	0.96	**M8**	919.3174	919.3230	6.09	$[M-2H]^{-2}$	*
		A4BF1G2	nd	-	-	-	
		A3F2G2	nd	-	-	-	
		A4G2Ga1	nd	-	-	-	
		FA4G3S(2Ac)1	nd	-	-	-	
		A4G3	nd	-	-	-	
		A2F2G2S(6)1	1170.9307	1170.9288	1.62	$[M-2H]^{-2}$	*
9.10	1.93	**FA2G2Ga2**	1114.3909	1114.4050	12.65	$[M-2H]^{-2}$	
		FA4F2G1	nd	-	-	-	
		FA3F2G(SO_4^{-2})1G1	nd	-	-	-	
		A4F1G3S(2Ac)1	nd	-	-	-	
		A3F1G3	nd	-	-	-	
		A4BG3	1264.9562	1264.9687	9.88	$[M-2H]^{-2}$	
		A2F2G2S(6)1	1170.9166	1170.9288	10.42	$[M-2H]^{-2}$	*
		A3G2G(*)1Ga1S(6)1	nd	-	-	-	
		A3G2G(*)1Ga1S(3)1	nd	-	-	-	
9.16	**1.80**	**M9**	1000.3449	1000.3495	4.60	$[M-2H]^{-2}$	*
		A3F3G2	1199.9453	1199.9497	3.67	$[M-2H]^{-2}$	*
		A4F2G2	nd	-	-	-	
		A3F3G(SO_4^{-2})1G1	nd	-	-	-	
		A4BF2G2	nd	-	-	-	
		A4F2G2S(2Ac)1	nd	-	-	-	
		FA2G2S(3)2	1243.4425	1243.4476	4.10	$[M-2H]^{-2}$	*
		A2F1G(SO_4^{-2})1G1S(6)1	1137.8875	1137.8783	8.09	$[M-2H]^{-2}$	*
		FA3F1G1Sg(3)1	1199.4552	1199.4395	13.09	$[M-2H]^{-2}$	*
		FA2F(2)1G(SO_4^{-2})1G1Sg(3)1	nd	-	-	-	
		A3F1G2S(6)1	1199.4552	1199.4395	13.09	$[M-2H]^{-2}$	*
		FA3G2S(6)1	1199.4552	1199.4395	13.09	$[M-2H]^{-2}$	*
		FA2G2Ga1S(3)1	1178.9237	1178.9263	2.21	$[M-2H]^{-2}$	*

GU	% Area	Glycan	Experimental m/z	Theoretical m/z	Error (ppm)	Ion	
		FA3F1G(SO_4^{-2})1G2	nd	-	-	-	
		FA3F1G3S(2Ac)1	nd	-	-	-	
		A3G3Ga1	nd	-	-	-	
9.23	**1.86**	**FA3F1G3**	1207.9369	1207.9472	8.53	$[M-2H]^{-2}$	
		FM5A1G1S(6)1	1077.3829	1077.3866	3.43	$[M-2H]^{-2}$	*
		M5A1F1G1S(6)1	1077.3829	1077.3866	3.43	$[M-2H]^{-2}$	*
		FA3F1G2S(3)1	1272.4879	1272.4685	15.25	$[M-2H]^{-2}$	*
		FA4F2G1	nd	-	-	-	
		FA3F2G(SO_4^{-2})1G1	nd	-	-	-	
9.42	1.21	FA3G(SO_4^{-2})1G2GlcNAc2	nd	-	-	-	
		FA3F2G2	1199.9377	1199.9497	10.00	$[M-2H]^{-2}$	*
		A2F(2)2G1Ga1S(6)1	1170.9095	1170.93	16.48	$[M-2H]^{-2}$	*
		M9	1000.3449	1000.3495	4.60	$[M-2H]^{-2}$	*
		A4F2G2	nd	-	-	-	
		A3F3G(SO_4^{-2})1G1	nd	-	-	-	
		A4BF2G2	nd	-	-	-	
		A4F1G3	nd	-	-	-	
9.54	5.53	A4G3Ga1	nd	-	-	-	
		FA2G2S(6)2	1243.4569	1243.4476	7.48	$[M-H]^{-2}$	*
		FA2F2G1Sg(3)1	1170.9166	1170.9288	10.42	$[M-2H]^{-2}$	*
		A3F1G2S(3)2	1344.9772	1344.9872	7.44	$[M-2H]^{-2}$	*
		FA3G2S(3)2	1344.9772	1344.9872	7.44	$[M-2H]^{-2}$	*
		FA3F1G2S(6)1	1272.4733	1272.4685	3.77	$[M-2H]^{-2}$	*
		M9	1000.3449	1000.3495	4.60	$[M-2H]^{-2}$	*
		FA3F3G2	nd	-	-	-	
		FA4F2G2	1301.4987	1301.4894	7.15	$[M-2H]^{-2}$	
		FA3F3G(SO_4^{-2})1G1	nd	-	-	-	
		FA4BF2G2	nd	-	-	-	
		FA4F2G2S(2Ac)1	nd	-	-	-	
9.68	3.21	**FA2G(SO_4^{-2})1G1S(3)2**	1283.4415	1283.4260	12.08	$[M-2H]^{-2}$	*
		FM5A1G1S(6)2	1222.9236	1222.9343	8.75	[M-2H]-2	*
		A3G3S(6)1S(1Ac)1	1374.0074	1373.9900	12.66	-	
		FA2F(2)2G1Sg(3)1	1170.9166	1170.9288	10.42	$[M-2H]^{-2}$	*
		M5A1F1G1S(6)2	1222.9236	1222.9343	8.75	[M-2H]-2	*
		FA2G2Ga1S(6)1	1178.9097	1178.9263	14.08	$[M-2H]^{-2}$	*
		FA2F2G2S(6)1	1243.9487	1243.9578	7.32	$[M-2H]^{-2}$	
		A3G2S(6)2	nd	-	-	-	

GU	% Area	Glycan	Experimental m/z	Theoretical m/z	Error (ppm)	Ion	
		A4F3G2	nd	-	-	-	
		FA4F2G2	nd	-	-	-	
		FA3F3G(SO_4^{-2})1G1	nd	-	-	-	
		FA4BF2G2	nd	-	-	-	
		FA4BF1G3	nd	-	-	-	
		A2F1G1Sg(6)1S(6)1	1170.4324	1170.4186	11.79	$[M-2H]^{-2}$	
		FA3F1G1S(3)1Sg(3)1	1344.9772	1344.9872	7.44	$[M-2H]^{-2}$	*
9.91	1.70	**A3F1G2S(6)2**	1344.9772	1344.9872	7.44	$[M-2H]^{-2}$	*
		FA3G2S(6)2	1344.9772	1344.9872	7.44	$[M-2H]^{-2}$	*
		FA3BG2S(3)2	1446.4998	1446.5269	18.73	$[M-2H]^{-2}$	*
		FA4G2S(3)2	1446.4998	1446.5269	18.73	$[M-2H]^{-2}$	*
		A3BG3Sg(3)1	1316.9713	1316.9741	2.13	$[M-2H]^{-2}$	*
		FA3G3S(6)1	1280.4749	1280.4659	7.03	$[M-2H]^{-2}$	*
		A3F1G3S(3)1	1280.4749	1280.4659	7.03	$[M-2H]^{-2}$	*
		A3F(2)1G2G(*)1Ga1	nd	-	-	-	
		FA3F2G3	1280.9520	1280.9761	18.81	$[M-2H]^{-2}$	
		FA4BF1G3	nd	-	-	-	
		A2G2S(6)3	1315.9741	1315.9663	5.93	$[M-2H]^{-2}$	
10.10	2.22	**FA2G(SO_4^{-2})1G1S(6)2**	1283.4121	1283.4260	10.83	$[M-2H]^{-2}$	*
		A4G3Sg(3)1	1316.9639	1316.9741	7.75	$[M-2H]^{-2}$	*
		FA2G2S(3)1S(2Ac)1	1285.4408	1285.4581	13.46	$[M-2H]^{-2}$	
		FA2G2S(3)1S(1Ac)1	nd	-	-	-	
		FA2G2Sg(3)1S(6)1	nd	-	-	-	
		M9Glc1	1081.3854	1081.3759	8.79	$[M-H]^{-2}$	*
10.25	1.01	**FA4G3Ga1**	1317.4625	1317.4843	16.55	$[M-2H]^{-2}$	
		A4G4Ga1	nd	-	-	-	
		A3F(2)2G2G(*)1Ga1	nd	-	-	-	
		M9Glc1	1081.3854	1081.3759	8.79	$[M-H]^{-2}$	
		FA4F3G2	nd	-	-	-	
		A4BF1G4	nd	-	-	-	
		FA2F1G1Sg(6)1S(6)1	1243.4569	1243.4476	7.48	$[M-H]^{-2}$	*
		A2F1G2S(6)2	925.6588	925.6611	2.48	$[M-H]^{-3}$	*
		FA2G2S(6)3	925.6588	925.6611	2.48	$[M-H]^{-3}$	*
		A2F1G(SO_4^{-2})1G1S(6)2	1283.4269	1283.4260	0.70	$[M-H]^{-2}$	*
10.40	1.25	**FA3F1G1S(3)1Sg(6)1**	1345.0072	1344.9872	14.87	$[M-H]^{-2}$	*
		A3BG2Sg(3)2	1389.4758	1389.4929	12.31	$[M-H]^{-2}$	*
		A3G2Ga1S(6)2	1352.9694	1352.9847	11.31	$[M-H]^{-2}$	*
		A3G3S(6)2	1352.9694	1352.9847	11.31	$[M-H]^{-2}$	*
		FA3F1G3S(6)1	1353.5126	1353.4949	13.08	$[M-H]^{-2}$	*
		FA3BG3Sg(3)1	926.3265	926.3330	7.02	$[M-H]^{-3}$	*
		FA3F2G2S(6)1	1345.4736	1345.4974	17.69	$[M-H]^{-2}$	

GU	% Area	Glycan	Experimental m/z	Theoretical m/z	Error (ppm)	Ion	
10.60	0.58	A3BF3G3	nd	-	-	-	
		A3F2G3S1-2Ac	nd	-	-	-	
		FA3F(2)3G3	1353.9805	1354.0051	18.17	$[M-2H]^{-2}$	*
		A2F2G2S(6)1Sg(3)1	1324.4694	1324.4740	3.47	$[M-2H]^{-2}$	
		FA3F1G2S(3)2	1426.0267	1426.0137	9.12	$[M-H]^{-2}$	*
10.83	1.24	FA3G(SO_4^{-2})1G2Lac2	nd	-	-	-	
		A4G2Sg(3)2	1389.4683	1389.4929	17.70	$[M-H]^{-2}$	*
		FA3F1G2S(6)2	1426.0267	1426.0137	9.12	$[M-H]^{-2}$	*
		FA2F2G2S(6)2	1389.5140	1389.5055	6.12	$[M-H]^{-2}$	
		FA3G3S(6)2	1426.0267	1426.0137	9.12	$[M-H]^{-2}$	*
		A3F1G3S(6)2	1426.0267	1426.0137	9.12	$[M-H]^{-2}$	*
11.02	2.64	A4F4G3	nd	-	-	-	
		FA3BF3G3	nd	-	-	-	
		FA3F2G3S(2Ac)1	1353.4900	1353.4949	3.62	$[M-H]^{-2}$	*
		A3F3G2Sg(6)1	1353.9805	1354.0051	18.17	$[M-H]^{-2}$	*
		FA3F2G2Sg(6)1	1353.9805	1354.0051	18.17	$[M-H]^{-2}$	*
		FA3F3G2Sg(3)1	1426.5303	1426.5239	4.49	$[M-H]^{-2}$	*
		FA3F2G3S(6)1	1426.5303	1426.5239	4.49	$[M-H]^{-2}$	*
		A2F(2)2G1Ga1Sg(3)2	nd	-	-	-	
11.19	1.50	FA4F3G3	nd	-	-	-	
11.41	0.33	**A3F1G2S(3)2Sg(6)1**	1498.5428	1498.5324	6.94	$[M-H]^{-2}$	*
		FA3G2S(3)2Sg(6)1	1498.5428	1498.5324	6.94	$[M-H]^{-2}$	*
		A3G3S(6)3	1498.5428	1498.5324	6.94	$[M-H]^{-2}$	*
		FA3F1G3S(6)2	1499.0272	1499.0426	10.27	$[M-H]^{-2}$	*
		FA3F2G2S(3)1Sg(3)1	1499.0272	1499.0426	10.27	$[M-H]^{-2}$	*
		FA3F(2)3G3S(3)1	999.3592	999.3661	6.90	$[M-H]^{-3}$	
11.52	0.78	A4F4G4	nd	-	-	-	
		FA4F4G3	1528.5516	1528.5737	14.46	$[M-2H]^{-2}$	
		FA2G2S(6)4	1534.5472	1534.5430	2.74	$[M-2H]^{-2}$	
		A3BG2Sg(3)2S(6)1	1023.0133	1023.0246	11.05	$[M-H]^{-3}$	*
		A4G2Sg(3)2S(3)1	1023.0133	1023.0246	11.05	$[M-H]^{-3}$	*
		FA2G2Ga1Sg(3)1Sg(6)1	1340.4454	1340.4689	17.53	$[M-2H]^{-2}$	
		FA2F2G2S(6)3	1023.0133	1023.0330	19.26	$[M-H]^{-3}$	
		A3F3G2Sg(3)1S(6)1	1499.0193	1499.0426	15.54	$[M-2H]^{-2}$	*
		FA3F2G2Sg(3)1S(6)1	1499.0193	1499.0426	15.54	$[M-2H]^{-2}$	*
		A4F1G3Sg(6)1	926.3328	926.3330	0.22	$[M-H]^{-3}$	*
		FA4F2G3S(6)1	1528.0465	1528.0635	11.13	$[M-2H]^{-2}$	

GU	% Area	Glycan	Experimental m/z	Theoretical m/z	Error (ppm)	Ion	
11.64	1.26	A4F1G(SO_4^{-2})1G2Lac2	nd	-	-	-	
		FA3G3S(6)3	1571.5725	1571.5614	7.06	$[M-2H]^{-2}$	*
		A3F1G3S(3)3	1571.5725	1571.5614	7.06	$[M-2H]^{-2}$	*
		A4BG3Sg(3)2	1047.7007	1047.7036	2.77	$[M-H]^{-3}$	*
		FA3F3G2Sg(6)1	1426.5380	1426.5239	9.88	$[M-2H]^{-2}$	*
		FA3F2G3S(3)2	1047.7007	1047.7119	10.69	$[M-H]^{-3}$	*
		A3F(2)2F(3)1G2G(*)1Ga1	nd	-	-	-	
11.95	0.45	FA4F4G4	nd	-	-	-	
		FA4F1G(SO_4^{-2})1G2Lac2	nd	-	-	-	
		FA3BG3S(6)3	1115.0688	1115.0649	3.50	$[M-H]^{-3}$	
		FA3F3G2Sg(3)1S(6)1	1572.0767	1572.0716	3.24	$[M-2H]^{-2}$	
12.06	1.36	**FA2BG2Sg(6)2S(6)1**	nd	-	-	-	
		A3F1G3S(6)3	1047.3622	1047.3718	9.17	$[M-H]^{-3}$	
		A4BG3Sg(3)1Sg(6)1	1047.7140	1047.7036	9.93	$[M-H]^{-3}$	*
		A3F3G2Sg(6)1S(6)1	999.0156	999.0260	10.41	$[M-H]^{-3}$	*
		FA3F2G2Sg(6)1S(3)1	999.0156	999.0260	10.41	$[M-H]^{-3}$	*
		FA3F2G3S(6)2	1047.7140	1047.7119	2.00	$[M-H]^{-3}$	*
		A4BF1G4Sg(3)1	1572.5808	1572.5692	7.38	$[M-2H]^{-2}$	
12.62	1.33	FA4F2G(SO_4^{-2})1G2Lac2	nd	-	-	-	
		FA4BG3Sg(6)1Sg(3)1	1096.4098	1096.3895	18.52	$[M-H]^{-3}$	
		FA3F(2)3G3S(6)2	1096.4098	1096.3979	10.85	$[M-H]^{-3}$	
12.73	0.55	FA4F4G(SO_4^{-2})1G2GlcNAc3	nd	-	-	-	
12.87	0.45	FA3'F(2)3G2G(*)1Ga1Sg(3)1	nd	-	-	-	
13.04	0.30	FA3'F(2)3G2G(*)1Ga1Sg(3)1	nd	-	-	-	
13.16	0.51	FA4F3G(SO_4^{-2})1G3GlcNAc4	nd	-	-	-	
		A4F4G3Sg(3)1S(3)1	1754.6228	1754.6377	8.49	$[M-H]^{-2}$	
13.29	0.53	**FA4F4G4S(6)1**	1169.7518	1169.7628	9.40	$[M-H]^{-3}$	
13.56	0.69	**FA4F2G3S(6)3**	1217.7722	1217.7685	3.04	$[M-H]^{-3}$	*
		A4F3G3S(3)3	1217.7722	1217.7685	3.04	$[M-H]^{-3}$	*
		A4F4G4S(6)2	1218.0872	1218.1087	17.65	$[M-H]^{-3}$	
		A3'F(2)2G2G(*)1Ga1Sg(6)2	nd	-	-	-	
14.58	0.74	**A4F1G4S(6)4**	1266.1235	1266.1144	7.19	$[M-H]^{-3}$	